CCD Photometry of Eclipsing Binary Star Systems in the Large and Small Magellanic Clouds

by

J.D. Pritchard

A thesis submitted in partial fulfillment of the
requirements of the degree of Doctor of Philosophy

UNIVERSITY OF CANTERBURY

Department of Physics and Astronomy

CHRISTCHURCH

NEW ZEALAND

CCD Photometry
of
Eclipsing Binary Star Systems
in the
Large and Small Magellanic Clouds

J.D. Pritchard

A thesis submitted in partial fulfillment of the
requirements of the degree of Doctor of Philosophy

For
Mum and Dad
who are always,
always
there.

Acknowledgments

I would first like to thank Alan Gilmore who was one of the first to help me at the telescope. He provided guidance and experience without which I might never have found my first star! At a much later stage, Alan also acquired observations on a number of nights and I thank him for that. Most of all though, I would like to thank Alan for his advice from time to time and his always friendly and helful nature.

I would like to thank Mohd Zambri Zainuddin who also acquired a number of observations for me as well as with me. His bubbly, almost comical nature was infectious and made long nights of observing pass quickly.

I feel I owe a great debt to Mike Clark and John Baker who between them kept the observatory and telescope operational dispite my best efforts to the contrary from time to time. I am sure I will never forget December the 24th 1994, when both Mike and John spent several hours trying to resurrect a telescope that had mysteriously ceased to function. In true testament to their expertise they succeded in their efforts to repair the faulty beast. Unfortunately, true to form for Mount John, that night was cloudy and no observations were possible that night. I also thank Mike Clark for the huge number of observations he made on my behalf.

I thank Peter Cottrell and John Hearnshaw for the many interesting and valuable discussions and for sharing with me their vast wealth of knowledge and experience over the past five years.

I gratefully acknowledge the assistance and support provide by the technical staff of the Department of Physics and Astronomy, and by Roger Govind and Mark Aitchison in particular.

To Jon-Paul Wells, David Frame, Tom King, Andrew Richards, Duncan McCloud, Steve Jamison, Jean-Phillipe Beaulieu and Phillipe Grison in particular, and all the other graduates students of the Department in general, I perhaps owe my sanity, for these brave and intrepid adventurers were kind enough to include me in their explorations of the extra-curricular opportunities abounding in these here parts.

I am thankful for the financial and logistical support afforded me by the Department of Physics and Astronomy, University of Canterbury and of course the University of Canterbury itself. I am also immeasurably indebted to the International Astronomical Union, the Royal Society of New Zealand, the Royal Society of New Zealand – Canterbury Branch, the Royal Astronomical Society of New Zealand and to Frank Bradshaw and Elizabeth Pepper Wood who all provided financial assistance which allowed me to spend three months studying at the Institut d'Astrophysique, Paris, France and to attend the Third Pacific Rim Conference on Recent Developements in Binary Star Research in Chaing Mai, Thailand. I also acknowledge financial support from the Marsden Fund which has permitted me to complete this degree to my own satisfaction without the insupportable burden of total financial ruin.

I am of course also thankful to the Institut d'Astrophysique, Paris, France who also provided no small measure of financial and logistical support during my three month visit.

Finally, to my supervisor William Tobin, whose door has always been open for me, I owe my greatest debt. William has worked ceaselessly and tirelessly to make me the scientist that I am. He has been a true mentor, but more than that, he has been a good friend. I especially appreciate the personal courtesy he has shown me, never more so than during those sometimes lonely three months in Paris when he often shared the companionship and happiness of his family with me. Thank you William.

Abstract

Double lined, eclipsing binaries are an important probe of stellar structure and evolution. Their study provides the most accurate data on the defining fundamental properties of stars, namely stellar masses, radii and luminosities.

Observations made at the Mount John University Observatory (MJUO) have yielded high precision, six colour CCD light curves and calibrated standard system Strömgren *uvby* and Cousins *VI* photometry for three Magellanic Cloud eclipsing binaries; HV 982 and HV 2241 in the Large Magellanic Cloud (LMC) and HV 1620 in the Small Magellanic Cloud (SMC). The masses, radii and luminosities for HV 1620 and HV 2241 have been determined by analysis of the light curves and standard system photometry in conjunction with IUE ultraviolet spectrophotometry and spectroscopic radial velocity curves obtained by other investigators. The masses, radii and luminosities for HV 982 have been estimated in conjunction with IUE ultraviolet spectrophotometry by adopting a distance for the system. No spectroscopic radial-velocity curves are available for HV 982 at this time.

Analysis of the calibrated standard system photometry, light curves and IUE spectrophotometry for the well-detached, 5.55335 d period HV 982 permits the determination of the effective temperatures of the two components of HV 982; $T_{\rm eff,1} = 24\,000 \pm 5\,000$ K and $23\,400 \pm 5\,000$ K. The large uncertainties result from the poorly defined reddening which in turn is primarily due to large uncertainty in the $(b-y)$ photometry resulting from observations obtained on only two nights, both of questionable quality. The fact that no spectroscopic radial-velocity curves are available means that neither the mass ratio nor the physical size of the system can be determined directly. The derived temperatures are nonetheless insensitive to reasonable ranges of the mass ratio (as deduced from the the form of the light curve) and of the physical size of the system (in order to be consistent with the distance to the LMC). Adopting a value of unity for the mass ratio and a distance modulus of $(m-M)_0 = 18.35 \pm 0.2$ mag allows the estimation of masses, radii and thus luminosities of the individual components of HV 982. They are $\mathcal{M}_1 = \mathcal{M}_2 = 9.1 \pm 3.2\,\mathcal{M}_\odot$, $\mathcal{R}_1 = \mathcal{R}_2 = 7.0 \pm 1.1\,\mathcal{R}_\odot$ and $\log[L_1/L_\odot] = 4.2\pm0.5$, $\log[L_2/L_\odot] = 4.1\pm0.5$. These properties correspond well to the expected properties of normal single stars as predicted by modern theoretical stellar evolution models. Moreover the position of the components of HV 982 in the Hertzsprung-Russell Diagram (HRD) implies the components are main sequence stars, although not far from the Terminal Age Main Sequence (TAMS), i.e. HV 982 is still relatively young, which is consistent with the fact that HV 982 is an eccentric orbit system. Apsidal motion with a period of 206 ± 6 yr has also been discovered and an improved ephemeris, including the effects of the apsidal motion has been derived.

Combined analysis of the MJUO photometry and light curves, the IUE spectrophotometry and the published spectroscopic radial-velocity curves permits a complete analysis and direct determination of the properties of the 3.62642 d period HV 1620. The analysis yields the following properties for the components of HV 1620: $T_{\rm eff,1} = 33\,000\pm4\,500$ K, $\mathcal{M}_1 = 20.9\pm0.4\,\mathcal{M}_\odot$, $\mathcal{R}_1 = 6.27\pm0.10\,\mathcal{R}_\odot$ and $\log[L_1/L_\odot] = 4.62\pm0.25$; $T_{\rm eff,2} = 24\,400\pm3\,500$ K, $\mathcal{M}_2 = 14.3\pm0.7\,\mathcal{M}_\odot$, $\mathcal{R}_2 = 11.3\pm0.2\,\mathcal{R}_\odot$ and $\log[L_2/L_\odot] = 4.53\pm0.25$. The system is found to be in a semi-detached configuration, with the cooler component filling its Roche lobe, while the hotter component is well-detached from its Roche lobe. Despite this evolved binary state, the properties of both components correspond well to those of normal single stars, implying that any mass transfer currently in progress is occuring at a rate slow enough that both components can retain at least the appearance of normal single stars. Comparison of the the observed spectral flux distribution with model flux distributions also yields the distance modulus, $(m-M)_0 = 18.6\pm0.3$ mag, which is in agreement with other measurements of the distance modulus for the SMC. An improved ephemeris has been determined.

Similarly, the combined analysis of the MJUO photometry and light curves, the IUE spectrophotometry and the published spectroscopic radial-velocity curves permits a complete analysis and direct determination of the properties of the 4.3426241 d period HV 2241. The effective temperatures, masses, radii and luminosities of the components of HV 2241 are $T_{\rm eff,1} = 27\,000\pm3\,000$ K, $\mathcal{M}_1 = 36.82\pm0.10\,\mathcal{M}_\odot$, $\mathcal{R}_1 = 16.1\pm0.2\,\mathcal{R}_\odot$ and $\log[L_1/L_\odot] = 5.10\pm0.20$ and $T_{\rm eff,2} = 20\,200\pm1\,500$ K, $\mathcal{M}_2 = 19.4\pm0.6\,\mathcal{M}_\odot$, $\mathcal{R}_2 = 13.9\pm0.1\,\mathcal{R}_\odot$ and $\log[L_2/L_\odot] = 4.49\pm0.13$. The distance modulus is 18.50 ± 0.16 mag, likewise in good agreement with other measurements of the distance modulus for the LMC. Like HV 1620, this system is found to be in a semi-detached configuration with the cooler component filling its Roche lobe. However the hotter component of HV 2241 is very close to filling its Roche lobe also. The above properties give stars that are somewhat under-luminous in comparison to normal single-star models and are not consistent with binary-star evolution models for very massive, short period systems. The derived properties can however be brought into agreement with current theory if there is a large ($\sim$12 percent) systematic error in the radial

velocity data for this star. (If there is a systematic error in one of the data sets, it seems most probable that it would be in the radial velocities since this data was obtained photographically on a 1-m telescope and a $M_V = 13.5$ mag star like HV 2241 must surely be close to the practical limit of such a system.) If on the other hand the properties derived here are accurate then it would appear that HV 2241 has been caught in an unprecedented evolutionary phase.

A new analysis procedure has been employed in order to investigate the nature of a selection of eight stars from the recently published *EROS catalogue of eclipsing binary stars in the bar of the Large Magellanic Cloud.* All eight stars are well-detached systems with obviously eccentric orbits. The results of the analysis show seven of the eight to be composed of young (i.e. main sequence), coeval components, in accord with theoretical models for binary star formation and evolution. Consideration of the position of the components of eighth system, EROS 1061, in the HRD leads to the suggestion that this system is composed of two pre-main sequence stars in the final stages of contraction down onto the zero-age main sequence.

Contents

Figures

Tables

Chapter 1

Introduction

Stars constitute the fundamental 'building block' of the Universe. The ability of Science to observe, interpret and make predictions about the Universe beyond the solar-system is based almost entirely on stars and empirical and theoretical understanding of them. The implications of this are far reaching, perhaps one of the most fundamental questions confronting science today is the age of the Universe. The hierarchy of methods by which the age of the Universe is measured are based upon the assumed properties of stars derived from stellar evolution and stellar pulsation theories. It is essential therefore that those models be as accurate and precise as possible. This requires that the theoretical models for all aspects of stars be tested against reality, across as wide a range of conditions as possible. In this thesis I present the results of research aimed at increasing the size of the global data base against which modern theoretical stellar astrophysical models, in particular those for stellar evolution, can be tested. This research centres on the investigation of eclipsing binary stars in the Magellanic Clouds.

The nature of the problem makes this task non trivial. It is not possible to examine a star from the 'comfort' of a laboratory, to subject it to variable conditions in order to see how it responds. Nor can we dismantle a star in order to investigate its inner workings. Instead we can only make observations of the motions of stars and of the radiation emitted at the surfaces of stars.[1] Although new technologies are forever improving and increasing the ways in which we can obtain and analyse such data, we are limited in the number of properties of stars which can be directly observed.

It is nevertheless possible to deduce a great deal from such limited data sources. Currently of interest in the literature, at least as far as evolutionary models are concerned, are the influences of model parameters such as helium abundance, opacity tables, mixing length and convective core overshooting. The data necessary to permit tests of theoretical models and to discriminate between models differing in these properties are the *mass*, *radius*, *luminosity* and *metal abundance* of individual stars. The components of *Close Binary Stars* represent a large fraction of all stars for which the above physical characteristics have been accurately determined. The research described in what follows centers on my efforts to determine the masses, radii and luminosities of the components of a number of eclipsing binaries, one of which is located in the *Small Magellanic Cloud* (SMC) while the remainder are members of the *Large Magellanic Cloud* (LMC).

In the first section of this introduction, I present a simplistic picture of exactly what an eclipsing binary is and an outline of historical aspects of the study of eclipsing binaries. I then go on to describe how eclipsing binaries are studied and elaborate on the applications of the results of such studies. In the following section I give a brief overview of the history and importance of the study of the Large and Small Magellanic Cloud galaxies. Following that, I discuss the research programme undertaken in the course of this degree. The last section of this chapter provides an overview of Charge-Coupled Device (CCD) detectors and in particular their application to astronomical purposes and a short introduction to the processing of CCD images.

In the following chapters I discuss the work conducted and present the results of the research toward those goals. Specifically, chapter 2 details aspects of the observations of three stars obtained at the Mount John University Observatory (MJUO), while chapter 3 describes the reduction[2] of the observations to produce light curves[3] and calibrated standard system photometry.[4] In chapter 4 I present a brief description of the model used in the analysis of the light curves and background information regarding the actual analysis

[1] Arguably, one might also include particles blown off by radiation pressure and released during the thermonuclear processes which produce the vast majority of the energy released by stars during the majority of stellar lifetimes, but apart from the sun, most stars are too distant for such sources to be of significant utility.

[2] Reduction is a somewhat generic term when applied to astronomy. Perhaps the broadest definition is simply *Reducing a large data set to a smaller, more meaningful set.* In my particular case this, for the most-part, means the measurement of the brightnesses of anywhere between 1 and perhaps 20 stars in a CCD image, in essence the reduction of some several hundred thousand numbers – the individual pixel values which make up the image – to a mere handful.

[3] Measurements of the brightness of an object (for example a star or a galaxy) as a function of time.

[4] Measurements of the brightness of object at particular wavelengths (or more precisely over a range of wavelengths defined by some bandpass). Photometry is also concerned with the relative brightness of an object at two (or more) wavelengths. Measurements at a single wavelength are generally called 'magnitudes', while relative brightnesses at two different wavelengths are termed 'colour indices'.

procedure. Chapter 5 deals with the analysis of the calibrated standard system photometry while chapter 6 presents final results obtained by combining the light curve and standard system photometry analyses with other data for the three stars taken from the literature. Chapter 6 also includes a discussion of these results in the light of current theoretical models for the evolution of both single stars and binary stars. Chapter 7 deals with results to date from on-going related research before a final discussion, including possibilities for the future, is presented in chapter 8.

1.1 Eclipsing binary star systems

An *eclipsing* binary star is merely the result of a fortuitous alignment of the orbital plane of the rather more commonplace binary star. However, due to the unique combination of the orbital motion and the variation in total light output due to eclipse phenomena[5] the study of eclipsing binaries is a particularly powerful tool for the investigation of stars in general.

1.1.1 What is an eclipsing binary

Binary stars in general form one of the most diverse and interesting class of stars known. Such diversity inevitably leads to endless classification, sub-classification, sub-sub-classification... In what follows, I do not attempt to review all that is known of binary stars but rather to take as direct a route as possible to the elucidation of the fundamental nature of *eclipsing* binaries.

The first requirement of a binary star for it to possibly be an *eclipsing* binary is that it be *gravitationally bound* – as against those who are merely located in the same general volume of space but whose individual motions will eventually carry them apart, or those that are merely chance alignments of two stars seen in the same direction but separated by large distances. The components of gravitationally bound systems, under the influence of their mutual gravitational attraction, will orbit about their common center of mass, obeying – at least to a very good first approximation – Kepler's Laws of orbital motion. Their systemic properties, in particular the orbital period and the separation of the components, range over several orders of magnitude, from systems with periods of small fractions of a day and correspondingly small separations (e.g. the *cataclysmic binary* HV And which has a period of $\sim$0.056 day, Ritter 1990) up to the most widely separated systems with periods of several hundreds of years (see for example Latham et al., 1991). In fact, it is difficult to place an upper limit on the orbital period, and hence the separation of the components of binary stars, since astronomers have only possessed the appropriate tools for measuring such phenomena for a relatively short period of history, i.e. a relatively small fraction of the longest orbital periods.

Figure 1.1 depicts a binary star system in a circular orbit as seen from two vantage points, one directly above the system in the sense that the two stars would then move in the plane of the sky or, as in this case, in the plane of the page, the other from an *angle of inclination* of $\sim$76° (see inset in figure 1.1). A circular orbit is of course a special case of orbital motion. More generally, the components of two body gravitationally bound systems move in elliptical orbits. However, consideration of a circular orbit can often be very instructive as some of the complications arising from the variable orbital speed and separation of the two components in elliptical orbits (see figure 1.2) are then obviously not present.

The only other requirement of a binary star in order for it to be an *eclipsing* binary is that its orbit be inclined at an appropriate angle to the observer's line of sight so that at some point in their orbital cycle, the motions of the two components carry first one in front of the other and then (usually[6]) vice-versa. Plainly, any gravitationally bound binary system is potentially an eclipsing binary, the controlling factor being the chance orientation of the orbital plane with respect to the observer.

1.1.2 Close Binaries

The separation of the two components of a binary star system plays an influential rôle in the evolution of both the individual component stars as well as the system as a whole. A binary star is classified as a *Close Binary* if the two components of the binary star are close enough together that the fact that they are in a binary star system will, at some point in time, have an important bearing on their evolution in that sense that their

[5] In fact only in the most simple of cases does the light vary only during an eclipse, more generally, the light can be constantly varying, although the eclipses are usually the most prominent features of the light curve.

[6] In exceptional circumstances it is conceivable that, for a particular combination of orbital eccentricity and inclination, at some longitudes of periastron only one eclipse per orbital cycle results while for at other longitudes of periastron the more usual two eclipses per cycle result, figure 1.2.

evolution will significantly differ from that of isolated stars of the same initial masses and compositions. Within this class of binary, there are a number of sub-classes, but a little background is required first.

If one imagines a small quantity of stellar matter moving away from the center of gravity of one of the stars (for whatever reason) toward the other, eventually the point will be reached where the gravitational attraction of the second star is stronger than that of the first, and the matter will be lost from the first and gained by the second. This is, in the most simplistic terms, what is called *Mass Exchange* or *Mass Transfer*.

Similarly a small quantity of stellar matter moving away from one of the stars in some other direction will reach a point where the gravitational attraction will not be great enough to overcome to centrifugal effects of the orbital motion of the system as a whole. In this case, the matter will likely be lost from the system entirely, a process not surprisingly termed *Mass Loss*.

Mass exchange and mass loss are perhaps the two main reasons why evolution of a star in a binary system may differ from that which would occur if the same star were isolated. Theoretical models predict that as stars evolve they pass through phases of rapid increase (and decrease) in their radii. This then provides the mechanism by which mass exchange and mass loss can result. In very massive stars ($\mathcal{M} \gtrsim 10\mathcal{M}_{\odot}$), stellar winds also provide a mechanism by which significant mass loss can occur.

The distance from each star at which the star's gravity is no longer sufficient to attract mass back to itself defines what is referred to as a *Critical Roche Lobe* or simply Roche lobe. Roche lobes in fact define three dimensional surfaces, much like a three-dimensional figure eight, surrounding the two components. The exact geometry of the each Roche lobe depends on the separation of the two components and upon the mass of each component. A more complete discussion of the concept of Roche lobes and the Roche model in general is given in section 4.1. The concept of Roche lobes allows for the classification of systems according to whether both, one or other, or neither star is contained within its respective Roche lobe:

- If both stars are sufficiently young that neither star has *yet* evolved to the point where it 'fills' its critical Roche lobe, the system is referred to as *detached*.
- When one or other of the components is essentially filling its Roche lobe, the system is labelled *semi-detached*.
- When both stars just fill their Roche lobes it is said to be a *contact* system.
- If one or both of the stars overflows their Roche lobe the system is termed a *common envelope* system since the whole binary will generally be surrounded by a gas cloud.

The different physical situations described above correspond to physical properties of binaries that are not directly observable. However, the classifications do correspond reasonably well with observable properties, i.e. the form of the light curve the systems. Detached systems tend to have relatively simple light curves, with little or no variation in light level outside of eclipse whereas the semi-detached, contact and common envelope systems tend to have light curves which vary continuously during the orbital cycle.

It should be obvious from figure 1.1 that the closer that the two components of the system are to each other, the greater the chance of eclipses resulting since eclipses will occur for an increasing range of inclination as the separation of the two components decreases. As a result, the vast majority of known eclipsing binaries have relatively short periods – of the order of 1 to 10 days – since the orbital period of the system is proportional to the separation of the components (as well as, but inversely, to their total mass – Kepler's 3rd Law). This means that most, if not all known eclipsing binaries are indeed close binaries.

1.1.3 Important processes in binary star systems

There are four main processes which affect the properties and evolution of the individual components of binary star systems, as well as the system as a whole. The processes are *Circularization* of the orbit, *Synchronization* of axial rotation with orbital rotation, *Mass Transfer* and *Mass Loss*.

Circularization of the orbit and synchronization of the axial rotation of the individual components with orbital rotation of the system arise out of 'tidal' interactions. The details of the mechanism responsible for the tidal interactions is the topic of ongoing discussion in the literature, e.g. Rieutord and Zahn (1997), Tassoul and Tassoul (1992) and most recently Keppens (1997). In spite of disagreements among the major proponents in the field regarding the precise details of the tidal interaction process, there is qualitative agreement regarding the overall consequences of the interactions. Circularization and synchronization proceed due to the dissipation of orbital and rotational energy by the tidal interactions. These changes have an effect on the geometry of the critical Roche lobes and thus alter the maximum size the components can attain before the onset of mass transfer and mass loss, although probably not by any greatly significant degree.

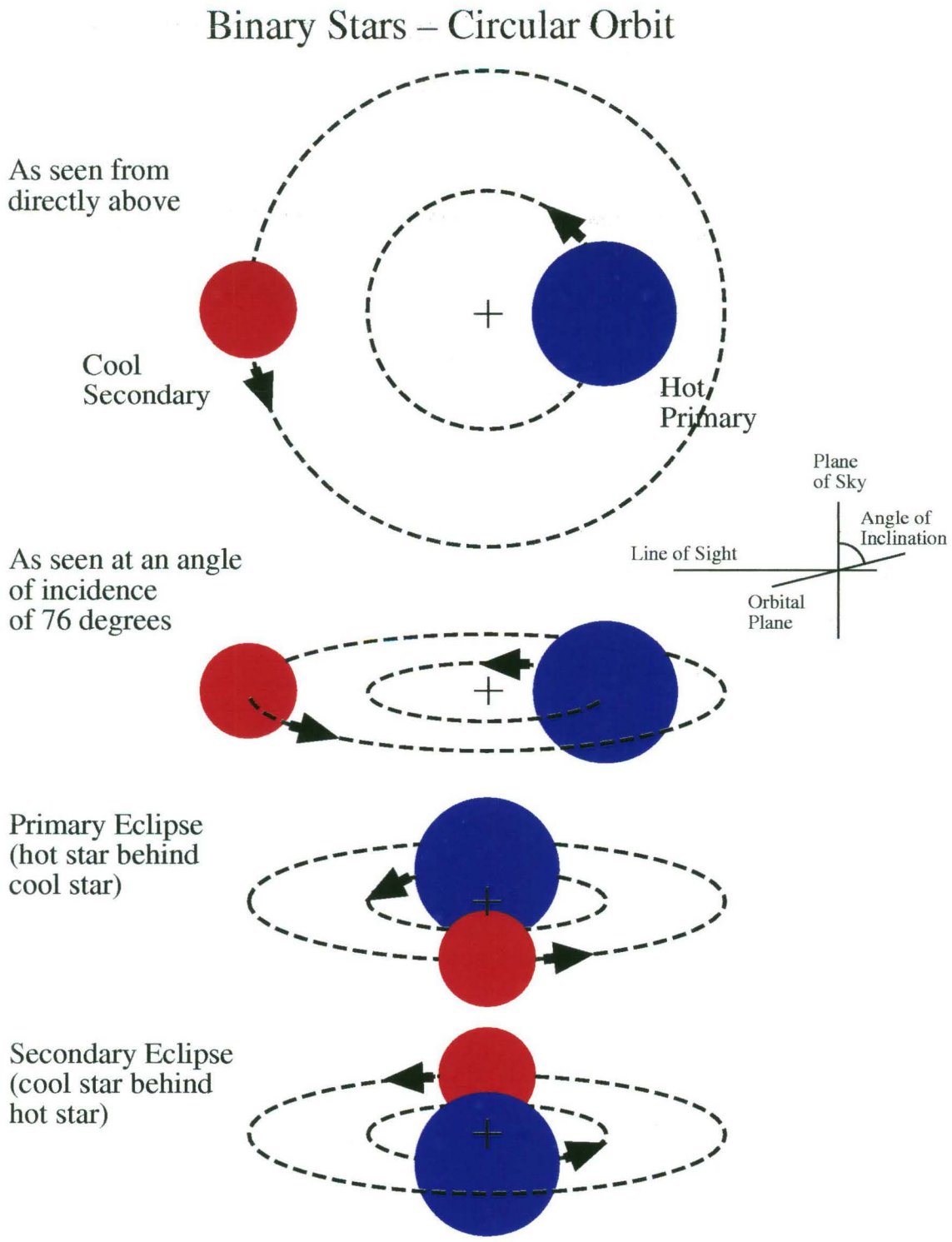

Figure 1.1: Four schematic representations of an eclipsing binary whose components are in circular orbits. At the top, the orbit is seen from a view point perpendicular to the plane of the orbit (i.e. an inclination of 0° – see inset). The lower three sketches view the system from an inclination of 76°, with the components at orbital phases corresponding to (second) *Quadrature*, *Primary* minimum and *Secondary* minimum. The + indicates the center of mass of the system. In this frame of reference the center of mass remains fixed, and the stars move in such a way so as that a line joining their individual centers of mass always passes through the systemic center of mass.

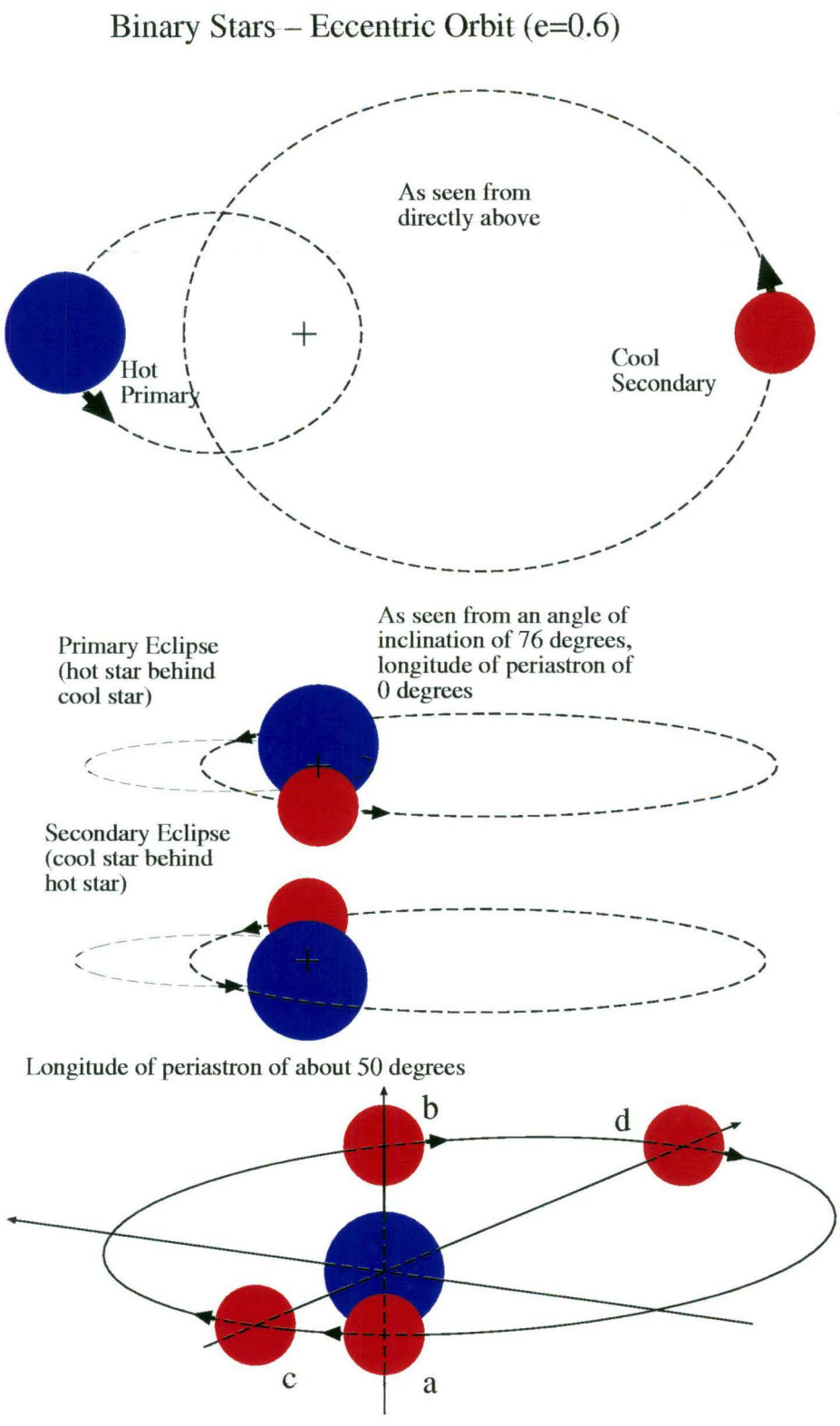

Figure 1.2: Four schematic representations of an eclipsing binary whose components are in eccentric (or elliptical) orbits. At the top, the orbit is seen from a view point perpendicular to the plane of the orbit (i.e. an inclination of 0°). The middle two views see the system from an inclination of 76° with a particular orientation of the major semi-axis (i.e. longitude of periastron). The components are shown at orbital phases corresponding to *Primary* and *Secondary* minima (upper middle and lower middle respectively). As in figure1.1, the + indicates the fixed center of mass of the system and the stars move in such a way so as that a line joining their individual centers of mass always passes through the systemic center of mass. The bottom view shows exactly the same system only from the frame of reference of the primary component and with a different orientation of the major semi axis. This figure illustrates an the interesting case of an eclipsing binary where only one eclipse per orbit occurs. The orbital phases labelled (a) and (b) indicate the phases when primary and secondary eclipses would usually occur. This unusual situation is merely due to the particular combination of orbital eccentricity and inclination and the longitude of periastron with respect to the line of sight. Points (c) and (d) indicate periastron and apastron respectively.

More importantly the rates at which circularization and synchronization proceed are determined by the characteristics of the components of the the binary and the binary system itself, in particular the masses, radii, luminosities, mass ratio and orbital period. The rates also depend on the internal structure of the individual stars. On the whole, synchronization occurs over a much shorter time scale than circularization. Thus studies of synchronization and circularization provide useful empirical insight into stellar structure (Claret et al., 1995).

Mass transfer and mass loss processes have the potential to affect the evolution of the individual components of a system as well as the system as a whole much more dramatically. During mass transfer phases significant fractions of the total mass of the system can be moved from one component to the other. Aside from altering the mass ratio of the system, mass transfer acts to redistribute angular momentum between the two components while mass loss is accompanied by the loss of angular momentum from the system. Both of these changes in angular momentum result in changing the separation of the components (or equivalently, the orbital period of the system). For example a system initially composed of $9\,\mathcal{M}_\odot + 8\,\mathcal{M}_\odot$ with an orbital period of 3.95 days will eventually end up as a $2.19\,\mathcal{M}_\odot + 11.46\,\mathcal{M}_\odot$ system with an orbital period of 18.41 days (de Loore and De Greve, 1992). Such dramatic changes in mass for the individual components must necessarily drastically alter their evolutionary path from that of isolated single stars. Recent studies of the evolution of close binary stars, including the effects of mass transfer and mass loss have been made by Doom and de Grève (1983), Doom (1984), Sybesma (1985; 1986a; 1986b), De Greve and Doom (1988), de Loore and De Greve (1992), De Greve and de Loore (1992) and De Greve (1993). A more general review of stellar evolution in binary star systems is that of Batten (1995).

1.1.4 Some historical notes

The variability of stars has been recorded for several centuries now (Strohmeier, 1977). Perhaps the earliest such record derives from Arabic sources which describe a 'new star in Scorpius' in the year 1006. Today there exists a region of intensive X-ray radiation in this direction, which is perhaps the remnant of a supernova explosion. Indeed the names of such stars – *nova* and super*nova* – derive from the Latin *novus* meaning new. Similarly, one need search no further than the name of certain stars to realize that the star's intrinsic variability has been noticed; β Persei's more familiar name *Algol* for example, likely derives from the Arabic *al-ghul* meaning 'demon' or 'changing' spirit.

It was however, only somewhat more recently that some stars, including Algol, were recognized as varying on a regular, or perhaps semi-regular, basis. In 1596, Fabricius noted the variability of o Ceti (Mira Ceti) but it wasn't until 1638 that Holwarda deduced that o Ceti was in fact varying periodically.

It was in 1786 that Pigott published the first summary of variable stars. His catalogue comprised 12 stars, eight of which were true variables, the remaining four being novae. A century later the number of catalogued variable stars had grown to 143. By the start of the twentieth century, that number had blossomed to some 700. With the high precision of today's technology, the difficulty is often to find a star which is NOT variable!

The history of eclipsing binaries tends to follow, and indeed at times, to lead the history of astronomy in general. Algol in fact turns out to be an eclipsing binary, a fact first deduced by Goodricke in 1783. Subsequently, many eclipsing binaries were identified by many astronomers, although little could be deduced from their light variations due to the lack of a means to accurately measure them. It wasn't until 1880 that Pickering was able to derive the elements[7] of a binary star from the analysis of its light curve derived from photometric measurements of the brightness of the star through-out its orbital period. Within ten years, spectroscopic methods were applied to the observation of eclipsing binaries, revealing the variation of radial velocity[8] in eclipsing binaries which of course results from their orbital motion. To this day, photometric light curves and spectroscopic radial velocity curves remain the basic data required for determination of the elements of eclipsing binaries.

It was in 1910 that Blazko, Russell and Shapley put determination of the elements of eclipsing binaries, via the analysis of eclipsing binary light curves, onto a theoretical foundation, albeit a rather simple model based on circular orbits and spherical stars. It wasn't until 1940 that Russell published a revised theory of eclipsing binary light curve analysis, which incorporated a process known as *rectification*. The new theory provided a means by which to account for the effects of ellipsoidal, rather than spherical components, which could have greater surface brightnesses on the hemispheres of the stars that faced each other (the *reflection* effect) and varying gravitational acceleration over the stellar surfaces (leading to *gravity darkening*):

[7]The 'elements' of a binary include the relative sizes and surface brightnesses of the two component stars of the binary system, eccentricity and inclination of the orbit of the system as well as the distance to the system.

[8]The radial velocity of an object is component of the object's velocity in the direction of the line of sight from the observer.

processes which had been shown to be important and whose theory had been developed by others in the intervening years. These processes generally act to complicate the form of the light curve, often to the point where the light is continuously varying, thus complicating interpretation of the light curve and the determination of elements. Rectification in essence 'corrected' a light curve distorted by the aforementioned effects into one with constant light outside of eclipse.

But of course, as with all science, the field continued to develop. As the quality of the observational data improved, and new and ever more subtle effects were found, new and ever more complicated models and theories were developed to explain the new phenomena. Computation by hand grew ever more laborious. Despite a well developed theoretical understanding of the process which influence the observed light of an eclipsing binary, the fully physical application of the theories was, to a large extent, entirely impractical. It was not until the advent of the modern computer that this sad state of affairs could be reversed.

In the late 1960s the first computer programs for the analysis of binary star light curves, implementing much more physical models, began to appear. Some of these original programs, or at least their direct descendants, survive to this day and have even become the standard in the field (e.g. the Wilson and Devinney program, see chapter 4). The basic functioning of these programs is as follows. The light output at each observed orbital phase is computed according to the model implemented by the program and then compared to the observed light at that orbital phase. After consideration of the differences between each observed and model light value, the parameters of the model are adjusted so as to reduce the overall discrepancy between the observations and the predictions of the model. However, even the incredible power of modern computers does not render the problem entirely trivial. Numerical techniques are generally required both in the computation of the model lights and in the determination of the corrections for the model parameters required to fit the observations. The determination of a solution is necessarily an iterative process and of course all of the standard problems associated with numerical algorithms, (e.g. solution convergence, uniqueness of the solution etc.) are applicable. Nevertheless with careful use these modern computer programs are incredibly powerful and in conjunction with certain other data, the elements of eclipsing binaries (i.e. the orbital inclination and eccentricity, the masses, radii and luminosities of the individual components and the distance to the system) can be determined to great accuracy (Andersen, 1991).

1.1.5 The study of eclipsing binaries

The study of eclipsing binaries has, in general, a seemingly simple goal – *The determination of the basic characteristics of the individual components if the system*, i.e. the mass, radius, luminosity and perhaps the chemical composition of each star. As with any research effort, it is the required observations and subsequent analysis of the resultant data that is the tricky part.

The frequency of eclipsing binaries and their variety means that useful data can probably be obtained by all possible observational techniques. However, probably the most useful data is that provided by *standard system photometry*,[9] *photometric light curves* and *spectroscopic radial velocity curves*. With these three data sets, along with modern analysis tools, the desired properties of the components can, at least in theory, be completely determined. Standard system photometry provides information on the temperatures of the stars, photometric light curves provide information about the relative physical geometry of the system, while spectroscopic radial velocity curves set that onto an absolute scale. The problem is however sufficiently complicated that the three data sets are best treated as a whole, rather that as individual, isolated sets. If analyzed individually, each data set will in general yield formally different results, with no clear indication of which result is the better, or how to combine or average the individual results into a single result. Other observational data, such as ultraviolet spectrophotometry, can help to improve the precision of or confidence in the derived properties of the component stars, or may help to provide a more complete picture of the system and the processes of importance that the system is undergoing.

What can be learnt from the study of eclipsing binaries?

Obviously the mass, radius and luminosity of each of the component stars can be determined, provided of course that appropriate data is available. In addition, the study of eclipsing binaries can provide useful information about stellar structure, atmospheres and evolution as well as permitting the determination of the distance to the star, and hence any other stars that maybe associated with the binary if, for instance, the binary star is a member of cluster or perhaps a galaxy other than the Milky Way.

[9] Calibrated magnitudes and colour indices (such as the Strömgren c_1 index). The most appropriate photometric system to use is dependent on the kind of stars the binary system to be observed is composed of.

Binaries with eccentric orbits display a phenomenon known as apsidal motion. This is a process whereby the system as a whole actually rotates and is seen as a rotation of the major semi-axis (see figure 1.2). There are several causes for the motion including a general relativistic term. But in general, in the case of binary star systems, the dominant term is caused by the divergence of the stars from spherical symmetry due to tidal interactions between the two components of a system and rotational distortion. Study of eccentric-orbit eclipsing binaries displaying apsidal motion thus can provide information on the internal structure of the stars, i.e. the variation of the matter density through the interior of the star.

As one star moves across the face of the other during an eclipse the eclipsing star is in fact acting as a kind of a scanner and can thus provide information of the structure of the atmosphere of the eclipsed star and any processes that might be occurring in the atmosphere of the eclipsed star. In the special case where a large, extended star eclipses a much more compact and hotter star (e.g. ζ Aurigae, K5 Iab + B7 V), if the orbital plane is so inclined that the smaller star moves across the larger at relatively high latitudes then the light from the smaller star will likely be seen through the atmosphere of the larger which will likely provide information on the chemical makeup of the atmosphere of the giant star which may well have consequences on evolution as well as mass exchange and mass loss processes.

Determination of the temperature and luminosity of a star locates it, in most cases, unambiguously on the Hertzsprung-Russell diagram and hence specifies its evolutionary state. Most theories on the origins of binary stars imply that the two stars should share the same age since they are presumed to form at the same time. Therefore determination of the temperature and luminosity of the two components of a binary star system should correspond to two stars of the same age. If the stars are of different initial mass then they will evolve at differing rates, but they should nonetheless correspond to stars of the same age. Such data for *detached* binaries[10] can thus be used to test the validity of theoretical models for stellar evolution.

Once the intrinsic properties of the stars are known absolutely, the intrinsic luminosity can be compared with the observed luminosity from which the distance to the binary star can be, almost trivially, determined.

The above uses to which the results of the study of eclipsing binaries may be put is but a sample. A recent review by Guinan (1993) provides a more complete and in depth discussion of the many and varied uses to which eclipsing binary star data may be put.

Why the study of eclipsing binaries is useful

Detailed verification of modern theoretical astrophysical models for stellar structure, atmospheres and evolution are essentially based on the observations of little more than a handful of stars in our own Galaxy, the Milky Way. And in fact there are only a relatively small number of stars for which the fundamental parameters (mass, radius, luminosity) are known to any great accuracy (Andersen, 1991)[11]. Almost all of this data has been provided by the study of eclipsing binaries. The stars in the Milky Way however, represent a rather limited sample in terms of chemical composition. Variations in composition lead to rather subtle influences on the properties of individual stars, however such effects can have far reaching consequences[12]. Thus we must look to stars with significantly different compositions in order to verify the theoretical models over as broad a range of stellar parameters as possible. For this purpose, the stars in the Large and Small Magellanic Clouds offer a wonderful opportunity since modern technology has now made possible observations of sufficient quality that theoretical models can be tested against empirical observations with the appropriate rigour.

In addition, the ability to determine the distance for individual systems to great accuracy (Tobin et al., 1997) and with very little reliance on theory or empirical calibration is of great importance since, apart from a rather small number of the closest stars to earth, distances can in general only be determined via statistical relationships and usually rely rather more heavily upon either theoretical models of one sort or another or on empirical calibrations. One example is distance determinations for Globular Clusters where the apparent magnitude of the Main Sequence Turn Off Point is compared with the intrinsic magnitude for stars at the appropiate stage of evolution, as derived either from theoretical evolution and structure models or from an empirical calibration. Another is distances based on empirical Cepheid Period-Luminosity (PL) relationships where an assumption is made that extra-galactic Cepheids obey the same PL relationship as Galactic Cepheids. With the recent advent of technology of a sufficient standard to permit observations of the appropriate precision of eclipsing binary stars in local group galaxies, the whole cosmological distance

[10] Systems which have undergone some significant degree of mass exchange or loss are unsuitable for such purposes since these processes affect the apparent age of the stars, and mean that the stars can no longer be expected to appear to be of the same age.

[11] Andersen (1991) presents data for 45 binary systems, i.e. 90 individual stars, with masses and radii determined to better than 2 percent for which single-star evolutionary models can be presumed valid.

[12] Differences in chemical composition may go a long way toward reducing the scatter, and hence bring into better agreement, the many determinations of the Hubble Constant (Beaulieu and Sasselov, 1997).

scale can be put on a much firmer basis than is currently achieved with the present methods for extra-galactic distance indicators. The accuracy of individual eclipsing binary distances may also be of use as a probe of the structure of the Magellanic Clouds (e.g. Bell et al., (1991; 1993)).

1.2 The Magellanic Clouds

The Large Magellanic Cloud (LMC) and the Small Magellanic Cloud (SMC) are the two nearest galaxies to the Milky Way, at approximately 50 and 60 kpc from the Galaxy respectively. In the summary to his review of the literature at the time, Westerlund (1990) wrote,

> The Magellanic Clouds play a fundamental role in a number of fields of astronomical research. Their distances are most relevant to the extragalactic distance scale. Their relative proximity offers exceptional opportunities for detailed studies of their stellar and interstellar content. They serve therefore as testing grounds for modern astrophysical theories in particular concerning the chemical evolution of stars and galaxies.

The study of the Magellanic Clouds spans more than 100 years. Their nature as separate galaxies from our own Galaxy appears to have first been surmised by Abbe (1867). One of the most famous, and perhaps important, results to have come from the study of the Magellanic Clouds is the discovery of the Period-Luminosity (PL) relationship for Cepheids by Leavitt (1912). To this day, and well into the foreseeable future, the PL relationship plays a crucial rôle in extragalactic distance determinations and the distances to the Clouds themselves form the cornerstone of the extragalactic distance scale, so important to the truly grand questions concerning the nature, origin and future of the Universe itself.

Research during the past few decades has concentrated on the questions of the distance to and the structure, kinematics and composition of the Clouds, in the ultimate hope of better understanding their evolutionary history and future. As a consequence the innumerable number of studies of the Clouds have employed wide and varied methods and techniques. The Clouds have been studied from radio to X-ray frequencies from probably every southern ground-based observatory as well as from satellite observatories such as the *International Ultraviolet Explorer* (IUE), *Infra-Red Astronomical Satellite* (IRAS) and most recently the *Hubble Space Telescope* (HST).

The Clouds and the Galaxy almost certainly form an interacting three body system and it is probable that this interaction has led to their somewhat irregular appearance. Recent studies indicate that the LMC is in fact probably a disk galaxy seen nearly edge on, although a little distorted thus giving rise to its irregular appearance. The SMC on the other hand seems more likely to be a true irregular galaxy. Studies of the H I distribution in and around the Clouds show much larger complexes associated with the galaxies than is indicated by the visible component of the galaxies. Furthermore these studies reveal the presence of a 'bridge' of matter between the two Clouds and a 'stream' of matter extending out from the Clouds. Recent numerical simulations have had great success reproducing the observed gas distributions of these structures by modelling the gravitational interactions between the Clouds and the Galaxy as the Clouds orbit about each other and about the Galaxy as a bound system (Gardiner et al., 1994). These results are extremely promising, however large uncertainties surround most of the initial conditions governing the simulations and many critical assumptions, although apparently reasonable enough, are made a priori without strong observational evidence for their validity. Nevertheless, the Galaxy and Magellanic Clouds are clearly linked and their interactions likely have a strong bearing on the evolution of all three galaxies. In a sense the three galaxies form binary systems which are, in some ways, analogous to the close binary star systems already described.

Despite their close association and the resulting interactions between the Clouds and the Galaxy, their current evolutionary states differ due of course to differences in their evolutionary histories. An important consequence of apparently different rates and conditions of star formation is that the three galaxies now have quite different chemical makeups. The proportion of the total mass of the LMC which is composed of metals[13] differs from that of the Galaxy by a factor of approximately 2.5 (Pagel, 1993). In the SMC, metals are approximately 10 times less abundant than in the Galaxy (Pagel, 1993). According to theory, these differences have important consequences for stellar structure and evolution.

The review by Westerlund is the most recent attempt to summarise research on the Magellanic Clouds. An earlier review is that of Buscombe et al. (1954). Table 1.1 presents a summary of general properties for the LMC and SMC (reproduced from Westerlund, 1990).

[13] All elements heavier than Hydrogen and Helium are, in astronomy, termed *metals*. Metals are (mostly) the products of stellar evolution via thermonuclear proceeses.

Table 1.1: General properties of the Large and Small Magellanic Clouds, reproduced from Westerlund (1990).

	LMC	SMC
V	0.1 mag	2.3 mag
$B-V$	+0.55 mag	+0.50 mag
$(m-M)_0$	18.5 mag	18.9 mag
Distance	50 kpc	60 kpc
Diameter on sky	24°	7°
Tilt	45°	...
Optical center	$5^{\rm h}24^{\rm m}, -69.8°$	$0^{\rm h}48^{\rm m}, -73.2°$
Total Mass[a]	$6 \times 10^9 \mathcal{M}_\odot$	$1.5 \times 10^9 \mathcal{M}_\odot$
HI mass[b]	$5 \times 10^8 \mathcal{M}_\odot$	$5 \times 10^8 \mathcal{M}_\odot$
Gas/Dust ratio[c]	4	17

[a] $\mathcal{M}_{\rm Gal} \approx 10^{11} \mathcal{M}_\odot$
[b] $\mathcal{M}_{\rm H\,I_{Gal}} \approx 10^9 \mathcal{M}_\odot$ i.e. $\mathcal{M}_{\rm H\,I}/\mathcal{M}_{\rm Total} \approx 0.33/0.08/0.01$ for the SMC/LMC/Galaxy.
[c] Relative to the Galactic gas/dust ratio

1.2.1 Eclipsing binaries in the Magellanic Clouds

The earliest studies of eclipsing binaries in the Magellanic Clouds derive from the Harvard College Observatory's (HCO) Magellanic Cloud project carried out over a period of some seventy years, beginning in 1898 and ending in the early seventies (Gaposhkin, 1970). The project was based on photographic surveys consisting of some 4000 plates. It was conducted under the auspices of such notables as E. Pickering, H. Shapley and S.I. Gaposhkin[14]. Aside from the pioneering work of Leavitt, Gaposhkin (1970) claims the following achievements from the project: the discovery, cataloguing and investigation of 3323 variable stars and the 'establishment beyond reasonable doubt' of the existence of star streams connecting the Clouds and the Milky Way, the determination of distance moduli ($(m-M)_0$) to the Clouds (18.38±0.02 mag for the LMC and 19.15±0.03 for the SMC – quoted uncertainties here are internal only), the 'absence' of tilt of the Clouds in the conventional sense, the existence of mini-clusters and the topography of the LMC.

Of the 3323 variable stars discovered by the HCO project, one hundred and eight were positively identified as eclipsing binaries. Ephemerides were determined and photographic light curves were presented (Shapley and Nail, 1953; Wetzel, 1953; Gaposchkin, 1965; Payne-Gaposchkin and Gaposchkin, 1966; Gaposhkin, 1970; Payne-Gaposchkin, 1971; Gaposhkin, 1977). Until recently these catalogues represented the majority of the known eclipsing binaries in the Magellanic Clouds. The low precision of the photographic light curves (several hundredths of a magnitude) however renders these data unsuitable for the determination of accurate elements. In spite of this H.N. Russell carried out light curve analyses of one LMC[15] and three SMC eclipsing binaries based on observations 'communicated to the writer [Russell] by Mrs. NAIL' (Russell, 1956). Russell's analysis was based on nomographic techniques applied to the rectified data. For each of the four systems analysed, Russell obtained several solutions which correspond to different initial assumptions regarding the nature of the system, i.e. 'grazing transit', 'equal radii' and 'grazing occultation'. For these reasons any comparison between Russell's results and the work here are not of great significance and no comparison has been attempted.

Herczeg (1982) presents the first *photoelectric* light curve for a Magellanic Cloud eclipsing binary, again HV 2241.[16] More recently, Davidge (1987; 1988) obtained and analysed three colour UBV photoelectric light curves of five Magellanic Cloud eclipsing binaries (HV 2241, HV 2765 and HV 5943 in the LMC,[17] HV 1620 and HV 1669 in the SMC). Photographic spectroscopic radial velocity curves have been obtained for four Magellanic Cloud eclipsing binaries (HV 2241 and HV 2543 in the LMC, HV 1620 and AzV 73 in the SMC, Niemela and Bassino, 1994).

The advent of the CCD detector has made possible more detailed study of individual binary systems in the Clouds. With CCD detectors accurate photometry is possible with 1-m class telescopes while accurate spectroscopic radial velocity curves can be obtained with 4-m class telescopes. Jensen, Clausen and Giménez (Jensen et al., 1988) secured complete or partially complete two colour BV CCD light curves for

[14] Mr Gaposhkin is also known to have adopted the slight different spelling of his name of 'Gaposchkin' from time to time.
[15] In fact the LMC eclipsing binary analysed by Russell was HV 2241, one of the stars investigated in this thesis.
[16] The 'popularity' of observing HV 2241 in the LMC is no doubt due to the fact that it is the brightest eclipsing binary in the LMC.
[17] The name of these stars, as so often is the case, derives from and/or is in recognition of the circumstances surrounding their 'discovery'. The label 'HV' is simply an acronym for *Harvard Variable*, reflecting the fact that these stars were first recognised as variable stars by the Harvard College Observatory's Magellanic Cloud project.

Table 1.2: Distance moduli for selected Local Group Galaxies (reproduced from van den Bergh, 1992).

Galaxy	$(m-M)_0$ [mag]	D [kpc]
LMC	18.45±0.1	49
SMC	18.80±0.15	58
NGC 6822	23.66±0.2	540
NGC 185	23.96±0.25	620
NGC 147	24.09±0.25	660
M31	24.3±0.1	725
M32	24.3	725
NGC 205	24.3	725
IC 1613	24.42±0.13	765
M33	24.5±0.2	795

six Magellanic Cloud eclipsing binaries (HV 5936, HV 6029 and HV 12634 in the LMC, HV 1876, HV 2016 and HV 2226 in the SMC). The analysis of these light curves for two of these systems, in conjunction with spectroscopic radial velocity curves subsequently obtained on the Anglo-Australian Telescope, has been published (HV 2226 Bell et al., 1991 and HV 5936 Bell et al., 1993). The group responsible for these efforts continue this programme, obtaining both CCD light curves and spectroscopic radial velocity curves for further eclipsing binaries in both Clouds (Clausen, 1996). In 1989, Tobin initiated a long term project to obtain CCD light curves of Magellanic Cloud eclipsing binaries (e.g. Tobin, 1994, also section 1.3.1 below).

Recently, both IUE SWP ultraviolet spectrophotometry ($\lambda\lambda$1150-2000 Å, Bradstreet, 1995) and HST spectrophotometry ($\lambda\lambda$1150-7075 Å, Guinan, 1996) has been obtained for about ten Magellanic Cloud eclipsing binaries. Because only the brightest, hottest stars in the Clouds are observable, the majority of their energy output is in the ultraviolet, hence short wavelength observations are required in order to accurately determine the effective temperatures of the stars. Accurate temperatures are required in order to establish empirically the mass/luminosity relationship.

In the early 1990's several large projects searching for dark matter using the microlensing technique (see section 1.3.2) were initiated. Two of these projects, EROS[18] and MACHO[19], use the dense star fields of the Magellanic Clouds to search for the elusive microlensing events. As a consequence, these two projects generate light curves for several million stars in the Magellanic Clouds. More than 40 000 of these have been discovered to be variable (Cook, 1996). Several catalogues of selections of these variable stars have been published (Grison et al., 1995; Beaulieu et al., 1995; Alcock et al., 1995; Alcock et al., 1996b; Alcock et al., 1996a). The catalogue by Grison et al. lists 78 newly identified LMC eclipsing binaries which essentially doubles the number of previously known eclipsing binaries in the LMC. The MACHO group are yet to publish a catalogue of eclipsing binaries found in their data. The other catalogues are of Cepheid, RR Lyrae and R Coronae Borealis stars. As Cook points out, the huge number of high precision light curves with excellent phase coverage are revolutionising the study of Magellanic Cloud eclipsing binaries, and of course other types of stars as well as the Clouds themselves.

Magellanic Cloud eclipsing binaries are of particular interest because being located in the Clouds they are of course of low metallicity. Eclipsing binaries in the Clouds therefore provide unprecedented opportunities for the study of the rôle metallicity plays in determining stellar structure, evolution and mass loss. Additionally, eclipsing binaries should permit the determination of the distance moduli with high accuracy i.e. ±0.15 mag or better (Giménez et al., 1994; Tobin et al., 1997).

1.2.2 The distance to the Magellanic Clouds

The Magellanic Clouds play a fundamental rôle in calibrating the cosmic distance ladder. They are the closest Galaxies to our own galaxy, the Milky Way, by an order of magnitude (or 4 mag in $(m-M)_0$ – see table 1.2). Distances to all other galaxies are therefore measured *relative* to the distance to the Clouds[20] or at least via a series of relative measures with the Clouds at the very base. Clearly then it is essential that the distances to the Clouds be known with as much certainty and accuracy as possible.

Table 1.3 summarises recent determinations of the distances the the LMC (using seven different methods

[18]Expérience de Reserche d'Objets Sombres (e.g. Aubourg et al., 1993).
[19]MAssive Compact Halo Objects (e.g. Alcock et al., 1993).
[20]In practice, primarily the *Large* Magellanic Cloud.

Table 1.3: Distance moduli for the LMC and SMC determined by various methods based on various objects (reproduced from Westerlund, 1997.) The mean values are the unweighted means of the values for the different methods; the errors indicate the scatter between the individual values. Clusters are omitted because of the uncertainties still prevailing in the fitting procedures.

	LMC		SMC	
	$(m-M)_0$	n	$(m-M)_0$	n
Cepheids	18.53±0.03	17	18.93±0.04	6
RR Lyraes	18.37±0.04	10	18.83±0.03	3
Mira stars	18.46±0.08	4		
OB stars	18.35±0.07	2	19.05±0.07	2
Red stars	18.42±0.15	1		
SN 1987A	18.50±0.04	5		
Novae	18.70±0.23			
Mean values	18.48	7	18.94	3

Table 1.4: Distance moduli for the LMC based on Supernova 1987A (reproduced from Westerlund, 1997).

Author	Method	$(m-M)_0$
Panagia et al. (1991)		18.53±0.13
Hanuschik & Schmidt-Kaler (1991)	shell expansion	18.47±0.18
Schmidt-Kaler, (1992)	Baade's method, ring expansion and ring light propagation parallax	18.38±0.07
McCall (1993)	based on Panagia et al.	18.52±0.13
Crotts et al. (1995)	light echoes, circular ring	18.61±0.11

and/or kinds object) and the SMC (using three different methods and/or kinds of object). While apparently accurate estimates of $(m-M)_0$ can be obtained by considering a single class of object, as indicated by the quoted (internal) errors, clearly systematic errors, as yet unaccounted for, mean that the true uncertainty in the distance is more likely of the order of 10 percent, rather than the typical ~3 percent often quoted. The major source of these systematic errors undoubtably arises from an imcomplete understanding of the phenomenon being used to measure the distances. Distance determinations based on Cepheids for example have to date assumed a Galactic Period-Luminosity relationship. The subtle, yet possibly important influence of metallicity is thus unaccounted for. Needless to say, resolving these uncertainties is the subject of much active research (Beaulieu and Sasselov, 1997).

SN 1987A on the other hand presents an unprecented opportunity to measure the distance to the LMC more directly than is possible for the majority of the other methods which rely either on imperfect models or a-priori empirical assumptions. Table 1.4 presents five recent determinations of the distance to the LMC based on observations of SN 1987A. Clearly there is good agreement amongst the individual determinations which have largely been made using independent data sources and a variety of techniques.

As noted above, eclipsing binaries in the Magellanic Clouds have the potential to allow the determination of the distance moduli with high accuracy i.e. ±0.15 mag or better for each object (Giménez et al., 1994; Tobin et al., 1997). Furthermore, the distance moduli are determined directly: they do not depend on a succession of calibration steps, unlike most other methods. Distances for two eclipsing binary systems, one in each Cloud, have recently been determined. Bell et al. (1991; 1993) find distance moduli of 18.6±0.3 for HV 2226 in the SMC and 18.1±0.3 mag for HV 5936 in the LMC. These are the first such measurements of notable accuracy for individual systems. They cite their spectroscopic radial-velocity data which was obtained in poor seeing conditions as the main factor resulting in the less than optimum accuracy in their determinations.

1.3 Research programme

The aim of the research programme undertaken is the investigation of stellar properties with a view to gaining a better understanding of stellar structure and evolution. Eclipsing binaries in the Magellanic Cloud have been investigated since eclipsing binaries potentially provide the most accurate data on stellar properties while stars in the Magellanic Clouds provide the opportunity to study stars of significantly different chemical

Table 1.5: Location of the Mount John University Observatory and other southern hemisphere observatories.

Observatory	Longitude	Latitude	Altitude (m)
MJUO	170° 27′ 54″ E	43° 59′ 14″ S	1027
Mount Stromlo Obs., Mount Stromlo, Aust.	149° 00′ 30″ E	35° 19′ 12″ S	767
SAAO, Sutherland, S.A.	20° 56′ 39″ E	32° 22′ 46″ S	1771
AAO, Siding Spring, Aust.	149° 03′ 42″ E	31° 16′ 24″ S	1149
CTIO, Cerro Tololo, Chile	70° 48′ 53″ W	30° 09′ 57″ S	2215
ESO, Cerro La Silla, Chile	70° 43′ 48″ W	29° 15′ 24″ S	2282

compositions from that of Galactic stars. In the pursuit of this aim I have become involved with two projects. The major component of this research has been as part of the ongoing *Mount John University Observatory Magellanic Cloud Eclipsing Binary*, or MJUO MCEB, project. The goal of my involvement with this project has been to acquire and analyse CCD observation of three Magellanic Cloud eclipsing binaries. Over the period December 1993 to February 1994 I visited the Institut d'Astrophysique de Paris, France (IAP) where I became involved with the EROS project. Here the hope was to find new eclipsing binaries suitable for further study from MJUO.

1.3.1 The Mount John University Observatory Magellanic Cloud Eclipsing Binary project

My involvement with the MJUO MCEB project continues and builds on previous efforts by by West, Duncan, Watson, Gilmore and of course Tobin (e.g. West, 1991; Duncan, 1991; West et al., 1992; Watson et al., 1992; Tobin et al., 1993a; Duncan et al., 1993). The primary objective of the MJUO MCEB programme is to obtain high accuracy standard system photometry and multi-bandpass light curves of eclipsing binary star systems in the Magellanic Clouds. The purpose of this is to determine the fundamental stellar parameters of the individual components of the systems by the analysis of these data in conjunction with other data, including spectroscopic radial velocity curves and ultraviolet to visible spectrophotometry, obtained by collaborators and other investigators. These fundamental stellar data for the low metallicity stars of the Magellanic Clouds can then be compared with the predictions of appropriate theoretical stellar structure and evolution models, in order to empirically check the validity of such low metallicity models, which are at present untested but important, for example, for the modelling of the evolution of external galaxies, which vary greatly in metallicity.

The MJUO MCEB project was started in 1989 by the principal investigator Dr. William Tobin and continues a tradition of binary star research at the University of Canterbury and the MJUO. In the mid sixties several students from the University of Pennsylvania, Philadelphia, Pennsylvania, U.S.A., made photoelectric observations of eclipsing binaries for their Ph.D. projects (e.g. Chambliss, 1967a,1967b; Leung, 1974; Guinan 1977). In 1971 Mochnacki and Marsh obtained masters degrees for their theses entitled *The W Ursae Majoris Systems: Interpretation of Light Curves and Line Profiles* (Mochnacki, 1971) and *Semi-detached close binary systems* (Marsh, 1971). Mochnacki also published several papers (e.g. Mochnacki and Doughty, 1972a,1972b). Finally, in 1982, Buckley gained his masters degree for his thesis on *Observations and interpretation of some neglected eclipsing binaries.*

The MJUO is ideally suited for studies of the Magellanic Clouds. At the latitude of the observatory (43° 59′ 14″ S) worthwhile CCD photometry of stars in both the LMC and the SMC can be carried out year round. The airmasses never exceed ~2.9 for the LMC and ~2.4 for the SMC. This fact coupled with the relatively high availability of telescope time (compared with major international observatories) means that long term programmes are relatively easy to carry out at MJUO.

Observations of Magellanic Cloud eclipsing binaries for the present project were first acquired in 1990. These first observations were made by Tobin, Duncan, West and Gilmore using the MJUO 60cm Boller & Chivens telescope, the then newly purchased Photometrics CCD system (see section 2.1.2) and a set of glass BVI filters. Calibrated standard system BVI photometry and complete light curves with reasonable phase coverage were secured during 1990 for five systems, LMC:HV 2208 and SMC:HV 12634 (West et al., 1992), LMC:HV 2274 (Watson et al., 1992), LMC:HV 12484 (Tobin et al., 1993a) and SMC:HV 1761 (Duncan et al., 1993). The precision of the data obtained in this initial campaign was 'in general no better than 1-2 percent' (Duncan et al., 1993), while the uncertainty in the zero points of the photometry 'probably did not exceed 0.1-mag' (Duncan et al., 1993).

I became involved with the project toward the end of 1992. In an effort to improve upon the earlier efforts a number of instrumentation and procedural changes were implemented:

- Observations were shifted from the 60-cm Boller & Chivens telescope to the 1-m McLellan telescope. Obviously the greater light gathering power of the 1 m telescope permits, in theory at least, shorter exposures, better signal and/or the observation of fainter objects.

- The BVI filters were replaced with a six filter set based on *uvby* of the Strömgren four colour system and V and I of the Cousins $UBVRI$ system (hereafter, the MJUO *uvbyVI* photometric system – see section 2.1.4). The *uvby* photometry allows far more accurate estimation of stellar properties than BVI photometry for the early-type (i.e. late O- early B-type) stars that Magellanic Cloud eclipsing binaries invariably consist of.

- Use of a newly constructed, purpose-built Photometer Head which allows real-time telescope guiding and computer-controlled filter selection. The guiding facility allows for longer exposures (necessary for the intermediate bandwidth *uvby* filters, especially for the shorter wavelengths. The computer-controlled filter wheel reduces the probability of observer errors and mechanical breakdown or fault (see section 2.1.3).

- Use of alternative image reduction software. The stellar images from the 1990 observations are clearly non-circularly symmetric, probably due to atmospheric refraction, tracking errors and seeing conditions. The reduction package used to reduce these images (ROMAFOT) however utilises a circularly symmetric Point Spread Function (PSF) for the estimation of magnitudes (see section 1.4.1 below). This presumably leads to an image-dependent systematic error in the magnitude estimates of stars in the image. Primarily for this reason DAOPHOT II which permits non-circularly symmetric PSFs was used for image reduction.

- Generally improved observation and reduction procedures, based on the experience gained during the 1990 campaign, were continually developed.

With these improvements in place a second observational campaign was begun in November of 1992 and carried on until March of 1995. The vast majority of the observations during this phase of the programme were been made by myself, although observations were also made by Tobin, Clark, Gilmore and Zambri (see chapter 2). Calibrated standard system Strömgren $(b-y)$, $\mathrm{m_1}$ and $\mathrm{c_1}$ and Cousins V and $(V-I)$ photometry (see chapter 5) and complete differential magnitude light curves (of varying degrees of phase coverage) have been secured in the six colour *uvbyVI* system for three Magellanic Cloud eclipsing binaries: HV 982 and HV 2241 in the LMC and HV 1620 in the SMC (see chapter 3). These data result from the reduction and analysis of some 2800 CCD images. The light curves and calibrated photometry have been analysed in conjunction with IUE SWP ultraviolet spectrophotometry (also chapter 5) and where available spectroscopic radial velocity curves to finally yield masses, radii and luminosities for the individual components of the three systems, which have been compared with theoretical evolutionary models (chapter 6). For the two systems for which spectroscopic radial velocity curves are available, HV 1620 and HV 2241, distances to the systems have also been determined.

1.3.2 Expérience de Recherche d'Objets Sombres

The *Expérience de Recherche d'Objets Sombres* (EROS) is a major French collaboration aimed at detecting baryonic matter (i.e. the so-called dark matter) in the halo of the Milky Way. According to the General Theory of Relativity, when any massive body passes in front of a light source, the light's path will follow the local distortion of the space-time continuum caused by the gravitational field of the body. For particular alignments of light source, massive body and observer, an amplification of the observed light as seen by the observer will result, the so-called microlensing effect. A modern treatment of the theory and its application to Galactic halo dark matter searches using the stars of the Magellanic Clouds as potential source objects is presented by Paczynski (1986). Dark matter has been suggested as the cause of the observed flat galactic rotation curves which are at odds with the expected rotation curves given the masses and distribution of that mass as deduced from the observable components of galaxies, namely stars. EROS is but one of (at least) eight collaborations in search of Galactic halo dark matter.

The first phase of the EROS project is now complete. It consisted of two complementary programmes aimed at photometrically detecting microlensing events caused by dark matter in the Milky Way's halo passing in front of stars in the Large Magellanic Cloud. The first programme involved the photographic monitoring of about 4 million LMC stars over a $5.2^\circ \times 5.2^\circ$ area (centered on $\alpha = 05\mathrm{h}\ 20\mathrm{mn}, \delta = -68^\circ\ 30'$, J2000.0) using the ESO 1 m Schmidt telescope. One hour exposures in two colours (blue and red) were taken no more frequently than nightly. This approach is primarily sensitive to massive lens objects ($10^{-4}\mathcal{M}_\odot \leq$

$\mathcal{M} \leq 1\mathcal{M}_{\odot}$) and microlensing events lasting from one day to a few months. The other programme involved a 16 chip CCD mosaic camera mounted on a 40 cm $f/10$ reflector telescope. This setup had a field of view of $0.4° \times 1.1°$ and for three observing seasons (1991-92 to 1993-94) was centered on the bar of the LMC ($\alpha = 05\text{h}\,23.5\text{mn}, \delta = -69°\,36'$, J2000.0) while during 1994-95 was centered on an SMC field ($\alpha = 0\text{h}\,50\text{mn}, \delta = -73°\,15'$, J2000.0). This programme yielded some 250 000 light curves. As compared with the photographic programme, the CCD programme is sensitive to lens objects with masses in the range $5\times10^{-8}\mathcal{M}_{\odot} \leq \mathcal{M} \leq 5\times10^{-4}\mathcal{M}_{\odot}$ and to shorter duration events since many (up to 46) measurements per night were acquired.

No microlensing events have been detected in the CCD data (Aubourg et al., 1995) but two possible events have been identified in the photographic data (Ansari et al., 1996). Uncertainty surrounds the interpretation of these two events as microlensing events. The possibility that the stars are 'new types of irregular variable stars' can not yet be ruled out. Complementary observations are therefore in progress in the hope of resolving remaining uncertainties.

Clearly the project generates vast quantities of data. The usefulness of this data extends far beyond 'merely' the detection of dark matter. As noted above, I spent 3 months visiting the IAP where I worked with members of the EROS group. My motivation for this collaboration was to identify new LMC eclipsing binaries suitable for further, more accurate observation from MJUO. The EROS catalogues of eclipsing binaries (Grison et al., 1995) and Cepheids (Beaulieu et al., 1995) are a direct consequence of this collaboration. Unfortunately, very few if any of the EROS eclipsing binaries are suitable for observation from MJUO due to the very crowded fields they reside in.

Nevertheless further analysis of the EROS eclipsing binary light curves has been undertaken in an effort to identify especially interesting systems from which other investigators with access to sites with better seeing conditions may profit in observing. The analysis effort has also proved exceedingly useful, first of all, in coming to terms with the analysis software, and later as something of an experimental test bed for software and procedural development. If nothing else it has provided a wealth of experience in the analysis and interpretation of a wide plethora of eclipsing binary light curves.

The results of my analysis of eight of the EROS systems are presented in chapter 7.

1.4 CCDs in Astronomy

In the time since 1975 when Charge-Coupled Devices (CCDs) were first used for astronomical observations (Jacoby, 1990), something of a revolution has occurred. In the span of about ten years CCDs became the detector of choice for optical astronomy at all major observatories around the world. In the following ten years, advancements in CCD technology have extended the useful range of application of the CCD and further cemented the central rôle that CCDs play in modern astronomy.

The utility of the CCD for astronomical observations is immense. Of primary import are the following properties:

- **It is an area detector**: a CCD image is a two-dimensional record of the pattern of light incident upon its surface.
- **Linear response**: the measured signal is directly proportional, within the operational limits of the given CCD chip and associated electronics, to the quantity of light incident upon it.
- **High quantum efficiency**: the fraction of the light which is incident upon the chip that is actually detected is relatively high, compared with photographic emulsions and photomultiplier tubes in particular.
- **Low intrinsic noise levels**: again, compared with photographic emulsions and photoelectric photometers, the noise is relatively low.
- **Broad spectral response**: the spectral response of CCDs is intrinsically fairly broad, typically ranging from $\lambda\lambda 400 - 900$ nm. In recent times a number of fabrication techniques[21] have been developed in order to extend the operational spectral region both shortward and longward.
- **Image digitisation**: the fact that the image is composed of a regular array of picture elements or 'pixels' means that the resulting image is ideally suited for computer analysis.

[21] For example coating the CCD's surface with an ultraviolet sensitive fluorescent film, 'thinned' CCDs and 'back-illuminated CCDs.'

The work described in this thesis is based largely on data obtained via CCD observations specifically for this programme of research. Data not obtained with CCDs includes visual observations (e.g. historical times of minima taken from the literature), photographic and digital two-dimensional photon-counting observations (radial velocity curves), photomultiplier tube observations (standard star photometry) and television camera observations (IUE spectrophotometry).

Although the properties of CCDs described above make CCD detectors useful for all manner of observations, the CCD observations obtained for this thesis are based entirely on direct imaging for the purpose of measuring the brightnesses of the stars imaged, i.e. *photometry*.

1.4.1 Extracting photometry from CCD images: I

The digital format of the CCD image lends itself ideally to computer analysis. To this end a number of highly sophisticated computer software packages have been developed over the years since CCDs were first used for astronomical purposes, including DAOPHOT II (Stetson, 1987; Stetson et al., 1989), ROMAFOT (Buonanno et al., 1983) and DOPHOT (Schechter et al., 1993).

There are essentially two approaches to the extraction of photometry from CCD images, *Synthetic Aperture Photometry* and *Profile Fitting Photometry*. The appropriate method for a given image is largely dependent on the number of stars in the image and their relative proximity to each other. DAOPHOT II which comes as a standard package with MIDAS[22], provides for the extraction of photometry from CCD images by both methods. DAOPHOT II has been used extensively throughout the course of the research described here and although the following is no doubt heavily coloured by that experience, the basic principles are common to all such packages.

Synthetic aperture photometry usually involves the counting of the total signal within some radius of the stellar centroid and the correction for the background sky level. In this way the technique is directly analogous to photomultiplier tube photometry where real apertures are used to restrict the light incident upon the photo-cathode. The background sky level at the actual position of the star is of course impossible to measure, therefore it must be estimated in some way. The estimation scheme adopted by DAOPHOT II uses an estimate of the modal[23] sky value derived from an annulus centered on the star of sufficient radius so as not to include any (significant amount of) light from the star in question.

For sparsely populated fields (see figure 1.3) synthetic aperture photometry is perfectly adequate for the extraction of photometry from CCD images. Synthetic aperture techniques become inadequate only when fields are sufficiently crowded (e.g. figure 1.3) that apertures of appropriate size can not be fitted around the stars of interest without the light from nearby field stars contaminating the measurement. Photometry of high precision can nevertheless be obtained via profile fitting techniques.

Profile fitting photometry relies on either the prior knowledge of, or the ability to determine, the characteristic two dimensional intensity profile or *Point Spread Function* (PSF) of a point source in a given image. The actual PSF is a function of the optical system, including the atmosphere, through which the image was acquired and the telescope tracking history of the observation. Thus in general, each CCD image has its own characteristic PSF. The total signal in a given pixel of the CCD is then assumed to be the sum of a sky background contribution plus contributions from the PSFs of nearby stars. Once an appropriate PSF for a given image has been determined, that PSF is 'fitted' to the observed image profiles of objects in the image by scaling the PSF and adjusting the centroid of the PSF so as to minimise the residuals between the observed signal and the model PSF plus sky background in each pixel. The measured light for the object is then proportional to the volume under the PSF. In this scheme, the determination of the sky background contribution in each pixel is perhaps one of the most difficult aspects. In DAOPHOT II the sky is estimated as the synthetic aperture photometry sky measurement.

Profile fitting photometry is an extremely powerful tool for the extraction of *differential* photometry from a CCD image. In most cases, any difference between the true image profile and the model PSF used to calculate the photometry will likely result in a systematic difference between the true magnitude and the calculated magnitude. But this systematic difference is most likely to scale with the light level, corresponding to a constant offset in magnitude. In calculating a differential magnitude between two stars in an image, this constant offset will cancel, providing an excellent estimate of the true differential magnitude. This simple explanation will generally fail when the image profile varies with position on the CCD, if the crowding is extreme or if the CCD has a non-linear response.

[22] MIDAS is the acronym for the *Munich Image and Data Analysis System*. As the name suggests MIDAS is an integrated collection of software specifically designed for the processing of astronomical images and data.

[23] The *mode* of the sky values in the annulus is computed as three times the *mean* minus two times the *median*.

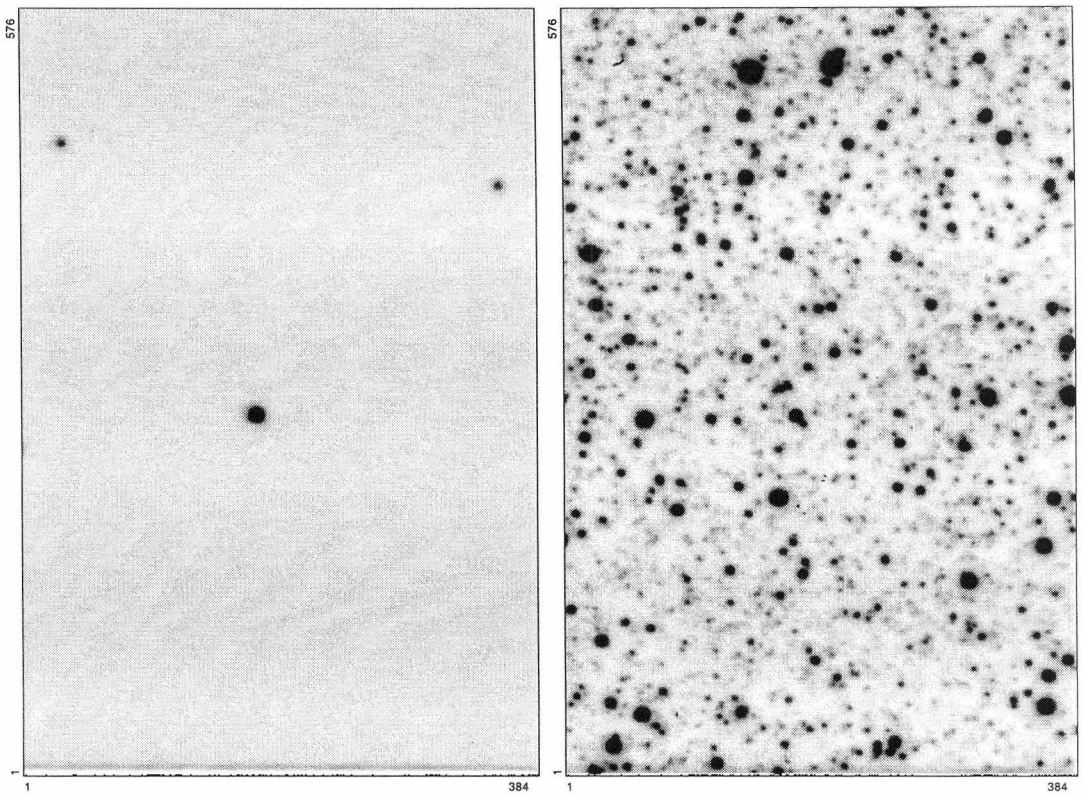

Figure 1.3: Example fields, on the left a sparse field with three stars within the $4' \times 6'$ field of view of the CCD, and on the right a rather more crowded field with $\sim$1 500 stars in the image.

To obtain *absolute* photometry in crowded fields both synthetic aperture and profile fitting photometry must be used. In the simplest cases, a relatively isolated star in an image can be used to establish the relationship between the synthetic aperture photometry and profile fitting photometry for that image. In more complicated cases where there are no suitable isolated stars, a more sophisticated approach is required (see section 3.3.1).

More detailed descriptions of the both synthetic aperture photometry and profile fitting photometry techniques and procedures are given in section 3.2.

Chapter 2

Observations

Observations as part of the research programme for this Ph.D. thesis, within the context of the MJUO MCEB programme, were begun in July of 1992. The programme was allocated of the order of twelve nights per month telescope time during 1992 and 1993, but due to the increased demand for time on the Mount John University Observatory McLellan 1m telescope, was allocated only about seven nights per month in 1994 and 1995. In total from July 1992 until Mar 1996 296 nights were allocated to the programme.

The following chapter describes the procedures for getting starlight from the point at which it arrives at the telescope into a format suitable for analysis at the University of Canterbury. I begin by giving a description of the telescope and instrumentation employed for all observations obtained at Mount John University Observatory for this project between mid 1992 and early 1996. In section 2.2 I give details of the initial process by which the three eclipsing binaries, stars whose observations constitute the bulk of the observational effort, were selected. Section 2.3 describes the general procedure adopted for the acquisition of stellar images.

2.1 Instrumentation

Direct imaging CCD observations were made at Mount John University Observatory, Lake Tekapo, New Zealand (longitude 170° 27′ 54″ E, latitude 43° 59′ 14″ S) using the McLellan 1m reflecting telescope at $f/7.7$ cassegrain focus. Observations were for the most part obtained by the author. In addition Messrs M. Clark, A.C. Gilmore, W. Tobin and M. Zambri obtained observations which form part of the data set embodied in this work. Observations were made in a six colour photometric system based on the well-known Strömgren *uvby* and Cousins *UBVRI* systems (see fig 2.3). The detector used for all observations was a computer-controlled Thomson TH 7882 CDA CCD chip housed in an evacuated, cryogenically cooled dewar with a quartz entrance window through which the incoming star light passed before arriving at the CCD. Between the telescope and the detector was a purpose built *photometer head* which incorporated computer-controlled filter selection and offset guiding.

The following sections give details of the above systems, but first, it will perhaps be useful to provide a detailed description of the light and data path:

- Having arrived at the top of earth's atmosphere the light then suffers perhaps the greatest degree of degradation during its passage from origin to analysis, as it passes through the atmosphere to arrive at the primary mirror of the telescope.

- In the telescope the light undergoes two reflections by aluminium-coated mirrors. It then passes through two correcting lenses in the chimney baffle before leaving the telescope. The correcting lenses provide an unaberrated wide field of view at the image plane.

- Next in the optical train is the photometer head. In the photometer head the light is passed through a filter in order to select only a small spectral region of the flux distribution.

- The light then passes through the quartz entrance window of the CCD dewar before finally striking the silicon substrate of the CCD itself, where individual photons are absorbed, thus creating electron/hole pairs. The electrons are trapped and held in the potential wells of the pixels until the CCD is read out.

- The *Analogue* signal generated by the ensemble of electrons collected by each pixel is first amplified before being converted to a *Digital* signal. It is then sent to the controlling computer which stores the image in RAM memory.

- Prudent observers will then write the image to hard-disk, before subsequently writing it to half-inch, 9-track tape, ready for transportation from Observatory back to Christchurch.

- At the University of Canterbury, the image is read off tape. Finally, the image is converted from the format it was written to tape in, to the *Flexible Image Transport System* or FITS format, suitable for input into analysis packages such as MIDAS. At this time clock corrections (see section 2.1.2), Heliocentric Julian Day number, airmass and other useful data for the image are calculated and added to the FITS header.

2.1.1 Telescope

Observations were made on the Mount John University Observatory McLellan 1m Telescope. A full history of the telescope design and construction and aspects of its performance was recently published to mark the ten year anniversary of the telescope (Tobin and Evans, 1996). The telescope mechanics were designed and built, for the most part, by the technical staff, in particular Graeme Kershaw, of the then Department of Physics, University of Canterbury while the optics were respectively designed and fabricated by Norman Rumsey and Garry Nankivell of the Physics and Engineering Laboratory of the former Department of Scientific and Industrial Research. The telescope was constructed between 1980 and 1985. First light was achieved during March of 1986 and the telescope was officially opened on the 11th of July of the same year.

The telescope uses Dall-Kirkham optics, i.e. an ellipsoidal, concave primary mirror combined with a spheroidal convex secondary. The focal length of the primary mirror is 3.5m but in combination with one or other of the two secondary mirror units available, the resulting cassegrain focal ratios are $f13.5$ and $f7.7$. The optical configuration provides relatively long equivalent focal ratios with a physically compact design, the Cassegrain foci for the two systems being no more than $\sim$3.2m from the secondary mirror. The $f13.5$ system was designed with the (at the time of the design of the telescope) primary purpose of the telescope, namely spectroscopy and photoelectric photometry, in mind. Since such observations usually involve observation of only one star at a time, no particular effort was made to minimize off-axis aberrations. By contrast, the $f7.7$ system was designed for wide-field-of-view applications and thus incorporates two correcting lenses in the chimney baffle which act to reduce off-axis aberrations. The result is a reasonably uniform field of view over a reasonable area in the focal plane, certainly large enough to accommodate most standard CCD chips. The optical design of the telescope make it the second largest Dall-Kirkham in the world, the largest being the 1.5m coudé auxiliary feed telescope at La Silla in Chile, but the 1.5m telescope is suitable for axial images only.

The telescope has an equatorial, torque-tube type mounting which provides practically unrestricted pointing ability. However this versatility of the telescope in fact leads to the possibility of observing the same celestial coordinates from **two** orientations. The import of this is that the two different orientations lead to a rotation of 180° of the image on the CCD, assuming the CCD itself is not remounted rotated by 180° which is entirely possible. This obviously has consequences on ensuring that the observed fields are always observed at the same chip location and with the same field orientation (the importance of this is discussed in section 2.3.3). The specification of the two orientations has, in the past lead to confusion, and so it may be useful to here take the time to clarify this confusion.

The first requirement is to specify a point of reference. As good a choice as any is that the telescope cage is *physically* to the west of the pier and pointing to the zenith. If from this point the telescope is driven to the declination of the object to be observed *without* passing through the South Celestial Pole i.e. $-90°$ S (or the North Celestial pole for that matter if if were possible to do so without having the primary mirror fall out of the telescope!) then I label the orientation of the telescope *North of the Pole*. In this orientation driving the telescope by pressing the N(orth) button on the telescope hand paddle will indeed drive the telescope northward.

If on the other hand the telescope is driven first past the declination of the object, then through the South Celestial Pole and then, continuing in the same direction, to the appropriate declination, then I label the orientation of the telescope *South of the Pole*. In this orientation driving the telescope by pressing the N(orth) button on the telescope hand paddle will in fact drive the telescope southward, at least until the telescope passes through the South Celestial Pole.

At all times, the digital readout on the console remains correct. In particular, the right ascension readout jumps by twelve hours as appropriate as the telescope passes through the South Celestial Pole.

These labellings are entirely equivalent to the labels *West of the Pier* (equivalent to North of the Pole) and *East of the Pier* (equivalent to South of the Pole). However it must be noted that the telescope can be *physically* west of the pier and yet still be oriented in the East of the Pier mode, and vice versa. Similarly the telescope can be pointing above the South Celestial Pole and yet still be oriented in the South of the Pole mode. Herein lies the possibility of confusion, but I hope the above helps to clarify rather than confuse the situation.

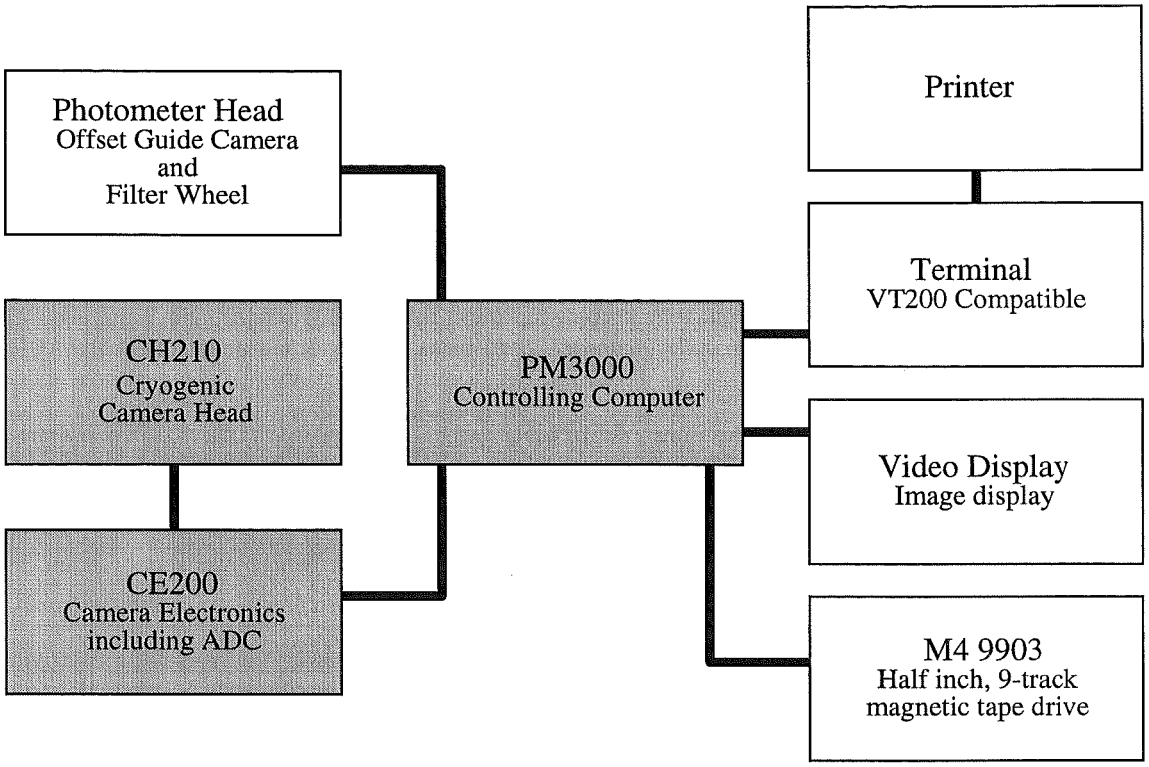

Figure 2.1: A schematic of the various components which together constitute the MJUO Photometrics PM3000 CCD system. The CCD chip and the amplifier electronics are housed in the CH210 cryogenically-cooled, bottom-looking camera head. The CE200 contains the ADC and other electronics. The system is controlled by the PM3000 computer via standard VT200 compatible terminals. Image display is provided by RS170 video monitors. Images are archived to 1600 bpi 9-track, half-inch tape by the M4 9903 streaming tape drive. Also indicated are the printer with which a complete and permanent record of all computer screen output could be kept and the Photometer Head, also controlled by the PM3000 system.

The 1m mirror is semi-regularly re-aluminized and occasionally more often when for one reason or another if it has become particularly dirty. It is hard to imagine that differences in the reflective coating could have a significant effect on the definition of the instrumental photometric system, except of course for the zero point. Certainly no obvious effect is seen in the obtained data.

Throughout the period during which the observations were obtained, the telescope suffered from a guiding problem of the following nature. If the telescope had been driven northward for some time (i.e. pressing the N(orth) button, ignoring the complications of telescope orientation described above), and then it was desired to drive southward, there would be an initial period – of the order of one or two seconds[1] – during which the telescope drive motors would certainly be driving, the Declination indicators on the telescope control console would be ticking over, but the telescope was quite plainly not in motion, as testified by the fact that the stellar image on the guide camera monitor remained perfectly stationary. By contrast, once the telescope eventually began to move southward, if one then desired to drive the telescope northward, the telescope would begin moving in that direction immediately, however, after about half a second the telescope would become stationary for a period of one or two seconds again, before it would then restart its motion. The effect was a function of the telescope torque loading, so that at different positions of the telescope the effect ranged from bad to worse.

2.1.2 Detector

The CCD detector system used for all observations obtained for this project at Mount John University Observatory was a cryogenically cooled, overcoated Thomson TH 7882 CDA CCD. The chip and cryostat form part of a system purchased from Photometrics Ltd. of Tucson, Arizona, USA in 1988 (Tobin, 1991b; Tobin, 1991a). Figure 2.1 shows a schematic of the various components of the system. The chip comprises 384×576-pixels, each of which is 23 μm square. The CH210 camera head was bolted to the photometer head which was in turn bolted to the telescope, thereby placing the CCD at the Cassegrain focus

[1]This duration (and those that follow) applied at stepper motor drive speed 2. At speed 1, the effect would last longer, while at all higher speeds the effect is essentially unobservable.

of the McLellan 1m telescope at focal ratio $f7.7$. This configuration produces a plate scale of approximately 26.8 arcsec mm^{-1} and thus 0.616 $arcsec^2$ per pixel. The total field of view is therefore approximately 3.8×5.8 arcmin. The CCD is controlled by a PM3000 computer system based on the Motorola 68020 chip which also provides image manipulation and display capabilities. The PM3000 is run under a FORTH [2] Operating System.

The camera and computer system arrived from the supplier in December of 1988. It was commissioned in May of the following year after extensive investigation of its linearity (Pollard, 1989a) and spectral response as a function of operating temperature (Pollard, 1989b). Subsequently other properties of the system have been investigated including the temperature sensitivity of the CE200 camera electronics unit (Gilmore and Tobin, 1989), the stability of the various time keeping systems (Tobin, 1989) and the gain, noise and other related characteristics (Tobin, 1991a). The main results of these investigations applicable to the MJUO MCEB programme are:

- The chip is linear over intensity ranges of 10 ADU (Analogue to Digital Units) to 15 900 ADU to better than 0.5%. In fact it is likely linear to much higher count levels but the analogue to digital converter or ADC (an ADC76KG) is only 14-bit, thus the maximum representable integer is 16 383.

- Low signal level exposures suffer from electrical pick-up of the 50Hz mains power supply signal. The detected signal is $\sim 9e^-$ peak-to-peak.

- For short exposures (less than ~1 second), shutter-speed variations cause relatively large uncertainty in measured signal levels. It is found that regions of the chip nearest the edges can be exposed for upto 20 milliseconds less than central regions due to the finite speed of the shutter's blade mechanism.

- The optimum operating temperature of the CCD is dependent on the wavelength to be observed at as well as on the exposure duration (since this determines the accumulated dark current). Practical constraints however mean that operating temperatures are limited to the range −50°C to −150°C. In general lower temperatures produce higher efficiency at shorter wavelengths. The dark current is essentially negligible (of the order of 1 electron per pixel per minute) below temperatures of ~ −30°C, above which there is a sharp rise in the measured count rate.

- Experimentally, the count level in the DARK images is found to correlate with telescope dome temperature. This is believed to be due to temperature dependence of the electronics inside the CE200 electronics box, which includes the analogue to digital converter. The net result is that the fat zero[3] is a function of temperature (0.7 ADU/°C). The gain on the other hand is found to be independent of the temperature of the CE200 unit (Gilmore and Tobin, 1989).

- The time keeping clock module of the CCD's controlling computer is known to run fast at a rate of ~1 part in 10^5 different from that of *Coordinated Universal Time* (UTC). While this is unlikely to produce errors of practical importance for the calculation of exposure durations, if not accounted for it will have non-negligible consequences for determination of the epoch of an observation at levels of accuracy of the order of 0.0001 Julian day (i.e. 9 seconds). Procedures for dealing with the clock drift are described below in section 2.1.2.

- The signal gain G (ADU/e^-), (and hence inverse gain, $Q = G^{-1}$, base level noise[4] B_e (e^-) and chip readout time) can be set to a number of different values via the FORTH gain parameter `cgain`. Different `cgain` settings affect the maximum observable light levels before exceeding the limits of the 14-bit ADC. It therefore also affects the level of truncation or digitization noise since the output signal for each pixel is represented by descrete (14-bit binary) numbers rather than an analogue signal.

The MJUO chip is of particularly high cosmetic quality. Figure 2.2 presents the V FLAT FIELD images from 1992-Nov-03 (derived from image `T2770013`) and 1995-Oct-23 (derived from images `T8960001` and `T8990005`). FLAT FIELD images essentially show the response of each individual pixel to the same amount of incident light and therefore constitute maps of response sensitivity (see section refsecObsFlatFields). A number of interesting features can be identified in the images:

[2] A lesser known but rather powerful computer programming and instrument control language. The FORTH 'bible' is called Starting FORTH (Brodie and Forth Inc., 1987).

[3] In practice the ADC outputs a non zero reading for zero signal input, the so-called *fat zero*.

[4] Base level noise is the low-signal-level readout noise which in general differs from the readout noise at higher signal levels.

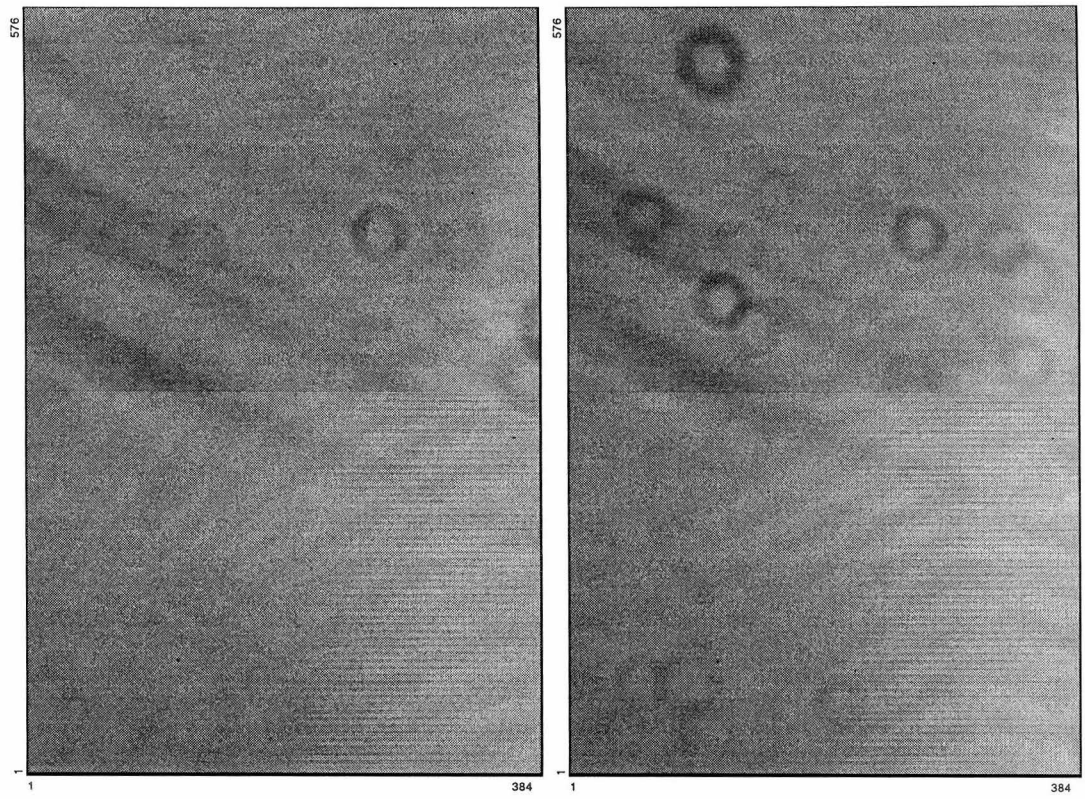

Figure 2.2: Two V FLAT FIELD images acquired close to the beginning (1992-Nov-03 on the left, `ff921103V` derived from image `T2770013`) and end (1995-Oct-23 on the right, `ff951023V` derived from images `T8960001` and `T8990005`) of the observing programme. The circular features are 'shadow rings' caused by dust specks on the cryostat entrance window or elsewhere.

- Most obviously the chip appears to be composed of two halves. This is presumably a result of the conversion of the chip by Photometrics from its original frame transfer mode to the operational full chip mode.
- Running from the top left toward the bottom right at an angle of $\sim 30°$ are 'stripes' believed to be polishing marks.
- In the bottom right quarter of the chip, there appears to be a spatial periodic variation of the sensitivity, with adjacent rows having high and low sensitivities.
- A number of 'cold' pixels (i.e. single or small groups of just a couple of pixels whose sensitivity is much lower than their immediate surroundings) are evident; properties of the most obvious cold pixels (MIDAS coordinates[5] and the factor (F) by which the sensitivity is down with respect to the local mean) are (Col_{MIDAS},Row_{MIDAS},F) (112,88,0.92), (364,256,0.75), (277,535,0.75). The factors have been determined by examination of the individual pixel values in the V FLAT FIELD image from 1992-Nov-03 and are thus only indicative rather than being the statistical means from a sample. Examination of V FLAT FIELD image from 1994-Dec-26 (derived from images `T6040027` and `T6070013`) shows that the factors vary from image to image by perhaps $1 - 2\%$.

The quantum efficiency of the chip, as quoted by Photometrics, is plotted in figure 2.3 and tabulated in table F.8. Figure 2.12 presents representative FLAT FIELD images in u and I. The most obvious difference between the images is the apparent granularity of the u FLAT FIELD as compared with the I FLAT FIELD. This is not caused by digitization noise since, as explained in section 2.3.3, all FLAT FIELD exposure times were adjusted so as to produce a mean signal level of 10000 ADU in the individual DARK subtracted images from which the final medianed image was constructed. I believe the granulation is a real effect caused by greater variations in sensitivity from pixel to pixel. The cold pixels are also generally more obvious in the u image. Examination of the pixel values of the cold pixels in the two images shown in figure 2.12 indicates

[5]When an image is converted in to the internal MIDAS BDF format with either of the MIDAS commands `intape/fits` or `indisk/fits`, a coordinate transformation with respect to the PM3000 coordinate system is applied as follows: $Col_{\mathrm{MIDAS}} = 384 - Row_{\mathrm{PM3000}}$ and $Row_{\mathrm{MIDAS}} = Col_{\mathrm{PM3000}}$.

that the factor by which the sensitivity of the cold pixels is reduced is a function of the wavelength of the incident light, but it is not a trivial relationship. For the three cold pixels identified above the factors are 0.65, 0.75, 0.77 for u and 0.96, 0.88, 0.80 for I.

For the acquisition of all scientific images obtained for the current phase of the MJUO MCEB programme, the system was operated at a chip temperature of approximately $-110°$ C and at FORTH gain parameter `cgain=100`. The thermostat control is able to maintain the desired chip temperature to an accuracy of $\sim \pm 0.2°$ C. `cgain=100` leads to an inverse gain of $4.31 \pm 0.06\, e^-$/ADU and a base-level noise of $7.1 \pm 0.1\, e^-$ (Tobin, 1991a). The normal full-chip set-up and read-out time at this gain is approximately 14 seconds.

Drift of the PM3000's clock

As described above, the time keeping clock of the PM3000 computer (giving PM3000-time) is known to drift with respect to UTC. The drift turns out to be a general trend to run a little quickly by of the order of 0.4 of a second per day, although experience shows that the rate can vary by several tenths of a second per day from time to time. Examination of the clock-drift data base shows that the drift rate has also been known to reverse entirely on occasion.

This drift has implications for epoch-critical observations, such as those of eclipsing binaries, since the various times recorded in the image header information will in general be inaccurate, and, unless corrected for, may introduce an apparent random error, which is however entirely correctable.

The adopted procedure for dealing with this problem was as follows. At regular intervals (perhaps as often as daily) the current PM3000-time was compared with UTC. Effectively, three sources of UTC were available at MJUO at the time of the observations: the 'Industrial Research Limited Talking Clock', VNG/WWV/WWH (Australia) broadcast time signals available via a loudspeaker system and an oven-controlled crystal oscillator clock maintained by Dr. D.J. Sullivan of Victoria University, Wellington, New Zealand (this clock was regularly synchronised with UTC using the VNG/WWV/WWH signals and is found to drift relative to UTC by less than one millisecond per day). The difference between PM3000-time and UTC, the so called clock-drift data, was recorded for subsequent entry in a database used by the Christchurch-based tape reading software (see section 2.3.6). In practice, as long as one was confident that the drift had been well behaved over the duration of a given observing run, which one could ensure by checking on a daily basis, clock-drift data from the beginning of the run prior to any observations and at the end of the run after all observations was found to be sufficient for the purposes of calculating the appropriate corrections since the correction was calculated by a simple linear interpolation based on the two bracketing clock-drift data (or extrapolation based on the two most recent clock-drift data).

At first glance, this might seem like a large amount of effort to go to when the PM3000 clock could simply be reset to be equal to UTC each night (or as often as desired) in order to maintain accuracy of recorded information in image headers. There are however a number of justifications for this effort. First, should an individual forget to make such corrections, accurate times can nevertheless be determined from data provided prior to and subsequent to the observers own observations. In addition, keeping track of the behavior of the clock drift provides a diagnostic which could conceivably indicate more general problems concerning the PM3000's performance.

CCD signal noise

From simple theory, the noise in the CCD signal from a single pixel is taken to be comprised of two components, readout noise (R_e) in electrons and intrinsic noise in the signal itself. The signal noise is usually assumed to be Poisson, but in reality there is a non-Poisson noise component which is proportional to signal level. Mathematically the variance in the CCD signal can thus be expressed as:

$$\sigma^2 = G^2 B_e^2 + GS + cS^2 \tag{2.1}$$

where G is the system gain (i.e. the number of electrons corresponding to one digital unit), B_e the base-level readout noise which is equal to the low-signal-level readout noise, S is the signal and c is a curvature term introduced to account for the slightly non-Poisson nature of the noise in the signal.

Note that the above is of course the noise in the total signal from the pixel which comprises the signal one is trying to determine (e.g. stellar flux) plus other spurious sources such as cosmic ray events and thermal or dark current.

2.1.3 Photometer Head

The Photometer Head was designed and built by the Department of Physics and Astronomy at the University of Canterbury (Tobin et al., 1993b). It was first used in September of 1992, and has been used for essentially all observations obtained in the context of the MJUO MCEB programme since. Only the initial surveys made just before the commissioning of the photometer head did not utilize it.

Most of the functions of the photometer head are controlled by the PM3000 computer thus providing an integrated environment for the observer in that essentially all aspects of actually making an exposure, once the desired field has been acquired, are controlled by one computer. Aside from convenience, this has important benefits in terms of reducing the number of possible errors that might otherwise occur if the photometer head was controlled by an auxiliary computer, provided the programmer is kind enough to reduce the requirements for making an exposure to, essentially, a single keystroke.

The most important features of the instrument are the computer controlled filter wheel and offset guide camera. The computer controlled filter wheel allows automatic selection of the appropriate filter. Once the appropriate covers have been attached, the photometer head is to all intents and purposes a sealed unit. This cuts down on possible problems due to dust or other undesirable contaminants (e.g. metal splinters from manually mounted filter holders) which might impair image quality or instrument performance, as experienced in the 1990 observational campaign where filters, which were mounted on modified Pentax bayonet camera lens mounts, were manually changed for each exposure. The offset guide camera makes possible accurate guiding for long-duration exposures, thereby opening up opportunities to observe far fainter systems than is possible without guiding. Acceptable signal to noise levels can be maintained even for observations in intermediate bandpass photometric systems such as the Strömgren system used here in the MJUO MCEB programme for which, aside from transmitting only a narrow spectral region, absolute transmission levels are typically low (peak transmissions of the MJUO Strömgren filters, as measured by the Omega Optical Inc., Brattleboro, Vermont, USA, are 0.43, 0.51, 0.75 and 0.68 for u, v, b and y respectively.)

2.1.4 Filters

Initially, observations were made with a V filter approximating the V of the Cousins $UBVRI$ photometric system. The V filter was constructed from 2mm of Schott GG495 filter glass oiled to 3mm of BG39. A set of image quality glass and/or interference filters approximating $uvby$ of the Strömgren photometric system and I of the Cousins $UBVRI$ photometric system was purchased from Omega Optical Inc., Brattleboro, Vermont, USA. Delivery of the $uvby$ and I filters took somewhat longer than anticipated. As a result, for HV 982 and HV 1620 somewhat more observations were obtained with the V filter than was initially anticipated would be the case. While the result is a rather large number of V observations in comparison with the other bandpasses for these two targets, the resulting light curves are, if nothing else fairly complete and rather esthetically pleasing! Indeed M.S. Bessell (private communication) argues that observations of V are in general more practical than y since the exposure time will be significantly less, and yet there is little to be gained astrophysically from y that can not be found with V, especially for the hot stars where there are few lines in this spectral region. It is never the less desirable to have reasonable phase coverage in both V and y for the purposes of calibration. Unfortunately this was realized at a rather late stage. As a result the V light curve for HV 2241 is composed of somewhat less observations than one would ideally like.

The filters were mounted in a circular filter wheel that held eight filters in total. The remaining two spaces were occupied, for the most part, by a clear-glass focus-plate and the H_α filter supplied by Greenhill & Watson, University of Tasmania, for a side project of observations of GX1+4 (Greenhill et al., 1995). The filter wheel was housed in the photometer head which, as described above (section 2.1.3), provided the means by which filter selection was computer controlled. The filters obtained from Omega were manufactured to be as nearly as possible of the same optical thickness so that the same telescope focus was reasonably appropriate for all filters. A clear-glass plate was therefore added to the V filter in order to produce the same optical thickness as well.

Derived characteristics of the resulting bandpasses after convolution of the filter spectral transmission functions (as measured by Omega), the mean spectral quantum efficiency of a TH7882 CCD chip (as provided by Photometrics) and the effect of two reflections from an aluminium mirror (Allen, 1976) are given in table 2.1. Figure 2.3 presents the convolved bandpasses and the TH7882 quantum efficiency graphically. Also included in figure 2.3 for comparison are 'standard' representations of the standard system bandpasses taken from the literature ($uvby$ from Schaifers and Voight, 1982a; V and I from Bessell, 1990). The excellent match between our 'measured' bandpasses and the standard bandpasses is a direct consequence of the effort that went into the initial specification of the filter transmission functions. Such a good match is

Table 2.1: Characteristics of the MJUO *uvbyVI* photometric system and of the 'standard' bandpasses (*uvby* pg. 329, *V* pg. 211 and *I* pg 310 Straižys, 1992).

	MJUO		Standard	
Filter	$\bar{\lambda}$ [nm]	$\Delta\lambda$ [nm]	$\bar{\lambda}$ [nm]	$\Delta\lambda$ [nm]
u	346.6	26.6	350.0	30.0
v	410.0	13.7	411.0	19.0
b	465.9	12.8	467.0	18.0
y	548.2	24.0	547.0	23.0
V	544.2	67.0	550.5	83.0
I	794.6	86.2	790.0	150.0

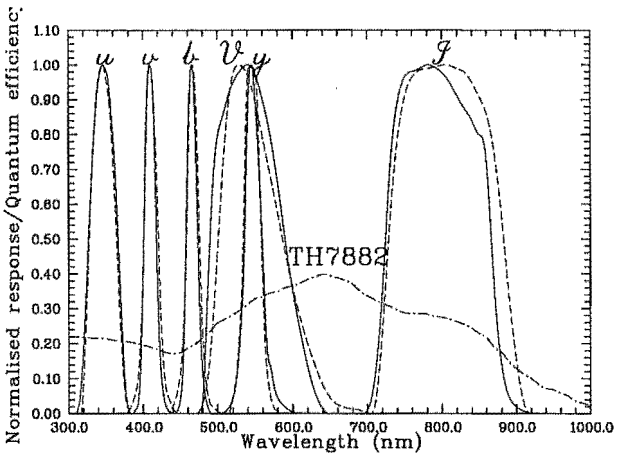

Figure 2.3: Normalised response functions of the MJUO *uvbyVI* photometric system. The solid lines represent the MJUO bandpasses and include the effects of the *filter* transmissions, the *detector* sensitivity and the effect of two *reflections* from aluminium mirrors. No atmosphere effect has been included. The dashed lines represent 'standard' bandpasses (*uvby* pg. 57 from Schaifers and Voight, 1982a; *V* and *I* from Bessell, 1990).

desirable so that non-linear terms in transformation equations from instrumental to standard photometric systems are kept to a minimum if not made entirely negligible.

Scattered light from filters

In images with large signal to noise it is plainly obvious that there are scattered light problems. Figure 2.4 shows a composite image of 'typical' *uvbyVI* images made up from 61×61-pixel cutouts of the same star (DM −26 1339) from six individual observations. The u, v, b, and y images were obtained on the night of 1995-Sep-19 while the V and I images were obtained on the night of 1995-Feb-12. The images have been flat-fielded and sky-background normalised[6]. By adjustment of the exposure durations, signal levels in all six images are approximately equal.

It is interesting to note the different patterns generated by the scattered light for the different filters;

- For b, where the problem is perhaps most obvious, the scattered light forms a ring, which looks not unlike the shadow rings produced by dust motes on the surface of the entrance window of the CCD's dewar. The center of the ring is offset to the left and down from the stellar centroid.
- For v a similar, though less obvious ring is formed whose center is slightly above the stellar centroid.
- For y the stellar image is surrounded by a diffuse 'cloud'.
- There is no particularly obvious problem for the u, V or I filters.

[6]Sky-background normalisation here means that a representative sky value – as measured by the MIDAS command `Magnitude/circle` centered on the stellar centroid in each image – has been subtracted so that all six images then have a sky backgorund of approximately zero.

It is clear that these features are generated by the filters since the only difference in the optical system between the u, v, b and y images and between the V and I images is the change of filter. The patterns of scattered light are stable. In fact, essentially no change is seen in the patterns during the three years of observations with the filters.

To quantify the significance of the problem I attempted to estimate the amount of light scattered relative to that in the central stellar profile. Synthetic aperture photometry for an aperture centered at the position of the stellar centroid for the original (flat-fielded) image gives a measure of the total light in the stellar image. Synthetic aperture photometry for the image after subtraction of a fitted *Point Spread Function* (PSF)[7] gives a measure of the amount of light scattered by the filter since the subtraction of the fitted PSF should leave behind essentially only the scattered light. If $m_{\rm Ori}$ is the magnitude measured in the original image and $m_{\rm PSF}$ is the magnitude measured in the PSF subtracted image then the fraction of light scattered by the filter ($F_{\rm Scat}$) is given by,

$$F_{\rm Scat} = 10^{\frac{m_{\rm Ori} - m_{\rm PSF}}{2.5}}. \tag{2.2}$$

Figures 2.5 and 2.6 show composite images made up of the 61×61-pixel cutouts of the PSF subtracted images of standard stars observed on the nights of 1995-Feb-12 (*VI* observations) and 1995-Sep-19 (*uvby* observations) respectively (See figures B.2 and B.7 for the non-subtracted images). The bandpass of each observation is indicated to the lower-left of each cutout image. For convenience of display, the images have been sky-background normalized, as above. The circle centered on the stellar centroid for each image represents the 37.5″ diameter aperture for which the PSF-subtracted and non-subtracted synthetic-aperture photometry was compared.

It is obvious from examination of figures 2.5 and 2.6 that for bigger PSF radii, more of the scattered light is, without doubt, included in the look-up table of the PSF and hence the measured scattered light will be less than it truly is. This will contribute to the scatter amongst the measurements. Thus, the measured fractions of scattered light, as summarized in table 2.2 should be treated as indicative only.

For *synthetic aperture photometry*, the scattered light will, in general introduce a seeing-dependent systematic error, unless the aperture is big enough to include essentially all of the scattered light. For smaller apertures, particularly in v and b where the light is scattered to large distances from the stellar centroid the true magnitude will be systematically underestimated by the measured magnitude. There should be no significant problem for differential photometry within a given image since the systematic error should be the same for each measured magnitude in the image. This is because one would expect both the seeing and the fraction and pattern of scattered light to be constant within a single image. Only if crowding is such that some measured magnitudes include the scattered light from nearby field stars would this not be true. But if that is the case, profile fitting photometry is probably more appropriate anyway. For absolute photometry, where magnitudes measured in separate images are compared, the statistics presented in table 2.2 would indicate that the amount of scattered light can vary by as much as ∼4%. This is probably an overestimate of the true variation due to the analysis procedure. It probably reflects more the variation of the amount of scattered light included in the PSF as the PSF radius is varied. As above, if the aperture is sufficiently big, so as to include all scattered light, there should be no significant error.

For *profile fitting photometry* the situation is similar. If the PSF radius is set large enough, the PSF, in particular the look-up table component thereof, will include the effect of the scattered light. If not the estimated magnitude will include a systematic error. Once again for differential photometry within a given image, the systematic error should be the same for each estimated magnitude and hence cancel out in the differential magnitude. For absolute photometry between images, since the zero point of the profile fitting photometry for each image must be tied down by synthetic aperture photometry (at least for DAOPHOT II), provided large enough apertures are employed, again no significant errors should result.

2.2 Target Selection

Possible targets for observation were chosen from the catalogues of Gaposchkin (1965), Gaposhkin (1970; 1977) and Payne-Gaposchkin (1971). Field surveys through filters approximating the U, B and I bandpasses of the *UBVRI* system for 11 possible targets were carried out in mid 1992 (see table 2.3). Eight of the 11 are located in the LMC, the other three in the SMC. Of the 11, three have been the subject of further research, namely HV 982 and HV 2241 in the LMC and HV 1620 in the SMC.

Observations of HV 982 and HV 1620 began in November of 1992. The choice of these two targets was based on several factors. Both are relatively bright ($m_{\rm pg}$∼14.4 and ∼14.3 respectively), and the published

[7]For details of the extraction of photmetry from CCD images the reader is referred to section 3

Table 2.2: Synthetic-aperture photometry for PSF subtracted and non-subtracted images. The amount of light remaining after the PSF subtractions is indicative of the scattered light from the filters. The the table gives, as percentages, the statistics for the fraction of the total light scattered by the filters.

Filter	$\bar{x}$	σ	Min	Max	n
u	0.72	0.21	0.34	1.25	27
v	1.78	0.62	0.81	3.46	27
b	4.05	0.81	2.49	5.78	27
y	3.18	0.89	1.29	5.58	29
V	1.04	0.56	1.42	2.48	62
I	1.39	0.97	0.19	4.23	62

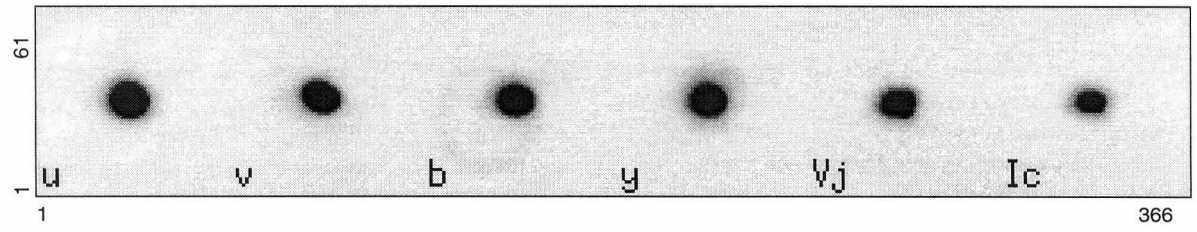

Figure 2.4: Typical stellar images in $uvbyVI$. This is a composite image constructed from 61×61 pixel cutouts form six individual exposures in each of the six $uvbyVI$ filters. The star is DM −26 1339, the exposure times are 180.0, 180.0, 150.0, 80.0, 10.0 and 10.0 seconds in $uvbyVI$ respectively.

light curves indicated relatively well separated systems. Furthermore, HV 1620 was chosen since it would then be possible to make a qualitative comparison between our data and analysis and the photoelectric light curves and analysis of Davidge (1988). In addition, it was observationally convenient to have a target in each of the Clouds since when one was at high airmass, the other would not be.

Subsequently, in the middle of 1993, HV 2241 was added to the list of programme stars. The primary reason for the choice of this star was the low degree of crowding in the field making this target particularly suitable for observations on nights of questionable quality. Davidge (1987) has also published photoelectric light curves and an analysis for this star.

Additionally, spectroscopic radial-velocity curves were known to exist for HV 1620 and HV 2241 (Niemela, 1986). These observations and a more complete analysis has also since been summarized by Niemela and Bassino, (1994).

HV 982 appears to have first been recognized as an eclipsing binary by Payne-Gaposchkin (1971) who determined a period of 5.335268 d. Gaposhkin (1970; 1977) provides a tabulation and plot of a photographic light curve for HV 982 as well as 13 times of minima derived from 507 observations. The minima span the period 1897-1949. The plotted light curve is obviously asymmetric in that the secondary minimum does not occur at an orbital phase corresponding to 0.5, indicative of an eccentric system.

Gaposchkin (1965) provides tabulated and plotted photographic light curves for the 3.6265 d period eclipsing binary HV 1620. He also notes that HV 1620 is the brightest eclipsing variable in the SMC. He calculated $\mathcal{R}_1 = 9.3\mathcal{R}_\odot$ and $\mathcal{R}_2 = 8.7\mathcal{R}_\odot$. As noted above Davidge (1988) obtained (three colour UBV) photoelectric light curves for HV 1620. He also obtained classification spectra from which he estimated the MK type of the primary component to be O9 III-V. He was thus able to derive the following dimensions for the components of HV 1620; $\mathcal{M}_1 = 13^{+8}_{-5}\mathcal{M}_\odot$, $\mathcal{R}_1 = 9^{+2}_{-1}\mathcal{R}_\odot$, $\mathcal{M}_2 = 9^{+6}_{-4}\mathcal{M}_\odot$ and $\mathcal{R}_2 = 9^{+2}_{-2}\mathcal{R}_\odot$. He also found that 'the secondary component is very close to filling its Roche lobe and it is possible that the system is semi-detached'. Niemela and Bassino (1994) obtained spectroscopic radial velocity curves. They were also able to make MK classifications of both components, O9 V+O9.5 III.[8] Adopting Davidge's orbital inclination and volume radii they determine $\mathcal{M}_1 = 16.8\mathcal{M}_\odot$, $\mathcal{R}_1 = 11.4\mathcal{R}_\odot$, $\mathcal{M}_2 = 21.3\mathcal{M}_\odot$ and $\mathcal{R}_2 = 10.9\mathcal{R}_\odot$.

Tabulated and plotted photographic light curves for the 4.3426 d eclipsing binary HV 2241 are given by Gaposhkin (1970; 1977) who also notes a 'distortion on the left shoulder of m_2 (the secondary minimum)'.

[8]Note that Niemela and Bassino (1994) labelled the O9.5 III star as the primary component due to its spectrum possessing stronger lines. In the present work the O9.5 III star corresponds to the secondary component. The present labelling is thus the same labelling adopted by Davidge (1988). The difference in labelling is inconsequential and arises simply from alternative adoptions for the zero point Epoch in the orbital ephemeris.

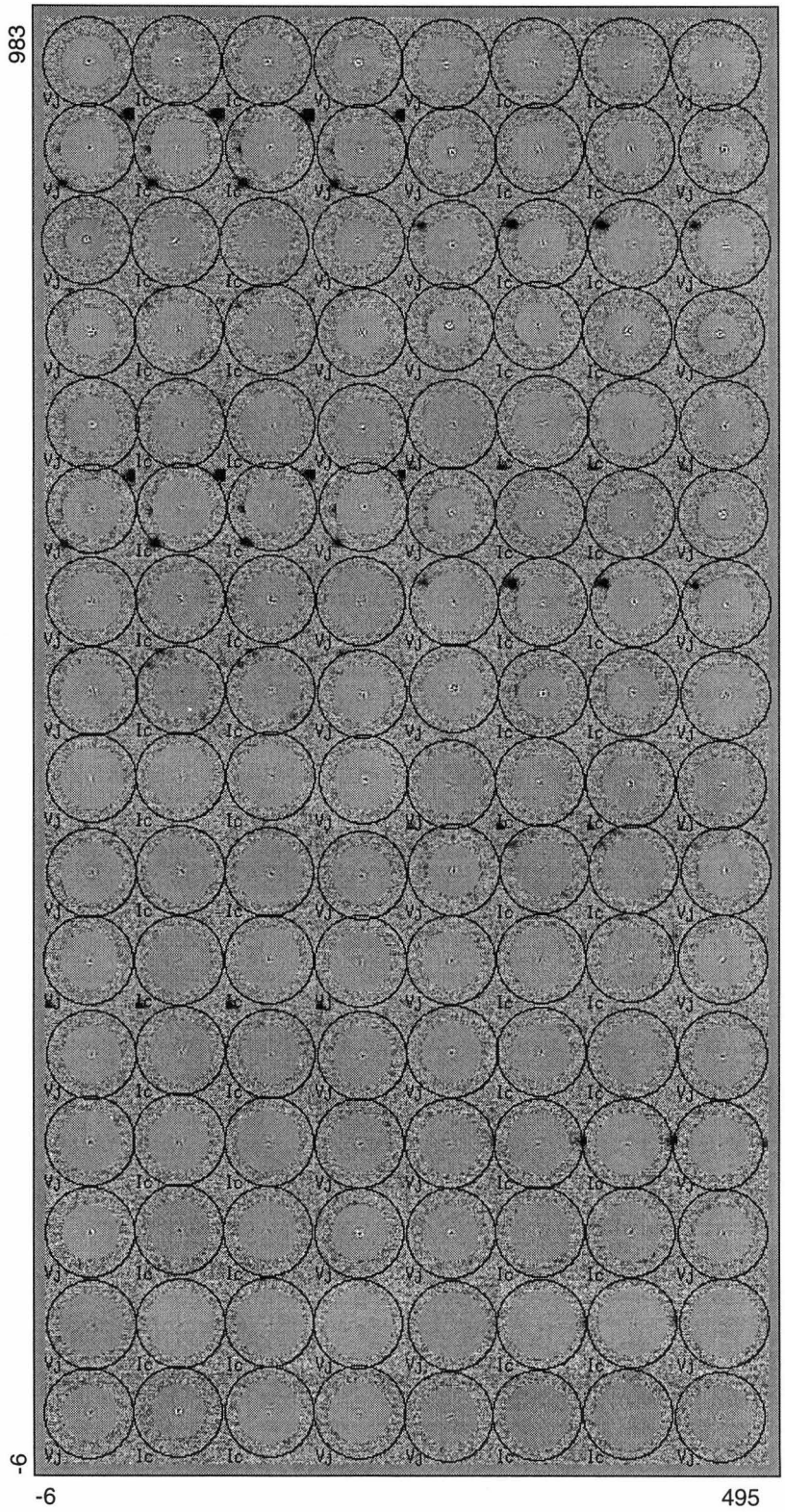

Figure 2.5: PSF subtracted composite image (VI). The data is from the night of 1995-Feb-12. The stars are the various standard stars observed on that night. The ring centered on the stellar centroid in each cutout corresponds to a $37.5''$ diameter aperture. A similar composite image made up from the non subtracted images is presented in figure B.2.

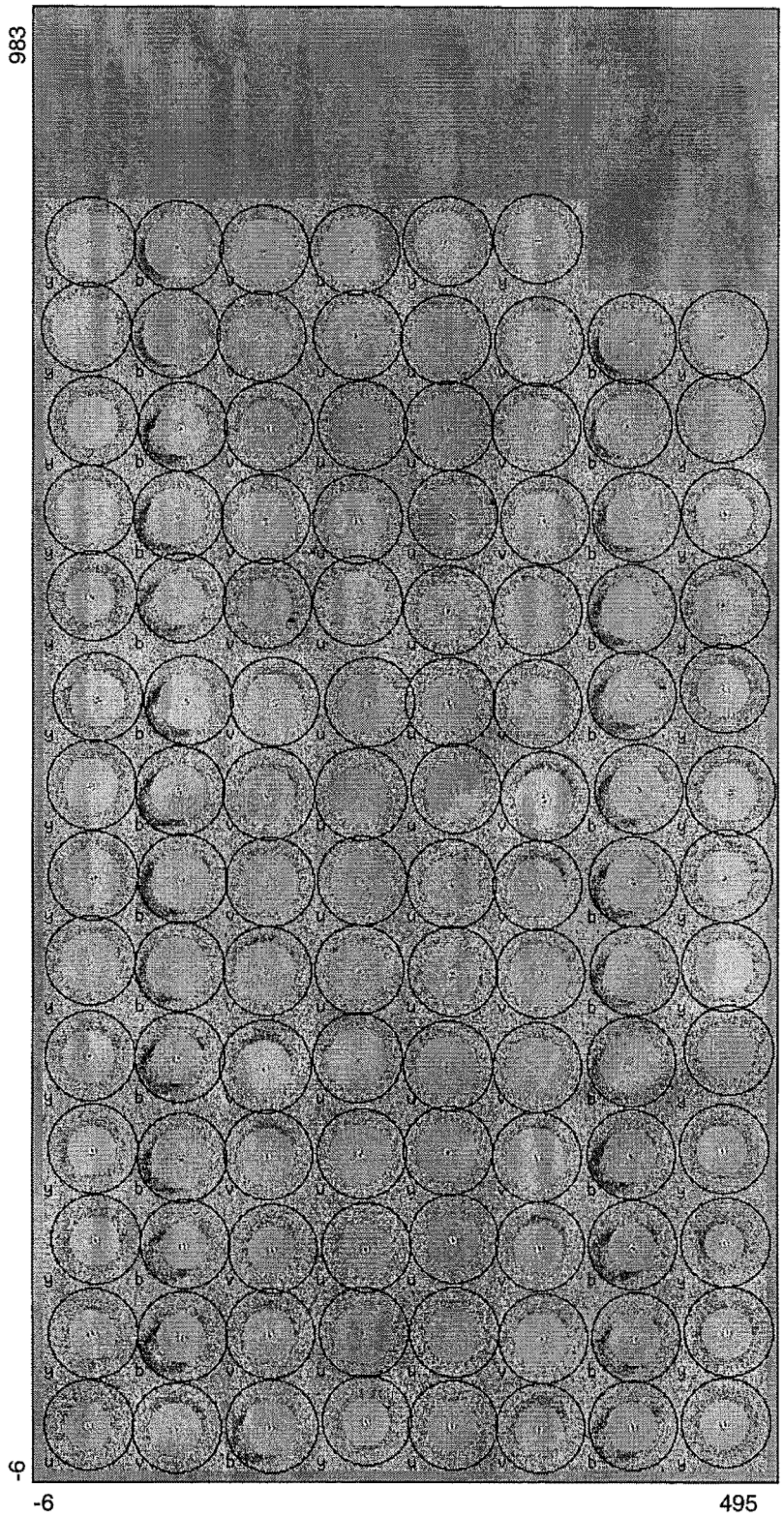

Figure 2.6: PSF subtracted composite image (*uvby*). The data is from the night of 1995-Sep-19. The stars are the various standard stars observed on that night. The ring centered on the stellar centroid in each cutout corresponds to a $37.5''$ diameter aperture. A similar composite image made up from the non subtracted images is presented in figure B.2. Non-smooth background outside the PSF subtracted region (the very smooth circular area centered on each stellar centroid) is caused by light scattered by the filters. It is particularly evident in the *b* images and to a lesser extent in the *v* and *y* images.

Table 2.3: Basic data for the possible targets surveyed. All coordinates measured by Gilmore and Kilmartin (1994; 1996), m_{pg} magnitudes (at maximum light) and periods taken from Gaposchkin (1965), Gaposhkin (1970; 1977) and Payne-Gaposchkin (1971).

	J2000.0			Period	Airmass	
	R.A.	Declination	m_{pg}	(days)	Max	Min
LMC						
HV 936	05 20 04.01	-69 36 38.4	14.1	10.032	1.11	2.50
HV 982	05 29 52.27	-69 09 22.9	14.4	5.335	1.10	2.54
HV 2241	04 57 15.84	-66 33 56.0	13.5	4.343	1.08	2.85
HV 2348	05 09 40.78	-69 20 26.7	14.2	1.990	1.11	2.53
HV 2401	05 16 41.73	-67 07 42.4	14.5	2.945	1.09	2.78
HV 2543	05 27 27.56	-67 11 55.7	12.1	4.829	1.09	2.77
HV 2765	05 39 53.43	-69 15 35.3	14.0	2.149	1.11	2.53
HV 5943	05 34 20.93	-66 44 22.4	14.2	3.663	1.08	2.83
SMC						
HV 1620	00 54 38.64	-72 32 04.8	14.3	3.627	1.14	2.24
HV 1876	01 01 52.29	-72 21 51.0	14.8	2.758	1.14	2.25
HV 2016	01 06 24.15	-72 12 45.4	14.3	2.954	1.13	2.26

Table 2.4: The adopted field positions and orientation for HV 982, HV 1620 and HV 2241. The row and column of the so-called 'Optimum Target Position' in both the PM3000 and and MIDAS coordinate systems are given as well as the telescope orientation (N/S), either North or South of the Celestial Pole. When an image is converted in to the internal MIDAS BDF format with either of the MIDAS commands `intape/fits` or `indisk/fits`, a coordinate transformation with respect to the PM3000 coordinate system is applied as follows: $Col_{\rm MIDAS} = 384 - Row_{\rm PM3000}$ and $Row_{\rm MIDAS} = Col_{\rm PM3000}$, i.e. the image is rotated and the origin is shifted from what is the top right-hand corner in the PM3000 system to the bottom left-hand corner in the MIDAS system.

	PM3000		MIDAS		
Variable	Row	Col	Row	Col	N/S
HV 982	142	221	163	142	S
HV 1620	272	210	174	272	S
HV 2241	452	274	110	452	N

Davidge (1987) determined $\mathcal{M}_1 = 20^{+14}_{-8}\mathcal{M}_\odot$, $\mathcal{R}_1 = 13^{+3}_{-2}\mathcal{R}_\odot$, $\mathcal{M}_2 = 12^{+9}_{-5}\mathcal{M}_\odot$ and $\mathcal{R}_2 = 12^{+3}_{-2}\mathcal{R}_\odot$ from his UBV photoelectric light curves and spectral classification of the primary (O8.5 III), while Niemela and Bassino (1994) determine $\mathcal{M}_1 = 34.3\mathcal{M}_\odot$, $\mathcal{R}_1 = 15.1\mathcal{R}_\odot$, $\mathcal{M}_2 = 17.3\mathcal{M}_\odot$ and $\mathcal{R}_2 = 13.5\mathcal{R}_\odot$ and classify the components as O7 V+O8 V-III.

Given the little data available for the bright and apparently well-detached HV 982 it is clearly a suitable target for study. The uncertainty surrounding the nature of HV 1620 and HV 2241 make them similarly suitable for observation. The effort to observe these three stars and to reduce and analyse those observations constitutes the primary focus of the research presented in this thesis. The adopted field placings and orientations for all observations are presented in figures 2.7, 2.8 and 2.9 and in table 2.4. Details regarding the photometric reduction of the CCD images obtained are given in the sections that follow and the analysis of the resulting data is discussed in the chapters that follow.

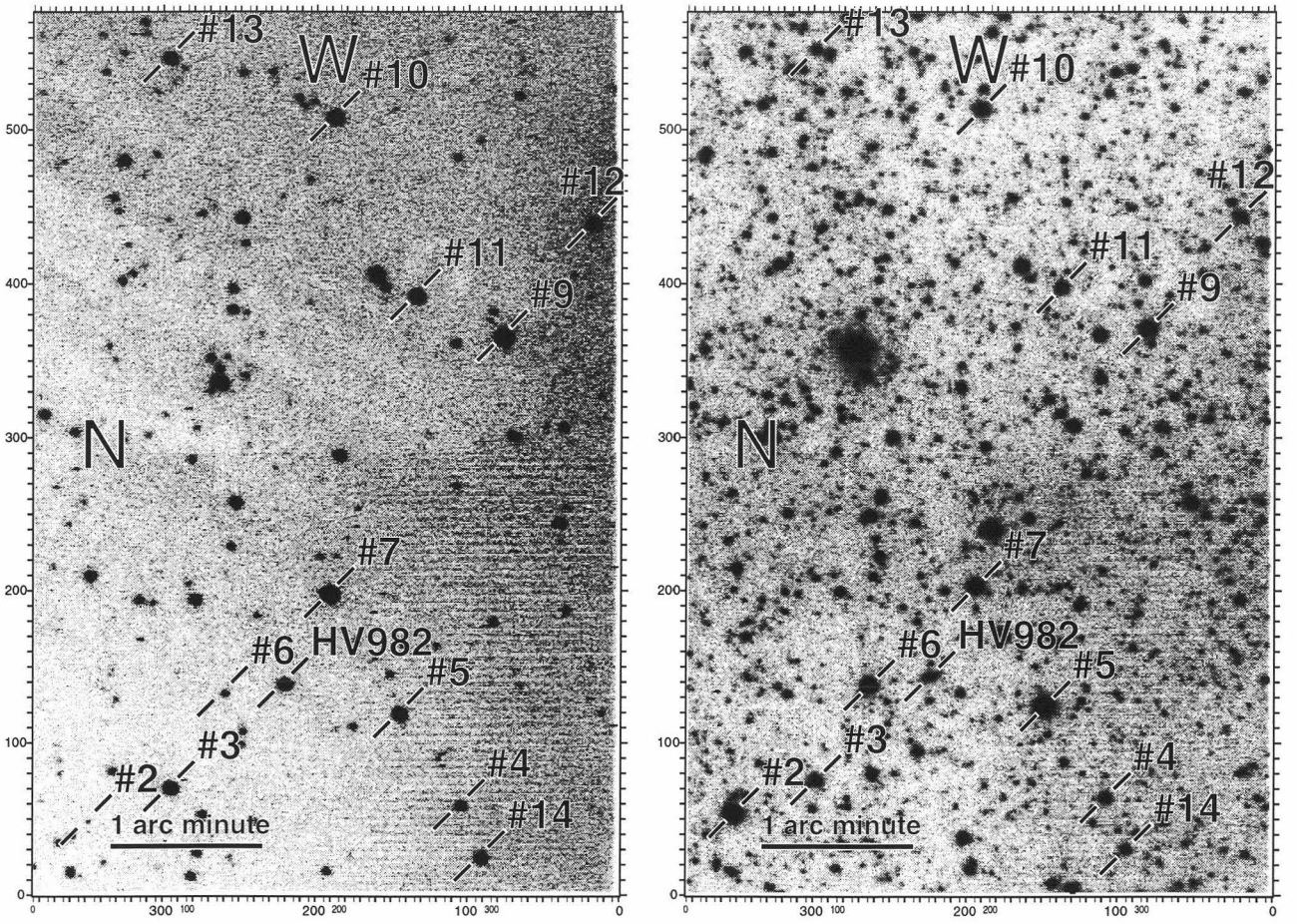

(a) u (b) I

Figure 2.7: The adopted field positioning for HV 982. The telescope orientation is *South of the Pole* (see section 2.1.1). HV 982 and the 13 stars selected as possible $Comparison/Check$ stars are indicated (numbered #2 to #14). The finally adopted $Comparison$ stars were #10 for u, v and b and #4 for y, V and I while the light from stars #12 and #14 was combined to form a $Check$ star. Both u and I fields are provided in order to give an indication of crowding at the longer wavelengths and of the colours of the stars. The numbers around the edges give the PM3000 and MIDAS coordinates: On the vertical axis in these figures the numbers give the PM3000 row but the MIDAS column whereas the numbers across the bottom give the PM3000 column (larger numbers, right to left) but the MIDAS row (smaller numbers, left to right).

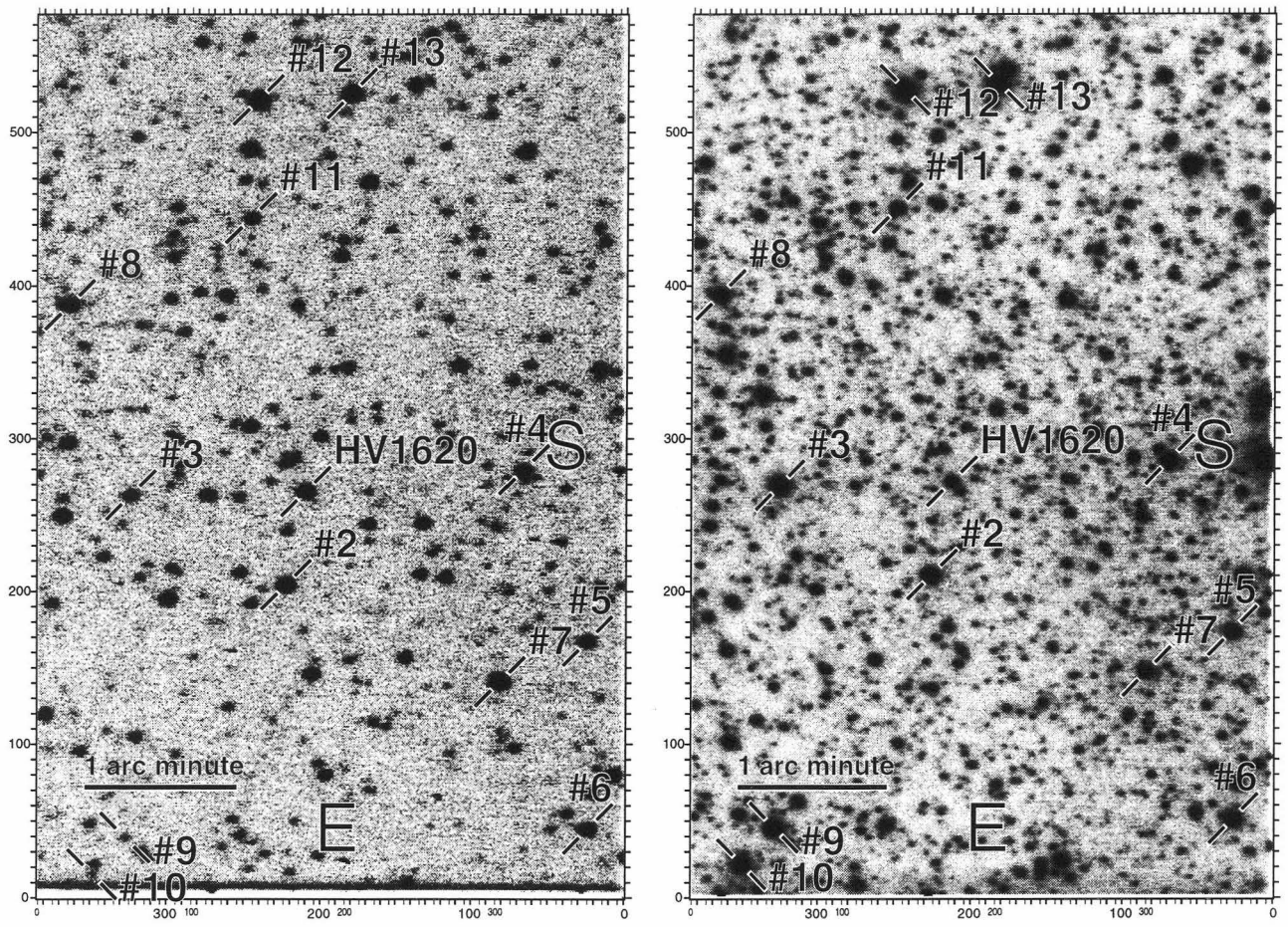

(a) u (b) I

Figure 2.8: The adopted field positioning for HV 1620. The telescope orientation is *South of the Pole* (see section 2.1.1). HV 1620 and the 12 stars selected as possible $Comparison/Check$ stars are indicated. Light from stars #8 and #12 was combined to give the finally adopted $Comparison$ while the light from stars #3 and #13 was combined to form a $Check$ star. Both u and I fields are provided in order to give an indication of crowding at the longer wavelengths and of the colours of the stars. The numbers around the edges give the PM3000 and MIDAS coordinates: On the vertical axis in these figures the numbers give the PM3000 row but the MIDAS column whereas the numbers across the bottom give the PM3000 column (larger numbers, right to left) but the MIDAS row (smaller numbers, left to right).

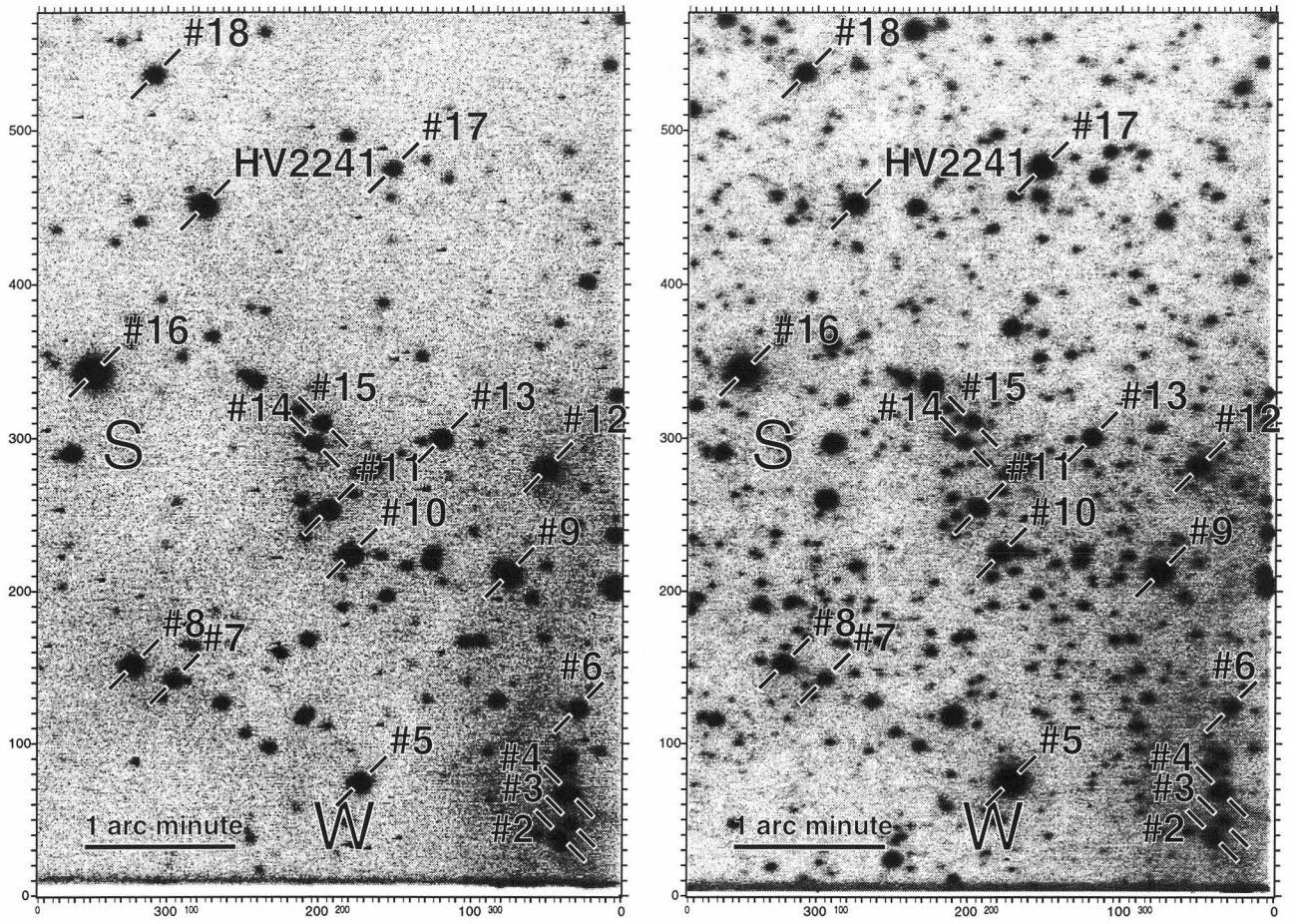

(a) u (b) I

Figure 2.9: The adopted field positioning for HV 2241.The telescope orientation is *North of the Pole* (see section 2.1.1). HV 2241 and the 17 stars selected as possible $Comparison/Check$ stars are indicated. The adopted $Comparison$ was star #10. A $Check$ star was derived from stars #11 and #13. Both u and I fields are provided in order to give an indication of crowding at the longer wavelengths and of the colours of the stars. The numbers around the edges give the PM3000 and MIDAS coordinates: On the vertical axis in these figures the numbers give the PM3000 row but the MIDAS column whereas the numbers across the bottom give the PM3000 column (larger numbers, right to left) but the MIDAS row (smaller numbers, left to right).

2.3 Observational Procedure

Because of the nature of the programme of research, namely an ongoing, long-term project, it is necessary to have a well defined observational procedure. During the first six months of my enrollment I was fortunate to participate in a world-wide, longitude coordinated observation campaign for Sanduleak-3.[9] This project provided my first practical experience in astronomy and the observing procedure I developed for the eclipsing binary project is derived directly from the procedure developed by Tobin for the Sanduleak-3 project and on the experience I gained during that project. As a result, the basic procedure was well defined almost from the beginning of observations for the eclipsing binary project. During the slightly more than three years that observations were made, although I was continually refining the computer software which in essence defined the procedure, the underlying philosophy of the procedure remained essentially unchanged.

For the benefit of Mike Clark, William Tobin, Mohd Zambri Zainudden and Alan Gilmore who all made a significant number of observations for me, as well as for my own benefit, I also codified the procedure in an 'Observing Guide'. The guide describes all relevant procedures for obtaining a complete data set from which meaningful scientific data can eventually be extracted. These include:

Procedures for each run

- Obtaining clock-drift data.
- Checking the mounting and orientation of the CCD dewar and photometer head on the telescope.
- Checking on the cleanliness of the filters and CCD dewar entrance window, cleaning if necessary.
- Focusing the photometer head offset guide camera so it is in focus when the telescope is in focus.
- Aligning the finder-scopes with the CCD's field of view.

Procedures for each night's observations

- DARK images (see below, section 2.3.2).
- FLAT FIELD images (see below, section 2.3.3).
- Telescope focusing.

Procedures for each exposure

- The acquisition and archiving of each observation (see below, section 2.3.4)

Observations for the programme separated naturally into two sub-programmes. One for the acquisition of data from which to construct differential photometry light curves, the other for the acquisition of data with which to calibrate the MJUO photometric system and hence transform the MJUO photometry onto the standard systems. The differences between observations for these two programmes are mainly in the philosophy of 'what to observe when' and are described in section 2.4 below. Both programmes are however based on the same procedures for obtaining a single exposure, which is what is described in the following sections.

Before getting to stellar observations however, there are a number of significant considerations which must be seen to. CCD images suffer from a number of systematic problems which must be corrected for before scientifically meaningful data can be extracted from them. In essence, the CCD signal is composed of a number of the stellar light source signals and a number of other additional sources, such as the DARK current. The variation of sensitivity from pixel to pixel must also be corrected for. Fortunately the correction procedure is relatively straightforward. The usual procedure, and certainly the procedure adopted in this work, is to correct the stellar exposures by either the subtraction of or the division by other images exposed under particular conditions.

Before describing the individual procedures for obtaining each of the images required in order to obtain the final corrected stellar image it will be useful to describe in detail the actual CCD camera and electronics system and the practical workings of each individual exposure. Having typed into the PM3000 computer the appropriate command to initiate an exposure the following occurs:

[9] By utilizing telescopes at a number of observatories located at various longitudes around the world, provided the weather is kind, it is possible to obtain essentially continuous observations of objects rather than the more usual eight or so hours obtainable in one night from a single observatory. As part of such a project coordinated by Dr. H.E. Bond of the Space Telescope Science Institute, William Tobin, Mike Clark and myself observed the Pre-Planetary Nebula Sanduleak-3 between May 6^{th} and 17^{th}, 1992.

- A 'flash ring' of 8 green LEDs, which is part of the mechanical shutter assembly, is illuminated for (unless otherwise specified) 70ms. This flash deposits ~300 electrons in each pixel of the CCD. The purpose of the preflash is to avoid problems associated with reduced transfer efficiency at low signal levels. The noise in the normal 70ms flash ring signal is found to be 18-19 electrons per pixel (Tobin, 1992).

- The mechanical shutter assembly is then opened to admit light. If the FORTH command `obs` is used to start the exposure the PM3000 computer is then unusable during the exposure. If on the other-hand the FORTH command `expose` is used then the PM3000 returns to the prompt once the exposure has begun. The shutter remains open until either the specified exposure time has elapsed (`obs`) or the FORTH command `readout` is issued. In the case of `expose` and `readout`, the PM3000 waits for the tick of the second before starting the flash ring preflash and then opening the shutter and closing the shutter at the end of the exposure. The difference between the recorded exposure start and finish times therefore includes the time preflash time during which the shutter was closed. The true exposure duration is therefore the difference between the recorded exposure start and finish times minus the preflash duration.

- The CCD is read out and the resulting signal is processed by the CE200 electronics unit. This includes the analogue to digital conversion. The resulting signal is then sent to the PM3000 computer for display, processing and writing to half inch 9-track tape for transport to Christchurch.

2.3.1 BIAS images

BIAS images record the zero duration i.e. zero signal, exposure. They do however include the signal from the flash ring preflash, unless of course this is turned off. They also include the effect of the temperature sensitive fat zero offset from the ADC.

BIAS images were obtained immediately after each exposure. The mean of the 50×50 pixel central region of the chip is calculated and stored in the header information of the current exposure. If a DARK subtraction (see below) is to be made the BIAS level of the current exposure is compared to the BIAS level of the DARK exposure. If these two levels differ by a (`cgain` dependent) amount, a warning is given. This is necessary since, as described above, the BIAS level is a function of, among other things, the temperature of the CE200 camera electronics unit. Thus as the temperature in the dome varies during the night so will the BIAS level.

BIAS images were in general not archived.

2.3.2 DARK images

DARK images are usually used to correct for the *thermal current* during an exposure. But at cryogenic operating temperatures, the thermal current is only ~1 electron per pixel per minute, so even for the longest exposure durations (20 minutes) used for the observations made for this project, the resulting dark current is only of the order of 5% of the signal deposited in each pixel by the flash ring preflash. Therefore for practical purposes a single 10 second DARK image was used to correct images of all exposure durations. The actual DARK used was in fact the median[10] of three individual 10 second dark images.

DARK subtraction was automatically applied to each FLAT FIELD or stellar observation made when the various FORTH commands specifically defined for the programme (see section 2.3.5) were used. When BIAS level warnings were given due to differences between the DARK bias level and the bias level of the image from which the DARK was to be subtracted, usually the subtraction was allowed to continue, but a new DARK image was subsequently acquired before the acquisition of any further FLAT FIELD or stellar images. DARK images used for DARK subtraction of FLAT FIELD or stellar images were archived to tape as part of the data set.

Figure 2.10 presents a typical DARK image. Noteworthy are the extremely dark and bright regions across the bottom and right hand margins of the chip, the two dark vertical stripes running from top to bottom about one third and three quarters of the way across the chip, and the dark stripe about 10 pixels long toward the top center of the chip. The dark and bright margin regions are presumably a problem introduced during the

[10]The FORTH command `median` computes a 'median' image from three input images. The pixel values of the median image are the medians of the three individual values of the corresponding pixel in the three input images. Medianing provides an effective means by which cosmic rays and other spurious signals can be eliminated from the images. Since the CCD detects ~9 cosmic rays events per minute, cosmic ray free images are otherwise generally possible only for very short exposures which for other reasons are often impractical.

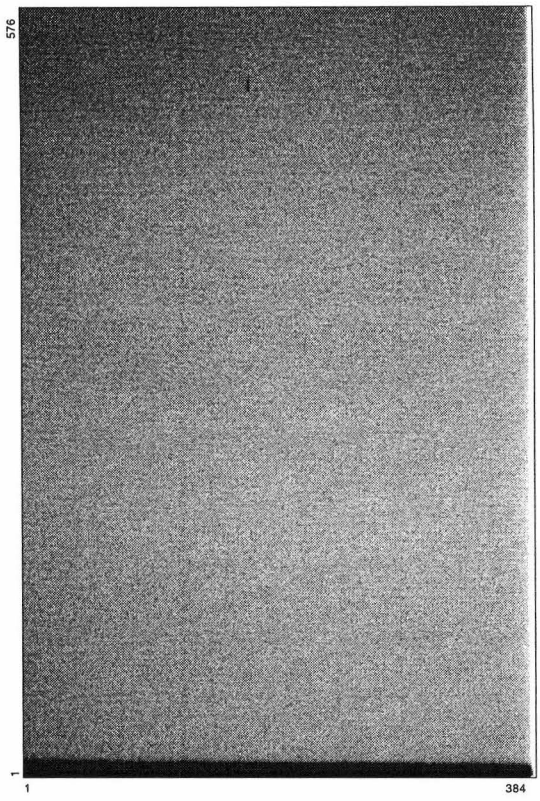

Figure 2.10: A typical DARK image (frame T4760001 from 1994-Jun-08). The exposure time was 10.0-sec, `cgain=100`. The mean, standard deviation, minimum and maximum of the pixel values in the region [10,10:374,566] of the image are 416.2, 4.6, 379 and 433.

readout of the chip since similar structure exists in all images, whether the image is composed from the entire frame or a restricted region of the chip. These features mean that data from these two regions is effectively unusable. The other three features are not known to cause any significant problem being adequately dealt with by the adopted DARK subtraction and flat fielding procedures.

2.3.3 FLAT FIELD images

We adopted the use of *dome* FLAT FIELD images, as opposed to *sky* FLAT FIELD images, mostly due to considerations of convenience, practicality and reliability (in that it is not possible to guarantee that suitable skies will be available at appropriate times). Dome FLAT FIELD images were obtained by illuminating a white-coloured board with either a 1 200 W theatrical spot lamp or a 5 W Halogen torch bulb lamp, depending on the filter for which the FLAT FIELD was being obtained. Further, the white board was painted with a low reflectivity black paint outside of the telescope beam path, to reduce the contribution from scattered light. Sharpened annuli added to the chimney baffle and skirt also help to reduce the amount of scattered light arriving at the CCD.

For the most part, FLAT FIELD images were obtained before the start of and at the conclusion of each night's observations. The main reason being that should contaminants, such as dust motes, enter the light path (i.e. end up on the entrance window of the CCD's dewar) it would still be possible to flat field subsequent images with an appropriate FLAT FIELD image. On occasion, usually when observations were made for only a restricted time, (having been ended early due to deteriorating weather conditions, having been started late due to initial weather conditions being unsuitable or for whatever other reason) only one set of FLAT FIELD images were obtained and/or archived to tape. Since a full set of FLAT FIELD images for all six bandpasses used for observations required of the order of one and a half hours to acquire, mainly due to the required exposure time for u, practical considerations, particularly with MJUO observer/technicians in mind who are not normally resident on the mountain, mean that it may not always be convenient or indeed possible to obtain before and after FLAT FIELD images every night without using dark time that might better be used for stellar observations. A reasonable approach for future work might be beginning and end of **run** – rather than night – FLAT FIELD images. As can be seen in figure 2.11, which shows the ratio of V FLAT FIELD images obtained at the start of observations in the 1992 and toward the end of observations in 1995

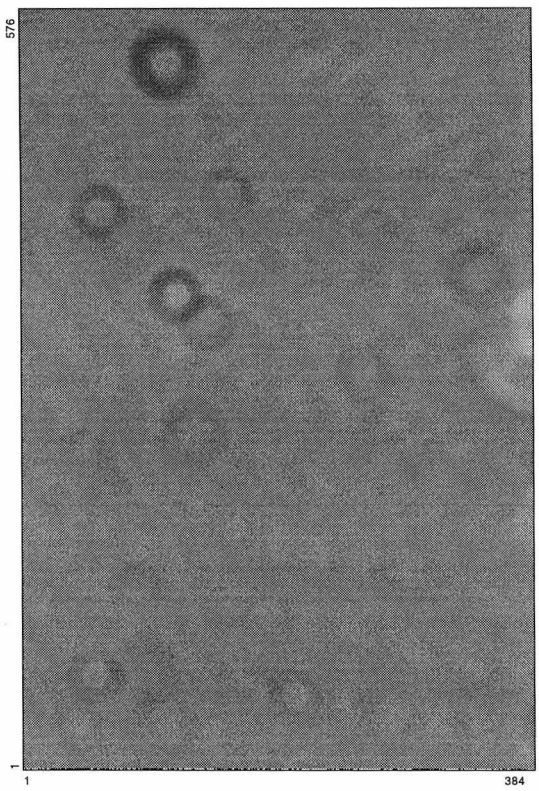

Figure 2.11: The ratio of the two images shown in figure 2.2 (`ff921103V` divided by `ff951023V`). It is pleasing to see that essentially all of the structure evident in the original FLAT FIELD images has divided out, the only significant differences between the images being produced by dust motes on the interior face of the quartz entrance window of the cryostat dewar. The mean, standard deviation, minimum and maximum of the pixel values in the region [10,10:374,566] of the image are 1.0000 , 0.0063 , 0.9589 and 1.0970 .

(figure 2.2), pixel sensitivity is rather stable, the only significant differences between the two images being caused by the accumulation of dust (mainly) on the inside of the entrance window of the CCD's dewar and the development of one cold pixel (located at (MIDAS) coordinates (151,215) with a reduced sensitivity of $\sim$0.9 that of surrounding pixels) during the three year period. The implications of this are that beginning- and end-of-run FLAT FIELD images should be more than adequate. Precautions should however be taken to watch for new contaminants in the optical path. This could be achieved quite simply by obtaining a single V FLAT FIELD image which, without neutral density filters attenuating the 1 200 W lamp, requires only a 3 deci-second exposure, which could then be compared with the archived beginning-of-run V FLAT FIELD. Any new contaminants would be immediately obvious in the ratio of the two images, and new FLAT FIELD images could be acquired if deemed necessary due to the presence of new contaminants.

For each filter, three individual DARK subtracted dome FLAT FIELD images were acquired. The exposure time for each filter was adjusted each night so as to produce as nearly as possible, a mean signal level of 10 000 ADU in each pixel in each individual exposure. Neutral density filters were used to attenuate the 1 200 W theatrical lamp where necessary so that resultant exposure durations were at least 10 seconds. Typical exposure times were 700, 45, 60, 50, 15 and 200 seconds for *uvbyVI* respectively. Each of the three individual images were then multiplied by an appropriate number so as to insure that all three *formally* had the same mean of 10 000 ADU per pixel. Ensuring the original image had a mean close to 10 000 ADU in the first place reduces truncation errors caused by the integer image representation employed by the PM3000 computer. The medianed image was computed from these scaled images. In general only this medianed image was retained and archived to tape for further use in the reduction process. Unlike the earlier work described in (Duncan, 1991; West, 1991; West et al., 1992; Watson et al., 1992; Tobin et al., 1993a; Duncan et al., 1993; West et al., 1992) stellar images were not flat fielded 'at the telescope', but rather as a preliminary step of the reduction procedure (see section 3.1.2). This was to avoid truncation errors since PM3000 images are stored as integer numbers rather than real numbers. The final FLAT FIELD images for flat-fielding the stellar images from a given nights observations were computed as the sum of the before- and after-observations median FLAT FIELD images, divided by the mean pixel value in this summed image, so that on average the stellar images are divided by a pixel value of unity.

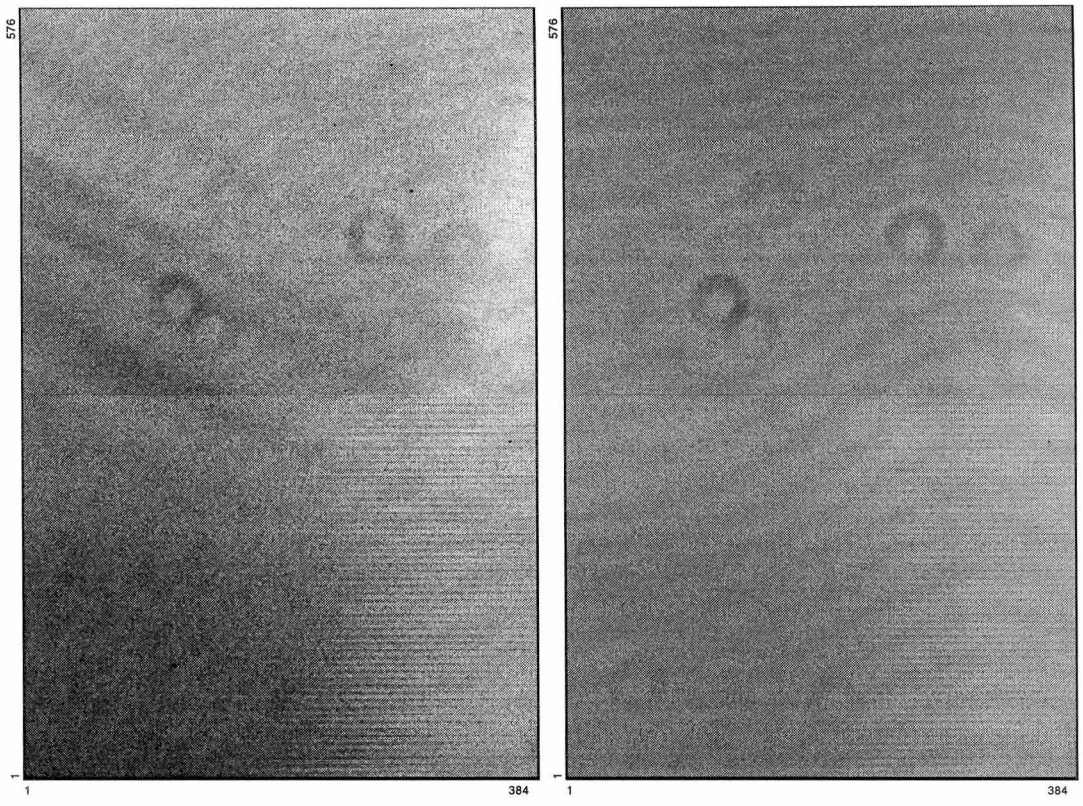

Figure 2.12: The image on the left is a u FLAT FIELD while that on the right is an I FLAT FIELD. The difference between the two images is indicative of differences in the spectral dependence of the response of the CCD.

Problems with Flat Fielding

At the time of carrying out the observations, no definitive solution to the problem of correcting for inter-pixel variable quantum efficiency was (and indeed is still not) known. While the high spatial frequency variations are believed to be adequately accounted for in the adopted flat fielding procedure, the same can not be said for lower spatial frequencies. The result of this is that differential photometry between two stars in a single image will in general be a function of their exact locations on the chip. On the Boller & Chivens telescope, differential photometry accuracy was limited to no better ~ 4 percent. No thorough investigation of the problem has yet been made for the McLellan 1m telescope, but due to a number of improvements (e.g. sharpened annuli in the chimney baffle to reduce scattered light) it is hoped that the problem is less significant. In any case, this leads to certain constraints on the most desirable means for carrying out stellar observations as will be described in section 2.3.4.

2.3.4 Stellar images

Because of the remaining uncertainties regarding the flat fielding procedure (section 2.3.3), stellar observations were acquired with target objects located at predefined 'Optimum Target Positions'. Each of the three primary programme stars (HV 982, HV 1620 and HV 2241) had such a position defined. Every effort was made to ensure that the stellar centroid was located at this position in every exposure. Additionally, it was of course also important to ensure that the telescope was always oriented (either above or below the south celestial pole) as appropriate for each target (see section 2.1.1).

For differential photometry within a single image any remaining error in the flat fielding procedure is thereby reduced to a (unknown) systematic offset in the differential magnitude. If the above precautions are adopted the offset in two images of the same field will not significantly differ. Thus, for the construction of photometric light curves this effect will without doubt affect the **apparent overall level** of the differential magnitude, but it will not have any effect on the **shape** of the light curve.

For calibrating the instrumental photometric system against standard systems, the same philosophy applies. Any difference in local quantum efficiency unaccounted for by the flat fielding procedure, will be absorbed by the transformation equations, provided that all observations from one night – for which one would naturally determine one set of transformation equations – be obtained at one Optimum Target Po-

sition. From night to night however, such a restriction is not necessary. Changing the Optimum Target Position from one night to another is basically equivalent to the calibration of separate systems, as if one had simply switched detectors. How much one can combine sets of data obtained at several Optimum Target Positions to obtain transformation coefficients depends on the exact nature of the remaining deficiencies in the flat fielding procedure. This is discussed in section 5.2.1.

Stellar observations were made at all reasonable opportunities, irrespective of seeing conditions. Observations made in conditions of poor quality can always be eliminated from the analysis at a later point, but if those observations were never made, one obviously does not have that luxury.

DARK subtracted stellar images were written to half inch 9-track magnetic tape for archiving and transport to Christchurch.

2.3.5 FORTH Acquisition Software : *file jdp*

The nature of astronomy, working in conditions where the observer is often cold and/or tired means that when observing, astronomers are perhaps more prone to making mistakes than would otherwise be the case under more ideal circumstances. It is thus desirable to utilize computers to automate as much of the process as is possible, while still providing full control over the observations. This philosophy underlies my efforts to design, develop and implement a suite of acquisition software. The software is of course designed specifically for the MCEB programme, but many of its features are of more general use to other observers.[11]

The FORTH operating system of the PM3000 computer provides a powerful environment for instrument control. FORTH programming is based on the definition of 'words' which perform simple tasks. More complicated commands can then be constructed by defining new words which simply invoke a series of previously defined words. Such an environment is particularly useful when a series of tasks need to be performed many times, or when varied combinations of a wide variety of tasks need to be performed.

The result of my efforts to design an integrated set of commands is that under ideal conditions (i.e. the telescope is already focused and pointing in the correct direction), an entire night's differential photometry observations, including appropriate DARK and FLAT FIELD images can be made with of the order of ten commands, if observations are required in just one bandpass. For each additional bandpass, two more commands, one for FLAT FIELD images and one for stellar exposures, must be remembered, but these are simply commands with a common root either prefixed or appended with the appropriate filter name. For example a medianed (see 2.3.3) FLAT FIELD image, derived from three individual FLAT FIELD images, each with an exposure time of 700-decisec, for the I filter bandpass would be produced by `700 Icflats` while for V the appropriate command to produce the final FLAT FIELD image based on 150-decisec exposures would be `150 Vjflats`. Each command resulting in an exposure also displays the image graphically on the display monitor and calculates and displays appropriate useful statistics from which the observer can determine if the image is useful or not and therefore whether the image should be recorded to tape or not. Additionally, the observer is led through a series of yes/no prompts which result in writing the image to hard disk for semi-permanent storage and finally to tape for 'permanent' storage and transfer to Christchurch.

With a number of different observers making observations, and the desire to make observations in as standard a manner as possible (for the various reasons described in the sections above), given the actual complexity of the observational procedure when coupled to the necessity of implementing it via a computer, such a suite of software is extremely useful if not essential. The quality of the resulting data (see following chapters) is, in my mind, in no small part due to careful thought and much effort at this most fundamental level.

2.3.6 Christchurch-based tape reading software

A suite of software for the transfer of images from half-inch, 9-track tape to the local computer system (and from thence to the world!) is provided on the VAX/VMS cluster of the University of Canterbury. A number of useful and important functions and features are performed/provided by this software:

- The primary function of the tape reading software is, of course, the reading of the original tape file and thence the conversion of the file format and writing to disk of each image. The file format on the original 9-track tape is an idiosyncratic format specific to the Photometrics PM3000 FORTH system. The file is written to disk directly in FITS format, suitable for input into analysis packages such as MIDAS.

[11] During the *Jupiter/Shoemaker-Levy 9 Impact* event in July of 1994, I acted as a technical observer/assistant to the visiting astronomer who was part of a world-wide observational effort. Adaptations of my software were used extensively for that effort.

- At the time the file is written to disk, the correction to the recorded observation times for the drift of the clock of the CCD's controlling computer (see section 2.1.2), the Heliocentric correction, airmass (see appendix A) and other useful information are calculated and written into the header structure of the FITS file.
- Provided appropriate information is included in the file headers of the image and maintained in a master 'Object List' file, the software appends relevant information regarding each observation of a given object to an 'Observing Log' file. This is an incredibly useful feature.
- A 'Tape Log' file summarizing each image file read on a given tape is produced each time the tape is read, another incredibly useful feature.
- Auxiliary software is provided which will output a PostScript file version of images, including relevant parameters of the observation. Such files can be sent directly to PostScript printers and are also suitable for direct encapsulation in documents such as this one. Figures 2.7, 2.8, and 2.9 are examples, although a small amount of subsequent editing has been done in order to add the identifications of the objects of interest and the orientation compass.

2.4 Observational Programmes

Observations for this project naturally divided themselves into two programmes, one from which to construct differential magnitude light curves and one from which transformations from the instrumental photometric system to the standard photometric systems could be determined. The latter of course required all-sky photometric conditions, conditions that are all too infrequent at MJUO. Almost all other nights on which observations were possible were devoted to differential photometry observations.

2.4.1 Observations for Differential Photometry

On most nights, observations were made of only one target, although two targets during the course of one night was not uncommon, usually splitting the night in half between the two targets. Once all six filters were in use, the six filters would usually be cycled through, however emphasis was given to u, and I observations (and in the case of HV 982 and HV 1620, V as well). Observations would typically be acquired in a sequence such as $VIuVIvVIuVIbVIuVIyVIuVIv\ldots$, thus accumulating light curves somewhat denser in u, V and I. Of course phase coverage in the various filters to date was considered in devising an appropriate observation sequence for a given night.

For accurate determination of the geometrical properties of an eclipsing binary system, one precise curve with high density phase coverage is probably sufficient. Emphasis was given to the u and I in order to obtain such a curve and to in addition provide the widest spectral base line which provides information regarding the relative temperatures of the two components, as manifest in the different relative depths of primary and secondary eclipses in the different bandpasses.

MJUO's latitude and the declination of the targets (see table 2.3) means that the maximum airmass obtained by any of the three targets was no greater than 2.85. Therefore, given that differential extinction effects for target, comparison and check stars will be insignificant given the rather small field of view of the CCD, observations were made at all airmasses for the programmes stars since seeing at MJUO was found to be only slightly correlated with airmass (Pritchard, 1993). Atmospheric and dome turbulence play much more dominant rôles in determining the seeing at MJUO.

In slightly less than three years of observing (1992-Nov to 1995-Mar) more than 2200 images were obtained (HV 982:1081, HV 1620:760 and HV 2241:391). The reduction of this data is described in section 3.3.

2.4.2 Observations for Calibration Photometry

Initial efforts quickly showed that obtaining observations from which to calibrate all six bandpasses in one night was impractical for a number of reasons. In order to avoid exceeding the 14-bit integer limit of the ADC as well as saturation of the CCD itself, secondary standard stars must be used since all primary standards are too bright, especially given the desire to have exposure durations of at least 10 seconds to reduce scintillation noise and errors associated with the finite speed of the shutter mechanism (see section 2.1.2) to acceptable levels. On the other-hand, since one wishes to observe as many standard stars as possible in a given night it is desirable that the standards be as bright as possible so as to minimize the required exposure durations,

without going below 10 seconds. The significantly greater total transmission of the wider bandpass V and I filters, as compared with the *uvby* filters means that the brightest stars meeting the above criteria have V magnitudes of about 10.0 and 8.0 for VI and *uvby* respectively. Thus a star suitable for *uvby* observations will be too bright for VI observations while an appropriate VI star will be so faint as to make *uvby* exposure durations prohibitively long. Furthermore, since the programme stars are all likely OB-type stars and therefore rather blue in colour, best results will be obtained if the standard stars observed are of similar colours. Reliable, homogeneous photometric catalogues in the standard Cousins $UBVRI$ and Strömgren *uvby* systems of such stars are of limited availability in the literature. The number of such stars for which good photometry[12] standard system exists for *both* systems is a rather small subset of the above. Final standard star observing lists and photometry were taken from Kilkenny and Menzies (1989), Menzies et al. (1989), Menzies, Marang and Westerhuys (1990), Landolt (1983; 1992), Graham (1982) and Bessell (1995) for VI and Kilkenny and Laing (1992), Kilkenny (1977; 1977a; 1977b), Cousins (1987), Kilkenny and Hill (1975), Graham (1972), Graham and Slettebak (1973) Bessell and Wickramasinghe (1978) for *uvby*.

For standard stars the basic observing sequences for VI and *uvby* observations were $VIIV$ and *uvbyybvu* respectively.[13] Since the transformation equations in general rely on observed colour terms (see section 5.1.2) but the observations can not be made simultaneously, such sequences have the advantage of providing a pair of measurements for each colour that are in a sense averaged over airmass.

For programme stars, which are of course somewhat fainter than most secondary standards and therefore require exposure durations of the order of 20 minutes for *uvb*, 12 minutes for y and 7 minutes for VI in order to collect suitable signal levels, time did not permit two measurements of each star on a given night especially for the *uvby* observations. Indeed it was quite a feat to observe all three targets and a suitable number of standard stars in a given night.

For the purposes of calibration, airmass is rather more critical than is the case for differential photometry. Therefore programme stars were observed at as small airmasses as practical given the limitations of any given night. Standard stars were observed at appropriate airmasses so as to ensure that the programme star airmasses would be bracketed by standard stars. Similarly for stellar colours.

At the conclusion of observations for this project, data of suitable quality for calibration had been acquired on eight separate nights: (*VI*) 1994-Dec-26, 1995-Feb-12, 1995-Sep-02, 1995-Sep-03 and 1995-Oct-23 and (*uvby*) 1995-Sep-18, 1995-Sep-19 and 1995-Oct-25. The reduction of this data is described in section 3.4 while the analysis is detailed in chapter 5.

2.5 Image quality

A number of factors influence the final quality of a CCD image, including atmospheric seeing, the accuracy of the tracking of the telescope during long duration exposures, and the optical quality of the telescope, filters and any other optical components in front of the CCD in the optical path.

At MJUO, observations are possible, and indeed worth while, over a wide range of atmospheric conditions. The seeing thus varies over a corresponding range. On the best nights the seeing approaches $1''$. Stellar images are so (positionally) stable that damped oscillations of the telescope, (of maximum amplitude of $\sim 0.1''$) as the telescope comes to rest after minor pointing corrections due to inaccuracies in telescope tracking, can be seen in the guide-star image. Of the $\sim$200 nights I observed, such conditions prevailed on probably $\sim$10 occasions. On lesser quality nights, poor seeing can result from intrinsically small stellar images (in terms of the width of their profile) that are positionally very unstable on very short time scales, so that the guide-star image is seen to 'dance' about. Typically, the instantaneous position of the centroid of the guide star might deviate from its mean position by of the order of one or two seconds of arc on time scales of fractions of a second. Such seeing presumably results from a relatively clear but rather turbulent atmosphere. Alternatively, the image can be positionally very stable but simply of large width. This presumably results from a fairly stable atmosphere, but one where the light suffers a relatively large amount of scattering during its passage through the atmosphere. On the worst nights the seeing is characterized by both of these effects. The seeing at MJUO can vary dramatically over time scales as short as 1 hour.

[12] Here, 'good photometry' typically means that each individual standard star has been observed somewhere between five and ten times in each bandpasses over a time period typically measured in years, and that the standard deviations of the resulting standard system photometry are less that 0.01 mag.

[13] In what follows I will from time to time refer to 'measurements' of the instrumental magnitudes and colours by which I will be implying the magnitudes and colours derived either from one V observation and one I observation for VI while for *uvby* the implication will be magnitudes and colours derived from one u, one v, one b and one y observation.

As discussed in section 2.1.3, the photometer head provides an offset guide camera which allows adjustments to the telescope's pointing to account for inaccuracies in tracking and changes in the atmosphere to be performed in real time. Inaccuracies in tracking are most probably due to effects associated with flexure of the telescope, since on 'good' nights, the required corrections tend to be rather systematic, always in one or two of the four possible directions. Moreover, the required corrections tend to fade to zero as the meridian is approached, and then 'grow back' again, except in the opposite direction, as the telescope moves away from the meridian again. Atmospheric variations causing changes in atmospheric refraction can also have dramatic effects (at the several arc-second level) on the apparent position of the stellar images.

Aside from the optical quality of the telescope's mirrors and lenses, the filters, the entrance window of the CCD's dewar and the CCD itself, all of which are factors essentially beyond my control, probably the most important contribution to image quality is the cleanliness of those surfaces, especially the ones closest to the focal plane, i.e. the entrance window and the filters. Shadow rings, caused by dust on the inside surface of the entrance window can be plainly seen in FLAT FIELD images (figures 2.2 to 2.12). Dust on the inside window can only be dealt with by opening the cryostat to clean the system. Such a job would be best done by the supplier (Photometrics) and thus would involve the CCD system being unavailable for a lengthy period of time. Until recently the Photometrics CCD system used for this project was the only CCD detector available at MJUO, thus given the usage demands on the system, this was not a viable option. It is however possible to clean the external surface of the entrance window. Once cleaned at, for example, the beginning of an observing run, the CCD, photometer head, telescope system is sufficiently 'dust-tight' that was seldom necessary to clean it again for the duration of the run.

Chapter 3

Photometric reduction

A CCD image is, in general, comprised of anywhere from several thousand to several million numbers, in the case of the MJUO CCD some $384 \times 576 = 221\,184$ integers. Each represents the measured incident light at the location of the corresponding pixel (or perhaps bin of pixels). For most purposes, these raw numbers are too complex to interpret directly. *Reduction* of a CCD image is the process of deriving a smaller set of *meaningful* numbers from the raw CCD image. In general it includes procedures for accounting and/or correcting for the ADC fat-zero or BIAS and thermal currents (DARK subtraction) as well as inter-pixel variable quantum efficiency (Flat Fielding) and of course, in the case of photometry, the actual extraction of photometric magnitudes for objects of interest in the image.

This chapter describes the procedures, the philosophy behind their development, and the results of the reduction of the raw CCD images acquired for this thesis. In particular I describe the biasing and flat-fielding procedures, then I discuss general aspects of the two primary methods of extracting photometry from CCD images, *Synthetic Aperture Photometry* and *Profile Fitting Photometry*. Next I discuss the reduction of the slightly more than 2000 images from which the *differential magnitude* light curves of the three Magellanic Cloud Eclipsing Binaries observed at MJUO have been constructed (the analysis of these light curves is presented in chapters 4 and 6). Finally I discuss the reduction of the more than 600 images from which transformation equations from the MJUO *uvbyVI* instrumental photometric system to the relevant standard system magnitudes and colours will be derived (chapter 5). Ultimately, the transformation equations are required to calculate the standard system photometric magnitudes, colors and indices for the three systems studied. This data, along with IUE spectrophotometry will be used to determine the temperatures of the stars (also in chapter 5).

3.1 Preparing raw images for reduction

Before actually measuring the flux of each object of interest in a given CCD image, several corrections to the raw image must (or at least should) be made in order to help achieve the best photometric quality. At each step, a new image is created.

3.1.1 Correcting for BIAS and Thermal Current – DARK Subtraction

Correction for the BIAS and thermal current were achieved by the subtraction of a single DARK image. DARK subtraction was performed immediately after image acquisition at the telescope, as described in section 2.3.2.

3.1.2 Correcting for inter-pixel variable quantum efficiency – Flat Fielding

As described in section 2.3.3, FLAT FIELD images were generally acquired both immediately before and immediately after each night's observations. When both start-of-night and end-of-night FLAT FIELD images were available for a given night, the two FLAT FIELD images were first summed together to produce a 'mean' FLAT FIELD image. Obviously when only either start-of-night or end-of-night FLAT FIELD images were available, that single image was used as the FLAT FIELD image. There is a small number of nights which, for a variety of reasons, have no FLAT FIELD images. For these nights, FLAT FIELD images from the next most recent night were used. As discussed in section 2.3.3 this is unlikely to have introduced any significant errors. The FLAT FIELD image was then scaled such that the mean value of the pixels was 1. Flat fielded *Stellar* images were then obtained simply by dividing the raw stellar image by the scaled FLAT FIELD image.

3.2 Extracting photometry from CCD images: II

As discussed in section 1.4.1, the digital format of the CCD image lends itself ideally to computer analysis, but not all methods are equal. When work on image reduction commenced in late 1992, there were two options for profile fitting photometry available here at the University of Canterbury, ROMAFOT and DAOPHOT II, both provided as standard MIDAS packages. The reduction of images acquired during the 1990 observation campaign had been made with ROMAFOT utilizing a Moffat function in a circularly symmetric, analytic PSF (West et al., 1992). Asymmetric stellar images often result from the less than ideal seeing conditions regularly experienced at MJUO and telescope tracking imperfections, thus improved precision of the photometric reduction would be expected from a reduction package which would better account for this. DAOPHOT II not only permits non-circularly symmetric PSFs, but combines analytic and empirical components into the image PSF. It is primarily for these reasons that DAOPHOT II has been employed for photometric reduction of the CCD images in this thesis.

DAOPHOT II has found wide appeal amongst the astronomical community, without doubt due to its availability, versatility, adjustable level of sophistication to suit the application and, perhaps most importantly, the dedication of its author, Peter Stetson, to the development as well as the documentation of the package. DAOPHOT II has been used almost exclusively in the course of the research described in this thesis and so naturally many of the details in what follows are specific to DAOPHOT II, although the general philosophies will be common to most such packages.

3.2.1 Synthetic Aperture Photometry

For what follows it is useful to state the following definition. Synthetic aperture photometry calculated by the DAOPHOT II command PHOTOMETRY produces magnitudes (m) related to the measured flux (or counts C) by the following relation:

$$m = 25 - 2.5 \log_{10} [C] . \tag{3.1}$$

The choice of the aperture size can be critical but the nature of the CCD image means that the appropriate choice can be made with a degree of hindsight, not generally available with traditional, at the telescope photometry using real apertures and photomultipliers. In general the appropriate aperture size is dependent on a number of factors including the seeing and the accuracy of the telescope tracking during a given exposure. The final choice of aperture size is invariably a trade-off between choosing a large enough aperture to include essentially all of the stellar signal but not so large that noise from the sky background dominates. Also potentially critical is the specification of the stellar centroid, although the larger the aperture, the less critical this element.

A sensible approach provided by DAOPHOT II is the capacity of the synthetic aperture photometry routine to compute photometry for up to twelve aperture sizes simultaneously, so that the dependence of the signal level and signal noise on aperture size can be investigated systematically. The final choice of the appropriate aperture size could then depend on some quantitative criterion rather than subjective judgment. Possible criteria are the plateau aperture size of the curves of growth (see figure 3.17) or perhaps the aperture size which produces transformations to standard system photometric systems with the least scatter.

3.2.2 Profile Fitting Photometry

Profile Fitting techniques allow for the extraction of precise photometry in crowded fields where synthetic aperture photometry is inappropriate. In general, the derived photometry is *internally* but not necessarily *externally* accurate, which is to say that differential magnitudes of stars within a single image are of high precision, but the zero point is not generally well defined. The zero point can only be determined via aperture photometry of an uncrowded star in the image and the relationship between the aperture photometry magnitude and the profile fit magnitude for that star.

Perhaps the most critical aspect of profile fitting photometry is the specification of the model PSF. In the main, there are two schools of thought, analytic and empirical representations. Analytic function PSFs are particularly useful in the case of undersampled images, but integration of the function to estimate the total light can be time consuming and accurate representation of the true image profile may be difficult to achieve with a reasonable parameterization. Empirical representations, usually derived from interpolating within the observed image profile of an isolated star or stars in the image, generally provide for fast computation of the required integrations but are poorly suited to undersampled images where systematic errors from the interpolation within the finite grid over-which the PSF is defined become significant (Stetson, 1987).

DAOPHOT II allows for a number of options in the definition of the image PSF. Moreover, it is in general composed of two components, an analytic, two-dimensional function plus an 'empirical look-up-table' of corrections between the 'true' image profile and the analytic first approximation component. This so-called *hybrid* PSF offers adequate flexibility for the modeling of complex PSFs while maintaining some hope of reasonably accurate interpolations for critically sampled or slightly undersampled images. The versions of DAOPHOT II used in this thesis allow for several options for both the analytic function component (including Gaussian, Lorentz, Moffat and Penny functions) and the look-up-table component (it can be constant for the image, allowed to vary as a function of position or turned off all together).

The DAOPHOT package also provides a number of options for the actual profile fitting algorithm which vary in their level of sophistication. Least sophisticated is the PEAK algorithm, a single-star profile fitting algorithm. Next on the 'ladder of sophistication' is the NSTAR routine which can simultaneously fit profiles to groups of up to 60 stars at a time. At the top of the ladder[1] is the stand-alone executable ALLSTAR which can simultaneously fit profiles to *all* of the stars specified in the image. ALLSTAR does not however include routines for finding stars in the image or generating PSFs. It thus relies on some external package to provide preliminary photometry as well as a PSF. Not surprisingly though, DAOPHOT II is ideal for producing the required input.

The following provides an overview of the philosophy and implementation of a typical image reduction procedure, in terms of the DAOPHOT II routines, used to extract photometry from CCD images. I also outline the workings of some of the DAOPHOT II routines which perform the various tasks. It is provided simply to give the following sections some context and is therefore by no means a complete description. For more detailed descriptions, the reader is referred to the DAOPHOT II section of the MIDAS manuals (Stetson, 1994a) and/or the various articles devoted to these issues (Stetson, 1987; Stetson et al., 1989; Stetson, 1992; Stetson, 1994b).

- The first step is to create a list (or lists) of objects for which one desires photometry. The DAOPHOT II command FIND performs this function. This routine convolves a one dimensional Gaussian function of user specified Full Width at Half Maximum (FWHM) with the rows of the image at each pixel in the image. 'Found' objects are those for which the correlation between the image and the Gaussian are greater than some (user specified) threshold. The centroid is estimated as the local maximum of the correlations.

- Synthetic aperture photometry (DAOPHOT II command PHOTOMETRY) can then be computed for this list of stars. The profile fitting algorithms all require initial guesses for the stellar brightnesses as well as the sky background which are provided by PHOTOMETRY.

- A list (not necessarily different from the first list) containing the PSF stars, i.e. the stars upon which the PSF for the image is to be based, is required. The DAOPHOT II routine PICK will provide a list, sorted by order of brightness, of 'suitable' candidates. Some editing of this file may be required since the selection criteria employed by PICK are not especially sophisticated.

- A representative PSF for the image can now be constructed. This is achieved with the DAOPHOT II routine PSF.

- Profile fitting photometry can now be calculated using either PEAK or ALLSTAR. If NSTAR is to be used, a further step is required to sort the stars in the groups that will be simultaneously fitted.

The above procedure, employing PEAK for the profile fits, is essentially the procedure used for reduction of the differential photometry data. More sophisticated procedures revolve around redeterminations of the PSF from 'cleaned' images:

- Once the initial photometry has been computed it can be used along with the PSF to create a 'subtracted' image, an image where the fitted PSF for each star is subtracted from the original data. In fact ALLSTAR creates such an image as a matter of course. If PEAK or NSTAR were used for the profile fits then the subtracted image can be computed with the DAOPHOT II routine SUBSTAR.

- Using FIND the subtracted image can be searched for faint stars hidden in the wings of brighter stars in the original image.

[1] Actually, the next generation in the DAOPHOT profile fitting software development has been created (Stetson, 1994b). Named ALLFRAME it (apparently) simultaneously fits profiles to all the specified stars in any number of frames of the same field. Like ALLSTAR it too relies on preliminary photometry derived by DAOPHOT II (or for that matter ALLSTAR) as well as the DAOPHOT II PSF. At the time of writing, the availability of ALLFRAME is unclear.

- Synthetic aperture photometry to provide initial guesses for profile fitting routines would then be computed for these newly found stars (PHOTOMETRY).
- If PEAK is being used for the profile fits then profile fitting photometry for the stars in the subtracted image should be calculated by fitting the original PSF to the the observed profiles in the subtracted image. The resulting photometry could then be subtracted from the original image. Improved photometry for the original list of stars is then obtained by fitting the PSF to the stars in this new image.
- Alternatively, if one of the simultaneous multiple profile fitting routines (NSTAR or ALLSTAR) are being used it makes more sense to proceed as follows. Profile fitting photometry for the stars in the subtracted image should be calculated directly by fitting the PSF to the observed profiles in the subtracted image. This photometry could then be appended to the photometry file from the original image, and photometry for the entire list (original image list plus subtracted image list) can then be computed.
- Whichever routine is used, a refined PSF can now be constructed by subtracting all but the PSF stars from the original image and recomputing the PSF with the DAOPHOT II routine PSF.
- Refined photometry can then be computed based on this refined PSF.
- This procedure can be iterated until the user is satisfied with the resulting photometry.

In general, the simultaneous multiple profile fitting routines NSTAR and ALLSTAR produce much superior quality photometry as compared with the (as Stetson himself puts it) obsolete PEAK. However in images where there are large numbers of stars, the required CPU time can be prohibitive. With the phenomenal developments in computing power in recent times, such issues become less of a concern. During the course of this degree, I have seen computing speeds increase by probably more than a factor of ten. Nonetheless, the ultimate purpose of the extracted photometry should not be forgotten and a procedure commensurate with the final requirements should be employed.

3.3 Differential Photometry

The primary aims for the programme were to produce high accuracy light curves. As described in chapter 2, observations were made in the Mount John University Observatory six colour *uvbyVI* photometric system, which is based on the *uvby* filters of the Strömgren system, and the V and I filters of the Cousins $UBVRI$ system. Given the crowded fields all three programme and potential comparison and check stars are located in profile fitting photometry was required.

3.3.1 Procedure

Two versions of DAOPHOT II were used, being those that were part of the standard MIDAS distributions of 91NOV and 92NOV, although in all likelihood the source code was exactly the same. Reductions were computed on the VAX/VMS systems of the Computer Services Center of the University of Canterbury.

Initial reductions employed the crude reduction procedure described above. PSFs were determined from a small number of field stars (typically 3 for HV 982, 12 for HV 1620 and 13 for HV 2241). No PSF cleaning passes (see above) were made. Profile fits were calculated individually (DAOPHOT II routine PEAK) rather than by simultaneous multiple profile fits (the NSTAR routine of DAOPHOT II or ALLSTAR) and only for the programme star plus a small number of field stars (13 for HV 982, 13 for HV 1620 and 17 for HV 2241) deemed of possible use as comparison or check stars. This procedure produced satisfactory results for HV 2241 and for the shorter wavelength bandpasses for HV 982 and HV 1620 where the effects of crowding are not so severe. However it was particularly evident in preliminary V and I light curves of HV 982 and in preliminary I light curves of HV 1620 that Nearby-Field-Stars (NFSs) were significantly affecting the precision of the extracted photometry.

Nearby-Field-Star corrections

Stars within a distance comparable with the FWHM of the image profile of any star of interest are almost certain to reduce the precision of the extracted photometry for that star. Since the FWHM varies as a function (primarily) of seeing, this is a somewhat loose definition. In practical terms it amounts to stars closer than

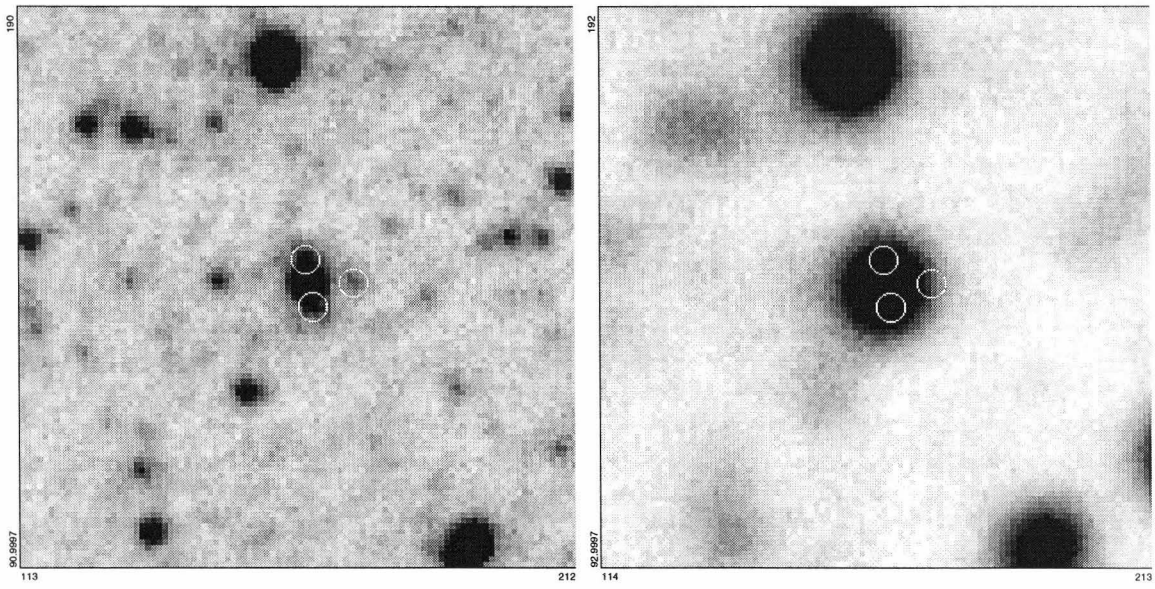

Figure 3.1: 100×100 pixel regions centered on the centroid of HV 982 for images acquired in good (T3750009, left) and bad (T4230011, right) seeing conditions. The FWHM for the good seeing image is 2.″06 while for the bad seeing image it is 7.″03. The filter used is V. The positions of the three NFSs are indicated by the circles. (North is to the top, East to the left.)

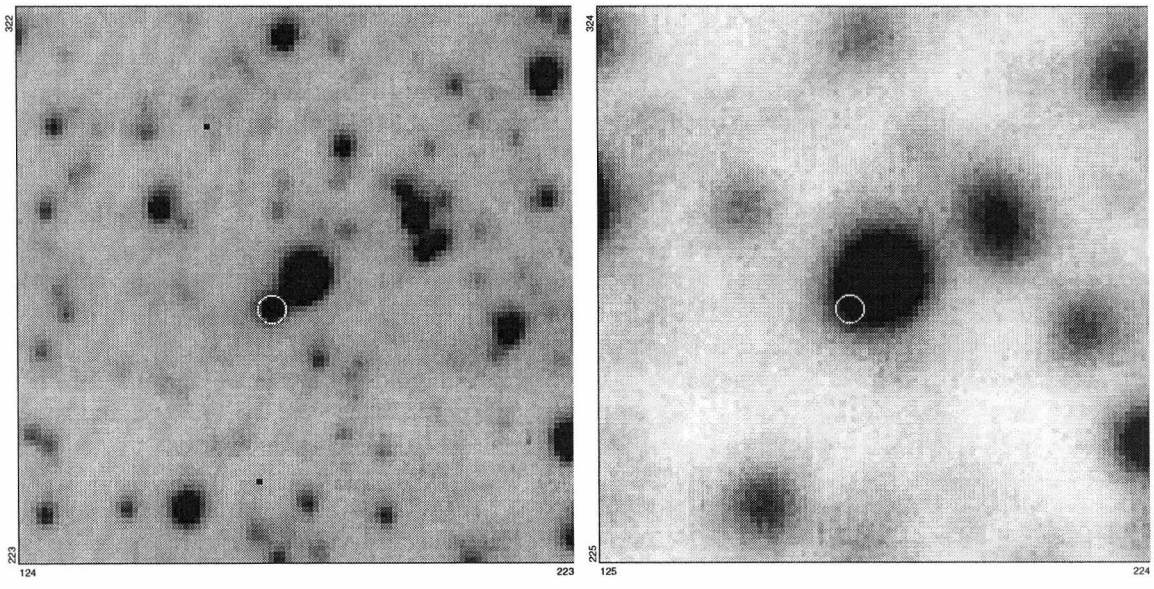

Figure 3.2: 100×100 pixel regions centered on the centroid of HV 1620 for images acquired in good (S1600003, left) and bad (T4250024, right) seeing conditions. The FWHM for the good seeing image is 1.″96 while for the bad seeing image it is 6.″54. The filter used is V. The position of the NFS is indicated by the circle. (North is to the top, East to the left.)

about 10 pixels or $\sim 6''$. Accordingly, the inaccuracies introduced by NFSs are also largely dependent on the seeing of a given image.

Figures 3.1 and 3.2 present views of the 100×100-pixel regions centered on the target star for V images obtained in good and bad seeing conditions for HV 982 and HV 1620 respectively. NFSs which most significantly affect the photometry of the target stars are circled in the good seeing images. The positions of the NFSs in the bad seeing images are also indicated by the same circles, although it is difficult to distinguish the NFSs from the targets.

For HV 982, three NFSs are of significance, one directly north, one directly south and one directly west of HV 982. In V, these stars are approximately 2.9, 2.8 and 3.4 magnitudes fainter than HV 982 outside of eclipse. For HV 1620 one NFS star to the south-east, $\sim$2.5 magnitudes fainter than HV 1620 outside of eclipse, is of greatest significance. The primary reason for photometric inaccuracies caused by NFSs occurs when the light from the NFSs can not be separated from that of the target. In general, as the seeing degrades, this becomes more and more of a problem.

Figures 3.3 and 3.4 present perspective plots of the central 30×30-pixel regions of the images in figures 3.1 and 3.2. Also presented are similar plots for images with fitted profiles for the target star subtracted. These plots show that in conditions of good seeing (FWHM= $2''.06$ for the HV 982 good seeing image and FWHM= $1''.96$ for the HV 1620 good seeing image), the relatively simple approach of the DAOPHOT II PSF fitting routine `PEAK` does a reasonable job of isolating the light of the target star from that of the NFSs, although in both cases the central intensity of the target has been slight overestimated. However, when the seeing is significantly worse (FWHM = $7''.03$ for the HV 982 bad seeing image and FWHM = $6''.54$ for the HV 1620 bad seeing image) the image profile of the target is so extended that `PEAK` is unable to separate the light from the target from that of the NFSs. The result is that the extracted magnitude is somewhat brighter than the true magnitude since it combines light from several stars, rather than only the star of interest.

The adopted NFS correction procedure was, like the initial profile fitting procedure, somewhat rudimentary. For HV 982, the mean positions of the three NFSs relative to the position of HV 982 and the mean brightnesses of the three NFSs relative to the mean of three field stars, known to be relatively constant, were determined from $\sim$50 images acquired in good seeing conditions. Once initial photometry (as above) had been extracted from the image the fitted PSF for HV 982 was subtracted from the image (producing a 'target-subtracted' image). The DAOPHOT II command `FIND` was used to search for the NFSs in the target-subtracted image. For each of the three NFSs, if found by `FIND`, profile fitting photometry was calculated. If not located by `FIND` the mean relative position and brightness plus the position of the HV 982 and the magnitudes of the three field stars for the frame (established in the initial `PEAK` photometry) were used to estimate the position and brightness of the NFS in the given frame. PSFs for the NFSs were then subtracted from the original image based on either the fitted or estimated photometry (producing a 'NFS-subtracted' image). Photometry for HV 982 was recalculated from the NFS-subtracted image. Such an approach, where mean photometry is adopted when the NFSs can not be independently located and fitted by profiles, is desirable because for a significant fraction of the images, the seeing is so poor that there is no trace of the NFSs in the target-subtracted image that one might hope to `FIND` and hence subsequently deal with in a manner such as that described in section 3.2.2.

Figure 3.5 presents composite images made up from 60×60-pixel cutouts of the various frames made during the reduction procedure. The first cutout shows the original flat fielded image. Next is the same image but with the initial profile fit for HV 982 subtracted out, i.e. the target-subtracted image. The bright white region at the position of HV 982 (which of course corresponds to a low light level in this negative image) is a clear indication that too much light has been subtracted, i.e. the central intensity, and hence the total magnitude, of HV 982 has been over-estimated. The fitted profiles for all three found and fitted NFSs are then subtracted from this image to give the third image in the sequence. The fourth cutout is taken from the NFS-subtracted image, i.e. the original image with the NFSs subtracted. The last cutout in the sequence has the target subtracted after fitting the PSF to the NFS-subtracted image. While it is evident that the magnitude of HV 982 is still being over estimated, the error is certainly smaller than before correcting for the NFSs. Figure 3.6 shows a similar sequence for the bad seeing image from figure 3.1 except that since the NFSs were not found in the target subtracted image, and therefore not fitted with profiles, there is no cutout showing the subtraction of the target and then the NFSs, i.e. there is no image cutout corresponding to the middle image of figure 3.5. Again the reduction in the over-estimation of the magnitude of HV 982, as evidenced by the reduced over-subtraction of the fitted profile, is clear (compare the second and fourth cutouts).

This correction procedure has been applied to V and I images only. In u, v and b the NFSs are much fainter relative to HV 982. Their influence on the profile fits to HV 982 is therefore not significant compared to other sources of random error. For y images, an NFS correction would likely improve the accuracy. How-

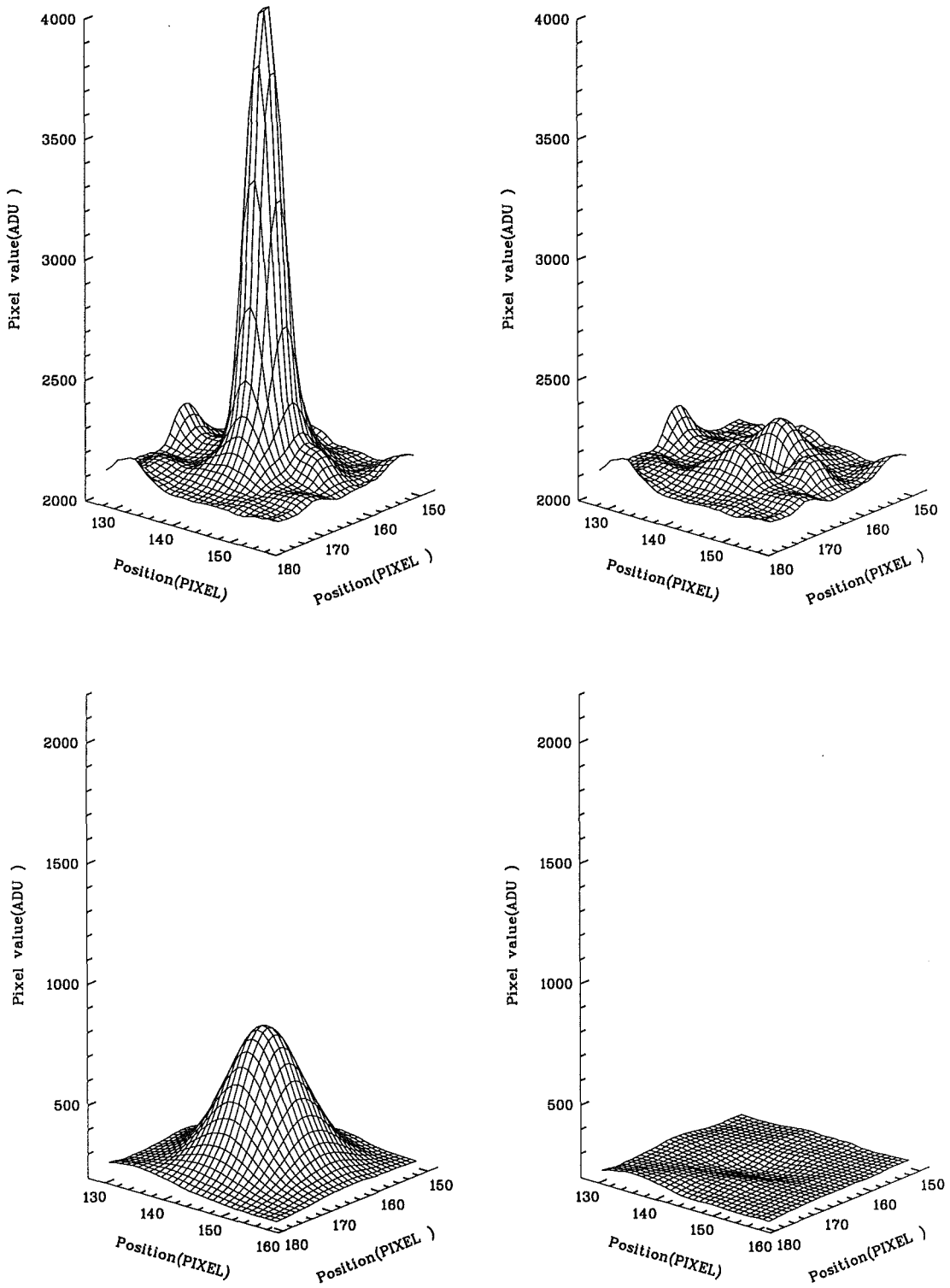

Figure 3.3: Perpsective plots of V HV 982 images in good (top) and bad (bottom) seeing conditions (the same images as in figure 3.1). Shown are the original images (left) and the HV 982 subtracted images. Both images are shown at the same vertical scale and the data has been tinned into 2×2 bins for display purposes. In the good seeing image, the three NFSs are clearly visible after the subtraction of HV 982's fitted profile. In the bad seeing image, the light from the NFSs has been included in the fit of HV 982 and hence no trace is left of the NFSs in the subtracted image. Note that the differing background levels are unrelated to the seeing but rather result from different lunar phases during the respective observations.

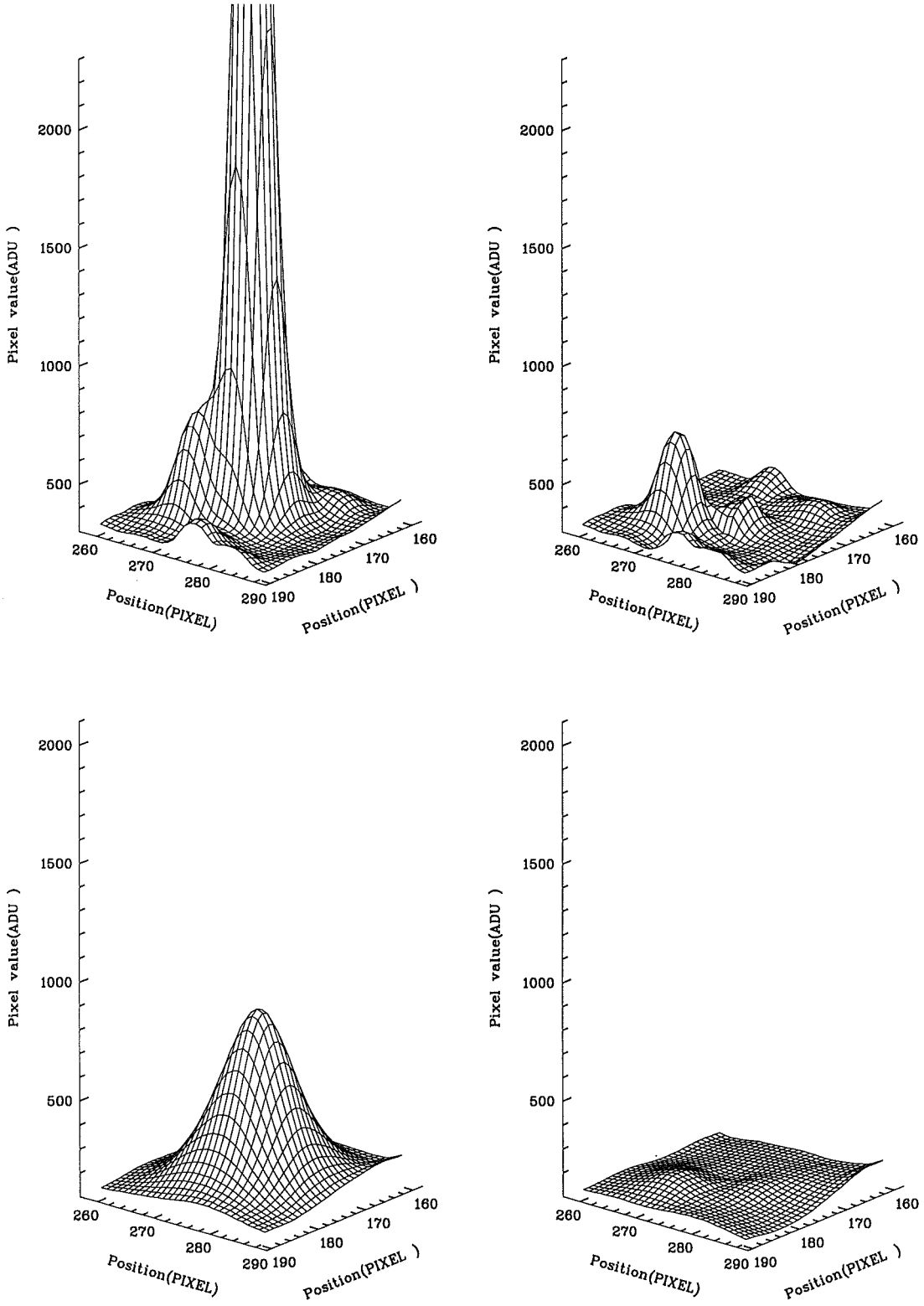

Figure 3.4: Perspective plots of V HV 1620 images in good (top) and bad (bottom) seeing conditions (the same images as in figure 3.2). Shown are the original images (left) and the HV 1620 subtracted images. Both images are shown at the same vertical scale and the data has been binned into 2×2 bins for display purposes. In the good seeing image, the NFS is clearly visible after the subtraction of HV 1620's fitted profile. In the bad seeing image, the NFS is only just discernible.

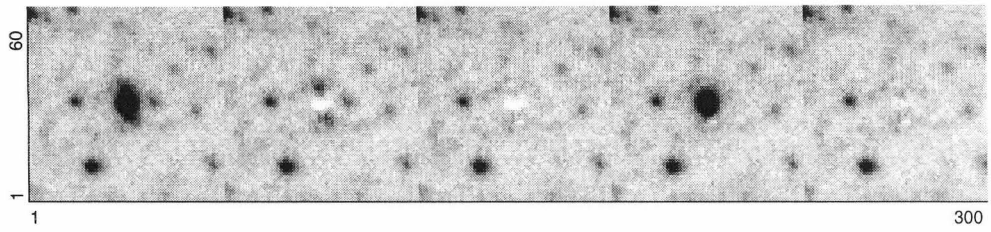

Figure 3.5: A composite image composed from 60×60-pixel regions centered on HV 982 showing various stages of the reduction procedure for the good seeing image from figure 3.1. The first cutout shows the original flat fielded image, next is the same image but with the initial profile fit for HV 982 subtracted out i.e. the target-subtracted image. The fits for all three found and fitted NFSs are then subtracted from this image to give the third in the sequence (the target-then-NFS-subtracted image). The fourth is the original image with the NFSs subtracted, i.e. the NFS-subtracted image. Finally, the fifth in the sequence has the target subtracted after fitting the profile to the NFS-subtracted image (the NFS-then-target-subtracted image). The improved photometry is clearly indicated by the significant reduction in the over-subtracted central region of HV 982 (compare the third and fifth cutouts)

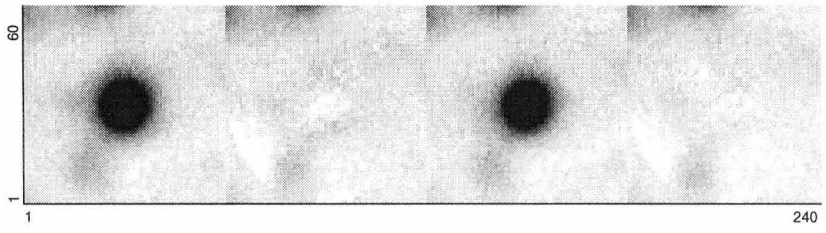

Figure 3.6: A composite image composed from 60×60-pixel regions centered on HV 982 showing various stages of the reduction procedure for the bad seeing image from figure 3.1. The sequence is the same as for figure 3.5 except that since the NFSs were not found in the target subtracted image, and therefore not profile fitted, there is no cutout showing the subtraction of the target and then the NFSs, i.e. there is no image cutout corresponding to the middle image from the good seeing composite. As for figure 3.5, the over-subtraction in the center of the image profile of the target has been reduced implying more accurate photometry.

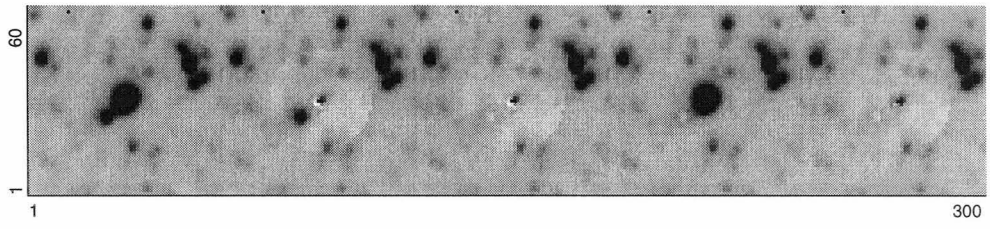

Figure 3.7: A composite image composed from 60×60-pixel regions centered on HV 1620 showing various stages of the reduction procedure for the good seeing image from figure 3.2. The sequence is the same as that of figure 3.5, i.e. the original flat fielded image, the target-subtracted image, the target-then-NFS-subtracted image, the NFS-subtracted image and then the NFS-then-target-subtracted image. The profile fit to HV 1620 has clearly been improved (yielding improved photometry) however a significant residual, in this case in the sense of an 'under-subtraction', remains. PSF cleaning passes would likely improve the fit. The obvious circular pattern centered on the centroid of HV 1620 in the cutouts with the fitted profile for HV 1620 subtracted indicates that the sky-background has been over estimated.

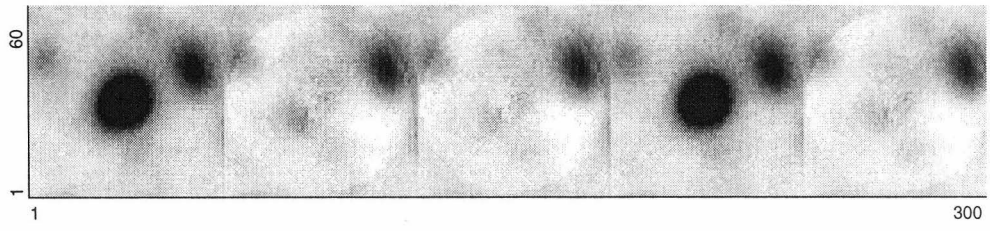

Figure 3.8: A composite image composed from 60×60-pixel regions centered on HV 1620 showing various stages of the reduction procedure for the bad seeing image from figure 3.2. The sequence is the same as that of figure 3.5, i.e. the original flat fielded image, the target-subtracted image, the target-then-NFS-subtracted image, the NFS-subtracted image and then the NFS-then-target-subtracted image. Comparing target-then-NFS-subtracted and NFS-then-target-subtracted images, a marginal improvement is just evident. Once again the over estimate of the sky-background is clearly indicated by the circular pattern resulting from the subtraction of the fitted profiles for HV 1620. For both the good and bad seeing images, this is likely a consequence of the high density of field stars with $\sim 20''$.

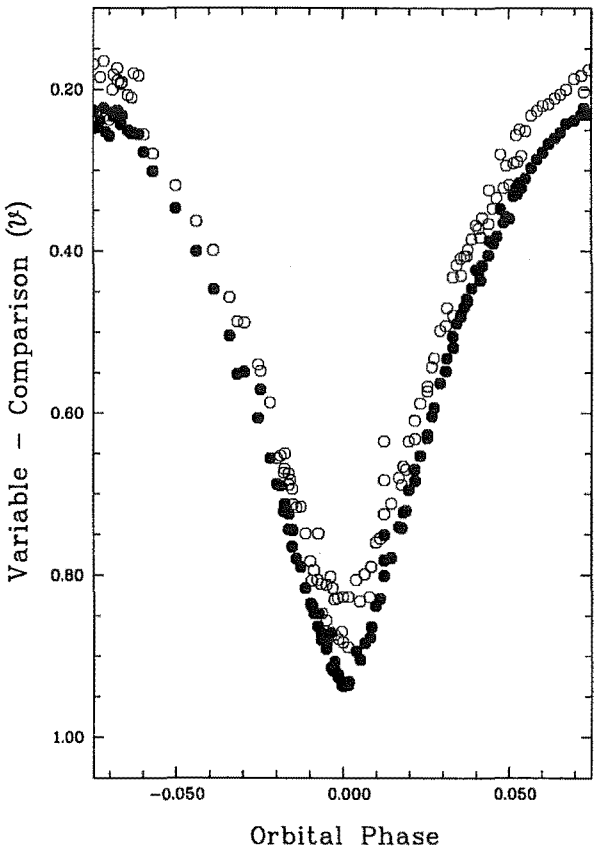

Figure 3.9: The V primary minimum for HV 982. Shown are both the 'uncorrected' (open circles) and *Nearby-Field-Star* corrected (filled circles) differential photometry. The two curves are plotted at exactly the same scale and offset. The lower light level in the NFS corrected curve is therefore real.

Table 3.1: Preliminary *Comparison* and *Check* stars. The star numbers are as indicated in figures 2.7 to 2.9.

	u	v	b	y	V	I
			HV 982			
Comparison	#12	#4	#4	#4	#4	#4
Check	#14	#12	#12	#12	#12	#12
			HV 1620			
Comparison	#3	#8	#3	#8	#3	#8
Check	#8	#11	#8	#11	#8	#11
			HV 2241			
Comparison	#11	#11	#11	#11	#11	#11
Check	#10	#10	#10	#10	#10	#10

ever due to the small number of y images and hence the difficulties in determining reliable mean positions and brightness, I did not feel the effort required would be warranted by the improvement in accuracy.

Figure 3.9 presents both 'uncorrected' (open circles) and 'corrected' (filled circles) V differential photometry during primary eclipse for HV 982. The improvement due to the NFS correction is clearly seen. The corrected curve is much tighter than the uncorrected curve. This is especially obvious at the minimum. Also of note is the overall lower level of the corrected curve showing that even for images of good seeing, the NFS correction provides a significant improvement.

A similar procedure was employed for HV 1620. Once initial photometry had been calculated for HV 1620, the DAOPHOT II FIND command was used to locate the NFS in an image with the fitted profile of HV 1620 subtracted. HV 1620's NFS was found more reliably than was the case for the HV 982 NFSs due to it being significantly brighter than the HV 982 NFSs and a little further away from HV 1620 than the HV 982 NFSs were from HV 982. Once located, the frame PSF was fitted and then the fitted profile for the NFS was subtracted from the original image. Photometry of HV 1620 was then recalculated from the NFS-subtracted image. Unfortunately this effort did not provide the expected improvement in the quality of the I curve. Most probably improved precision could be obtained by re-reducing using a rather more sophisticated procedure based on one of the simultaneous multiple profile fitting routines (NSTAR or ALLSTAR). Due to the available computing resources at the time that reductions were carried out, it was not clear that the possible improvements warranted the required effort. An NFS correction has only been applied to I images for HV 1620. Although figures 3.7 and 3.8, which show various stages of the reduction procedure applied to the good and bad seeing images of figure 3.2, clearly demonstrate that the V photometry for HV 1620 is affected by the presence of the NFS, once again, for the present purposes, the likely improvements do not justify the effort that would be required to re-reduce the 403 V images of HV 1620.

Based on the more recent experience gained reducing the programme star images for the calibration photometry, I expect that the precision of all of the differential photometry could be improved upon by re-reducing the original images with a more sophisticated procedure based on the simultaneous multiple profile fitting algorithms. But for the present purposes I do not feel that that effort is warranted.

3.3.2 Selection of *Comparison* and *Check* stars

As indicated above, photometry was extracted from each CCD image for the programme star and a number of field stars which were hoped would be of use as *Comparison* or *Check* stars. Possible comparison and check stars were initially chosen based on their colour and magnitude relative to the programme star by examination of the initial U and I field surveys (see section 2.2). Preliminary *Comparison* and *Check* stars were selected based on the stability of the differential photometry between the possible candidates at various stages during the period of observations as the light curves for each programme star in each filter became more complete. Much of the light curve analysis is based on the light curves derived from these preliminary selections (table 3.1). The final selection of *Comparison* and *Check* stars was based on a more rigorous examination of the stability of the differential photometry between the possible candidates and after searching the resulting light curves for systematic effects due to seeing and airmass once the observation programme was finished and all images had been reduced.

- **HV 982**: For each pair of stars, the sample was first restricted to a self consistent set of observations for which the differential photometry for that pair of stars was within three standard deviations of the mean value. The rms scatter of these samples were then compared for each possible pairing of stars. This procedure indicated a number of pairings for which the rms scatter was less than 0.01 mag, but no single pair of stars could be found for all six bandpasses for which this was true.

  Averaging the light from two stars should provide a less noisy signal, provided the noise intrinsic to each signal is random and uncorrelated. Thus the light from stars #12 and #14 (see figure 2.7) was added together to form one reference signal, the '*Check*' star. Two *Comparison* stars were used, star #10 for the u, v and b observations and star #4 for the y, V and I observations. This proved necessary because for the longer wavelengths, the nearby field star to the west of #10 significantly affects the precision of the photometry for star #10 while the low signal level from star #4 at shorter wavelengths reduced the precision of the photometry for that star.

  Figure 3.10 shows plots of the adopted $Comparison - Check$ photometry versus the image FWHM for each observation. Observations for which the adopted $Comparison - Check$ differential photometry lies more than three standard deviations from the mean were rejected and were not included in further light curve analysis. No clear trends are evident, except for in the I photometry. Despite this trend in I, no further observations were rejected at this stage. The seeing dependence here is most probably in the photometry of star #12 (one of the *Check* stars), caused by the field star $\sim 5''$ to the north west. Thus the photometry of the *Comparison* (star #4) and hence the $Variable - Comparison$ differential photometry is unlikely to be influenced by the systematic error in the photometry of star #12.

- **HV 1620**: Although a number of *Comparison/Check* pairs produced excellent differential photometry with rms scatters well below 0.01 mag, no one pair was entirely suitable for all six bandpasses. After a thorough investigation, stars #3 and #8 seemed most promising and were adopted as *Check* and *Comparison* respectively for V. For the other five bandpasses, in order to improve signal to noise, the fluxes from #8 and #12 were combined to form a *Comparison* signal and fluxes from #3 and #13 were combined for the *Check* signal. Combined signals were not used for V because the signal levels are such that signal to noise for stars #3 and #8 is quite adequate and stars #12 and #13 are likely to have saturated the CCD for the observations obtained in better seeing conditions (FWHM$\leq 2''.5$).

  Figure 3.11 show plots of the adopted $Comparison - Check$ photometry versus the FWHM of the HV 1620 images. Again, no clear trends are evident except for in the I photometry. This is likely due to the influence of the nearby field stars of stars #12 and #13. I observations with Full Width at Half Maximum in excess of $5''.0$ were therefore excluded from further light curve analysis.

- **HV 2241**: For HV 2241, the choice of the *Comparison* was clear, star #10 (see figure 2.9) was adopted for all bandpasses. A *Check* star was derived from stars #11 and #13. No trends in the $Comparison - Check$ photometry with respect to the image FWHM are evident in figure 3.12, as would be expected for the much less crowded field of HV 2241.

$Variable - Comparison$ and $Comparison - Check$ differential photometry is tabulated in appendix A. Table 3.3 presents relevant statistics of the *Variable*, *Comparison* and *Check* star photometry and the $Variable - Comparison$ and $Comparison - Check$ differential photometry. For comparison, table 3.2 presents the quoted rms precisions of the $Variable - Comparison$ and $Comparison - Check$ photometry from the observations made in 1990 as part of the MJUO MCEB programme. It is pleasing to note the overall general improvement in the achieved rms precisions.

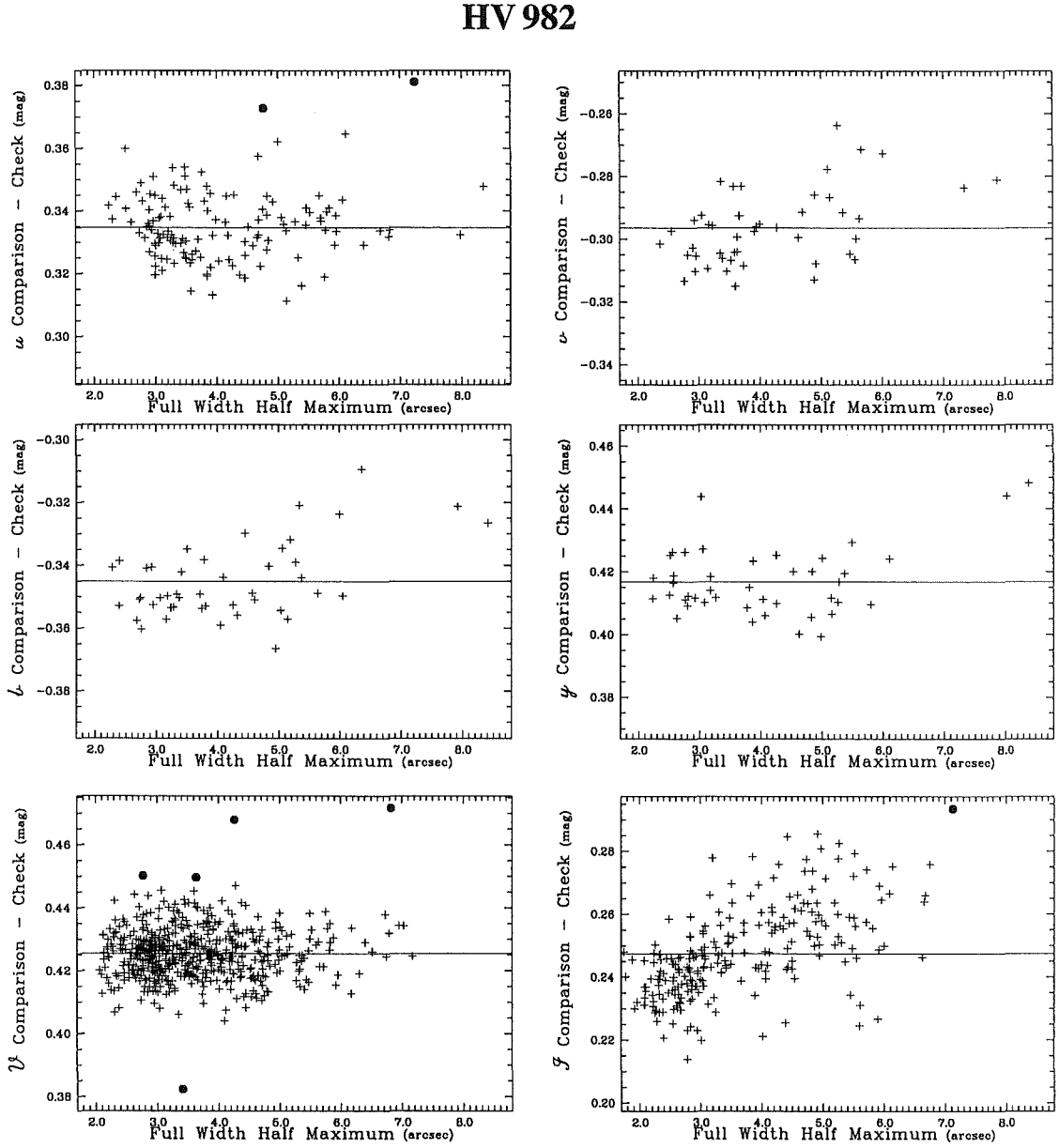

Figure 3.10: Plots of the *Comparison* − *Check* differential photometry versus the Full Width at Half Maximum for HV 982. Crosses (+) indicate the adopted photometry, filled circles indicate photometry rejected based on being more than three standard deviations from the mean. The seeing dependence of the I data is most probably caused by contamination of the photometry of check star #12 by the field star $\sim 5''$ to its north west.

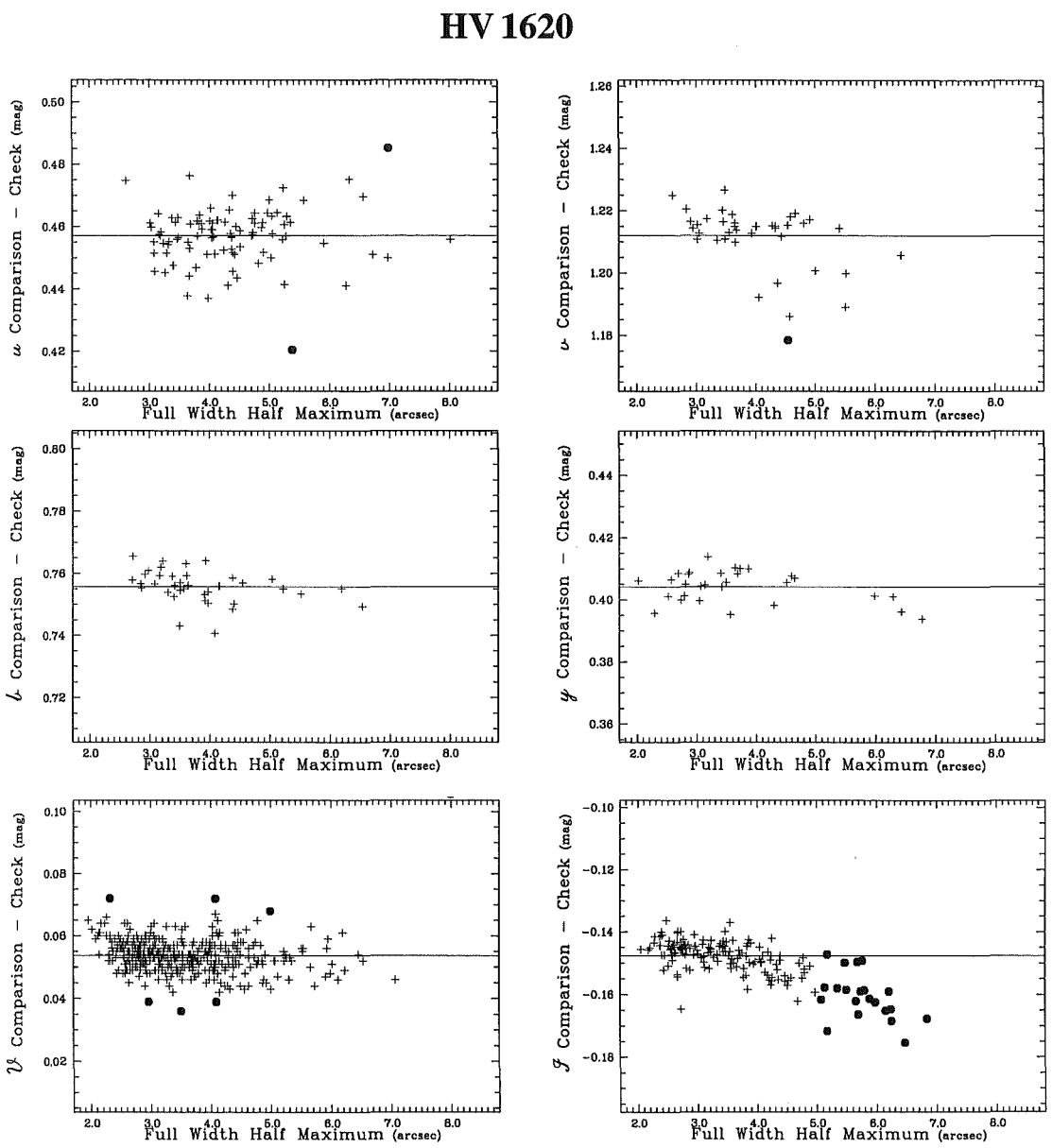

Figure 3.11: Plots of the *Comparison − Check* differential photometry versus the Full Width at Half Maximum for HV 1620. Crosses (+) indicate the adopted photometry, filled circles indicate photometry rejected based on being more than three standard deviations from the mean. In addition for I, observations with FWHM greater than 5.″0 have also been rejected.

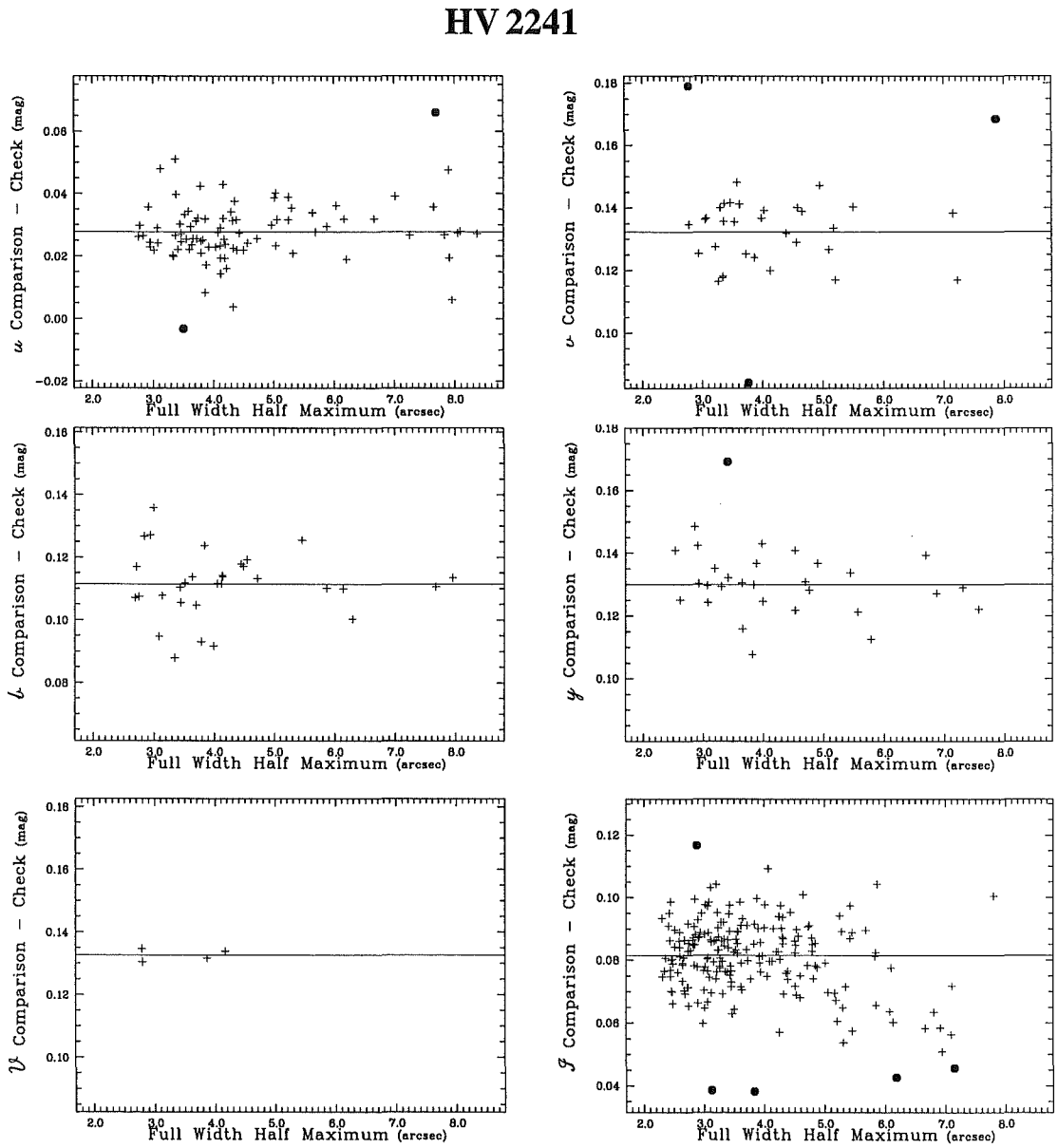

Figure 3.12: Plots of the *Comparison − Check* differential photometry versus the Full Width at Half Maximum for HV 2241. Crosses (+) indicate the adopted photometry, filled circles indicate photometry rejected based on being more than three standard deviations from the mean.

Table 3.2: RMS precisions of $Variable - Comparison$ and $Comparison - Check$ differential photometry from the 1990 observational campaign. The column *Paper* refers to the article in the *CCD photometry of variable stars in the Magellanic Clouds* series.

	B		V		I		
Variable	$V-C$	$C-C$	$V-C$	$C-C$	$V-C$	$C-C$	Paper
HV 2208	0.02	0.030	0.015	0.013	0.015	0.012	(West et al., 1992)
HV 12634	0.02	0.021	0.02	0.016	0.015	0.020	(West et al., 1992)
HV 2274	0.015	0.026	0.01	0.028	0.01	0.018	(Watson et al., 1992)
HV 12484	0.018	0.027	0.014	0.012	0.028	0.012	(Tobin et al., 1993a)
HV 1761	0.031	0.035	0.017	0.020	0.032	0.016	(Duncan et al., 1993)

Table 3.3: Detailed properties of the $Variable-Comparison$ $(V-C)$ and $Comparison-Check$ $(C-C)$ differential photometry and light curves. The *Number of frames* rows give both the number of observations retained for the final light curve analysis and the total number of observations made in each bandpass. Only the observations included in the final light curve analysis data sets are included in the calculations of the rms precisions. The $V-C$ standard deviations are with respect to preliminary *WD95* light curve solutions.

	u	v	b	y	V	I
			HV 982			
Signal Levels[a]						
$Variable$	14.48	14.67	14.32	14.12	12.86	14.32
$Comparison^{(\#4)}$	15.57	14.66	14.22	13.94	12.69	13.99
$Comparison^{(\#10)}$	13.89	13.60	13.18	12.90	11.61	12.97
$Check^{(\#12)}$	14.55	14.72	14.35	14.14	12.87	14.30
$Check^{(\#14)}$	14.84	14.96	14.66	14.44	13.17	14.71
Phase	0.2535	0.2548	0.2483	0.2558	0.2464	0.2518
Frame	t4880037	t6420002	t4880034	t6420001	t3730004	t4880036
RMS precisions						
Number of frames	132/139	48/48	45/45	44/44	565/582	205/248
$\sigma_{(V-C)}$	0.016	0.018	0.021	0.015	0.011	0.014
$\sigma_{(C-C)}$[b]	0.010	0.012	0.012	0.011	0.007	0.013
			HV 1620			
Signal Levels[a]						
$Variable$	13.77	14.47	13.86	13.49	12.60	13.53
$Comparison^{(\#8)}$	14.46	13.68	12.96	12.49	11.66	12.40
$Comparison^{(\#12)}$	13.33	12.16	11.39	10.90	10.07	10.68
$Check^{(\#3)}$	15.31	14.85	13.49	12.51	11.71	11.59
$Check^{(\#13)}$	13.67	13.39	12.21	11.41	10.61	10.75
Phase	0.2596	0.7620	0.7662	0.7540	0.2560	0.2544
Frame	t4810018	t3960004	t3960005	t3960002	t4810016	t4810015
RMS precisions						
Number of frames	92/100	38/39	32/37	26/30	359/411	141/162
$\sigma_{(V-C)}$	0.018	0.018	0.017	0.015	0.012	0.017
$\sigma_{(C-C)}$[c]	0.008	0.009	0.006	0.005	0.005	0.005
			HV 2241			
Signal Levels[a]						
$Variable$	12.96	13.20	12.69	12.50	12.25	12.53
$Comparison^{(\#10)}$	13.26	13.54	13.02	14.41	12.54	12.94
$Check^{(\#11)}$	13.80	13.96	13.48	13.32	12.79	13.44
$Check^{(\#12)}$	14.23	14.30	13.88	13.72	13.38	13.82
Phase	0.2705	0.2747	0.2830	0.2911	0.6032	0.2809
Frame	t5680008	t5680010	t5680014	t5680019	t8300013	t5680013
RMS precisions						
Number of frames	86/88	31/34	31/31	29/30	4/4	208/213
$\sigma_{(V-C)}$	0.016	0.016	0.015	0.012	0.007	0.017
$\sigma_{(C-C)}$[d]	0.008	0.009	0.011	0.009	0.002	0.011

[a]The frames listed above were chosen based on being the images with the 'best' seeing at phases close to maximum light for each binary. Reported in instrumental magnitudes $\approx 25 - 2.5\log_{10}$[ADU above background].

[b]Star #10 was used for the *Comparison* for u, v and b while star 4 was used for y, V and I. Light from stars #12 and #14 were combined to form the *Check*.

[c]For u, v, b, y and I the *Comparison* star was derived by combining the light from stars #8 and #12 while the light from stars #3 and #13 was combined to produce the *Check*, for V stars #8 and #3 were used directly for *Comparison* and *Check* respectively.

[d]Star #10 was used for the *Comparison* while the light from stars #11 and #13 were combined to provide the *Check*.

3.3.3 Light Curves

The differential photometry for the programme stars resulting from the above procedures has been phased according to the following ephemerides:

- **HV 982**: The ephemeris of Payne-Gaposchkin (1971),

$$\begin{array}{rcl} \text{Time of primary minimum} & = & \text{HJD2429189.469} + 5.335268 \times E. \end{array} \quad (3.2)$$

- **HV 1620**: An ephemeris derived from the ephemerides of Payne-Gaposchkin and Gaposchkin (1966) and Davidge (1988),

$$\begin{array}{rcl} \text{Time of primary minimum} & = & \text{HJD2446426.468} + 3.626408 \times E. \end{array} \quad (3.3)$$

- **HV 2241**: An ephemeris derived from the times of minima from Gaposhkin (1977),

$$\begin{array}{rcl} \text{Time of primary minimum} & = & \text{HJD2413876.814} + 4.342640 \times E. \end{array} \quad (3.4)$$

All subsequent analysis of the light curves is based on these ephemerides. New ephemerides based on the above plus data derived from the analysis of the light curves are presented in section 6.1. Figures 3.13, 3.14 and 3.15 present $Variable - Comparison$ $(V - C)$ and $Comparison - Check$ $(C - C)$ light curves in all six colours for all three observed binaries.

- **HV 982**: The light curve of HV 982 is much like that of the Galactic eclipsing binary VV Pyxidis (Andersen et al., 1984). Clearly the system is currently well detached. Furthermore, the unequally spaced minima and the unequal durations of eclipse indicate that the system is in an eccentric orbit. The system is thus a relatively young system since the orbit has not yet been circularized by tidal interactions. The nearly equal depths of the two minima, from the ultraviolet (u) to infrared (I) indicate that the two components of the system are of very nearly the same temperature. The overall depth of the eclipses ($\sim$0.7 mag) indicates that the eclipses are nearly total and hence that the inclination must be close to 90°.

- **HV 1620**: HV 1620 presents a light curve of the classical Algol type, similar in form to that of the LMC eclipsing binary HV 5936 (Bell et al., 1993). Unlike HV 982's flat out of eclipse plateaux, the light is continuously varying. In V the deeper (primary) eclipse has a depth of $\sim$0.55 mag while the secondary has a depth of $\sim$0.35 mag (as measured from maximum light). The relative depths of the eclipses is wavelength dependent as would be expected for components of significantly different temperatures. The u curve has a primary eclipse deeper than the secondary by slightly more than 0.2 mag where as the corresponding difference is just slightly more than 0.1 mag for the I curve. The small scatter in the $Comparison - Check$ photometry in all filters (except u) is pleasing.

- **HV 2241**: HV 2241 also presents a light curve of the classical Algol type, not unlike that of the SMC eclipsing binary HV 2226 (Bell et al., 1991). HV 2241 has deep eclipses, in I $\sim$0.85 mag and $\sim$0.50 mag for the primary and secondary minima respectively. As for HV 1620, there is a dependence of the relative depths of the two minima on the wavelength of the observations. The difference in depth between the two minima in u is $\sim$0.45 mag whereas for I it is $\sim$0.35 mag. Again the implication is that the two components are of significantly different temperature.

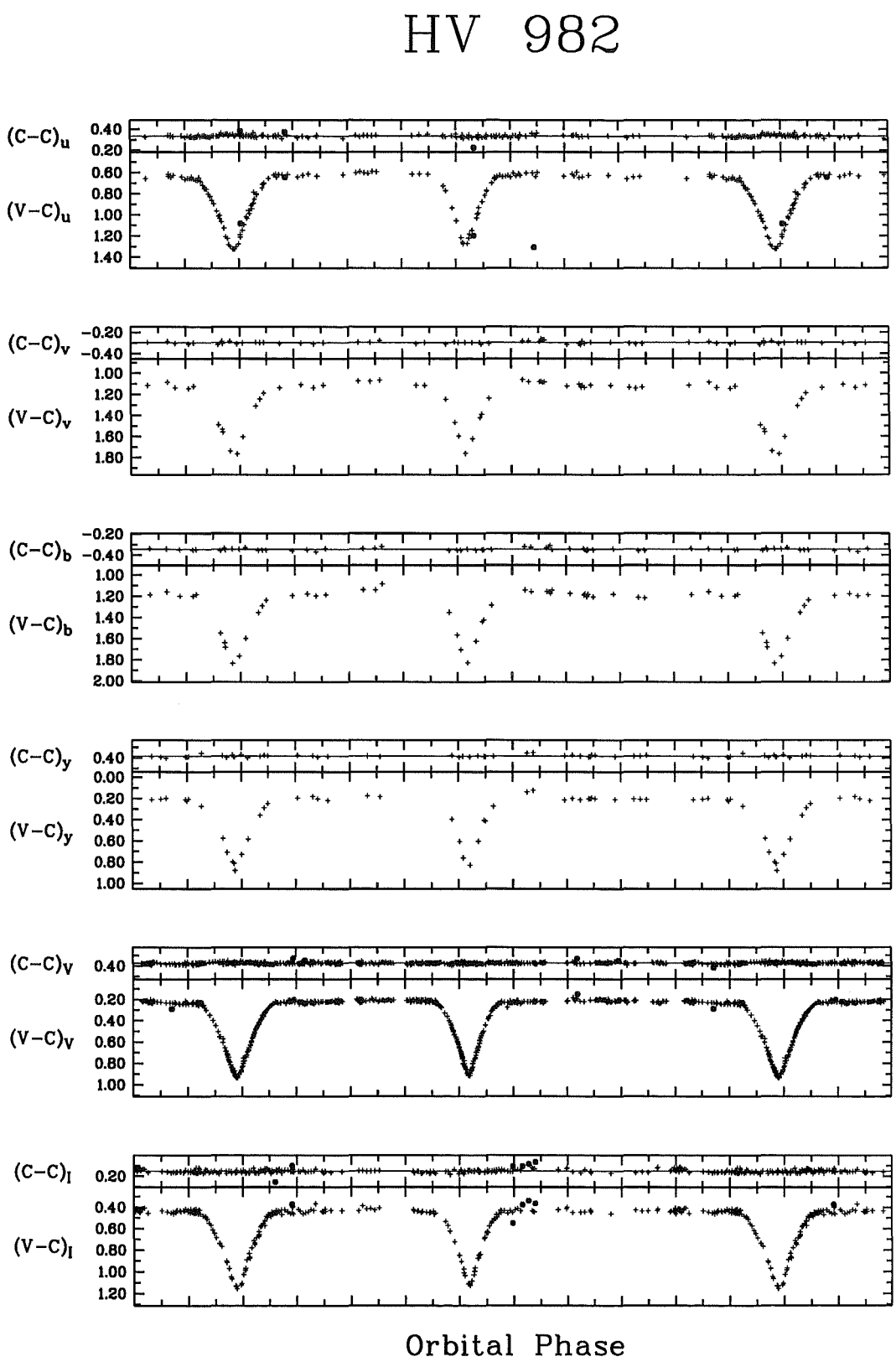

Figure 3.13: Six colour *uvbyVI* light curves for HV 982. $Variable - Comparison$ $(V - C)$ and $Comparison - Check$ $(C - C)$. Crosses represent individual observations, filled circles are observations excluded from the analysis (see text).

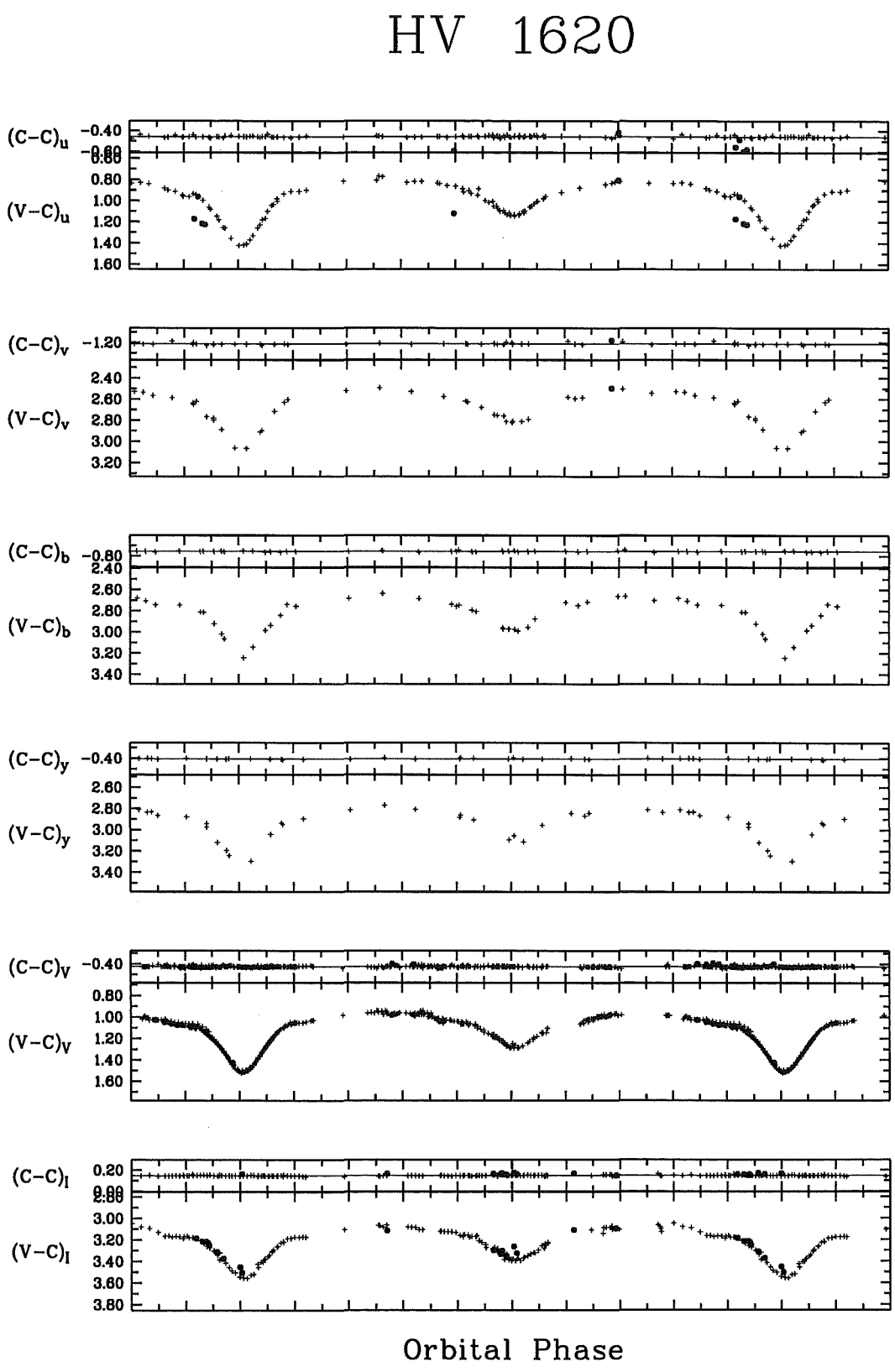

Figure 3.14: Six colour *uvbyVI* light curves for HV 1620. $Variable - Comparison$ $(V-C)$ and $Comparison - Check$ $(C-C)$. Crosses represent individual observations, filled circles are observations excluded from the analysis (see text).

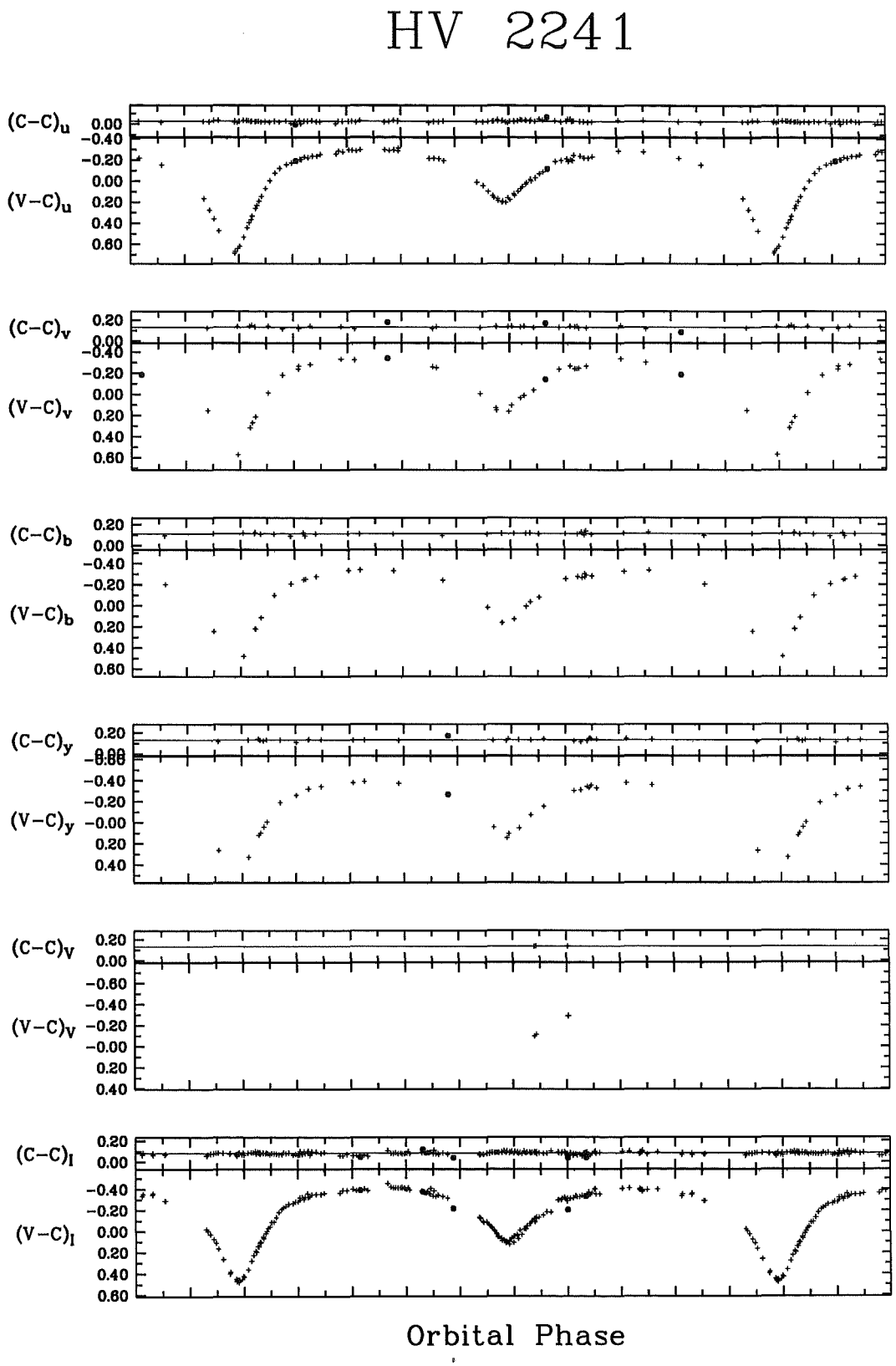

Figure 3.15: Six colour *uvbyVI* light curves for HV 2241. $Variable - Comparison$ $(V-C)$ and $Comparison - Check$ $(C-C)$. Crosses represent individual observations, filled circles are observations excluded from the analysis (see text).

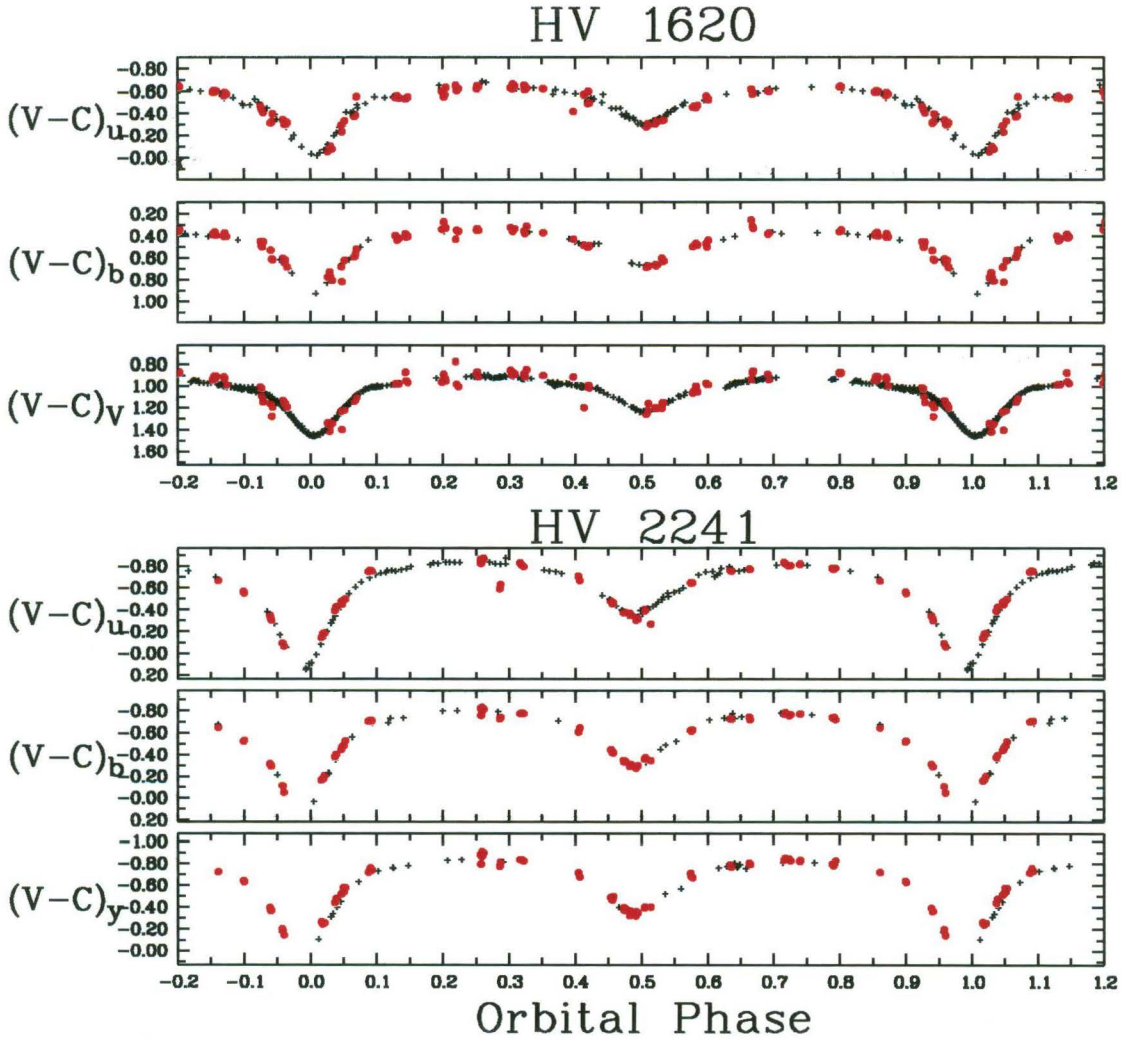

Figure 3.16: Comparison of MJUO (black crosses) and Davidge (red filled circles) light curves. The Davidge curves are UBV thus for comparison the MJUO u, b and V curves are plotted for HV 1620 (top) and the MJUO u, b and y curves (since only four V observations were made) are plotted for HV 2241 (bottom). The Davidge photometry has been arbitrarily offset in both phase and level so that the two data sets lie over the top of each other. The improved phase coverage, particularly in u and I (see figures 3.14 and 3.15) for both stars and in V for HV 1620, and quality of the MJUO light curves is immediately apparent.

Comparison with Davidge's light curves

Tim Davidge of the DAO kindly provided photocopies of his original differential photometry tables for HV 1620 and HV 2241 upon which Davidge (1987; 1988) are based. Figure 3.16 presents plots of the Davidge UBV light curves along with u, b and V light curves for HV 1620 and u, b and y light curves for HV 2241 from the present work. Aside from the improvement in precision of the current light curves over the photoelectric light curves of Davidge, the far greater phase coverage, particularly in u and I (and also V for HV 1620), represents a not insignificant improvement. Furthermore the fact that the CCD photometry has been obtained in the intermediate bandpass Strömgren system, which is much better suited to the study of early-type stars than the UBV system, also represents a significant improvement in the available data for these systems.

3.4 Calibration Photometry

As with the differential photometry DAOPHOT II was utilized for all reductions. But in contrast to the differential photometry where profile fitting photometry was most suitable, for the calibration photometry,

Table 3.4: The aperture and sky annulus radii used for all of the calibration synthetic aperture photometry. Apertures 1 to 12 are labelled A1 through AC, while the inner and outer sky annulus radii are labeled IS and OS.

Aperture	Radius (pixels)	Diameter (arcsec)
A1	12.10	15.0
A2	14.11	17.5
A3	16.13	20.0
A4	17.75	22.0
A5	19.36	24.0
A6	20.16	25.0
A7	20.97	26.0
A8	22.59	28.0
A9	24.19	30.0
AA	26.21	32.5
AB	28.23	35.0
AC	30.24	37.5
IS	35.00	43.4
OS	45.00	55.8

synthetic aperture photometry is required because photometry from different frames must be compared on an absolute scale. As explained in section 3.2, even if profile fitting photometry is used, if one wishes to compare photometry from separate images, the zero point of the photometry can only be determined by synthetic aperture photometry. Synthetic aperture photometry also helps avoid systematic errors that may occur if the original photometry was obtained photoelectrically, i.e. with *real* apertures, and the catalogue photometry for a particular star includes the contribution from a nearby companion.

While measuring synthetic aperture photometry is a straightforward procedure for the standard stars which generally lie in sparsely populated fields (often they are the only significant stars within the field of view of the chip), it does present reduction problems for the programme stars due to the much more crowded fields the programme stars lie in.

3.4.1 Standard Stars

The choice of the appropriate aperture size is influenced by several factors. The bigger the aperture, the more of the star's light we measure. Bigger apertures also reduce systematic errors arising from, for example, tracking errors and seeing variations. However when considering the programme stars, the bigger the aperture, the more field stars it is liable to contain, and thus the larger the contribution to the uncertainty from them. In order to investigate the effect of varying the aperture diameter, photometry was computed for the 12 aperture diameters listed in table 3.4. 'Curves of growth' which plot the measured magnitude as a function of aperture diameter are presented in figure 3.17. As the aperture diameter is increased, more and more of the star's light is included in the measurement and so the measured magnitude decreases (brightness increases). Eventually however the point is reached when essentially all of the light is included and the measured magnitudes plateau. For larger diameters noise from the large number of pixels now included in the summation of the light is liable to begin to dominate. Such plots provide a simple but effective way to obtain a first estimate of the most appropriate size for the aperture. They also permit easy identification of possible problems in the observed data, e.g. stars with companions (for which aperture size choice will be critical) or stars whose photometry for one reason or another 'blows up' (i.e. PHOTOMETRY can not determine a meaningful measurement and thus reports 99.999 for some or all apertures).

From figure 3.17, it can be seen that the photometry for all ~600 standard star images is well behaved, at least for apertures between 15 and 37.5 arc-seconds. It is noteworthy that the rate of growth of the extracted photometric magnitudes as a function aperture diameter varies from filter to filter. This is no doubt related to the variable amount of scattered light from the different filters, as discussed in section 2.1.4. Indeed the steepest gradients (b and y) correspond to the filters suffering most from scattered light problems.

Instrumental magnitudes ($m_{\rm inst}$) are derived from the DAOPHOT II synthetic aperture magnitudes ($m_{\rm raw}$) via the following equation,

$$m_{\rm inst} = m_{\rm raw} + 2.5 \log_{10}[\rm Exp], \tag{3.5}$$

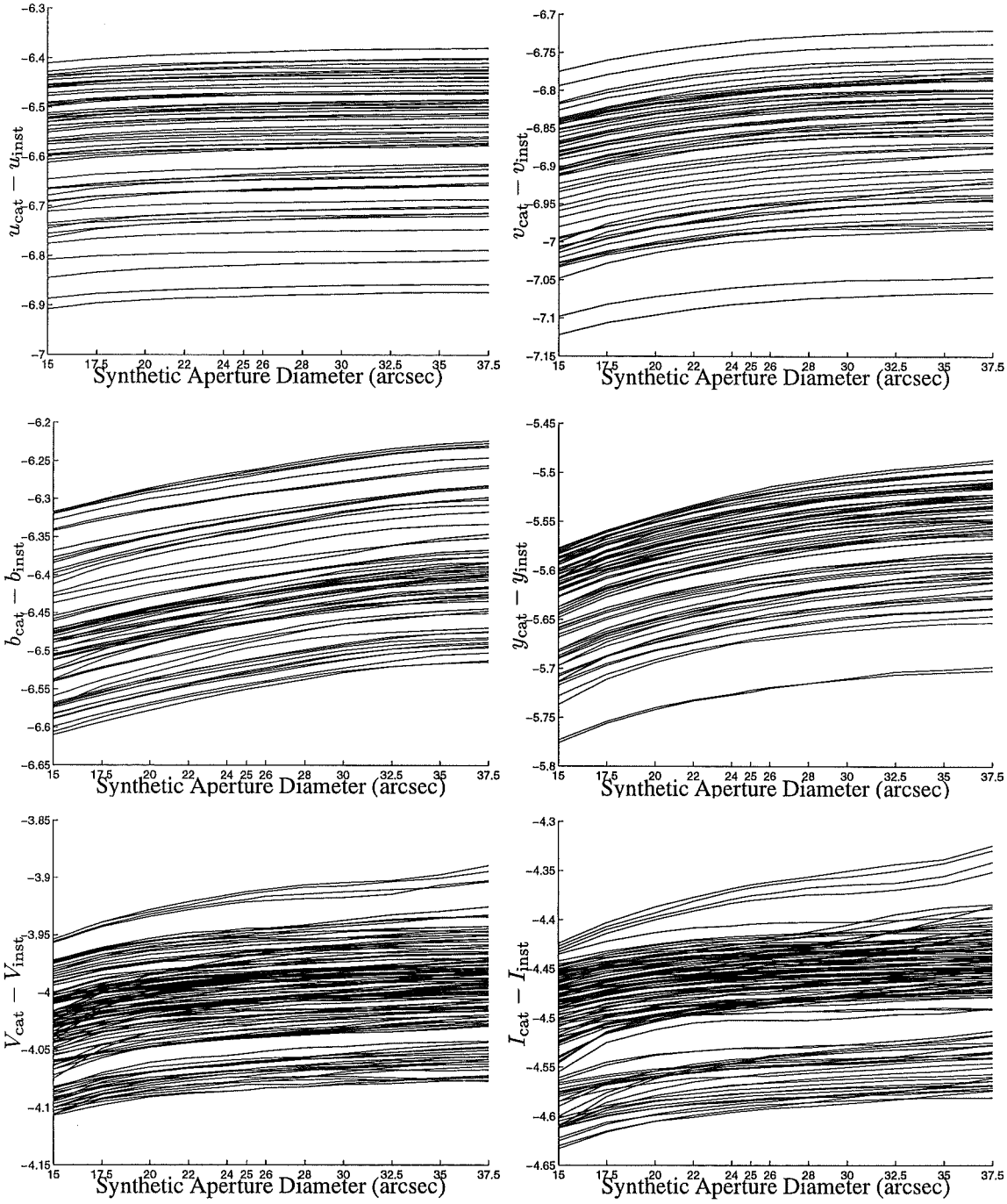

Figure 3.17: Curves of growth. The plots show the DAOPHOT II extracted aperture photometry as a function of synthetic aperture diameter for the six bandpasses ($uvbyVI$) for the standard stars observed at MJUO. Plotted is the difference between the *instrumental* magnitudes and the catalogue magnitude ($y_{\rm cat} = V{\rm cat}$ is adopted, the remaining Strömgren magnitudes are then derived from the standard colours and indices while the I magnitude is simply derived from the V magnitude and the $(V - I)$ color). Each line corresponds to one observation of one standard star. The above figures include all observations obtained in the current project. The spread in each figure represents the effect of atmospheric extinction. The varying gradient of growth from curve to curve is indicative of the amount of scattered light from the different filters, steepest gradients corresponding to the filters which scatter the most light (b and y). The greatest variation in gradient from image to image within a given filter, particularly at small diameters, is seen in V and I and probably results from variable seeing on different nights.

where Exp is the exposure duration in seconds.

The curves of growth (figure 3.17) indicate that apertures larger than ~20 arc-seconds produce stable photometry. The scatter of the residuals between transformed and catalogue standard star photometry (as determined from preliminary transformation equations, see chapter 5) shows a shallow minimum at or close to a diameter of 24 arc-seconds for all magnitudes and colours. Based mainly on these two indicators the 24 arc-second aperture diameter photometry was adopted. This is perhaps a somewhat smaller aperture than typically employed in the original photometry with which the standard systems were established, e.g. Cousins (1987) writes:

> A relatively large (one minute of arc) diaphragm was used most of the time to reduce the risk of errors due to seeing and guiding (e.g. telescope shake), which could affect the zero point ties. When measuring the fainter stars, with good seeing, a smaller diaphragm was preferred.

However it is a reasonable compromise between an aperture large enough to include all of the light from the star concerned and to minimize systematic errors between transformed and catalogue photometry caused by the inclusion or otherwise of field stars in the apertures of the standard stars and one small enough so as to minimize errors introduced by contaminating light from field stars for the programme stars. The adopted standard star photometry is tabulated in section B.2 of appendix B. Flat-fielded images of the standard stars for all eight nights on which useful calibration observations were made are presented in section B.1 of the same appendix. The analysis of this photometry to derive transformation equations from the MJUO *uvbyVI* photometric system to the relevant standard systems is presented in chapter 5.

3.4.2 Programme Stars

In order to derive magnitudes, colours and indices for the programme stars in the standard systems, based on the transformations derived from the photometry of the observed standard stars as described above, the raw magnitudes of the programme stars must be measured in exactly the same fashion as for the standard stars, i.e. synthetic aperture photometry. However, all three programmes stars lie in fields so crowded that even the smallest apertures considered for the measurement of the standard stars would be contaminated by light from one or several nearby field stars, even in the ultraviolet u bandpass. Thus, a rather more sophisticated approach for the photometric reduction procedure was required, combining aspects of profile fitting photometry and synthetic aperture photometry.

The job is straightforward in principle, but difficult and rather CPU intensive in practice. By subtracting the fitted profiles of all stars (except the actual target) within a region slightly larger than the largest aperture diameter used by PHOTOMETRY (usually the 'Outer Sky' (OS) radius), synthetic aperture photometry of the target star alone can be extracted. For the best accuracy, simultaneous multiple profile fitting routines were required. Furthermore, as compared with profile fitting for differential photometry, one must go to slightly more trouble to ensure that the PSF for the frame is indeed a good representation of the observed profiles of stellar images in the frame since, for this application, systematic differences between the PSF for the frame and the true image profile will not cancel out as they do for differential photometry.

Given the less-than-ideal seeing conditions in which the programme star calibration observations were obtained, implementation of the above procedure required multiple PSF cleaning passes as described in section 3.2.2. Up to four passes were required for the the most crowded y, V and I fields of HV 982 and HV 1620 before all stars which could possibly affect the synthetic aperture photometry of the programme stars were adequately fitted. ALLSTAR was used for calculating the profile fits. Sections B.5, B.6 and B.7 present representative images and perspective plots of the 100×100-pixel regions centered on the programme stars for the original flat-fielded frames and the frames after subtraction of all (including the programme star) fitted profiles for the three programme stars.

Chapter 4

Analysis of Photometric Light Curves I. Techniques and preliminary solutions

As discussed in chapter 1, eclipsing binaries, at present, provide the most accurate data on stellar fundamental properties such as mass, radius and luminosity. The derivation of such properties relies heavily on the analysis and interpretation of photometric light curves and spectroscopic radial-velocity curves.

Modern techniques for analysing photometric light and/or spectroscopic radial-velocity curves are based around the adjustment of the parameters of a model binary star system so as to minimize the difference between the observed light and/or radial-velocity curves and those predicted by the model. Once satisfactory agreement between the observations and the model has been achieved, the properties of the real system are assumed to be the same as those of the model system.

Some preliminary modeling of the well detached system HV 982 was carried out with the EBOP program which implements the Nelson-Davis-Etzel model (see Etzel (1993) and references therein), but this was soon abandoned in favor of the more general Wilson and Devinney Synthetic Light Curve Program (hereafter *WD*) (Wilson and Devinney, 1971; Wilson and Biermann, 1976; Wilson, 1979; Wilson, 1990; Wilson, 1992a; Wilson, 1992b; Wilson, 1993b; Wilson, 1994). The *WD* program is based on a more sophisticated and more general model and is thus better suited to the analysis of the more complicated light curves of HV 1620 and HV 2241. Since the above cited references provide a complete and detailed description of the *WD* program and its use, it is unnecessary to attempt to provide a comprehensive description here. Nonetheless, the first three sections of this chapter provide an overview of those aspects and features of the *WD* program most pertinent to this research. Following them is a section describing the use of the *WD* program to derive preliminary solutions for the three programme stars HV 982, HV 1620 and HV 2241. These preliminary solutions have been used to investigate systematic effects in the differential photometry and in the derivation of the effective temperatures of the components of each binary system (chapter 5). Final solutions are derived and discussed in chapter 6.

The *WD* code is continuously evolving as new physics or options are added and bugs are discovered and corrected. It is therefore useful to specify exactly the version of the code used, and discussed in this thesis. The basic code – which includes the differential corrections and light curve main programs (DC and LC) and all the necessary subroutines – was obtained directly from R.E. Wilson in June 1995. A number of corrections – including the complete substitution of updated subroutines – have subsequently been made to the code according to instructions from Wilson. This code will hereafter be referred to as *WD95*. A number of further developments and innovations have been made to the basic code but these will be discussed in appendix C.

4.1 The Roche Model and the physical basis of the Wilson & Devinney Model

The *WD95* **program** is based on a 'physical' **model** which characterizes binary star systems with (nominally) 30 parameters – see section 4.2. In the most general terms the model is based on the Roche Model (e.g. Kopal, 1959) generalized to include non-synchronous and/or eccentric orbits (Wilson, 1979). The main features of the Roche Model are that the gravitation field of the binary system is approximated by that of two point masses while the surfaces of the two components are specified by the so-called equipotential surfaces. Because of the high degree of central concentration of mass in real stars, the point-mass approximation is found to provide an adequate representation of the gravity field at the stellar surfaces (Wilson, 1994). The equipotential surfaces are the surfaces defining constant total potential energy. The total potential is generally composed of two components, gravitational plus centrifugal generated by the orbital motion of the binary system.

For completeness and convenience, the main results as presented in the initial sections of chapter three of *Close Binary Systems* (Kopal, 1959) are summarized below. It is first necessary to define a reference frame. The origin of a right handed Cartesian coordinate frame is placed at the center of gravity of the 'primary' component of the system ($\mathcal{M}_1$). The X-axis passes through the centers of gravity of both components and

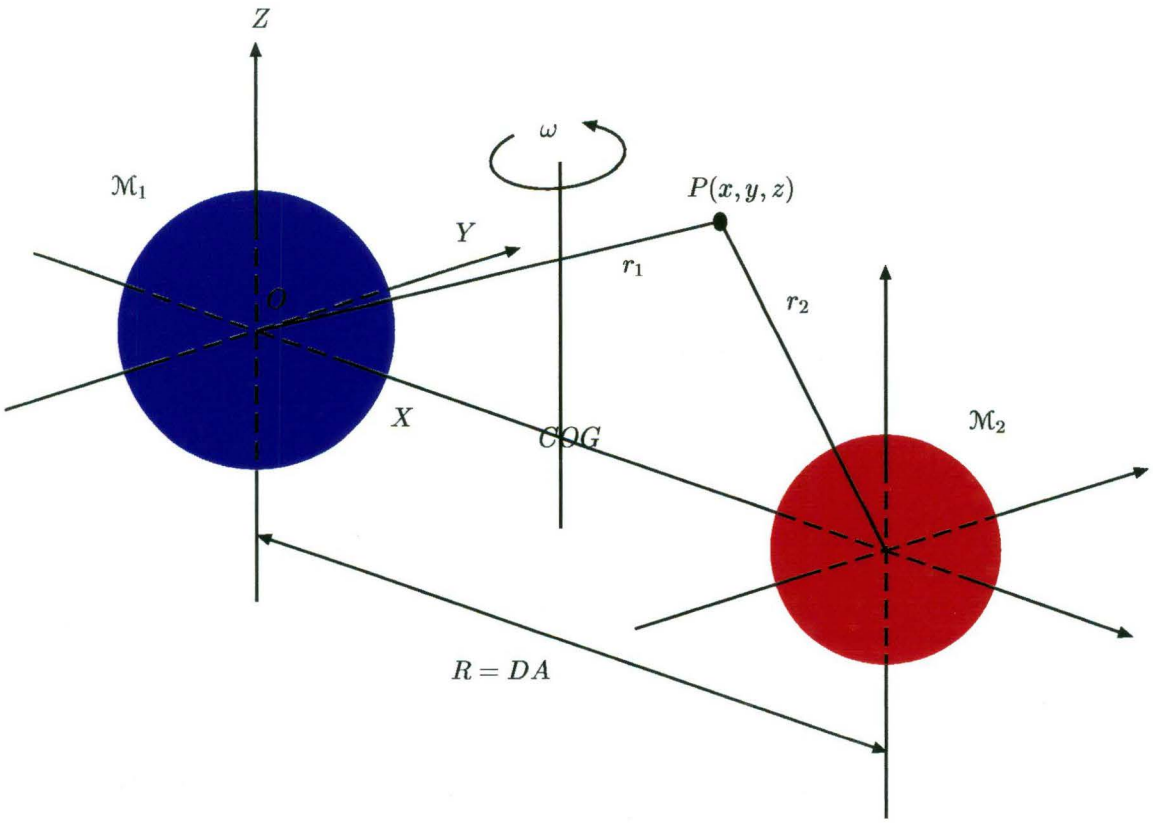

Figure 4.1: The geometry of the Roche Model of a binary star system.

the Z-axis is perpendicular to the plane of the orbit. The center of gravity (COG) of the system is then at the coordinates given by

$$(x, y, z) = \left(\frac{\mathcal{M}_2 R}{\mathcal{M}_1 + \mathcal{M}_2}, 0, 0 \right), \tag{4.1}$$

where $\mathcal{M}_2$ is the mass of the 'secondary' component and R[1] is their separation. This geometry is illustrated in figure 4.1. In the case of circular orbits R is identical to the major semi-axis of the relative orbit (A) and $D \equiv 1$, but for eccentric orbits – discussed below – this is not generally the case. The total potential (Ψ) at an arbitrary point $P(x, y, z)$ is given by,

$$\Psi(x, y, z) = G\frac{\mathcal{M}_1}{r_1} + G\frac{\mathcal{M}_2}{r_2} + \frac{\omega^2}{2}\left\{ \left(x - \frac{\mathcal{M}_2 R}{\mathcal{M}_1 + \mathcal{M}_2} \right)^2 + y^2 \right\}, \tag{4.2}$$

where G is the Universal Gravitational constant, ω the angular velocity of the system about an axis perpendicular to the XY-plane and passing through the center of gravity of the system and

$$\begin{aligned} r_1^2 &= x^2 + y^2 + z^2, \\ r_2^2 &= (R - x)^2 + y^2 + z^2. \end{aligned} \tag{4.3}$$

The surfaces of the two components are then defined by surfaces of constant potential – often referred to as *Roche Equipotentials*.

The earliest versions of the *WD* program were based directly upon the Roche Model. The potential was dealt with via the modified, dimensionless potential Ω (Kopal, 1959; Wilson and Devinney, 1971),

$$\Omega = \frac{A\Psi}{G\mathcal{M}_1} - \frac{\mathcal{M}_2}{2\mathcal{M}_1(\mathcal{M}_1 + \mathcal{M}_2)} = \frac{1}{r} + q\left\{ \frac{1}{\sqrt{(r^2 - 2r\lambda + 1)}} - r\lambda \right\} + \frac{(1+q)}{2} r^2 (1 - \nu^2) \tag{4.4}$$

[1] In the original edition of *Close Binary Systems* this R is given the symbol r, but this is easily confused with the r defined in equation (0-2) of *Close Binary Systems* hence I make the indicated substitution. This also implies the replacement of r by R in equation 4.2 (corresponding to equation (0-1) of *Close Binary Systems*) in the term involving the masses in the angular velocity term and in the definition of r_2, equation 4.3 (which corresponds to (0-2) of *Close Binary Systems*).

where q is the mass ratio ($\mathcal{M}_2/\mathcal{M}_1$) and

$$\begin{array}{rclcl} x & = & Ar\cos\phi\sin\theta & = & Ar\lambda, \\ y & = & Ar\sin\phi\cos\theta & = & Ar\mu, \\ z & = & Ar\cos\theta & = & Ar\nu. \end{array} \tag{4.5}$$

Note that r is thus in units of the major semi-axis (A). The angular velocity (ω) has been assumed to be equal to the Keplerian velocity (i.e. $\sqrt{G(\mathcal{M}_1+\mathcal{M}_2)/R^3}$), hence the above is applicable to the case of circular, synchronous orbits.

The *WD95* program deals with a form of the modified potential generalized to include non-synchronous rotation and eccentric orbits (Wilson, 1979),

$$\Omega = \frac{1}{r} + q\left[(D^2+r^2-2r\lambda D)^{-1/2} - \frac{r\lambda}{D^2}\right] + \frac{1}{2}F_1^2(1+q)r^2(1-\nu^2) \tag{4.6}$$

where, as above, D is the instantaneous separation of the components in units of the major semi-axis (i.e. $D = R/A$) and F is the ratio of rotational to orbital angular velocity. Equation 4.6 applies to the first component (i.e. $\mathcal{M}_1$), when treating the second ($\mathcal{M}_2$), the origin should be moved to the center of gravity of that component and the resulting potential (Ω') is then related to the above by

$$\Omega' = \frac{\Omega}{q} + \frac{q-1}{2q}. \tag{4.7}$$

The above is not exact. Wilson (1979) points out:

> A generalization of the binary potential to include eccentric orbit effects was given recently by Avni (1976). Strictly speaking, such a potential does not exist, because the force field is time-dependent and therefore nonconservative. However if a binary can readjust to equilibrium on a time scale which is short compared to that on which the forces vary, one can define an effective potential locally at each point of the orbit, without significant inconsistency, as Avni has done. The time scale of principal interest here is that for free non-radial oscillations, which will normally be shorter than an orbital period.[2]

4.2 Main features of the *WD95* program

The program consists of two main routines, `LC` which computes synthetic light and radial-velocity curves, and `DC` which computes parameter corrections to improve the agreement between model and observations. `DC` can simultaneously deal with multiple bandpass light curve observations as well as radial velocity observations. The advantage of this approach is that 'global' parameters, such as the mass ratio, the effective temperatures and radii of the individual components etc can be determined from all of the information contained in the complete data set rather than determining several values from the analysis of each curve individually and then having to adopt some mean of the individual values.

The program can deal with a number of morphological binary types; detached, semi-detached, contact (but restricted to synchronous circular orbits), double-contact, over-contact and X-ray binaries. Different morphologies are specified via a `Mode` of operation. Specific physical constraints are then placed on the system and its components according to the selected `Mode`. The modes of greatest relevance here are the detached configuration (`Mode=2`) and the semi-detached configurations (`Mode=4` and `Mode=5`).

The program allows for nominally thirty of the parameters to be determined from the light curves by the differential corrections main routine `DC`. The actual number of variable parameters is dependent on the mode of operation – since in some modes certain parameters are redundant (e.g. in most modes the luminosity of the secondary component is coupled to the luminosity of the primary star and the effective temperatures of the two components) – and upon the number of curves being analysed simultaneously. In general, the adjustable parameters are as follows:

- **Spots:** An arbitrary number of circular spots can be added to each component. Each spot is characterized by 4 parameters, the Latitude and Longitude of the spot center, the angular radius of the spot, and the temperature factor of the spot. The parameters of any two of the spots can be solved for by `DC`.

[2]For example, the free non-radial oscillation time scale for the Sun is of the order of one hour.

- **Longitude of Periastron** (ω)**:** Defined such that 90° corresponds primary eclipse occurring at periastron.
- **Orbital Inclination** (i)**:**
- **Phase of Primary Conjunction:** Merely a parameter to allow for an offset in the zero point of the ephemeris with which the observations have been phased.
- **Orbital Eccentricity** (e)**:**
- **Mass Ratio** (q)**:** The ratio of the mass of the secondary to that of the primary, i.e. $\mathcal{M}_2/\mathcal{M}_1$.
- **Orbital Major Semi-Axis** (A)**:** of the relative orbit, in units of $\mathcal{R}_\odot$.
- **Systemic Radial Velocity** (V_γ)**:**
- **Effective Temperatures** ($T_{\rm eff}$)**:** for each component.
- **Surface Potentials** (Ω)**:** for each component.
- **Stellar Luminosities** (L)**:** for each component for each bandpass.
- **Gravity Darkening Exponents:** for each component. For radiative envelopes the exponent is expected to be unity while for convective envelopes the exponent should be somewhat smaller, perhaps ~0.3 (Wilson, 1992b). An exponent of unity means that the bolometric flux is proportional to the local gravity, while zero would mean that the flux is constant over the surface.
- **Bolometric Albedo coefficients:** for each component. The bolometric albedo coefficients specify the ratio of re-radiated bolometric energy to received bolometric energy. For radiative envelopes the exponent is expected to be unity while for convective envelopes the exponent should be somewhat smaller, perhaps ~0.5 (Wilson, 1992b).
- **Axial to Orbital Rotation Rate ratios:** The ratio of the axial rotation rate to the mean orbital rotation rate for each component.
- **Limb-darkening Coefficients:** for each component for each bandpass. Limb-darkening is treated by the application of either a linear or a logarithmic limb-darkening law (see equations D.13 and D.15). The x coefficients can be solved for. There is no scope for solving for the y coefficient in the standard version of the program but it is possible to customize exactly which parameters are solved for (Wilson, 1992a).
- **Third-Light:** for each bandpass.

Intuitively, the 30 parameters of the *WD95* program can be divided up into a four 'natural' groups:

- The *relative* geometry of the model is specified by the Eccentricity (e), Mass Ratio (q) and the Surface Potentials ($\Omega_{1,2}$). Note that the radii of the two components are not parameters of the model. They must be derived from the mass ratio and surface potentials.
- The *absolute* geometry is then tied down by the Period (P) and the Major Semi-Axis (A).
- Aspect-dependent parameters are the Longitude of Periastron (ω) and the Inclination (i). These parameters specify the observer's viewpoint.
- Given the above parameters, the exact form of the light curve will then depend on the effective temperatures of the two components ($T_{\rm eff,1,2}$), the wavelength (λ), component Axial Rotation Rates, Gravity Darkening, Albedo, Limb-darkening and Third Light contributions and any hot or cold spots on the stellar surfaces.

In the standard version of the *WD95* code, the stellar atmospheres can be modeled by one of two options, either black-bodies or via an approximation derived from interpolations within the stellar atmosphere tables of Carbon and Gingerich (1969). A third option due to Milone and collaborators (Milone, 1993) provides for the atmospheres to be interpolated from lookup tables derived from the Kurucz stellar atmosphere models (Kurucz, 1993). The relevant subroutine was obtained from Milone and incorporated into the *WD95* code obtained from Wilson.

The numerical precision of the interpolation of the light over the stellar surfaces is adjustable through grid-fineness parameters for each component.

Two options are provided for calculating the effect of mutual irradiation and reflection between the two components. The simpler and faster option uses a 'corrected inverse square law' (Wilson, 1993a) while the more detailed option is based on a 'rigorous treatment of the geometric and irradiation heating problems for the binary star reflection effect' (Wilson, 1990).

4.3 Parameter adjustment

When optimizing the parameters of a model, the set of parameters which can meaningfully be determined from a given set of data is often restricted. With a program such as the *WD* program, careful consideration must therefore be given to exactly which of the ~30 parameters should be solved for from a given set of light and/or radial velocity curves, and which should be adopted from theory and/or consideration of other available information.

Without radial-velocity curves, it is not meaningful to solve for the orbital major semi-axis, since in general the light curves alone provide no information about the absolute dimensions of a system.

The mass ratio is an interesting case. In general the mass ratio is only weakly correlated with the light curves. In most cases it is most accurately determined from radial-velocity curves. However, in the case of semi-detached systems (Wilson, 1994) where the relative size of the lobe filling star gives precise information regarding the location of the inner Lagrangian point, the mass ratio is well defined by the light curves since they provide all of the information regarding the physical geometry of the system.

In general it is not meaningful to solve for the effective temperatures of both components of a binary star using the *WD* program alone. Differential light curves really only give information regarding the relative surface brightness. Certainly differential light curves at several wavelengths provide information about the absolute temperature scale, but in my experience the correlation is only very weak, at least for very hot stars over the spectral range of the work considered in this thesis (Strömgren u (λ350nm) to Cousins I (λ790nm)).

Without independent information regarding the individual stellar luminosities there is no conceivable reason to decouple the calculation of the luminosity of the secondary component from that of the primary and the respective effective temperatures. In any case, unless the light curves are calibrated in some sense, the luminosities act only as scaling factors by which the overall level of the calculated light curve can be made equal to that of the observations.

Tidal interactions act both to circularize orbits and to synchronize the rates of orbital and axial rotation (i.e. axial to orbital rotation rate ratios are unity). However, in eccentric orbits where the instantaneous orbital velocity is continuously varying, it is more likely that the axial and orbital rotation rates are pseudo-synchronized, i.e. synchronized at the periastron rate (Claret et al., 1995). In this case the axial to orbital rotation rate ratios are given by the following simple relation (Avni, 1976),

$$F_1 = F_2 = \frac{\omega_{\rm axial}}{\bar{\omega}_{\rm orb}} = \frac{\omega_{\rm peri}}{\bar{\omega}_{\rm orb}} = \sqrt{\frac{1+e}{(1-e)^3}}. \tag{4.8}$$

The gravity darkening exponents and bolometric albedo coefficients are probably best set according to theoretical considerations while the limb-darkening coefficients should be taken from theoretical stellar atmosphere models.

The question of third-light must be investigated on a case by case basis. Certainly there is reason to believe that in the rather crowded fields of the Magellanic Clouds, especially for the EROS stars which are of course located in the bar of the LMC, the failure of the reduction procedure to account for all the neighbours and thus give rise to third-light is a very real possibility.

Whether spots are required or not also must be investigated on a case by case basis. For the Magellanic Clouds, only eclipsing binaries consisting of early type stars are likely to be bright enough to be usefully observable. Spots are usually associated with chromospheric and/or magnetic activity in cooler, late-type stars with convective envelopes. Such spots are thus unlikely to be necessary for modeling light curves of Magellanic Cloud eclipsing binaries. It should however be noted that the spot formalism may be a useful tool for dealing with binaries whose light curves display the O'Connell effect.[3] In this case it must of course be remembered that the spot (or spots) is only being used as a means to obtain a better fit between model and observations. The interpretation of such spot (or spots) is thus far from obvious.

[3]The O'Connell effect refers to the phenomenon whereby the brightness maxima following the two eclipses are not equal (Davidge and Milone, 1984).

The actual adjustment scheme employed by DC is based on the calculation of differential corrections determined via linear least squares analyses. The majority of the derivatives required by the computations are evaluated numerically. DC itself does NOT provide for automated iteration but instead performs only one iteration at a time so as to force the user to consider the progress of convergence toward a solution. For each iteration performed by DC, in addition to providing differential corrections for each parameter being optimized, the program reports the standard error for each of the suggested corrections, the correlation coefficients between each of the adjusted parameters and the total weighted sum of the squares of the residuals.

DC also requires the specification of the expected random error of each observation for each light or radial-velocity curve included in the optimization. These random errors influence the relative weight given to the different curves as well as the reported standard errors of the adjusted parameters and the weighted sum of the squares of the residuals. As pointed out by Wilson (1979), it is therefore important to ensure that these random errors are set carefully, especially when both light and radial velocity data is included in the analysis. It should also be noted that the weighted sums of the squares of the residuals for two iterations with different values for the expected random errors can not be directly compared.

4.4 Preliminary fits to the MJUO light curves

In the course of deriving final parameters for the three programme stars, numerous preliminary fits to the HV 982, HV 1620 and HV 2241 light curves were computed. The effects of alternative physical approximations (e.g. the simple or the detailed reflection calculations and the proximity corrections to radial velocities) and different methods of parameter adjustment were investigated. Solutions over ranges of mass ratios were also sought.

All optimizations were performed using all six light curves for each programme star simultaneously. The individual curves have not been fitted individually although in hindsight, this would have been a useful exercise since it might provide information regarding such factors as third-light and its influence in the individual bandpasses. For HV 1620 and HV 2241, optimizations both with and without the spectroscopic radial-velocity curves (Niemela and Bassino, 1994) were obtained.

In addition to providing insight into the nature of parameter space and the uniqueness of computed solutions and how well determined they are, preliminary solutions have also been used to derive calibrated photometry at specific reference phases and for the determination of the stellar effective temperatures (chapter 5).

4.4.1 When has the iterative process converged?

The objective of numerical optimization algorithms (such as the *WD95* program) is (usually) to obtain the set of model parameters, the so-called 'optimal' parameter set, which best represents a given set of data. The optimal parameter set usually corresponds to the parameter set which minimizes the difference between the physical observables and those predicted by the model, as judged, for instance, by the (weighted) sum of the squares of the residuals between observations and model.

The very nature of numerical optimization procedures, as applied to non-linear problems, means that given one parameter set which is believed to be optimal, it is not generally possible to be completely certain that there does not exist some other better parameter set. It is necessary therefore to adopt a priori an appropriate criterion for convergence.

The most common criterion for convergence found in the literature, at least as far as the *WD95* program is concerned, is that the suggested parameter corrections converge to 'utterly negligible' values (Wilson, 1983). This has usually been taken to mean suggested corrections for each parameter smaller than the standard error associated with the parameter. It has long been known however that correlations between the parameters being optimized can cause problems for convergence for some binaries (Wilson and Biermann, 1976). Wilson and Biermann suggest a method (the Method of Multiple Subsets [MMS]) by which problems due to parameter correlation can be circumvented. The MMS involves breaking large sets of parameters with strong correlations into smaller subsets which avoid strong correlations between the parameters being optimized. Differential corrections are calculated and applied for each subset in turn until the suggested corrections for all parameters of all subsets are negligible and the optimization procedure is deemed to have converged. According to Wilson and Biermann, the MMS approach is useful for dealing with problems caused by a large number of high correlations rather than a few *very* high correlations for which convergence should not be too severely affected even when iterating the full parameter set.

For the light curve analysis of the three programme stars, all parameters to be optimized in a given solution were generally adjusted simultaneously rather than by the MMS. This method of parameter adjustment

leads to relatively quick convergence toward the vicinity of the (presumably) optimal solution. However, once close to the optimal solution, the suggested parameter corrections did not converge to 'utterly negligible' values in comparison with the corresponding standard errors. The suggested parameter corrections in fact remained of the order of the standard errors. Thus the convergence criterion usually employed was that the suggested parameter corrections all be simultaneously smaller (but not necessarily 'utterly negligibly' smaller) than their respective standard errors for two consecutive iterations. The 'adopted solution' is then the parameter set corresponding to the first of the two converged iterations. Subsequent iterations did not necessarily fulfill the convergence criterion. But by continuing to iterate from the adopted solution, further solutions could eventually be found. The individual parameters which were optimized were not found to differ significantly (i.e. in comparison to the reported standard errors) amongst the various adopted solutions. Furthermore as the iterations proceed, the rms scatter of the adjusted parameters generally tended toward the level of the reported standard errors.

Examination of the correlation matrices reported by DC revealed that strong correlations (correlation coefficients in excess of 0.2) existed between several pairs of parameters for all three binaries. Correlations were particularly strong between the orbital inclination and the mass ratio, the orbital inclination and the surface potentials, the mass ratio and the surface potentials and, for the eccentric system HV 982, between the eccentricity and the longitude of periastron. To investigate if these correlations were significantly affecting the computed solutions, new solutions were obtained employing the MMS. The resulting MMS solutions obtained by iteratively correcting adopted solutions according to the above criterion did not differ significantly from the original solutions. Other MMS solutions were obtained by iterative correction of initial parameter sets which were located in parameter space a significant distance from the the previous solutions. In these tests it was found that in some cases, the MMS was less practical and lead to solutions which, both by visual inspection and in terms of the weighted sum of the squares of the residuals, were clearly inferior. In the particular case of HV 1620, numerous local minima are located relatively close to the global minimum. The MMS iterations tended to become 'trapped' in local minima. The full parameter set iterations on the other hand were always found to be able to 'escape' the local minima and eventually find their way to the global minimum, although not necessarily by the first solution corresponding to the adopted convergence criterion. A discussion of such behavior during an extended number of iterations with the *WD* code is given by de Landtsheer (1983) with reply from Wilson (1983). The magnitude of the problem experienced here however does not appear to be nearly as severe as that in the example provided by de Landtsheer.

The experience gained here seems to indicate that problems due to parameter correlation are best dealt with by optimizing larger parameter sets simultaneously so as to 'dilute' the effect of the correlations. When smaller subsets are optimized concurrently, as per the MMS, for the cases of the three programme stars studied here, strong correlations between even one pair of parameters tend to dominate when mixed in with only one or two other parameters. Furthermore, smaller subsets are less able to take large 'leaps' across parameter space in order to escape local minima.

4.4.2 Uncertainties in the derived parameters

Uncertainty in the assumed parameters of the binary systems derive from several sources. There are of course the 'internal' uncertainties associated with the quality of the observations and their ability to constrain the adopted model. Then there is uncertainty arising from questions of the uniqueness of a solution derived by the numerical algorithm: has the true global minimum been located, or has the solution become trapped in merely a local minimum? Finally, further uncertainty derives from systematic errors arising from the physical validity or otherwise of the adopted model.

From a thorough investigation using synthetic light curves smeared with noise, Popper (1984) suggests that 'multiplying internal mean errors by a factor of 3 will lead to results that, statistically, do not overestimate the accuracy with which the parameters of a system are derived'. On the other hand, based on similar tests Davidge (1987) came to the conclusion that multiplication of the reported standard errors by the factor of three was unnecessary, at least as far as his analysis of HV 1620 and HV 2241 was concerned.

As noted in the previous section, close examination of the behavior of the parameters being optimized as further iterations are carried out to obtain subsequent solutions, suggests that the solution is well defined by the light curves within the uncertainty indicated by the standard errors. To put it another way, once a local minimum has been reached, the iterations will indeed 'bounce around' within that minimum, but the range of values taken on by the parameters is in most cases, well characterized by the reported standard errors. The weighted sum of the squares of the residuals does not vary significantly from iteration to iteration.

To test for the uniqueness of the solutions derived by DC, solutions for all three programme stars were obtained starting from several initial parameter sets. The initial parameters were varied arbitrarily over

appropriate ranges. For HV 1620 and HV 2241, the same solutions were obtained, within the uncertainty of the reported standard errors irrespective of the starting parameter sets, thus lending confidence that the final adopted solutions for these two stars do indeed correspond to solutions at the global minimum. There is less confidence in the identification of the global minimum for HV 982. Different initial parameter sets led to different local minima, from which the iterations were unable to escape (at least not within of the order of 100 iterations). The optimized parameters derived from the various minima differ by significantly more than the reported standard errors, most especially so for the surface potentials. The typical weighted sum of the squares of the residuals however differs by less than 1 per cent. A deeper investigation of parameter space, perhaps by means of a systematic search using a two parameter grid (e.g. mass ratio and the surface potential of one of the components (Davidge, 1987)), would probably be required before the final parameters for HV 982 could be determined with greater confidence from the light curve analysis alone. However, spectroscopic radial-velocity curves for HV 982 are likely to be available soon (Clausen, 1996). Substantial further effort in the modeling of the system is thus probably not warranted until those data become available.

A study of the physical validity of the Wilson and Devinney model is beyond the scope of the current research. Systematic errors arising from the model are thus, for the moment, assumed to be negligible in comparison with the uncertainties discussed above.

Thus, unless otherwise stated, the standard errors reported by DC are generally adopted where appropriate as estimates of the uncertainty in the derived model parameters. For other derived quantities for which no standard errors are reported by DC, the uncertainties have been estimated by consideration of the rms scatter of the quantity obtained from a large number of iterations within the immediate vicinity of the (assumed) global minimum. Quantities for which DC does not report standard errors include the surface potentials of components which fill their Roche lobes and the masses of the individual components of each system. The critical surface potentials are calculated directly and are dependent on the mass ratio and the ratios of axial to orbital rotation rate. The masses of the individual components of each system are computed via the values of the major semi-axis, the orbital period, the mass ratio and Kepler's 3rd law.

4.4.3 General considerations and specific implementation

Since the individual components are all expected to be early-type OB stars, the gravity-darkening and albedo coefficients were set as appropriate, according to theory, for radiative atmospheres, i.e. equal to unity.

The logarithmic limb-darkening law (see equation D.15) was used for all computations. Limb-darkening coefficients derived from Kurucz (1993) stellar atmosphere models for $Z = [-0.3]$ and $Z = [-0.5]$ were used for the LMC stars (HV 982 and HV 2241) and the SMC star (HV 1620) respectively. Coefficients for each iteration were interpolated from $T_{\rm eff}/\log[g]$ grids computed for each of the instrumental bandpasses over the full grid of stellar atmosphere models available, see appendix D.

Suggested corrections to the surface potentials of the secondary components of HV 1620 and HV 2241 often resulted in surface potentials smaller than the critical surface potentials, i.e. stars larger than their Roche Lobes. No solutions (according to the above convergence criterion) were found when the surface potential of the secondary component of either system was optimized under *WD95* `Mode=2` (i.e. the detached configuration). By relaxing the convergence criterion by not requiring that two consecutive iterations produce suggested corrections smaller than the standard errors but accepting any single iteration for which the suggested corrections were smaller than the standard errors, solutions could be found. However the resulting optimized secondary component surface potentials were within the reported standard errors of the critical surface potentials. These results agree with the findings of Davidge who used mass-ratio/secondary-component-surface-potential parameter space searches to establish that HV 2241 was best modeled by a semi-detached configuration (Davidge, 1987) while HV 1620 was best modeled by a detached configuration, although the resulting surface potential of the secondary component was equal to the critical surface potential within the uncertainties (Davidge, 1988). Based on these findings, the *WD95* `Mode=5` configuration (i.e. semi-detached systems with the secondary star filling its Roche lobe) was adopted for most of the modeling of both HV 1620 and HV 2241. The light curves for HV 982 are clearly more evocative of a well detached configuration (`Mode=2`). No solutions were ever found with the surface potential of either component significantly close to the critical values.

The Milone `ATM` subroutine option, which provides for interpolation within lookup tables for corrections of blackbody fluxes to model-atmosphere fluxes was used throughout. As for the limb-darkening coefficients, appropriate files for the instrumental bandpasses of the observations were created from the appropriate Kurucz (1993) stellar atmosphere models as required.

HV 1620 and HV 2241 were assumed to have circular orbits. Axial rotation rates were assumed to be synchronous with the orbital rotation rates. In accord with the obvious indicators present in the light curve

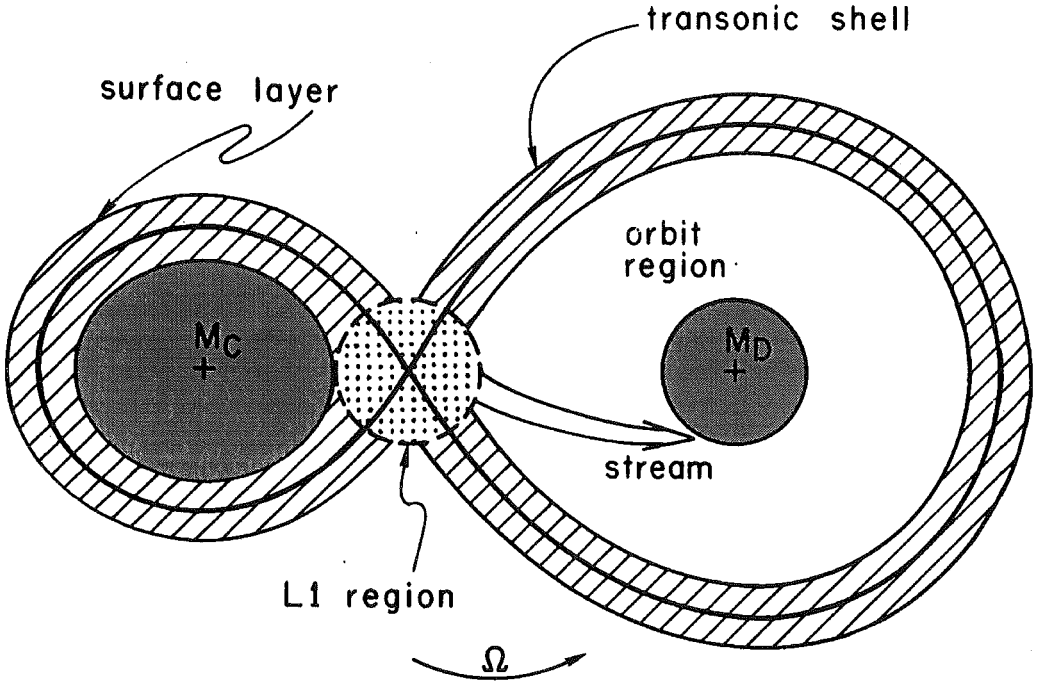

Figure 4.2: Schematic diagram of the various regimes involved in the mass transfer process. The direction of flow of the mass stream is shown, flowing from Contact component (M_C), through the 'L1 region' and onto the Detached component (M_D). The direction of orbital rotation is indicated by Ω. This figure has been reproduced from Lubow and Shu (1975) who give a full explanation of the meaning of the identified regimes.

of HV 982 – i.e. the unequal durations and spacing (in phase) of the minima – the orbit for this star was assumed to be eccentric. The axial rotation rate was thus set according to equation 4.8, corresponding to synchronization of the axial and orbital rotation rates at periastron.

The luminosity of the secondary was always left coupled to the luminosity of the primary and the effective temperatures of the two components (i.e. `IPB=0`). The numerical derivatives were computed using the symmetrical-derivatives option (i.e. `ISYM=1`).

Preliminary solutions plainly indicated that the light curves of HV 1620 and HV 2241 are asymmetric in the sense that the maximum of light following primary minimum is slightly brighter than that following secondary minimum, the so-called O'Connell effect (Davidge and Milone, 1984). For HV 1620 the effect amounts to a difference of $\sim$0.02 mag for u and $\sim$0.01 mag for the other five observed bandpasses while for HV 2241 the differences are $\sim$0.05 mag in u and $\sim$0.03 mag for the other five bandpasses. This effect was noted by Davidge (Davidge, 1987) for HV 2241 but not identified by him in his less-precise light curve of HV 1620. As a means to model this O'Connell effect, solutions with spots were computed. For each binary, one spot was located on the equator (i.e. in the notation of the *WD95* model, latitude 90°.0) of the primary star at (*WD95* model) longitude 270°.0, i.e. corresponding to the spot being directly visible at the quadrature point corresponding to maximum light following the primary minimum. The temperatures of the spot were set at 10% above the local effective temperature. The net effect of the spot is to increase the light output relative to the unspotted model for phases when the spot is visible. Spot diameters of $\sim$30° for HV 1620 and $\sim$25° for HV 2241 were found to model the observed asymmetries well. Both binaries have secondary components which fill, or at least are very close to filling, their Roche lobes. Mass transfer from secondary to primary is therefore possible. According to the models of Lubow and Shu (1975; 1976), given the approximate mass ratios and primary component radii of both systems ($q\approx$0.7 and $\mathcal{R}_1/A\approx$0.2 for HV 1620 while $q\approx$0.5 and $\mathcal{R}_1/A\approx$0.4 for HV 2241), any mass stream will result in a 'direct impactor' scenario rather than the formation of an accretion disk. This will likely result in a so-called 'hot-spot'. However the expected position of this hot-spot does not coincide with that of the spot used to model the observed O'Connell effect. Hot-spots resulting from direct impact mass accretion are located at equatorial latitudes but closer to (*WD95* model) longitudes of 30° (see figure 4.2). It is therefore unclear what physical interpretation to attach to the spots or indeed how to account for the observed O'Connell effect.

Spectroscopic radial velocity data (Niemela and Bassino, 1994) was included in the analysis for HV 1620 and HV 2241 thus permitting the determination of the major semi-axes of the orbits and hence the absolute

physical sizes of the systems. Radial-velocity curves are normally integral to the unambiguous determination of the mass ratio, but for these two semi-detached binaries given the relative precision of the light curves and the radial-velocity curves, the photometric mass ratio is to be preferred (see section 4.3 above).

The detailed reflection effect option was found to be necessary for HV 1620 and HV 2241 as the simpler treatment resulted in the need to calculate blackbody to stellar atmosphere corrections at unrealistically high temperatures (e.g. 60 000 K) which exceeds the interpolation range of the Kurucz stellar atmosphere models and thus results in practical difficulties. Two reflections were found to be adequate to compute the effect to suitable accuracy. Increasing the number of reflections did not significantly alter the computed light values. For HV 982, given the negligible departures from spherical geometry of the components, the simpler treatment of the reflection effect is entirely adequate.

The observed differential magnitudes were converted into light values in the following way;

$$l_{\bar{\lambda},\mathrm{i}} = 10^{m_{\bar{\lambda},\mathrm{i}} - m_{\bar{\lambda},1}} \tag{4.9}$$

where $l_{\bar{\lambda},\mathrm{i}}$ is the light value corresponding to the i^{th} differential magnitude observation ($m_{\bar{\lambda},\mathrm{i}}$) made in the bandpass denoted by $\bar{\lambda}$. $m_{\bar{\lambda},1}$ is simply the first observation listed in the the original data file. By definition, $l_{\bar{\lambda},1}$ is unity.

To summarize:

HV 982: The parameters which were optimized by the differential corrections program were the eccentricity, the longitude of periastron, the phase offset, the inclination, the temperature of the secondary component, the surface potentials of both components and the luminosity of the primary component. Solutions were obtained for mass ratios of 0.90, 1.00 and 1.10 over a temperature range of the primary component of 18,000 K to 30,000 K in steps of 1000 K.

The mass ratio can not be meaningfully determined from the light curve analysis alone. Spectroscopic radial-velocity curves must be obtained to set this parameter directly. However, mass ratios significantly differing from 1 can be eliminated on the physical basis that the similar depth of the light curve minima indicates nearly equal temperatures for the two components. Since the orbit is eccentric, HV 982 is likely comparatively young and both components are probably still main sequence stars. According to theoretical models, two main sequence stars of nearly the same temperature will necessarily also be of nearly the same mass, assuming they are to be of the same age as required by most binary star evolutionary scenarios.

The major semi-axis also can only be determined directly via analysis of radial-velocity curves. However by adopting a distance modulus to the LMC and thus to HV 982 itself, the major semi-axis can be estimated by requiring the model light output, corrected for distance and interstellar extinction, to be equal to the observed light at earth. Adopting $(m - M)_0 = 18.35$ mag (Schmidt-Kaler, 1993), the appropriate major semi-axis is then $\sim 34\,\mathrm{R}_\odot$.

The temperature range above is appropriate under the assumption that the system is composed of OB-type stars which is consistent with the apparent magnitude of the star assuming HV 982 is indeed a member of the LMC. The ratio of the effective temperature of the secondary component ($T_{\mathrm{eff},2}$) to that of the primary component ($T_{\mathrm{eff},1}$) at any given $T_{\mathrm{eff},1}$ (within the range investigated) is found to be well defined by the light curves and insensitive to the mass ratio (again within the range investigated). Using these preliminary fits it is thus possible, in conjunction with the IUE spectrophotometry and calibrated standard system photometry, to determine a reliable estimate of the effective temperatures of the two components. This is the subject of chapter 5.

The eccentricity, the longitude of periastron and the inclination can be expected to be well defined by the light curves, independent of the mass ratio and effective temperatures.

For a given mass ratio, the surface potentials of the two components are well defined by the light curves. However, until the mass ratio can be determined, the true values of the surface potentials are indeterminate. The radii, or at least the relative radii (i.e. $\mathcal{R}_\mathrm{i}/A$), on the other hand, which in the *WD* model are derived from the surface potentials, are indicated by the inter- and intra-eclipse durations. The radii are thus less correlated with the mass ratio.

Figure 4.3 presents typical plots of the observations, model light curves and residuals between the observed $Variable - Comparison$ differential photometry and the models. Plots of the residuals versus seeing (figure 4.4) and airmass were examined. No obvious or significant trends are evident in the plots against airmass indicating that any differential extinction resulting from the different colours of the programme and the comparison star is insignificant. However in the plots against seeing, clear systematic effects are present in the *uvby* data. Residuals in the sense of observations minus model become increasingly negative with increasing FWHM. This is likely due to contamination of the photometry of HV 982 by the three nearby field stars (see section 3.3.1). As the seeing becomes worse, more of the light from the field stars contaminates the estimation of the brightness of the programme star. The brightness of the programme star is thus

overestimated, the magnitude becomes more negative, and so the residual becomes likewise more negative. Linear corrections to the $Variable - Comparison$ *uvby* differential photometry have thus been applied according to,

$$(V-C)'_u = (V-C)_u + 0.008 \times (\mathrm{FWHM} - 4.38) \quad (4.10)$$
$$(V-C)'_v = (V-C)_v + 0.011 \times (\mathrm{FWHM} - 4.18) \quad (4.11)$$
$$(V-C)'_b = (V-C)_b + 0.013 \times (\mathrm{FWHM} - 4.31) \quad (4.12)$$
$$(V-C)'_y = (V-C)_y + 0.015 \times (\mathrm{FWHM} - 3.80) \quad (4.13)$$

where $(V-C)_u$, $(V-C)_v$, $(V-C)_b$ and $(V-C)_y$ are the original differential magnitudes, $(V-C)'_u$, $(V-C)'_v$, $(V-C)'_b$ and $(V-C)'_y$ are the corrected differential magnitudes and the FWHM are in seconds of arc. In V and I, where a more sophisticated reduction procedure was employed in an effort to account for the contamination of the nearby field stars, systematic effects in the residuals are seen only for extreme seeing conditions (FWHM$\geq$6.″0 for V and FWHM$\geq$5.″0 for I). These observations have therefore been excluded from further analysis.

HV 1620 and HV 2241: Due to the similarity of the light curves for HV 1620 and HV 2241 and indeed of the component stars themselves (hot early type stars with the cooler secondary component filling its Roche Lobe) the light curves of the two systems were analysed in much the same fashion.

The spectroscopic radial-velocity curves of Niemela and Bassino (1994) were included in the analysis. The precision of these data is not high. The observations were made photographically with a 1-m telescope. Niemela and Bassino quote rms scatters with respect to radial-velocity curve fits of between $\sim$20 and $\sim$30 km s^{-1}. Several of the measured velocities are derived from a single spectral line and were excluded from the analysis. Observations at phases close to conjunctions when blending effects in the spectra make the accurate measurement of radial velocities for the individual components difficult were also excluded. The *WD95* 'proximity corrections' option for the radial-velocity curves was included. The exclusion of the observational data points close to conjunction however means that including the proximity corrections makes no significant difference to the derived optimized parameters. The distortions to the radial-velocity curves arise because the observed spectral lines are in some sense a weighted mean of the velocity across the surface of the star which of course varies due to the rotation of the star. When the entire star is visible, the weighted mean velocity approximates that of the center of mass of the star, whose radial velocity varies sinusoidally (assuming the orbit is circular). During an eclipse, the star in front acts as a scanner across the surface of the star being eclipsed. During ingress to the eclipse, the observed radial velocity thus becomes increasingly weighted by the trailing limb of the occulted star, which due to rotation, is moving away from the observer, hence the radial velocity remains more positive than the center of mass radial velocity of the component being eclipsed. During egress, the radial velocity starts out strongly weighted by the leading limb of the component now exiting eclipse, which is rotating toward the observer, and hence produces an observed radial velocity much more negative than that of the center of mass. As the star emerges from eclipse, more of the surface becomes visible and the velocity tends toward that of the center of mass of the star. A small effect can be seen in the model radial-velocity curves for HV 1620 (figure 4.5). The distortions are much more clearly evident in the model radial-velocity curves of HV 2241 (figure 4.7).

The parameters optimized were generally the major semi-axis, the phase offset, the inclination, the mass ratio, the temperature of the secondary component, the surface potential and luminosity of the primary component, the systemic velocity and the radius of the spot on the primary component. Solutions were obtained over temperature ranges of the primary component of 20,000 K to 36,000 K in steps of 1000 K for both stars. As for HV 982, the temperatures of the components of HV 1620 and HV 2241 will be determined in chapter 5 in conjunction with the IUE spectrophotometric and standard system photometric data.

For HV 1620 and HV 2241, the mass ratio is insensitive to temperature since it is determined via the geometry of the light curve (see section 4.3). The mass ratios were thus determined both photometrically (i.e. using the differential light curves only) and by including the spectroscopic radial-velocity curves of Niemela and Bassino. With appropriate relative weightings derived from the scatter amongst the residuals between observations and model, the two approaches yielded the same mass ratios within the uncertainties. This is most probably due to the much heavier weighting given to the photometry which is consistent with its much smaller internal scatter. Considering a large sample of preliminary solutions, the indicated mass ratios are roughly 0.68$\pm$0.01 for HV 1620 and 0.53$\pm$0.01 for HV 2241 where the uncertainties here are indicative of the total range of solution mass ratios. Solutions were also found for a range of adopted mass ratios at intervals of 0.05 centered on those indicated above. The mass ratio corresponding to the minimum of the sum of the squares of the residuals was for both stars, to within the accuracy of the grid, the same as those indicated by the solutions when the mass ratio was solved for. For HV 2241, the current mass

ratio is in good agreement with those obtained by Davidge (1987) (0.54±0.12) and Niemela and Bassino (0.50±0.03). For HV 1620, the agreement between the current determination and those of Davidge (1988) (0.604±0.024) and Niemela and Bassino (0.79±0.09) is not quite as favorable but is still reasonable. The disagreement with Davidge is possibly related to the different *WD* `Mode` used by Davidge: he solved for a detached configuration.

The inclination and surface potentials are well defined given the well defined mass ratios since they are largely determined by the geometry of the light curves and are only weakly correlated with the effective temperatures (at least over the applicable temperature range) as evidenced by the correlation coefficients reported by the *WD95* program.

The major semi-axes and the systemic velocities are specified by the spectroscopic radial velocities and can be expected to be uncorrelated with temperature. Thus the overall scale of the system is well defined, provided of course that the radial velocities are not systematically in error.

Figures 4.5 and 4.7 present typical plots of the observations, model light curves and residuals between the observed $Variable - Comparison$ differential photometry and the models for HV 1620 and HV 2241 respectively. Plots of the residuals versus seeing (figures 4.6 and 4.8) and airmass were examined. As for HV 982 no obvious or significant trends are evident in the plots against airmass.

For HV 1620 the plots against seeing indicate systematic errors in the $Variable - Comparison$ b, y, V and I differential photometry for the worst seeing. This is likely due to the contamination of the HV 1620 photometry by the nearby field star $\sim 6''$ to the south-east. The contamination is apparently only significant for observations with FWHM$\geq 5\farcs0$ which is due no doubt to the nearby field star being relatively more distant from HV 1620 as compared with the nearby field stars of HV 982. The u and v data appear free of such effects presumably due to the much lower signal level of the nearby field star at the shorter wavelengths. On the basis of these plots b, y, V and I observations with FWHM$\geq 5\farcs0$ have been excluded from further analysis. In the V residuals there is clearly some systematic problem for the 22 observations with FWHM$\leq 2\farcs4$. The majority of these observations were obtained on the night of 1993-Sep-07. Inspection of the 1993-Sep-07 images reveals that the pixels at the image core of both the $Comparison$ and $Check$ stars are saturated or very close to being so. Thus all observations obtained on the night of 1993-Sep-07 have also been excluded from further analysis. In the I residuals there are five observations with FWHM$\sim 2\farcs6$ but with large, negative residuals (one has a residual of -0.057 and so is not shown in figure 4.6). The orbital phases of these observations are close to zero, i.e. primary eclipse. Figure 4.5 shows a systematic deviation of the model I light curve from the observations during primary eclipse. This hints at the possibility of a small infrared excess for the system. A possible source for such an excess is a gas envelope surrounding the system created during periods of mass exchange between the components. Such a mechanism is consistent with the observed I magnitude being most significantly affected at the lowest total light levels (i.e. primary eclipse). An alternative possibility is a 'third-light' contribution either by a physical third companion star in the system or simply an unresolved nearby field star, in either case the third star would necessarily be much fainter and cooler than the two eclipsing components.

For HV 2241, only I shows any indication of a seeing dependent systematic error. The error likely results from contamination of the photometry of the comparison star (star #10) by the field star $\sim 5''$ to the north. A linear correction given by

$$(V-C)'_I = (V-C)_I - 0.004 \times (\mathrm{FWHM} - 4.5) \tag{4.14}$$

has therefore been applied to the $Variable - Comparison$ I differential photometry (here $(V-C)_I$ is the original differential magnitude, $(V-C)'_I$ the corrected differential magnitude and the FWHM is in seconds of arc). Note that over the observed range of FWHM, this correction amounts to no more than ± 1 per cent (i.e. ± 0.01 mag).

The differential photometry tabulated in tables A.1 to A.18 includes the linear corrections to the $Variable-Comparison$ differential photometry as detailed above. Likewise the rms residuals ($\sigma_{(V-C)}$ and $\sigma_{(C-C)}$) summarized in table 3.3 derive from the corrected photometry and the restricted data sets. The corrected differential photometry under the above selection criteria represent the *finalized* data sets for the light curve analysis. Final elements and properties of the systems and their components along with a full discussion will be presented in chapter 6.

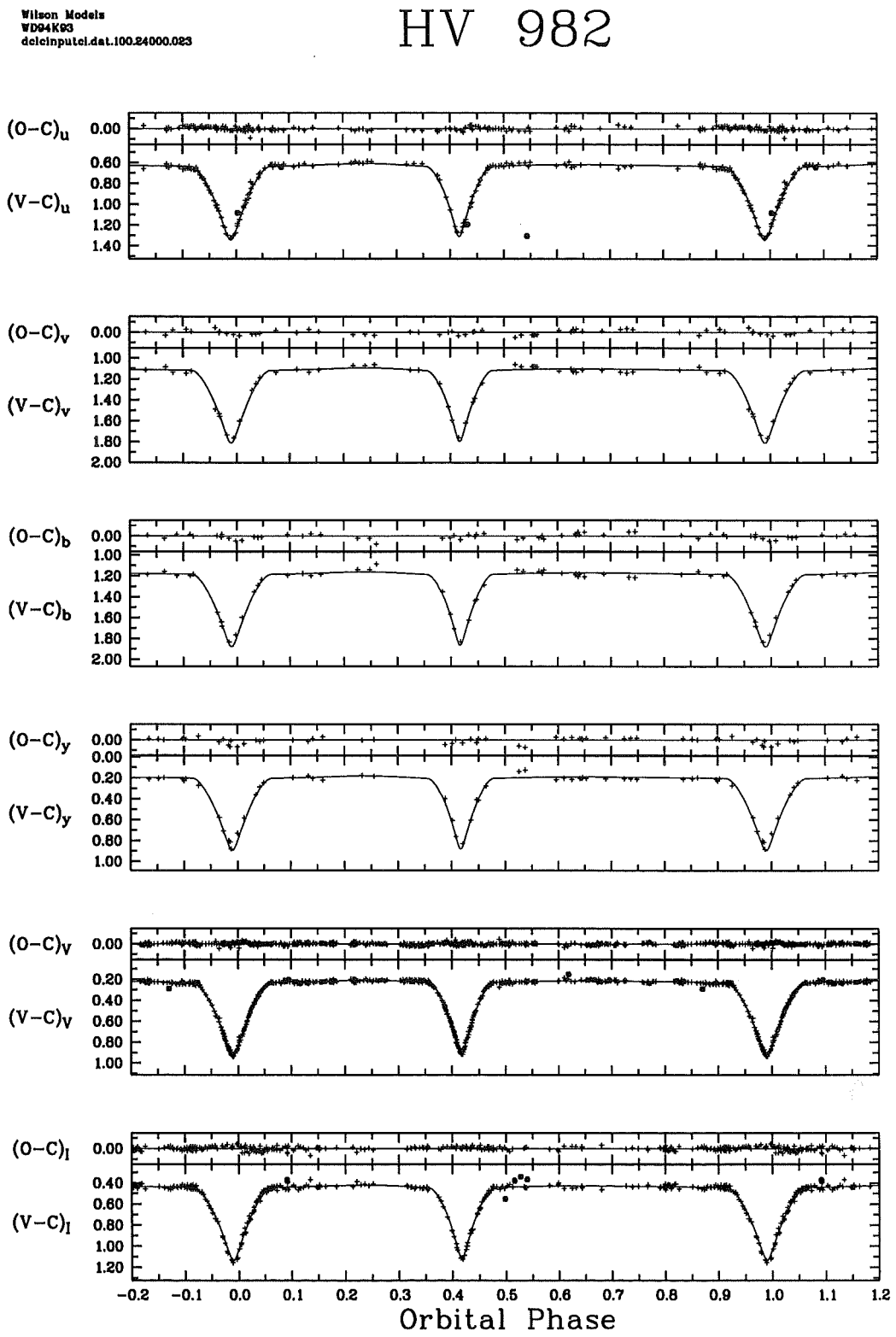

Figure 4.3: A typical preliminary *WD95* fit to the light curves for HV 982. Plotted are the $Variable - Comparison$ differential light curve observations [$(V - C)$ – crosses indicate data points included in the optimization, filled circles indicate excluded points], model light curves (lines) and residuals between Observations and model Computations [$(O - C)$] for each bandpass ($uvbyVI$).

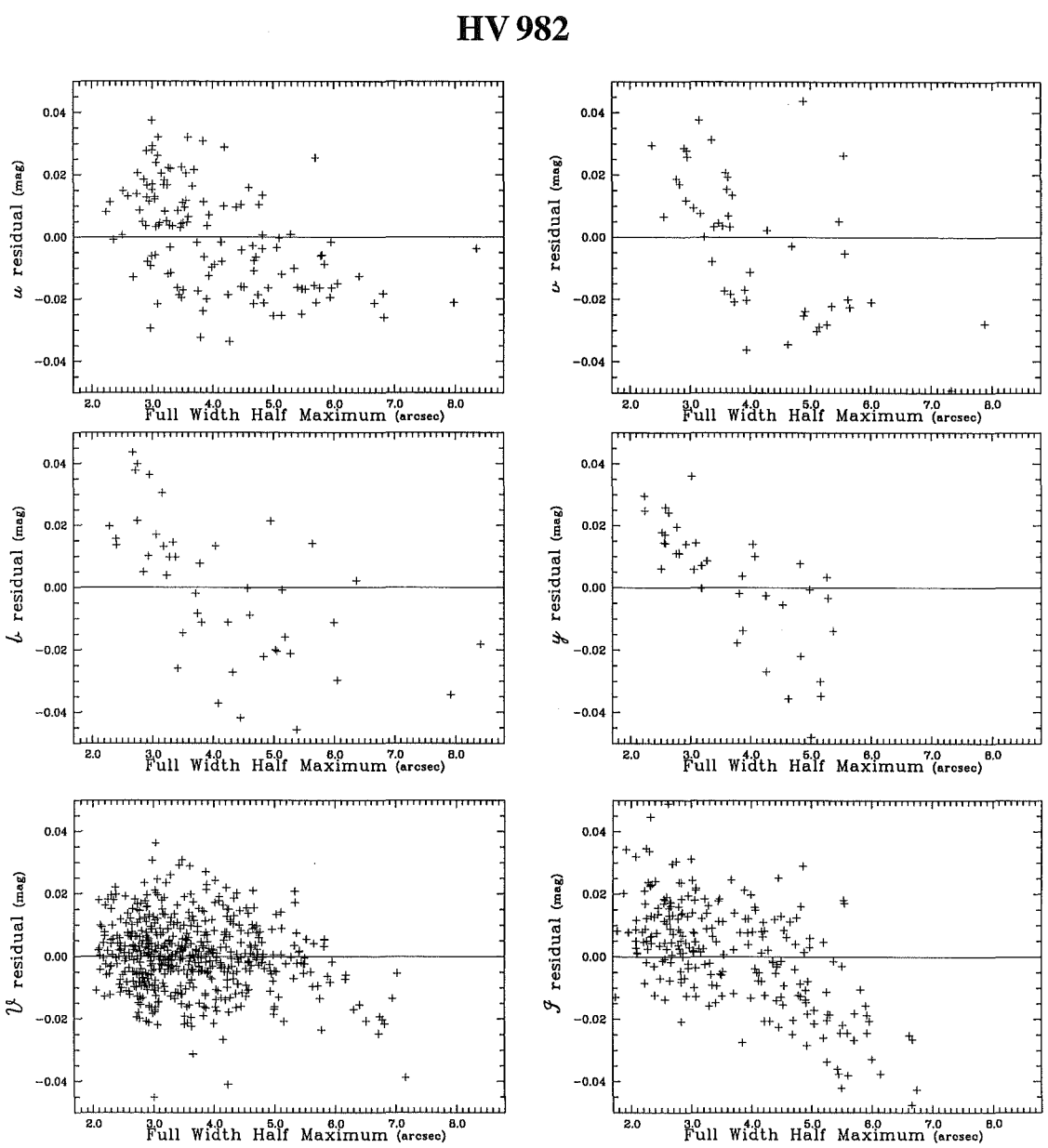

Figure 4.4: Plots of residuals between the observed $Variable - Comparison$ differential photometry and *WD95* synthetic light curves versus the Full Width at Half Maximum for HV 982. Trends in residuals as a function of FWHM are clearly evident in the b and y data and perhaps also in the u and v data. Linear corrections have thus been applied to the $uvby$ $(V - C)$ photometry for further analysis (equations 4.10 to 4.13). In V, observations with FWHM greater than about $6.0''$ appear to be systematically in error and are thus excluded from further analysis. Similarly in I, observations with FWHM greater than $5\overset{''}{.}0$ have been excluded from further analysis.

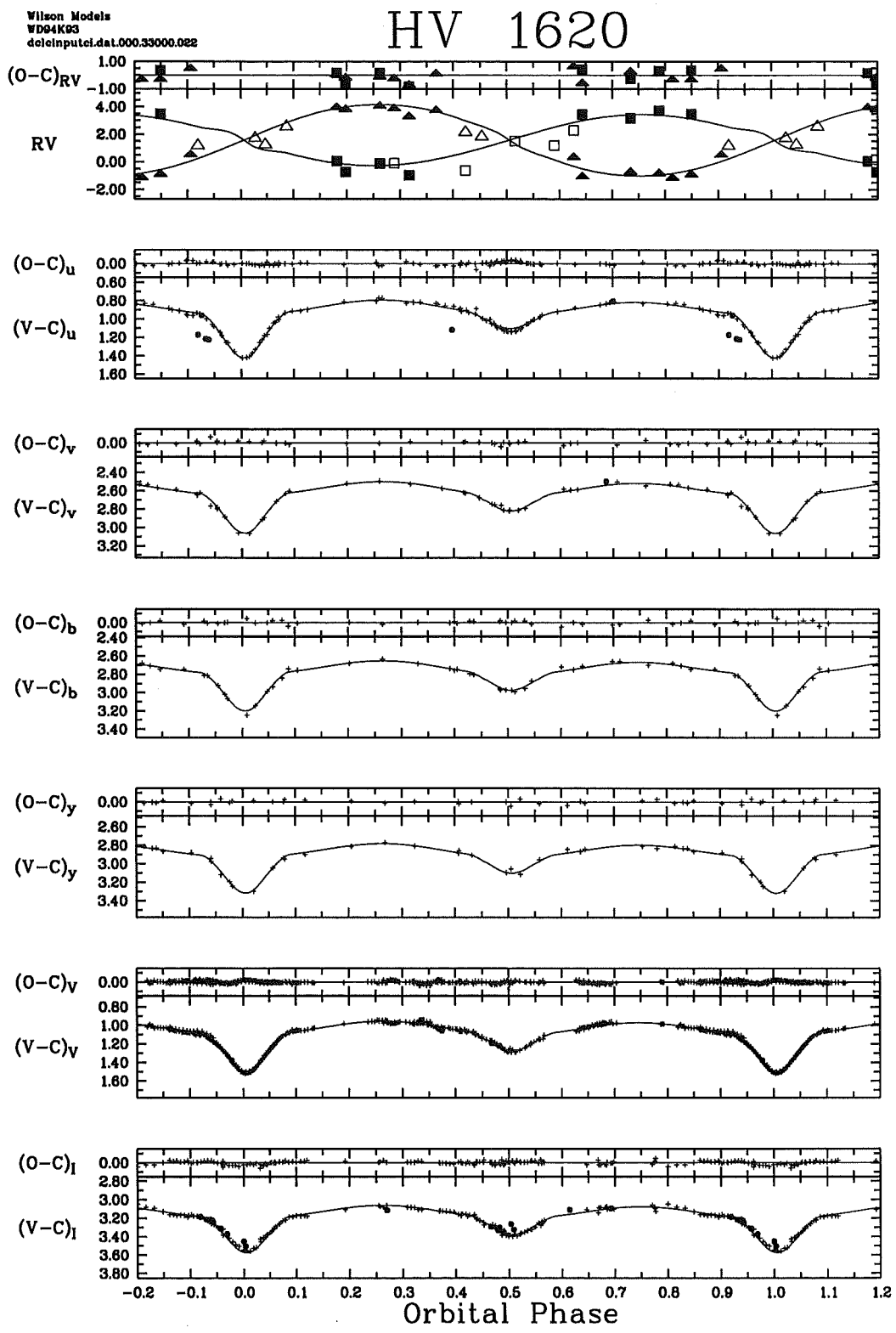

Figure 4.5: A typical preliminary *WD95* fit to the light curves for HV 1620. Plotted are the $Variable - Comparison$ differential light curve observations [$(V - C)$ – crosses indicate data points included in the optimization, filled circles indicate excluded points], model light curves (lines) and residuals between Observations and model Computations [$(O - C)$] for each bandpass ($uvbyVI$). Also shown are the spectroscopic radial-velocity curves (Niemela and Bassino, 1994) (RV – squares for primary component and triangles for secondary component, filled symbols for points included in optimizations, open symbols for excluded points) and residuals to the fit. The RVs are plotted in units of 100 km s^{-1}. The slight departures from sinusoidal curves of the model RV curves of the occulted components about conjunction (i.e. for the primary at orbital phase ~0. and for the secondary at orbital phase ~0.5) result from the so-called proximity effect (see text). The rms scatters of the radial velocity residuals are 51 and 39 km s^{-1} for primary and secondary curves respectively.

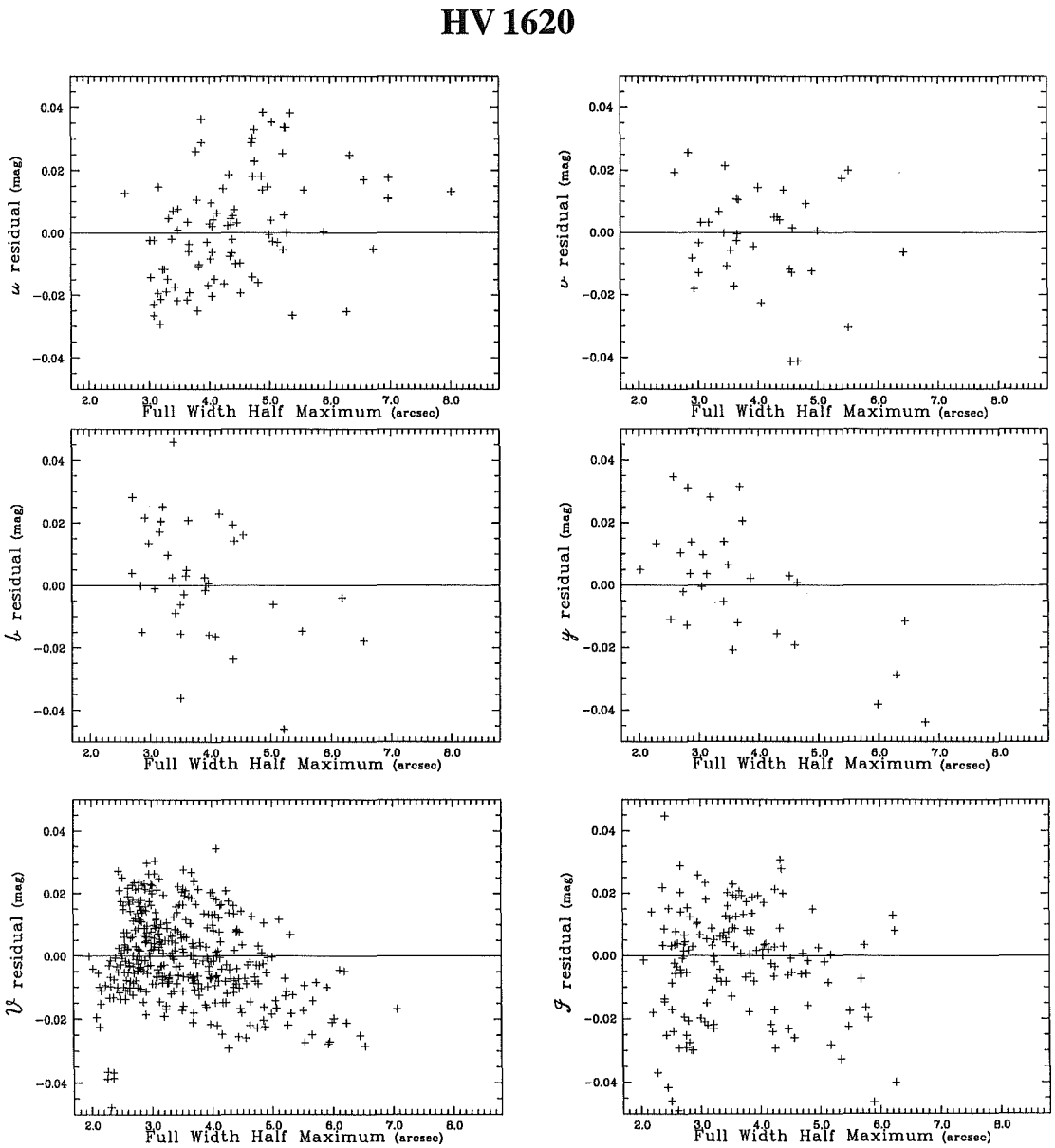

Figure 4.6: Plots of typical residuals between the observed *Variable − Comparison* differential photometry and *WD95* synthetic light curves versus the Full Width at Half Maximum for HV 1620. Clearly, systematic errors affect the b, y, V and I differential photometry for the worst seeing, i.e. FWHM greater than about $5\farcs0$. These observation are thus excluded from further analysis.

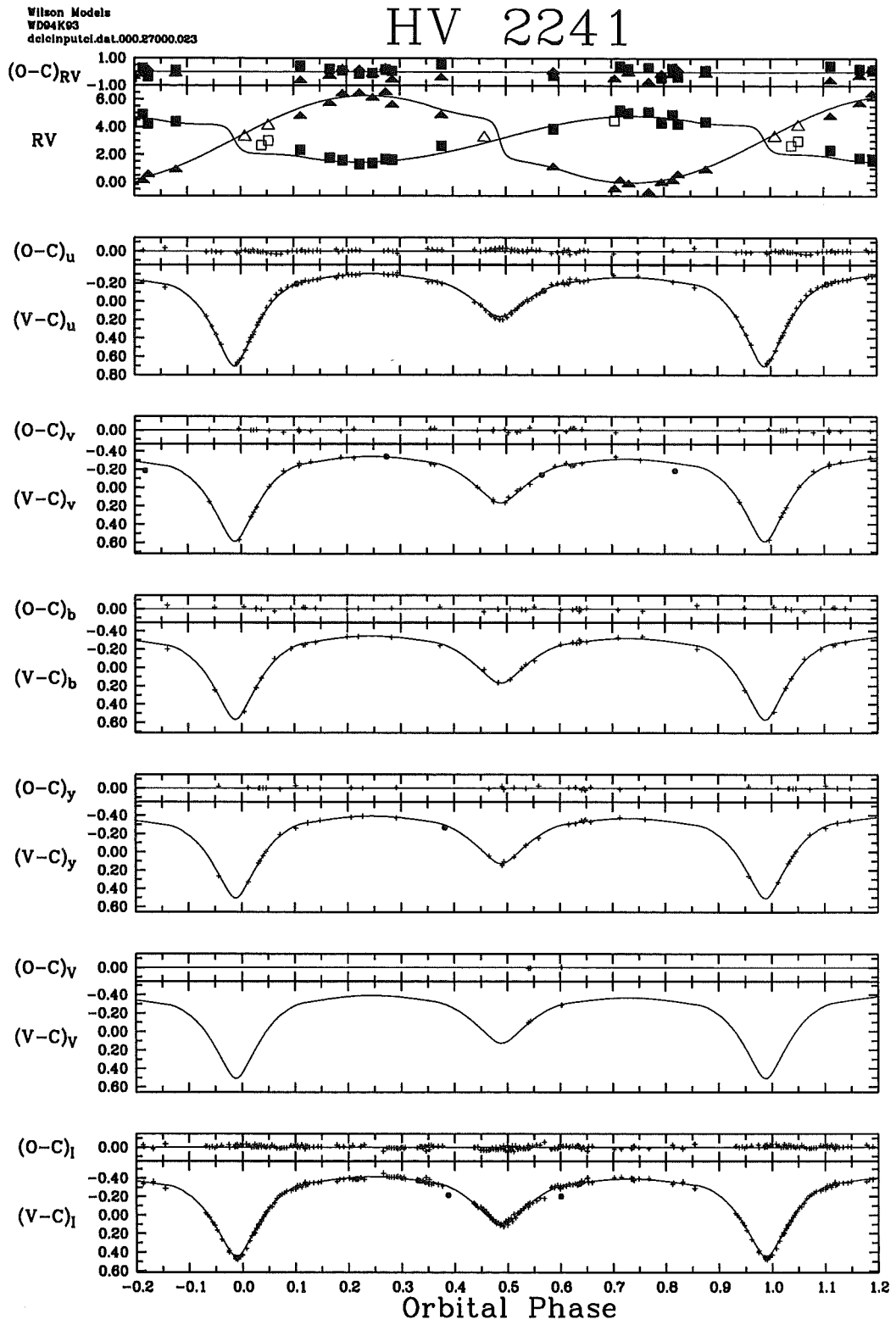

Figure 4.7: A typical preliminary *WD95* fit to the light curves for HV 2241. Plotted are the $Variable - Comparison$ differential light curve observations [$(V - C)$ – crosses indicate data points included in the optimization, filled circles indicate excluded points], model light curves (lines) and residuals between Observations and model Computations [$(O - C)$] for each bandpass ($uvbyVI$). Also shown are the spectroscopic radial-velocity curves (Niemela and Bassino, 1994) (RV – squares for primary component and triangles for secondary component, filled symbols for points included in optimizations, open symbols for excluded points) and residuals to the fit. The RVs are plotted in units of 100 km s^{-1}. The departures from sinusoidal curves of the model RV curves of the occulted components about conjunction (i.e. for the primary at orbital phase $\sim$0. and for the secondary at orbital phase $\sim$0.5) result from the so-called proximity effect (see text). The rms scatters of the radial velocity residuals are 29 and 32 km s^{-1} for primary and secondary curves respectively.

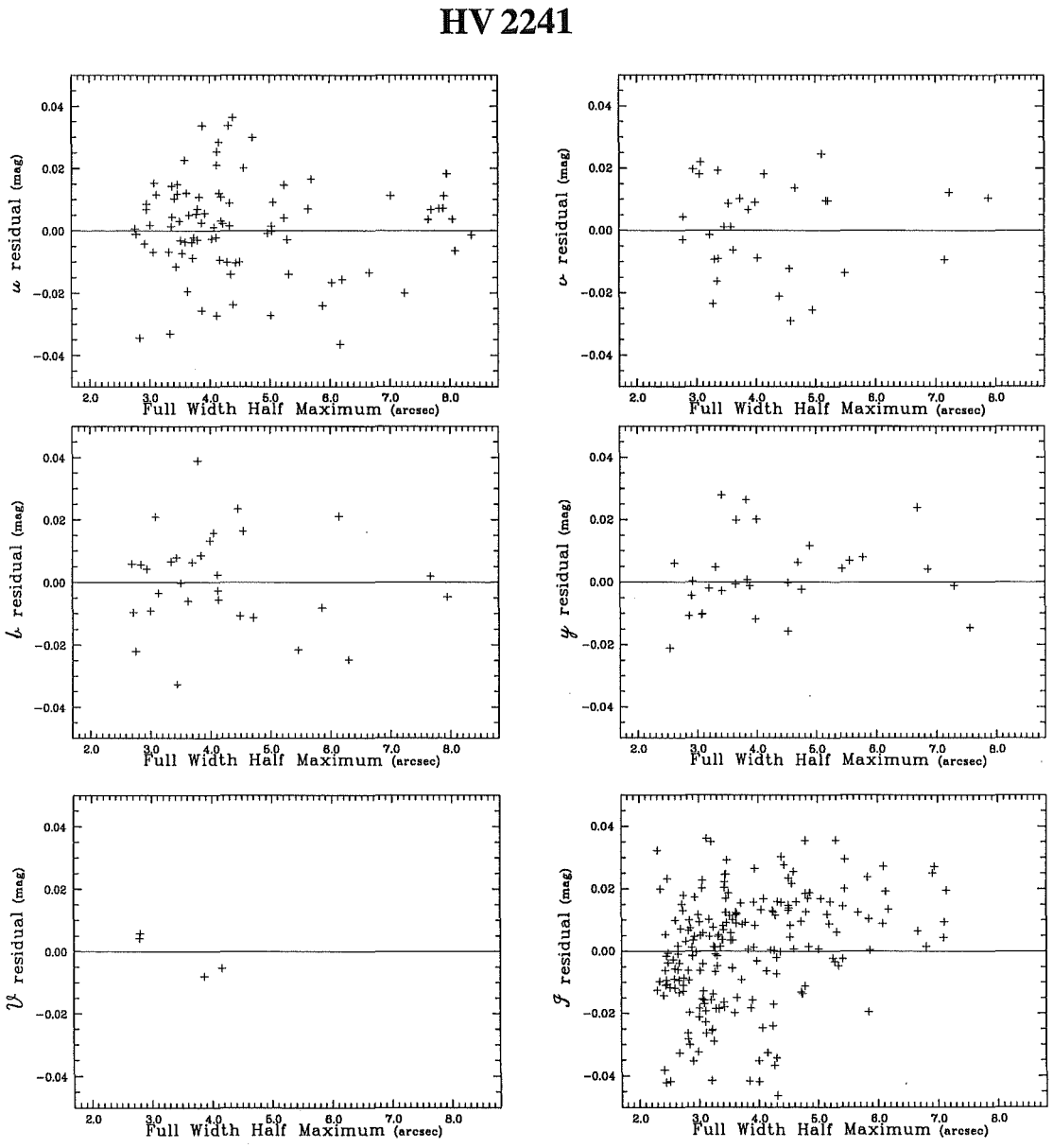

Figure 4.8: Plots of typical residuals between the observed *Variable − Comparison* differential photometry and *WD95* synthetic light curves versus the Full Width at Half Maximum for HV 2241. The residuals are apparently free of systematic errors, except for the I data. A linear correction has thus been applied to correct the I photometry for the slight positive gradient w.r.t. the FWHM (equation 4.14).

Chapter 5

Analysis of Calibration Photometry

The calibration of a given instrumental photometric system in terms of a standard system (or systems) is a highly non-trivial problem. From deciding on the appropriate photometric system to use, to the careful matching of the instrumental response functions to the standard response functions, to obtaining the observations, to the final step of computing the transformation equations, the effort is fraught with complexities and subtleties. Crawford (1993) writes,

> ...there are the effects of rotation, emission, double or multiple stars, line shape, spots, flares, shells, disks, the interstellar matter, variable background, the faintness of our object, seeing, filter leaks, filter cut-off characteristics, filter shapes, time, temperature, atmospheric absorption, clouds, the detector and telescope changes and characteristics, and so on. It all seems designed to trap us with many pitfalls.

All of these aspects have a bearing on the ultimate achievable quality of photometry. It is therefore obviously important that plenty of careful thought be given to exactly what it is that one wishes to use photometry for and to the best means to achieving that goal.

The ultimate goal to which the calibrated standard system photometry obtained for this project is to be applied is the determination of the interstellar reddenings in the direction of the programme stars and the determination of the effective temperatures of the programme stars through the fitting of the observed fluxes to theoretical ones. To this end the MJUO *uvbyVI* photometric system was established. The *uvby* photometry is ideal for measuring the reddening via the intrinsic $(b-y)/c_1$ relationship for OB-type stars. Combining the *uvby* with the extended spectral baseline given by the inclusion of the Cousins I bandpass should lead to improved reliability in the effective temperature determinations. The inclusion of the V bandpass in addition to Strömgren y provides a check on the Strömgren photometry. Because of its generally greater total transmission, the V bandpass also offers the practical advantage of better signal to noise with shorter exposure durations. There is no significant loss of astrophysical information due to the broader bandpass since the stellar spectra of OB-type stars are largely featureless over the spectral range of the V and y bandpasses.

The extraction of instrumental magnitudes from the CCD images obtained for calibration of the Mount John University Observatory *uvbyVI* photometric system was described in section 3.4. In the first section of this chapter, theoretical transformation equations are derived in full. Then transformation equation coefficients are derived from the standard star observations. Next, standard system photometry, i.e. magnitudes, colours and indices are derived for the three programme stars HV 982, HV 1620 and HV 2241. IUE SWP spectrophotometry of the three programme stars is then presented. Following that, total and foreground reddenings of the programme stars are determined and the adopted interstellar extinction laws are presented. Absolute, bandpass integrated fluxes for the standard *uvby* and *UBVRI* systems are then derived from standard system photometry and convolutions of the standard bandpasses with the Kurucz (1993) model stellar atmosphere for Vega. Spectral flux distributions for the programme stars, derived from preliminary light curve fits, are then compared with the dereddened IUE spectrophotometry and absolute *uvbyVI* fluxes and the absolute temperatures of the programme stars are determined.

5.1 Definition of the transformations equations

5.1.1 Generalized transformation equations

Ultimately, for each bandpass (denoted in the following by $\bar{\lambda}$, the *mean wavelength* of the bandpass, see equation D.43) a transformation from an observed instrumental magnitude ($m_{\bar{\lambda},\mathrm{inst}}$) to the standard system magnitude ($M_{\bar{\lambda}}$) is required. The derivation that follows is based on the model outlined by Harris et al. (1981).

Considering first the effect of the atmosphere, the following relationship between the *observed* instrumental magnitudes ($m_{\bar{\lambda},\mathrm{inst}}$) and the *extra-atmospheric* instrumental magnitudes ($m_{\bar{\lambda},\mathrm{inst},0}$) is assumed,

$$m_{\bar{\lambda},\mathrm{inst}} = m_{\bar{\lambda},\mathrm{inst},0} + k_{\bar{\lambda}}X, \tag{5.1}$$

where $k_{\bar{\lambda}}$ is the atmospheric extinction and X is the airmass of observation. Second-order terms in the extinction can be easily incorporated in this model simply be defining,

$$k_{\bar{\lambda}} = k'_{\bar{\lambda}} + k''_{\bar{\lambda}}(m_{\bar{\lambda}_3} - m_{\bar{\lambda}_4})_{\mathrm{inst},0}, \tag{5.2}$$

where $(m_{\bar{\lambda}_3} - m_{\bar{\lambda}_4})_{\mathrm{inst},0}$ is an extra-atmospheric instrumental colour (e.g. $(V-I)$), preferably at the time of observation.

Once extra-atmospheric instrumental magnitudes have been determined from the observations, these must be *transformed* to the standard system. The transformation between the extra-atmospheric instrumental magnitude and standard system magnitude ($M_{\bar{\lambda}}$) is defined by the following,

$$m_{\bar{\lambda},\mathrm{inst},0} = \sum_{i=0} \alpha_{\bar{\lambda},i} M^i_{\bar{\lambda}} + \sum_{j=1} \beta_{\bar{\lambda},j}((m_{\bar{\lambda}_3} - m_{\bar{\lambda}_4})_{\mathrm{inst},0})^j. \tag{5.3}$$

As per Harris et al. (1981), equations 5.1 and 5.3 can be combined, yielding,

$$m_{\bar{\lambda},\mathrm{inst}} = \sum_{i=0} \alpha_{\bar{\lambda},i} M^i_{\bar{\lambda}} + \sum_{j=1} \beta_{\bar{\lambda},j}((m_{\bar{\lambda}_3} - m_{\bar{\lambda}_4})_{\mathrm{inst},0})^j + k_{\bar{\lambda}}X. \tag{5.4}$$

For the transformation of an instrumental colour ($m_{\bar{\lambda}_1,\mathrm{inst}} - m_{\bar{\lambda}_2,\mathrm{inst}}$) to the corresponding standard system colour ($M_{\bar{\lambda}_1} - M_{\bar{\lambda}_2}$), generalizing equation 5.1 gives,

$$\begin{aligned} (m_{\bar{\lambda}_1,\mathrm{inst}} - m_{\bar{\lambda}_2,\mathrm{inst}}) &= (m_{\bar{\lambda}_1,\mathrm{inst},0} + k_{\bar{\lambda}_1}X_{\bar{\lambda}_1}) - (m_{\bar{\lambda}_2,\mathrm{inst},0} + k_{\bar{\lambda}_2}X_{\bar{\lambda}_2}), & (5.5)\\ &= (m_{\bar{\lambda}_1,\mathrm{inst},0} - m_{\bar{\lambda}_2,\mathrm{inst},0}) + (k_{\bar{\lambda}_1}X_{\bar{\lambda}_1} - k_{\bar{\lambda}_2}X_{\bar{\lambda}_2}), & (5.6)\end{aligned}$$

where the $k_{\bar{\lambda}_\mathrm{i}}$ are the extinction coefficient and the $X_{\bar{\lambda}_\mathrm{i}}$ are the airmasses of the observations in the $\bar{\lambda}_\mathrm{i}$ bandpasses. Ideally, the observations of the two magnitudes should be made simultaneously so that $X_{\bar{\lambda}_1} = X_{\bar{\lambda}_2}$ but this is not possible with the Mount John University Observatory CCD system. However if the observations are close enough that the difference between the two airmasses is small, then considering the mean airmass of the two observations $\bar{X}_{\bar{\lambda}_1\bar{\lambda}_2}$, the following approximation is plausible,

$$(m_{\bar{\lambda}_1,\mathrm{inst}} - m_{\bar{\lambda}_2,\mathrm{inst}}) \approx (m_{\bar{\lambda}_1} - m_{\bar{\lambda}_2})_{,\mathrm{inst},0} + k_{\bar{\lambda}_1\bar{\lambda}_2}\bar{X}_{\bar{\lambda}_1\bar{\lambda}_2}. \tag{5.7}$$

where $k_{\bar{\lambda}_1\bar{\lambda}_2}$ is the extinction term for the colour $(m_{\bar{\lambda}_1} - m_{\bar{\lambda}_2})$ (i.e. $k_{\bar{\lambda}_1\bar{\lambda}_2} = k_{\bar{\lambda}_1} - k_{\bar{\lambda}_2}$) since

$$(m_{\bar{\lambda}_1,\mathrm{inst}} - m_{\bar{\lambda}_2,\mathrm{inst}}) \equiv (m_{\bar{\lambda}_1} - m_{\bar{\lambda}_2})_{,\mathrm{inst},0} \tag{5.8}$$

Reexamining equation 5.4 with equation 5.7 it is evident that,

$$m_{\bar{\lambda},\mathrm{inst}} = \sum_{i=0} \alpha_{\bar{\lambda},i} M^i_{\bar{\lambda}} + \sum_{j=1} \beta_{\bar{\lambda},j}((m_{\bar{\lambda}_3,\mathrm{inst}} - m_{\bar{\lambda}_4,\mathrm{inst}}) - k_{\bar{\lambda}_3\bar{\lambda}_4}\bar{X}_{\bar{\lambda}_3\bar{\lambda}_4})^j + k_{\bar{\lambda}}X, \tag{5.9}$$

and generalizing equation 5.9 gives,

$$\begin{aligned} (m_{\bar{\lambda}_1,\mathrm{inst}} - m_{\bar{\lambda}_2,\mathrm{inst}}) &= \sum_{i=0}\left[\alpha_{\bar{\lambda}_1,i}M^i_{\bar{\lambda}_1} - \alpha_{\bar{\lambda}_2,i}M^i_{\bar{\lambda}_2}\right] + \\ &\quad \sum_{j=1}\left\{\beta_{\bar{\lambda}_1,j}\left[(m_{\bar{\lambda}_3,\mathrm{inst}} - m_{\bar{\lambda}_4,\mathrm{inst}}) - k_{\bar{\lambda}_3\bar{\lambda}_4}\bar{X}_{\bar{\lambda}_3\bar{\lambda}_4}\right]^j\right\} - \\ &\quad \sum_{j=1}\left\{\beta_{\bar{\lambda}_2,j}\left[(m_{\bar{\lambda}_3,\mathrm{inst}} - m_{\bar{\lambda}_4,\mathrm{inst}}) - k_{\bar{\lambda}_3\bar{\lambda}_4}\bar{X}_{\bar{\lambda}_3\bar{\lambda}_4}\right]^j\right\} + \\ &\quad (k_{\bar{\lambda}_1}X_{\bar{\lambda}_1} - k_{\bar{\lambda}_2}X_{\bar{\lambda}_2}), & (5.10)\\ &\approx \sum_{i=0}\alpha_{\bar{\lambda}_1\bar{\lambda}_2,i}(M_{\bar{\lambda}_1} - M_{\bar{\lambda}_2})^i + \\ &\quad \sum_{j=1}\beta_{\bar{\lambda}_1\bar{\lambda}_2,j}\left[(m_{\bar{\lambda}_3,\mathrm{inst}} - m_{\bar{\lambda}_4,\mathrm{inst}}) - k_{\bar{\lambda}_3\bar{\lambda}_4}\bar{X}_{\bar{\lambda}_3\bar{\lambda}_4}\right]^j + \\ &\quad k_{\bar{\lambda}_1\bar{\lambda}_2}\bar{X}_{\bar{\lambda}_1\bar{\lambda}_2}. & (5.11)\end{aligned}$$

5.1.2 The adopted transformation equations for the MJUO photometric system

The Mount John University Observatory *uvbyVI* photometric system is of course based on the Strömgren *uvby* system and on V and I of the Cousins $UBVRI$ system. Transformations from the observed, instrumental u, v, b, y, V and I magnitudes to the standard V magnitude and colour indices ($(V-I)$, $(b-y)$, $\mathrm{c_1}$ and $\mathrm{m_1}$) are thus required. However, the physical meaning of the various terms in the transformation equations for the non-standard Strömgren colours $(u-b)$ and $(v-b)$ are more obvious than for the more usual indices $\mathrm{c_1}$ and $\mathrm{m_1}$. It is therefore simpler to derive transformations for these two colours and to derive transformed $\mathrm{c_1}$ and $\mathrm{m_1}$ indices from the transformed colours than to derive transformations for the $\mathrm{c_1}$ and $\mathrm{m_1}$ indices directly.

Various forms of the transformation equations were investigated (see section 5.2 below) before adopting the following equations derived from equations 5.9 and 5.11. For the colours $(V-I)$, $(b-y)$, $(v-b)$ and $(u-b)$,

$$(V_{\rm inst}-I_{\rm inst}) = \alpha_{(V-I)}+(V-I)+\beta_{(V-I)}(V_{\rm inst}-I_{\rm inst})+(1-\beta_{(V-I)})k_{(V-I)}\bar{X}_{(V-I)} \quad (5.12)$$

$$(b_{\rm inst}-y_{\rm inst}) = \alpha_{(b-y)}+(b-y)+\beta_{(b-y)}(b_{\rm inst}-y_{\rm inst})+(1-\beta_{(b-y)})k_{(b-y)}\bar{X}_{(b-y)}, \quad (5.13)$$

$$(v_{\rm inst}-b_{\rm inst}) = \alpha_{(v-b)}+(v-b)+\beta_{(v-b)}(v_{\rm inst}-b_{\rm inst})+(1-\beta_{(v-b)})k_{(v-b)}\bar{X}_{(v-b)}, \quad (5.14)$$

$$(u_{\rm inst}-b_{\rm inst}) = \alpha_{(u-b)}+(u-b)+\beta_{(u-b)}(u_{\rm inst}-b_{\rm inst})+(1-\beta_{(u-b)})k_{(u-b)}\bar{X}_{(u-b)}. \quad (5.15)$$

while for the V magnitude,

$$y_{\rm inst} = \alpha_y+V+\beta_y\left[(b_{\rm inst}-y_{\rm inst})-k_{(b-y)}\bar{X}_{(b-y)}\right]+k_yX_y, \quad (5.16)$$

$$V_{\rm inst} = \alpha_V+V+\beta_V\left[(V_{\rm inst}-I_{\rm inst})-k_{(V-I)}\bar{X}_{(V-I)}\right]+k_VX_V, \quad (5.17)$$

give the transformations from both $y_{\rm inst}$ and $V_{\rm inst}$. In addition it is not unreasonable to transform from $I_{\rm inst}$ to I directly,

$$I_{\rm inst} = \alpha_I+I+\beta_I\left[(V_{\rm inst}-I_{\rm inst})-k_{(V-I)}\bar{X}_{(V-I)}\right]+k_IX_I. \quad (5.18)$$

Note that only first order colour and extinction terms have been retained and that $\alpha_{\bar{\lambda},1}\equiv 1$, which is equivalent to assuming a linear response of the detector, has been adopted. It is convenient to list the following two definitions,

$$\mathrm{c_1} = (u-v)-(v-b), \quad (5.19)$$

$$\mathrm{m_1} = (v-b)-(b-y). \quad (5.20)$$

Transformed $\mathrm{m_1}$ indices can be calculated from the transformed $(v-b)$ and $(b-y)$ colours according to equation 5.20, transformed $\mathrm{c_1}$ indices can be calculated from

$$\mathrm{c_1} = (u-b)-2(v-b). \quad (5.21)$$

'Catalogue' values for the non-standard Strömgren colours can be derived from the standard $(b-y)$, $\mathrm{c_1}$ and $\mathrm{m_1}$ colour indices as follows:

$$(u-b) = \mathrm{c_1}+2\mathrm{m_1}+2(b-y), \quad (5.22)$$

$$(v-b) = \mathrm{m_1}+(b-y). \quad (5.23)$$

Magnitudes in the MJUO photometric system bandpasses

Since the photometry is ultimately to be used to define the spectral flux distributions of the programme stars, it is obviously desirable to define 'standard system magnitudes' for each observed bandpass in addition to the one magnitude derived above, namely V. Once again, these are simply derived from the standard system magnitude and colour indices. It is necessary to a priori adopt some means by which to place the Strömgren system on an absolute scale. Adopting $y\equiv V$,[1] after a trivial amount of algebra, the following are obtained:

$$I = V-(V-I), \quad (5.24)$$

[1] Investigations using synthetic photometry derived from the Kurucz (1993) stellar atmosphere models show that over the range of temperature applicable to the programme stars (i.e. 20000K to 40000K), the systematic error introduced in the adoption of $y\equiv V$ is likely of the order of several thousandths of a magnitude. This is in accord with the claim by Crawford (1975a) that the V apparent visual magnitude defined by the standard star data of Crawford and Barnes (Crawford and Barnes, 1970) is '...essentially (within ± 0.01 mag) the same magnitude system as V of the UBV system (Johnson and Morgan, 1953).'

$$y = V, \tag{5.25}$$
$$b = V + (b - y), \tag{5.26}$$
$$v = V + 2(b - y) + \mathrm{m}_1, \tag{5.27}$$
$$u = V + 3(b - y) + 2\mathrm{m}_1 + \mathrm{c}_1. \tag{5.28}$$

5.2 Determination of the transformation equation coefficients

Determination of the transformation equations effectively reduces to the solution of the systems of simultaneous equations. For example, rewriting equation 5.17 as follows,

$$((V_{\mathrm{inst}} - I_{\mathrm{inst}}) - (V - I))_i = \alpha_{(V-I)} + \beta_{(V-I)}(V_{\mathrm{inst}} - I_{\mathrm{inst}})_i + (1 - \beta_{(V-I)})k_{(V-I)}\bar{X}_{(V-I),i}, \tag{5.29}$$

where i indexes the N observations from which the unknown transformation coefficients ($\alpha_{(V-I)}$, $\beta_{(V-I)}$ and $k_{(V-I)}$) are to be determined, it is immediately obvious that this equation can be written in the form of the matrix equation,

$$AX = B \tag{5.30}$$

where,

$$A = \begin{bmatrix} 1 & (V_{\mathrm{inst}} - I_{\mathrm{inst}})_1 & \bar{X}_{(V-I),1} \\ 1 & (V_{\mathrm{inst}} - I_{\mathrm{inst}})_2 & \bar{X}_{(V-I),2} \\ \vdots & \vdots & \vdots \\ 1 & (V_{\mathrm{inst}} - I_{\mathrm{inst}})_N & \bar{X}_{(V-I),N} \end{bmatrix}, \tag{5.31}$$

$$X = \begin{bmatrix} \alpha_{(V-I)} \\ \beta_{(V-I)} \\ (1 - \beta_{(V-I)})k_{(V-I)} \end{bmatrix}, \tag{5.32}$$

$$B = \begin{bmatrix} ((V_{\mathrm{inst}} - I_{\mathrm{inst}}) - (V - I))_1 \\ ((V_{\mathrm{inst}} - I_{\mathrm{inst}}) - (V - I))_2 \\ \vdots \\ ((V_{\mathrm{inst}} - I_{\mathrm{inst}}) - (V - I))_N \end{bmatrix}. \tag{5.33}$$

Therefore the transformation equation coefficients are simply the solution of the matrix inversion problem,

$$X = A^{-1}B. \tag{5.34}$$

Since the matrix will generally be over-determined, i.e. there will be many more rows in A and B than in X, the solution must be found in a least squares sense. It is a straightforward exercise to vectorize all of the relevant transformation equations in this way. The numerical computation and visualization software package MATLAB was used extensively for the investigation of the behavior of the derived transformation coefficients as different forms of the transformation equations were tested and as different sets of data were used in different combinations.

The best results, in terms of the minimum scatter of the residuals between the transformed and catalogue standard star photometry were obtained when the data from the five VI nights and the three *uvby* nights were combined together into two large data sets. For each transformation equation the combined data sets were used to determine a single value of the β coefficients, but nightly values of the α or zero-point coefficients and k (i.e. extinction) coefficients.

Obviously, atmospheric extinction can be expected to vary from night to night. It's not necessarily quite so obvious however that the zero-point coefficient should vary from night to night since the most obviously variable component of the optical system, i.e. the atmosphere has supposedly already been accounted for via the extinction coefficient. However contributions to variations in the zero-point coefficients can be expected from changes in the transmission, reflection or detection efficiency of the other components in the optical system, namely the filters, mirrors and detector. Certainly the reflectivity of the mirror can be expected to vary over long time-scales as the aluminium coating cyclically becomes tarnished and is re-applied (section 2.1.1). While the spectral response of the detector is generally not expected to vary significantly either over time or from pixel to pixel, as discussed in section 2.3.3 the flat-fielding procedure is known not to fully correct for low spatial frequency variations of the quantum efficiency. Thus photometry obtained at various locations on the chip can reasonably be expected to require different zero-point corrections. During any

given night of calibration observations, each observation was made with the star as nearly as possible at the same position, however from night to night, different positions on the chip were quite deliberately selected in order to check for such systematic effects. The possibility of variation of the transmission efficiency of the filters can not be excluded, but any significant variations over the applicable time-scale seem unlikely.

A single β coefficient for each transformation makes sense since the β coefficients embody most of the differences between the instrumental and standard system response functions. As discussed above, while the overall level of the various transmission, reflection and detection efficiencies can reasonably be expected to vary over time-scales of nights to months, or as a function of the position of the chip used, the spectral dependence of the various functions, especially over the bandwidths of the overall bandpasses can reasonably be expected not to vary significantly.

However it was found that some of the extinction coefficients formally varied from night to night by significantly more than would be expected from variations in the transmission of the atmosphere alone. For example, the y extinction coefficient for the night of 1995-Sep-18 was found to be $\sim$0.44 while the following night it was $\sim$0.18, and slightly more than a month later on the 25th of October it was $\sim$0.14. Similar trends were seen in all of the *uvby* extinction coefficients. Moreover, the high extinction coefficients were correlated with lower zero-point coefficients (5.19, 5.43 and 5.45 respectively for y for the three nights). Similar trends of surprisingly large nightly variations in the extinction coefficients correlated with compensating adjustments in the zero-point coefficients were also identified in the *VI* results.

Despite such obvious effects in the coefficients, in general, no particularly obvious trends are evident in plots of magnitude, colour, Coordinated Universal Time (UTC) or seeing against airmass for each observation (see figures B.9 to B.11) or in plots of the residuals between transformed and catalogue standard star photometry against UTC, airmass, colour, magnitude and telescope orientation (see figures B.12 to B.16).

Nonetheless, the variations in the extinction coefficients and zero-points are most likely to be artifacts of the less-than-ideal data sets upon which the determinations rely. Due to observational constraints, apart from one night when 58 standard star measurements were obtained (1995-Feb-12), the number of measurements was in general $\sim$30 or less. Furthermore, due to the shortage of suitable faint blue standard stars with well defined and reliable standard system photometry, the number of different standard stars observed on any given night was only $\sim$10. In order to investigate this problem, the residuals between transformed and catalogue standard star photometry based on 'mean' transformation equation coefficients were examined. Mean coefficients were estimated in the following way. The β coefficients (i.e. the colour coefficients) determined from the least squares fits as above were adopted. One representative extinction coefficient for each transformation was adopted for all nights. Zero-point coefficients were calculated so as to set the mean of the residuals to zero. The scatter of the resulting residuals does not differ significantly from that obtained from the least squares fits. Moreover the resulting standard system photometry for the programme stars differs insignificantly between the two methods. Therefore the mean transformation equation coefficients have been adopted. The following two sections provide summary tables of the adopted transformation equation coefficients and other data regarding the determinations for the *VI* and *uvby* photometry respectively.

Clearly, a more complete study based on a larger data base is required before full confidence in the accuracy and precision of transformations from the MJUO *uvbyVI* instrumental photometric system to the standard photometric systems is possible.

5.2.1 *VI* standard star photometry

The adopted V, I and $(V-I)$ mean transformation equation coefficients are listed in table 5.1. Further information regarding the standard star calibration photometry is tabulated in table 5.2.

Table 5.3 summarizes the information regarding the exclusion of certain observations from the determination of the transformation coefficients. The reasons for the exclusion of THPE-B (variable), THPE-E (misidentified) and Feige 110 (extreme airmass) are self-evident. DM -24 3988 and DM -07 3477 were excluded based on their consistently large residuals between their transformed and catalogue photometry. This is likely due to the fact that their catalogue photometry (Menzies et al., 1990) is not especially well defined. The Menzies et al. (1990) catalogue is in fact the compilation of photometry from a 'pilot survey' only. As a result, the I photometry for DM -24 3988 is based on one measurement only while the V photometry is based on just four. Obviously this leads to some doubt as to the precision and accuracy of the catalogue photometry for this star and therefore its suitability as a standard star. In the case of DM -07 3477, although the photometry is based on a larger number of measurements (6 and 24 for I and V respectively), the quoted standard deviation for the $(V-I)$ photometry is 0.031 mag, which likewise casts doubts over the suitability of this star as a standard.

Examining the residuals listed in table 5.2, it is clear that the V photometry is more reliable than both

Table 5.1: Adopted V, I and $(V-I)$ *mean* transformation equation coefficients for the five nights of 1994-Dec-26, 1995-Feb-12, 1995-Sep-02, 1995-Sep-03 and 1995-Oct-23. These coefficients derive from the $24''$ synthetic aperture.

	Coefficient	$V-I$	V	I
α	1994-Dec-26	−0.5782	3.8335	4.4108
	1995-Feb-12	−0.5616	3.8067	4.3674
	1995-Sep-02	−0.5349	3.8130	4.3466
	1995-Sep-03	−0.5173	3.8231	4.3397
	1995-Oct-23	−0.5423	3.8654	4.4064
β		−0.0566	0.0246	0.0786
k		0.0500	0.1500	0.1000

Table 5.2: Further information regarding the *VI* standard star observations. The columns give the (MIDAS) row and column of the location at which all stars where positioned, the telescope orientation (N for *North of the Pole*, S for *South of the Pole*, see section 2.1.1), the number of different standard stars observed on a given night (N_S), number of measurements included in the transformation equation coefficient determinations (N_M) and the standard deviations of differences between the transformed and catalogue magnitudes and colour. The last row of the table lists results for the combined data set.

Date	Row	Col	N/S	As	N_S	N_M	σ_{V-I}	σ_V	σ_I
1994-Dec-26	163	142	S	HV 982	9	32	0.030	0.006	0.031
1995-Feb-12	174	271	S	HV 1620	11	58	0.035	0.015	0.038
1995-Sep-02	110	452	N	HV 2241	7	20	0.029	0.017	0.028
1995-Sep-03	110	452	N	HV 2241	11	30	0.040	0.008	0.040
1995-Oct-23	110	452	N	HV 2241	8	21	0.033	0.012	0.032
Overall					19	161	0.034	0.012	0.035

the I and the $(V-I)$ photometry. This can likely be attributed to short time scale variations in the strengths of three atmospheric absorption features. The I bandpass, extending from about 700nm to 900nm includes two strong water molecule absorption bands (centered at λ720nm and λ820nm) and the Fraunhoffer A band (O_2) at λ760nm.

5.2.2 *uvby* standard star photometry

The adopted V, $(b-y)$, $(v-b)$ and $(u-b)$ mean transformation equation coefficients are listed in table 5.4. Further information regarding the standard star calibration photometry is tabulated in table 5.5.

Table 5.6 summarizes the information regarding the exclusion of certain observations from the determination of the transformation coefficients. Full details are given below,

- **1995-Sep-18**
  The $(b-y)$ residual for the first *uvby* measurement of E710 is exceptionally large in comparison with all other $(b-y)$ residuals. Although no obvious cause can be established, a procedural error at the time of observation can not be ruled out. The relevant observing log is confusing and does not lend confidence. For consistency, observations in all four bandpasses for this measurement have been excluded from the coefficient determinations.

- **1995-Sep-19**
  Weather conditions deteriorated rather quickly soon after completing the HV 982 observations at approximately UTC15:10. Examination of the residuals between the transformed y[2] magnitude and the catalogue V magnitude indicate observations up until approximately UTC15:30 are unaffected by the change in the sky conditions, however the appearance of cloud at or around UTC15:30 significantly degrades the y photometry thereafter. Thus all observations obtained after UTC15:30 have been excluded from the determinations of the transformation equation coefficients.

[2] Although $y_{\rm inst}$ is transformed to V and so one should technically write '...the transformed V magnitude...', to avoid confusion with the $V_{\rm inst}$ to V transformation it is convenient to write '...the transformed y magnitude...' where it is implicitly understood that the quantity being considered is the V magnitude obtained from the transformation of the instrumental y photometry.

Table 5.3: This table lists the frames excluded from the *VI* transformation coefficient determinations.

Date	Frame	Identity	Filter	Reason for exclusion
1994-Dec-26	T6040033	THPE-B	*V*	Known variable[a]
	T6040034	THPE-B	*I*	Known variable
	T6040035	THPE-B	*I*	Known variable
	T6040036	THPE-B	*V*	Known variable
	T6050005	THPE-E	*V*	Misidentified?[b]
	T6050006	THPE-E	*I*	Misidentified?
	T6050007	THPE-E	*I*	Misidentified?
	T6050008	THPE-E	*V*	Misidentified?
	T6060018	DM −24 3988	*V*	Anomalous Residual
	T6060019	DM −24 3988	*I*	Anomalous Residual
	T6060020	DM −24 3988	*I*	Anomalous Residual
	T6060021	DM −24 3988	*V*	Anomalous Residual
	T6070001	DM −24 3988	*V*	Anomalous Residual
	T6070002	DM −24 3988	*I*	Anomalous Residual
	T6070003	DM −24 3988	*I*	Anomalous Residual
	T6070004	DM −24 3988	*V*	Anomalous Residual
1995-Feb-12	T8220009	DM −24 3988	*V*	Anomalous Residual
	T8220010	DM −24 3988	*I*	Anomalous Residual
	T8220011	DM −24 3988	*I*	Anomalous Residual
	T8220012	DM −24 3988	*V*	Anomalous Residual
	T8260001	DM −07 3477	*V*	Anomalous Residual
	T8260002	DM −07 3477	*V*	Anomalous Residual
	T8260003	DM −07 3477	*I*	Anomalous Residual
	T8260004	DM −07 3477	*I*	Anomalous Residual
	T8260033	DM −07 3477	*V*	Anomalous Residual
	T8260034	DM −07 3477	*I*	Anomalous Residual
	T8260035	DM −07 3477	*I*	Anomalous Residual
	T8260036	DM −07 3477	*V*	Anomalous Residual
1995-Sep-02	T8730020	THPE-B	*V*	Known variable
	T8730021	THPE-B	*I*	Known variable
	T8730022	THPE-B	*I*	Known variable
	T8730023	THPE-B	*V*	Known variable
	T8730024	THPE-E	*V*	Misidentified?
	T8730025	THPE-E	*I*	Misidentified?
	T8730026	THPE-E	*I*	Misidentified?
	T8730027	THPE-E	*V*	Misidentified?
1995-Sep-03	T8750012	Feige 110	*V*	Extreme Airmass (2.737)
	T8750013	Feige 110	*I*	Extreme Airmass (2.713)
	T8750014	Feige 110	*I*	Extreme Airmass (2.692)
	T8750015	Feige 110	*V*	Extreme Airmass (2.671)
1995-Oct-23	T8960015	THPE-B	*V*	Known variable
	T8960016	THPE-B	*I*	Known variable
	T8960017	THPE-B	*I*	Known variable
	T8960018	THPE-B	*V*	Known variable
	T8960024	THPE-E	*V*	Misidentified?
	T8960025	THPE-E	*I*	Misidentified?
	T8960026	THPE-E	*I*	Misidentified?
	T8960027	THPE-E	*V*	Misidentified?
	T8980007	THPE-E	*V*	Misidentified?
	T8980008	THPE-E	*I*	Misidentified?
	T8980009	THPE-E	*I*	Misidentified?
	T8980000	THPE-E	*V*	Misidentified?

[a]From the literature, THPE-B turns out to be the 5.4129 day period eclipsing binary RW Phe, (see Landolt (1992)).

[b]The residuals between the catalogue and transformed magnitude are typically of the order of 1.5-mag, prompting the suspicion that this star has been misidentifed.

Table 5.4: Adopted V, $(b-y)$, $(v-b)$ and $(u-b)$ *mean* transformation equation coefficients for the three nights of 1995-Sep-18, 1995-Sep-19 and 1995-Oct-25. These coefficients derive from a $24''$ synthetic aperture.

Coefficient		$b-y$	V	$v-b$	$u-b$
α	1995-Sep-18	0.7684	5.5034	0.2846	−0.3592
	1995-Sep-19	0.7593	5.4576	0.2772	−0.3877
	1995-Oct-25	0.7608	5.4303	0.2613	−0.3930
β		−0.0110	−0.0889	0.0297	−0.0183
k		0.0800	0.1600	0.1300	0.4400

Table 5.5: Further information regarding the *uvby* standard star observations. Column definitions as for table 5.2.

Date	Row	Col	N/S	As	N_S	N_M	σ_{b-y}	σ_V	σ_{v-b}	σ_{u-b}
1995-Sep-18	110	452	N	HV 2241	10	24	0.010	0.030	0.012	0.018
1995-Sep-19	163	142	N	HV 982[a]	11	23	0.009	0.012	0.011	0.013
1995-Oct-25	163	142	N	HV 982[a]	8	11	0.009	0.012	0.011	0.012
Overall					15	58	0.009	0.020	0.011	0.015

[a] This is the standard position for HV 982, but NOT the standard telescope orientation.

- **1995-Oct-25**
  The v observation of E902 is contaminated by a cosmic ray hence its exclusion from the $(v-b)$ coefficient determinations. The two u observations lead to exceptionally large $(u-b)$ residuals, hence their exclusion from the $(u-b)$ coefficient determinations.

5.2.3 Residuals between catalogue photometry and transformed photometry

Figure 5.1 presents the residuals between the catalogue photometry and the transformed photometry for the standard stars as a function of UTC. Plots of the residuals versus other parameters – including airmass, colour, magnitude, hour angle and declination – are presented in section B.4.

In figure 5.1 the plots for each transformation are scaled appropriately so as to include all of the data, thus leading to different scales for each transformation. In section B.4 the plots are presented at a standardised scale to ease direct comparison between the transformations and to show more clearly the detailed behaviour of the majority of the residuals, especially in the cases where the desire to include all of the observations leads to extreme plot scales (i.e. V and $(V-I)$) in figure 5.1. Measurements excluded from the determinations of the transformation equation coefficients are circled.

No significant trends are evident in the $(V-I)$, V, I, $(u-b)$, $(v-b)$ or $(b-y)$ residuals (see figure 5.1 and figures B.12, B.13 B.14, B.15, B.16 and B.17).

For the y transformation residuals, the dramatic increase in atmospheric extinction (due to cloud) at around UTC15:30 on 1995-Sep-19 is very evident. It is interesting to note that there is no corresponding effect evident in the colours for that night. A slight gradient in the residuals for 1995-Oct-25 is also evident. Small empirical corrections to the y transformed photometry for the programme stars observed on 1995-Oct-25 (HV 1620 and HV 2241) have therefore been applied (see section 5.3).

Table 5.6: This table lists the frames excluded from the *uvby* transformation coefficient determinations.

Date	Frame	Identity	Filter	Reason for exclusion
1995-Sep-18	T6950028	E710	u	Anomalous Residual
	T6950029	E710	b	Anomalous Residual
	T6950030	E710	v	Anomalous Residual
	T6950031	E710	y	Anomalous Residual
	T8880030	E301	u	Saturated Exposure
1995-Sep-19	T8910022	E302	u	Cloud
	T8910023	E302	v	Cloud
	T8910024	E302	b	Cloud
	T8910025	E302	y	Cloud
	T8910026	E302	y	Cloud
	T8910027	E302	b	Cloud
	T8910028	E302	v	Cloud
	T8910029	E302	u	Cloud
	T8910030	E301	u	Cloud
	T8910031	E301	b	Cloud
	T8910032	E301	v	Cloud
	T8910033	E301	y	Cloud
	T8910034	E301	y	Cloud
	T8910035	E301	b	Cloud
	T8910036	E301	v	Cloud
	T8910037	E301	u	Cloud
	T6650001	E301	y	Cloud
	T6650002	E301	y	Cloud
1995-Oct-25	T9000034	E902	v	Cosmic Ray
	T9000035	E902	u	Anomalous Residual
	T9010001	E902	u	Anomalous Residual

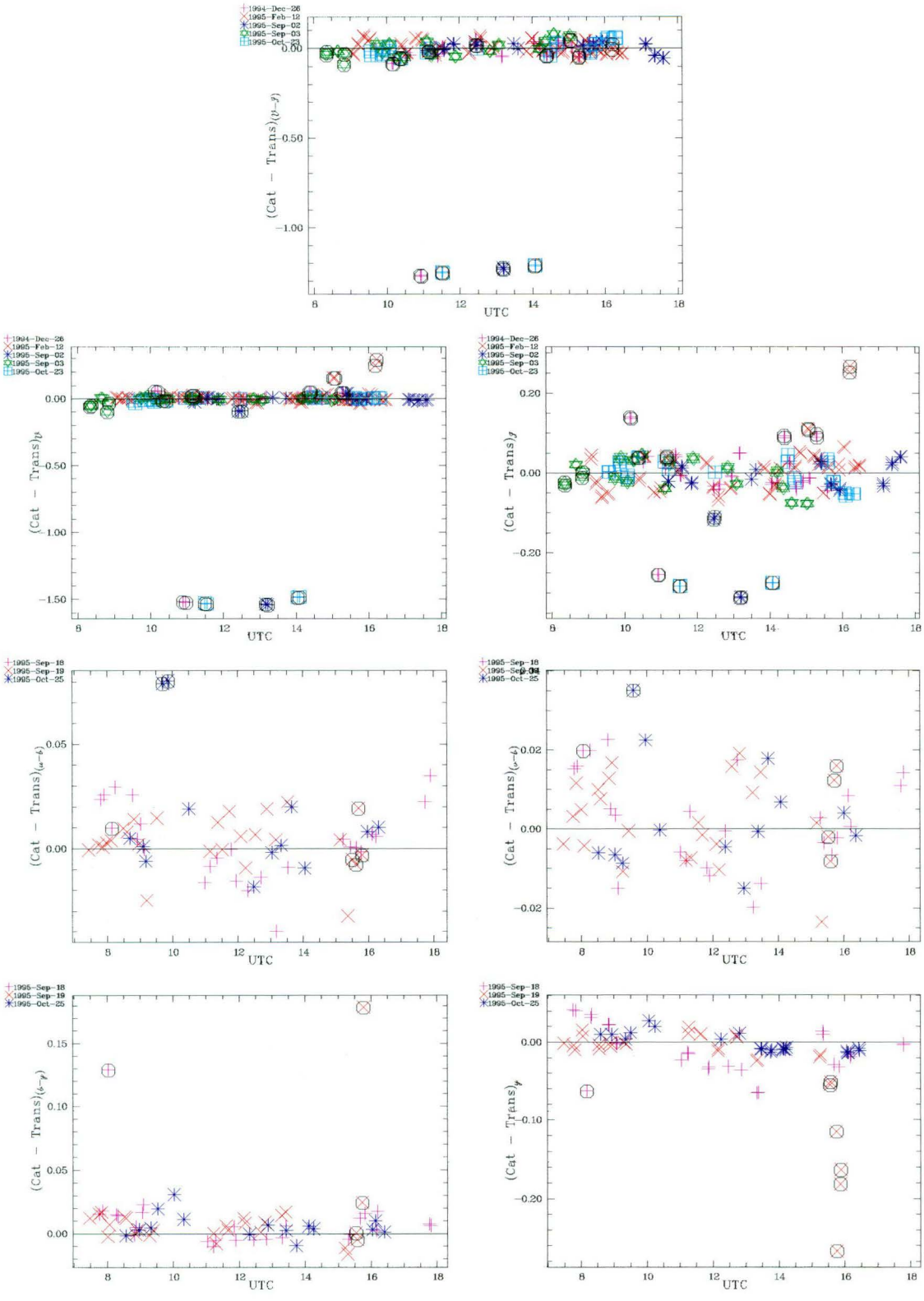

Figure 5.1: Residuals between the transformed magnitudes (V, I and $y = V$) and colours ($V - I$, $b - y$, $v - b$ and $u - b$) and the catalogue values. Plots for each transformation are shown at various vertical scales so as to include all observations. Plots at a standardized vertical scale are given in section B.4. Circled points indicate observations excluded from the transformation equation coefficient determinations.

5.3 Standard system photometry for the programme stars

To compare theoretical stellar flux distributions with observed flux distributions in order to determine the effective temperatures of the components of a eclipsing binary star, obviously all observed fluxes should ideally be obtained at a single epoch (or equivalently a specific orbital phase) and these should be compared with theoretical flux distributions appropriate to that epoch (orbital phase). Given the *WD95* program, computation of the theoretical flux distributions at any arbitrary orbital phase is relatively straightforward (see appendix C). However, practical considerations mean that the observations will in general be obtained over a range of epochs. Observational constraints are most restrictive for the IUE observations. Only one observation is available for each of the three programme stars and the observations were acquired at essentially arbitrary epochs (see table 5.20). The *uvby* and *VI* calibration observations were also acquired at arbitrary epochs (i.e. whenever photometric conditions prevailed). Furthermore the *uvby* and *VI* observations are made non-simultaneously. Thus each individual observation was acquired at a unique epoch. Therefore, for complete consistency, all of the data should be 'corrected' for the variation of light (according to the observed light curve) to some common epoch (orbital phase). The adopted solution is to apply corrections to the observed instrumental *uvby* and *VI* magnitudes thereby giving the magnitudes that *would* have been observed had all of the observations been made at an epoch (orbital phase) corresponding to the orbital phase of the epoch of the IUE observations. These corrected instrumental magnitudes can then be transformed to the standard systems (according to the transformations derived in the previous section) giving standard system photometry at the phases of the IUE observations.

It is also convenient to derive standard system photometry at some more generally useful phase, i.e. the phase corresponding to maximum light. For all three programme stars maximum light corresponds to the quadrature point following primary minimum.

The required corrections between the instrumental magnitude at the observed phase and at any given reference phase for each bandpass ($\Delta_{\bar{\lambda}}$) can be derived from preliminary light curve fits calculated with the *WD95* program (see section 4.4). Defining,

$$\Delta_{\bar{\lambda},\phi=\phi_{\rm obs}} = m_{WD95,\bar{\lambda},\phi=\phi_{\rm ref}} - m_{WD95,\bar{\lambda},\phi=\phi_{\rm obs}}, \tag{5.35}$$

then the instrumental magnitude that would have been observed, had the observation been made at an epoch corresponding to orbital phase $\phi_{\rm ref}$ is simply,

$$m_{{\rm inst},\bar{\lambda},\phi=\phi_{\rm ref}} = m_{{\rm inst},\bar{\lambda},\phi=\phi_{obs}} + \Delta_{\lambda,\phi=\phi_{\rm obs}}. \tag{5.36}$$

The preliminary fits need only be good fits in the sense of minimizing the residuals between the computed and observed light curves. The parameters sets need not represent physically realistic stars since these fits are being used only to estimate relative magnitudes between different orbital phases. No physical interpretation has been, nor should be, made based on these parameter sets.

The raw photometry for HV 982, HV 1620 and HV 2241 is tabulated in tables 5.7, 5.8 and 5.9 respectively. These data represent *Synthetic Aperture Photometry* extracted from the CCD images according to the methods outlined in section 3.4. Also tabulated for each observation is the image file name, the Heliocentric Julian date and the corresponding orbital phase of mid exposure, the filter, the exposure duration (Exp), the airmass (X) and the corrections from the observed phases to the phases of the IUE observations ($\Delta_{\rm IUE}$) and to the phase of Maximum Light ($\Delta_{\rm ML}$).

Rearranging equations 5.12, 5.13, 5.14, 5.15, 5.16, 5.17 and 5.18, and accounting for the phase corrections (Δ) gives the following relations,

$$(V-I) = (1-\beta_{(V-I)})\left[(V_{\rm inst}-I_{\rm inst}) + (\Delta_V-\Delta_I) - k_{(V-I)}\bar{X}_{(V-I)}\right] - \alpha_{(V-I)}, \tag{5.37}$$

$$(b-y) = (1-\beta_{(b-y)})\left[(b_{\rm inst}-y_{\rm inst}) + (\Delta_b-\Delta_y) - k_{(b-y)}\bar{X}_{(b-y)}\right] - \alpha_{(b-y)}, \tag{5.38}$$

$$(v-b) = (1-\beta_{(v-b)})\left[(v_{\rm inst}-b_{\rm inst}) + (\Delta_v-\Delta_b) - k_{(v-b)}\bar{X}_{(v-b)}\right] - \alpha_{(v-b)}, \tag{5.39}$$

$$(u-b) = (1-\beta_{(u-b)})\left[(u_{\rm inst}-b_{\rm inst}) + (\Delta_u-\Delta_b) - k_{(u-b)}\bar{X}_{(u-b)}\right] - \alpha_{(u-b)}, \tag{5.40}$$

$$V = y_{\rm inst} + \Delta_y - \alpha_y - \beta_y\left[(b_{\rm inst}-y_{\rm inst}) + (\Delta_b-\Delta_y) - k_{(b-y)}\bar{X}_{(b-y)}\right] - k_yX_y, \tag{5.41}$$

$$V = V_{\rm inst} + \Delta_V - \alpha_V - \beta_V\left[(V_{\rm inst}-I_{\rm inst}) + (\Delta_V-\Delta_I) - k_{(V-I)}\bar{X}_{(V-I)}\right] - k_VX_V, \tag{5.42}$$

$$I = I_{\rm inst} + \Delta_I - \alpha_I - \beta_I\left[(V_{\rm inst}-I_{\rm inst}) + (\Delta_V-\Delta_I) - k_{(V-I)}\bar{X}_{(V-I)}\right] - k_IX_I. \tag{5.43}$$

where the α, β and k coefficients are taken from tables 5.1 and 5.4. Application of the above relations to the data in tables 5.7, 5.8 and 5.9 results in the transformed photometry given in tables 5.10 and 5.11. The

finally adopted standard system photometry is tabulated in tables 5.12 and 5.13. The adopted photometry is calculated as the weighted means (equation 5.44) of the individual nightly photometry listed in tables 5.10 and 5.11. Tables 5.12 and 5.13 also list the errors of the means calculated according to equation 5.45.

$$\bar{x} = \frac{\sum_{i=1}^{n} w_i x_i}{\sum_{i=1}^{n} w_i} \tag{5.44}$$

$$\sigma_{\bar{x}} = \sqrt{\frac{\sum_{i=1}^{n} w_i (x_i - \bar{x})^2}{(n-1)\sum_{i=1}^{n} w_i}} \tag{5.45}$$

For the *VI* photometry, equal weight was given to all observations except for the measurements for HV 1620 for the night of 1995-Sep-02 which were excluded entirely from the calculations of the means. Examination of the first I image from 1995-Sep-02 (T8730034) indicates that a large amount of scattered light was incident on the CCD during the exposure, possibly a result of the fluorescent lights in the telescope dome being accidentally turned on during the exposure. Although no obvious problem can be identified in the second I image from 1995-Sep-02 (T8730035), the deviation of the transformed magnitude for this observation from the mean of the others by approximately half a magnitude can not be a result of random error. Figure B.28 graphically illustrates the peculiar nature of image T8730034. For comparison, the other I image (figure B.29) as well as the two V images (figures B.27 and B.30) from that night are also presented.

For the *uvby* photometry, half weight was given to the 1995-Sep-18 measurements. Independent observations made by other observers working at MJUO cast doubts on the photometric quality of that night. Empirical corrections of $+0.010$ mag and -0.008 mag for HV 1620 and HV 2241 respectively for the night of 1995-Oct-25 were applied to the transformed V magnitudes to account for the small but significant drift in the atmospheric transmission identified in section 5.2.3.

It is clear that for the *VI* photometry, the scatter between the two measurements of V, I and $(V-I)$ on a given night is generally less than the night-to-night scatter. The two measurements of V for a given star on a given night typically vary by several thousandths of a magnitude, while from night to night they tend to differ by several hundredths. In the *uvby* photometry the errors of the mean adopted photometry are apparently correlated with the crowdedness of the programme star fields. The smallest errors are achieved for HV 2241 – the least crowded of the programme star fields – the largest errors pertain to HV 982 – the most crowded of the programme star fields – with HV 1620 somewhere in between. These two trends indicate that the accuracy of the photometry is limited by the precision of the reduction procedure used to extract the instrumental magnitudes from the CCD images. Moreover, the achievable precision of the reduction procedure is closely associated with the seeing in which the image was acquired. In good seeing conditions, faint field stars which contaminate the synthetic aperture photometry of the programme stars can be more reliably accounted for via the profile fitting routines since they will be less blended and have generally higher signal to noise ratios.

In general, the quoted errors of the means in tables 5.12 and 5.13 undoubtedly underestimate the true uncertainty in the adopted photometry, especially for HV 2241. This is particularly true for the *uvby* photometry, which is derived from just two measurements for HV 982 and HV 2241 and three for HV 1620. More realistic total uncertainties are obtained by combining (quadratically) the internal errors of the means and the overall rms scatters of the residuals between the transformed and catalogue photometry for the standard stars (see tables 5.2 and 5.5) which reflect the uncertainty arising from transformation errors.

For HV 1620 and HV 2241, there is agreement within the uncertainties between the adopted V magnitudes derived from the *VI* photometry and the *uvby* photometry. But for HV 982 there is a difference of 0.066 magnitudes which is only agreement at the 2σ level.

Clearly significantly more data would be required to improve the standard system photometry for the three programme stars.

Table 5.7: Instrumental photometry for HV 982 for calibration. Listed for each observation is the image file name, the Heliocentric date and the corresponding orbital phase computed from the ephemeris of section 3.3.3, the filter, the extracted raw magnitude ($m_{\rm raw}$) and the instrumental magnitude ($m_{\rm inst}$, equation 3.5), the airmass (X) and the corrections from observed phase to the phases of the IUE observation ($\phi_{\Delta_{\rm IUE}} = 0.5592$) and of Maximum Light ($\phi_{\Delta_{\rm ML}} = 0.25$).

Image	HJD −2 400 000.0	Phase	Filter	Exp	$m_{\rm raw}$	$m_{\rm inst}$	X	$\Delta_{\rm IUE}$	$\Delta_{\rm ML}$
				1994-Dec-26					
T6050022	49712.9940	0.7655	V	400.0	12.081	18.586	1.105	0.000	−0.012
T6050023	49712.9991	0.7665	I	400.0	12.729	19.234	1.105	0.000	−0.011
T6050024	49713.0041	0.7674	I	400.0	12.708	19.213	1.106	0.000	−0.011
T6050025	49713.0092	0.7684	V	400.0	12.084	18.589	1.107	0.000	−0.012
				1995-Feb-12					
T8220021	49760.9862	0.7608	V	400.0	12.093	18.598	1.206	0.000	−0.012
T8220022	49760.9913	0.7617	I	400.0	12.651	19.156	1.215	0.000	−0.011
T8220023	49760.9963	0.7627	I	400.0	12.657	19.162	1.224	0.000	−0.011
T8220024	49761.0014	0.7636	V	400.0	12.101	18.606	1.233	0.000	−0.012
				1995-Sep-18					
T8860025	49979.0823	0.6390	u	1200.0	13.861	21.559	1.317	0.004	−0.010
T8860026	49979.0966	0.6417	v	1200.0	13.975	21.673	1.283	0.004	−0.008
T8860027	49979.1110	0.6444	b	1200.0	13.511	21.209	1.252	0.004	−0.009
T8860028	49979.1224	0.6465	y	700.0	13.233	20.346	1.231	0.003	−0.009
				1995-Sep-19					
T8910010	49980.0817	0.8263	u	1200.0	13.637	21.335	1.312	−0.006	−0.020
T8910011	49980.0961	0.8290	v	1200.0	13.852	21.550	1.278	−0.005	−0.017
T8910012	49980.1104	0.8317	b	1200.0	13.347	21.045	1.247	−0.004	−0.017
T8910013	49980.1219	0.8338	y	700.0	13.155	20.268	1.227	−0.004	−0.016

Table 5.8: Instrumental photometry for HV 1620 for calibration. Listed for each observation is the image file name, the Heliocentric date and the corresponding orbital phase computed from the ephemeris of section 3.3.3, the filter, the extracted raw magnitude ($m_{\rm raw}$) and the instrumental magnitude ($m_{\rm inst}$, equation 3.5), the airmass (X) and the corrections from observed phase to the phases of the IUE observation ($\phi_{\Delta_{\rm IUE}} = 0.1540$) and of Maximum Light ($\phi_{\Delta_{\rm ML}} = 0.2559$).

Image	HJD −2 400 000.0	Phase	Filter	Exp	$m_{\rm raw}$	$m_{\rm inst}$	X	$\Delta_{\rm IUE}$	$\Delta_{\rm ML}$
				1994-Dec-26					
T6040029	49712.8965	0.2490	V	400.0	11.936	18.441	1.192	0.065	0.000
T6040030	49712.9016	0.2504	I	400.0	12.367	18.872	1.197	0.062	0.000
T6040031	49712.9067	0.2518	I	400.0	12.308	18.813	1.204	0.062	0.000
T6040032	49712.9117	0.2532	V	400.0	11.941	18.446	1.210	0.065	0.000
				1995-Feb-12					
T4300024	49760.9066	0.4880	V	400.0	12.190	18.695	1.476	−0.231	−0.296
T4300025	49760.9117	0.4894	I	400.0	12.591	19.096	1.492	−0.235	−0.297
T4300026	49760.9167	0.4908	I	400.0	12.598	19.103	1.507	−0.238	−0.300
T4300027	49760.9218	0.4922	V	400.0	12.275	18.780	1.523	−0.239	−0.304
				1995-Sep-02					
T8730033	49963.1118	0.2471	V	400.0	11.916	18.421	1.138	0.064	−0.001
T8730034	49963.1169	0.2485	I	400.0	12.417	18.922	1.138	0.062	0.000
T8730035	49963.1219	0.2499	I	400.0	12.839	19.344	1.138	0.062	0.000
T8730036	49963.1270	0.2513	V	400.0	11.878	18.383	1.139	0.065	0.000
				1995-Sep-03					
T8750016	49963.8852	0.4604	V	400.0	12.112	18.617	1.449	−0.142	−0.207
T8750017	49963.8903	0.4618	I	400.0	12.534	19.039	1.435	−0.145	−0.207
T8750018	49963.8954	0.4632	I	400.0	12.538	19.043	1.421	−0.151	−0.213
T8750019	49963.9005	0.4646	V	400.0	12.111	18.616	1.408	−0.157	−0.222
				1995-Oct-23					
T8960028	50013.9920	0.2775	V	400.0	11.943	18.448	1.140	0.065	0.000
T8960029	50013.9971	0.2790	I	400.0	12.432	18.937	1.141	0.061	−0.001
T8960030	50014.0022	0.2804	I	400.0	12.445	18.950	1.142	0.061	−0.001
T8960031	50014.0073	0.2818	V	400.0	11.964	18.469	1.143	0.064	−0.001
				1995-Sep-18					
T8850018	49978.9022	0.6014	u	1200.0	13.539	21.237	1.305	−0.048	−0.118
T8850019	49978.9165	0.6053	v	1200.0	13.762	21.460	1.277	−0.045	−0.111
T8850020	49978.9308	0.6093	b	1200.0	13.289	20.987	1.252	−0.041	−0.107
T8850021	49978.9423	0.6124	y	700.0	13.061	20.174	1.235	−0.038	−0.103
				1995-Sep-19					
T8890033	49979.9125	0.8800	u	1200.0	13.444	21.142	1.279	−0.042	−0.112
T8890034	49979.9269	0.8839	v	1200.0	13.743	21.441	1.254	−0.038	−0.104
T8890035	49979.9412	0.8879	b	1200.0	13.255	20.953	1.231	−0.039	−0.105
T8890036	49979.9527	0.8910	y	700.0	12.978	20.091	1.216	−0.041	−0.106
				1995-Oct-25					
T9010009	50015.9541	0.8186	y	700.0	12.872	19.985	1.140	0.018	−0.047
T9010010	50015.9662	0.8219	b	1200.0	13.152	20.850	1.138	0.016	−0.050
T9010011	50015.9810	0.8260	v	1200.0	13.619	21.317	1.139	0.011	−0.055
T9010012	50015.9958	0.8301	u	1200.0	13.310	21.008	1.142	0.003	−0.067

Table 5.9: Instrumental photometry for HV 2241 for calibration. Listed for each observation is the image file name, the Heliocentric date and the corresponding orbital phase computed from the ephemeris of section 3.3.3, the filter, the extracted raw magnitude ($m_{\rm raw}$) and the instrumental magnitude ($m_{\rm inst}$, equation 3.5), the airmass (X) and the corrections from observed phase to the phases of the IUE observation ($\phi_{\Delta_{\rm IUE}} = 0.8207$) and of Maximum Light ($\phi_{\Delta_{\rm ML}} = 0.2389$).

Image	HJD −2 400 000.0	Phase	Filter	Exp	$m_{\rm raw}$	$m_{\rm inst}$	X	$\Delta_{\rm IUE}$	$\Delta_{\rm ML}$
				1994-Dec-26					
T6060006	49713.0640	0.1807	V	200.0	11.695	17.448	1.144	0.046	−0.025
T6060007	49713.0668	0.1814	I	200.0	12.164	17.917	1.148	0.043	−0.024
T6060008	49713.0696	0.1820	I	200.0	12.147	17.900	1.152	0.044	−0.023
T6060009	49713.0723	0.1826	V	200.0	11.698	17.451	1.155	0.048	−0.023
				1995-Feb-12					
T8230009	49761.0576	0.2324	V	300.0	11.262	17.455	1.448	0.070	−0.001
T8230010	49761.0616	0.2333	I	300.0	11.727	17.920	1.463	0.066	−0.001
T8230011	49761.0654	0.2342	I	300.0	11.720	17.913	1.478	0.066	−0.001
T8230012	49761.0694	0.2351	V	300.0	11.265	17.458	1.493	0.071	0.000
				1995-Sep-02					
T8740013	49963.1892	0.7782	V	400.0	10.952	17.457	1.144	0.029	−0.042
T8740014	49963.1943	0.7794	I	400.0	11.410	17.915	1.138	0.028	−0.039
T8740015	49963.1993	0.7805	I	400.0	11.413	17.918	1.132	0.027	−0.040
T8740016	49963.2044	0.7817	V	400.0	10.957	17.462	1.126	0.027	−0.044
				1995-Sep-03					
T8760005	49963.9466	0.9526	V	200.0	12.415	18.168	2.034	−0.522	−0.593
T8760006	49963.9500	0.9534	I	200.0	12.786	18.539	2.013	−0.515	−0.582
T8760007	49963.9531	0.9541	I	200.0	12.787	18.540	1.993	−0.521	−0.588
T8760008	49963.9565	0.9549	V	200.0	12.428	18.181	1.973	−0.544	−0.615
				1995-Sep-18					
T8880018	49979.1912	0.4631	u	1200.0	12.702	20.400	1.098	−0.322	−0.408
T8880019	49979.2056	0.4664	v	1200.0	13.137	20.835	1.090	−0.372	−0.448
T8880020	49979.2199	0.4697	b	1200.0	12.666	20.364	1.085	−0.395	−0.468
T8880021	49979.2314	0.4723	y	700.0	12.419	19.532	1.083	−0.411	−0.482
				1995-Oct-25					
T9020004	50016.1164	0.9660	y	700.0	12.594	19.707	1.086	−0.665	−0.736
T9020005	50016.1283	0.9687	b	1200.0	12.886	20.584	1.084	−0.702	−0.775
T9020006	50016.1419	0.9719	u	1000.0	13.230	20.730	1.083	−0.796	−0.882
T9020007	50016.1542	0.9747	v	1000.0	13.619	21.119	1.085	−0.780	−0.856

Table 5.10: Transformed VI calibration photometry for phases corresponding to both the phases of the IUE observations and the phases of Maximum Light for each programme star. Observations on each night consisted of a $VIIV$ sequence, hence the two listed values for each observation date. The IUE phases are 0.5592, 0.1591 and 0.8265 for HV 982, HV 1620 and HV 2241 respectively. Maximum Light occurs at the quadrature following primary minimum. The photometry from 1995-Sep-02 for HV 1620 is bracketed to indicate that it is not to be trusted and has thus been excluded from the calculations of the final photometry.

	IUE Phase			Max Light Phase		
Date	$V-I$	V	I	$V-I$	V	I
			HV 982			
1994-Dec-26	−0.165	14.603	14.767	−0.166	14.592	14.757
	−0.140	14.605	14.744	−0.141	14.594	14.734
1995-Feb-12	−0.092	14.625	14.716	−0.093	14.614	14.696
	−0.091	14.629	14.719	−0.092	14.618	14.709
			HV 1620			
1994-Dec-26	0.062	14.501	14.438	0.060	14.440	14.380
	0.129	14.501	14.373	0.127	14.441	14.314
1995-Feb-12	0.063	14.443	14.379	0.061	14.382	14.320
	0.138	14.511	14.373	0.136	14.450	14.314
1995-Sep-02	(−0.054)	(14.510)	(14.563)	(−0.056)	(14.449)	(14.505)
	(−0.539)	(14.484)	(15.021)	(−0.541)	(14.423)	(14.963)
1995-Sep-03	−0.003	14.442	14.444	−0.005	14.381	14.385
	−0.016	14.432	14.447	−0.018	14.371	14.388
1995-Oct-23	−0.031	14.485	14.516	−0.034	14.424	14.457
	−0.024	14.504	14.528	−0.026	14.443	14.470
			HV 2241			
1994-Dec-26	0.025	13.507	13.481	0.020	13.431	13.410
	0.047	13.510	13.462	0.042	13.434	13.393
1995-Feb-12	−0.002	13.519	13.521	−0.008	13.443	13.450
	0.008	13.516	13.509	0.002	13.440	13.438
1995-Sep-02	−0.008	13.519	13.527	−0.014	13.443	13.457
	−0.007	13.525	13.531	−0.012	13.449	13.460
1995-Sep-03	0.011	13.535	13.524	0.006	13.459	13.453
	0.009	13.535	13.525	0.004	13.459	13.454

Table 5.11: Transformed $uvby$ calibration photometry for phases corresponding to both the phases of the IUE observations and the phases of Maximum Light for each programme star. Observations on each night consisted of a $uvby$ sequence, hence only one listed value for each observation date in contrast to the VI photometry (table 5.10). The IUE phases are 0.5592, 0.1591 and 0.8265 for HV 982, HV 1620 and HV 2241 respectively. Maximum Light occurs at the quadrature following primary minimum.

	IUE Phase				Max Light Phase			
Date	$b-y$	V	$v-b$	$u-b$	$b-y$	V	$v-b$	$u-b$
				HV 982				
1995-Sep-18	0.005	14.716	0.006	0.140	0.004	14.705	0.007	0.139
1995-Sep-19	−0.074	14.669	0.053	0.108	−0.075	14.658	0.054	0.107
				HV 1620				
1995-Sep-18	−0.050	14.493	0.011	0.033	−0.052	14.433	0.011	0.030
1995-Sep-19	0.015	14.461	0.041	0.014	0.013	14.401	0.041	0.011
1995-Oct-25	0.020	14.464	0.043	0.029	0.018	14.404	0.043	0.026
				HV 2241				
1995-Sep-18	0.001	13.517	0.058	−0.019	0.000	13.441	0.055	−0.033
1995-Oct-25	0.001	13.502	0.045	−0.040	0.000	13.426	0.042	−0.054

Table 5.12: The adopted V and I magnitudes and the $(V-I)$ colours derived from the VI photometry. The photometry is computed at the IUE phases and at the phases of Maximum Light for the programme stars. The IUE phases are 0.5592, 0.1591 and 0.8265 for HV 982, HV 1620 and HV 2241 respectively. Maximum Light occurs at the quadrature following primary minimum. The adopted values are the weighted means of the data in table 5.10. Observations from the night of 1995-Sep-18 were given half weight due to doubts concerning the photometric quality of the night. Below each magnitude and colour is the standard error for the mean (bracketed) and the total adopted uncertainty (the quadratic sum of the standard errors and the rms scatters of the residuals between the transformed and catalogue photometry for the standard stars which are listed at the bottom of the table).

	IUE Phase			Max Light Phase		
Variable	$V-I$	V	I	$V-I$	V	I
HV 982	−0.122	14.615	14.736	−0.123	14.604	14.726
	(±0.032)	(±0.011)	(±0.021)	(±0.032)	(±0.011)	(±0.021)
	±0.047	±0.016	±0.041	±0.047	±0.016	±0.041
HV 1620	0.040	14.477	14.437	0.038	14.416	14.379
	(±0.037)	(±0.018)	(±0.033)	(±0.037)	(±0.018)	(±0.033)
	±0.050	±0.022	±0.048	±0.050	±0.022	±0.048
HV 2241	0.010	13.521	13.510	0.005	13.445	13.439
	(±0.010)	(±0.005)	(±0.014)	(±0.010)	(±0.006)	(±0.014)
	±0.035	±0.013	±0.038	±0.035	±0.013	±0.038
RMS scatter of standard star residuals						
	±0.034	±0.012	±0.035	±0.034	±0.012	±0.035

Table 5.13: The adopted V magnitudes and $(b-y)$, $(v-b)$, $(u-b)$, $\mathrm{m_1}$ and $\mathrm{c_1}$ colour indices derived from the $uvby$ photometry. The photometry is computed at the IUE phases and at the phases of Maximum Light for the programme stars. The IUE phases are 0.5592, 0.1591 and 0.8265 for HV 982, HV 1620 and HV 2241 respectively. Maximum Light occurs at the quadrature following primary minimum. The adopted V magnitudes and $(b-y)$, $(v-b)$, $(u-b)$ colours are the weighted means of the data in table 5.10. The $\mathrm{m_1}$ and $\mathrm{c_1}$ indices are the means of values calculated from the individual colours from each night (table 5.11) according to equations 5.20 and 5.21. Below each magnitude/index is the standard error for the mean (bracketed) and the total adopted uncertainty (the quadratic sum of the standard errors and the rms scatters of the residuals between the transformed and catalogue photometry for the standard stars which are listed at the bottom of the table).

Variable	$b-y$	V	$v-b$	$u-b$	$\mathrm{m_1}$	$\mathrm{c_1}$
			IUE Phase			
HV 982	−0.048	14.685	0.037	0.118	0.085	0.045
	(±0.037)	(±0.022)	(±0.022)	(±0.015)	(±0.059)	(±0.059)
	±0.038	±0.030	±0.025	±0.021	±0.060	±0.061
HV 1620	0.004	14.469	0.036	0.024	0.032	−0.048
	(±0.019)	(±0.009)	(±0.009)	(±0.006)	(±0.010)	(±0.021)
	±0.021	±0.022	±0.014	±0.016	±0.016	±0.026
HV 2241	0.001	13.507	0.049	−0.033	0.049	−0.131
	(±0.000)	(±0.007)	(±0.006)	(±0.010)	(±0.005)	(±0.002)
	±0.009	±0.021	±0.013	±0.018	±0.013	±0.016
			Max Light Phase			
HV 982	−0.049	14.674	0.038	0.117	0.087	0.042
	(±0.037)	(±0.022)	(±0.022)	(±0.015)	(±0.059)	(±0.059)
	±0.038	±0.030	±0.025	±0.021	±0.060	±0.061
HV 1620	0.002	14.408	0.036	0.021	0.034	−0.051
	(±0.019)	(±0.009)	(±0.009)	(±0.006)	(±0.010)	(±0.021)
	±0.021	±0.022	±0.014	±0.016	±0.016	±0.026
HV 2241	0.000	13.431	0.046	−0.047	0.047	−0.140
	(±0.000)	(±0.007)	(±0.006)	(±0.010)	(±0.005)	(±0.002)
	±0.009	±0.021	±0.013	±0.018	±0.013	±0.016
			RMS scatter of standard star residuals			
	±0.009	±0.020	±0.011	±0.015	±0.012	±0.016

5.4 Interstellar Extinction

Before the flux levels of the stars can be used to determine the stellar temperatures by comparison with theoretical model flux distributions derived from the *WD95* light curve solution and the Kurucz theoretical stellar atmosphere models, the photometric magnitudes and the IUE fluxes must be dereddened.

First the total reddening or color excess ($E(B-V)$) suffered by each of the three stars must be determined. Then the fraction of the total reddening due to foreground extinction (i.e. within the Galaxy) must be determined. Finally, interstellar extinction laws must be applied to calculate the color excess and thus the dereddened magnitudes and fluxes at each observed wavelength.

5.4.1 Total Reddenings

Figure 5.2 shows the $(b-y)$-c_1 plane with empirical and theoretical loci. The empirical relations are taken from Crawford (1975a; 1978; 1979) and represent the intrinsic relations for main sequence B-, A- and F-type stars. The theoretical $(b-y)$ and c_1 indices have been calculated by convolving appropriate bandpasses with the theoretical model atmosphere spectral flux distributions (Kurucz, 1993) and are calibrated relative to the theoretical model atmosphere spectral flux distribution and standard system photometry for Vega (see appendix D). Shown are the relations for $\log[g] = 4.0$ for Galactic, LMC and SMC metallicities. The excellent agreement between observation and theoretical predictions based on theoretical stellar atmosphere models, particularly for early type stars, is evident.

Figure 5.3 presents detailed comparisons of the $(b-y)$-c_1 relations between the models at Galactic and Magellanic Cloud metallicities for the full complement of Kurucz theoretical stellar atmosphere models (i.e. at 11 values of $\log[g]$ ranging from 0.0 to 5.0). For the bluest stars, ($(b-y) \lesssim 0.0$), i.e. the Main Sequence OB-type stars, it is clear that the metallicity dependence of the $(b-y)$-c_1 relation is very weak. Furthermore, the dependence of the relation on $\log[g]$ (or equivalently luminosity class) is likewise extremely weak. Significant departures from the empirical relation only occurs for $\log[g]$ less than 3.5, i.e. luminosity class I and II stars, in accord with the findings of Crawford (1978). The $(b-y)$-c_1 plane is thus ideal for the determination of the reddenings for luminosity class V-III OB-type stars since the *intrinsic* or reddening-corrected indices ($(b-y)_0$ and c_0) and hence $E(B-V)$ (via a suitable transformation from $E(b-y)$) can be unambiguously determined from the observed indices ($(b-y)$ and c_1) by moving back to the intrinsic relationship along the direction of the reddening slope (e.g. $E(c_1) = 0.20E(b-y)$ (Crawford, 1975b) as adopted here).

Total reddenings for the three programme stars were estimated by examination of the $(b-y)$ and c_1 indices and comparing them with empirically determined intrinsic indices (Crawford, 1975a; Crawford, 1978; Crawford, 1979). The $(b-y)$ and c_1 indices corresponding to the phases of the IUE observations were used (table 5.13). Reddening-corrected $(b-y)$ and c_1 indices (i.e. $(b-y)_0$ and c_0) for the programme stars were determined by the intersection of the $(b-y)$-c_1 reddening slopes ($E(c_1) = 0.20E(b-y)$, (Crawford, 1975b)) which pass through the observed $(b-y)$-c_1 points and linear interpolations between the empirical intrinsic data. The colour excess in $(b-y)$ is then given by $E(b-y) = (b-y) - (b-y)_0$ and the colour excess in $(B-V)$ is derived from $E(b-y)$ according to $E(b-y) = 0.74E(B-V)$, (Crawford, 1975b). The procedure is depicted graphically in figure 5.4.

The relations given by Crawford are, of course, for single stars. Some systematic error must therefore arise from the application of these relations to the observed indices of binary stars. Consider the $(b-y)$ colour. The observed $(b-y)$ of a binary star is given by,

$$(b-y) = -2.5\log_{10}\left[\frac{f_{b,1}+f_{b,2}}{f_{y,1}+f_{y,2}}\right] + c_{b-y} + E(b-y) \tag{5.46}$$

where $f_{y,1}$ and $f_{b,1}$ are the intrinsic (i.e. reddening-corrected) y and b fluxes at Earth from the primary component in the direction of the observer, $f_{y,2}$ and $f_{b,2}$ are the intrinsic y and b fluxes at Earth from the secondary component in the direction of the observer, c_{b-y} is simply a constant which sets the zero-point and $E(b-y)$ is the reddening. The relative light (or flux) levels from the two components of a binary as a function of phase for any given wavelength (i.e. $f_{y,1}/f_{y,2}$ and $f_{b,1}/f_{b,2}$) can however be obtained directly from the output of the *WD95* LC program. Note that although the observed magnitudes are affected by interstellar extinction, in the light ratios (derived from light curve fits to the observed light curves) the interstellar extinctions cancel since for a given bandpass the interstellar extinction can be expected to be the

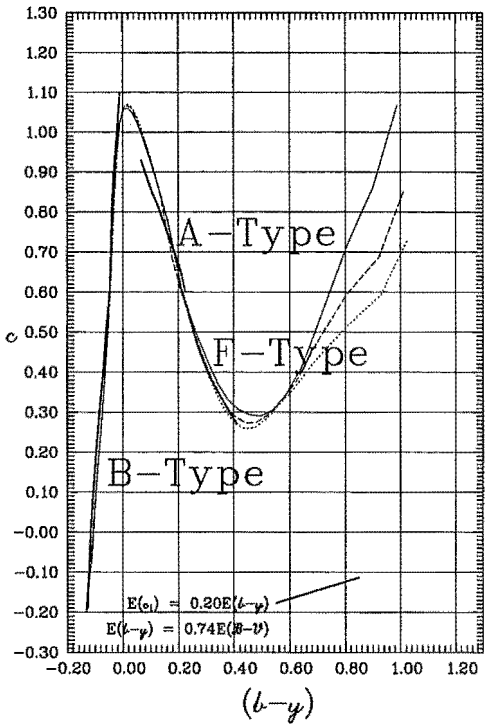

Figure 5.2: The intrinsic relation between $(b-y)$ and c_1. The heavy solid lines are the empirical calibrations for B-, A- and F-type stars (Crawford, 1975a; Crawford, 1978; Crawford, 1979). The light solid, dashed and dotted lines are derived from the theoretical stellar atmosphere models (Kurucz, 1993) with $\log[g] = 4.0$ and at metallicities appropriate for the Galaxy (Kurucz model ip00k2, i.e. abundance [0.0]), the LMC (im03k2, i.e. abundance $[-0.3]$) and the SMC (im05k2, i.e. abundance $[-0.5]$) respectively. The reddening slope is indicated in the lower portion of the figure (Crawford, 1975b).

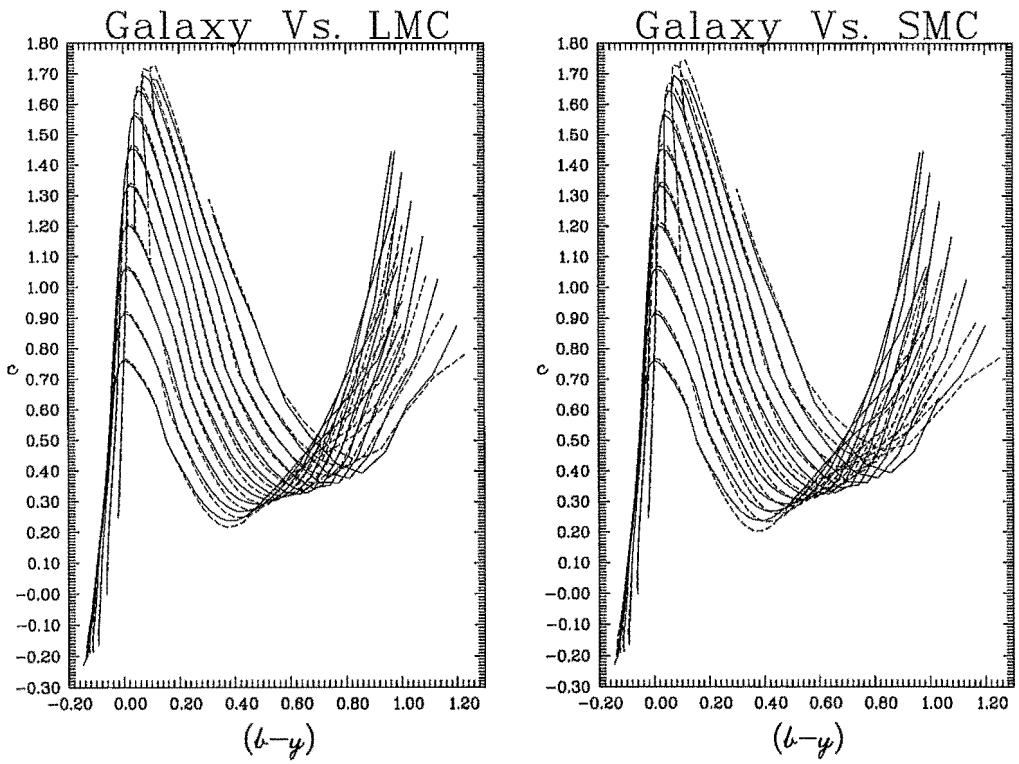

Figure 5.3: Comparison of the $(b-y)$-c_1 plane for Galactic vs LMC (left) and SMC (right) metallicities. The solid lines are the Galactic relationships while the dotted lines are the those for the Clouds. The various lines plotted are for the various values of $\log[g]$, from 0.0 to 5.0 in steps of 0.5. At $(b-y) = 0.4$ the lines correspond to the gravities with 0.0 at the top and 5.0 at the bottom.

same for both components of the binary. Rearranging equation 5.46 gives,

$$(b-y) = -2.5\log_{10}\left[\frac{f_{b,1}}{f_{y,1}}\right] + c_{b-y} + E(b-y) - 2.5\log_{10}\left[\frac{1+\frac{f_{b,2}}{f_{b,1}}}{1+\frac{f_{y,2}}{f_{y,1}}}\right], \quad (5.47)$$

$$= (b-y)_1 - 2.5\log_{10}\left[\frac{1+\frac{f_{b,2}}{f_{b,1}}}{1+\frac{f_{y,2}}{f_{y,1}}}\right], \quad (5.48)$$

or

$$(b-y)_1 = (b-y) + 2.5\log_{10}\left[\frac{1+\frac{f_{b,2}}{f_{b,1}}}{1+\frac{f_{y,2}}{f_{y,1}}}\right], \quad (5.49)$$

and similarly

$$(b-y)_2 = (b-y) + 2.5\log_{10}\left[\frac{1+\frac{f_{b,1}}{f_{b,2}}}{1+\frac{f_{y,1}}{f_{y,2}}}\right], \quad (5.50)$$

where $(b-y)_1$ and $(b-y)_2$ are estimates the reddened colours of the primary and secondary components respectively that would be observed if it were possible to measure the light from each component individually. Similar relationships can be derived for the c_1 indices of the primary and secondary components ($c_{1,1}$ and $c_{1,2}$),

$$c_{1,1} = c_1 + 2.5\log_{10}\left[\frac{\left(1+\frac{f_{u,2}}{f_{u,1}}\right)\left(1+\frac{f_{b,2}}{f_{b,1}}\right)}{\left(1+\frac{f_{v,2}}{f_{v,1}}\right)^2}\right], \quad (5.51)$$

$$c_{1,2} = c_1 + 2.5\log_{10}\left[\frac{\left(1+\frac{f_{u,1}}{f_{u,2}}\right)\left(1+\frac{f_{b,1}}{f_{b,2}}\right)}{\left(1+\frac{f_{v,1}}{f_{v,2}}\right)^2}\right], \quad (5.52)$$

where c_1 is the observed index for the binary and $f_{u,1}$, $f_{u,2}$, $f_{v,1}$ and $f_{v,2}$ are the u and v intrinsic fluxes for the individual components of the binary star from LC. Using the above expressions, total reddenings can be derived in the usual manner for the individual components of each binary star.

Table 5.14 tabulates the adopted observed binary star $(b-y)$ and c_1 indices (taken from table 5.13), the computed indices for the individual components (derived from preliminary *WD95* light curve fits) and the corresponding $E(B-V)$ values for the three programme stars. Also tabulated are the intermediate values of $(b-y)_0$, c_0 and $E(b-y)$. Uncertainties for the total reddening have been estimated by determining the total reddenings for points corresponding to the extreme values of the $(b-y)$ and c_1 indices given the uncertainties in $(b-y)$ and c_1. The estimated uncertainty in the empirical relation for the B-type stars of ± 0.005-mag (Crawford, 1978) has been accounted for in the estimates of the uncertainties of the derived indices and reddenings. It is worth reiterating that the quoted uncertainties, based as they are on small numbers of measurements of both programme stars and standard stars should be considered as indicative rather than formally accurate in any statistical sense. In practice the reddenings determined from the individual components do not differ significantly from the values obtained from the observed indices of the binary stars. The largest variation between the two reddenings, that for HV 1620, is consistent with the uncertainty in the flux ratios: for HV 1620, the uncertainty in the f_b and f_y values are of the order of 1.5 percent.

5.4.2 Foreground Reddenings

The foreground component of the total reddening ($E(B-V)_{\rm Gal}$) in the direction of each of the three programme stars has been recently determined by Tobin (1997a). Subjectively-weighted means were calculated from estimates based on the H I surveys of Schwering and Israel (1991) (both Magellanic Clouds) and McGee and Newton (1982) (SMC) and on stellar photometry, Oestreicher et al. (1995) (LMC). Schwering and Israel provide coarse resolution (48′) foreground $E(B-V)$ maps covering the Clouds permitting estimation of $E(B-V)_{\rm Gal}$ for all three programme stars. The foreground reddening toward HV 1620 (SMC) was also estimated by integration of the low velocity component of the H I line profiles of McGee and Newton giving the Galactic H I column densities which were converted into $E(B-V)$ reddenings via the Galactic $N({\rm H\,I})/E(B-V) = 4.8\times10^{21}$ atom cm^{-2} mag^{-1} ratio (Bohlin et al., 1978). The McGee

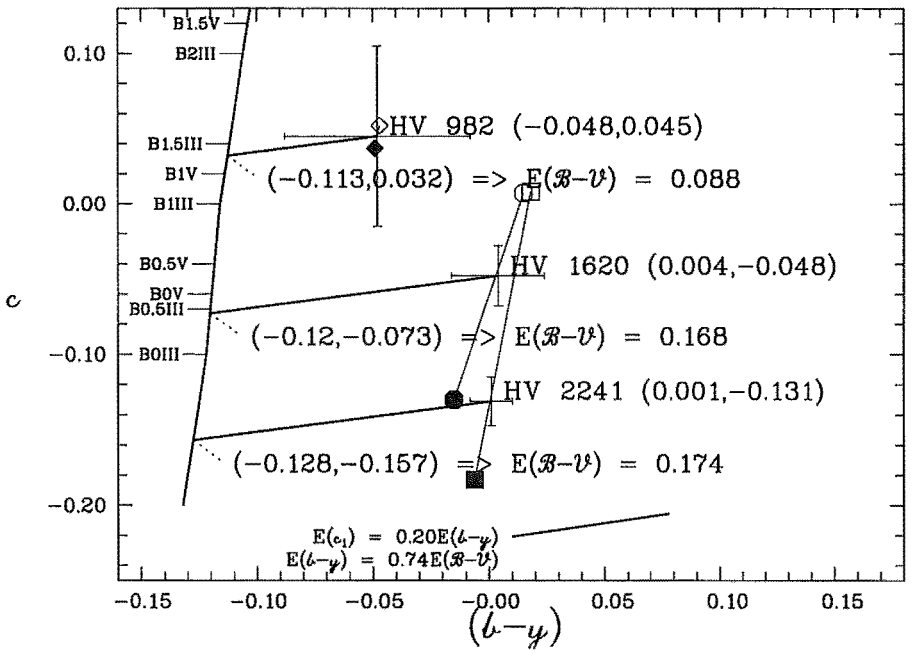

Figure 5.4: Determination of $E(B-V)$ for HV 982, HV 1620 and HV 2241. The adopted extinction laws are $E(c_1) = 0.20E(b-y)$ and $E(b-y) = 0.74E(B-V)$ (Crawford, 1975b). Also shown are the points corresponding to the deconvolved colours of the individual components: diamonds for HV 982, circles for HV 1620 and squares for HV 2241, filled symbols for primary components. The approximate intrinsic colours of early luminosity class V and III B-type stars are labelled (Crawford, 1978). The uncertainties in the observed photometry are indicated by the error bars.

Table 5.14: Total reddenings for HV 982, HV 1620 and HV 2241. The adopted extinction laws are $E(c_1) = 0.20E(b-y)$ and $E(b-y) = 0.74E(B-V)$ (Crawford, 1975b). The 'Binary' $(b-y)$ and c_1 are the observed indices, corrected to the orbital phases corresponding to the epochs of the IUE observations, according to the methods described in section 5.3. The 'Primary' and 'Secondary' indices are derived from deconvolution of the observed light from the binary using *WD95* preliminary light curve solutions.

Star	$(b-y)$	c_1	$(b-y)_0$	c_0	$E(b-y)$	$E(B-V)$
			HV 982			
Binary	−0.048	0.045	−0.113	0.032	0.065	0.088
Primary	−0.049	0.037	−0.114	0.024	0.065	0.087
Secondary	−0.047	0.052	−0.112	0.039	0.065	0.088
	±0.038	±0.061	±0.012	±0.065	±0.055	±0.068
			HV 1620			
Binary	0.004	−0.048	−0.120	−0.073	0.124	0.168
Primary	−0.015	−0.130	−0.127	−0.152	0.112	0.152
Secondary	0.015	0.007	−0.117	−0.019	0.132	0.179
	±0.021	±0.026	±0.007	±0.025	±0.027	±0.038
			HV 2241			
Binary	0.001	−0.131	−0.128	−0.157	0.129	0.174
Primary	−0.006	−0.183	−0.138	−0.209	0.132	0.179
Secondary	0.018	0.008	−0.117	−0.019	0.135	0.183
	±0.009	±0.016	±0.007	±0.020	±0.015	±0.025

Table 5.15: Foreground reddening for HV 982, HV 1620 and HV 2241. For each star the individual estimates derived from the work of various authors are listed in addition to the finally adopted values. Also listed are the total reddenings to the programme stars (from table 5.14) and for comparison the reddenings to infinity in the directions of the programme stars.

Method	Resolution	HV 982	HV 1620	HV 2241
H I	48′	0.07	0.10	0.10
(Schwering and Israel, 1991)		±0.01	±0.01	±0.01
H I	15′		0.076	
(McGee and Newton, 1982; Bohlin et al., 1978)			±0.02	
Stellar Photometry	10′	0.050		0.066
(Ostreicher et al., 1995)		±0.02		±0.02
Adopted Foreground		0.06	0.09	0.085
$E(B-V)$		±0.02	±0.02	±0.02
Total $E(B-V)$		0.088	0.168	0.174
		±0.068	±0.038	±0.025
To infinity		0.110	0.174	0.187
		±0.035	±0.035	±0.035

and Newton data have a 15′ resolution. A PC computer program (obtained from Oestreicher) was also used to determine $E(B-V)_{\rm Gal}$ for HV 982 and HV 2241. The computer program corresponds to the LMC foreground reddening maps of Oestreicher et al. Table 5.15 tabulates the various estimates and the adopted means.

Tobin has also derived reddenings to infinity for all three stars. For HV 1620 in the SMC, the H I profile of McGee and Newton were integrated over SMC velocities and converted to a reddening using the gas-to-dust ratio $N({\rm H\,I}) = 59{\times}10^{21}[E(B-V)]$ atom cm^{-2} mag^{-1} (Bessell, 1991). For HV 982 and HV 2241 in the LMC, the 14.5′ resolution H I profiles of McGee and Milton (1966) were integrated over LMC velocities and converted to a reddening using the gas-to-dust ratio $N({\rm H\,I})/E(B-V) = 20{\times}10^{21}$ atom cm^{-2} mag^{-1} (Koorneef, 1982). These 'Cloud' reddenings are then added to the adopted foreground reddenings to give the reddenings to infinity.

Comparison of the total reddenings, the foreground reddenings and reddenings to infinity (table 5.15) for the three programme stars suggest that HV 1620 and HV 2241 are located toward the rear of the gas in the SMC and LMC respectively. Because of the large uncertainty in the reddening in the direction of HV 982, it is not possible to comment on the location of HV 982. In fact the situation is somewhat reversed, the foreground reddening and reddening to infinity in fact place upper and lower limits on the reddening to HV 982 (i.e. $E(B-V)_{\rm HV\,982} = 0.09 \pm 0.06$ rather than 0.088 ± 0.068) although the differences are only just significant.

5.4.3 Interstellar extinction laws

For the Galaxy, $R = A_V/E(B-V) = 3.1$ is adopted (Howarth, 1983). The mean Galactic interstellar extinction law of Seaton (1979) is adopted. The ratios of interstellar extinction ($A_{\bar{\lambda}}$) to colour excess ($E(B-V)$) – i.e. $\chi = A_{\bar{\lambda}}/E(B-V) = R + E(\lambda - V)/E(B-V)$ – are calculated according to the expressions provided by Howarth (1983) (equations (3) & (4)) and Seaton (1979) (table 2),

$$\begin{array}{lll}
0.00 \le x \le 1.83 & \chi_{\rm Gal} = (R-3.1) + [(1.86 - 0.48x)x - 0.1]x \\
1.83 \le x \le 2.75 & \chi_{\rm Gal} = R + 2.56(x-1.83) - 0.993(x-1.83)^2 \\
2.75 \le x \le 3.65 & \chi_{\rm Gal} = (R-3.2) + 1.56 + 1.048x + 1.01/((x-4.60)^2 + 0.280) \\
3.65 \le x \le 7.14 & \chi_{\rm Gal} = (R-3.2) + 2.29 + 0.848x + 1.01/((x-4.60)^2 + 0.280) \\
7.14 \le x \le 10.0 & \chi_{\rm Gal} = (R-3.2) + 16.17 - 3.20x + 0.2975x^2
\end{array} \qquad (5.53)$$

where $x = 1\,000/\lambda$ and λ is in units of nm.

For the Large Magellanic Cloud, $R = 3.1$ is adopted (Koorneef, 1982). For wavelengths shorter than 278 nm (corresponding to $x \geq 3.6$) the 'Average LMC curve' from table III of Fitzpatrick (1986) is adopted

Table 5.16: Adopted ratios of interstellar extinction to colour excess (χ) for Strömgren *uvby* and Cousins $UBVRI$ bandpasses. Mean wavelengths of the bandpasses ($\bar{\lambda}$) are in nm, $x = 1000/\bar{\lambda}$. The Galactic and LMC ratios are the same due to the adoption of the same value of $R = 3.1$ and the same extinction law (Seaton, 1979) for $x \leq 3.6$. The SMC ratios differ due to the adoption of $R = 2.7$. The adopted SMC extinction law is the same as the mean Galactic law for $x \leq 2.75$.

Bandpass	$\bar{\lambda}$	x	$\chi_{\rm Gal}$	$\chi_{\rm LMC}$	$\chi_{\rm SMC}$
u	347	2.886	4.8	4.8	4.6
v	411	2.434	4.3	4.3	3.9
b	467	2.142	3.8	3.8	3.4
y	546	1.832	3.1	3.1	2.7
U	361	2.774	4.6	4.6	4.5
B	441	2.266	4.0	4.0	3.6
V	551	1.814	3.1	3.1	2.7
R	658	1.519	2.5	2.5	2.1
I	806	1.241	1.8	1.8	1.4

(equation 5.54),

$$\begin{aligned} 3.6 \leq x \leq 5.9 \quad & \chi_{\rm LMC} = R - 0.69 + 0.89x + \frac{2.55}{\left[x - \frac{4.608^2}{x}\right]^2 + 0.994^2} \\ x \geq 5.9 \quad & \chi_{\rm LMC} = R - 0.69 + 0.89x + \frac{2.55}{\left[x - \frac{4.608^2}{x}\right]^2 + 0.994^2} + 0.50[0.539(x-5.9)^2 + 0.0564(x-5.9)^3] \end{aligned} \tag{5.54}$$

For longer wavelengths the Galactic law as above is adopted.

For the Small Magellanic Cloud, $R = 2.7$ is adopted (Bouchet et al., 1985). For wavelengths shorter than 346 nm (corresponding to $x \geq 2.75$) $\chi_{\rm SMC}$ is estimated via a linear interpolation between the values tabulated in table 2 of Prévot et al. (1984). For longer wavelengths the Galactic law as above is adopted.

The adopted extinction laws are plotted in figure 5.5. Table 5.16 tabulates the adopted ratios of interstellar extinction to colour excess for the *uvby* and $UBVRI$ bandpasses.

Uncertainty in the extinction laws derives from the uncertainties in both R and in the shape of the extinction curve (i.e. $E(\lambda - V)/E(B - V)$). Within the Milky Way, R typically ranges from 3.0 to 3.3 for early-type stars, however R can be as large as 6 in the densest regions of dark nebulae and H II regions (Straižys, 1992). The shape of the extinction curves is most uncertain for ultraviolet wavelengths, i.e. at wavelengths shorter than ~200 nm, with particular uncertainty surrounding the strength or, as in the case of the SMC, the existence of the so-called 2175 Å bump. Studies of individual stars indicate that the cosmic scatter of the shape of the Galactic extinction curve may be as large as 0.66 at λ155 nm (Savage et al., 1985), although at longer wavelengths (λ300 nm) the scatter is significantly less (~0.2-0.3) (Fitzpatrick, 1986). Within the LMC, a significant difference is seen in the shape of the extinction curve for stars in and near to (i.e. within ~0.5°) the 30 Doradus nebula (Fitzpatrick, 1986).

Given an observed magnitude ($m_{\bar{\lambda}}$) of an object in one of the Magellanic Clouds, with total colour excess $E(B-V)_{\rm Tot}$ and a Galactic foreground component of $E(B-V)_{\rm Gal}$ then the reddening-corrected magnitude ($m_{0,\bar{\lambda}}$) is given by,

$$m_{0,\bar{\lambda}} = m_{\bar{\lambda}} - \chi_{\bar{\lambda},{\rm Gal}} E(B-V)_{\rm Gal} - \chi_{\bar{\lambda},{\rm MC}}(E(B-V)_{\rm Tot} - E(B-V)_{\rm Gal}) \tag{5.55}$$

where $\chi_{\bar{\lambda},{\rm MC}}$ is either $\chi_{\bar{\lambda},{\rm LMC}}$ or $\chi_{\bar{\lambda},{\rm SMC}}$ as appropriate.

5.5 Calibrated fluxes

In order to compare visual fluxes estimated from the standard system photometry and the IUE spectrophotometry with theoretical spectral flux distributions, the estimated 'magnitudes' for each bandpass must first be converted into calibrated fluxes.

5.5.1 Calibration

The calibrated fluxes corresponding to observed standard system 'magnitudes' have been determined by a number of investigators, (e.g. Heber et al., 1984; Bessell, 1979; Underhill, 1981). However, since none of these sources provide a single, consistent set of fluxes for all six of the bandpasses used in the current

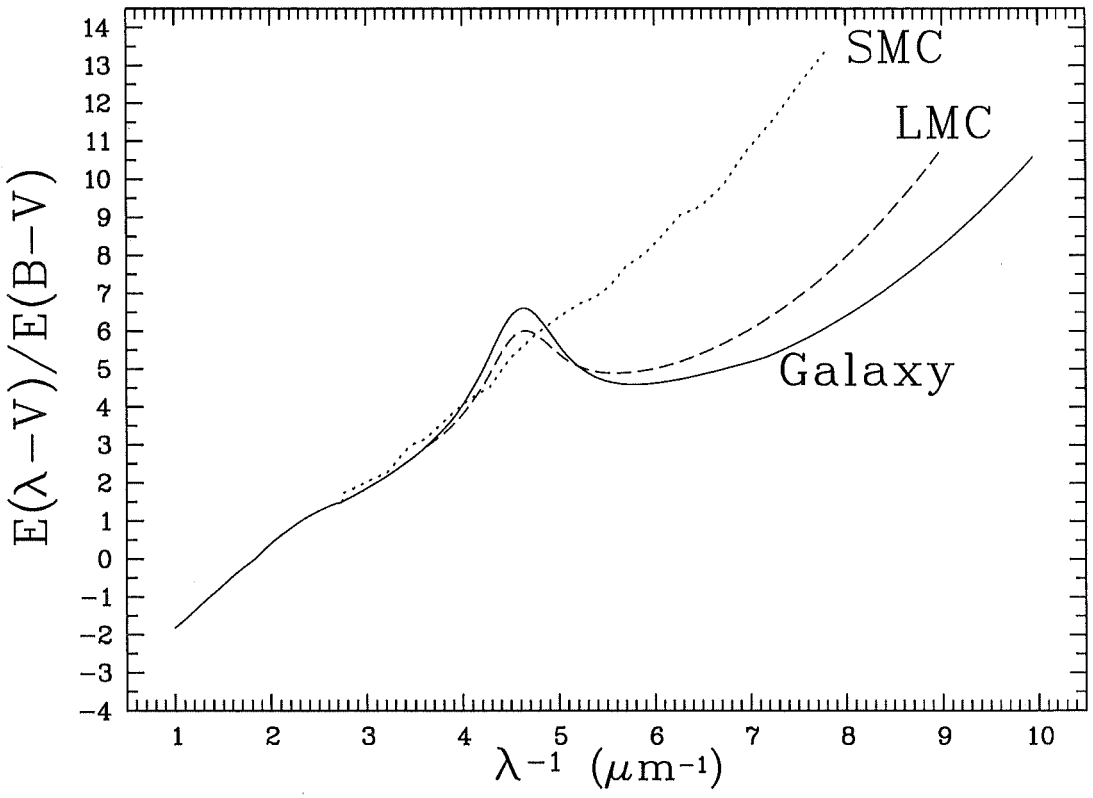

Figure 5.5: Adopted extinction laws. The solid line is that for the Galaxy (Seaton, 1979), the dashed is that for the mean LMC extinction curve (Fitzpatrick, 1986), while the dotted line is for the SMC (Prévot et al., 1984). Note that the LMC extinction of Howarth (Howarth, 1983) lies about halfway between the adopted LMC and SMC curves.

Table 5.17: Calibrated fluxes for *uvby* and Cousins *UBVRI* bandpasses. The adopted 'standard magnitudes' for Vega ($m_{\rm Vega}$) are derived from the following adopted magnitudes and colour indices: $V_{\rm J} = 0.03$, $(U-B)_{\rm J} = 0.00$, $(B-V)_{\rm J} = 0.00$, $(V-R)_{\rm J} = -0.04$, $(V-I)_{\rm J} = -0.06$ (Johnson, 1965): $y = V$ (adopted): $(b-y) = 0.004$, $\rm m_1 = 0.159$ and $\rm c_1 = 1.089$ (Crawford et al., 1972). The Johnson $(V-R)_{\rm J}$ and $(V-I)_{\rm J}$ are transformed into the $(V-R)_{\rm C}$ and $(V-I)_{\rm C}$ of the Cousins system according to the transformations $(V-R)_{\rm C} = 0.73(V-R)_{\rm J} - 0.03 = -0.06$ and $(V-I)_{\rm C} = 0.713(V-I)_{\rm J} = -0.04$ (Bessell, 1979). Calibrated fluxes ($f_{\bar{\lambda},m_{\bar{\lambda}}=0}$) in units of 10^{-9}erg cm^{-2}s^{-1}Å^{-1} for $m_{\bar{\lambda}} = 0^{\rm m}00$ for each bandpass are tabulated from Heber et al. (1984), Bessell (1979), and Underhill (1981) and for the new results derived here.

	$\lambda_{\rm eff}$	Adopted $m_{\rm Vega}$	Heber (1984)	Bessell (1979)	Underhill (1981)	This work
u	346	1.442	11.46		12.05	12.40
v	411	0.195	8.42		9.85	8.82
b	466	0.034	5.65		5.74	5.93
y	545	0.030	3.60		3.69	3.75
U	366	0.03	4.16	4.19		4.26
B	436	0.03	6.17	6.60		6.51
V	545	0.03	3.58	3.61		3.71
R	641	0.09		2.25		2.35
I	798	0.07		1.22		1.19

work, a new calculation of the flux calibration was made. The method of Heber et al. (1984) was adopted. Bandpass weighted fluxes for Vega ($f_{\bar{\lambda},\rm Vega}$) are calculated by convolving the bandpass response functions with the theoretical spectral flux distribution of Vega (Kurucz (1993) model FVEGA.PCK from CDROM13, $T_{\rm eff} = 9550$ K, $\log[g] = 3.95$ and $[{\rm M/H}] = -0.5$) scaled to give the observed flux *at Earth* from Vega of $f_\lambda = 3.46{\times}10^{-9}$erg cm^{-2}s^{-1} Å^{-1} at λ555.6 nm (Mégessier, 1995). Calibrated fluxes corresponding to $m_{\bar{\lambda}} = 0.00$ mag are then derived from the standard system photometry for Vega via,

$$f_{\bar{\lambda},m_{\bar{\lambda}}=0} = 10^{\frac{m_{\bar{\lambda},\rm Vega}}{2.5}} f_{\bar{\lambda},\rm Vega}. \tag{5.56}$$

where $m_{\bar{\lambda},\rm Vega}$ is the standard system magnitude for Vega for the bandpass. Table 5.17 tabulates the derived calibrated fluxes as well as those of Heber et al. (1984), Bessell (1979), and Underhill (1981) for comparison and to give an indication of the uncertainties in the calibration. Corresponding fluxes between the four calibrations generally agree within 5% except for the u flux between Heber et al. (1984) and the new calculation which differ by of the order of 10%. The differences between the new calibration and that of Heber et al. (1984) can be attributed to a) a more recent theoretical atmosphere model for Vega with slightly different parameters (the model used by Heber et al. (1984) had $T_{\rm eff} = 9\,400$ K, $\log[g] = 3.95$ and $[{\rm M/H}] = -0.0$), b) a slightly different $f_{\lambda=555.6\ \rm nm}$, and c) different bandpass response functions. The theoretical atmosphere model for Vega used here is one of the nine models favored by Castelli and Kurucz (1994) and corresponds to $E(B-V) = 0.00$ mag and solar Helium abundance for Vega. The newer model improves the agreement between the theoretical model and observations, particularly in the ultraviolet (Castelli and Kurucz, 1994) which explains the larger difference between the Heber et al. (1984) and the new u calibration. The new calibration is therefore to be preferred.

The observed flux ($f_{\bar{\lambda}}$) for any star with observed magnitude ($m_{\bar{\lambda}}$) is then given by,

$$f_{\bar{\lambda}} = 10^{\frac{m_{\bar{\lambda}}}{-2.5}} f_{\bar{\lambda},m_{\bar{\lambda}}=0} = 10^{\frac{m_{\bar{\lambda}}-m_{\bar{\lambda},\rm Vega}}{-2.5}} f_{\bar{\lambda},\rm Vega}. \tag{5.57}$$

For a reddened star in either of the Magellanic Clouds with total colour excess $E(B-V)_{\rm Tot}$ and a Galactic foreground component of $E(B-V)_{\rm Gal}$, the reddening corrected flux ($f_{0,\bar{\lambda}}$) is given by,

$$f_{0,\bar{\lambda}} = 10^{\frac{m_{\bar{\lambda}}-\chi_{\bar{\lambda},\rm Gal}E(B-V)_{\rm Gal}-\chi_{\bar{\lambda},\rm MC}(E(B-V)_{\rm Tot}-E(B-V)_{\rm Gal})}{-2.5}} f_{\bar{\lambda},m_{\bar{\lambda}}=0} = 10^{\frac{m_{0,\bar{\lambda}}}{-2.5}} f_{\bar{\lambda},m_{\bar{\lambda}}=0}, \tag{5.58}$$

where $\chi_{\bar{\lambda},\rm Gal}$ and $\chi_{\bar{\lambda},\rm MC}$ are the appropriate ratios of interstellar extinction to colour excess for the Galaxy and whichever Cloud the star resides in (see section 5.4.3).

5.5.2 Calibrated fluxes for the programme stars at the IUE phases

V and I magnitudes are taken from tables 5.12 and 5.13 while b, v and u magnitudes are estimated from the adopted photometry (tables 5.12 and 5.13), adopting $y{\equiv}V$ and the following equations,

$$b = (b-y) + V, \tag{5.59}$$

Table 5.18: Calibrated fluxes in the *uvbyVI* bandpasses for the three programme stars HV 982, HV 1620 and HV 2241. Listed are the observed magnitudes ($m_{\bar{\lambda}}$), the observed fluxes ($f_{\bar{\lambda}}$), the reddening-corrected magnitudes ($m_{0,\bar{\lambda}}$) and the reddening-corrected fluxes ($f_{0,\bar{\lambda}}$). The fluxes are in units of erg cm^{-2}s^{-1}Å^{-1}. V_{uvby} and V_{VI} refer to the V magnitudes derived from the *uvby* and *VI* photometry respectively.

	$m_{\bar{\lambda}}$	$f_{\bar{\lambda}}$	$m_{0,\bar{\lambda}}$	$f_{0,\bar{\lambda}}$
		HV 982		
u	14.756	1.553×10^{-14}	14.334	2.291×10^{-14}
v	14.674	1.191×10^{-14}	14.297	1.685×10^{-14}
b	14.637	8.288×10^{-15}	14.302	1.128×10^{-14}
V_{uvby}	14.685	4.960×10^{-15}	14.412	6.380×10^{-15}
V_{VI}	14.615	5.291×10^{-15}	14.344	6.788×10^{-15}
I	14.736	1.521×10^{-15}	14.576	1.764×10^{-15}
		HV 1620		
u	14.496	1.973×10^{-14}	13.707	4.084×10^{-14}
v	14.508	1.388×10^{-14}	13.819	2.616×10^{-14}
b	14.472	9.648×10^{-15}	13.864	1.688×10^{-14}
V_{uvby}	14.469	6.052×10^{-15}	13.979	9.508×10^{-15}
V_{VI}	14.477	5.008×10^{-15}	13.992	9.394×10^{-15}
I	14.437	2.004×10^{-15}	14.162	2.581×10^{-15}
		HV 2241		
u	13.475	5.052×10^{-14}	12.640	1.090×10^{-13}
v	13.557	3.332×10^{-14}	12.812	6.620×10^{-14}
b	13.508	2.344×10^{-15}	12.846	4.312×10^{-14}
V_{uvby}	13.507	1.468×10^{-14}	12.967	2.415×10^{-14}
V_{VI}	13.521	1.449×10^{-14}	12.986	2.372×10^{-14}
I	13.510	4.706×10^{-15}	13.193	6.302×10^{-15}

$$v = (v-b)+(b-y)+V, \tag{5.60}$$

$$u = (u-b)+(b-y)+V. \tag{5.61}$$

In the case of V there are two values, one derived from the VI photometry, the other from the *uvby* photometry. Rather than averaging the values, both are retained in the analysis to give an indication of the uncertainties. Observed and dereddened magnitudes and fluxes are tabulated for the three programme stars HV 982, HV 1620 and HV 2241 in table 5.18. Dereddened magnitudes are calculated according to equation 5.55 with the total and foreground colour excess taken from tables 5.14 and 5.15 and the ratios of interstellar extinction to colour excess taken from table 5.16. Observed and dereddened fluxes are calculated from equations 5.57 and 5.58 with $f_{\bar{\lambda},m_{\bar{\lambda}}=0}$ taken from table 5.17.

5.5.3 IUE Ultraviolet Spectrophotometry

Collaborator E.F. Guinan acquired IUE satellite low-resolution uv spectra with the SWP camera and large entrance aperture for the three programme stars, as detailed in tables 5.19 and 5.20. The spectra were reprocessed with the Final Archive (NEWSIPS) software in order to obtain improved spectral resolution and to correct for the variation of the camera sensitivity with temperature and time (Garhart, 1992; Nichols and Linsky, 1996). The uncertainty in the reprocessed fluxes is estimated to be ~5 per cent (Imhoff, 1996). Figure 5.6 presents the observed spectral flux distributions. Also shown in figure 5.6 are the three bandpasses (UV_4, UV_5 and UV_6) used to calculate representative uv flux levels for comparison with the theoretical spectral flux distributions. The bandpasses were selected so as to be relatively free of significant absorption features.

Dereddened fluxes ($f_{0,\bar{\lambda}}$) for each bandpass (denoted by its mean wavelength $\bar{\lambda}$) are derived from the observed fluxes ($f_{\bar{\lambda}}$) via,

$$f_{0,\bar{\lambda}} = 10^{\frac{\chi_{\bar{\lambda},\mathrm{Gal}}E(B-V)_{\mathrm{Gal}}-\chi_{\bar{\lambda},\mathrm{MC}}(E(B-V)_{\mathrm{Tot}}+E(B-V)_{\mathrm{Gal}})}{2.5}} f_{\bar{\lambda}} \tag{5.62}$$

where once again $\chi_{\bar{\lambda},\mathrm{Gal}}$ and $\chi_{\bar{\lambda},\mathrm{MC}}$ are the appropriate ratios of interstellar extinction to colour excess for

Table 5.19: IUE UV Spectrophotometry

Variable	Image	Mid-Exposure Date	Time (UT)	Exposure (sec)
HV 982	SWP 50009	1994-Day-044 (Feb-13)	13:52:28	5999.691
HV 1620	SWP 50613	1994-Day-113 (Apr-23)	10:07:42	5999.481
HV 2241	SWP 52968	1994-Day-337 (Dec-03)	06:33:45	2399.177

Table 5.20: IUE UV Spectrophotometry. Listed are the Julian Day Number (JD), the Heliocentric Julian Corrections (HCC), the Heliocentric Julian Day Number (HJD) and the orbital phase (computed according to the ephemerides in section 3.3.3).

Variable	Image	JD −2400000	HCC	HJD −2400000	Phase
HV 982	SWP 50009	49397.11282	−0.00037	49397.1125	0.5592
HV 1620	SWP 50613	49465.95673	−0.00039	49465.9563	0.1540
HV 2241	SWP 52968	49689.78732	0.00012	49689.7874	0.8207

the Galaxy and whichever Cloud the star resides in (see section 5.4.3), $E(B-V)_{\rm Tot}$ is the total colour excess and $E(B-V)_{\rm Gal}$ is the foreground component of the total colour excess.

Figure 5.7 presents representative 'pictures' of the three programme stars at orbital phases corresponding to mid-IUE-exposure. For all three stars the observed light at these phases is clearly composed of significant contributions from both components. Fortunately though, the analysis and interpretation is not complicated by eclipse phenomena.

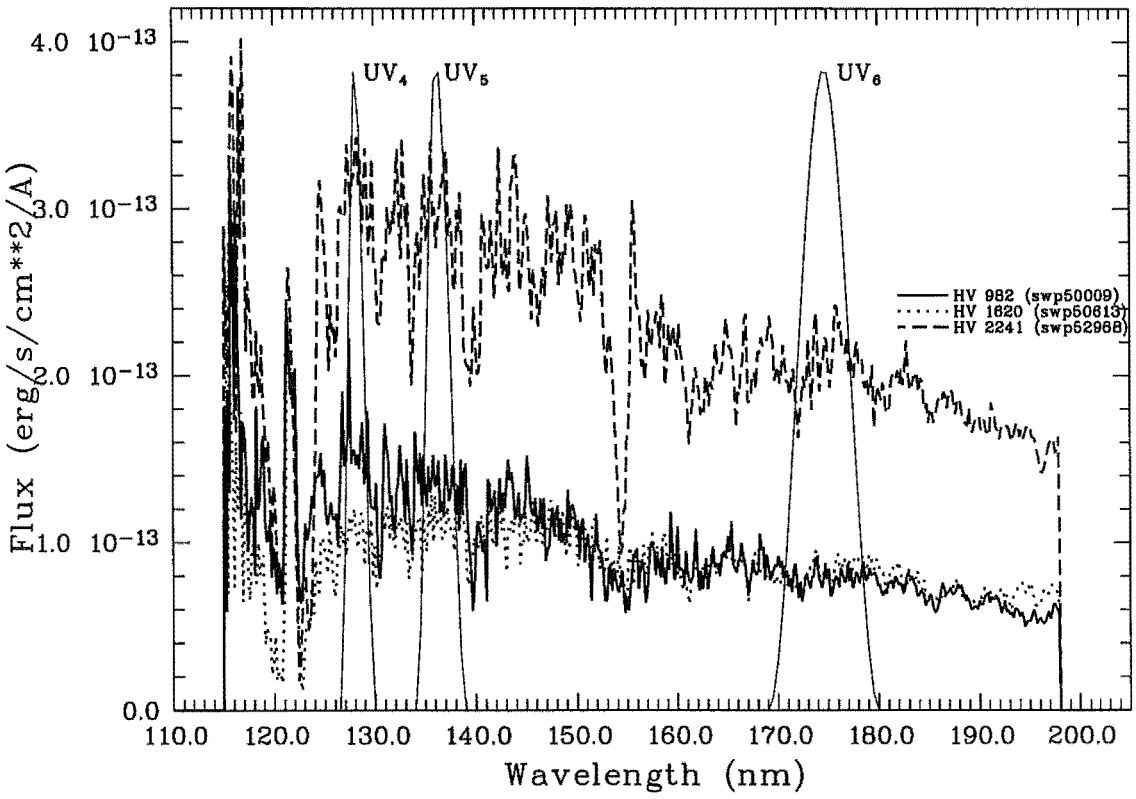

Figure 5.6: IUE SWP spectra of HV 982, HV 1620 and HV 2241. Also shown are the three bandpasses (labeled UV_4, UV_5 and UV_6) used to measure monochromatic fluxes for comparison with theoretical model flux distributions.

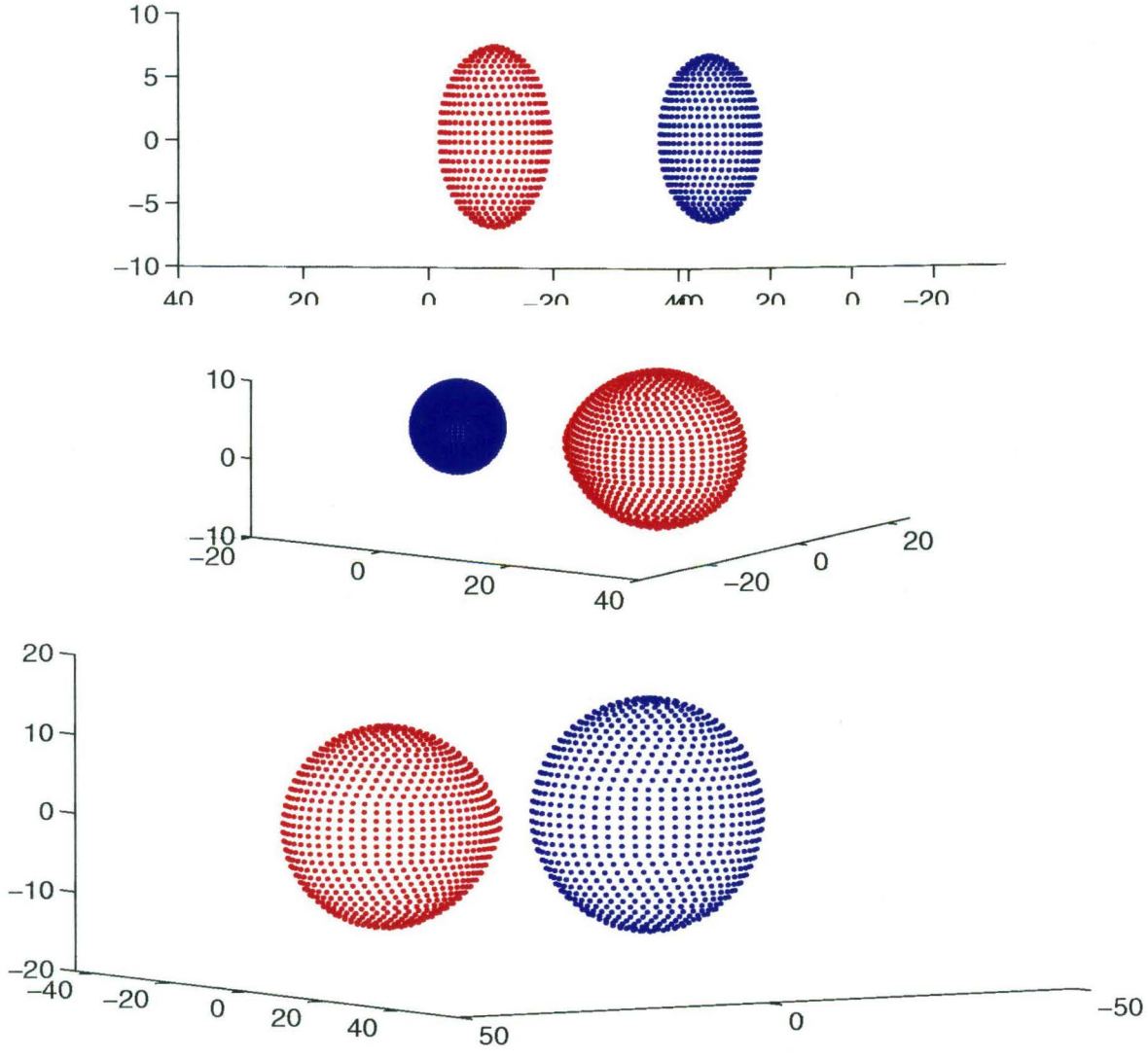

Figure 5.7: These show the physical orientation of the three systems HV 982, HV 1620 and HV 2241 (from top to bottom respectively) at the times of observation by the IUE. The plots are generated by MATLAB from output derived from the *WD95* code. Due to as yet misunderstood subtleties of the MATLAB plotting package, these renderings are not completely accurate. The HV 982 picture appears to have been stretched in the vertical during the generation of the encapsulated postscript file while doubt remains as to whether the inclination is being correctly accounted for for all three, which has the greatest consequences for HV 1620 whose inclination is furtherest from 90°. Nevertheless the pictures are believed to depict the relative positions and sizes of the components reasonably accurately.

5.6 Temperature determination

By comparison of *theoretical* spectral flux distributions – derived from the *WD95* program and the Kurucz theoretical stellar atmosphere spectral flux distributions – with the *observed* spectral flux distributions – from the IUE observations and the calibrated standard system photometry – the effective temperatures of the individual components of each of the three programme stars can be determined.

The relative surface brightness of the two components of a binary system is, in general, well defined by the light curve. With the adoption of an effective temperature of one of the components, the corresponding effective temperature of the other component is then likewise well defined. Preliminary *WD95* light curve solutions for a range of primary component effective temperatures were thus determined and theoretical spectral flux distributions corresponding to each solution were computed for the phase of the IUE observation for each of the three programme stars. The theoretical spectral flux distributions are derived by integrating the light over the visible surface of each component of the binary at each wavelength of interest. For the current purposes spectral flux distributions were computed from $\lambda 100$ to $\lambda 1000$ nm. By using a program derived from the *WD95* program the correct relative flux from each component is included in the sum. Additionally, effects such as the so-called reflection effect and the variation of the local effective temperature (and hence surface flux intensity) across the surface of each component due to tidal and rotational distortions are thus included in the calculations. The more non-spherical a component the more important such effects become. Full details of the calculation of the theoretical spectral flux distributions are given in appendix C.1.

Bandpass integrated fluxes corresponding to the observed *uvbyVI* and the three ultraviolet bandpass (see figure 5.6) fluxes were computed for the theoretical spectral flux distributions by convolving the adopted standard system (see appendix F) and ultraviolet UV_4, UV_5 and UV_6 response functions with the computed spectral flux distributions. The three ultraviolet bandpasses were also convolved with the dereddened IUE fluxes to give 'observed' fluxes for each of the ultraviolet bandpasses. The nine theoretical fluxes were then compared with the observed fluxes to determine the effective temperature most consistent with the observations. The theoretical flux as calculated is, in some sense, an average of the emergent flux over the surface of the of both components *at the surface of the star*. This is slightly inconsistent because the two components of each binary are at slightly different distances from the observer. But of course, in practice, given the total distance between observer and binary, the error introduced by the slight difference in the distance to each component is utterly negligible. The reddening free observed flux at Earth for each bandpass ($f_{\bar{\lambda},\mathrm{Obs}}$ [$\mathrm{W\,m^{-1}\,m^{-2}}$]) is related to the corresponding theoretical light at the surface of the star ($\mathcal{L}_{\bar{\lambda},\mathrm{Th}}$ [$\mathrm{W\,m^{-1}\,ster^{-1}}$]) according to the following relation,

$$f_{\bar{\lambda},\mathrm{Obs}} = \frac{\mathcal{L}_{\bar{\lambda},\mathrm{Th}} d\Omega}{d^2 d\Omega} \tag{5.63}$$

where d is the distance between observer and binary, at this stage in meters if $f_{\bar{\lambda},\mathrm{Obs}}$ and $\mathcal{L}_{\bar{\lambda},\mathrm{Th}}$ have the units as above. By definition, the distance modulus $(m - M)$ is,

$$(m - M)_{\bar{\lambda}} = 5 \log_{10}[d] - 5 \tag{5.64}$$

provided d is now measured in parsec. Using equation 5.63 to eliminate d from equation 5.64 gives,

$$(m - M)_{\bar{\lambda}} = 2.5 \log_{10}[\mathcal{L}_{\bar{\lambda},\mathrm{Th}}] - 2.5 \log_{10}[f_{\bar{\lambda},\mathrm{Obs}}] - 5 \log_{10}[3.085678] - 85 \tag{5.65}$$

since there are 3.085678×10^{16} m per parsec.

In general the ratio of the theoretical flux to the the observed flux, or equivalently, the distance modulus estimate, at any given wavelength will vary as a function of the effective temperature or, as in the case of binary stars, as a function of the particular combination of effective temperatures of the two components of the model used to compute the theoretical flux. The inter agreement between distance modulus estimates calculated at a number of different wavelengths therefore gives some indication of the overall agreement between the observed and theoretical flux distributions. Formally, the best estimate of the effective temperatures of the two components of the binary star is given by the model with the minimum internal scatter between the distance modulus estimates.

For the three programme stars, as described in section 4.4, preliminary *WD95* light solutions were obtained over a range of primary star temperatures. Corresponding spectral flux distributions were then calculated. The nine distance modulus estimates derived from the *uvbyVI* photometry and the three ultraviolet bandpasses were compared to estimate the appropriate combination of effective temperatures for the component stars. The I flux for HV 1620 was found to be slightly excessive and could only be estimated well at the

Table 5.21: The adopted effective temperatures of the primary components of the three programme stars. Also listed for HV 1620 and HV 2241 are the mean distance moduli derived from the individual estimates from each bandpass (UV_4, UV_5, UV_6, u, v, b, V, I) corresponding to the adopted temperatures (I not used for HV 1620).

Star	$T_{\rm eff,1}$	$T_{\rm eff,2}$	$(m-M)$
HV 982	23000	22400	...
	±5000	±5000	...
HV 1620	33000	24400	18.6
	±4500	±3500	±0.3
HV 2241	27000	20200	18.50
	±3000	±1500	±0.16

expense of good agreement at all other eight bandpasses. Thus the effective temperatures for HV 1620 were re-estimated excluding the I flux. (Discussion of the possible reasons for and implications of this apparent infrared excess will be left to section 6.1.)

Log/log plots of the observed and theoretical fluxes were also compared visually for goodness of fit and to gain some estimate of the uncertainty in the estimate of the effective temperatures. Figures 5.8, 5.9, 5.10 show plots of the observed and theoretical fluxes for small ranges of primary component effective temperature, centered on the adopted effective temperature for each of the three programme stars. For a given value of the reddening the effective temperature of the primary component can be estimated to within $\pm 1000 - 2000$ K. However the uncertainties in the reddening lead to somewhat larger total uncertainties in the effective temperatures. The adopted effective temperatures are listed in table 5.21. Uncertainties for the primary component effective temperatures ($T_{\rm eff,1}$) have been estimated by determining the effective temperatures corresponding to the extreme values of the reddening indicated by the uncertainties in the adopted total reddenings (table 5.14). The uncertainties listed in table 5.21 for the secondary component effective temperatures ($T_{\rm eff,2}$) are based on the range of $T_{\rm eff,2}$ corresponding to the range of $T_{\rm eff,1}$ given by the indicated uncertainties. Of course the effective temperatures of the two components of each system are strongly correlated. The $T_{\rm eff,2}$ corresponding to an adopted $T_{\rm eff,1}$, and vice versa is well defined by the light curves. The standard errors for the $T_{\rm eff,2}$ parameter corrections reported by the *WD95* program are typically of the order of 50 K for HV 982, 80 K for HV 1620 and 70 K for HV 2241 and these probably better represent the uncertainty in the $T_{\rm eff,2}$ which corresponds to a given adopted $T_{\rm eff,1}$.

Also tabulated in table 5.21 are the mean distance moduli derived from the individual estimates from each bandpass (UV_4, UV_5, UV_6, u, v, b, V, I) corresponding to the adopted temperatures for HV 1620 and HV 2241. (Without spectroscopic radial-velocity curves the distance to HV 982 can not be determined directly.) The quoted uncertainties for the distance moduli again are simply derived by considering the range of the distance moduli corresponding to the uncertainty in the effective temperatures. No allowance has been made for the contribution to the uncertainty in the distance moduli from the uncertainties in the major semi-axes of the systems and the surface areas of the individual components of each system. The standard errors on the major semi-axes reported by the *WD95* program are of the order of 2% and 1% for HV 1620 and HV 2241 respectively which correspond to contributions of 0.04 and 0.02 mag to the uncertainties in the respective distance moduli, which are not significant compared to the uncertainties due to the uncertainties in the effective temperatures. It should be noted though that an uncertainty of 5% in the major semi-axis corresponds to an uncertainty of 0.1 mag which, if added quadratically, would increase the uncertainty in the HV 2241 distance modulus to 0.19 mag. The derived distance moduli are in reasonable accord with other estimates derived by other investigators using a variety of techniques and types of indicators (see section 1.2.2).

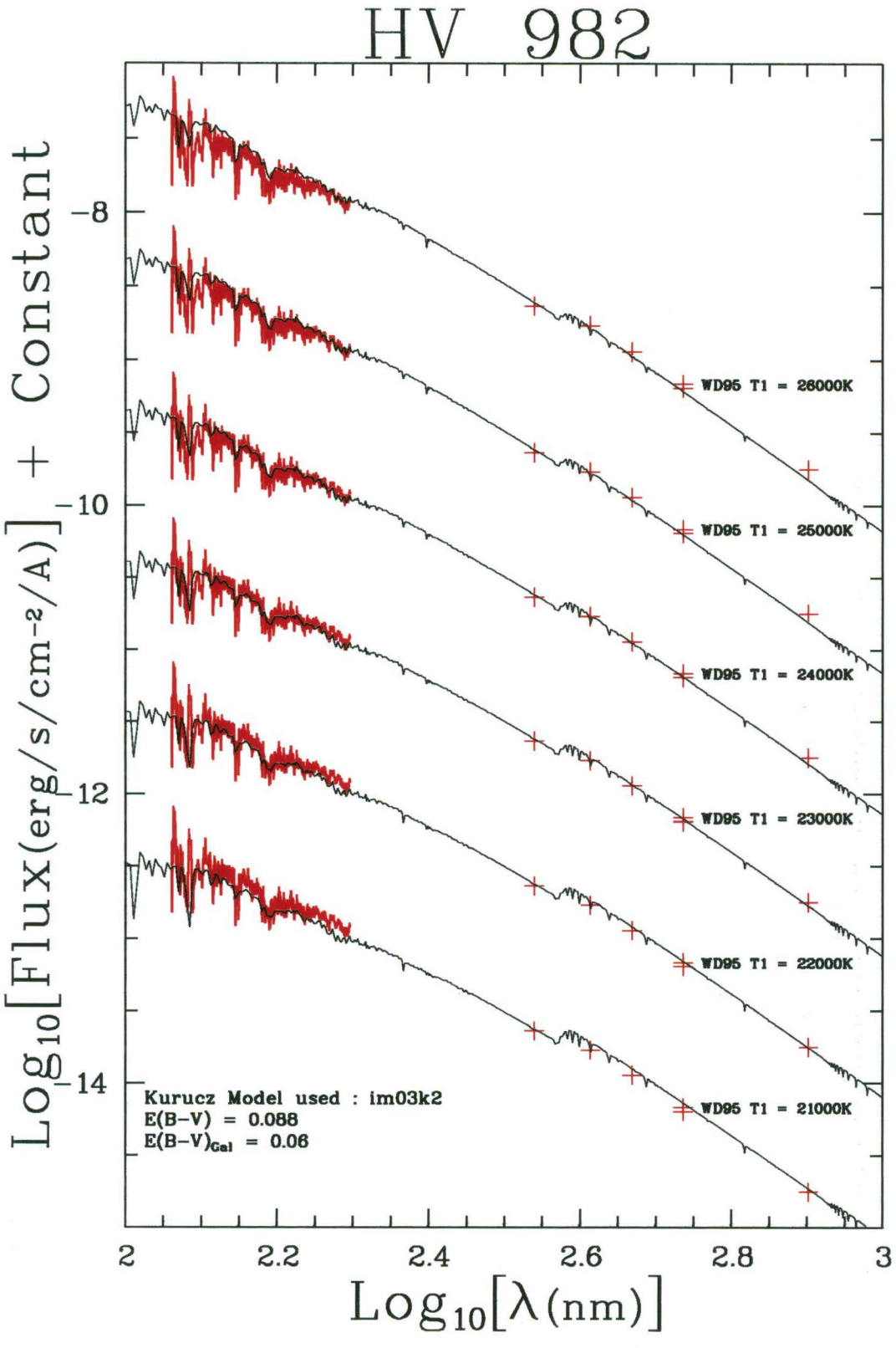

Figure 5.8: Observed and theoretical spectral flux distributions for HV 982. The thick solid lines are the dereddened IUE SWP spectrophotometry. The crosses indicate the observed u, v, b, V and I fluxes (there are two crosses for V, corresponding to the V fluxes derived independently from the *uvby* and *VI* photometry). The thin solid lines are the theoretical spectral flux distributions derived from the *WD95* program and the Kurucz theoretical stellar atmosphere models. The bottom-most observed fluxes are displayed at actual dereddened signal level. The ones above are then offset by 1,2,3... The theoretical fluxes have been scaled by the mean of the individual scale factors between the nine observed and theoretical fluxes (UV_4, UV_5, UV_6, u, v, b, V_{uvby}, V_{VI} and I).

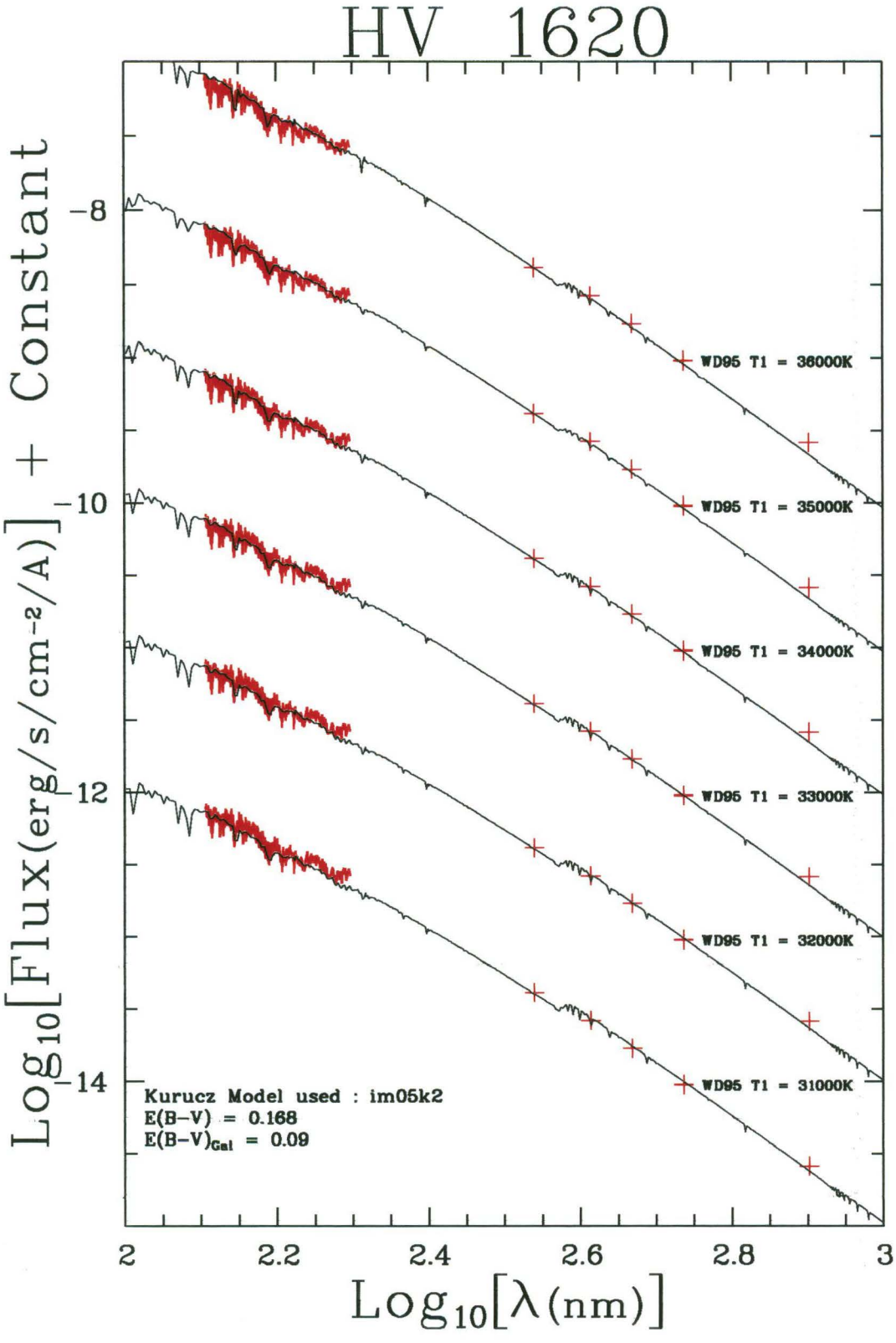

Figure 5.9: Observed and theoretical spectral flux distributions for HV 1620. The thick solid lines are the dereddened IUE SWP spectrophotometry. The crosses indicate the observed u, v, b, V and I fluxes (there are two crosses for V, corresponding to the V fluxes derived independently from the *uvby* and *VI* photometry). The thin solid lines are the theoretical spectral flux distributions derived from the *WD95* program and the Kurucz theoretical stellar atmosphere models. The bottom-most observed fluxes are displayed at actual dereddened signal level. The ones above are then offset by 1,2,3... The theoretical fluxes have been scaled by the mean of the individual scale factors between the eight observed and theoretical fluxes (UV_4, UV_5, UV_6, u, v, b, V_{uvby} and V_{VI}).

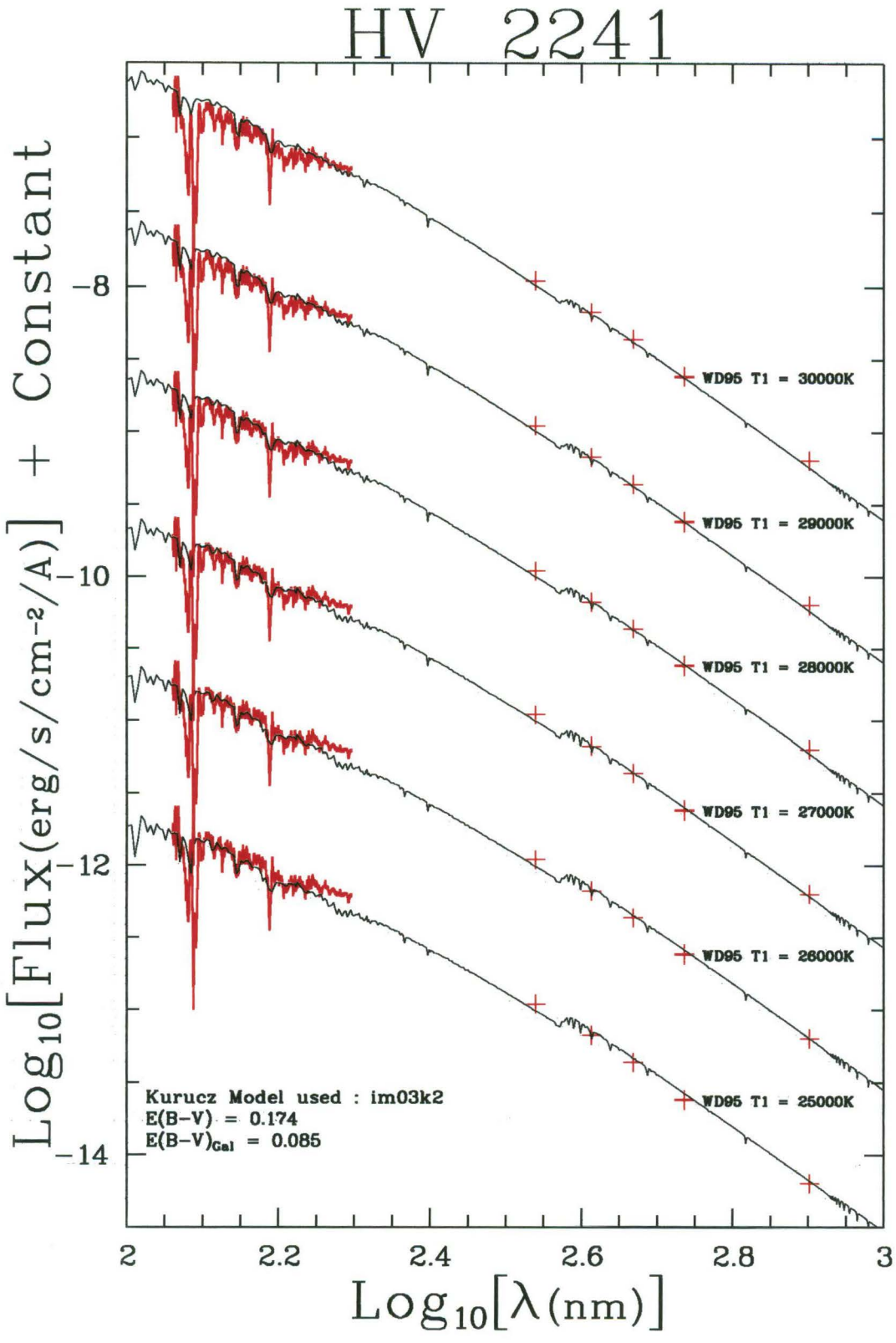

Figure 5.10: Observed and theoretical spectral flux distributions for HV 2241. The thick solid lines are the dereddened IUE SWP spectrophotometry. The crosses indicate the observed u, v, b, V and I fluxes (there are two crosses for V, corresponding to the V fluxes derived independently from the *uvby* and *VI* photometry). The thin solid lines are the theoretical spectral flux distributions derived from the *WD95* program and the Kurucz theoretical stellar atmosphere models. The bottom-most observed fluxes are displayed at actual dereddened signal level. The ones above are then offset by 1,2,3... The theoretical fluxes have been scaled by the mean of the individual scale factors between the nine observed and theoretical fluxes (UV_4, UV_5, UV_6, u, v, b, V_{uvby}, V_{VI} and I).

Chapter 6

Analysis of Photometric Light Curves II. The MJUO MCEB light curves

With the effective temperatures derived from the fitting of model spectral flux densities to the observed spectral flux densities, final solutions to the photometric light and spectroscopic radial-velocity curves of HV 1620 and HV 2241 can now be derived. For HV 982, without spectroscopic radial-velocity curves, the mass ratio and total size of the system can not be determined directly, but indicative dimensions can be derived by adopting a distance modulus and making assumptions based on theoretical stellar evolutionary models.

Combining published times of minima with the times derived from the present observations extends the temporal baseline from which new, improved ephemerides can be derived for all three binaries. Note however that all analysis and calculations of orbital phase in this thesis are based on the ephemerides presented in section 3.3.3. In the case of HV 982 this analysis leads to the identification of the phenomenon of apsidal motion.

6.1 MJUO light curves – Final solutions and discussion

6.1.1 HV 982

As often mentioned in the preceding chapters, absolute masses and radii for HV 982 can not be determined until spectroscopic radial-velocity curves are available. Given the observational requirements for obtaining such data, that effort has been left to other investigators with better access to large telescopes such as those of the European Southern Observatory.

Some useful information can (and has) nevertheless be obtained from the analysis of the light curves. As argued previously the mass ratio probably does not differ greatly from unity. This arises from the observational evidence of very nearly equal-depth minima implying stars of very similar temperature and the observed orbital eccentricity which implies relatively young, i.e. main-sequence, stars. Binary star formation scenarios generally require coeval components while stellar evolution theory requires that two stars of the same age and very nearly the same temperature should be of very nearly the same mass.

Under this assumption, *WD95* solutions were obtained for primary effective temperatures ranging from 18 000 to 30 000 K at mass ratios of 0.90, 1.00 and 1.10. In computing these solutions the orbital eccentricity, longitude of periastron, orbital phase offset, orbital inclination, effective temperature of the secondary component, surface potentials of both components and luminosity of the primary were optimized. Synthetic spectral flux densities were computed using a computer program based on the *WD95* LC program and model stellar atmospheres with metal abundance [−0.3] (Kurucz, 1993). Effective temperatures for the two components of HV 982 have been estimated by comparison of the synthetic spectra and the observed spectral flux density: dereddened IUE SWP uv spectrophotometry and calibrated Strömgren *uvby* and Cousins VI photometry. The resulting adopted effective temperatures, $24\,000 \pm 5\,000$ K for the primary component and $23\,400 \pm 5\,000$ K for the secondary component, are insensitive to the mass ratio over the range 0.90 to 1.10. The large uncertainties in the temperatures derive primarily from the uncertainties in the reddening ($E(B-V) = 0.09 \pm 0.06$) which in turn arise from the uncertainties in the standard system photometry (tables 5.12 and 5.13), in particular $(b-y) = -0.048 \pm 0.038$. The primary cause of these large uncertainties is the difficulty in extracting accurate synthetic aperture photometry in extremely crowded fields. This difficulty is exacerbated by the fact that the Strömgren standard system photometry is based on only two measurements of each of the four instrumental *uvby* magnitudes obtained during two nights, both of questionable photometric quality. It should of course be pointed out that given the effective temperature of one component, the effective temperature of the other is well defined by the light curves with an uncertainty more of the order of ±200 K, however for a given reddening, the uncertainty arising from the flux matching procedure is still of the order of ±1 000 K. Clearly, further work is required in order to refine the temperature estimations for this star.

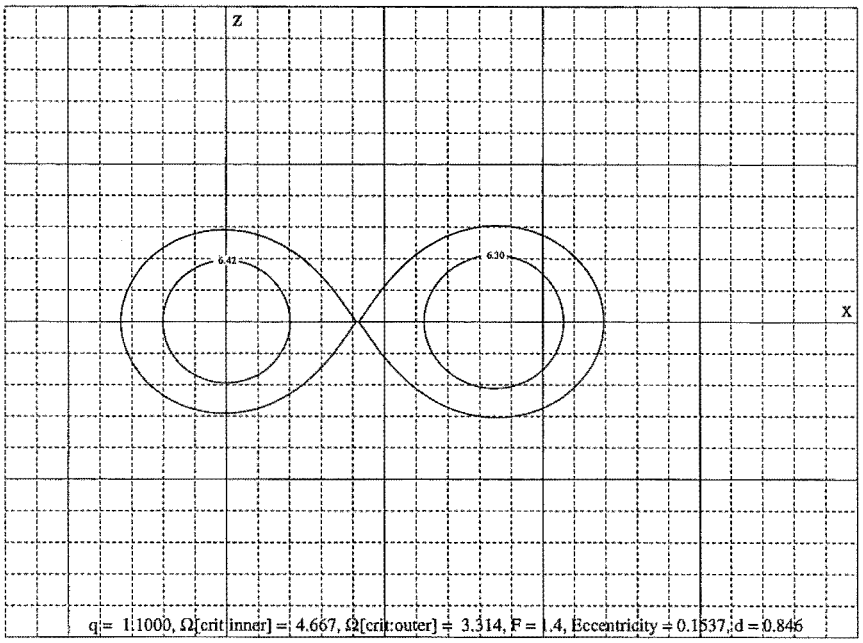

Figure 6.1: Representative schematic of the surfaces of HV 982 in the XZ plane (i.e. the plane perpendicular to the orbital plane) at periastron. The surfaces of the two components are indicated by the two potentials labelled 6.42 and 6.30. Also shown are the critical Roche lobes.

The geometric and aspect-dependent parameters of the *WD95* model, namely the orbital eccentricity, relative radii (i.e. $\mathcal{R}/A$), longitude of periastron and orbital inclination are similarly largely insensitive to the mass ratio. Estimates of these parameters, along with uncertainties, are listed in table 6.1. Figure 6.1 shows representative solution surface potentials and the corresponding critical Roche lobes at periastron. Both components of HV 982 are clearly still well inside their critical Roche lobes.

The phase offset is also well defined by the light curves, although it is correlated with the eccentricity and longitude of periastron. It is however of no physical interest since it merely allows for a zero-point offset in the orbital ephemeris. Its interpretation for a circular orbit is straightforward, it simply denotes the phase of mid-primary minimum. For an eccentric orbit, at least in the *WD95* formulation, its interpretation is not so obvious since the model has been formulated such that if the phase offset is held constant, as the longitude of periastron is varied, the phases of both mid-primary and mid-secondary minima vary accordingly.

Representative times of primary and secondary minima (T_1 and T_2) during the period of observations have thus been determined simply by adopting the orbital phases of minima indicated by tabulations of the light output from preliminary *WD95* solutions in steps of 0.0001 in orbital phase (table 6.1). Plotting the residuals between observed times of minima (see table 6.2) and those predicted by the linear ephemeris – e.g. equation 3.2) – it is immediately apparent, when the two representative minima are combined with the 13 minima between 1897 and 1949 reported by Gaposhkin (1977), that HV 982 displays apsidal motion[1]. It is therefore desirable to determine a new ephemeris taking the apsidal motion into account. A full solution requires the determination of the eccentricity (e), a reference value of the longitude of periastron (ω_0), the rate of advance of the longitude of periastron ($\dot{\omega}$), the orbital inclination (i), a reference epoch (T_0) and the anomalistic period[2] (P_a). Under the assumption the apsidal motion is secular then the longitude of periastron is given by equation (1) of Giménez & Garcia-Pelayo (1983),

$$\omega = \omega_0 + \dot{\omega}E \tag{6.1}$$

where E is the epoch (elapsed cycles) as measured from the time when $\omega = \omega_0$ at time T_0. Adopting the values of e, i, ω_0 and T_0 from preliminary light curve solutions (table 6.1), Tobin (1997b) has recently determined the sidereal period[3] (P_s) and anomalistic period by fitting the observed times of minima with equation (20) of Giménez and Garcia-Pelayo (1983)[4] using the Levenberg-Marquardt method (Press et al.,

[1] Apsidal motion describes the phenomenon of the secular precession of the longitude of periastron. In effect the binary system as a whole rotates.

[2] The *anomalistic* period is the time interval between successive periastron passages.

[3] The *sidereal* period is the mean time interval between successive primary (or secondary) eclipses.

[4] Giménez & Bastero (1995) have revised the work of Giménez & Garcia-Pelayo (1983), extending the truncated series expansion

Table 6.1: Geometric parameters and ephemeris for HV 982. The apsidal period of 75 200 ± 2 300 day is equal to 206 ± 6 yr.

Parameter	*Value*
Derived from light curve analysis	
Eccentricity, e	0.155 ±0.002
Relative Radii, $\mathcal{R}_1/A$	0.197 ±0.002
$\mathcal{R}_2/A$	0.215 ±0.002
Inclination, i	88°.7 ±0°.5
Longitude of periastron, ω_0	223°.0 ±2°.0
Representative primary (deeper) minimum, T_1	HJD 2449335.38655 ±0.00008
Representative secondary (shallower) minimum, T_2	HJD 2449337.66684 ±0.00008
Derived from timings 1897–1996	
T_0 (Eq. 20, Giménez & Garcia-Pelayo 1983)	HJD 2449335.17745 ±0.00008
Sidereal period, P_s	5.335220 d ±0.000003
Anomalistic period, P_a	5.335599 d ±0.000011
Rate of advance of Longitude of periastron, $\dot{\omega}$	0.000446 rad/cycle ±0.000003
Apsidal period, U	75 200 d ±2 300
Estimated dimensions	
Mass, $\mathcal{M}_1$	$9.1 \pm 3.2\,\mathcal{M}_\odot$
$\mathcal{M}_2$	$9.1 \pm 3.2\,\mathcal{M}_\odot$
Mean Radius, $\mathcal{R}_1$	$7.0 \pm 1.0\,\mathcal{R}_\odot$
$\mathcal{R}_2$	$7.0 \pm 1.0\,\mathcal{R}_\odot$
Mean Surface Gravity, $\log[g_1]$	3.7 ± 0.08
$\log[g_2]$	3.7 ± 0.08
Luminosity, $\log[L_1/L_\odot]$	$4.garc00.5$
$\log[L_1/L_\odot]$	4.1 ± 0.5

Table 6.2: Observed times of minima for HV 982. Times are taken from Gaposhkin (1977). Representative minima during the period of observations have also been determined from the preliminary light curve analysis. The type of minima is indicated by either 'P' for primary or 'S' for secondary. The uncertainty in the Gaposhkin timings is likely of the order of 90 min while the uncertainties in the two new times of minima are 40 sec.

HJD	Cycle	P/S	Reference
2413946.555	−6633	P	Gaposhkin
2417590.584	−5950	P	Gaposhkin
2423875.527	−4772	P	Gaposhkin
2425849.645	−4402	P	Gaposhkin
2426060.243	−4363	S	Gaposhkin
2426412.253	−4297	S	Gaposhkin
2426577.631	−4266	S	Gaposhkin
2427786.315	−4039	P	Gaposhkin
2429189.469	−3776	P	Gaposhkin
2429629.338	−3694	S	Gaposhkin
2431304.630	−3380	S	Gaposhkin
2432070.603	−3236	P	Gaposhkin
2433153.625	−3033	P	Gaposhkin
2449335.38655	0	P	This work
2449337.66684	0	S	This work

1980). For the Gaposhkin timings, an uncertainty of 90 min, which is considered representative based on analysis of other systems (Watson et al., 1992; Tobin et al., 1993a), was adopted. The rate of advance of the longitude of periastron is given by,

$$\dot{\omega} = 2\pi \left(1 - \frac{P_{\rm s}}{P_{\rm a}}\right), \tag{6.2}$$

and the apsidal period (U) is given by,

$$U = \frac{2\pi}{\dot{\omega}} P_{\rm a} = \frac{P_{\rm a}^2}{P_{\rm s} - P_{\rm a}} \tag{6.3}$$

The new values for $P_{\rm s}$, $P_{\rm a}$, U and $\dot{\omega}$ are also reported in table 6.1. Figure 6.2 shows the residuals between the observed times of minima and those predicted by the linear ephemeris of,

$$\begin{array}{rcl} \text{Time of primary minimum} & = & \text{HJD2449335.17745} \;+\; 5.335220\times E. \end{array} \tag{6.4}$$

Also shown are the residuals between the predicted times of minima according to equation (20) of Giménez and Garcia-Pelayo with the new values for the various parameters and the above linear ephemeris. The full ephemeris for HV 982 is given by equation (20) of Giménez and Garcia-Pelayo substituting numerical values reported in table 6.1.

In systems like HV 982, apsidal motion is primarily a consequence of the deviation from spherical symmetry caused by rotational and tidal distortions. There is also a General Relativistic component, but this is generally only a small contribution to the total effect. Accurate determinations of the apsidal period, orbital eccentricity and component masses and radii of eccentric binary stars permit detailed comparisons of internal structure of real stars and those predicted by theory (e.g. Claret and Giménez 1993). HV 982 is only the second extragalactic eclipsing binary for which apsidal motion has been confirmed (Pritchard et al., 1994). While the above apsidal motion parameters are probably accurate enough for a useful comparison between observation and theory, accurate spectroscopic radial-velocity curves are needed to specify the masses and radii with sufficient accuracy to make such a comparison meaningful since the structure constant depends on $\mathcal{R}^5$.

The *WD95* luminosities of the components, and in particular of the primary, act merely as scaling factors due to the way in which the observed differential magnitudes were converted into light values for input into

for equation (20) to terms up to the sixth power of the eccentricity. They note however that equation (20) is nonetheless accurate to terms up to the fifth power of the eccentricity.

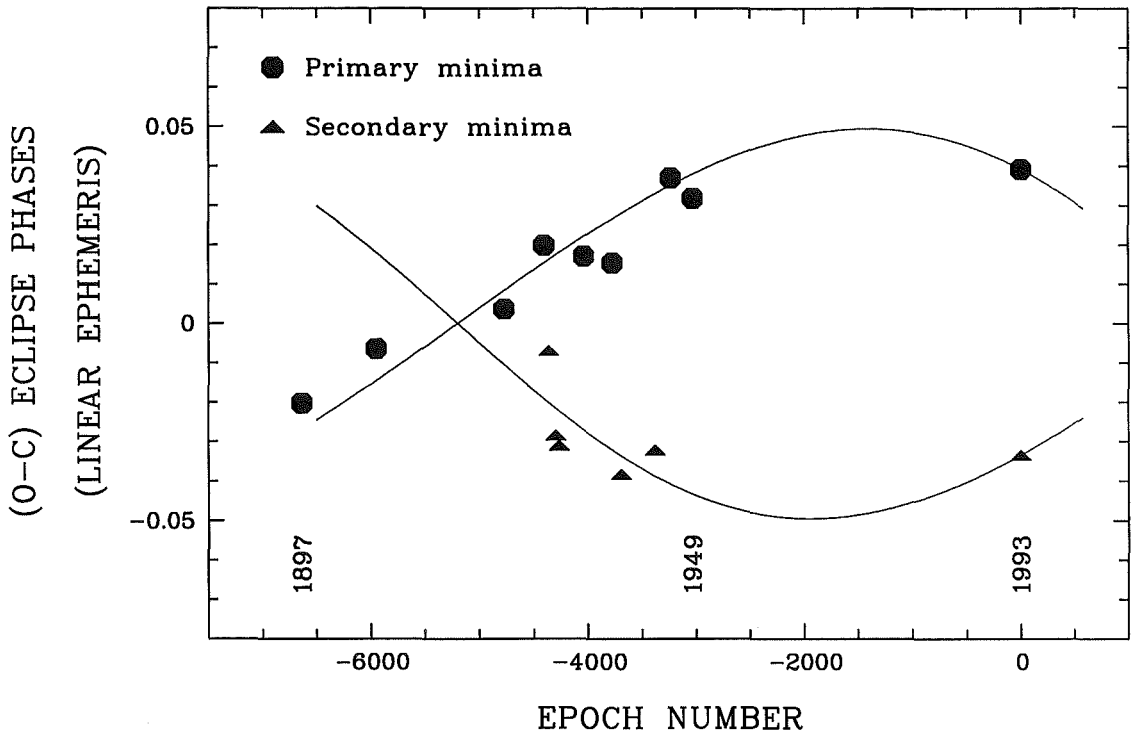

Figure 6.2: Apsidal motion analysis of HV 982. The deviations of a century of observed timings from a linear ephemeris (equation 6.4, points) should be compared with the fit (full lines) corresponding to the parameters reported in table 6.1. The rms deviation of the older, photographic timings about the fitted curves is actually 60 minutes, similar to the 90 minutes assumed in determining the full ephemeris.

the *WD95* DC program. Thus while the ratio between the primary and secondary component luminosities are meaningful, inter-comparison between the bandpasses, or interpretation of the overall, level is not.

As discussed in section 5.4.1 the $(b-y)$ colours and c_1 indices of the individual components of HV 982 have been derived (table 5.14) from the the relative light levels from the two components in each bandpass as provided by LC. This can also be done by convolving appropriate bandpass spectral response functions with the individual component spectral flux densities which are generated as a matter of course when the binary-system spectral flux densities are generated. In either case, adopting the empirical relations for MK classification of Crawford (1978) for main-sequence B-type stars allows the estimation of the MK types of the components of HV 982. From their c_1 indices, both components turn out to be either B1 V or B1.5 III stars with an uncertainty of half an MK subclass. This classification is clearly seen graphically in figure 5.4. Temperatures corresponding to these MK classifications ($T_{\rm eff,B1\,V} = 25\,400$ and $T_{\rm eff,B1\,III} = 24\,000$, Schaifers and Voight 1982, $T_{\rm eff,B1\,V-III} = 26\,500$ Straižys 1992) are in good agreement with those derived by the flux fitting procedure.

Adopting a distance modulus of 18.35 mag (Schmidt-Kaler, 1993), the major semi-axis, and therefore the absolute scale of the system, can be estimated by forcing the distance corrected theoretical flux to equal the observed flux at Earth. It is thus possible to make gross estimations of the masses, radii and $\log[g]$ values of the stars which can be compared with expected properties both empirically and theoretically. If the uncertainty in the distance modulus is ± 0.2 mag then the uncertainty in the major semi-axis (from this source alone) is of the order of 10 percent while the uncertainty in the total mass of the system is approximately 30 percent. The appropriate major semi-axis is found to be $34 \pm 3\,\mathcal{R}_\odot$. From Kepler's third law, given the orbital period of 5.3353220 days the corresponding total mass of the system is $18.2 \pm 5.5\,\mathcal{M}_\odot$. If the mass ratio is assumed to be 1.0 ± 0.1 then the uncertainty in the individual masses is ~35 percent and the masses themselves are $\mathcal{M}_1 = \mathcal{M}_2 = 9.1 \pm 3.2\,\mathcal{M}_\odot$. From the light curve solutions the radii are of the order of $\mathcal{R}_1 = \mathcal{R}_2 = 7.0 \pm 1.1\,\mathcal{R}_\odot$. The uncertainty in the radii includes contributions from both the uncertainty arising from the light curve analysis itself (some 5 percent) and the uncertainty in the distance modulus (a further 10 percent). The $\log[g]$ values (where g is in cgs units) predicted by the light curve solutions are 3.70 ± 0.08.

Figure 6.3 shows the points corresponding to the above dimensions in the $\log[T_{\rm eff}]/\log[L/L_\odot]$ plane.

Also shown are theoretical evolutionary tracks for stars with metal abundances ranging from $Z = 0.001$ to $Z = 0.020$ and initial masses ranging from 7 to 25 $\mathcal{M}_{\odot}$(Schaller et al., 1992; Schaerer et al., 1993; Charbonnel et al., 1993). The $Z = 0.008$ abundance models are most appropriate for LMC stars. From this graph it is apparent that both components are most probably still main-sequence stars, although clearly not so very far away from the Terminal Age Main-Sequence (TAMS). This result is in agreement with the above MK estimations based on the reddening-corrected c_1 values and the calibration of Crawford (1978).

These dimensions are also in general agreement with empirical values for B1 V and B1.5 III stars according to the tabulations of Straižys (1992). Furthermore, the similarity of the two components of HV 982 is consistent with their having the same age, as required by standard theories for binary-star formation and evolution.

When accurate spectroscopic radial-velocity curves are available and the uncertainty in the temperatures has been reduced, HV 982 will provide an excellent case study for comparison with theoretical models for stellar evolution and structure.

6.1.2 HV 1620

The analysis of the calibrated photometry and the IUE spectrophotometry in conjunction with preliminary light curve analysis (chapter 5) lead to the determination of the effective temperatures of the two components ($T_{\rm eff,1} = 33\,000 \pm 4\,500$ K and $T_{\rm eff,2} = 24\,400 \pm 3\,000$ K). These temperatures are in excellent agreement with those obtained by Davidge (1988) who adopted $T_{\rm eff,1} = 33\,400$ K based on spectral classification, and derived $T_{\rm eff,2} = 24\,900 \pm 1\,550$ K from light curve analysis. Niemela and Bassino (1994) suggest temperatures of 35 900 and 32 900 K for primary and secondary components based on spectral classifications alone. The implication is that the effective temperature of the secondary component, derived from spectral classification, is in some way less reliable.

The remaining properties of the system have been determined from the analysis of the light curves and the radial-velocity curves (Niemela and Bassino, 1994) with the *WD95* program. Solutions were sought while optimising the major semi-axis, inclination, mass ratio, effective temperature of the secondary component (the effective temperature of the primary was fixed at the value determined from the flux matching) and the surface potential of the primary component. Based on the findings of preliminary analyses, the binary was assumed to be in a semi-detached configuration with the secondary component filling its Roche lobe. This may in some way explain the apparently less reliable effective temperature estimation from the spectral classification. Some understanding of this may be gained by recognising the fact that the greater the distortion of a star (i.e. the less spherical the star) the greater the variation of local effective gravity and hence local temperature over the surface of the star. While the effective temperature and surface gravity vary from their mean values by no more than 1 and 0.3 percent respectively over the surface of the primary component, they can differ from the mean values by as much as 40 and 25 percent over the surface of the secondary. These large deviations, which are in the sense of a cooler temperature and weaker gravity, occur over small a region near the cusp of the Roche lobe, i.e. at the inner Lagrangian point (L1). The maximum temperature and gravity occur at the poles of the star and are only some 6 and 3 percent bigger than the respective mean values. The corresponding rms scatters (as percentages of the mean values) are 0.3 and 0.01 percent for the primary component and 6 and 3 percent for the secondary component. The effective temperature and gravity clearly vary over the surface of the more distorted secondary to a much larger degree than is the case for the primary. This must complicate the interpretation of spectra in terms of MK type because features in the spectra may not necessarily be representative of the entire photosphere in the same way that they are for undistorted stars. In particular the hotter regions of the secondary, which are of course also the most luminous, may produce spectral features indicative of a hotter temperature. But this will not correspond to the appropriate effective temperature since this is representative of the total emitted energy, and clearly the cooler regions will radiate less energy than the hotter regions.

Preliminary analysis also indicated the presence of a small, but significant O'Connell effect, in the sense that the light maximum following the primary minimum is brighter than that following secondary minimum by ~0.02 mag in u and ~0.01 mag in v, b, y, V and I. In an effort to model this effect, solutions with a 'hot spot' located on the primary component, such that it was directly visible at the brightest orbital phase, were obtained. Spotted solutions were able to significantly improve the fit, reducing the weighted sum of the squares of the residuals by approximately 10 percent. The O'Connell effect is therefore asserted to be real and not merely some artifact of the observations. For a spot temperature 10 percent hotter than the local effective temperature, the required spot radius was found to be ~30° which would cover less 7 percent of the surface of the primary component. However the modelling of the effect with the *WD95* spot formalism does not provide any particular insight into the cause of the effect since it is difficult to imagine a physical

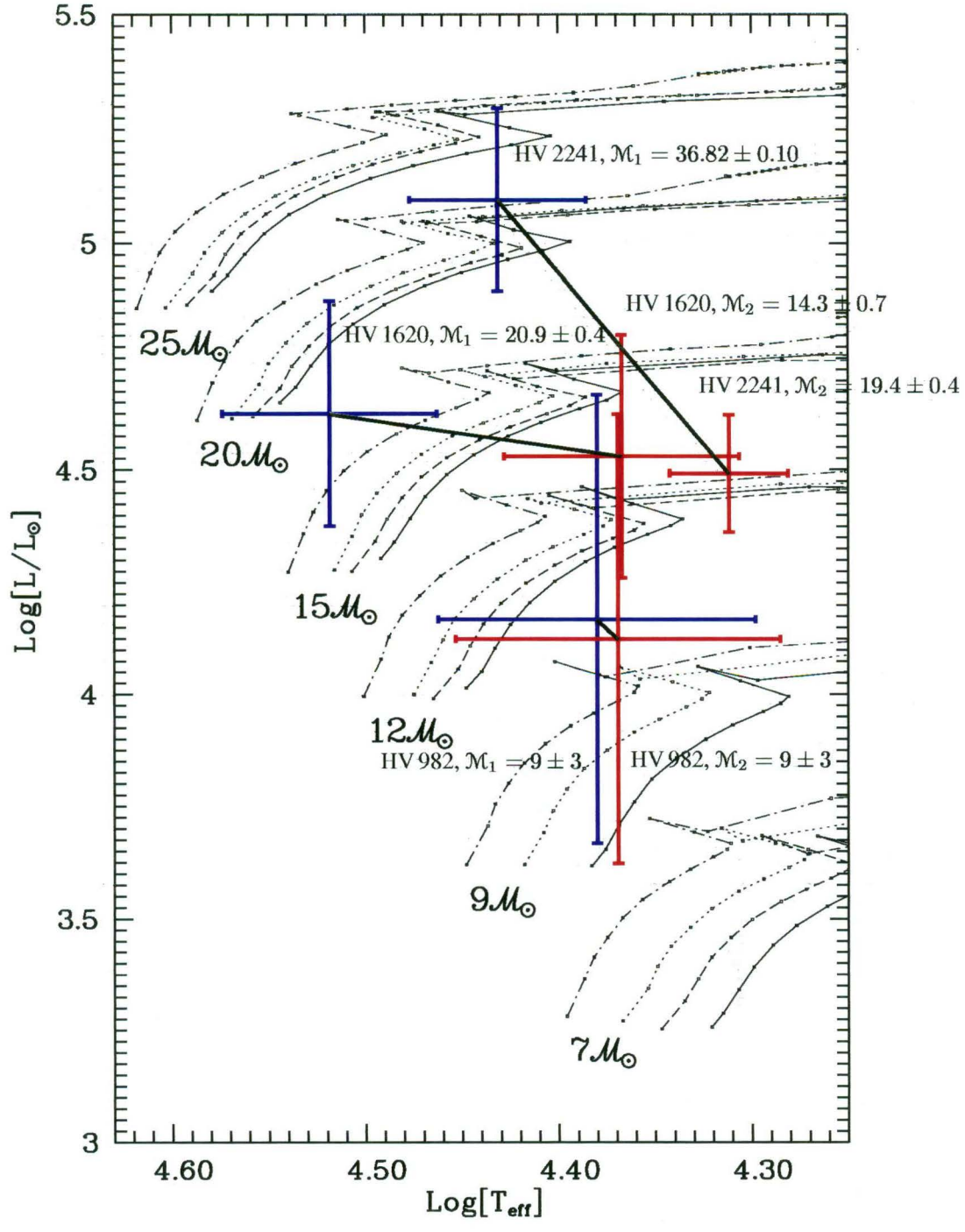

Figure 6.3: The components of the three programme stars are shown in the $\log[T_{\rm eff}]/\log[L/L_\odot]$ plane. For comparison, theoretical evolutionary tracks for single stars with metal adundances (by mass) $Z = 0.001$ (dot-dash), $Z = 0.004$ (dotted), $Z = 0.008$ (dashed) and $Z = 0.020$ (full lines) and initial masses ranging from 7 to 25 $\mathcal{M}_\odot$ (Schaller et al., 1992; Schaerer et al., 1993; Charbonnel et al., 1993) are also plotted (note that there is no 9 $\mathcal{M}_\odot$ model for $Z = 0.008$, There is a 10 $\mathcal{M}_\odot$ model, but for the sake of clarity this has not been plotted). The $Z = 0.020$ models of course represent solar abundances, while the $Z = 0.008$ models are appropriate for LMC stars. SMC stars have adundances between $Z = 0.001$ and $Z = 0.004$. The derived masses for each component of each system are labelled and the two components of each system are joined by a line. Error bars indicate the uncertainty in the derived properties. The uncertainty in the temperatures, due primarily to the uncertainty in the photometry, contribute the most to the total uncertainties. Clearly the uncertainties are far too great to discirminate between metallicity effects.

Table 6.3: Final values for the optimised parameters of HV 1620 from the analysis of the light and radial-velocity curves. Uncertainties have been estimated after consideration of the standard errors reported by the *WD95* program, the rms scatter amongst ensembles of solutions, according to the adopted convergence criterion (see section 4.4.1), and differences between solutions for models both with and without a spot to model the O'Connell effect. The uncertainty in the effective temperatures is dominated by the uncertainty in the reddening. For a given value of $T_{\rm eff,1}$ the uncertainty in $T_{\rm eff,2}$ is of the order of 100 K.

Parameter	Value
Period, P	3.62642 ± 0.00001 d
Reference epoch T_0	HJD2449345.7476 $\pm$ 0.0004
Major semi-axis, A	$32.5 \pm 0.8\,\mathcal{R}_\odot$
Inclination, i	$77\overset{\circ}{.}10 \pm 0\overset{\circ}{.}4$
Mass ratio, q	0.68 ± 0.03
Effective Temperature, $T_{\rm eff,1}$	$33\,000 \pm 4\,500$ K
$T_{\rm eff,2}$	$24\,400 \pm 3\,500$ K
Surface Potential, Ω_1	5.89 ± 0.10
Ω_2	3.21 ± 0.06
Mass, $\mathcal{M}_1$	$20.9 \pm 0.4\,\mathcal{M}_\odot$
$\mathcal{M}_2$	$14.3 \pm 0.7\,\mathcal{M}_\odot$
Mean Radius, $\mathcal{R}_1$	$6.27 \pm 0.10\,\mathcal{R}_\odot$
$\mathcal{R}_2$	$11.30 \pm 0.2\,\mathcal{R}_\odot$
Luminosity, $\log[L_1/L_\odot]$	4.62 ± 0.25
$\log[L_1/L_\odot]$	4.53 ± 0.27
Mean Surface Gravity, $\log[g_1]$	4.162 ± 0.005
$\log[g_2]$	3.490 ± 0.005

mechanism for generating such a spot. It must also add to the uncertainty surrounding the derived parameters of the system. The optimised parameters for solutions without a hot spot generally differ significantly (if the standard errors reported by *WD95* are indeed reasonable estimators of the uncertainty in the optimised parameters) from those of solutions with hot spots. Furthermore, the O'Connell effect could presumably be modelled equally well by any number of combinations of appropriately located hot or cool spots on one or other or both components. Each model would presumably also lead to another different set of solutions. Clearly no analysis of HV 1620, or any other binary with an O'Connell effect in its light curve, can be considered definitive until a physical process can be identified as the cause for the O'Connell effect and its consequences appropriately modelled in the light curve analysis. The O'Connell effect is, therefore, clearly deserving of further investigation.

Final values for the optimised parameters and derived properties of HV 1620 and its components are listed in table 6.3. Although these parameters are taken from the solutions with a hot spot to model the O'Connell effect, the uncertainties have been estimated after consideration of the standard errors reported by the *WD95* program, the rms scatter amongst ensembles of solutions, according to the adopted convergence criterion (see section 4.4.1), and differences between the solutions for models both with and without a spot to model the O'Connell effect. The derived masses and radii are in reasonable agreement with those obtained by Davidge (1988) ($\mathcal{M}_1 = 13^{+8}_{-5}\,\mathcal{M}_\odot$ and $\mathcal{R}_1 = 9^{+2}_{-1}\,\mathcal{R}_\odot$, $\mathcal{M}_2 = 9^{+6}_{-4}\,\mathcal{M}_\odot$ and $\mathcal{R}_2 = 9^{+2}_{-2}\,\mathcal{R}_\odot$) except that the radius of the primary determined here is apparently significantly smaller. Clearly, given the much higher quality MJUO light curves with generally far superior phase coverage, the present results represent a significant improvement in the accuracy and precision with which these fundamental parameters for HV 1620 are known. They are also in reasonable agreement with the results obtained by Niemela and Bassino (1994) ($\mathcal{M}_1 = 21.3 \pm 1.4\,\mathcal{M}_\odot$ and $\mathcal{R}_1 = 10.9\,\mathcal{R}_\odot$, $\mathcal{M}_2 = 16.86 \pm 1.1\,\mathcal{M}_\odot$ and $\mathcal{R}_2 = 11.4\,\mathcal{R}_\odot$[5])

Figure 6.4 presents a representative schematic of the potential surfaces of the components of HV 1620. Also indicated is the critical Roche lobe for the primary component. It is clear that the primary component of HV 1620 is well inside its critical Roche lobe.

The MK type of of the secondary component can be estimated from its reddening-corrected c_1 index (i.e. c_0) derived from the deconvolved $(b-y)$ colour and c_1 index (see table 5.14 and figure 5.4) and the

[5]Niemela and Bassino (1994) do not quote uncertainties for their masses or radii. The uncertainties on the masses have therefore been calculated by propagating the uncertainties in K_1 and K_2. Uncertainties in the radii have not been estimated as the radii are derived from the Davidge solution, hence the radii of Niemela and Bassino are more diffiuclt to estimate uncertainties for than is the case for their masses.

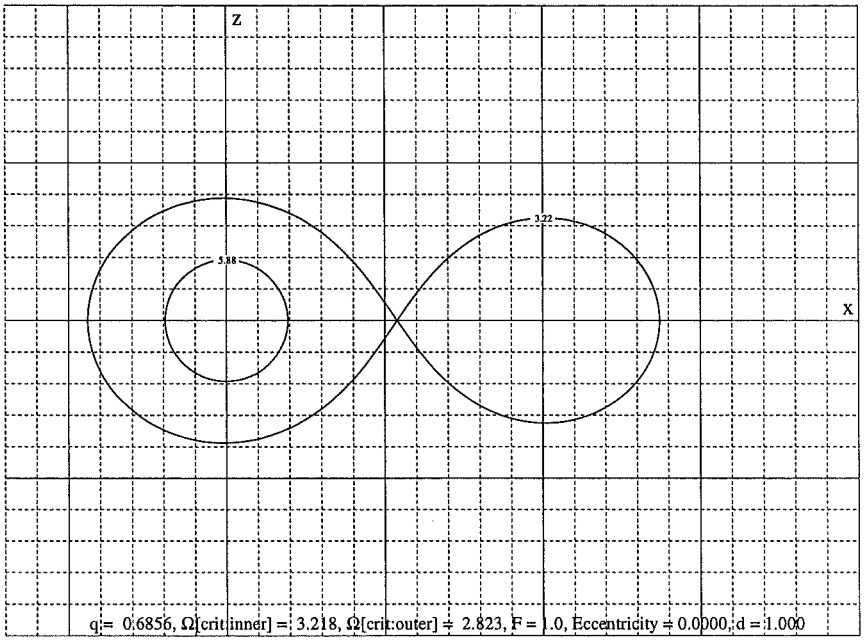

Figure 6.4: Representative schematic of the surfaces of HV 1620 in the XZ plane (i.e. the plane perpendicular to the orbital plane). The primary component (on the left) at a surface potential of 5.88 is clearly well inside its critical Roche lobe while the secondary component fills its Roche lobe at a potential of 3.22.

intrinsic relationship (Crawford, 1978). It is either a B1 V or a B1 III star. The $\log[g]$ of 3.490 ± 0.005 (table 6.3) is more consistent with a sub-giant classification hence the luminosity class III classification is to be preferred. From the photometry, the MK type of the primary component can not be estimated with any great precision. It is clearly earlier than B0 (see figure 5.4), i.e. an O-type star. However the Strömgren photometric colours and indices are not sufficiently sensitive to MK type for O-type stars to allow a reliable estimation of MK type. Indeed investigations of interstellar reddening make the assumption that O-type stars have 'nearly identical intrinsic colours' (Crawford, 1975b). The $\log[g]$ of the primary component derived from the light curve analysis (4.162 ± 0.005) does indicate a luminosity class V star, but much more than this can not be deduced from the photometry alone. Spectral classifications have however been made by Davidge (1988) (primary only, O9 III-V) and by Niemela and Bassino (1994) (O9 V+O9.5 III).[6] Thus the photometric indicators are in reasonable agreement with the spectroscopic classifications. However, as noted above, effective temperature estimates based on spectral classification of distorted stars (i.e. stars which fill or are close to filling their Roche lobes) appear to be less reliable than estimates obtained from, for example, light curve fits. It is worth noting that the adopted parameters of HV 1620 correspond to the larger, cooler secondary having a greater total luminosity than the smaller, hotter primary at wavelengths longer than $\lambda \sim 300$ nm which is consistent with the observation by Niemela and Bassino that,

> ...the lines of one component appear stronger, but He II lines are seen more often in the spectrum of the fainter lined component.

Figure 6.3 plots the points corresponding to the dimensions from table 6.3 in the $\log[T_{\rm eff}]/\log[L/L_{\odot}]$ plane. Hilditch and Bell (1987) found that the primary components of OB-type semi-detached systems tend to be apparently about halfway through their main-sequence lifetimes whilst the secondary components tend to be oversized, and hence over-luminous, for their Zero Age Main Sequence (ZAMS) masses. Certainly the primary star seems to fit this pattern however the secondary is not significantly over-luminous for its mass, in fact the masses, radii and temperatures (and hence luminosities) of both components are in reasonable agreement with the single-star models. On the other hand, the positions of the two components in this diagram clearly show that the less-massive secondary component is apparently more evolved than the primary component, contradicting single-star stellar evolutionary theory under the assumption of coeval components. This state of affairs is observationally well known for the Algol class of binary, although archetypical Algols are generally composed of much later-type stars and have much smaller mass ratios. The apparently

[6]Note that the star labelled the primary by Niemela and Bassino (1994) corresponds to the secondary component in the present work.

Table 6.4: Observed times of minima for HV 1620. Times are taken from Payne-Gaposchkin and Gaposchkin (1966) (PG&G) and Davidge (1988). A representative minimum during the period of observations has been determined from the preliminary light analysis. The number of orbital cycles prior to the new minimum is given in the Cycle column.

HJD	Cycle	Reference
2432537.326	−4635	PG&G
2446426.468	−805	Davidge
2449345.7477	0	This work

contradictory evolutionary state is however reasonably well understood in terms of modern binary star evolution theories (e.g. Doom 1984, Sybesma 1985, 1986a, 1986b, de Loore and De Greve 1992) which predict that the less-massive secondary was in fact initially the more-massive component. In accord with standard evolutionary theory, this star evolved more quickly and consequently expanded to meet its Roche lobe first. At that point in time mass transfer commenced and continued to the point where the initially more-massive component is now the less massive. Given the currently semi-detached state of the system, it is possible that mass transfer is still in progress. The reasonable agreement with single-star properties, albeit for stars of different ages, indicates that any mass transfer is occurring at a rate slow enough that both components are able to readjust to resemble normal single stars. However, because of this complicated evolutionary history, neither component can be expected to be truly representative of normal single stars. The derived properties of the components of HV 1620 thus do not, and will never, allow rigorous tests of single-star stellar evolution.

The primary import of the study of non-well-detached systems such as HV 1620 is the determination of the distance to the star. For Magellanic Cloud binaries this allows for independent confirmation of the distance to the galaxy itself and may also permit probing of the internal structure of the Clouds if sufficiently accurate data can be obtained. For the current work on HV 1620, the uncertainty in the calibrated standard system photometry is the main contribution to the fairly large uncertainty in the distance modulus derived in chapter 5 (see table 5.21), providing the stated radial-velocity uncertainties are accepted at face value.

An improved ephemeris for HV 1620 has been derived by combining results from the current work with published data for the star. Observed times of minima are available from Payne-Gaposchkin and Gaposchkin (1966) and Davidge (1988) and a representative primary minimum during the period of observations has been determined from the preliminary light curve analysis (see table 6.4). The Davidge time of minimum has an uncertainty of 10 minutes. It is unclear what uncertainty should be attached to the time of minimum provided by Payne-Gaposchkin and Gaposchkin (1966) since it is undoubtedly a mean derived from several individual observations. From investigations of the uncertainty of reported timings from earlier epochs for other systems (Watson et al., 1992; Tobin et al., 1993a), an uncertainty of 90 minutes on the original individual times of minimum would probably be representative. An uncertainty of 45 minutes, which would thus not seem unreasonable, then gives about equal weighting to the Davidge (1988) and Payne-Gaposchkin and Gaposchkin (1966) points in an uncertainty-weighted linear regression determination of the period. After several trial regressions of the data, attaching various uncertainties to the Payne-Gaposchkin and Gaposchkin (1966) point, the following ephemeris is adopted as being representative of all of the available data,

$$\begin{array}{rcrcrl} \text{Time of} & = & \text{HJD2449345.7476} & + & 3.62642\times\text{E} & \\ \text{primary} & & \pm\ 0.0004 & \pm & 0.00001 & \quad (6.5) \\ \text{minimum} & & & & & \end{array}$$

6.1.3 HV 2241

The effective temperatures of the components of HV 2241 derived in chapter 5 by spectral flux fitting are $T_{\rm eff,1} = 27\,000 \pm 3\,000$ K and $T_{\rm eff,1} = 20\,200 \pm 1\,500$ K. Table 6.5 lists the corresponding optimized and derived parameters determined from the analysis of the light curves and the radial-velocity curves of Niemela and Bassino (1994) for this primary-component temperature. As noted in section 4.4, HV 2241 displays the O'Connell effect in its light curves. Like HV 1620 it is in the sense of a brighter maximum following primary minimum as compared to the maximum following secondary minimum. The effect is slightly larger for HV 2241 than for HV 1620, ~0.05 mag in u and ~0.03 mag in the other bandpasses. The parameters in table 6.5 correspond directly to those for solutions for models with a spot. For a spot 10 percent hotter than the local effective temperature, the required spot radius was ~25°, i.e. approximately 5 percent of the total surface area of the primary component. The uncertainties have been estimated after

Table 6.5: Final values for the optimized parameters of HV 2241 from the analysis of the light and radial-velocity curves. Uncertainties have been estimated after consideration of the standard errors reported by the *WD95* program, the rms scatter amongst ensembles of solutions, according to the adopted convergence criterion (see section 4.4.1), and differences between solutions for models both with and without a spot to model the O'Connell effect. The uncertainty in the effective temperatures is dominated by the uncertainty in the reddening. For a given value of $T_{\rm eff,1}$ the uncertainty in $T_{\rm eff,2}$ is of the order of 200 K.

Parameter	Value
Period, P	4.3426241 ± 0.0000016 d
Reference epoch T_0	HJD2449477.7285 $\pm$ 0.0009
Major semi-axis, A	$42.9 \pm 0.5\,\mathcal{R}_\odot$
Inclination, i	$85\overset{\circ}{.}3 \pm 0\overset{\circ}{.}6$
Mass ratio, q	0.53 ± 0.01
Effective Temperature, $T_{\rm eff,1}$	$27\,000 \pm 3\,000$ K
$T_{\rm eff,2}$	$20\,200 \pm 1\,500$ K
Surface Potential, Ω_1	3.25 ± 0.03
Ω_2	2.93 ± 0.02
Mass, $\mathcal{M}_1$	$36.82 \pm 0.10\,\mathcal{M}_\odot$
$\mathcal{M}_2$	$19.4 \pm 0.6\,\mathcal{M}_\odot$
Mean Radius, $\mathcal{R}_1$	$16.1 \pm 0.2\,\mathcal{R}_\odot$
$\mathcal{R}_2$	$13.9 \pm 0.1\,\mathcal{R}_\odot$
Luminosity, $\log[L_1/L_\odot]$	5.10 ± 0.20
$\log[L_1/L_\odot]$	4.49 ± 0.13
Mean Surface Gravity, $\log[g_1]$	3.588 ± 0.005
$\log[g_2]$	3.440 ± 0.005

consideration of the standard errors reported by the *WD95* program, the rms scatter amongst ensembles of solutions, according to the adopted convergence criterion (see section 4.4.1), and differences between the solutions for models both with and without a spot to model the O'Connell effect. Paradoxically, despite the larger size of the effect, the differences between the parameters derived from light curve solutions for models with and without a spot are less pronounced than for HV 1620 as indicated by the generally smaller uncertainties in the masses, radii and surface potentials. Note that the uncertainty in the temperatures and hence the luminosities are dominated by the uncertainty in the reddening.

The adopted effective temperatures differ significantly from those derived by Davidge (1987) ($T_{\rm eff,1} = 34\,500 \pm 2\,500$ K from spectral classification and $T_{\rm eff,2} = 25\,580 \pm 1\,880$ K from light curve analysis) and Niemela and Bassino (1994) ($T_{\rm eff,1} = 40\,000$ and $T_{\rm eff,1} = 37\,000$, both from spectral classification). On the other hand, the adopted $T_{\rm eff,1}$ does agree well with that derived by Guinan (1995) ($T_{\rm eff,1} = 28\,000 \pm 700$ K, from analysis of the IUE spectrophotometry and Davidge photometry). Furthermore, it should be noted that the $T_{\rm eff,2}$ implied by preliminary solutions at $T_{\rm eff,1} = 34\,000$ and $T_{\rm eff,1} = 35\,000$ K are in agreement with the $T_{\rm eff,2}$ obtained by Davidge. This implies (as was found for HV 1620) that it would not be possible to obtain light curve solutions with the effective temperatures of both components consistent with the temperatures implied by the spectral classifications of Niemela and Bassino. The maximum local effective temperatures and gravities of both components are again at the poles and are 4 and 2 percent and 7 and 3 percent larger than the mean values of local effective temperature and gravity of the primary and secondary components respectively. In contrast to HV 1620, *both* components have much lower local effective temperatures and gravities in the most distorted regions nearest the L1 point, 9 and 5 percent cooler and weaker for the primary and 40 and 26 percent cooler and weaker for the secondary. Again these large variations in the local properties of the atmospheres may go some way toward explaining the large discrepancies between the temperature estimates based on the spectral classifications and those derived in the present work by fitting the the observed flux from the far uv to the near infrared to theoretical spectral flux distributions. Finally the masses and radii for the components of HV 2241 are in reasonable accord with those derived by Niemela and Bassino which are based on their radial-velocity curve analysis and Davidge's light curve analysis. They obtain $\mathcal{M}_1 = 34.3$ and $\mathcal{M}_2 = 17.3$,and $\mathcal{R}_1 = 15.1$ and $\mathcal{R}_2 = 13.5$ (in solar units). The inter-agreement between the present analysis and that of other investigators where the same data is used suggests that no obvious analysis or interpretational mistakes have been made by any of the investigators. This does not of course rule out the possibility of systematic errors in the common data that has been analyzed.

Figure 6.5 presents a schematic of representative surface potentials in the XZ plane. The primary

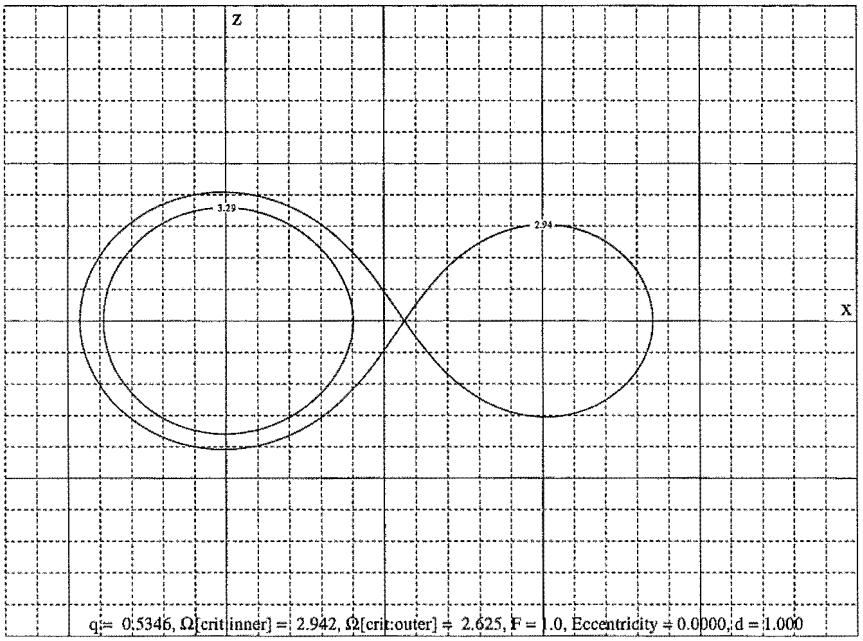

Figure 6.5: Representative schematic of the surfaces of HV 2241 in the XZ plane (i.e. the plane perpendicular to the orbital plane). The primary component at a surface potential of 3.29 is very close to filling its critical Roche lobe. The secondary component does fill its Roche lobe at a potential of 2.94.

component is on the left, the secondary component, which fills its Roche lobe, is on the right. The primary component's Roche lobe is also shown and it is clear that the primary component is very close to filling its Roche lobe and shows a non-negligible degree of distortion from a spherical geometry. This may help to explain the above discrepancies between the effective temperatures. It was noted in the previous section that the effective temperature of the secondary component of HV 1620 derived from spectroscopic classification (Niemela and Bassino, 1994) did not agree with those derived from the light curve analysis. This was ascribed to complications arising from the distortion of the secondary component. In HV 2241 the primary is sufficiently close to filling its Roche lobe that it too is somewhat distorted.

The evolutionary status of the components of HV 2241 should also be noted. Figure 6.3 shows the points corresponding to the dimensions from table 6.5 in the $\log[T_{\rm eff}]/\log[L/L_{\odot}]$ plane. It is immediately obvious that, unlike the components of HV 982 and HV 1620, both components of HV 2241 are (grossly) under-luminous for their ZAMS masses, even allowing for the substantial uncertainties, or equivalently, the derived effective temperatures do not correspond to those of single stars for the masses and radii obtained from the light curve and radial-velocity curve analysis.

This situation can not easily be explained in terms of binary star evolution models. The most appropriate models for comparison, given the total mass of the system, the mass ratio, the orbital period and the semi-detached nature of the system derived in the current analysis, are the $40+20\,\mathcal{M}_{\odot}$ and $40+30\,\mathcal{M}_{\odot}$ models of Sybesma (1986b). But neither of these models predict the under-luminous states derived here. Furthermore these models do *not* predict the mass ratio reversal seen for the lower mass systems, e.g. the $20+18\,\mathcal{M}_{\odot}$ and $20+16\,\mathcal{M}_{\odot}$ models of Sybesma (1986a) which are more appropriate for HV 1620. For the more massive systems (i.e. binaries with primaries initially in excess of $\sim 33\,\mathcal{M}_{\odot}$), during semi-detached phases, it is always the more-massive component which fills its Roche lobe (although in the $40+20\,\mathcal{M}_{\odot}$ model the system passes through a contact phase) and this component does not lose sufficient mass (at least not during the mass transfer phase) that it becomes the less-massive component of the system. This, of course is contradictory to light curve analysis of HV 2241 which shows the less-massive secondary component to be filling its Roche lobe, but not the more massive primary component. The primary however is rather close to doing so and the system is possibly merely slightly perturbed from a contact state. No stable light curve solutions could be found for the primary component Roche lobe filling configuration, i.e. *WD95* `mode=4` option. For this reason contact solutions (*WD95* `mode=6`) were not sought.

Again we are forced to consider the possibility of a systematic error in the temperature determination. The reddening-corrected c_1 index for the primary component of HV 2241 is bluer than that of HV 1620's primary (table 5.14) which implies that HV 2241's primary should have an effective temperature greater than that HV 1620's primary (i.e. in excess of 33,000 K). The lower temperature of 27 000 K is derived from the

flux fitting procedure and it is principally the IUE spectrophotometry which forces the lower temperature. There is however considerable uncertainty surrounding the form of the interstellar extinction law in the far-ultraviolet. Moreover, the extinction is known to vary significantly from star to star. For stars in the SMC, the extinction can range from the SMC 'mean' law (figure 5.5) to distinctly Galactic laws (Lequeux, 1997). In the LMC, the 30 Doradus region is known to have stronger far-ultraviolet extinction than the LMC mean (Fitzpatrick, 1986). The LMC interstellar extinction law of Howarth (1983) implies greater far-ultraviolet extinction than that of Fitzpatrick. In the $E(\lambda - V)/E(B - V)$ vs. λ^{-1} plane (see figure 5.5) it lies about midway between Fitzpatrick's LMC curve and the SMC curve (Prévot et al., 1984). Fitzpatrick argues that Howarth's law is strongly influenced by the 30 Doradus region, which is not representative of the rest of the LMC hence his assertion that his more Galactic like LMC extinction curve is more appropriate for LMC stars in general. In accord with this view, the Fitzpatrick 'Average LMC curve' has been adopted for HV 2241 since HV 2241 is well removed from the 30 Doradus region. However, if Howarth's LMC extinction law is used, rather than Fitzpatrick's, then all other things being equal, the $T_{\rm eff,1}$ derived from the flux fitting is 30 000 K rather than 27 000 K. Clearly, systematic errors in the treatment of the interstellar extinction could possibly be a contributing factor to the apparent discrepancies between derived temperatures and the anomalous evolutionary state.

However, the temperature scale alone can not be the problem. The physical scale of the system is set by the light and radial-velocity curve analysis. It is directly proportional to the amplitude of the radial-velocity curves and is thus weakly correlated with the mass ratio. It is largely insensitive to effective temperature. Thus, by adopting $T_{\rm eff,1} = 35\,000$ K as per Davidge, the radii, masses and effective temperatures of both components would then be in reasonable agreement with the single-star evolutionary models. But by the same token the distance modulus derived from the synthetic spectral flux distributions (section 5.6) would then increase by ~0.6 mag to ~19.2 mag. This increased distance modulus is clearly inconsistent with other LMC distance determinations (e.g. Westerlund 1990, van den Bergh 1992, de Vaucouleurs 1993, Schmidt-Kaler 1993) which range between 18.3 and 18.5 mag. To bring the distance modulus into accord with the accepted range would require a ~25 percent reduction in the physical size of the system. The theoretical radial-velocity curves would then be grossly inconsistent with the observations of Niemela and Bassino and furthermore the masses in this scaled down system ($\mathcal{M}_1 = \sim 15.5\,\mathcal{M}_\odot$ and $\mathcal{M}_1 = \sim 8.2\,\mathcal{M}_\odot$) would then be too small for the theoretical single-stars of the appropriate radii and temperatures, or equivalently, the stars would now be *over*-luminous for their masses and temperatures. At $T_{\rm eff,1} = 30\,000$ K the distance modulus would be 18.8 mag which again is a little large. But the size of the system need only be 12 percent smaller to reduce the distance modulus back down to the more consistent value of 18.5 mag. Moreover, the masses and radii of the two components would then correspond well to those of $25\,\mathcal{M}_\odot$ star nearing the TAMS and a $13\,\mathcal{M}_\odot$ star perhaps just slightly evolved past the TAMS. Finally, this reduction in mass probably puts this system into the range for which the binary star evolution models do predict mass ratio reversal and Roche lobe filling secondary components. Needless to say though, the theoretical radial-velocity curves would still clearly be incompatible with the observations. A reduction in the scale of the system thus requires that some systematic error has been made in the measurement of the radial velocity curves for this system. Further observations are thus required in order to resolve the uncertainties surrounding this system. To this end, Hubble Space Telescope spectrophotometry from $\lambda\lambda 300 - 1000$ nm has been recently secured by collaborators which should help reduce uncertainty in the effective temperatures of the components of HV 2241. In addition, the observed O'Connell effect also requires physical explanation and subsequent modelling, as was pointed out above in the case of HV 1620. Again this adds to the uncertainty and difficulty in analysing and interpreting non-well-detached systems and reinforces the obvious preference for well-detached systems like HV 982 which not only have the potential to provide more accurate astrophysical data (of current use) but are less difficult to model and interpret.

In spite of the remaining uncertainties it is still possible to derive an improved ephemeris for this system. Combining observed times of minima from Gaposhkin (1977), Davidge (1987) and a representative primary minimum during the period of observations derived from preliminary light curve solutions (see table 6.6), the following ephemeris is derived from an uncertainty-weighted linear regression,

$$\begin{array}{rcrcl} \text{Time of primary minimum} & = & \text{HJD2449477.7285} & + & 4.3426241 \times E. \\ & & \pm\ 0.0009 & \pm & 0.0000016 \end{array} \qquad (6.6)$$

Table 6.6: Observed times of minima for HV 2241. Times are taken from Gaposhkin (1977) and Davidge (1988). A representative minimum during the period of observations has been determined from the preliminary light analysis. The number of orbital cycles prior to the new minimum is given in the Cycle column.

HJD	Cycle	Reference
2413876.814	−8198	Gaposhkin
2416816.768	−7521	Gaposhkin
2424824.683	−5677	Gaposhkin
2426453.220	−5302	Gaposhkin
2427456.309	−5071	Gaposhkin
2427786.315	−4995	Gaposhkin
2429219.388	−4665	Gaposhkin
2430322.446	−4411	Gaposhkin
2430665.492	−4332	Gaposhkin
2431681.586	−4098	Gaposhkin
2432024.604	−4019	Gaposhkin
2432919.292	−3813	Gaposhkin
2446424.8644	−703	Davidge
2449477.7285	0	This work

Chapter 7

Analysis of Photometric Light Curves III. The EROS EB light curves

The EROS Eclipsing Binary Catalogue (Grison et al., 1995) presents two colour, photometrically calibrated light curves for 79 eclipsing binaries in the bar of the LMC. One of the 79 is the previously recognized eclipsing binary HV 2436. The remaining 78 are new identifications. As part of an ongoing programme of research into LMC variable stars and eclipsing binaries in particular, an investigation of the binary systems based on the analysis of the EROS light curves utilizing the *WD95* program is underway. The light curve analysis is now complete for the majority of the systems. The main purpose of the investigation is to identify interesting members of the catalogue suitable for further observation.

The calibrated light curves are, in most cases, the only data currently available for these systems. The light curves are generally well sampled but the intrinsic scatter is relatively large, typical rms scatters of residuals between observations and model light curve fits range from $\sim$0.015 mag for the brighter systems ($V \approx 15$ mag) to $\sim$0.08 mag for the fainter systems ($V \approx 18$ mag). Systematic errors may affect the overall photometric calibrations at the 0.1-0.2 mag level while crowding or other effects can affect the EROS photometry of individual stars by greater amounts (Grison et al., 1995). The accuracy of the analysis is thus restricted and results for any particular star must be interpreted cautiously. Of more value will be overall trends that may indicated by the ensemble once the analysis for all systems is complete.

The investigation has, to date, been carried out by a group of six researchers; W. Tobin, L.B. Keep, A. Batten, L. Skuljan, Mohd Zambri, and of course the author. This chapter presents details of the new analysis procedure developed by the group in order to carry out the investigation of the EROS eclipsing binaries and results from the analysis of the light curves of eight of the EROS eclipsing binaries with obviously eccentric orbits.

7.1 Absolute parameters for the EROS systems

Usually, the determination of the mass and radius of each component of an eclipsing binary system requires the analysis of, at least, both photometric light curves and spectroscopic radial velocity curves. This is because light curves alone contain information about the *relative* geometry of the system (i.e. the ratios between the radii of the components and their separation) but not about the *absolute* scale of the system which in general can only be determined directly from radial velocity curves.

However, for the binaries of the EROS catalogue, the fact that they all reside in the LMC means that, for the purposes of this investigation, it can be assumed that the distance to the stars is known. Thus for any combination of two model stars of a specific geometry, the absolute scale can be set by requiring that the total luminosity from the model stars placed at the known distance and corrected for interstellar extinction corresponds to the 'observed' luminosity as given by the calibrated photometry.

Unfortunately the analysis of the light curves alone leads to a large number of equally valid (in a purely least-squares sense) solutions spanning a wide range of mass ratios and effective temperatures. Thus theoretical single-star evolutionary models (Schaerer et al., 1993) are used to eliminate physically (or at least theoretically) unrealistic solutions giving much tighter constraints on the derived properties of the systems and their components.

The basis of the EROS light curve analysis procedure was pioneered by L.B. Keep and W. Tobin during Keep's Fourth Year Honours Project research (Keep, 1995). The procedure as applied to each system is straightforward. For any reasonable choice of mass ratio ($q = \mathcal{M}_2/\mathcal{M}_1$) for a particular system and effective temperature for the primary component ($T_{\rm eff,1}$), it is usually trivial to find a *WD95* solution for the remaining parameters, in general the orbital inclination, the effective temperature of the secondary component ($T_{\rm eff,2}$), the surface potentials of both components and the monochromatic luminosities of the primary component for both the $B_{\rm E}$ and $R_{\rm E}$ observations. For eccentric systems the orbital eccentricity and longitude of periastron should also be optimized.

The major semi-axis (A) can now be determined by requiring that the luminosity of the model system placed at the distance of the LMC is equal to observed apparent luminosity. Of course the luminosity of

the binary is not observed directly, however 'observed' monochromatic luminosities for each component at each observed wavelength[1] can be derived from the *WD95* monochromatic luminosities (L1 and L2) determined by the light curve analysis. These are 'apparent' luminosities since the zero point is defined by the observed calibrated apparent photometry which of course includes the effects of distance and interstellar extinction. The total monochromatic luminosity of the system for each bandpass is easily calculated from the monochromatic luminosities of the individual components (see below, section 7.1.1). These luminosities are independent of the absolute scale of the system.

The *WD95* program also reports the surface area of each component of the binary. Thus multiplying the surface areas by the monochromatic surface flux intensities appropriate for the adopted $T_{\rm eff,1}$ and derived $T_{\rm eff,2}$ will give the 'absolute' monochromatic luminosities of the individual components of the binary and hence the binary as a whole. The surface flux intensities are derived from model stellar atmospheres (Kurucz, 1993) by convolving the appropriate spectral response functions of the EROS $B_{\rm E}$ and $R_{\rm E}$ bandpasses with the stellar atmospheres. In order to compare these absolute luminosities with the apparent luminosities, they must be corrected for the known distance to the binary and for the effects of interstellar extinction[2] (see below, section 7.1.2). Clearly the corrected absolute luminosities can be made numerically equal to the apparent luminosities simply by scaling the surface areas, which is achieved by scaling the major semi-axis i.e. the physical size of the system (see below, section 7.1.3).

The resulting pair of stars however will not generally correspond to realistic stars. For the assumed $T_{\rm eff,1}$, the derived masses, radii and $T_{\rm eff,2}$ will generally not match those predicted by theoretical stellar evolution models. However by adjusting the $T_{\rm eff,1}$ and re-determining the masses, radii and $T_{\rm eff,2}$ from the light curve analysis it is generally possible to find a particular value of $T_{\rm eff,1}$ for which the effective temperature, mass and radius of the *primary* component is consistent with the theoretical models. This follows from the relationship between surface flux intensity and effective temperature. Since the surface flux intensity scales with the effective temperature, the major semi-axis scales inversely with the effective temperature – as the star becomes cooler, it needs to have a greater surface area, i.e. a larger radius, in order to produce the observed luminosity. Since the relative radii ($\mathcal{R}/A$) are specified by the light curve, the radii are adjusted by scaling the major semi-axis.

Similarly, it is generally possible to find a particular value of $T_{\rm eff,1}$ for which the derived effective temperature, mass and radius of the *secondary* component is consistent with the theoretical models. In general though, the $T_{\rm eff,1}$ which produces the theoretically consistent primary component will not be the same as the $T_{\rm eff,1}$ which produces the theoretically consistent secondary component. However it is possible to find a specific mass ratio for which the two values for $T_{\rm eff,1}$ are equal.

So to summarize, the analysis procedure involves a systematic search of parameter space which we parameterize in terms of the mass ratio (q) and primary component effective temperature ($T_{\rm eff,1}$). We search for the particular combination of q and $T_{\rm eff,1}$ for which the masses and radii of the two components and secondary component's effective temperature derived from the analysis of the light curves are consistent with the predictions of theoretical stellar evolutionary models. A detailed guide to the use of the computer software and its implementation in the analysis procedure is included in appendix E.

The calculation of the two monochromatic luminosities for each component and the major semi-axis scale factor therefrom are detailed in the next three subsections. The adopted convergence criterion is then given and a discussion of the systematic errors and overall uncertainties in the derived parameters are presented in the following three subsections.

7.1.1 Calculation of the *WD95* monochromatic luminosities and the EROS indices from L1 and L2

In order to make use of the calibrated EROS photometry, the monochromatic luminosities reported by the *WD95* program (namely L1 and L2) – which are in user-defined units units – must be related to the actual observed magnitudes.

[1]The observations have, of course, been made through non-negligibly broad bandpasses defined by the spectral transmission functions of the atmosphere and the $B_{\rm E}$ and $R_{\rm E}$ filters, the spectral reflectivity of the telescope mirrors and the spectral response of the detector (see section F.3). The monochromatic wavelength corresponding to these bandpasses is therefore not well defined since the *effective* wavelength of the bandpass is dependent on the spectral profile of the incident radiation, i.e. the stellar spectral flux densities (see equation F.3). For the temperature range of interest (10 000-30 000 K) the effective wavelengths range from 479 nm to 482 nm for $B_{\rm E}$ and from 650 nm to 654 nm. The *mean* wavelengths (equation F.1) of the bandpasses ($\bar{\lambda}_{B_{\rm E}} = 490$ nm, $\bar{\lambda}_{R_{\rm E}} = 670$ nm) were adopted as the representative monochromatic wavelengths for the two bandpasses in the light curve analysis before the investigation of the effective wavelength as a function of $T_{\rm eff}$. Obviously, in retrospect it would have been more consistent to have adopted representative wavelengths within the applicable ranges. Fortunately, systematic errors resulting from the use of the less appropriate mean wavelengths are negligible, see section 7.1.6 below.

[2]Equivalently the apparent luminosities could be corrected for distance and extinction and compared to the absolute luminosities.

The procedure adopted for converting the observed EROS *magnitudes*[3] ($m_{\bar{\lambda}}$) into *lights* ($\mathtt{l}_{\bar{\lambda}}$) (as required by the *WD95* program) is to 'normalize' by the observed light of the first observation listed in the photometric light curve data file for each binary. The light value for the i^{th} observation is thus calculated as follows,

$$\mathtt{l}_{\bar{\lambda},\mathrm{i}} = 10^{(m_{\bar{\lambda},1\mathrm{st}} - m_{\bar{\lambda},\mathrm{i}})/2.5}. \tag{7.1}$$

The above definition then defines the units of the light and the luminosity within the *WD95* program. Wilson (1992b) makes the following definition. If the *light* is equal to 1.0, then for an isotropically radiating star, the integrated light over a sphere with a 'sufficiently' large radius, i.e. the monochromatic luminosity ($L_{\bar{\lambda}}$), is 4π. Thus a star for which the *WD95* program reports a luminosity of 4π will have a magnitude in the corresponding EROS photometric system exactly equal to $m_{\bar{\lambda},1\mathrm{st}}$.

Ultimately for comparison with the theoretical evolutionary models it is more convenient to express the *WD95* monochromatic luminosities ($\mathtt{L1}_{\bar{\lambda}}$ and $\mathtt{L2}_{\bar{\lambda}}$) in magnitudes in the EROS $B_{\mathrm{E}}/R_{\mathrm{E}}$ photometric system. In practice, all comparisons between light curve solution model stars and theoretical evolution model stars is carried out in the $T_{\mathrm{eff}}/m_{B_{\mathrm{E}}}$ plane. Thus, the *Luminosity-calculated apparent magnitude* of the primary component, $m_{\mathrm{L1},\bar{\lambda}}$, is the magnitude of the primary component as determined from the luminosity ($\mathtt{L1}_{\bar{\lambda}}$) reported by the *WD95* program and the observed magnitude of the star at the phase of light normalization ($m_{\bar{\lambda},1\mathrm{st}}$),

$$m_{\mathrm{L1},\bar{\lambda}} = m_{\bar{\lambda},1\mathrm{st}} - 2.5 \times \log_{10}\left[\frac{\mathtt{L1}_{\bar{\lambda}}}{4\pi}\right]. \tag{7.2}$$

This is essentially the magnitude that would be observed if an isotropically radiating, single star of the same total luminosity were placed at the same distance from the observer and suffered the same interstellar extinction as the binary star. Of course a directly analogous definition applies for the *Luminosity-calculated apparent magnitude* of the secondary component $m_{\mathrm{L2},\bar{\lambda}}$.

7.1.2 Calculation of the *WD95* monochromatic luminosities and the EROS indices from the Stellar Surface Areas

More generally, as compared with the previous section, the monochromatic luminosity ($L_{\bar{\lambda}}$) of a star is simply given by,

$$L_{\bar{\lambda}} = Area \times \mathcal{F}_{\bar{\lambda}}, \tag{7.3}$$

where $Area$ is the surface area of the star and $\mathcal{F}_{\bar{\lambda}}$ is the *physical* flux at wavelength $\bar{\lambda}$. Once again it is more convenient to consider EROS $B_{\mathrm{E}}/R_{\mathrm{E}}$ system magnitudes rather than luminosities thus we begin by defining the *absolute* magnitude ($M_{SA,\bar{\lambda}}$), as derived from consideration of the surface area, in the bandpass with effective wavelength $\bar{\lambda}$ by,

$$M_{SA,\bar{\lambda}} = c_{\bar{\lambda}} - 2.5\log_{10}\left[Area \times \mathcal{F}_{\bar{\lambda}}\right], \tag{7.4}$$

where $c_{\bar{\lambda}}$ sets the zero point and must be calibrated in some way.

Now the stellar atmosphere models (Kurucz, 1993) provide stellar *astrophysical* fluxes ($\mathcal{F}_{\mathrm{A}}$) which are related to physical fluxes simply by,

$$\mathcal{F} = \pi\mathcal{F}_{\mathrm{A}}, \tag{7.5}$$

while the Wilson code reports a dimensionless quantity proportional to the surface area of the each component of the binary (SA_1 and SA_2). The surface area ($Area_{\mathrm{j}}$) of component $\mathrm{j} \in (1,2)$ ($\mathrm{j} = 1$ primary, $\mathrm{j} = 2$ secondary) is,

$$Area_{\mathrm{j}} = \left(A \times \mathcal{R}_{\odot}\right)^2 \times SA_{\mathrm{j}}, \tag{7.6}$$

where A is the major semi-axis in units of the solar radius ($\mathcal{R}_{\odot}$) of the binary. Hence the absolute magnitude of the $\mathrm{j}^{\mathrm{t}}\mathrm{h}$ component in the bandpass denoted by $\bar{\lambda}$ is,

$$\begin{aligned} M_{SA,\bar{\lambda},\mathrm{j}} &= c_{\bar{\lambda}} - 2.5\log_{10}\left[\left(A \times \mathcal{R}_{\odot}\right)^2 \times SA_{\mathrm{j}} \times \pi\mathcal{F}_{\mathrm{A},\bar{\lambda},\mathrm{j}}\right], \\ &= c_{\bar{\lambda}} - 2.5\log_{10}\left[A^2 \times SA_{\mathrm{j}}\right] + 2.5\log_{10}\left[\pi\mathcal{R}_{\odot}^2 \frac{\mathcal{F}_{\mathrm{A},\bar{\lambda},\mathrm{j}}}{\mathcal{F}_{\mathrm{A,Vega},\bar{\lambda}}}\mathcal{F}_{\mathrm{A,Vega},\bar{\lambda}}\right], \end{aligned}$$

[3]The EROS catalogue (Grison et al., 1995) of course provides light curves in two colours from the observations in the B_{E} and R_{E} filters respectively. It is more convenient, and less confusing, to discuss the EROS photometry generically rather than explicitly referring to B_{E} and R_{E} magnitudes, luminosities etc. To this end a $\bar{\lambda}$ subscript is attached to the various quantities to indicate their applicability to both bandpasses. Of course, in the instances where the different bandpasses require individual treatment this will be provided.

$$= c_{\bar{\lambda}} - 2.5\log_{10}\left[A^2 \times SA_{\rm j}\right] - 2.5\log_{10}\left[\frac{\mathcal{F}_{{\rm A},\bar{\lambda},{\rm j}}}{\mathcal{F}_{{\rm A,Vega},\bar{\lambda}}}\right] - 2.5\log_{10}\left[\pi\mathcal{R}_\odot^2\mathcal{F}_{{\rm A,Vega},\bar{\lambda}}\right],$$

$$= c'_{\bar{\lambda}} - 2.5\log_{10}\left[A^2 \times SA_{\rm j}\right] - M_{{\rm Kurucz},\bar{\lambda},{\rm j}}, \quad (7.7)$$

where,

$$c'_{\bar{\lambda}} = c_{\bar{\lambda}} - 2.5\log_{10}\left[\pi\mathcal{R}_\odot^2\mathcal{F}_{{\rm A,Vega},\bar{\lambda}}\right], \quad (7.8)$$

and, by definition,

$$M_{{\rm Kurucz},\bar{\lambda},{\rm j}} = -2.5\log_{10}\left[\frac{\mathcal{F}_{{\rm A},\bar{\lambda},{\rm j}}}{\mathcal{F}_{{\rm A,Vega},\bar{\lambda}}}\right]. \quad (7.9)$$

$\mathcal{F}_{{\rm A},\bar{\lambda},{\rm j}}$ is the astrophysical flux for either the primary (j = 1) or secondary (j = 2) component in the bandpass denoted by $\bar{\lambda}$, i.e. either the $B_{\rm E}$ or $R_{\rm E}$ bandpass.

$$\mathcal{F}_{{\rm A},\bar{\lambda},{\rm j}} = \frac{\int_0^\infty S_{\bar{\lambda}}(\lambda)\mathcal{F}_{\rm A}(\lambda, T_{{\rm eff},{\rm j}}, \log[g_{\rm j}])d\lambda}{\int_0^\infty S_{\bar{\lambda}}(\lambda)d\lambda} \quad (7.10)$$

where $S_{\bar{\lambda}}(\lambda)$ is the spectral response of the bandpass denoted by $\bar{\lambda}$ and $\mathcal{F}_{\rm A}(\lambda, T_{{\rm eff},{\rm j}}, \log[g_{\rm j}])$ is the astrophysical spectral flux density for a model atmosphere with effective temperature $T_{{\rm eff},{\rm j}}$ and effective gravity $\log[g_{\rm j}]$ which are tabulated by Kurucz (1993). The normalization factor in equation 7.9 ($\mathcal{F}_{{\rm A,Vega},\bar{\lambda}}$) is the bandpass integrated flux from the atmosphere model for the approximately A0V star Vega≡ α Lyrae≡HD 172167≡HR 7001 (namely CDROM13/FLUXES/FVEGA.PCK, for which $T_{\rm eff} = 9550\,{\rm K}$ and $\log[g] = 3.95$). The above formulation is convenient since it is able to make use of tabulations of $M_{{\rm Kurucz},\bar{\lambda}}$ compiled from stellar atmosphere models (Kurucz, 1993). The tables are parameterized in terms of $T_{\rm eff}$ and $\log[g]$. $M_{{\rm Kurucz},\bar{\lambda}}$ values are linearly interpolated within the $T_{\rm eff}/\log[g]$ grid.

Calibration is straightforward. Adopting $M_{B_{\rm E}} = M_{R_{\rm E}} = 0.53\,{\rm mag}$ for Vega entirely specifies the $c_{\bar{\lambda}}$ constants in equation 7.4 for these two bandpasses. This is appropriate because the EROS $B_{\rm E}/R_{\rm E}$ photometric system has been calibrated such that a star with colour $(B-V) = 0.0\,{\rm mag}$ also has $(B_{\rm E} - R_{\rm E}) = 0.0$. Moreover,

$$V = B_{\rm E} - 0.47(B_{\rm E} - R_{\rm E}), \quad (7.11)$$

$$(B-V) = 0.92(B_{\rm E} - R_{\rm E}), \quad (7.12)$$

(Grison et al., 1995). Now, for Vega, $V = 0.03\,{\rm mag}$ and $(B-V) = 0.00\,{\rm mag}$ (Johnson, 1965) while the parallax of Vega is $\pi = 0''.126$ (Code et al., 1976), therefore since,

$$d = \frac{1\,{\rm AU}}{1\,{\rm pc}\tan[\pi/2]} \approx \frac{9.698\times10^{-6}}{\pi} = 7.94\,{\rm pc}, \quad (7.13)$$

then $(m-M)_0 = 5\log_{10}[d] - 5 = -0.50\,{\rm mag}$ and $M_V = 0.53\,{\rm mag}$. The radius of Vega is $2.76\,\mathcal{R}_\odot$ (Code et al., 1976) so the surface area (in solar units, which is equivalent to the $A^2\times SA$ term in equation 7.7) is simply $4\pi\times2.76^2$. Adopting $M_{SA,\bar{\lambda}} = M_V$ and substituting into equation 7.7 gives,

$$c_{\bar{\lambda}} = 0.53 + 2.5\log_{10}\left[4\pi \times 2.76^2\right] = 5.48\,{\rm mag}. \quad (7.14)$$

In order to relate these absolute magnitudes($M_{SA,\bar{\lambda},{\rm j}}$) to the observed apparent magnitudes ($m_{{\rm L1},\bar{\lambda}}$ and $m_{{\rm L2},\bar{\lambda}}$) the distance and reddening for the stars must be corrected for. Writing,

$$m_{SA,\bar{\lambda},{\rm j}} = M_{SA,\bar{\lambda},{\rm j}} + W_{\bar{\lambda}} \quad (7.15)$$

where the effects of distance and reddening have been combined into the single factor,

$$W_{\bar{\lambda}} = (m-M)_0 + \frac{A_{\bar{\lambda}}}{E(B-V)}E(B-V). \quad (7.16)$$

Combining $W_{\bar{\lambda}}$ and $c_{\bar{\lambda}}$ into one constant – for each bandpass – ($W'_{\bar{\lambda}}$) we finally have the *Surface-Area-calculated apparent magnitude*, $m_{SA,\bar{\lambda}}$ given by,

$$m_{SA,\bar{\lambda},{\rm j}} = -2.5 \times \log_{10}\left[A^2 \times SA_{\rm j}\right] + M_{{\rm Kurucz},\bar{\lambda},{\rm j}} + W'_{\bar{\lambda}}. \quad (7.17)$$

For the EROS bandpasses ($B_{\rm E}$ & $R_{\rm E}$) the distance/reddening/calibration factors used in all of the analysis were as follows;

$$W'_{B_{\rm E}} = c'_{\bar{\lambda}} + 18.35 + 3.65 \times 0.08 = 24.125, \quad (7.18)$$

$$W'_{R_{\rm E}} = c'_{\bar{\lambda}} + 18.35 + 2.47 \times 0.08 = 24.030. \tag{7.19}$$

The distance modulus for the LMC ($(m - M)_0 = 18.35$ mag) is taken from Schmidt-Kaler (1993), the colour excess ($E(B-V) = 0.08$ mag) is taken from Caldwell and Laney (1991) while the ratios of interstellar extinction to colour excess ($\chi_{\bar{\lambda}} = A_{\bar{\lambda}}/E(B-V)$) are taken from Seaton (1979) It has thus been implicitly assumed that the Galactic and LMC interstellar extinction laws in the visible and the values for $R = A_V/E(B-V)$ for the Galaxy and the LMC are identical.

7.1.3 Calculation of the Major Semi-Axis Scaling Factors

At each iteration with the *WD95* DC program the *Luminosity-calculated apparent magnitude* and *Surface-Area-calculated apparent magnitude* for each component for each bandpass can be computed. Considering one bandpass and one component at a time these two magnitudes will not generally be numerically equal. However they can be made numerically equal simply by 'scaling' the system, i.e. adjusting the major semi-axis (A). The following outlines the calculation of the so-called 'scaling-factor' (SF), the factor by which the major semi-axis must be multiplied in order to bring the Surface-Area-calculated apparent magnitude ($m_{SA,\bar{\lambda}}$) into agreement with the Luminosity-calculated apparent magnitude ($m_{{\rm L},\bar{\lambda}}$).

Defining $m_{SA_{\rm correct},\bar{\lambda}}$ as the value for the Surface-Area-calculated apparent magnitude with the major semi-axis scaled such that $m_{SA_{\rm correct},\bar{\lambda}}$ is equal to $m_{{\rm L},\bar{\lambda}}$ and introducing the scaling factor SF defined by the following relation,

$$m_{SA_{\rm correct},\bar{\lambda},{\rm j}} = -2.5 \times \log_{10}\left[\left(SF_{\bar{\lambda},{\rm j}} \times A\right)^2 \times SA_{\rm j}\right] + M_{{\rm Kurucz},\bar{\lambda},{\rm j}} + W'_{\bar{\lambda}}, \tag{7.20}$$

then obviously,

$$m_{SA_{\rm correct},\bar{\lambda},{\rm j}} = -2.5 \times \log_{10}\left[A^2 \times SA_{\rm j}\right] + M_{{\rm Kurucz},\bar{\lambda},{\rm j}} + W'_{\bar{\lambda}} - 5 \times \log_{10}\left[SF_{\bar{\lambda},{\rm j}}\right] \tag{7.21}$$

i.e.

$$m_{SA_{\rm correct},\bar{\lambda},{\rm j}} = m_{SA,\bar{\lambda},{\rm j}} - 5 \times \log_{10}\left[SF_{\bar{\lambda},{\rm j}}\right] \tag{7.22}$$

and hence

$$SF_{\bar{\lambda},{\rm j}} = 10^{\frac{m_{SA,\bar{\lambda},{\rm j}} - m_{{\rm L},\bar{\lambda},{\rm j}}}{5}} \tag{7.23}$$

The four individual scale factors, one for each component for each bandpass, will not generally be numerically equal. In practice they are found to differ by of the order of a few percent and the scale factor applied was simply the mean of the four individual estimates. For a particular component, the agreement between the $B_{\rm E}$ and $R_{\rm E}$ factors is indicative of how well the adopted stellar atmosphere model is estimating the relative flux levels at the two wavelengths. However it may also indicate any problems with the photometry in one or other of the bandpasses, e.g. significant third light in one bandpass but not the other. In this case it might be expected that the differences between the two scale factors for both components were of a similar nature. For a particular bandpass, disagreements between the scale factors for the two components are indicative of the accuracy of the stellar atmosphere models in predicting the true flux ratios for the stars at different temperatures.

7.1.4 The adopted convergence criterion for the *WD95* analysis

For the analysis of the EROS light curves, iterations were deemed to have converged upon the first instance at which the suggested parameter corrections were all simultaneously smaller than their respective standard errors. The stronger criterion employed in the analysis of the MJUO light curves, that two consecutive iterations have all suggested parameter corrections smaller than the corresponding standard errors, was not adopted here. The main reason for this was that due to the generally lower quality of the EROS photometry (as compared with the MJUO photometry) the more stringent criterion was not felt to be warranted.

7.1.5 Other particulars of the *WD95* EROS light curve analysis

As noted above, *WD95* solutions to the EROS light curves are obtained by optimizing the orbital inclination (i), the effective temperature of the secondary component ($T_{\rm eff,2}$), the surface potentials of both components (Ω_1 and Ω_2) and the monochromatic luminosities of the primary component for both $B_{\rm E}$ and $R_{\rm E}$ bandpasses ($L_{1,B_{\rm E}}$ and $L_{1,R_{\rm E}}$ and $L_{2,B_{\rm E}}$ and $L_{2,R_{\rm E}}$). For eccentric systems, i.e. all eight systems to be discussed in the next section, the orbital eccentricity (e) and longitude of periastron (ω) are also be optimized. The mass

ratio ($q = \mathcal{M}_2/\mathcal{M}_1$) and effective temperature of the primary component ($T_{\rm eff,1}$) are held constant in any given iteration.

Generally solutions are sought first assuming a detached configuration (*WD95* `Mode=2`). Semi-detached (`Mode=4` and `Mode=5`) or contact configurations (`Mode=3`) are reverted to if warranted, i.e. if either or both surface potentials are consistently close to (i.e. of the order of the corresponding standard errors) the relevant critical Roche lobe potentials.

Monochromatic luminosities were always coupled to the effective temperatures (`IPB=0`). The blackbody approximation to stellar atmosphere radiant intensities are adopted for all the EROS light curve analysis (`IFAT1=IFAT2=0`. At the time the analysis was commenced, the Kurucz model atmosphere subroutine was not yet available to us, and it was unclear how to evaluate the appropriateness or otherwise of the Wilson approximations. Therefore since we felt that we at least knew what we were dealing with by adopting the blackbody approximation we chose to work with that).

WD95 grid-fineness parameters (`N1` and `N2`) of 15 are generally adopted and the reflection effect is treated by the simple geometric approach (`MREF=1`. The proximity effect corrections are of no consequence, since radial-velocity curves are not included in the analysis. The symmetrical derivatives option is employed
(`IPB=1`). As noted above, limb-darkening coefficient are obtained by interpolation within $T_{\rm eff}$/log[g] grids derived by convolving the measured spectral response functions of the EROS $B_{\rm E}$ and $R_{\rm E}$ bandpasses with the Kurucz stellar atmosphere models. The gravity darkening and albedo coefficients are set at their theoretical values for radiative atmospheres as appropriate for these undoubtedly early-type stars (i.e. both unity, `g1=g2=1` and `A1=A2=1`). The axial rotation rates are assumed to be synchronized with the orbital rotation (`F1=F2=1`), except for the eccentric systems for which the axial rotation rates are assumed to be synchronized to the orbital rotation rates at periastron (see equation 4.8).

The need for third light and/or spots to optimize the model fits must, of course be judged on a case by case basis. Spots, in the classic sense, are however unlikely given the EROS binaries are all composed of hot, early-type stars, and the precision if the photometry is certainly insufficient to permit identification of subtle asymmetries in the light curves, such as those collectively labelled the O'Connell effect, which might otherwise be usefully modeled by the spot formalism, as was done for HV 1620 and HV 2241.

The *WD95* noise parameters (`Sigma`) for the individual light curves are set after consideration of the residuals to light curve fits. This is necessarily an iterative process, although only one, and perhaps sometimes two iterations are required to obtain self-consistent estimates of the rms standard deviations. In general, all observations were ascribed equal weight in the chi-squared minimization analysis, although it is occasionally necessary to eliminate obviously flawed data from further analysis.

7.1.6 Uncertainties in the derived parameters

The main sources of uncertainty in the derived parameters are likely to derive from both random and systematic errors. Purely systematic errors include the approximation of the real stellar atmospheres by blackbodies in the *WD95* light curve analysis and the assumption that the real stars are well modeled by the adopted theoretical models. The light curves and the photometric calibration contain elements of both random and systematic errors, as does the adoption of the mean distance to the LMC for the individual stars within the LMC.

The blackbody atmosphere approximation is likely to cause the largest errors for systems with components of very different temperatures, since even the blackbody model will predict the same surface flux from two stars of the same temperature. The magnitude of the error is however non-trivially temperature and wavelength dependent (see figure 7.1). The stars in the catalogue are all relatively hot, early-type stars, only five have a $(B-V)$ index greater than 0.5 mag so the relevant effective temperature range is ~10 000 to ~30 000 K. For the $B_{\rm E}$ and $R_{\rm E}$ bandpasses, the error in the estimation of the flux over this temperature range is typically ~20 percent but, as just noted, it is really the relative error at two different temperatures rather than the absolute error at a particular temperature that matters. Furthermore given the mean wavelengths of the $B_{\rm E}$ and $R_{\rm E}$ bandpasses, 490 and 670 nm respectively, the filters are both sampling over a relatively small range of the Rayleigh-Jeans tail of the spectral flux distributions of the stellar atmospheres. Errors are thus not as large as they might otherwise be, e.g. for bandpasses much nearer the Balmer discontinuity. This source of error will primarily lead to errors in the effective temperatures, but the error in temperature corresponding to a given error in the flux estimates again is non-trivial. A full investigation, e.g. by the comparison of solutions using various atmosphere models in the *WD95* analysis is not warranted in this case given the exploratory nature of this investigation.

Systematic errors arising from the estimation of the stellar fluxes by the flux intensities of blackbodies at

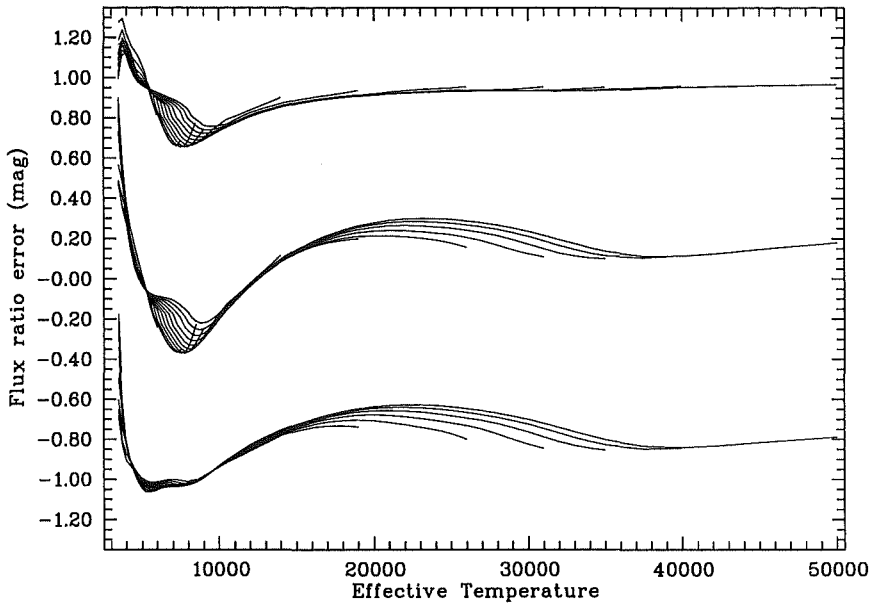

Figure 7.1: Ratios of Kurucz stellar atmosphere model fluxes to blackbody fluxes. The ratios are shown in units of magnitudes, so the deviation from zero indicates the approximate error in proportional terms. Three sets of ratios are shown, from bottom to top, $R_{\rm E}$ ($\bar{\lambda} = 670$ nm), $B_{\rm E}$ ($\bar{\lambda} = 490$ nm) and for the ratio of $B_{\rm E}$ to $R_{\rm E}$. For each set, the individual lines correspond to the gravities of the atmosphere models, which range from $\log[g] = 0.0$ to $\log[g] = 5.0$ in steps of 0.5. The $R_{\rm E}$ set are offset by -1.0 mag and the $B_{\rm E}$ to $R_{\rm E}$ set are offset by $+1.0$ mag.

the *mean* wavelengths of the bandpasses, rather than the *effective* wavelengths, or even better by convolving the bandpasses with blackbody spectral flux densities, are negligible. More importantly though, the differences between surface flux intensities estimated from Blackbody flux intensities at the mean wavelengths and by convolving the bandpass spectral response functions typically differ at the 1 percent level for $B_{\rm E}$ and the 0.5 percent level for $R_{\rm E}$. Furthermore, as above, it is only the relative error between two flux estimations at different temperatures or at different wavelengths that matters. If realistic stellar atmospheres were being used rather than blackbodies this error would persist, although it would presumably also be negligible as in the case of the blackbodies.

Systematic errors resulting from use of theoretical single-star evolutionary models to discriminate between 'realistic' and 'non-realistic' solutions to the light curves also are difficult to assess quantitatively. It seems probable that the the models are least appropriate for more evolved stars, since these are more likely to be in semi-detached or even contact systems and thus in complicated evolutionary states possibly involving mass transfer or mass accretion. In any case, it is perhaps the systems most at odds with the theoretical models that will prove most interesting since they thus defy standard explanations.

As noted above, systematic errors (in the EROS photometry) may affect the overall photometric calibrations (i.e. the zero point) at the 0.1-0.2 mag level while crowding or other effects can affect the EROS photometry of individual stars by greater amounts (Grison et al., 1995). To account for this essentially random uncertainty an uncertainty of ± 0.2 mag in the EROS photometry has been adopted (which also includes a contribution due to uncertainty in the distance modulus since it is most convenient to simply lump them together). This photometric uncertainty of course implies an uncertainty in the Luminosity-calculated apparent magnitudes of the components since they are calibrated by the EROS photometry and this leads ultimately to uncertainty in the effective temperatures ($T_{\rm eff,1}$ and $T_{\rm eff,2}$), the masses ($\mathcal{M}_1$ and $\mathcal{M}_2$) and all linear dimensions and related quantities (i.e. the major semi-axis, radii, effective surface gravity) as follows[4]. Writing,

$$m_{\rm L} = m_{\rm L_0} \pm \delta_{m_{\rm L}}, \tag{7.24}$$

then

$$\begin{aligned} SF &= 10^{\frac{M_{SA} - m_{\rm L_0} \mp \delta_{m_{\rm L}}}{5}} \\ &= 10^{\frac{M_{SA} - m_{\rm L}}{5}} \times 10^{\frac{\mp \delta_{m_{\rm L}}}{5}} \end{aligned}$$

[4]For the sake of clarity, subscripts referencing bandpass and component have been omitted

$$= 10^{\frac{\mp\delta m_{L_0}}{5}} \times SF_0. \quad (7.25)$$

$$(7.26)$$

Hence

$$A_{\rm correct} = SF \times A, \quad (7.27)$$

$$= 10^{\frac{\mp\delta m_{L_0}}{5}} \times SF_0 A \quad (7.28)$$

where A is the 'current' major semi-axis and $A_{\rm correct}$ is the major semi-axis for which m_{SA} will be equal to $m_{\rm L}$.

Now Kepler's third Law gives

$$\frac{4\pi^2 A^3}{P^2} = G(\mathcal{M}_1 + \mathcal{M}_2) \quad (7.29)$$

where $\mathcal{M}_1$ and $\mathcal{M}_2$ are the masses of the primary and secondary stars respectively. This leads directly to

$$\mathcal{M}^{\pm}_{1(2)} = 10^{\frac{\mp 3\times\delta m_{\rm L}}{5}} \times \mathcal{M}_{1(2)}. \quad (7.30)$$

In particular, a photometric uncertainty of 0.2 mag implies an ~10 percent uncertainty in the major semi-axis, and hence the radii also, and an ~30 percent uncertainty in the masses. The corresponding uncertainty in the temperatures is less directly obtained. It is estimated by examination of the range of temperatures of the *WD95* light curve solutions corresponding to the allowable range of mass. It is worth reiterating that the relative temperatures of the two components of a system are reasonably well defined by the light curves and thus the uncertainties in the two temperatures are correlated. The uncertainty in the mass ratio is estimated as the range of mass ratio over which the $T_{\rm eff,1}$ which produces the theoretically consistent primary component does not differ by more than its uncertainty from the $T_{\rm eff,1}$ which produces the theoretically consistent secondary component.

The surface potentials are of course directly correlated with the mass ratio, so uncertainty in the mass ratio directly corresponds to uncertainty in the surface potentials. However the relative radii are not strongly correlated with the mass ratio, and so the uncertainty in the radii derives primarily from the uncertainty in the semi major-axis only.

The remaining parameters determined from the light curve analysis, i.e. the orbital inclination and for eccentric systems the orbital eccentricity and longitude of periastron are not strongly correlated with the absolute size of the system and are generally weakly correlated with mass ratio over the typical ranges of uncertainty in the mass ratio. The uncertainty in these parameters has therefore been estimated after considering the standard errors reported by the *WD95* DC program and the ranges of values obtained for the parameters for solutions over the range of acceptable mass ratios.

7.2 Derived parameters for eight of the EROS systems

Table 7.1 tabulates the parameters finally adopted for eight of the EROS systems analyzed by the author. The observed light curves, representative light curve fits and the residuals between observations and the fits are presented in figures 7.4 through 7.11. All eight systems are detached, eccentric binaries, specifically chosen for these properties. The remaining 71 systems either have been analyzed by other members of the group, or will be in due course.

The parameters have been determined according to the procedure described in the previous section. Systematic parameter-space searches, parameterized by mass ratio and primary component effective temperature, were conducted to find the pair of component stars for each system that are simultaneously consistent with the photometrically calibrated, two colour light curves (Grison et al., 1995), theoretical evolutionary models for single-stars (Schaerer et al., 1993) and the known distance of the LMC ($(m-M)_0 = 18.35$ Schmidt-Kaler 1993[5]). The major semi-axis is determined by requiring the distance and reddening corrected monochromatic luminosities of the model binary system to be equal to the observed monochromatic luminosities of the system. For these eccentric systems the axial rotation rates were assumed to be synchronised to the orbital rotation rates at periastron (see equation 4.8). The gravity darkening and albedo

[5]The Schmidt-Kaler (Schmidt-Kaler, 1993) value for the distance modulus was adopted early in the EROS light curve analysis project, i.e. at a time when it was a very new determination. Other, including more recent, distance determinations also based on SN 1987A generally tend toward slightly larger values i.e. 18.50 mag, see table 1.4. Nevertheless, a value of 18.35 mag is generally consistent, within the quoted errors with these larger values

coefficients were set at their theoretical values for radiative atmospheres as appropriate for these undoubtedly early-type stars (i.e. both unity). Limb-darkening coefficients were interpolated within $T_{\rm eff}/\log[g]$ grids derived by convolving the measured spectral response functions of the EROS $B_{\rm E}$ and $R_{\rm E}$ bandpasses with stellar atmosphere models (Kurucz, 1993). The remaining parameters of the *WD95* model, namely the orbital inclination and eccentricity, the longitude of periastron, the effective temperature of the secondary component, the surface potentials of both components and the monochromatic luminosities for the primary component for both the $B_{\rm E}$ and $R_{\rm E}$ observations, were optimised using the *WD95* differential corrections (DC) program.

As has been pointed out elsewhere (e.g. Tobin et al. 1997), results for individual stars should be treated with a healthy degree of caution since large errors can be present in the photometry of individual stars. It is overall trends amongst the stars in the catalogue and subsets thereof that are of more value. In this vein it is worth making a few comments regarding the properties of this particular subset of EROS eclipsing binary systems.

Firstly the periods range from just over two days to almost ten. The upper limit is really due to well known observational bias. Longer period binaries, whose components are thus necessarily relatively further apart, are seen as eclipsing binaries only for orbital inclinations increasingly close to 90°. Hence, statistically, shorter period binaries are more likely to be discovered since easily detected deep eclipses will occur for wider ranges of orbital inclination. At the other end of the scale EROS1035 is however interesting for the fact that its period is so short and yet it is still found in an eccentric orbit.

Three systems, EROS 1060, EROS 1063 and EROS 1066 are, at first glance, curious in that their secondary components, i.e. the components occulted at the less deep minima, are of greater effective temperature than the primary component occulted during the deeper minimum. This is no great physical mystery however, but simply due to their eccentricity and the current physical orientation of the orbit (inclination and longitude of periastron). In circular orbits the minimum where the hotter component is occulted is the deeper minimum because the same fractional area of each component is occulted during each eclipse. Since the hotter component will have the greater surface flux, the light will be reduced by more when it is occulted. In eccentric orbits however, the fractional area occulted during the two eclipses is no longer equal in general, hence a greater total reduction in light can occur when the cooler component is occulted if the orbit is oriented such that a greater area of the cooler component is occulted during its eclipse.

Each of the eight systems consist of two fairly similar components. All of the derived mass ratios are unity, within the uncertainties, the effective temperatures are generally quite similar, as are the individual radii.

All of the components of the eight systems lie within the main sequence band when plotted in the Hertzsprung-Russell diagram, (figure 7.2). Since these systems are well detached it is reasonable to expect that the properties of the individual components will conform to standard models for normal single stars. All but one of the systems, namely EROS 1061 ($4.3\,\mathcal{M}_{\odot} + 3.8\,\mathcal{M}_{\odot}$), appear to have components which are as expected for normal, coeval single stars. EROS 1061 appears to be anomalous. The secondary component is less massive, larger in size, but due to being somewhat cooler, slightly less luminous in comparison to the primary. Standard single-star evolutionary models predict that more massive stars always have larger radii than coeval less massive stars, at least while while on the main-sequence, and as has been noted earlier, standard scenarios for binary star creation generally require simultaneous creation of the two components. At a mass ratio of 1.1 rather than 0.9, which is within the uncertainty, according to the light curve solutions for this mass ratio, the then more massive, larger and apparently more evolved secondary component would still be cooler and less luminous than the primary component and would thus remain inconsistent with the coeval assumption. Alternatively, the apparent properties of the two components derived here, i.e. their positions in the Hertzsprung-Russell diagram, are qualitatively consistent with theoretical evolutionary models for *pre*-main sequence stars (Iben, 1965) with the two components in the final stages of their contraction down onto the ZAMS (see figure 7.3). In this case, the derived masses are likely to be systematically in error since these have been set by requiring that the derived stellar properties be consistent with those of post ZAMS stars. The derived temperatures and radii, and hence the luminosities, on the otherhand are determined largely by the form of the light curve and so the positions of the components in the luminosity vs. effective temperature Hertzsprung-Russell diagram are probably not significantly in error. In any case, EROS 1061 thus clearly appears to present an interesting case for further study. It should also be noted that EROS 1061 has a quite large eccentricity, 0.429 ± 0.018, despite its relatively short period of 4.528 days. EROS 1063 also has a noteworthy eccentricity 0.36 ± 0.03. Unfortunately, not all of these systems are suitable for followup investigation from MJUO due to their crowded fields and the typical atmospheric conditions experienced at MJUO. In fact the majority of the EROS eclipsing binaries fall into this catagory. However, by coincidence, the most interesting system presented here, EROS 1061, maybe one of the few for which accurate photometry would be possible from MJUO. It may thus warrant further study.

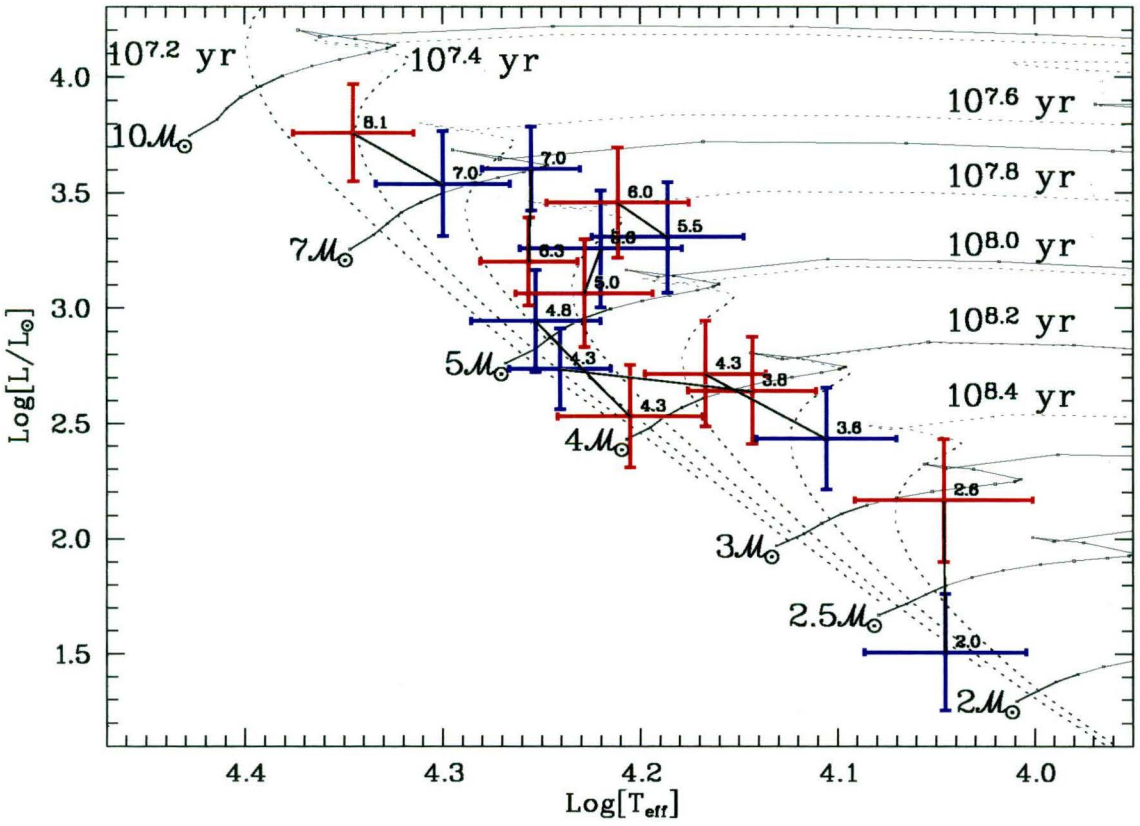

Figure 7.2: Eight well detached, eccentric EROS binary systems in the $\log[T_{\rm eff}]/\log[L/L_\odot]$ plane. Also plotted are theoretical evolutionary models for metal abundance $Z = 0.008$ for ZAMS masses from 2 to 10 $\mathcal{M}_\odot$ (solid lines) and corresponding isochrones for ages from $10^{7.2}$ to $10^{8.4}$ yr (dotted lines) (Schaerer et al., 1993). The individual components are labelled by their masses (in solar units) and the two components of each system are joined by lines. All of the systems appear to lie within the main-sequence band, within the uncertainties indicated by the error bars. All binaries, bar one (EROS 1061, $4.3\,\mathcal{M}_\odot + 3.8\,\mathcal{M}_\odot$) appear to have components of the same ages, within the uncertainties.

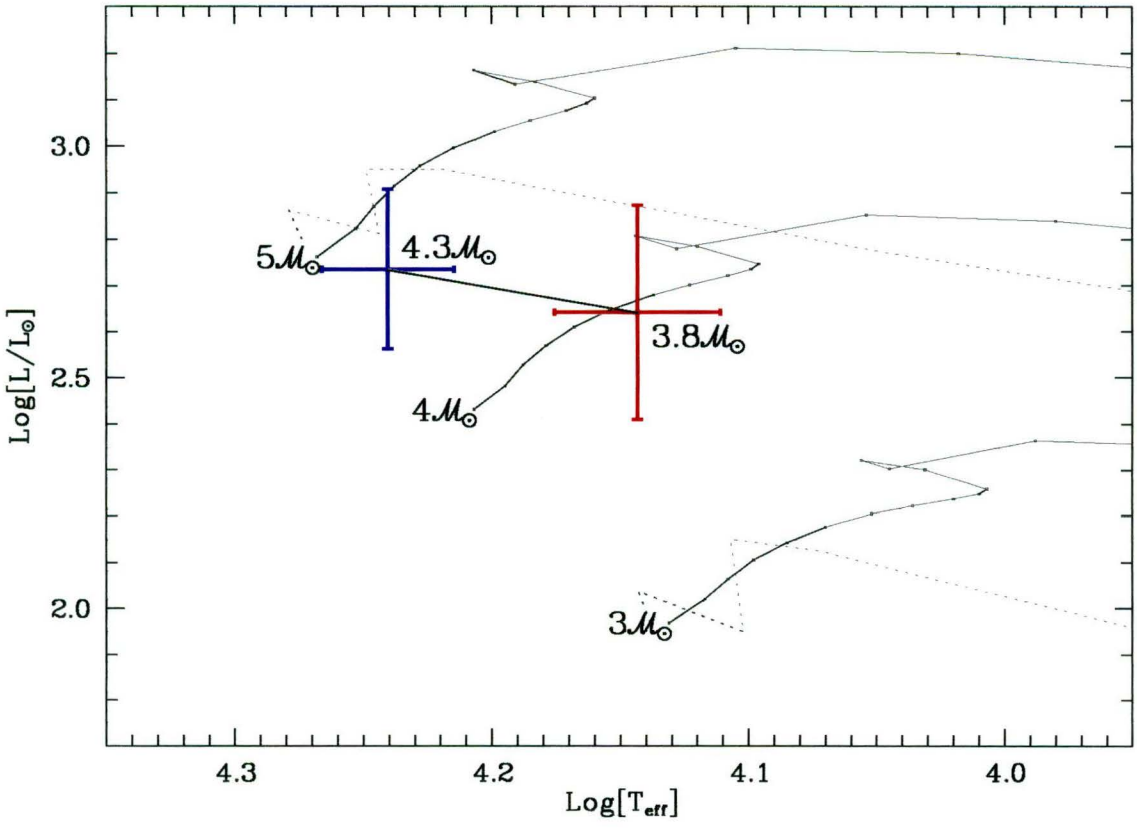

Figure 7.3: EROS 1061 shown by itself in the $\log[T_{\rm eff}]/\log[L/L_{\odot}]$ plane along with the post-ZAMS theoretical evolutionary models for metal abundance $Z = 0.008$ for ZAMS masses from 3, 4 and 5 $\mathcal{M}_{\odot}$ (solid lines) as in figure 7.2 (Schaerer et al., 1993) and also the 3 and 5 $\mathcal{M}_{\odot}$ pre-ZAMS theoretical evolutionary models (dotted lines, Iben, 1965). The individual components are labelled by their masses (in solar units). The 3 $\mathcal{M}_{\odot}$ pre-ZAMS model takes less than 2×10^6 yr to evolve from $\log[T_{\rm eff}] = 3.95$ to the ZAMS while the 5 $\mathcal{M}_{\odot}$ pre-ZAMS model takes less than 4.5×10^5 yr. By comparison stars of masses of the order of 5 $\mathcal{M}_{\odot}$ spend $\sim 10^8$ yr on the main sequence. The derived effective temperatures and luminosities of the components of EROS 1061 are clearly consistent with EROS 1061 being composed of two pre-ZAMS stars of slightly different masses (more-massive pre-ZAMS stars contract faster than less massive-ones) in the final stages of contraction down onto the ZAMS.

Table 7.1: Adopted parameters for eight well-detached, eccentric EROS eclipsing binary systems. Periods (P) and Epochs of Primary Minimum (T_0) are taken from Grison et al. (1995). The remaining parameters (the mass ratio (q), the effective temperatures of the primary and secondary components ($T_{\rm eff,1}$ and $T_{\rm eff,2}$), the major semi-axis (A), the orbital eccentricity (e) and inclination (i), the longitude of periastron (ω) and the masses and radii of each component ($\mathcal{M}_1$, $\mathcal{M}_2$, $\mathcal{R}_1$ and $\mathcal{R}_2$)) are derived from analysis of the calibrated light curves and by requiring that the mass, radius and luminosity of both components of each system be consistent with single-star theoretical evolutionary models. Uncertainties are estimated according to the methods described in section 7.1.6. The σ values listed in the last column are the standard deviations of the residuals between the observations and model light curves corresponding to the adopted properties.

	P	T_0	q	$T_{\rm eff,1}$	$T_{\rm eff,2}$	A	e	ω	i	$\mathcal{M}_1$	$\mathcal{M}_2$	$\mathcal{R}_1$	$\mathcal{R}_2$	$\sigma^{B_{\rm E}}_{R_{\rm E}}$
Star	d]	HJD		K	K	$\mathcal{R}_\odot$		°	°	$\mathcal{M}_\odot$	$\mathcal{M}_\odot$	$\mathcal{R}_\odot$	$\mathcal{R}_\odot$	mag
1035	2.088	2448662.040	1.3	11 100	11 100	11.4	0.09	115.	84.	2.0	2.6	1.53	3.3	0.077
	±0.004	±0.004	±0.3	±1 000	±1 100	±1.1	±0.07	±20.	±3.	±0.6	±0.8	±0.15	±0.3	0.071
1052	3.388	2448661.4092	0.9	16 450	16 600	21.9	0.130	89.2	85.6	6.3	6.0	5.3	3.9	0.047
	±0.002	±0.0010	±0.5	±1 500	±1 300	±2.2	±0.015	±0.7	±0.4	±1.9	±1.7	±0.5	±0.4	0.019
1053	3.5700	2448662.8907	0.9	17 900	16 032	20.5	0.260	130.	84.7	4.8	4.3	3.1	2.4	0.036
	±0.0015	±0.0011	±0.3	±1 300	±1 300	±2.0	±0.018	±30.	±0.3	±1.4	±1.3	±0.3	±0.2	0.044
1060	4.423	2448660.777	1.1	15 400	16 300	26.	0.05	103.	75.4	5.5	6.0	6.3	6.7	0.045
	±0.005	±0.003	±0.3	±1 300	±1 300	±3.	±0.03	±7.	±0.6	±1.6	±1.8	±0.6	±0.7	0.024
1061	4.538	2448663.634	0.9	17 400	14 000	23.2	0.429	335.	84.2	4.3	3.8	2.6	3.6	0.060
	±0.006	±0.003	±0.2	±1 000	±1 000	±2.1	±0.018	±7.	±0.7	±1.3	±1.2	±0.2	±0.4	0.057
1063	4.723	2448661.947	1.2	12 800	14 700	23.6	0.36	73.4	84.8	3.6	4.3	3.4	3.5	0.042
	±0.002	±0.002	±0.4	±1 000	±1 000	±2.5	±0.03	±1.7	±0.3	±1.1	±1.3	±0.3	±0.4	0.042
1066	5.604	2448664.2955	1.2	20 000	22 100	33.	0.234	95.5	84.00	7.0	8.1	4.9	5.2	0.024
	±0.003	±0.0012	±0.3	±1 500	±1 500	±3.	±0.016	±0.6	±0.13	±2.1	±2.4	±0.5	±0.5	0.018
1074	9.145	2448668.830	0.9	18 000	18 000	44.	0.252	107.1	84.4	7.0	6.3	6.5	4.1	0.019
	±0.015	±0.002	±0.3	±1 000	±1 000	±4.	±0.015	±1.1	±0.4	±2.1	±2.1	±0.6	±0.4	0.018

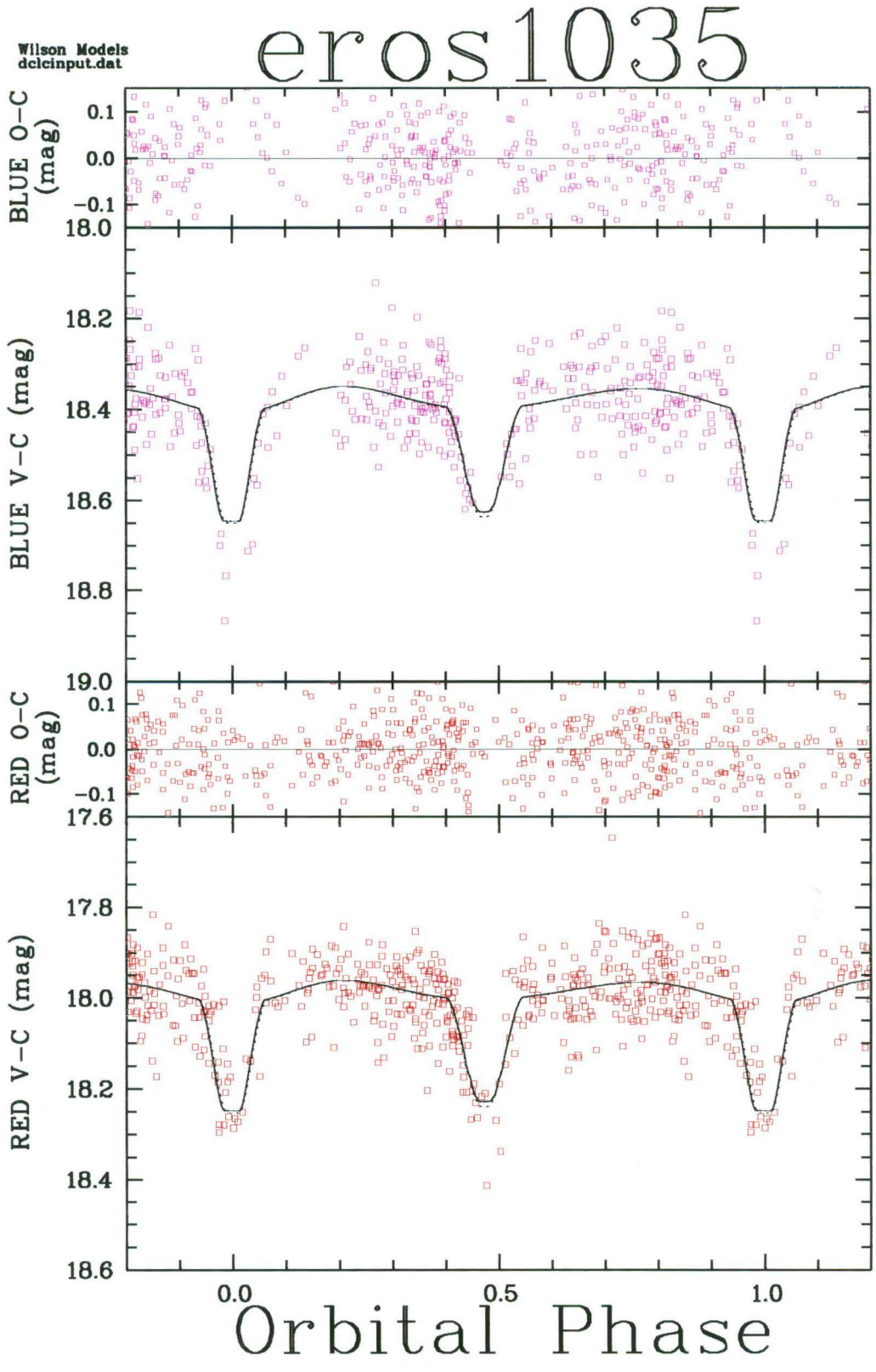

Figure 7.4: Light curve fit for EROS 1035. Both $B_{\rm E}$ (Blue) and $R_{\rm E}$ (Red) observed light curves are shown. Overplotted are model light curves corresponding to the adopted parameters tabulated in table 7.1. Also plotted are the residuals between observations and the models for both bandpasses ($\sigma_{B_{\rm E}} = 0.077$ and $\sigma_{R_{\rm E}} = 0.071$ mag). The noise in the photometry results from both its intrinsically low brightness and crowding by a nearby field star.

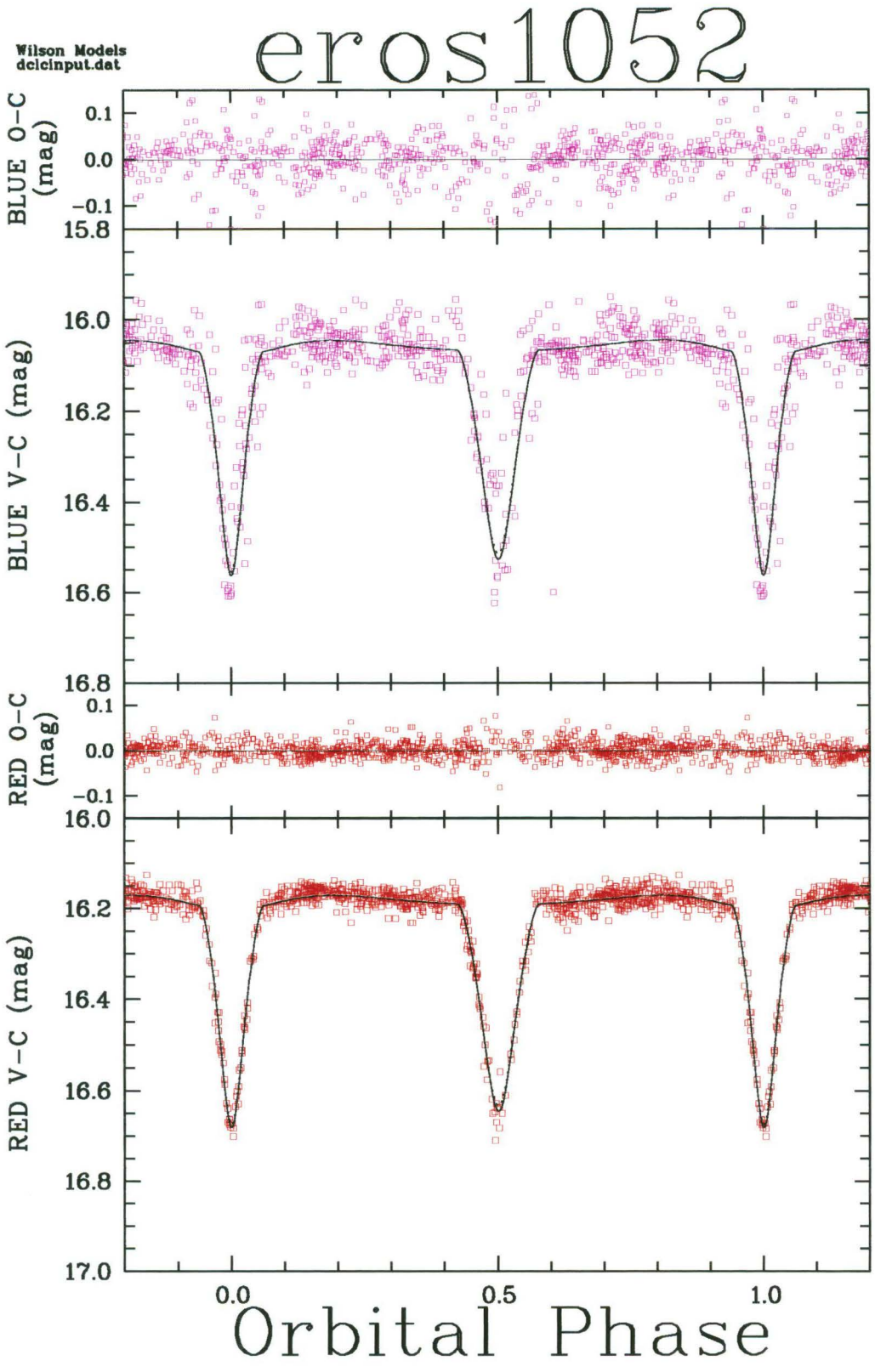

Figure 7.5: Light curve fit for EROS 1052. The standard deviations for the residuals between observations and the models are $\sigma_{B_E} = 0.047$ and $\sigma_{R_E} = 0.019\,mag$. This system is clearly one of those for which the B_E photometry 'often drifted brightwards' (Grison et al., 1995). The reasons for this drift are not known. The problem applies to all B_E light curves for stars located on certain of the CCDs which comprised the 16-chip mosaic camera used for the EROS observations.

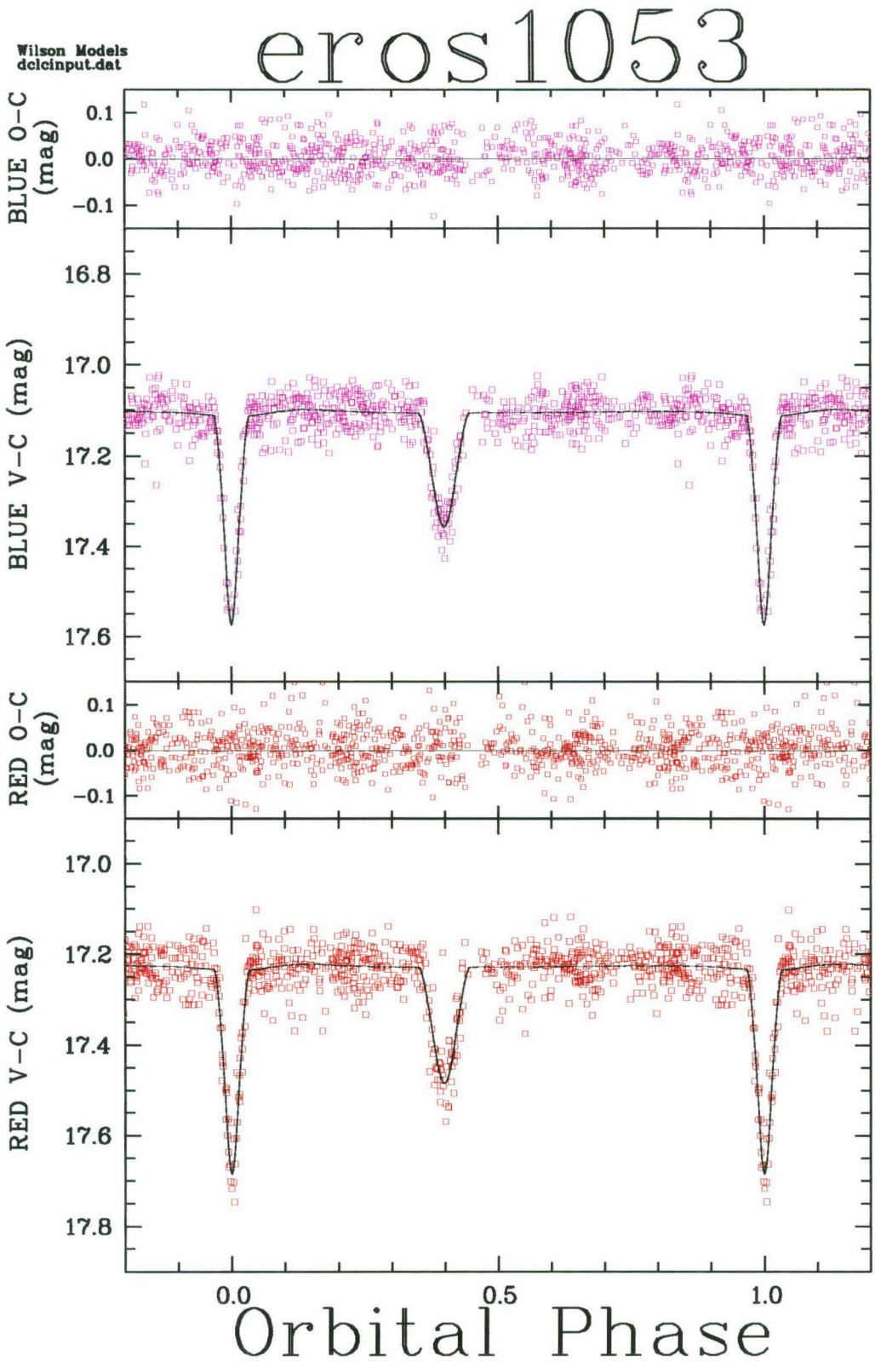

Figure 7.6: Light curve fit for EROS 1053. The standard deviations for the residuals between observations and the models are $\sigma_{B_E} = 0.036$ and $\sigma_{R_E} = 0.044$ mag. The slightly noiser R_E light curve is no doubt caused by crowding problems.

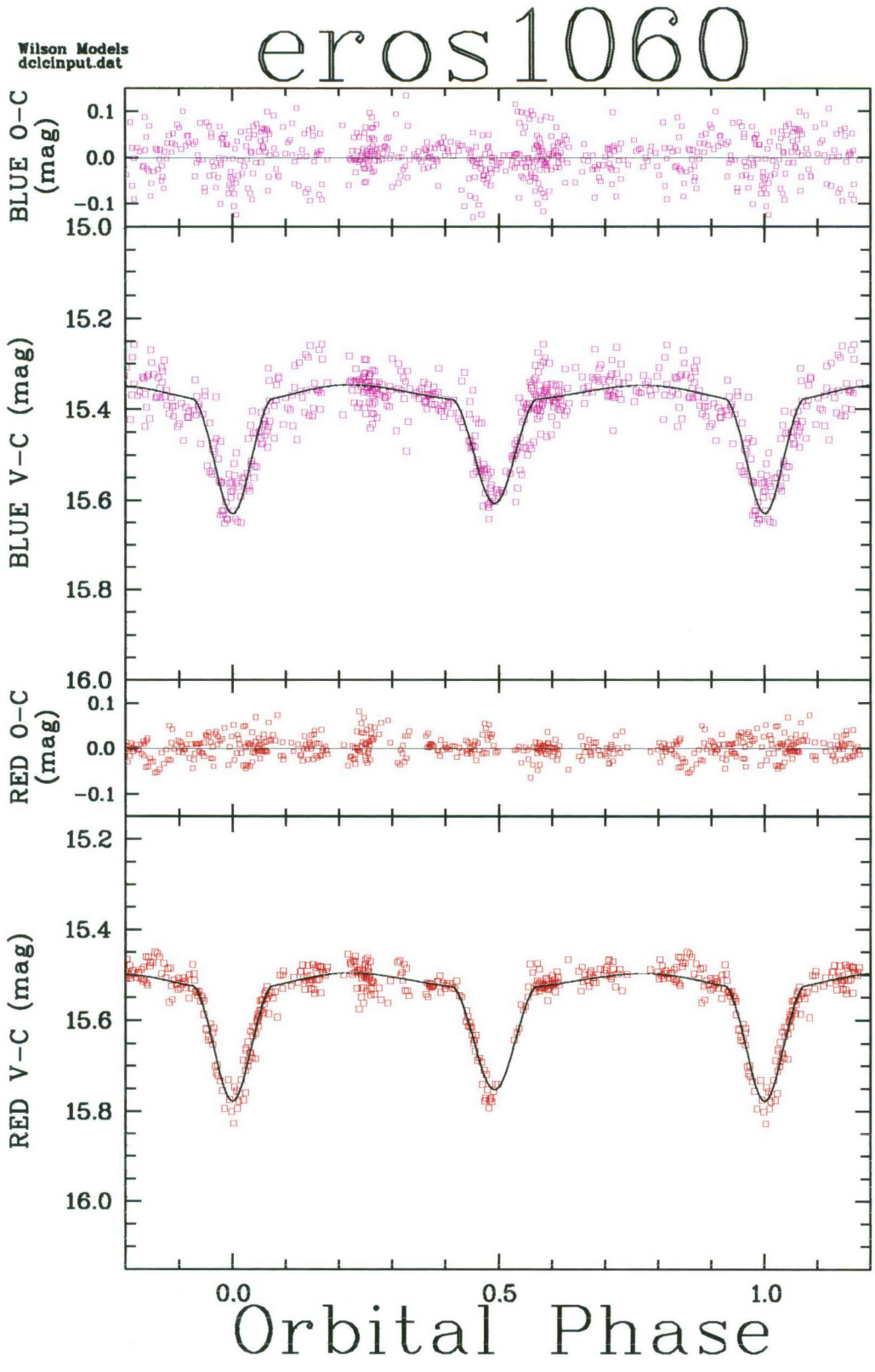

Figure 7.7: Light curve fit for EROS 1060. The standard deviations for the residuals between observations and the models are $\sigma_{B_E} = 0.045$ and $\sigma_{R_E} = 0.024$ mag. Like EROS 1052, this star is located on one of the CCDs with problematic B_E photometry.

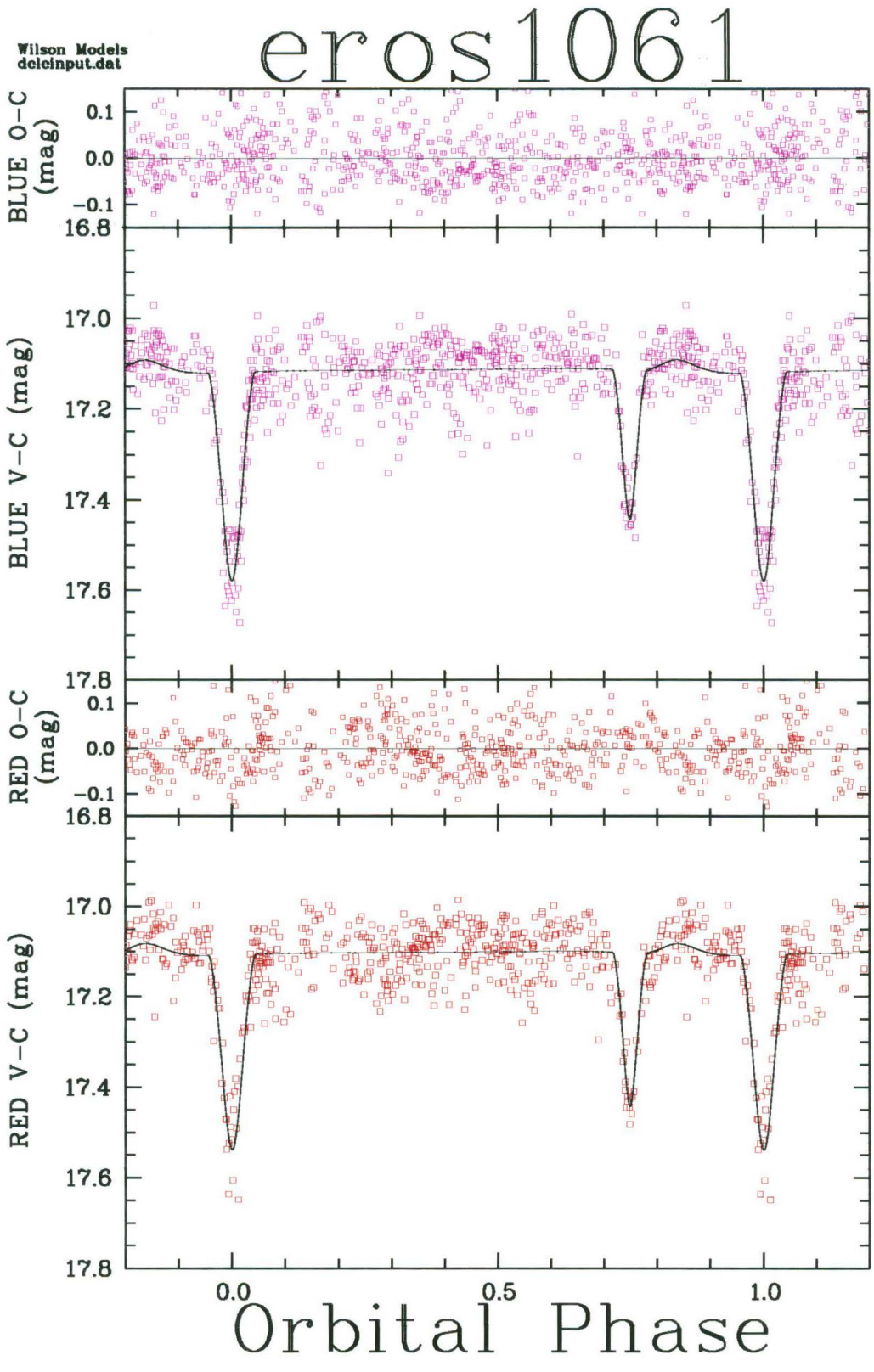

Figure 7.8: Light curve fit for EROS 1061. The standard deviations for the residuals between observations and the models are $\sigma_{B_{\rm E}} = 0.060$ and $\sigma_{R_{\rm E}} = 0.057$ mag.

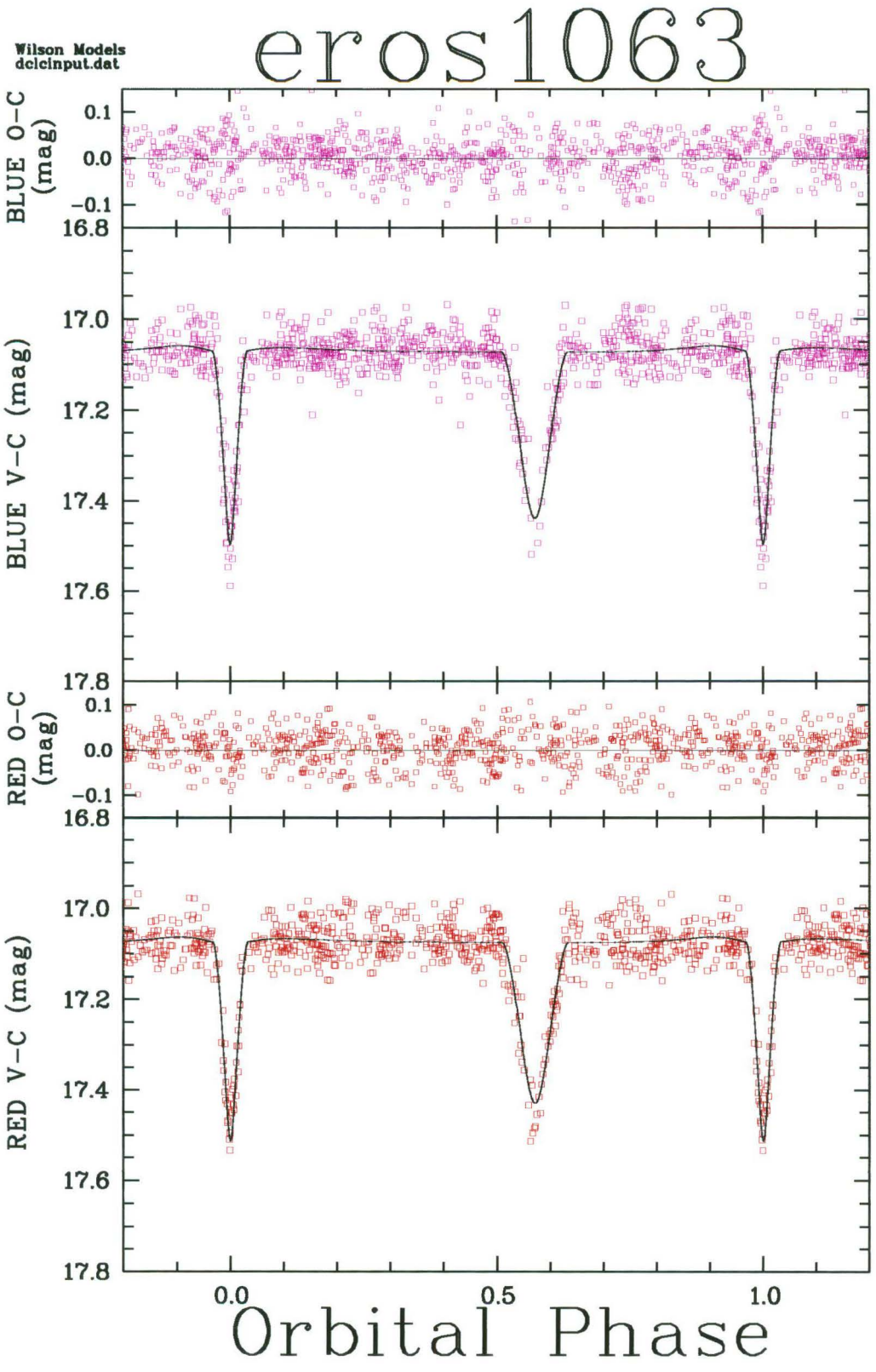

Figure 7.9: Light curve fit for EROS 1063. The standard deviations for the residuals between observations and the models are $\sigma_{B_E} = 0.042$ and $\sigma_{R_E} = 0.042$ mag.

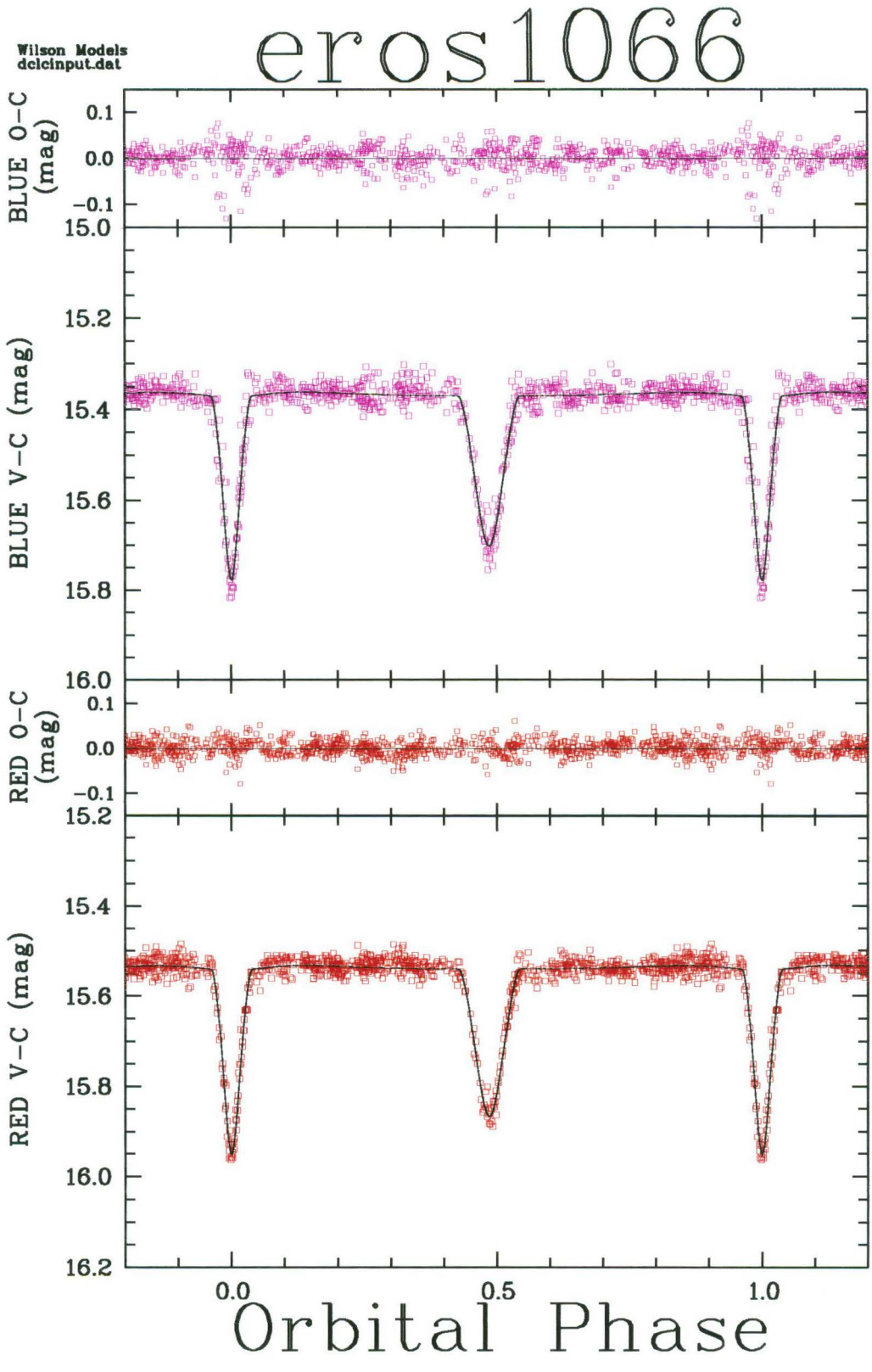

Figure 7.10: Light curve fit for EROS 1066. The standard deviations for the residuals between observations and the models are $\sigma_{B_E} = 0.024$ and $\sigma_{R_E} = 0.018$ mag.

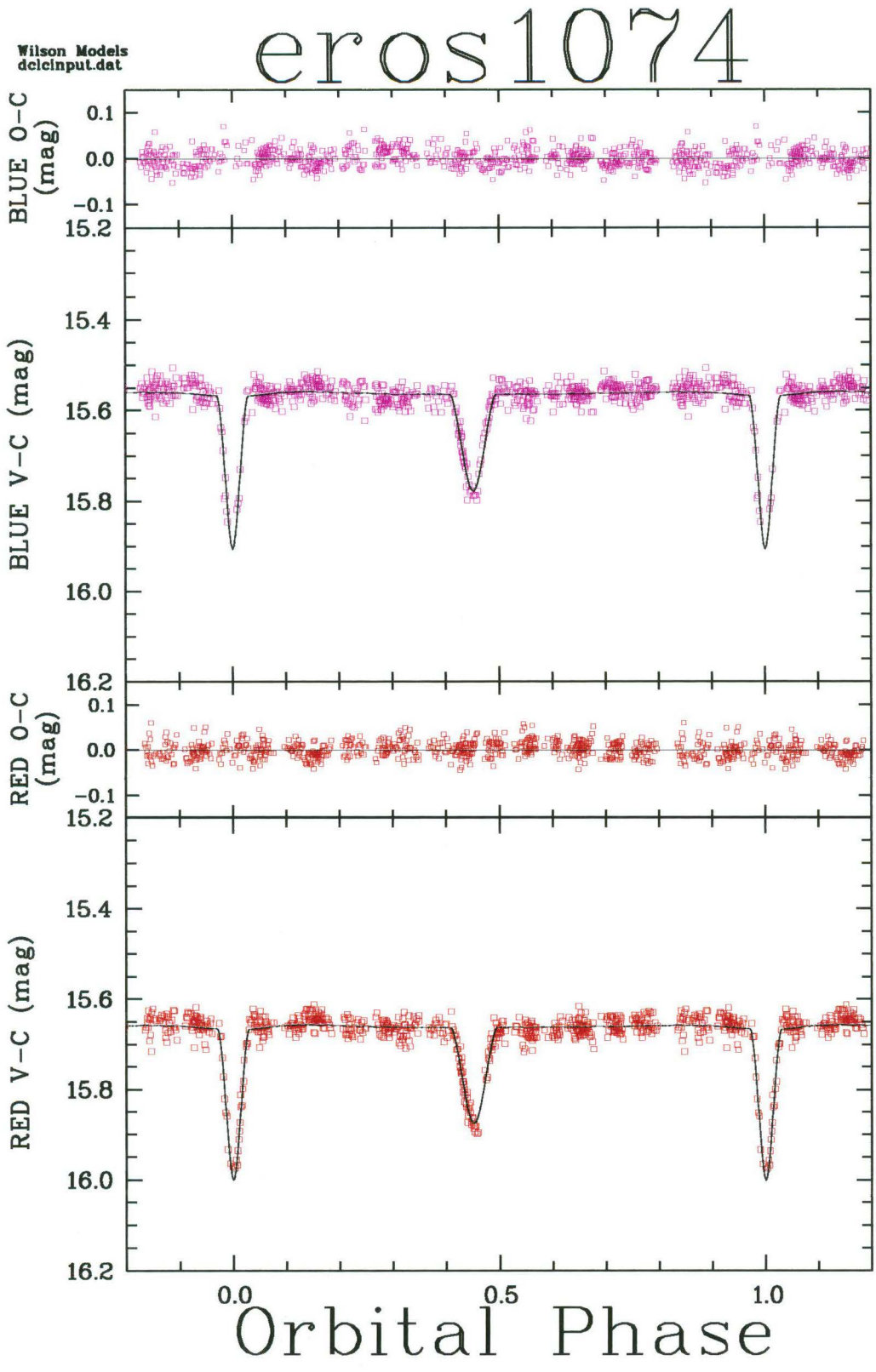

Figure 7.11: Light curve fit for EROS 1074. The standard deviations for the residuals between observations and the models are $\sigma_{B_E} = 0.019$ and $\sigma_{R_E} = 0.018$ mag.

Chapter 8

Concluding remarks

The primary goal of the thesis research programme undertaken was the investigation of stellar properties through the observation, analysis and interpretation of eclipsing binaries and by comparison of the empirically-determined properties of the individual component stars of the binary systems with theoretical models for structure and evolution for both single-stars and interacting binary star systems. This goal has been achieved.

A full analysis of two systems, HV 1620 in the Small Magellanic Cloud and HV 2241 in the Large Magellanic Cloud, has been made. The properties for the systems (see tables 6.3 and 6.5) have been determined through the analysis of the calibrated standard system photometry and accurate CCD light curves obtained at MJUO in conjunction with IUE spectrophotometry obtained by collaborators and published spectroscopic radial-velocity curves. These results are not the first to be determined for these two systems but they do significantly improve upon the precision and accuracy of previous work. Moreover the analysis conducted here is the first to incorporate all the available data in one internally consistent procedure. Both stars are found to be in semi-detached configurations with the cooler components filling their Roche lobes. Thus, due to the probability that these stars have undergone significant mass transfer and mass loss, the strictest test of theoretical models for the evolution of normal single-stars, i.e. comparison of masses, radii and luminosities of coeval theoretical stars with the observed values, is inappropriate. Indeed it is questionable that the components of evolved interacting binaries should necessarily correspond to normal single-stars of the same age or otherwise. Certainly there are phases during binary-star evolution when mass transfer and mass loss occur at very fast rates and it is by no means obvious that either component could retain, or even appear to retain, the properties of a normal single star.

In comparing the properties of HV 2241 with theoretical evolutionary models for normal single stars, such a discrepancy indeed appears to be the case. Both components of HV 2241 are grossly under-luminous for their masses (see figure 6.3). Furthermore, the properties determined here are not consistent in detail with models of very massive binary star evolution. The possibility of errors in the analysis of the available data for this system is small since the independent analyses by various investigators of the same data produce essentially concordant results. The remaining possibilities are that either some large (of the order of 12 percent) systematic error has been made in the calibration of the photometry, spectrophotometry and/or the spectroscopic radial velocities, or HV 2241 has been caught at a particularly interesting, unprecendented evolutionary stage.

The properties of the components of HV 1620 on the other hand are entirely consistent with theoretical models for normal single stars and are in qualitative agreement with the details of the most appropriate binary star evolutionary models. Significant uncertainties nevertheless remain and prevent a detailed comparison between observation and theory in terms of the more subtle features of the theoretical models such as chemical composition. The major source of the uncertainty is the uncertainty in the temperature estimation which in turn derives ultimately from the uncertainty in the photometry and that surrounding the interstellar extinction and correction thereof for these stars. The appropriate interstellar extinction law to apply is very uncertain due to the great variation from star to star, especially shortward of $\sim$2 000 Å. In the visible the similarity of the Galactic and Magellanic Cloud extinction laws is well established. SMC stars with Galactic far-uv extinction curves are known (Lequeux, 1997). Mean extinction laws, as applied in section 5.4.3, can thus be grossly inappropriate for particular stars. As was shown for HV 2241, simply adopting the alternative LMC extinction law of Howarth implied a temperature 3 000 K (i.e. more than 10 percent) hotter than that derived using the Fitzpatrick law. Howarth's extinction law lies about midway between the LMC and SMC laws plotted in figure 5.5. If the extinction toward HV 1620 were Galactic-like, this would have a huge effect on the temperature derived for this star. In order to improve confidence in the temperatures derived from flux fitting procedures, spectrophotometry is required over as large a wavelength range as possible. To this end, HST spectrophotometry covering $\lambda\lambda$1150-7075 Å for ten Magellanic Cloud eclipsing binaries, including these two stars, has recently been obtained by collaborators (Guinan and coworkers).

A second eclipsing binary in the LMC, HV 982, has also been observed extensively. Prior to the current investigation, only photographic light curve data were available. As a result of the present research

programme standard system photometry and complete CCD light curves in six colours have been secured, with extensive phase coverage in three of them. IUE spectrophotometry obtained by collaborators has been used in conjunction with analyses of the light curves and photometry to estimate the temperatures of the components of HV 982. No spectroscopic radial-velocity data is yet available for this system although other investigators are known to be in the process of obtaining such. Because of this, a full analysis is not yet possible. Despite this limitation, masses, radii and luminosities have been estimated (see table 6.1). These properties are based on the adoption of the distance to HV 982 being equal to the mean distance to the LMC itself and upon the assumption of a mass ratio close to unity based on arguments resulting from the observed light curve form and binary star evolution models. They are in good agreement with the predictions of normal single-star models. The estimates of the temperatures of the components are largely insensitive to the uncertainties in the parameters that can not be determined at this time for lack of spectroscopic radial-velocity data. However, as for HV 1620 and HV 2241, large uncertainty in the reddening of HV 982 leads to large uncertainty in the temperatures. These current limitations on the data available for HV 982 make it particularly deserving of further investigation since it is without doubt a well-detached system, and hence suitable for comparison with single-star theoretical models once suitably accurate properties have been determined. Moreover, HV 982 is an eccentric system and we have shown that it undergoes apsidal motion characteristic of such systems. These properties permit the possibility of studies of stellar structure both through comparison of the observed and theoretical apsidal motion rates and by placing lower limits on orbit circularization timescales. HST spectrophotometry for this star has also been secured by Guinan and coworkers. This together with the (hopefully) soon to be available spectroscopic radial-velocity curves, and of course the CCD light curves presented here, should permit a more detailed study of HV 982 in the near future.

Masses, radii and luminosities have been determined for the components of a further eight LMC eclipsing binaries taken from the EROS catalogue of eclipsing binaries. A new analysis procedure which centers on the analysis of photometrically calibrated light curves has been used. No spectroscopic radial-velocity curves are required. The properties are determined by requiring that the components resemble normal single stars as prescribed by theoretical models. The distance to the stars must also be known. We have assumed that these eight stars all lie at the mean distance of the LMC galaxy. The light curves used are those published by the EROS microlensing collaboration. All eight systems are apparently well-detached and have noticeably eccentric orbits, as indicated by their light curves. Thus the component stars of all eight binaries can be assumed to be well represented by normal single-star models. The derived properties of seven of the systems are found to be in good agreement with the usual assumption of coeval formation of binary star components. The eighth system, EROS 1061, appears not to correspond to the normal models for binary star formation and evolution. It is suggested that EROS 1061 is a pre-main sequence system, with both components in the final stages of their contraction down to their ZAMS states. Pre-ZAMS stars show emission features in their spectra. Spectrograms need not be of great resolution in order to merely detect the prescence of emission lines which would support the proposal that EROS 1061 is pre-ZAMS. Recent work by other observers at MJUO suggests that this 17^{th} mag star is just beyond the current practical limit for spectroscopic study at MJUO. However this should not present great difficulties for even a 2-m class telescope and it may prove fruitful to apply for time on the Mt. Stromlo Observatory 1.9-m telescope. Clearly, EROS 1061 is a particularly interesting candidate for further investigation, and luckily, unlike a goodly fraction of the other EROS eclipsing binaries, its field is not too crowded to be usefully observed photometrically from MJUO where the typical seeing conditions make accurate photometry for extremely crowded fields the exception rather than the rule.

With recent success in gaining funding from the Marsden Fund[1] the future of the MJUO Magellanic Cloud Eclipsing Binary project seems bright. The immediate priority must be to reestablish the observing programme which has been on hold since March of 1996. Effort should focus on improving the achievable quality of the standard system photometry. A fundamental component of this is simply gaining more experience and a better understanding of the instrumental photometric system and its relation to the standard systems. Clearly, more observations of as many (secondary) standard stars as possible will aid in this purpose. I believe it will be fruitful to establish a sequence of local tertiary standards. Field stars in the images of the three targets already observed should prove useful. In particular, the comparison and check stars used in the differential photometry should be ideal since their long term stability is already known. Because single CCD images would thus include several standards, such sequences should dramatically improve the situation whereby due to lengthy exposure times for the programme stars, limited numbers of observations of a limited number of standards can be acquired a single night. Furthermore, several practical considera-

[1]The Marsden Fund is a major New Zealand grant scheme which is geared toward the support of 'curiosity driven scientific research'

tions, for example ensuring standards are observed at an adequate range of airmasses so as to bracket the programme star observations, will take care of themselves automatically since the standards would necessarily be observed at essentially the same airmasses as he programme stars as a matter of course. Systematic errors arising from the remaining flat-fielding uncertainties can be easily avoided simply by extending the practice of always observing the programme stars and the standard stars at the same chip position. Clearly the tertiary standard sequences must be calibrated against the existing secondary standards. The calibrating secondary standard (and programme) stars should always be observed at a the same specific position on the CCD (call it the 'calibration position'). The new tertiary standard stars should always be observed at the same individual positions relative to the calibration position. The transformed standard system photometry for the new standards will then always be systematically in error. However as long as the same systematic error is made every time these stars are observed, their relationship to the photometry for stars observed at the calibration position should remain unchanged. Thus photometry for stars observed at the calibration position will be on the standard system. Alternatively, it may prove fruitful to improve the flat-fielding technique so that reliable photometry can be obtained across the entire CCD chip area. Manfroid (1995; 1996) discusses an interesting empirical technique for correcting for the large scale variations of the sensitivity which may well be useful for the MJUO system.

Perhaps more importantly in terms of the future of the MJUO MCEB programme is the selection of new target stars. Efforts must be concentrated on unevolved, well-detached systems which ultimately provide the most stringent astrophysical results. The truly staggering data bases amassed by the various microlensing projects should provide an abundance of useful targets. As already pointed out, the eclipsing binary systems in the EROS catalogue generally lie in fields too crowded to be usefully observed from MJUO. But the EROS catalogue published to date is based only on the CCD observations of a very small region of the very crowded bar of the LMC. Presumably, the EROS Schmidt plate photographic survey which observed a much larger field should provide a goodly number of suitable candidates. In addition the MACHO and MOA collaborations have also been observing much more extended regions of the Clouds and thus they too should reveal an abundance of eclipsing binaries in less crowded fields. Of course, obtaining useful targets from these sources is contingent on the respective collaborations being willing and able to do so. Tentative enquiries in this respect made to date seem promising.

The future is bright, for it lies with the stars

Appendix A

Tables of Differential photometry

This appendix presents tables of differential photometry for the three programme stars observed at MJUO, HV 982, HV 1620 and HV 2241. There are six tables corresponding to the six bandpasses the stars were observed in for each star. Each table lists the following columns:

1. **Frame** The computer magnetic tape file name of the image. The first four characters, usually a letter followed by three digits identifies the physical tape, the last four digits identifies the specific image on the tape.

2. **Date** The Coordinated Universal Time (UTC) date the image was acquired.

3. **HJD−2400000.0)** The (modified) Heliocentric Julian Day number of mid-exposure. The begining and finishing times of each exposure are recorded in the image header at the time the image file is first created by the PM3000 CCD system.[1] At the time the image is read from tape to disk back in Christchurch, a correction for the known drift behaviour of the PM3000 clock is applied, the mid time of the exposure is calculated, the appropriate heliocentric correction is calculated and the heliocentric Julian Day number is added to the image header information (see section 2.3.6).

4. **Orbital Phase** The orbital phase, computed according to the ephemerides of section 3.3.3.

5. **X** The airmass. By default the airmass is calculated according to,

$$X = \sec[z] \cdot (1 - 0.0012 \cdot (\sec^2[z] - 1)) \tag{A.1}$$

   where z is of course the zenith distance and,

$$\sec[z] = (\sin[\phi_{\rm Obs}] \cdot \sin[\delta_\star] + \cos[\phi_{\rm Obs}] \cdot \cos[\delta_\star] \cdot \cos[HA_\star])^{-1} \tag{A.2}$$

   where $\phi_{\rm Obs}$ is the latitude of the telescope, $\delta_\star$ is the declination of the star being observed and $HA_\star$ is Hour Angle of the star at the time of the observation. If both start and finish times of the exposure are recorded in the image header then a 'mean' airmass is estimated according to,

$$\bar{X} = \frac{X_{\rm start} + 4X_{\rm mid} + X_{\rm finish}}{6} \tag{A.3}$$

   where $X_{\rm start}$, $X_{\rm mid}$, and $X_{\rm finish}$ are the instantaneous airmasses at the start, mid and finish times of the exposure (Stetson, 1989).

6. **T** The exposure duration in seconds.

7. **Row** and **Col** The MIDAS position of the stellar centroid of the target reported by the DAOPHOT II profile fitting photometry.

8. $\mathbf{m}_{\rm raw}$ The magnitude of target reported by the DAOPHOT II profile fitting photometry (PEAK) [mag].

9. $\sigma_{\mathbf{m}_{\rm raw}}$ The standard error on magnitude reported by the DAOPHOT II profile fitting photometry [mag].

10. **sky** The background sky level reported by the DAOPHOT II profile fitting photometry [ADU].[2]

11. **CHI** and **Sharp** The two 'image-peculiarity indices' reported by the DAOPHOT II profile fitting photometry.

[1] Exposure begining and finishing times are recorded provided the `expose` and `readout` commands are used to obtain the exposure. If instead `obs` is used, the start time and exposure duration (in deci-secs) are recorded in the header. Either way it is possible to compute the precise moment of mid-exposure.

[2] Actually, under the reduction procedure employed for the differential photometry, the sky background is determined during the synthetic aperture photometry step and is *not* redetermined at the time of the profile fit.

12. **V − C** The $Variable - Comparison$ differential magnitude [mag].

13. **C − C** The $Comparison - Check$ differential magnitude [mag].

14. **Seeing (FWHM)** The seeing, in terms of the 'mean' Full Width at Half Maximum [arcsec]. The mean FWHM is computed as,

$$\mathrm{FWHM} = 0.6164 \cdot \sqrt{\sigma_x \cdot \sigma_y}, \tag{A.4}$$

where σ_x and σ_y are the PSF half-widths of the analytic component of the PSF determined by DAOPHOT II and the factor 0.6164 converts from pixels to arcsec.

15. **ILCA** Acronym for Included in Light Curve Analysis. A 1 indicates this point was included in the final light curve analysis while a 0 indicates this point was excluded (see sections 3.3.2 and 4.4.3).

A.1 HV 982 differential photometry

Table A.1: HV 982 differential photometry – u.

Frame	Date	HJD −2400000.0	Orbital Phase	X	T	Row	Col	$m_{\rm raw}$	$\sigma_{m_{\rm raw}}$	sky	CHI	Sharp	$V-C$	$C-C$	Seeing (FWHM)	ILCA
T4070006	1993-Jun-26	49164.8445	0.0248	2.016	1200.0	165.16	135.49	15.172	0.008	49.49	1.21	0.015	0.897	0.336	4.14	1
T4070007	1993-Jun-26	49164.8627	0.0282	2.110	1200.0	167.30	141.76	15.598	0.010	49.69	1.16	0.006	0.859	0.325	5.33	1
T4070008	1993-Jun-26	49164.8843	0.0322	2.219	1200.0	162.88	140.94	15.391	0.010	47.19	1.25	0.003	0.815	0.322	4.71	1
T4070009	1993-Jun-26	49164.9239	0.0396	2.393	1200.0	*	*	*	*	*	*	*	*	*	*	0
T4070010	1993-Jun-26	49164.9434	0.0433	2.457	1200.0	163.06	141.85	15.413	0.009	35.85	1.18	0.013	0.713	0.335	4.51	1
T4070011	1993-Jun-26	49164.9595	0.0463	2.496	1200.0	162.36	141.85	15.485	0.009	31.86	1.12	−0.001	0.702	0.337	4.68	1
T4070012	1993-Jun-26	49164.9828	0.0507	2.525	1200.0	*	*	*	*	*	*	*	*	*	*	0
T4070013	1993-Jun-26	49165.0057	0.0550	2.520	1200.0	161.26	142.59	15.570	0.010	17.05	1.23	0.004	0.661	0.328	4.82	1
T3990008	1993-Jun-29	49167.9108	0.5995	2.374	1200.0	163.53	141.64	14.832	0.009	238.26	1.35	0.034	0.621	0.340	2.90	1
T3990013	1993-Jun-29	49167.9932	0.6149	2.523	1200.0	162.55	144.65	15.191	0.012	212.41	1.33	0.008	0.610	0.340	3.85	1
T3990014	1993-Jun-29	49168.0095	0.6180	2.504	1200.0	162.92	142.70	15.012	0.011	219.33	1.35	0.017	0.623	0.342	3.53	1
T3990015	1993-Jun-29	49168.0373	0.6232	2.435	1200.0	165.66	142.24	15.055	0.010	193.10	1.23	0.000	0.592	0.348	3.84	1
T4080011	1993-Jul-01	49169.8585	0.9646	2.158	1200.0	165.77	138.60	14.929	0.011	449.77	1.39	0.061	1.020	0.337	2.30	1
T4080012	1993-Jul-01	49169.8739	0.9674	2.235	1200.0	165.49	138.74	15.096	0.012	464.34	1.22	0.089	1.051	0.360	2.50	1
T4080015	1993-Jul-01	49169.8990	0.9721	2.348	1200.0	165.98	139.16	15.293	0.013	480.86	1.14	0.051	1.115	0.345	2.92	1
T4080016	1993-Jul-01	49169.9171	0.9755	2.417	1200.0	166.61	139.20	15.447	0.014	492.47	1.09	−0.002	1.196	0.349	2.76	1
T4080019	1993-Jul-01	49169.9465	0.9810	2.497	1200.0	166.34	139.16	15.599	0.017	501.97	1.20	0.048	1.270	0.336	2.60	1
T4080020	1993-Jul-01	49169.9624	0.9840	2.520	1200.0	165.91	139.33	15.600	0.019	502.26	1.29	0.051	1.285	0.346	2.68	1
T4080023	1993-Jul-01	49169.9892	0.9891	2.522	1200.0	165.32	139.99	15.665	0.017	497.21	1.06	0.029	1.314	0.351	2.96	1
T4080024	1993-Jul-01	49170.0171	0.9943	2.477	1200.0	165.23	140.40	15.628	0.018	479.74	1.12	0.091	1.293	0.338	3.09	1
T4080027	1993-Jul-01	49170.0441	0.9993	2.392	1200.0	164.41	140.71	15.579	0.015	452.83	1.03	0.037	1.268	0.354	3.28	1
T4080028	1993-Jul-01	49170.0612	0.0025	2.323	1200.0	163.93	141.55	15.342	0.014	428.93	1.23	0.050	1.198	0.331	2.83	1
T4080031	1993-Jul-01	49170.0823	0.0065	2.225	1200.0	162.91	141.76	15.275	0.014	397.53	1.25	0.066	1.137	0.338	3.05	1
T4080032	1993-Jul-01	49170.0971	0.0093	2.151	1200.0	162.05	141.99	15.133	0.012	372.54	1.25	0.068	1.083	0.337	2.97	1
T4080036	1993-Jul-01	49170.1243	0.0144	2.011	1200.0	160.85	142.74	14.994	0.008	319.76	0.96	0.040	1.024	0.344	3.10	1
T4060018	1993-Jul-01	49170.1491	0.0190	1.884	1200.0	158.83	142.92	14.871	0.009	268.02	1.17	0.034	0.978	0.341	3.16	1
T4060021	1993-Jul-01	49170.1730	0.0235	1.767	1200.0	157.46	143.12	14.698	0.008	211.69	1.23	0.038	0.933	0.329	3.00	1
T4060022	1993-Jul-01	49170.1891	0.0265	1.693	1200.0	160.61	143.63	14.563	0.009	171.76	1.62	0.051	0.876	0.343	2.78	1
T4060028	1993-Jul-01	49170.2765	0.0429	1.372	1200.0	163.73	141.79	14.133	0.007	22.49	2.00	0.051	0.731	0.341	2.51	1
T4060029	1993-Jul-01	49170.2922	0.0458	1.328	1200.0	163.44	141.60	14.065	0.006	114.39	1.63	0.060	0.694	0.345	2.35	1
T4060042	1993-Jul-02	49170.8203	0.1448	1.975	1200.0	165.11	138.74	14.341	0.009	467.77	1.59	0.072	0.616	0.342	2.23	1
T4100031	1993-Jul-04	49172.9321	0.5406	2.484	1200.0	164.59	140.30	15.366	0.020	777.23	1.25	−0.024	0.606	0.357	4.68	1
T4100032	1993-Jul-04	49172.9469	0.5434	2.511	1200.0	164.97	140.40	15.477	0.020	799.15	1.12	−0.026	1.314	−0.045	5.15	0
T4100033	1993-Jul-04	49172.9647	0.5467	2.526	1200.0	166.15	139.93	15.341	0.020	817.18	1.27	−0.017	0.642	0.339	4.82	1
T4100034	1993-Jul-04	49172.9809	0.5498	2.522	1200.0	165.81	139.71	15.400	0.020	827.37	1.17	−0.015	0.604	0.362	5.00	1

Table A.1 cont.: HV 982 differential photometry – u.

Frame	Date	HJD −2400000.0	Orbital Phase	X	T	Row	Col	$m_{\rm raw}$	$\sigma_{m_{\rm raw}}$	sky	CHI	Sharp	$V-C$	$C-C$	Seeing (FWHM)	ILCA
T4220027	1993-Jul-22	49190.9892	0.9251	2.383	1200.0	162.32	143.64	15.954	0.012	18.33	1.19	−0.004	0.661	0.344	6.06	1
T4220032	1993-Jul-22	49191.0468	0.9359	2.116	1200.0	160.32	144.52	16.214	0.014	19.94	1.26	−0.017	0.763	0.338	5.70	1
T4240025	1993-Jul-24	49193.0923	0.3193	1.854	1200.0	161.12	144.32	14.698	0.007	15.18	1.40	0.004	0.613	0.337	3.98	1
T4240035	1993-Jul-24	49193.1658	0.3331	1.530	1200.0	156.49	144.85	14.358	0.006	15.06	1.54	0.021	0.606	0.347	3.51	1
T4250010	1993-Jul-24	49193.2484	0.3486	1.282	1200.0	159.49	144.35	14.226	0.006	17.00	1.68	0.018	0.608	0.351	3.48	1
T4270006	1993-Jul-27	49196.0518	0.8740	2.019	1200.0	164.62	144.01	14.733	0.008	59.12	1.42	0.031	0.637	0.341	3.55	1
T4270021	1993-Jul-27	49196.1588	0.8941	1.526	1200.0	158.54	144.18	14.300	0.006	17.84	1.62	0.043	0.633	0.334	3.21	1
T4280012	1993-Aug-15	49214.8697	0.4011	2.519	1200.0	168.27	139.20	15.684	0.010	16.04	1.25	0.016	1.053	0.324	4.03	1
T4280018	1993-Aug-15	49214.9153	0.4096	2.414	1200.0	168.10	139.94	15.675	0.011	21.42	1.37	0.043	1.211	0.325	3.74	1
T4280019	1993-Aug-15	49214.9369	0.4137	2.329	1200.0	165.95	140.99	15.723	0.012	20.07	1.36	0.036	1.269	0.313	3.93	1
T4280024	1993-Aug-15	49214.9755	0.4209	2.145	1200.0	164.73	145.01	15.736	0.012	18.29	1.43	0.016	1.273	0.330	4.46	1
T4280025	1993-Aug-15	49214.9909	0.4238	2.066	1200.0	164.37	145.13	15.592	0.012	18.00	1.51	0.020	1.220	0.323	4.26	1
T4280030	1993-Aug-15	49215.0214	0.4295	1.909	1200.0	163.62	145.08	15.264	0.010	17.56	1.58	0.044	1.144	0.320	3.84	1
T4280031	1993-Aug-15	49215.0363	0.4323	1.834	1200.0	163.01	144.77	15.180	0.009	17.41	1.38	0.014	1.194	0.226	3.94	0
T4280036	1993-Aug-15	49215.0654	0.4378	1.697	1200.0	160.79	144.86	14.958	0.009	17.85	1.59	0.052	1.023	0.326	3.59	1
T4280037	1993-Aug-15	49215.0818	0.4408	1.625	1200.0	160.06	145.35	14.896	0.008	18.02	1.50	0.020	0.980	0.319	3.84	1
S1250003	1993-Aug-15	49215.1206	0.4481	1.476	1200.0	157.71	145.18	14.597	0.006	18.12	1.38	0.030	0.868	0.323	3.56	1
S1250007	1993-Aug-15	49215.1462	0.4529	1.394	1200.0	156.81	145.20	14.496	0.007	18.78	1.71	0.027	0.809	0.327	3.66	1
S1250009	1993-Aug-15	49215.1646	0.4564	1.341	1200.0	155.83	144.93	14.382	0.006	18.47	1.47	0.031	0.767	0.325	3.51	1
S1250012	1993-Aug-15	49215.1914	0.4614	1.276	1200.0	*	*	*	*	*	*	*	*	*	*	0
S1250015	1993-Aug-15	49215.2132	0.4655	1.231	1200.0	161.27	145.64	14.236	0.006	15.20	1.52	0.022	0.693	0.330	3.50	1
S1250018	1993-Aug-15	49215.2401	0.4705	1.186	1200.0	160.00	144.04	14.140	0.011	15.10	3.00	0.090	0.656	0.327	3.46	1
S1250019	1993-Aug-15	49215.2563	0.4736	1.164	1200.0	160.00	143.76	14.139	0.006	21.67	1.68	0.032	0.647	0.324	3.60	1
S1290002	1993-Aug-18	49218.0798	0.0028	1.600	1200.0	161.85	144.12	16.157	0.059	20.52	5.66	−0.244	1.108	0.381	7.24	0
S1290004	1993-Aug-18	49218.1130	0.0090	1.475	1200.0	163.34	140.43	15.524	0.009	18.49	1.22	0.008	1.111	0.329	6.41	1
S1290006	1993-Aug-18	49218.1374	0.0136	1.395	1200.0	164.28	142.32	15.470	0.010	19.65	1.39	−0.009	1.038	0.334	6.67	1
S1290008	1993-Aug-18	49218.1586	0.0175	1.335	1200.0	162.59	143.16	15.511	0.009	19.29	1.08	−0.005	0.982	0.334	6.83	1
S1290010	1993-Aug-18	49218.1842	0.0223	1.273	1200.0	158.78	143.92	15.139	0.009	18.47	1.47	−0.007	0.924	0.334	5.96	1
S1290012	1993-Aug-18	49218.2087	0.0269	1.224	1200.0	163.86	141.26	16.505	0.104	18.51	1.35	−0.009	0.801	0.365	6.11	1
S1290014	1993-Aug-18	49218.2363	0.0321	1.179	1200.0	157.30	140.80	15.099	0.010	19.42	1.65	−0.002	0.820	0.332	6.81	1
S1330002	1993-Aug-20	49220.0753	0.3768	1.596	1200.0	163.15	142.65	14.728	0.008	21.03	1.61	0.033	0.720	0.343	3.80	1
S1330004	1993-Aug-20	49220.0970	0.3808	1.512	1200.0	162.29	142.24	14.943	0.009	21.56	1.67	0.069	0.763	0.331	3.44	1
T0810009	1993-Sep-07	49237.8914	0.7161	2.250	1200.0	166.46	141.58	14.699	0.007	14.28	1.42	0.053	0.649	0.320	2.99	1
T0810013	1993-Sep-07	49237.9561	0.7282	1.921	1200.0	165.10	143.52	14.444	0.008	12.24	1.81	0.030	0.629	0.335	2.86	1
T0810018	1993-Sep-07	49238.0186	0.7399	1.627	1200.0	162.76	142.55	14.200	0.007	14.10	1.76	0.025	0.624	0.333	2.74	1
S1620005	1993-Sep-08	49238.8746	0.9004	2.315	1200.0	168.50	141.94	14.829	0.008	17.31	1.53	0.039	0.656	0.321	3.10	1
S1620007	1993-Sep-08	49238.8989	0.9049	2.200	1200.0	166.05	141.30	14.737	0.007	16.60	1.50	0.046	0.648	0.331	3.07	1
S1620009	1993-Sep-08	49238.9199	0.9089	2.094	1200.0	165.34	141.37	14.802	0.008	15.86	1.60	0.046	0.650	0.325	3.49	1
S1620011	1993-Sep-08	49238.9385	0.9123	1.997	1200.0	164.33	139.70	14.664	0.006	16.58	1.31	0.035	0.648	0.323	3.30	1

Table A.1 cont.: HV 982 differential photometry – u.

Frame	Date	HJD −2400000.0	Orbital Phase	X	T	Row	Col	$m_{\rm raw}$	$\sigma_{m_{\rm raw}}$	sky	CHI	Sharp	$V-C$	$C-C$	Seeing (FWHM)	ILCA
S1620013	1993-Sep-08	49238.9592	0.9162	1.891	1200.0	166.36	142.83	14.511	0.006	16.37	1.30	0.018	0.653	0.322	3.00	1
S1620015	1993-Sep-08	49238.9786	0.9199	1.795	1200.0	162.71	141.36	14.446	0.008	16.35	1.85	0.029	0.660	0.325	3.09	1
S1620017	1993-Sep-08	49238.9974	0.9234	1.708	1200.0	165.32	138.02	14.398	0.007	16.90	1.76	0.043	0.662	0.330	2.99	1
S1620019	1993-Sep-08	49239.0235	0.9283	1.595	1200.0	162.84	140.89	14.329	0.006	16.87	1.52	0.010	0.675	0.330	3.33	1
S1620021	1993-Sep-08	49239.0450	0.9323	1.512	1200.0	162.51	143.90	14.253	0.007	17.94	1.70	0.044	0.707	0.335	2.91	1
S1620023	1993-Sep-08	49239.0640	0.9359	1.446	1200.0	159.09	142.99	14.214	0.006	19.97	1.49	0.044	0.727	0.334	2.94	1
S1620025	1993-Sep-08	49239.0825	0.9393	1.388	1200.0	165.22	141.78	14.264	0.006	23.07	1.48	0.029	0.747	0.330	3.28	1
S1620027	1993-Sep-08	49239.1006	0.9427	1.337	1200.0	162.26	142.26	14.259	0.007	27.92	1.83	0.051	0.790	0.326	2.99	1
S1620029	1993-Sep-08	49239.1192	0.9462	1.290	1200.0	161.66	142.58	14.292	0.006	31.46	1.43	0.048	0.815	0.325	3.19	1
S1620031	1993-Sep-08	49239.1372	0.9496	1.251	1200.0	160.36	142.40	14.324	0.006	34.47	1.54	0.035	0.853	0.331	3.24	1
S1620033	1993-Sep-08	49239.1550	0.9529	1.217	1200.0	159.85	143.11	14.259	0.008	36.99	1.95	0.065	0.883	0.333	3.03	1
S1630004	1993-Sep-08	49239.1862	0.9588	1.169	1200.0	159.18	142.86	14.298	0.008	41.50	1.96	0.069	0.954	0.333	3.04	1
S1630006	1993-Sep-08	49239.2052	0.9623	1.147	1200.0	158.38	142.86	14.374	0.008	41.57	2.00	0.069	1.005	0.332	3.20	1
T4420033	1993-Sep-14	49245.1066	0.0684	1.282	1200.0	161.02	143.04	14.575	0.007	13.82	1.58	−0.005	0.620	0.341	4.75	1
T4420036	1993-Sep-14	49245.1351	0.0738	1.224	1200.0	161.37	143.38	14.554	0.006	14.60	1.34	−0.005	0.623	0.343	4.91	1
T4430003	1993-Sep-14	49245.1675	0.0799	1.173	1200.0	161.55	142.80	15.752	0.034	14.43	1.36	−0.004	0.629	0.311	5.14	1
T4430006	1993-Sep-14	49245.1960	0.0852	1.140	1200.0	161.40	142.96	15.547	0.029	14.76	1.37	−0.016	0.648	0.373	4.76	0
T4430009	1993-Sep-14	49245.2220	0.0901	1.120	1200.0	159.96	142.84	14.704	0.008	24.66	1.53	−0.002	0.628	0.345	5.68	1
T4440031	1993-Sep-16	49246.8773	0.4003	2.199	1200.0	164.02	142.79	15.518	0.010	22.21	1.24	0.020	1.050	0.354	3.48	1
T4460001	1993-Sep-16	49246.9428	0.4126	1.864	1200.0	160.84	143.47	15.551	0.012	17.43	1.53	0.031	1.258	0.345	4.15	1
T4460007	1993-Sep-16	49247.0096	0.4251	1.564	1200.0	162.03	145.11	15.256	0.010	15.36	1.59	0.015	1.182	0.345	4.28	1
T4460013	1993-Sep-16	49247.0972	0.4415	1.291	1200.0	160.57	143.35	14.567	0.008	15.06	1.73	0.028	0.921	0.348	3.30	1
T4460019	1993-Sep-16	49247.1757	0.4563	1.155	1200.0	160.14	142.28	14.138	0.006	15.19	1.62	0.063	0.753	0.345	2.99	1
S1880016	1993-Nov-22	49313.9098	0.9644	1.300	1200.0	161.33	143.57	14.831	0.009	68.39	1.60	0.060	0.999	0.347	3.41	1
S1880021	1993-Nov-22	49313.9874	0.9789	1.161	1200.0	160.94	141.30	15.458	0.010	48.31	1.26	0.054	1.218	0.352	3.75	1
S1880026	1993-Nov-22	49314.1122	0.0023	1.110	1200.0	158.57	142.49	14.804	0.007	16.63	1.43	0.034	1.184	0.346	3.90	1
T5780016	1994-Feb-23	49406.8944	0.3927	1.132	1200.0	157.16	140.40	14.812	0.009	143.36	1.50	−0.010	0.941	0.336	5.09	1
T5940019	1994-Mar-14	49426.0958	0.9916	1.849	1200.0	162.30	138.27	15.976	0.015	16.89	1.56	0.005	1.330	0.334	5.13	1
T5990033	1994-Mar-22	49433.9871	0.4707	1.478	1200.0	160.80	137.75	14.738	0.008	55.97	1.55	0.008	0.650	0.332	4.68	1
T5990036	1994-Mar-22	49434.0108	0.4751	1.566	1200.0	161.41	137.02	14.878	0.008	44.39	1.45	−0.004	0.643	0.338	5.05	1
T6000001	1994-Mar-22	49434.0389	0.4804	1.684	1200.0	162.32	137.30	15.149	0.010	26.75	1.54	−0.001	0.640	0.334	5.78	1
T6000004	1994-Mar-22	49434.0662	0.4855	1.811	1200.0	163.78	136.78	14.762	0.007	23.82	1.42	0.006	0.634	0.322	3.90	1
T6000008	1994-Mar-22	49434.0959	0.4911	1.959	1200.0	164.70	136.67	15.048	0.009	23.83	1.52	0.000	0.638	0.345	4.82	1
T6000011	1994-Mar-22	49434.1208	0.4958	2.089	1200.0	164.87	136.63	14.990	0.009	23.02	1.63	−0.007	0.629	0.326	4.47	1
T6000014	1994-Mar-22	49434.1444	0.5002	2.208	1200.0	165.68	137.84	15.230	0.011	18.53	1.79	0.022	0.641	0.320	4.38	1
T6000017	1994-Mar-22	49434.1718	0.5053	2.335	1200.0	165.55	137.30	15.465	0.011	19.50	1.52	−0.011	0.615	0.336	5.46	1
T6000020	1994-Mar-22	49434.2001	0.5106	2.441	1200.0	164.99	137.34	15.631	0.012	17.04	1.56	−0.001	0.638	0.337	5.28	1
T6000023	1994-Mar-22	49434.2252	0.5153	2.502	1200.0	164.85	137.86	15.594	0.013	43.26	1.55	0.002	0.621	0.316	5.39	1
T4760010	1994-Jun-08	49511.8529	0.0652	1.807	1200.0	163.01	137.80	14.426	0.008	70.72	1.72	0.022	0.615	0.332	3.26	1

Table A.1 cont.: HV 982 differential photometry – u.

Frame	Date	HJD −2400000.0	Orbital Phase	X	T	Row	Col	$m_{\rm raw}$	$\sigma_{m_{\rm raw}}$	sky	CHI	Sharp	$V-C$	$C-C$	Seeing (FWHM)	ILCA
T4760013	1994-Jun-08	49511.8774	0.0698	1.929	1200.0	163.77	137.86	14.620	0.008	38.21	1.64	0.037	0.636	0.330	3.42	1
T4760027	1994-Jun-08	49512.0855	0.1088	2.464	1200.0	168.46	144.06	15.223	0.009	17.06	1.36	0.008	0.643	0.319	4.46	1
T4760033	1994-Jun-08	49512.1353	0.1182	2.274	1200.0	167.10	144.67	15.146	0.009	17.25	1.49	0.001	0.629	0.332	4.66	1
T4770004	1994-Jun-08	49512.1891	0.1283	2.003	1200.0	164.07	145.79	15.331	0.010	18.09	1.46	0.007	0.623	0.319	5.76	1
T4770013	1994-Jun-08	49512.2726	0.1439	1.607	1200.0	158.80	146.19	14.581	0.007	18.47	1.49	0.010	0.633	0.332	4.18	1
T4770025	1994-Jun-14	49517.8628	0.1917	1.938	1200.0	164.59	136.99	14.997	0.008	22.19	1.34	0.023	0.614	0.314	3.57	1
T4790010	1994-Jul-29	49562.9026	0.6336	2.527	1200.0	167.52	139.85	15.123	0.007	16.20	1.18	−0.004	0.636	0.331	3.70	1
T4790016	1994-Jul-29	49562.9652	0.6453	2.404	1200.0	166.78	140.80	14.787	0.008	12.76	1.48	0.067	0.615	0.332	3.12	1
T4790022	1994-Jul-29	49563.1621	0.6822	1.496	1200.0	161.28	145.04	14.188	0.006	50.36	1.68	0.061	0.613	0.336	2.89	1
T4790035	1994-Jul-30	49563.9357	0.8272	2.484	1200.0	165.87	139.62	15.178	0.009	10.56	1.53	0.008	0.657	0.324	4.20	1
T6400004	1994-Jul-30	49564.1622	0.8697	1.486	1200.0	160.51	144.08	14.274	0.008	29.49	2.13	0.047	0.628	0.338	3.23	1
T6400007	1994-Jul-30	49564.1856	0.8741	1.409	1200.0	159.38	143.98	14.193	0.008	30.43	1.94	0.031	0.620	0.331	3.29	1
T6400010	1994-Jul-30	49564.2088	0.8784	1.342	1200.0	158.74	144.50	14.103	0.006	29.97	1.67	0.056	0.616	0.330	3.05	1
T6380004	1994-Aug-26	49591.0637	0.9119	1.579	1200.0	162.35	145.49	15.271	0.010	71.11	1.34	0.011	0.638	0.332	3.93	1
T4880017	1994-Sep-02	49598.0207	0.2158	1.680	1200.0	162.43	145.47	15.042	0.007	14.25	1.24	−0.006	0.615	0.341	5.84	1
T4880021	1994-Sep-02	49598.0592	0.2231	1.523	1200.0	160.63	145.46	14.960	0.007	13.95	1.28	−0.002	0.603	0.329	5.93	1
T4880025	1994-Sep-02	49598.0983	0.2304	1.392	1200.0	158.61	145.60	14.821	0.007	16.57	1.40	−0.003	0.614	0.340	5.80	1
T4880029	1994-Sep-02	49598.1378	0.2378	1.287	1200.0	157.19	145.31	14.736	0.006	13.92	1.28	0.003	0.621	0.339	5.95	1
T4880033	1994-Sep-02	49598.1792	0.2456	1.205	1200.0	161.60	142.53	14.608	0.008	14.38	1.65	0.000	0.600	0.337	5.70	1
T4880037	1994-Sep-02	49598.2217	0.2535	1.148	1200.0	160.80	143.16	14.484	0.006	15.20	1.35	0.000	0.602	0.341	5.47	1
T5610004	1994-Sep-03	49598.8756	0.3761	2.371	1200.0	164.54	144.19	15.451	0.010	18.63	1.27	−0.005	0.733	0.331	4.84	1
T5610024	1994-Sep-03	49599.2118	0.4391	1.156	1200.0	159.73	143.83	14.810	0.007	20.25	1.27	−0.007	0.993	0.329	4.59	1
T6460004	1994-Sep-04	49600.2188	0.6279	1.145	1200.0	158.84	143.75	13.891	0.006	19.34	1.79	0.041	0.635	0.327	2.90	1
T5690006	1994-Oct-02	49628.1860	0.8698	1.113	1200.0	159.14	141.77	14.572	0.008	17.60	1.67	0.001	0.624	0.340	5.52	1
T6080008	1994-Dec-30	49717.0096	0.5182	1.111	1200.0	161.23	142.12	15.247	0.009	19.86	1.40	0.006	0.657	0.348	8.35	1
T6080014	1994-Dec-30	49717.0700	0.5295	1.157	1200.0	162.69	141.43	15.650	0.011	19.85	1.32	0.000	0.635	0.332	7.98	1

Table A.2: HV 982 differential photometry – v.

Frame	Date	HJD −2400000.0	Orbital Phase	X	T	Row	Col	$m_{\rm raw}$	$\sigma_{m_{\rm raw}}$	sky	CHI	Sharp	$V-C$	$C-C$	Seeing (FWHM)	ILCA
T3990009	1993-Jun-29	49167.9331	0.6037	2.451	1200.0	162.80	141.40	14.758	0.009	265.05	1.28	0.047	1.106	−0.313	2.76	1
T3990016	1993-Jun-29	49168.0533	0.6262	2.378	1200.0	166.32	139.43	14.861	0.009	209.37	1.31	0.013	1.097	−0.306	3.39	1
T3990017	1993-Jun-29	49168.0697	0.6293	2.310	1200.0	164.07	142.54	14.907	0.009	188.83	1.30	0.016	1.112	−0.315	3.60	1
T3990018	1993-Jun-29	49168.0847	0.6321	2.240	1200.0	162.88	143.10	14.870	0.007	169.48	1.10	0.003	1.111	−0.283	3.69	1
T4090004	1993-Jul-02	49170.8757	0.1552	2.256	1200.0	161.86	138.29	14.605	0.009	601.86	1.23	0.012	1.095	−0.297	2.55	1
T4100035	1993-Jul-04	49172.9969	0.5528	2.502	1200.0	161.54	138.13	15.321	0.018	857.84	1.17	0.000	1.090	−0.286	4.89	1

Table A.2 cont.: HV 982 differential photometry – v.

Frame	Date	HJD −2400000.0	Orbital Phase	X	T	Row	Col	$m_{\rm raw}$	$\sigma_{m_{\rm raw}}$	sky	CHI	Sharp	$V-C$	$C-C$	Seeing (FWHM)	ILCA
T4100036	1993-Jul-04	49173.0131	0.5558	2.466	1200.0	160.36	138.21	15.405	0.022	853.00	1.32	0.014	1.091	−0.264	5.27	1
T4100037	1993-Jul-04	49173.0287	0.5588	2.418	1200.0	161.43	137.86	15.527	0.020	844.80	1.06	−0.004	1.106	−0.273	6.01	1
T4100038	1993-Jul-04	49173.0453	0.5618	2.356	1200.0	161.09	137.76	15.652	0.026	840.49	1.19	−0.024	1.100	−0.271	5.65	1
T4240030	1993-Jul-24	49193.1269	0.3258	1.690	1200.0	156.23	142.02	14.608	0.007	22.39	1.50	0.057	1.108	−0.307	3.53	1
T4250004	1993-Jul-24	49193.2084	0.3411	1.387	1200.0	159.04	142.42	14.444	0.006	22.47	1.49	0.039	1.105	−0.296	3.22	1
T4270011	1993-Jul-27	49196.0892	0.8810	1.829	1200.0	159.02	141.70	14.696	0.009	53.88	1.77	0.050	1.130	−0.304	3.59	1
T4270029	1993-Jul-27	49196.2214	0.9058	1.328	1200.0	153.55	141.45	14.664	0.006	23.14	1.33	0.031	1.130	−0.310	2.94	1
T0810010	1993-Sep-07	49237.9088	0.7193	2.165	1200.0	161.02	139.53	14.587	0.008	24.14	1.63	0.034	1.120	−0.303	2.90	1
T0810014	1993-Sep-07	49237.9713	0.7311	1.845	1200.0	155.16	140.53	14.561	0.007	20.22	1.54	0.033	1.132	−0.309	3.14	1
T0810019	1993-Sep-07	49238.0347	0.7429	1.562	1200.0	158.91	140.04	14.366	0.007	31.90	1.68	0.011	1.118	−0.305	2.95	1
T4440032	1993-Sep-16	49246.8924	0.4032	2.123	1200.0	159.75	140.01	15.409	0.014	27.45	1.92	0.091	1.585	−0.296	3.16	1
T4460002	1993-Sep-16	49246.9584	0.4155	1.788	1200.0	157.14	140.77	15.609	0.010	23.43	1.25	0.024	1.758	−0.296	3.94	1
T4460008	1993-Sep-16	49247.0272	0.4284	1.498	1200.0	158.52	142.28	15.255	0.010	22.34	1.56	0.034	1.619	−0.296	3.93	1
T4460014	1993-Sep-16	49247.1141	0.4447	1.254	1200.0	158.38	140.83	14.741	0.008	22.64	1.50	0.040	1.379	−0.310	3.46	1
T4460020	1993-Sep-16	49247.1920	0.4593	1.139	1200.0	158.42	140.76	14.364	0.007	21.81	1.65	0.037	1.223	−0.305	2.81	1
S1880017	1993-Nov-22	49313.9259	0.9674	1.264	1200.0	159.34	141.24	15.158	0.012	75.05	1.75	0.065	1.524	−0.282	3.36	1
S1880022	1993-Nov-22	49314.0035	0.9819	1.144	1200.0	159.68	139.26	15.440	0.012	54.09	1.49	0.044	1.730	−0.283	3.57	1
S1880027	1993-Nov-22	49314.1283	0.0053	1.118	1200.0	160.21	139.34	15.253	0.008	22.40	1.27	0.002	1.608	−0.299	4.62	1
T5780017	1994-Feb-23	49406.9119	0.3959	1.149	1200.0	159.67	139.34	14.999	0.010	161.78	1.39	0.002	1.472	−0.291	4.69	1
T5940009	1994-Mar-14	49425.9284	0.9602	1.255	1200.0	158.23	141.12	16.201	0.016	19.49	1.42	−0.017	1.497	−0.313	4.88	1
T5940012	1994-Mar-14	49425.9715	0.9683	1.360	1200.0	159.93	140.16	15.398	0.009	21.89	1.28	−0.012	1.572	−0.305	5.47	1
T5940020	1994-Mar-14	49426.1124	0.9947	1.932	1200.0	158.98	138.57	16.278	0.018	22.30	1.51	−0.034	1.774	−0.308	4.91	1
T5100008	1994-Apr-10	49452.9737	0.0294	1.625	1200.0	158.87	136.60	14.752	0.008	27.36	1.49	0.030	1.303	−0.293	3.67	1
T5100011	1994-Apr-10	49453.0151	0.0372	1.814	1200.0	159.61	136.35	14.803	0.008	27.82	1.63	0.017	1.241	−0.298	3.90	1
T5100014	1994-Apr-10	49453.0553	0.0447	2.017	1200.0	160.68	136.08	14.949	0.009	27.33	1.52	0.012	1.186	−0.295	3.99	1
T4760016	1994-Jun-08	49511.9012	0.0743	2.052	1200.0	160.51	137.51	15.545	0.009	36.40	1.17	0.015	1.131	−0.304	3.63	1
T4760030	1994-Jun-08	49512.1113	0.1137	2.378	1200.0	163.37	142.57	15.445	0.012	25.28	1.57	0.007	1.123	−0.300	5.57	1
T4770010	1994-Jun-08	49512.2322	0.1363	1.787	1200.0	158.66	143.00	15.297	0.008	23.16	1.13	−0.007	1.151	−0.307	5.55	1
T4790011	1994-Jul-29	49562.9176	0.6364	2.518	1200.0	163.34	138.63	14.875	0.007	24.27	1.33	0.033	1.125	−0.305	3.35	1
T4790017	1994-Jul-29	49562.9798	0.6481	2.347	1200.0	162.55	138.66	14.719	0.007	22.20	1.36	0.018	1.101	−0.292	3.05	1
T4790023	1994-Jul-29	49563.1768	0.6850	1.445	1200.0	158.54	141.44	14.351	0.007	60.48	1.70	0.064	1.102	−0.294	2.92	1
T4790036	1994-Jul-30	49563.9504	0.8300	2.445	1200.0	160.56	137.59	14.907	0.010	19.45	1.86	0.037	1.109	−0.293	3.66	1
T6380005	1994-Aug-26	49591.0800	0.9149	1.517	1200.0	159.61	142.54	15.432	0.011	119.69	1.19	0.028	1.118	−0.299	3.63	1
T4880018	1994-Sep-02	49598.0354	0.2186	1.617	1200.0	158.82	142.85	14.959	0.007	20.19	1.27	0.004	1.087	−0.292	5.35	1
T4880030	1994-Sep-02	49598.1526	0.2406	1.255	1200.0	154.93	142.34	14.913	0.006	20.70	1.13	−0.003	1.091	−0.293	5.62	1
T6420002	1994-Sep-02	49598.2477	0.2584	1.125	1200.0	159.22	141.23	14.669	0.007	109.10	1.23	0.000	1.075	−0.278	5.10	1
T5610006	1994-Sep-03	49598.8962	0.3799	2.282	1200.0	159.88	141.98	15.151	0.023	26.32	3.51	0.145	1.241	−0.309	3.73	1
T5610025	1994-Sep-03	49599.2271	0.4420	1.140	1200.0	158.24	141.96	15.015	0.009	28.08	1.59	0.020	1.422	−0.296	4.28	1
T6460005	1994-Sep-04	49600.2334	0.6306	1.132	1200.0	157.93	141.71	14.054	0.007	29.31	2.03	0.077	1.112	−0.301	2.36	1

Table A.2 cont.: HV 982 differential photometry – v.

Frame	Date	HJD −2400000.0	Orbital Phase	X	T	Row	Col	$m_{\rm raw}$	$\sigma_{m_{\rm raw}}$	sky	CHI	Sharp	$V-C$	$C-C$	Seeing (FWHM)	ILCA
T5690005	1994-Oct-02	49628.1713	0.8670	1.121	1200.0	157.92	139.56	14.805	0.009	23.34	1.69	0.007	1.096	−0.287	5.14	1
T6080010	1994-Dec-30	49717.0268	0.5214	1.119	1200.0	159.97	139.55	15.400	0.009	29.88	1.17	0.009	1.097	−0.284	7.33	1
T6080015	1994-Dec-30	49717.0865	0.5326	1.178	1200.0	161.68	140.12	15.610	0.012	28.98	1.38	−0.021	1.123	−0.281	7.88	1

Table A.3: HV 982 differential photometry – b.

Frame	Date	HJD −2400000.0	Orbital Phase	X	T	Row	Col	$m_{\rm raw}$	$\sigma_{m_{\rm raw}}$	sky	CHI	Sharp	$V-C$	$C-C$	Seeing (FWHM)	ILCA
T3990010	1993-Jun-29	49167.9539	0.6076	2.501	1200.0	163.42	140.97	14.132	0.006	532.01	1.23	0.035	1.156	−0.341	2.85	1
T3990019	1993-Jun-29	49168.1007	0.6351	2.161	1200.0	162.80	141.03	14.199	0.006	298.65	1.29	0.036	1.167	−0.350	3.37	1
T3990020	1993-Jun-29	49168.1164	0.6380	2.080	1200.0	161.87	141.90	14.146	0.008	249.46	1.71	0.055	1.185	−0.357	3.16	1
T3990021	1993-Jun-29	49168.1314	0.6408	2.003	1200.0	160.62	142.77	14.140	0.006	195.43	1.33	0.040	1.168	−0.350	3.18	1
T4090005	1993-Jul-02	49170.8905	0.1580	2.323	1200.0	162.72	140.68	14.040	0.008	1187.3	1.36	0.031	1.161	−0.339	2.40	1
T4070030	1993-Jul-04	49173.0606	0.5647	2.289	1200.0	161.30	138.96	14.846	0.017	1626.3	1.26	−0.001	1.168	−0.332	5.19	1
T4070031	1993-Jul-04	49173.0817	0.5687	2.188	1200.0	160.60	138.65	14.874	0.016	1440.1	1.15	−0.006	1.183	−0.324	5.99	1
T4070032	1993-Jul-04	49173.0973	0.5716	2.108	1200.0	159.80	137.43	15.108	0.019	1375.9	1.14	−0.008	1.201	−0.309	6.36	1
T4070033	1993-Jul-04	49173.1125	0.5745	2.030	1200.0	160.14	138.70	14.939	0.015	1314.8	1.10	−0.001	1.165	−0.350	6.04	1
T4270016	1993-Jul-27	49196.1254	0.8878	1.661	1200.0	159.29	141.78	14.035	0.007	51.68	1.83	0.051	1.183	−0.350	3.06	1
T4270034	1993-Jul-27	49196.2548	0.9121	1.251	1200.0	158.31	142.18	13.788	0.007	40.42	2.25	0.094	1.174	−0.353	2.39	1
T0810015	1993-Sep-07	49237.9881	0.7342	1.764	1200.0	161.53	140.33	13.922	0.007	42.64	1.95	0.054	1.192	−0.360	2.76	1
T0810020	1993-Sep-07	49238.0505	0.7459	1.502	1200.0	161.15	142.63	13.862	0.006	89.34	1.92	0.040	1.196	−0.358	2.68	1
T4440033	1993-Sep-16	49246.9074	0.4060	2.045	1200.0	160.20	140.81	14.879	0.011	53.08	1.94	0.104	1.692	−0.354	3.23	1
T4460003	1993-Sep-16	49246.9752	0.4187	1.709	1200.0	162.59	142.61	15.090	0.010	46.70	1.53	0.031	1.827	−0.344	4.09	1
T4460009	1993-Sep-16	49247.0548	0.4336	1.406	1200.0	162.65	141.73	14.495	0.009	46.10	1.88	0.064	1.612	−0.353	3.28	1
T4460015	1993-Sep-16	49247.1297	0.4476	1.223	1200.0	160.54	141.98	14.220	0.007	45.12	1.72	0.054	1.412	−0.349	3.33	1
T4460021	1993-Sep-16	49247.2068	0.4621	1.126	1200.0	160.89	142.14	13.894	0.007	45.96	2.09	0.080	1.266	−0.350	2.74	1
S1880018	1993-Nov-22	49313.9440	0.9708	1.228	1200.0	160.65	140.88	14.581	0.009	129.35	1.74	0.055	1.628	−0.335	3.50	1
S1880023	1993-Nov-22	49314.0209	0.9852	1.128	1200.0	159.24	142.00	14.693	0.011	84.42	2.10	0.093	1.823	−0.342	3.41	1
S1880028	1993-Nov-22	49314.1500	0.0094	1.133	1200.0	160.87	140.73	14.740	0.008	263.55	1.22	0.019	1.601	−0.330	4.45	1
T5780018	1994-Feb-23	49406.9295	0.3992	1.170	1200.0	161.64	142.06	14.759	0.010	296.30	1.39	0.003	1.576	−0.354	5.03	1
T5940010	1994-Mar-14	49425.9441	0.9632	1.290	1200.0	160.75	142.99	14.903	0.007	43.54	1.26	0.008	1.560	−0.357	5.14	1
T5940014	1994-Mar-14	49425.9903	0.9718	1.416	1200.0	162.40	142.43	15.935	0.015	43.22	1.46	0.000	1.700	−0.349	5.64	1
T5940021	1994-Mar-14	49426.1281	0.9977	2.014	1200.0	161.68	140.54	15.896	0.014	45.47	1.38	−0.003	1.781	−0.344	5.37	1
T5100009	1994-Apr-10	49452.9901	0.0325	1.697	1200.0	161.11	139.09	14.633	0.006	48.26	1.28	0.018	1.347	−0.354	3.74	1
T5100012	1994-Apr-10	49453.0303	0.0400	1.889	1200.0	162.21	138.76	14.238	0.007	56.34	1.70	0.034	1.285	−0.353	3.81	1
T5100015	1994-Apr-10	49453.0704	0.0475	2.096	1200.0	162.53	138.85	14.590	0.007	57.14	1.32	0.016	1.236	−0.353	4.25	1
T4760021	1994-Jun-08	49512.0148	0.0956	2.506	1200.0	159.50	139.37	14.587	0.006	51.37	1.27	0.012	1.192	−0.359	4.04	1

Table A.3 cont.: HV 982 differential photometry – b.

Frame	Date	HJD −2400000.0	Orbital Phase	X	T	Row	Col	$m_{\rm raw}$	$\sigma_{m_{\rm raw}}$	sky	CHI	Sharp	$V-C$	$C-C$	Seeing (FWHM)	ILCA
T4770001	1994-Jun-08	49512.1628	0.1233	2.139	1200.0	162.81	143.89	14.476	0.006	52.05	1.19	−0.004	1.181	−0.349	4.57	1
T4770011	1994-Jun-08	49512.2471	0.1391	1.717	1200.0	159.57	143.49	14.672	0.007	46.97	1.42	0.006	1.205	−0.367	4.95	1
T4790012	1994-Jul-29	49562.9324	0.6392	2.497	1200.0	163.88	139.51	14.084	0.005	42.74	1.45	0.042	1.188	−0.353	2.95	1
T4790018	1994-Jul-29	49562.9943	0.6508	2.283	1200.0	163.08	139.78	14.015	0.008	40.61	2.14	0.094	1.187	−0.351	2.72	1
T4790024	1994-Jul-29	49563.1915	0.6877	1.399	1200.0	159.72	142.73	13.834	0.007	113.33	1.94	0.061	1.163	−0.341	2.92	1
T4790037	1994-Jul-30	49563.9650	0.8327	2.395	1200.0	161.43	138.88	14.312	0.006	38.87	1.56	0.023	1.179	−0.338	3.78	1
T6380006	1994-Aug-26	49591.0949	0.9177	1.464	1200.0	161.41	142.43	15.802	0.020	314.17	1.28	0.025	1.177	−0.349	3.71	1
T4880022	1994-Sep-02	49598.0743	0.2259	1.469	1200.0	159.88	143.23	14.484	0.006	39.31	1.30	0.008	1.153	−0.339	5.27	1
T4880034	1994-Sep-02	49598.1940	0.2483	1.182	1200.0	162.41	141.74	14.316	0.005	38.48	1.15	−0.005	1.151	−0.335	5.05	1
T6420003	1994-Sep-02	49598.2625	0.2612	1.116	1200.0	162.28	142.22	14.301	0.024	5423.5	1.62	−0.024	1.098	−0.321	5.34	1
T5610009	1994-Sep-03	49598.9197	0.3843	2.168	1200.0	160.97	142.12	15.223	0.008	33.75	1.16	0.010	1.353	−0.356	4.32	1
T5610026	1994-Sep-03	49599.2419	0.4447	1.127	1200.0	161.38	143.67	14.720	0.007	92.61	1.27	0.008	1.444	−0.351	4.61	1
T6460006	1994-Sep-04	49600.2479	0.6333	1.121	1200.0	160.61	143.32	13.608	0.006	316.90	1.76	0.047	1.163	−0.341	2.28	1
T5690004	1994-Oct-02	49628.1567	0.8643	1.132	1200.0	160.26	140.70	14.292	0.005	40.36	1.18	−0.001	1.165	−0.340	4.84	1
T6080011	1994-Dec-30	49717.0416	0.5242	1.129	1200.0	164.32	141.20	15.085	0.009	47.94	1.26	−0.010	1.190	−0.321	7.92	1
T6080016	1994-Dec-30	49717.1019	0.5355	1.202	1200.0	163.14	142.88	15.106	0.009	46.63	1.31	0.000	1.211	−0.327	8.41	1

Table A.4: HV 982 differential photometry – y.

Frame	Date	HJD −2400000.0	Orbital Phase	X	T	Row	Col	$m_{\rm raw}$	$\sigma_{m_{\rm raw}}$	sky	CHI	Sharp	$V-C$	$C-C$	Seeing (FWHM)	ILCA
T3990007	1993-Jun-29	49167.8950	0.5965	2.303	700.0	163.18	142.65	13.819	0.007	645.12	1.72	0.065	0.197	0.419	2.57	1
T3990012	1993-Jun-29	49167.9717	0.6109	2.523	700.0	163.10	144.09	13.862	0.008	689.69	1.66	0.069	0.184	0.426	2.76	1
T3990025	1993-Jun-29	49168.1514	0.6446	1.905	700.0	160.68	144.25	13.825	0.007	174.30	2.07	0.070	0.190	0.412	2.92	1
T3990026	1993-Jun-29	49168.1610	0.6464	1.856	700.0	160.91	143.91	13.763	0.007	127.26	2.20	0.075	0.184	0.427	3.05	1
T4090006	1993-Jul-02	49170.9023	0.1602	2.369	700.0	162.52	144.13	13.798	0.010	1529.5	1.85	0.084	0.196	0.411	2.23	1
T4270023	1993-Jul-27	49196.1769	0.8975	1.465	700.0	158.61	144.58	13.722	0.012	90.29	3.81	0.183	0.197	0.409	2.80	1
T4270025	1993-Jul-27	49196.1894	0.8998	1.423	700.0	158.23	144.33	13.686	0.007	91.58	2.39	0.098	0.207	0.405	2.63	1
T4270027	1993-Jul-27	49196.2053	0.9028	1.375	700.0	158.01	144.48	13.658	0.010	91.75	3.34	0.138	0.188	0.413	2.51	1
T0810011	1993-Sep-07	49237.9368	0.7246	2.026	700.0	164.43	143.58	13.724	0.008	80.78	2.69	0.108	0.187	0.417	2.57	1
T0810016	1993-Sep-07	49238.0011	0.7366	1.708	700.0	163.88	145.93	13.649	0.008	77.21	2.63	0.105	0.190	0.416	2.57	1
T0810021	1993-Sep-07	49238.0624	0.7481	1.464	700.0	161.90	145.04	13.588	0.008	155.19	2.71	0.110	0.191	0.425	2.52	1
T4440034	1993-Sep-16	49246.9192	0.4082	1.989	700.0	160.59	143.63	14.642	0.011	114.66	2.10	0.129	0.751	0.414	3.18	1
T4460004	1993-Sep-16	49246.9873	0.4210	1.660	700.0	163.48	145.79	14.785	0.010	96.18	1.73	0.021	0.835	0.410	4.26	1
T4460010	1993-Sep-16	49247.0669	0.4359	1.372	700.0	163.90	143.90	14.171	0.011	100.15	2.85	0.113	0.594	0.418	3.18	1
T4460016	1993-Sep-16	49247.1420	0.4499	1.204	700.0	161.49	144.49	13.947	0.008	94.53	2.13	0.081	0.403	0.412	3.27	1
T4460022	1993-Sep-16	49247.2195	0.4645	1.118	700.0	162.29	144.94	13.704	0.009	97.25	2.88	0.130	0.261	0.412	2.81	1

Table A.4 cont.: HV 982 differential photometry – y.

Frame	Date	HJD −2400000.0	Orbital Phase	X	T	Row	Col	$m_{\rm raw}$	$\sigma_{m_{\rm raw}}$	sky	CHI	Sharp	$V-C$	$C-C$	Seeing (FWHM)	ILCA
S1880019	1993-Nov-22	49313.9571	0.9732	1.206	700.0	164.11	143.63	14.550	0.008	215.48	1.44	0.025	0.710	0.404	3.86	1
S1880024	1993-Nov-22	49314.0331	0.9875	1.120	700.0	164.63	145.96	14.591	0.010	128.43	1.87	0.056	0.880	0.408	3.78	1
S1880030	1993-Nov-22	49314.1642	0.0121	1.146	700.0	162.85	143.83	14.469	0.010	1196.0	1.07	0.008	0.595	0.400	4.63	1
T5780019	1994-Feb-23	49406.9414	0.4015	1.185	700.0	163.84	145.39	14.790	0.010	422.80	1.26	0.013	0.626	0.407	5.16	1
T5940011	1994-Mar-14	49425.9577	0.9657	1.321	700.0	163.00	145.73	14.466	0.007	108.80	1.38	0.008	0.593	0.420	4.84	1
T5940015	1994-Mar-14	49426.0513	0.9833	1.638	700.0	160.41	147.74	16.258	0.019	105.89	1.19	0.011	0.835	0.424	6.10	1
T5940016	1994-Mar-14	49426.0655	0.9859	1.701	700.0	160.62	147.82	15.199	0.009	112.39	1.08	0.000	0.843	0.410	5.80	1
T5940022	1994-Mar-14	49426.1405	1.0000	2.073	700.0	161.36	144.36	15.233	0.011	115.25	1.41	−0.009	0.754	0.429	5.49	1
T5100010	1994-Apr-10	49453.0029	0.0349	1.751	700.0	162.42	142.96	14.004	0.007	174.85	1.71	0.028	0.359	0.415	3.81	1
T5100013	1994-Apr-10	49453.0425	0.0423	1.946	700.0	163.50	142.61	14.011	0.007	196.72	1.81	0.029	0.289	0.423	3.87	1
T5100016	1994-Apr-10	49453.0824	0.0498	2.152	700.0	162.96	141.99	14.317	0.006	210.73	1.16	0.006	0.259	0.420	4.53	1
T4760024	1994-Jun-08	49512.0625	0.1045	2.513	700.0	159.16	141.46	14.502	0.007	95.72	1.45	0.016	0.204	0.425	4.25	1
T4770007	1994-Jun-08	49512.2112	0.1324	1.895	700.0	162.32	146.39	14.621	0.007	95.72	1.31	0.001	0.206	0.419	5.37	1
T4770012	1994-Jun-08	49512.2589	0.1413	1.669	700.0	160.09	146.21	14.008	0.006	89.78	1.65	0.033	0.208	0.406	4.07	1
T4790013	1994-Jul-29	49562.9449	0.6415	2.470	700.0	163.57	142.62	13.838	0.007	80.10	2.05	0.094	0.192	0.410	3.08	1
T4790019	1994-Jul-29	49563.0061	0.6530	2.232	700.0	163.18	142.39	13.769	0.008	80.90	2.61	0.110	0.184	0.426	2.55	1
T4790025	1994-Jul-29	49563.2036	0.6900	1.366	700.0	160.93	145.34	13.602	0.007	160.32	2.37	0.089	0.193	0.411	2.77	1
T6400001	1994-Jul-30	49563.9767	0.8349	2.353	700.0	160.43	141.45	14.078	0.014	74.47	3.66	0.022	0.215	0.411	4.04	1
T6380007	1994-Aug-26	49591.1405	0.9263	1.330	700.0	162.17	145.08	15.665	0.020	695.88	1.06	−0.017	0.260	0.444	3.02	1
T4880026	1994-Sep-02	49598.1101	0.2326	1.360	700.0	159.90	145.79	14.196	0.005	81.07	1.13	−0.002	0.198	0.417	5.28	1
T6420001	1994-Sep-02	49598.2337	0.2558	1.137	700.0	163.88	146.05	14.121	0.007	80.82	1.72	0.006	0.206	0.410	5.26	1
T5610011	1994-Sep-03	49598.9392	0.3880	2.073	700.0	161.04	146.04	15.058	0.008	74.51	1.25	0.003	0.414	0.424	5.00	1
T5610027	1994-Sep-03	49599.2538	0.4470	1.120	700.0	162.69	146.21	14.801	0.009	346.90	1.13	−0.002	0.426	0.412	5.15	1
T6460003	1994-Sep-04	49600.2072	0.6257	1.159	700.0	161.53	145.34	13.478	0.010	78.64	3.32	0.139	0.190	0.418	2.24	1
T5640035	1994-Oct-02	49628.0925	0.8523	1.215	700.0	162.99	143.33	14.087	0.006	284.22	1.34	0.000	0.221	0.406	4.82	1
T5690003	1994-Oct-02	49628.1447	0.8621	1.143	700.0	162.03	143.57	14.081	0.005	71.28	1.43	0.006	0.216	0.399	4.98	1
T6080012	1994-Dec-30	49717.0545	0.5266	1.140	700.0	164.20	145.45	15.136	0.009	86.82	1.22	0.004	0.201	0.444	8.02	1
T6080017	1994-Dec-30	49717.1144	0.5378	1.221	700.0	165.86	146.10	14.827	0.007	90.45	1.26	0.001	0.193	0.448	8.39	1

Table A.5: HV 982 differential photometry – V.

Frame	Date	HJD −2400000.0	Orbital Phase	X	T	Row	Col	$m_{\rm raw}$	$\sigma_{m_{\rm raw}}$	sky	CHI	Sharp	$V-C$	$C-C$	Seeing (FWHM)	ILCA
T0360006	1992-Nov-27	48953.9794	0.5019	1.155	400.0	164.65	142.00	13.183	0.003	142.94	1.22	0.004	0.230	0.428	4.80	1
T0360008	1992-Nov-27	48953.9976	0.5053	1.136	400.0	165.12	141.61	13.267	0.003	138.19	1.17	0.003	0.235	0.433	4.71	1
T0360009	1992-Nov-27	48954.0107	0.5078	1.125	400.0	162.85	141.66	13.335	0.003	132.16	1.26	0.003	0.239	0.431	5.11	1
T0360010	1992-Nov-27	48954.0300	0.5114	1.114	400.0	163.95	142.35	13.373	0.004	126.50	1.43	0.001	0.228	0.425	5.33	1

Table A.5 cont.: HV 982 differential photometry – V.

Frame	Date	HJD −2400000.0	Orbital Phase	X	T	Row	Col	$m_{\rm raw}$	$\sigma_{m_{\rm raw}}$	sky	CHI	Sharp	$V-C$	$C-C$	Seeing (FWHM)	ILCA
T0360011	1992-Nov-27	48954.0552	0.5161	1.105	400.0	164.27	141.96	13.442	0.003	137.34	1.09	−0.004	0.229	0.429	5.83	1
T0360012	1992-Nov-27	48954.0763	0.5201	1.104	400.0	165.88	140.74	12.785	0.003	138.06	1.31	0.007	0.221	0.422	3.21	1
T0360013	1992-Nov-27	48954.1099	0.5264	1.114	400.0	164.42	140.68	13.090	0.003	151.41	1.28	0.007	0.224	0.426	3.97	1
T0360014	1992-Nov-27	48954.1338	0.5308	1.130	400.0	164.95	140.15	13.050	0.003	177.30	1.26	0.002	0.224	0.425	4.00	1
T0360015	1992-Nov-27	48954.1607	0.5359	1.157	400.0	164.69	139.47	12.992	0.004	1866.32	1.11	0.003	0.228	0.427	3.89	1
T0360024	1992-Nov-28	48954.1759	0.5387	1.139	400.0	163.21	139.79	14.015	0.005	126.41	1.22	0.016	0.223	0.430	3.45	1
T0840002	1993-Jan-26	49014.0353	0.7583	1.213	400.0	167.72	140.68	13.242	0.003	129.79	0.98	−0.002	0.225	0.433	4.27	1
T0840003	1993-Jan-26	49014.0490	0.7609	1.239	400.0	162.85	141.81	13.357	0.004	128.27	1.48	−0.005	0.228	0.426	4.68	1
T0840004	1993-Jan-26	49014.0934	0.7692	1.341	400.0	163.54	141.86	13.188	0.003	131.76	1.07	0.003	0.234	0.426	4.22	1
T0840005	1993-Jan-26	49014.1063	0.7716	1.377	400.0	164.53	141.03	13.526	0.004	133.92	1.17	−0.001	0.240	0.421	5.33	1
T0840006	1993-Jan-26	49014.1163	0.7735	1.407	400.0	163.19	142.08	13.356	0.003	138.99	1.16	0.002	0.235	0.430	4.67	1
T0840007	1993-Jan-26	49014.1234	0.7748	1.430	400.0	163.12	143.93	13.428	0.003	143.05	1.14	0.004	0.233	0.433	5.03	1
T0840008	1993-Jan-26	49014.1346	0.7769	1.467	400.0	166.06	141.37	13.255	0.003	142.94	1.21	0.002	0.219	0.425	4.40	1
T0840009	1993-Jan-26	49014.1457	0.7790	1.506	400.0	160.17	142.53	13.338	0.003	148.16	1.21	−0.001	0.220	0.421	4.72	1
T0840010	1993-Jan-26	49014.1645	0.7825	1.578	400.0	161.48	142.90	13.398	0.003	175.54	0.94	0.003	0.221	0.419	4.65	1
T0840011	1993-Jan-26	49014.1709	0.7837	1.604	400.0	161.71	142.16	13.421	0.004	244.62	1.17	0.004	0.216	0.423	4.60	1
T0840018	1993-Jan-27	49014.9526	0.9302	1.120	400.0	167.09	141.63	12.690	0.004	122.55	1.84	0.037	0.277	0.430	2.73	1
T0840019	1993-Jan-27	49014.9668	0.9329	1.130	400.0	164.12	139.68	12.673	0.004	129.74	1.83	0.026	0.301	0.428	2.44	1
T0840020	1993-Jan-27	49015.0041	0.9399	1.170	400.0	163.46	142.07	12.847	0.003	129.05	1.35	0.011	0.347	0.438	2.78	1
T0840021	1993-Jan-27	49015.0368	0.9460	1.221	400.0	163.63	142.60	13.011	0.003	130.64	1.40	0.016	0.400	0.436	3.24	1
T0840022	1993-Jan-27	49015.0641	0.9511	1.276	400.0	164.99	142.55	13.192	0.003	144.23	1.31	0.009	0.447	0.440	3.64	1
T0840023	1993-Jan-27	49015.0892	0.9558	1.337	400.0	162.33	140.62	13.238	0.004	146.92	1.47	0.006	0.504	0.434	3.40	1
T0840024	1993-Jan-27	49015.1127	0.9602	1.405	400.0	162.03	141.41	13.579	0.004	161.34	1.22	0.008	0.549	0.442	4.38	1
T0840025	1993-Jan-27	49015.1344	0.9643	1.476	400.0	162.58	142.23	13.714	0.004	167.31	1.13	0.001	0.606	0.441	4.45	1
T0840026	1993-Jan-27	49015.1538	0.9679	1.547	400.0	164.19	141.88	13.668	0.005	190.24	1.54	−0.003	0.656	0.442	4.06	1
T0840027	1993-Jan-27	49015.1773	0.9723	1.643	400.0	164.79	141.95	13.921	0.005	535.23	1.02	0.001	0.713	0.437	3.90	1
T0840028	1993-Jan-27	49015.1835	0.9735	1.670	400.0	162.49	141.45	13.938	0.006	1330.99	1.01	−0.011	0.744	0.431	4.19	1
T0840029	1993-Jan-27	49015.1894	0.9746	1.696	400.0	162.95	141.57	14.070	0.013	3650.34	1.32	−0.014	0.765	0.447	4.28	1
T3600002	1993-Jan-28	49015.9196	0.1115	1.107	400.0	162.88	141.64	13.533	0.004	133.04	1.49	0.020	0.241	0.438	2.90	1
T3600003	1993-Jan-28	49015.9321	0.1138	1.111	400.0	162.79	142.05	12.902	0.003	131.53	1.52	0.036	0.227	0.436	2.47	1
T3600004	1993-Jan-28	49015.9491	0.1170	1.119	400.0	164.20	141.98	13.837	0.005	124.19	1.49	0.049	0.236	0.450	2.78	0
T3600005	1993-Jan-28	49015.9591	0.1189	1.126	400.0	162.69	142.41	14.124	0.006	123.88	1.49	0.021	0.236	0.444	2.63	1
T3600006	1993-Jan-28	49015.9997	0.1265	1.168	400.0	163.18	142.08	12.628	0.004	125.19	2.11	0.029	0.220	0.442	2.31	1
T3600007	1993-Jan-28	49016.0066	0.1278	1.177	400.0	163.84	142.21	12.717	0.004	126.05	1.91	0.025	0.229	0.434	2.78	1
T3600008	1993-Jan-28	49016.0124	0.1289	1.185	400.0	163.63	141.51	12.775	0.003	127.44	1.63	0.030	0.235	0.433	2.85	1
T3600009	1993-Jan-28	49016.0198	0.1302	1.197	400.0	163.72	141.40	12.808	0.004	128.79	2.07	0.005	0.234	0.440	3.03	1
T3600010	1993-Jan-28	49016.0264	0.1315	1.207	400.0	163.28	140.91	12.859	0.004	129.60	1.76	0.015	0.241	0.440	3.19	1
T3600011	1993-Jan-28	49016.0340	0.1329	1.221	400.0	163.90	141.81	12.924	0.003	133.88	1.14	0.012	0.241	0.442	3.52	1
T3600012	1993-Jan-28	49016.0431	0.1346	1.238	400.0	161.79	141.13	12.567	0.006	130.28	3.06	0.076	0.222	0.431	2.12	1

Table A.5 cont.: HV 982 differential photometry – V.

Frame	Date	HJD −2400000.0	Orbital Phase	X	T	Row	Col	$m_{\rm raw}$	$\sigma_{m_{\rm raw}}$	sky	CHI	Sharp	$V-C$	$C-C$	Seeing (FWHM)	ILCA
T3600013	1993-Jan-28	49016.0488	0.1357	1.249	400.0	162.07	140.67	12.860	0.004	129.65	1.90	0.054	0.229	0.430	2.20	1
T3600014	1993-Jan-28	49016.0721	0.1401	1.301	400.0	162.75	141.09	12.679	0.005	130.58	2.08	0.052	0.223	0.431	2.12	1
T3600015	1993-Jan-28	49016.0838	0.1422	1.330	400.0	162.58	141.27	13.906	0.006	128.41	1.69	0.061	0.230	0.436	2.32	1
T3600016	1993-Jan-28	49016.1188	0.1488	1.433	400.0	162.87	141.33	12.637	0.004	142.43	2.14	0.053	0.221	0.428	2.25	1
T3630001	1993-Jan-28	49016.1460	0.1539	1.528	400.0	163.10	142.06	12.711	0.004	202.38	1.76	0.031	0.224	0.432	2.33	1
T3630002	1993-Jan-28	49016.1541	0.1554	1.559	400.0	163.75	141.87	12.728	0.003	160.93	1.65	0.034	0.226	0.427	2.65	1
T3630003	1993-Jan-28	49016.1601	0.1566	1.583	400.0	163.79	141.54	12.721	0.004	162.52	1.96	0.047	0.222	0.430	2.41	1
T3630004	1993-Jan-28	49016.1662	0.1577	1.607	400.0	162.38	143.01	12.784	0.003	186.89	1.54	0.028	0.228	0.431	2.56	1
T3630005	1993-Jan-28	49016.1725	0.1589	1.634	400.0	163.04	142.34	12.730	0.004	266.53	1.92	0.040	0.223	0.436	2.45	1
T3630006	1993-Jan-28	49016.1789	0.1601	1.661	400.0	163.50	142.77	12.793	0.003	535.12	1.31	0.018	0.224	0.430	2.66	1
T3630007	1993-Jan-28	49016.1845	0.1611	1.686	400.0	162.56	142.18	12.783	0.004	1230.44	1.53	0.011	0.223	0.440	2.71	1
T3640001	1993-Jan-31	49018.9133	0.6726	1.107	400.0	160.88	141.77	13.049	0.003	268.10	1.06	0.009	0.221	0.424	3.85	1
T3640003	1993-Jan-31	49018.9228	0.6744	1.110	400.0	161.53	142.16	12.876	0.003	251.90	1.26	0.021	0.227	0.423	3.30	1
T3640005	1993-Jan-31	49018.9351	0.6767	1.116	400.0	161.71	141.47	13.055	0.003	231.52	1.30	0.007	0.221	0.421	3.59	1
T3640007	1993-Jan-31	49018.9499	0.6795	1.126	400.0	160.74	141.23	13.098	0.003	174.53	1.28	0.009	0.219	0.431	3.18	1
T3640009	1993-Jan-31	49018.9614	0.6816	1.135	400.0	161.90	141.98	13.537	0.005	143.96	1.50	0.023	0.225	0.428	3.12	1
T3640011	1993-Jan-31	49018.9713	0.6835	1.144	400.0	161.86	141.62	13.430	0.004	107.82	1.42	0.019	0.220	0.431	2.92	1
T3640013	1993-Jan-31	49018.9950	0.6879	1.172	400.0	162.44	142.01	13.731	0.004	81.62	1.27	0.023	0.213	0.439	3.33	1
T3640015	1993-Jan-31	49019.0025	0.6893	1.183	400.0	162.74	142.24	13.963	0.005	78.07	1.43	0.023	0.221	0.439	3.27	1
T3640018	1993-Jan-31	49019.0161	0.6919	1.204	400.0	163.31	142.20	14.233	0.006	71.88	1.49	0.014	0.217	0.443	3.45	1
T3640019	1993-Jan-31	49019.0274	0.6940	1.223	400.0	163.56	142.10	14.326	0.005	70.35	1.26	0.001	0.214	0.445	3.60	1
T3640021	1993-Jan-31	49019.0385	0.6960	1.245	400.0	164.10	141.67	14.180	0.005	81.80	1.31	0.007	0.208	0.450	3.64	0
T3640023	1993-Jan-31	49019.0487	0.6980	1.266	400.0	164.10	141.95	14.382	0.006	78.65	1.20	0.023	0.215	0.441	3.46	1
T3640025	1993-Jan-31	49019.0874	0.7052	1.362	400.0	162.74	141.14	12.900	0.003	157.69	1.20	0.010	0.204	0.423	3.41	1
T3640027	1993-Jan-31	49019.0938	0.7064	1.381	400.0	161.96	141.75	13.029	0.003	158.89	1.25	−0.007	0.211	0.424	3.89	1
T3640029	1993-Jan-31	49019.1014	0.7078	1.403	400.0	162.95	141.54	12.931	0.003	156.94	1.57	0.008	0.215	0.422	3.30	1
T3640031	1993-Jan-31	49019.1071	0.7089	1.421	400.0	163.02	141.05	13.574	0.004	159.59	1.30	0.025	0.204	0.429	3.47	1
T3640033	1993-Jan-31	49019.1159	0.7106	1.450	400.0	163.27	141.90	14.422	0.006	162.71	1.25	0.041	0.230	0.406	3.35	1
T3640035	1993-Jan-31	49019.1233	0.7119	1.475	400.0	162.92	141.90	13.799	0.005	170.73	1.36	0.008	0.219	0.423	3.71	1
T3730002	1993-Feb-19	49037.9413	0.2390	1.170	400.0	175.43	135.93	12.938	0.003	223.81	1.34	0.005	0.197	0.430	3.67	1
T3730003	1993-Feb-19	49037.9509	0.2408	1.183	400.0	163.33	141.59	12.799	0.003	187.00	1.45	0.012	0.205	0.423	3.13	1
T3730004	1993-Feb-19	49037.9807	0.2464	1.233	400.0	162.42	141.37	12.892	0.003	187.11	1.18	0.012	0.206	0.424	3.25	1
T3730005	1993-Feb-19	49038.0182	0.2535	1.316	400.0	163.12	141.59	12.965	0.003	208.39	1.18	0.009	0.212	0.428	3.55	1
T3730006	1993-Feb-19	49038.0395	0.2575	1.374	400.0	163.64	142.12	12.981	0.003	176.06	1.15	0.002	0.210	0.431	3.54	1
T3730007	1993-Feb-19	49038.0527	0.2599	1.413	400.0	164.07	141.83	13.028	0.003	177.64	1.24	0.008	0.208	0.435	3.79	1
T3730008	1993-Feb-19	49038.0668	0.2626	1.459	400.0	163.13	142.32	13.066	0.003	175.20	1.12	0.007	0.213	0.428	3.79	1
T3730009	1993-Feb-19	49038.0800	0.2650	1.506	400.0	163.75	143.03	13.119	0.003	168.92	1.14	0.008	0.210	0.433	3.92	1
T3730010	1993-Feb-19	49038.0953	0.2679	1.564	400.0	162.98	141.67	13.076	0.003	158.49	1.45	0.002	0.209	0.425	3.66	1
T3730011	1993-Feb-19	49038.1077	0.2702	1.614	400.0	161.39	140.55	13.174	0.003	147.65	1.06	0.006	0.205	0.426	3.95	1

Table A.5 cont.: HV 982 differential photometry – V.

Frame	Date	HJD −2400000.0	Orbital Phase	X	T	Row	Col	$m_{\rm raw}$	$\sigma_{m_{\rm raw}}$	sky	CHI	Sharp	$V-C$	$C-C$	Seeing (FWHM)	ILCA
T3730012	1993-Feb-19	49038.1242	0.2733	1.685	400.0	161.10	140.45	13.080	0.003	154.12	1.42	0.013	0.212	0.428	3.53	1
T3730013	1993-Feb-19	49038.1358	0.2755	1.738	400.0	162.09	141.77	13.141	0.004	158.96	1.56	0.011	0.213	0.426	3.48	1
T3730014	1993-Feb-19	49038.1530	0.2787	1.820	400.0	161.76	141.10	13.529	0.004	165.15	1.22	0.020	0.206	0.424	3.86	1
T3740002	1993-Feb-23	49041.8973	0.9805	1.134	400.0	164.46	142.59	13.230	0.007	142.68	2.80	0.093	0.839	0.428	2.40	1
T3740003	1993-Feb-23	49041.9122	0.9833	1.148	400.0	164.50	142.23	13.245	0.007	142.82	2.67	0.097	0.880	0.427	2.19	1
T3740004	1993-Feb-23	49041.9192	0.9846	1.156	400.0	168.85	141.84	13.258	0.007	143.56	2.70	0.074	0.891	0.433	2.23	1
T3740005	1993-Feb-23	49041.9273	0.9862	1.166	400.0	162.17	141.44	13.327	0.006	149.52	2.07	0.063	0.914	0.426	2.43	1
T3740006	1993-Feb-23	49041.9336	0.9873	1.174	400.0	162.59	141.12	13.435	0.005	156.81	1.71	0.040	0.918	0.430	2.69	1
T3740007	1993-Feb-23	49041.9393	0.9884	1.182	400.0	162.70	141.30	13.428	0.005	158.02	1.66	0.050	0.923	0.435	2.83	1
T3740008	1993-Feb-23	49041.9467	0.9898	1.193	400.0	162.64	141.53	13.493	0.005	164.44	1.65	0.039	0.932	0.425	2.96	1
T3740009	1993-Feb-23	49041.9546	0.9913	1.206	400.0	162.65	141.82	13.442	0.006	162.98	2.02	0.072	0.936	0.426	2.81	1
T3740010	1993-Feb-23	49041.9899	0.9979	1.275	400.0	163.18	141.47	13.418	0.005	179.82	1.61	0.041	0.877	0.446	3.07	1
T3740011	1993-Feb-23	49042.0414	0.0075	1.412	400.0	164.17	141.26	13.816	0.004	178.62	1.24	0.011	0.742	0.427	3.48	1
T3740012	1993-Feb-23	49042.0480	0.0088	1.433	400.0	163.25	140.71	13.856	0.004	174.86	1.09	0.011	0.721	0.432	3.61	1
T3740013	1993-Feb-23	49042.0622	0.0114	1.481	400.0	164.39	140.87	13.767	0.005	166.53	1.30	0.015	0.684	0.433	3.43	1
T3740014	1993-Feb-23	49042.0817	0.0151	1.553	400.0	164.79	141.60	15.125	0.011	164.24	1.38	0.025	0.631	0.440	3.86	1
T3740015	1993-Feb-23	49042.0888	0.0164	1.581	400.0	163.89	140.95	14.612	0.007	174.41	1.24	−0.006	0.604	0.439	4.16	1
T3750007	1993-Mar-08	49054.9217	0.4217	1.210	400.0	162.34	140.47	13.105	0.005	1902.71	1.51	0.026	0.858	0.427	2.20	1
T3750008	1993-Mar-08	49054.9381	0.4248	1.240	400.0	163.71	140.12	13.111	0.005	2008.34	1.51	0.040	0.805	0.426	2.29	1
T3750009	1993-Mar-08	49054.9455	0.4262	1.255	400.0	162.54	141.49	13.092	0.007	2104.56	1.88	0.041	0.780	0.420	2.06	1
T3750010	1993-Mar-08	49054.9724	0.4312	1.317	400.0	160.94	142.24	13.042	0.005	2236.35	1.47	0.029	0.698	0.426	2.13	1
T3750011	1993-Mar-08	49054.9838	0.4333	1.347	400.0	161.96	141.98	13.017	0.005	2269.61	1.32	0.042	0.660	0.431	2.29	1
T3750012	1993-Mar-08	49054.9946	0.4354	1.378	400.0	159.18	142.64	13.036	0.005	2497.59	1.35	0.029	0.640	0.424	2.13	1
T3750013	1993-Mar-08	49055.0073	0.4377	1.416	400.0	162.48	142.29	13.071	0.004	2720.86	1.08	0.001	0.582	0.420	2.60	1
T3750014	1993-Mar-08	49055.0148	0.4392	1.441	400.0	162.39	142.10	13.111	0.004	3165.73	0.96	0.012	0.561	0.424	2.57	1
T3750015	1993-Mar-08	49055.0227	0.4406	1.467	400.0	161.57	141.94	13.109	0.005	3213.88	1.34	0.014	0.542	0.422	2.45	1
T3750016	1993-Mar-08	49055.0283	0.4417	1.486	400.0	161.44	143.04	13.053	0.004	3051.73	0.94	0.004	0.523	0.417	2.46	1
T3750017	1993-Mar-08	49055.0344	0.4428	1.509	400.0	163.15	142.73	13.046	0.005	3062.46	1.26	0.021	0.511	0.419	2.46	1
T3750018	1993-Mar-08	49055.0428	0.4444	1.540	400.0	161.74	142.60	13.184	0.005	2982.44	1.10	0.013	0.498	0.422	2.53	1
T3750019	1993-Mar-08	49055.0628	0.4482	1.620	400.0	162.84	142.08	12.937	0.004	2565.79	1.06	−0.005	0.439	0.415	2.88	1
T3750020	1993-Mar-08	49055.0876	0.4528	1.729	400.0	161.97	141.29	12.923	0.005	2818.58	1.34	0.012	0.388	0.423	2.82	1
T3750021	1993-Mar-08	49055.0943	0.4541	1.761	400.0	161.70	141.57	13.134	0.005	3567.92	1.09	0.001	0.370	0.438	2.83	1
T3750023	1993-Mar-08	49055.1096	0.4569	1.835	400.0	161.86	141.70	12.976	0.004	3004.01	1.17	0.010	0.357	0.427	2.99	1
T3750024	1993-Mar-08	49055.1193	0.4587	1.883	400.0	163.28	143.78	12.958	0.004	3018.73	1.07	−0.002	0.316	0.428	3.08	1
T3750025	1993-Mar-08	49055.1308	0.4609	1.942	400.0	161.49	142.66	12.986	0.004	2984.59	1.04	0.000	0.305	0.427	3.08	1
T3750026	1993-Mar-08	49055.1385	0.4623	1.982	400.0	161.83	142.90	12.914	0.005	2964.18	1.28	0.001	0.292	0.429	3.04	1
T3750027	1993-Mar-08	49055.1446	0.4635	2.013	400.0	161.45	143.42	12.920	0.005	2972.08	1.41	−0.002	0.282	0.431	3.03	1
T3750028	1993-Mar-08	49055.1508	0.4646	2.045	400.0	161.63	143.26	12.946	0.004	2991.30	1.08	−0.007	0.276	0.420	3.10	1
T3870026	1993-Mar-26	49073.0849	0.8261	1.958	400.0	161.45	144.46	13.420	0.003	183.50	1.14	0.005	0.230	0.429	4.22	1

Table A.5 cont.: HV 982 differential photometry – V.

Frame	Date	HJD −2400000.0	Orbital Phase	X	T	Row	Col	$m_{\rm raw}$	$\sigma_{m_{\rm raw}}$	sky	CHI	Sharp	$V-C$	$C-C$	Seeing (FWHM)	ILCA
T3870027	1993-Mar-26	49073.0943	0.8278	2.007	400.0	161.68	144.35	13.643	0.004	182.20	1.24	0.000	0.232	0.426	5.13	1
T3870028	1993-Mar-26	49073.1052	0.8299	2.064	400.0	162.67	143.23	13.440	0.003	185.07	1.04	−0.002	0.226	0.430	4.63	1
T3870029	1993-Mar-26	49073.1110	0.8310	2.094	400.0	160.78	143.31	13.393	0.004	186.93	1.39	−0.001	0.221	0.432	4.56	1
T3870030	1993-Mar-26	49073.1169	0.8321	2.124	400.0	160.14	143.45	13.408	0.004	188.10	1.42	0.008	0.235	0.428	4.28	1
T3870031	1993-Mar-26	49073.1236	0.8333	2.159	400.0	161.05	144.28	13.396	0.004	189.75	1.31	0.008	0.214	0.433	4.53	1
T3870032	1993-Mar-26	49073.1298	0.8345	2.190	400.0	160.71	143.93	13.548	0.004	190.07	1.43	0.001	0.232	0.425	4.96	1
T3870033	1993-Mar-26	49073.1394	0.8363	2.238	400.0	159.61	143.77	13.905	0.005	187.99	1.27	0.001	0.210	0.439	5.76	1
T3880003	1993-Mar-27	49073.8642	0.9721	1.201	400.0	164.62	142.10	13.319	0.004	145.80	1.55	0.025	0.722	0.428	3.33	1
T3880004	1993-Mar-27	49073.8739	0.9740	1.217	400.0	161.53	140.65	13.454	0.004	150.13	1.46	0.017	0.744	0.428	3.68	1
T3880005	1993-Mar-27	49073.8840	0.9758	1.236	400.0	161.90	140.52	13.482	0.004	149.57	1.42	0.019	0.780	0.428	3.73	1
T3880006	1993-Mar-27	49073.8911	0.9772	1.250	400.0	161.35	140.21	13.605	0.004	147.91	1.24	−0.010	0.790	0.430	4.12	1
T3880007	1993-Mar-27	49073.8988	0.9786	1.266	400.0	162.50	140.61	13.520	0.003	146.54	1.07	0.008	0.816	0.430	3.72	1
T3880008	1993-Mar-27	49073.9188	0.9824	1.313	400.0	161.67	140.79	14.054	0.005	154.13	1.18	0.002	0.847	0.428	5.16	1
T3880009	1993-Mar-27	49073.9418	0.9867	1.375	400.0	162.80	140.84	14.001	0.004	166.49	1.03	−0.002	0.918	0.438	5.50	1
T3880010	1993-Mar-27	49073.9502	0.9883	1.400	400.0	163.62	140.57	13.975	0.005	168.67	1.17	0.003	0.926	0.432	5.20	1
T3880011	1993-Mar-27	49073.9592	0.9899	1.428	400.0	163.12	140.46	14.119	0.005	167.74	1.20	0.003	0.937	0.435	5.83	1
T3880012	1993-Mar-27	49073.9677	0.9915	1.456	400.0	163.93	140.74	14.021	0.005	171.96	1.25	0.002	0.932	0.433	5.53	1
T3880013	1993-Mar-27	49073.9858	0.9949	1.520	400.0	165.35	140.39	13.727	0.004	171.84	1.26	0.015	0.905	0.426	3.86	1
T3880014	1993-Mar-27	49073.9933	0.9963	1.549	400.0	161.63	144.10	13.840	0.004	165.30	0.99	0.001	0.884	0.428	4.45	1
T3880015	1993-Mar-27	49074.0037	0.9983	1.590	400.0	161.36	144.25	13.755	0.005	170.42	1.35	0.009	0.864	0.436	4.02	1
T3880016	1993-Mar-27	49074.0116	0.9998	1.623	400.0	161.87	144.40	13.847	0.004	168.79	1.11	0.013	0.838	0.432	4.33	1
T3880017	1993-Mar-27	49074.0180	0.0010	1.650	400.0	162.28	143.68	13.769	0.004	166.77	1.19	0.014	0.829	0.425	4.21	1
T3880018	1993-Mar-27	49074.0245	0.0022	1.678	400.0	160.73	144.10	13.744	0.005	167.85	1.44	0.003	0.801	0.438	4.22	1
T3880019	1993-Mar-27	49074.0358	0.0043	1.730	400.0	160.52	143.54	13.714	0.004	176.58	1.35	0.007	0.779	0.425	3.88	1
T3880020	1993-Mar-27	49074.0482	0.0066	1.788	400.0	161.15	143.93	13.567	0.005	173.76	1.70	0.028	0.741	0.435	3.67	1
T3880021	1993-Mar-27	49074.0554	0.0080	1.823	400.0	161.23	143.98	13.512	0.004	174.95	1.39	0.017	0.723	0.428	3.63	1
T3880022	1993-Mar-27	49074.0643	0.0096	1.867	400.0	161.41	144.74	13.612	0.004	181.92	1.17	0.020	0.695	0.433	3.84	1
T3880023	1993-Mar-27	49074.0734	0.0114	1.913	400.0	161.53	145.16	13.578	0.005	184.36	1.59	0.014	0.670	0.434	3.76	1
T3880024	1993-Mar-27	49074.0820	0.0130	1.957	400.0	160.57	144.78	13.642	0.004	183.26	1.07	0.000	0.653	0.428	4.38	1
T3880025	1993-Mar-27	49074.0937	0.0152	2.018	400.0	161.57	144.84	13.602	0.004	182.98	1.23	0.015	0.627	0.430	4.02	1
T3880026	1993-Mar-27	49074.1043	0.0171	2.073	400.0	161.14	146.28	13.722	0.005	184.19	1.50	0.011	0.593	0.428	4.43	1
T3880027	1993-Mar-27	49074.1139	0.0189	2.123	400.0	160.59	142.30	13.719	0.004	184.52	1.17	0.011	0.563	0.430	4.57	1
T3880028	1993-Mar-27	49074.1230	0.0206	2.170	400.0	160.49	142.38	13.575	0.004	182.26	1.34	0.002	0.548	0.430	3.97	1
T3880029	1993-Mar-27	49074.1349	0.0229	2.229	400.0	161.29	142.50	13.327	0.004	183.51	1.40	0.021	0.519	0.427	3.40	1
T3880030	1993-Mar-27	49074.1473	0.0252	2.289	400.0	160.24	142.69	13.422	0.004	182.68	1.30	0.001	0.478	0.436	3.81	1
T3880031	1993-Mar-27	49074.1565	0.0269	2.330	400.0	159.18	143.37	13.507	0.004	180.50	1.37	0.001	0.459	0.429	4.23	1
T3880032	1993-Mar-27	49074.1717	0.0298	2.393	400.0	159.44	142.88	13.553	0.004	182.31	1.23	0.001	0.423	0.433	4.47	1
T3880033	1993-Mar-27	49074.1786	0.0311	2.418	400.0	159.89	142.91	13.539	0.004	180.69	1.28	0.004	0.436	0.419	4.25	1
T3880034	1993-Mar-27	49074.1915	0.0335	2.460	400.0	159.24	143.34	13.330	0.004	174.56	1.40	0.014	0.405	0.429	3.63	1

Table A.5 cont.: HV 982 differential photometry – V.

Frame	Date	HJD −2400000.0	Orbital Phase	X	T	Row	Col	$m_{\rm raw}$	$\sigma_{m_{\rm raw}}$	sky	CHI	Sharp	$V-C$	$C-C$	Seeing (FWHM)	ILCA
T3880035	1993-Mar-27	49074.1990	0.0349	2.480	400.0	159.83	143.19	13.385	0.003	176.08	1.07	0.003	0.390	0.432	3.83	1
T3880036	1993-Mar-27	49074.2053	0.0361	2.495	400.0	159.71	142.76	13.419	0.003	177.69	1.12	0.010	0.381	0.425	3.98	1
T3880037	1993-Mar-27	49074.2172	0.0383	2.516	400.0	158.57	143.09	13.403	0.003	185.02	1.11	0.014	0.365	0.422	3.89	1
T3890001	1993-Mar-27	49074.2264	0.0400	2.527	400.0	162.38	143.13	13.334	0.004	197.70	1.39	0.013	0.360	0.420	3.65	1
T3890002	1993-Mar-27	49074.2331	0.0413	2.531	400.0	162.14	143.30	13.334	0.003	263.05	1.19	0.019	0.332	0.439	3.76	1
T3890003	1993-Mar-27	49074.2394	0.0425	2.533	400.0	162.57	143.53	13.360	0.004	570.73	1.17	0.007	0.329	0.428	3.96	1
T3890004	1993-Mar-27	49074.2457	0.0436	2.532	400.0	162.20	143.29	13.327	0.005	2033.79	1.10	0.002	0.322	0.438	3.83	1
T3890010	1993-Mar-28	49074.8870	0.1638	1.247	400.0	167.44	142.21	12.557	0.006	151.17	2.94	0.049	0.218	0.419	2.10	1
T3890011	1993-Mar-28	49074.9059	0.1674	1.288	400.0	168.11	141.64	12.633	0.004	151.87	1.94	0.042	0.215	0.434	2.39	1
T3890012	1993-Mar-28	49074.9256	0.1711	1.337	400.0	163.36	141.39	12.754	0.003	160.46	1.70	0.044	0.221	0.428	2.90	1
T3890013	1993-Mar-28	49074.9297	0.1719	1.347	100.0	162.60	141.50	14.272	0.007	38.83	1.75	0.060	0.218	0.427	2.67	1
T3890014	1993-Mar-28	49074.9313	0.1721	1.351	100.0	163.51	141.14	14.307	0.006	38.47	1.59	0.042	0.210	0.437	2.67	1
T3890015	1993-Mar-28	49074.9328	0.1724	1.355	100.0	163.64	141.47	14.293	0.007	38.12	1.66	0.061	0.215	0.415	2.80	1
T3890017	1993-Mar-28	49074.9344	0.1727	1.360	113.0	162.92	140.98	14.340	0.006	38.89	1.50	0.029	0.227	0.420	3.07	1
T3890018	1993-Mar-28	49074.9457	0.1748	1.393	100.0	163.66	141.35	14.176	0.006	37.05	1.56	0.057	0.219	0.418	2.18	1
T3890019	1993-Mar-28	49074.9472	0.1751	1.397	100.0	163.83	142.41	14.170	0.007	37.29	1.91	0.076	0.224	0.421	2.15	1
T3890020	1993-Mar-28	49074.9488	0.1754	1.402	100.0	165.22	141.60	14.151	0.008	37.75	2.00	0.087	0.212	0.424	2.22	1
T3890021	1993-Mar-28	49074.9503	0.1757	1.407	100.0	165.57	141.23	14.220	0.007	37.83	1.88	0.078	0.221	0.427	2.41	1
T3890022	1993-Mar-28	49074.9555	0.1767	1.423	100.0	164.98	141.35	14.249	0.007	37.93	1.69	0.036	0.228	0.426	2.59	1
T3890023	1993-Mar-28	49074.9571	0.1770	1.428	100.0	164.64	141.74	14.223	0.006	37.93	1.49	0.050	0.216	0.423	2.46	1
T3890024	1993-Mar-28	49074.9586	0.1773	1.433	100.0	164.99	141.84	14.219	0.006	37.85	1.59	0.047	0.214	0.422	2.61	1
T3890025	1993-Mar-28	49074.9602	0.1776	1.438	100.0	165.22	141.46	14.221	0.007	37.14	1.72	0.065	0.204	0.427	2.48	1
T3890026	1993-Mar-28	49074.9639	0.1783	1.451	100.0	164.91	142.00	14.202	0.007	37.39	1.81	0.065	0.232	0.418	2.34	1
T3890027	1993-Mar-28	49074.9655	0.1786	1.456	100.0	165.04	142.20	14.212	0.007	38.19	1.75	0.053	0.208	0.434	2.50	1
T3890028	1993-Mar-28	49074.9670	0.1788	1.461	100.0	165.30	141.71	14.302	0.007	37.41	1.85	0.045	0.220	0.425	2.65	1
T3890029	1993-Mar-28	49074.9686	0.1791	1.466	100.0	166.00	141.33	14.332	0.006	36.67	1.37	0.037	0.227	0.420	2.93	1
T3890030	1993-Mar-28	49074.9737	0.1801	1.484	100.0	162.01	140.18	14.357	0.006	37.92	1.41	0.019	0.213	0.428	3.20	1
T3890031	1993-Mar-28	49074.9753	0.1804	1.490	100.0	163.40	140.42	14.326	0.006	37.76	1.32	0.047	0.215	0.420	2.78	1
T3890032	1993-Mar-28	49074.9768	0.1807	1.495	100.0	163.30	140.88	14.307	0.006	36.99	1.51	0.057	0.215	0.417	2.72	1
T3890033	1993-Mar-28	49074.9784	0.1810	1.501	100.0	163.18	140.37	14.284	0.005	37.19	1.28	0.035	0.213	0.430	2.79	1
T3890034	1993-Mar-28	49074.9837	0.1820	1.523	400.0	163.21	140.68	12.751	0.003	157.29	1.68	0.041	0.214	0.425	2.92	1
T3890035	1993-Mar-28	49074.9915	0.1834	1.552	400.0	161.46	142.46	12.830	0.004	159.79	1.82	0.025	0.216	0.426	3.08	1
T3890036	1993-Mar-28	49074.9986	0.1848	1.580	400.0	162.64	142.16	12.908	0.003	161.74	1.60	0.023	0.221	0.426	3.45	1
T3770001	1993-Mar-28	49075.1411	0.2115	2.272	400.0	161.06	140.74	12.941	0.004	168.70	1.66	0.022	0.199	0.426	3.02	1
T3770002	1993-Mar-28	49075.1503	0.2132	2.315	400.0	162.09	142.58	12.956	0.004	170.70	1.60	0.034	0.215	0.419	3.06	1
T3770003	1993-Mar-28	49075.1579	0.2146	2.348	400.0	162.01	142.09	12.939	0.004	172.19	1.60	0.023	0.203	0.428	2.88	1
T3770004	1993-Mar-28	49075.1634	0.2156	2.368	100.0	160.96	145.12	14.660	0.007	42.12	1.39	0.039	0.199	0.420	3.46	1
T3770005	1993-Mar-28	49075.1649	0.2159	2.374	100.0	161.61	142.06	14.517	0.007	41.50	1.44	0.056	0.224	0.423	2.89	1
T3770006	1993-Mar-28	49075.1665	0.2162	2.381	100.0	161.53	141.93	14.543	0.007	41.29	1.58	0.018	0.221	0.419	3.00	1

Table A.5 cont.: HV 982 differential photometry – V.

Frame	Date	HJD −2400000.0	Orbital Phase	X	T	Row	Col	$m_{\rm raw}$	$\sigma_{m_{\rm raw}}$	sky	CHI	Sharp	$V-C$	$C-C$	Seeing (FWHM)	ILCA
T3770007	1993-Mar-28	49075.1680	0.2165	2.387	100.0	161.16	141.86	14.475	0.007	40.76	1.53	0.028	0.218	0.410	2.96	1
T3770008	1993-Mar-28	49075.1707	0.2170	2.397	100.0	160.68	143.02	14.493	0.007	41.80	1.63	0.060	0.203	0.433	2.77	1
T3770009	1993-Mar-28	49075.1722	0.2173	2.403	100.0	160.66	144.79	14.520	0.007	41.93	1.43	0.059	0.232	0.413	2.85	1
T3770010	1993-Mar-28	49075.1738	0.2176	2.408	100.0	160.55	142.54	14.489	0.008	41.99	1.78	0.086	0.210	0.418	2.75	1
T3770011	1993-Mar-28	49075.1753	0.2179	2.414	100.0	160.56	141.87	14.475	0.007	41.63	1.45	0.053	0.215	0.425	2.73	1
T3770012	1993-Mar-28	49075.1796	0.2187	2.429	100.0	160.41	143.09	14.537	0.006	41.96	1.33	0.040	0.214	0.422	2.92	1
T3770013	1993-Mar-28	49075.1811	0.2190	2.434	100.0	160.74	142.58	14.522	0.006	41.70	1.37	0.034	0.199	0.424	2.85	1
T3770014	1993-Mar-28	49075.1827	0.2193	2.439	100.0	160.23	142.26	14.550	0.007	42.01	1.48	0.057	0.228	0.426	2.89	1
T3770015	1993-Mar-28	49075.1842	0.2196	2.444	100.0	160.68	141.74	14.484	0.006	41.92	1.37	0.019	0.212	0.419	2.67	1
T3770016	1993-Mar-28	49075.1890	0.2204	2.459	100.0	160.73	142.57	14.535	0.007	43.58	1.56	0.061	0.209	0.421	2.93	1
T3770017	1993-Mar-28	49075.1905	0.2207	2.463	100.0	160.68	142.11	14.542	0.007	43.55	1.52	0.033	0.221	0.414	2.93	1
T3770018	1993-Mar-28	49075.1921	0.2210	2.467	100.0	160.40	141.96	14.552	0.007	43.13	1.51	0.040	0.204	0.442	3.11	1
T3770019	1993-Mar-28	49075.1936	0.2213	2.472	100.0	160.50	141.67	14.604	0.008	43.49	1.67	0.056	0.229	0.423	3.03	1
T3770020	1993-Mar-28	49075.1995	0.2224	2.488	400.0	164.04	142.08	13.015	0.003	181.84	1.40	0.034	0.215	0.428	3.05	1
T3770021	1993-Mar-28	49075.2057	0.2236	2.501	400.0	164.50	142.55	13.027	0.004	182.12	1.60	0.025	0.211	0.430	2.97	1
T3900008	1993-Apr-14	49091.8445	0.3422	1.255	400.0	165.64	142.92	12.551	0.004	137.35	2.26	0.054	0.222	0.428	2.28	1
T3900024	1993-Apr-14	49091.9137	0.3552	1.440	400.0	162.51	142.41	12.800	0.003	190.77	1.45	0.033	0.231	0.428	3.09	1
T3900025	1993-Apr-14	49091.9195	0.3563	1.459	400.0	162.74	142.80	12.749	0.003	195.09	1.69	0.050	0.238	0.425	2.88	1
T3900026	1993-Apr-14	49091.9264	0.3576	1.483	400.0	162.52	143.12	12.836	0.003	199.10	1.47	0.019	0.233	0.428	3.27	1
T3900027	1993-Apr-14	49091.9410	0.3603	1.536	400.0	163.47	143.38	12.902	0.003	199.44	1.34	0.025	0.245	0.428	3.31	1
T3900028	1993-Apr-14	49091.9474	0.3615	1.561	400.0	163.72	143.10	12.888	0.003	198.38	1.52	0.030	0.244	0.432	3.30	1
T3900029	1993-Apr-14	49091.9543	0.3628	1.589	400.0	162.73	143.11	12.899	0.003	200.57	1.19	0.015	0.251	0.425	3.33	1
T3900030	1993-Apr-14	49091.9607	0.3640	1.615	400.0	163.24	143.10	12.961	0.004	204.51	1.62	0.027	0.262	0.429	3.53	1
T3900031	1993-Apr-14	49091.9676	0.3653	1.644	400.0	163.33	143.75	12.951	0.003	205.35	1.35	0.020	0.265	0.434	3.50	1
T3900032	1993-Apr-14	49091.9732	0.3663	1.668	400.0	163.32	142.65	13.057	0.003	207.75	1.09	0.005	0.276	0.434	3.87	1
T3900033	1993-Apr-14	49091.9796	0.3676	1.697	400.0	163.76	143.32	13.075	0.003	211.11	1.40	0.016	0.278	0.435	3.76	1
T3920002	1993-Apr-14	49092.1519	0.3998	2.485	400.0	160.97	140.67	13.407	0.004	342.29	1.36	0.016	0.645	0.419	3.49	1
T3920003	1993-Apr-14	49092.1574	0.4009	2.497	400.0	161.02	141.31	13.338	0.003	342.37	1.16	0.017	0.654	0.417	3.15	1
T3920004	1993-Apr-14	49092.1633	0.4020	2.509	400.0	160.97	141.06	13.335	0.005	339.91	1.56	0.039	0.678	0.420	3.05	1
T3920005	1993-Apr-14	49092.1690	0.4030	2.517	400.0	161.13	140.64	13.364	0.004	339.68	1.42	0.025	0.693	0.430	3.11	1
T3920006	1993-Apr-14	49092.1746	0.4041	2.524	400.0	160.86	140.70	13.374	0.005	342.01	1.56	0.028	0.710	0.425	3.14	1
T3920007	1993-Apr-14	49092.1871	0.4064	2.533	400.0	159.27	140.69	13.967	0.005	357.14	1.15	0.002	0.748	0.434	4.25	1
T3920008	1993-Apr-14	49092.2015	0.4091	2.529	400.0	161.25	141.45	14.084	0.006	368.81	1.29	−0.010	0.778	0.432	4.16	1
T3920011	1993-Apr-15	49092.9498	0.5494	1.582	400.0	162.76	141.84	12.735	0.004	192.71	1.87	0.045	0.224	0.430	2.83	1
T3920012	1993-Apr-15	49092.9559	0.5505	1.606	400.0	163.19	142.10	12.750	0.004	188.69	1.78	0.036	0.224	0.429	2.92	1
T3920013	1993-Apr-15	49092.9614	0.5516	1.629	400.0	162.99	141.60	12.792	0.003	185.70	1.39	0.026	0.219	0.431	3.13	1
T3920014	1993-Apr-15	49092.9689	0.5530	1.662	400.0	163.26	141.80	12.746	0.003	179.61	1.60	0.035	0.224	0.430	2.89	1
T3920015	1993-Apr-15	49092.9754	0.5542	1.690	400.0	163.27	141.80	12.746	0.004	177.29	1.68	0.041	0.220	0.425	2.85	1
T3920016	1993-Apr-15	49092.9810	0.5552	1.716	400.0	163.05	141.96	12.839	0.004	182.37	1.84	0.039	0.234	0.425	3.15	1

Table A.5 cont.: HV 982 differential photometry – V.

Frame	Date	HJD −2400000.0	Orbital Phase	X	T	Row	Col	$m_{\rm raw}$	$\sigma_{m_{\rm raw}}$	sky	CHI	Sharp	$V-C$	$C-C$	Seeing (FWHM)	ILCA
T3920017	1993-Apr-15	49092.9866	0.5563	1.741	400.0	163.52	141.79	12.834	0.004	184.98	1.68	0.033	0.219	0.433	3.12	1
T3920018	1993-Apr-15	49092.9924	0.5574	1.769	400.0	163.74	142.15	12.805	0.004	183.43	1.95	0.047	0.222	0.432	2.92	1
T3920019	1993-Apr-15	49092.9978	0.5584	1.795	400.0	163.50	142.15	12.913	0.004	184.24	1.84	0.040	0.223	0.427	2.93	1
T3920020	1993-Apr-15	49093.0036	0.5595	1.823	400.0	163.91	142.22	12.835	0.004	185.50	1.79	0.045	0.220	0.437	3.02	1
T3920026	1993-Apr-17	49094.9311	0.9208	1.530	400.0	164.11	141.96	13.516	0.004	196.96	1.28	0.007	0.228	0.419	3.46	1
T3920027	1993-Apr-17	49094.9400	0.9224	1.564	400.0	164.28	142.56	13.772	0.004	203.91	1.19	0.002	0.232	0.429	4.28	1
T3920029	1993-Apr-17	49094.9457	0.9235	1.587	400.0	163.25	141.97	13.844	0.005	201.77	1.41	0.003	0.232	0.435	4.26	1
T3920028	1993-Apr-17	49094.9457	0.9235	1.587	400.0	163.25	141.97	13.844	0.005	201.77	1.41	0.003	0.232	−0.492	4.26	0
T3920030	1993-Apr-17	49094.9552	0.9253	1.626	400.0	163.43	142.08	13.952	0.005	204.35	1.21	−0.002	0.250	0.428	4.33	1
T3920031	1993-Apr-17	49094.9614	0.9264	1.653	400.0	164.24	141.94	13.996	0.005	201.90	1.10	0.002	0.254	0.424	4.39	1
T3940002	1993-Apr-18	49095.9027	0.1029	1.439	400.0	162.43	137.47	12.728	0.003	167.75	1.59	0.029	0.222	0.422	3.02	1
T3940003	1993-Apr-18	49095.9119	0.1046	1.470	400.0	163.20	140.95	12.731	0.003	171.90	1.41	0.017	0.223	0.422	3.24	1
T3940004	1993-Apr-18	49095.9181	0.1057	1.492	400.0	163.27	141.46	12.791	0.003	170.40	1.58	0.017	0.221	0.423	3.29	1
T3940005	1993-Apr-18	49095.9244	0.1069	1.515	400.0	159.97	142.68	12.836	0.003	174.98	1.58	0.009	0.221	0.424	3.42	1
T3940006	1993-Apr-18	49095.9302	0.1080	1.537	400.0	162.67	143.91	12.855	0.003	176.92	1.22	0.015	0.228	0.421	3.46	1
T3940007	1993-Apr-18	49095.9362	0.1091	1.560	400.0	163.49	141.95	12.837	0.004	179.69	1.68	0.010	0.223	0.428	3.27	1
T3940008	1993-Apr-18	49095.9420	0.1102	1.583	400.0	163.44	141.43	12.957	0.003	184.83	1.32	0.018	0.227	0.427	3.48	1
T3940009	1993-Apr-18	49095.9484	0.1114	1.609	400.0	163.87	141.84	12.875	0.004	180.72	1.80	0.025	0.221	0.428	3.33	1
T3940010	1993-Apr-18	49095.9545	0.1126	1.635	400.0	163.60	141.75	12.909	0.003	185.67	1.34	0.020	0.235	0.419	3.34	1
T3940011	1993-Apr-18	49095.9599	0.1136	1.658	400.0	163.84	141.86	13.034	0.003	189.13	1.11	0.008	0.228	0.425	3.82	1
T0010004	1993-Apr-21	49098.9466	0.6734	1.634	400.0	163.22	143.00	13.438	0.004	188.76	1.38	0.004	0.215	0.425	5.12	1
T0010005	1993-Apr-21	49098.9592	0.6758	1.689	400.0	163.97	143.91	13.429	0.004	188.75	1.27	0.001	0.198	0.438	5.00	1
T0010006	1993-Apr-21	49098.9745	0.6786	1.759	400.0	163.54	143.19	13.201	0.003	200.88	1.20	0.005	0.210	0.432	4.33	1
T1280002	1993-May-21	49128.9846	0.3035	2.227	400.0	162.80	140.34	13.174	0.003	222.08	1.30	0.011	0.212	0.420	3.79	1
T1280003	1993-May-21	49128.9902	0.3045	2.254	400.0	162.97	140.32	13.234	0.003	217.24	1.10	0.010	0.212	0.410	3.76	1
T1280004	1993-May-21	49128.9960	0.3056	2.281	400.0	162.62	140.44	13.303	0.003	206.01	1.08	0.011	0.213	0.417	3.66	1
T1280005	1993-May-21	49129.0138	0.3089	2.360	400.0	162.32	139.52	13.755	0.004	179.33	1.23	0.005	0.204	0.424	4.05	1
T1280006	1993-May-21	49129.0209	0.3103	2.389	400.0	161.56	139.44	13.907	0.004	171.71	1.06	0.009	0.215	0.411	4.30	1
T1280007	1993-May-21	49129.0273	0.3115	2.413	400.0	160.37	140.49	13.985	0.004	153.25	1.11	−0.003	0.223	0.413	4.45	1
T1280008	1993-May-21	49129.0332	0.3126	2.433	400.0	163.63	140.30	13.860	0.005	147.88	1.37	0.012	0.214	0.417	3.66	1
T1280009	1993-May-21	49129.0409	0.3140	2.457	400.0	164.01	141.84	13.086	0.003	253.40	1.38	0.003	0.208	0.427	3.37	1
T1280010	1993-May-21	49129.0487	0.3155	2.479	400.0	163.14	141.47	13.051	0.003	285.14	1.04	−0.001	0.205	0.427	3.76	1
T1280011	1993-May-21	49129.0560	0.3169	2.496	400.0	163.74	141.43	13.096	0.003	288.37	1.29	0.003	0.204	0.426	3.87	1
T1280012	1993-May-21	49129.0775	0.3209	2.528	400.0	163.12	142.04	12.965	0.002	285.55	1.02	−0.002	0.200	0.434	3.52	1
T1280013	1993-May-21	49129.0830	0.3219	2.531	400.0	163.35	141.15	12.979	0.003	286.77	1.35	−0.005	0.206	0.431	3.56	1
T1280014	1993-May-21	49129.0886	0.3230	2.533	400.0	163.11	141.53	12.954	0.003	281.78	1.21	0.004	0.207	0.425	3.47	1
T1280015	1993-May-21	49129.0972	0.3246	2.531	400.0	162.20	142.15	13.148	0.003	289.54	1.10	−0.001	0.212	0.421	4.04	1
T1280016	1993-May-21	49129.1032	0.3257	2.528	400.0	163.86	141.68	13.112	0.003	289.12	1.17	0.007	0.221	0.417	3.88	1
T1280017	1993-May-21	49129.1092	0.3268	2.521	400.0	162.80	141.39	13.128	0.004	301.03	1.38	0.001	0.207	0.422	4.03	1

Table A.5 cont.: HV 982 differential photometry – V.

Frame	Date	HJD −2400000.0	Orbital Phase	X	T	Row	Col	$m_{\rm raw}$	$\sigma_{m_{\rm raw}}$	sky	CHI	Sharp	$V-C$	$C-C$	Seeing (FWHM)	ILCA
T1280018	1993-May-21	49129.1187	0.3286	2.507	400.0	163.06	140.85	13.178	0.003	305.38	1.10	0.003	0.220	0.426	4.12	1
T1280019	1993-May-21	49129.1282	0.3304	2.487	400.0	161.87	141.10	12.980	0.003	309.28	1.19	−0.003	0.203	0.423	3.57	1
T1280020	1993-May-21	49129.1340	0.3315	2.473	400.0	163.25	140.30	12.978	0.003	303.04	1.14	0.006	0.209	0.424	3.60	1
T1280021	1993-May-21	49129.1411	0.3328	2.452	400.0	161.94	140.61	13.051	0.004	309.01	1.44	−0.001	0.209	0.436	3.84	1
T1280022	1993-May-21	49129.1471	0.3339	2.433	400.0	162.32	140.77	12.977	0.003	308.15	1.12	0.000	0.206	0.428	3.64	1
T1280023	1993-May-21	49129.1663	0.3375	2.361	400.0	162.11	141.30	13.043	0.003	302.25	1.23	−0.002	0.204	0.421	3.64	1
T1280024	1993-May-21	49129.1751	0.3392	2.324	400.0	162.38	141.13	13.136	0.003	311.05	1.14	0.001	0.217	0.430	4.23	1
T1280025	1993-May-21	49129.1810	0.3403	2.297	400.0	161.55	141.16	12.930	0.003	307.94	1.19	−0.007	0.208	0.418	3.53	1
T1280026	1993-May-21	49129.1886	0.3417	2.262	400.0	161.94	140.66	12.729	0.004	303.19	1.69	0.004	0.208	0.428	2.73	1
T1280027	1993-May-21	49129.1942	0.3428	2.234	400.0	162.10	140.64	12.766	0.003	302.32	1.58	0.012	0.222	0.420	2.92	1
T1280028	1993-May-21	49129.1998	0.3438	2.207	400.0	161.52	141.07	12.788	0.003	299.06	1.26	−0.010	0.210	0.430	3.03	1
T1280029	1993-May-21	49129.2053	0.3448	2.179	400.0	161.55	141.02	12.700	0.003	292.41	1.69	0.004	0.210	0.423	2.76	1
T1280030	1993-May-21	49129.2111	0.3459	2.150	400.0	161.39	140.71	12.759	0.003	286.12	1.52	0.014	0.210	0.428	2.99	1
T1280031	1993-May-21	49129.2168	0.3470	2.121	400.0	160.94	141.16	12.681	0.003	278.47	1.37	−0.002	0.215	0.429	2.79	1
T1280032	1993-May-21	49129.2225	0.3481	2.091	400.0	160.96	140.75	12.676	0.003	266.71	1.67	0.011	0.209	0.427	2.77	1
T1280033	1993-May-21	49129.2283	0.3492	2.060	400.0	159.85	141.42	12.740	0.003	259.24	1.50	0.009	0.213	0.424	2.93	1
T1280034	1993-May-21	49129.2349	0.3504	2.026	400.0	161.25	140.75	12.723	0.003	261.36	1.63	−0.002	0.219	0.428	2.90	1
T1280035	1993-May-21	49129.2412	0.3516	1.993	400.0	161.26	141.28	12.764	0.003	244.94	1.42	0.013	0.220	0.427	3.09	1
T2160003	1993-May-21	49129.2643	0.3559	1.875	400.0	161.23	141.62	12.680	0.003	244.18	1.58	0.011	0.210	0.427	2.92	1
T2160004	1993-May-21	49129.2700	0.3570	1.846	400.0	161.16	141.46	12.682	0.004	258.23	1.78	0.011	0.216	0.428	2.98	1
T2160005	1993-May-21	49129.2761	0.3581	1.816	400.0	159.68	141.86	12.660	0.003	325.50	1.70	0.014	0.225	0.426	2.81	1
T2160013	1993-May-22	49129.8805	0.4714	1.714	400.0	162.04	142.34	13.812	0.004	226.02	1.07	0.002	0.238	0.429	3.86	1
T2160014	1993-May-22	49129.8876	0.4727	1.747	400.0	161.55	141.64	13.723	0.004	225.51	1.10	−0.003	0.244	0.427	3.62	1
T2160015	1993-May-22	49129.8931	0.4738	1.773	400.0	162.57	142.36	13.198	0.003	226.15	1.01	0.015	0.236	0.422	3.51	1
T2160016	1993-May-22	49129.8989	0.4748	1.801	400.0	161.52	142.60	13.200	0.003	225.26	1.27	0.016	0.236	0.428	3.26	1
T2160017	1993-May-22	49129.9054	0.4761	1.833	400.0	160.88	142.33	13.182	0.003	223.95	1.27	−0.001	0.230	0.425	3.98	1
T2160018	1993-May-22	49129.9109	0.4771	1.860	400.0	162.27	142.08	13.484	0.004	223.56	1.30	0.008	0.231	0.425	3.86	1
T2160019	1993-May-22	49129.9163	0.4781	1.887	400.0	162.34	141.57	13.373	0.004	226.05	1.29	0.021	0.221	0.431	3.61	1
T2160027	1993-May-22	49130.0036	0.4945	1.887	400.0	162.14	143.50	13.422	0.003	246.64	1.04	0.003	0.225	0.429	4.60	1
T2160028	1993-May-22	49130.0092	0.4955	1.887	400.0	162.22	143.61	13.367	0.003	250.45	1.14	0.007	0.228	0.432	4.29	1
T2160029	1993-May-22	49130.0146	0.4965	1.887	400.0	161.73	142.80	13.573	0.004	242.42	1.13	0.002	0.234	0.423	4.74	1
T2160030	1993-May-22	49130.0208	0.4977	1.887	400.0	162.18	143.54	13.702	0.005	252.43	1.37	0.000	0.234	0.418	4.77	1
T2160031	1993-May-22	49130.0279	0.4990	1.887	400.0	163.13	143.10	13.397	0.004	250.94	1.35	−0.004	0.221	0.433	3.92	1
T2160032	1993-May-22	49130.0341	0.5002	1.887	400.0	161.56	143.56	13.509	0.004	252.98	1.39	0.006	0.222	0.424	4.19	1
T2160033	1993-May-22	49130.0397	0.5012	1.887	400.0	160.79	142.14	13.483	0.004	258.01	1.31	0.007	0.236	0.423	4.32	1
T2160034	1993-May-22	49130.0595	0.5049	1.887	400.0	160.91	143.03	13.830	0.005	264.58	1.29	0.006	0.226	0.429	4.82	1
T2160035	1993-May-22	49130.0684	0.5066	1.887	400.0	161.04	143.65	13.734	0.004	261.86	1.09	0.000	0.209	0.434	5.01	1
T2160036	1993-May-22	49130.0796	0.5087	1.887	400.0	163.48	143.35	13.483	0.003	282.61	1.11	0.006	0.216	0.432	4.40	1
T2160037	1993-May-22	49130.2288	0.5367	2.042	400.0	166.98	138.12	13.966	0.004	229.34	0.98	0.018	0.217	0.424	3.13	1

Table A.5 cont.: HV 982 differential photometry – V.

Frame	Date	HJD −2400000.0	Orbital Phase	X	T	Row	Col	$m_{\rm raw}$	$\sigma_{m_{\rm raw}}$	sky	CHI	Sharp	$V-C$	$C-C$	Seeing (FWHM)	ILCA
T2160038	1993-May-22	49130.2357	0.5380	2.007	400.0	162.41	140.40	13.975	0.004	224.58	1.05	0.014	0.210	0.422	3.02	1
T2160039	1993-May-22	49130.2413	0.5390	1.978	400.0	161.12	139.34	13.573	0.004	215.60	1.18	0.017	0.215	0.423	3.19	1
T2160040	1993-May-22	49130.2471	0.5401	1.948	400.0	162.03	141.70	13.835	0.005	209.17	1.46	0.030	0.229	0.415	2.97	1
T2160041	1993-May-22	49130.2527	0.5411	1.919	400.0	162.34	140.70	13.923	0.004	203.78	1.08	0.014	0.220	0.430	3.17	1
T2160042	1993-May-22	49130.2589	0.5423	1.887	400.0	162.11	141.07	13.767	0.004	193.80	1.07	0.001	0.220	0.416	3.74	1
T2160043	1993-May-22	49130.2651	0.5435	1.857	400.0	162.23	140.14	13.963	0.005	190.95	1.22	0.022	0.214	0.419	3.57	1
T3950016	1993-May-23	49131.2242	0.7232	2.052	400.0	163.45	141.01	12.754	0.003	252.69	1.24	0.002	0.214	0.419	2.96	1
T3950017	1993-May-23	49131.2301	0.7243	2.021	400.0	162.66	140.43	12.683	0.003	245.66	1.54	0.023	0.217	0.421	2.65	1
T3950018	1993-May-23	49131.2354	0.7253	1.994	400.0	162.69	139.76	12.652	0.004	235.80	2.06	0.038	0.206	0.424	2.57	1
T3950019	1993-May-23	49131.2407	0.7263	1.966	400.0	162.76	140.21	12.686	0.003	225.03	1.61	0.005	0.209	0.421	2.86	1
T3950020	1993-May-23	49131.2465	0.7274	1.937	400.0	163.10	139.92	12.674	0.003	221.15	1.53	0.015	0.213	0.426	2.80	1
T3980007	1993-May-29	49137.0544	0.8160	2.521	400.0	164.94	140.18	13.200	0.003	214.20	1.23	0.006	0.215	0.425	4.23	1
T3980008	1993-May-29	49137.0602	0.8171	2.525	400.0	166.90	140.57	13.397	0.004	199.03	1.21	−0.005	0.221	0.418	4.57	1
T3980009	1993-May-29	49137.0662	0.8182	2.527	400.0	162.15	139.55	13.502	0.004	196.14	1.17	0.004	0.218	0.420	5.00	1
T3980010	1993-May-29	49137.0717	0.8192	2.527	400.0	162.61	142.36	13.385	0.003	197.51	1.21	0.006	0.212	0.417	4.59	1
T3980011	1993-May-29	49137.0773	0.8203	2.525	400.0	162.46	142.59	13.358	0.003	198.36	1.12	0.002	0.210	0.421	4.54	1
T3980012	1993-May-29	49137.0829	0.8213	2.521	400.0	164.14	141.56	13.344	0.003	201.52	1.20	0.001	0.212	0.418	4.56	1
T3980013	1993-May-29	49137.0884	0.8224	2.515	400.0	164.30	141.90	13.432	0.004	208.35	1.18	−0.003	0.219	0.421	4.84	1
T3980014	1993-May-29	49137.0940	0.8234	2.507	400.0	164.43	141.07	13.225	0.004	210.05	1.33	−0.011	0.218	0.424	4.18	1
T3980015	1993-May-29	49137.1027	0.8251	2.490	400.0	162.16	142.63	13.549	0.004	211.13	1.28	−0.004	0.211	0.418	4.36	1
T3980016	1993-May-29	49137.1083	0.8261	2.478	400.0	162.53	143.27	13.536	0.003	214.00	1.08	0.001	0.219	0.418	4.53	1
T3980017	1993-May-29	49137.1180	0.8279	2.452	400.0	162.47	143.01	13.240	0.003	219.64	1.22	−0.002	0.226	0.417	4.21	1
T3980018	1993-May-29	49137.1248	0.8292	2.431	400.0	162.96	142.49	13.295	0.003	217.29	1.00	0.008	0.220	0.415	3.76	1
T3980019	1993-May-29	49137.1339	0.8309	2.399	400.0	162.34	142.79	13.484	0.004	214.54	1.25	−0.002	0.204	0.426	3.83	1
T3980020	1993-May-29	49137.1395	0.8320	2.378	400.0	161.84	142.42	14.088	0.005	211.76	1.22	0.003	0.226	0.407	4.12	1
T3980021	1993-May-29	49137.1521	0.8343	2.326	400.0	164.35	141.31	15.010	0.008	190.50	0.98	−0.007	0.238	0.419	3.81	1
T3980024	1993-May-30	49137.8493	0.9650	1.672	400.0	162.20	142.16	15.280	0.023	1959.09	1.11	0.033	0.571	0.413	3.01	1
T3980025	1993-May-30	49137.8760	0.9700	1.795	400.0	164.16	141.43	13.594	0.005	961.02	1.08	−0.002	0.688	0.416	3.18	1
T3980026	1993-May-30	49137.8819	0.9711	1.824	400.0	163.51	142.55	13.359	0.004	667.86	1.29	0.010	0.690	0.419	3.55	1
T3980027	1993-May-30	49137.8880	0.9722	1.854	400.0	163.16	141.51	13.564	0.005	813.08	1.15	−0.001	0.715	0.425	3.70	1
T3980028	1993-May-30	49137.8948	0.9735	1.888	400.0	163.98	142.36	13.394	0.005	766.65	1.31	0.018	0.725	0.421	3.19	1
T3980029	1993-May-30	49137.9011	0.9747	1.920	400.0	159.88	141.18	13.233	0.004	682.59	1.27	0.027	0.745	0.420	3.04	1
T3980030	1993-May-30	49137.9296	0.9800	2.067	400.0	160.26	141.80	13.611	0.005	724.51	1.25	0.011	0.835	0.423	3.70	1
T3980031	1993-May-30	49137.9354	0.9811	2.097	400.0	159.77	141.32	13.647	0.006	747.98	1.51	0.018	0.847	0.424	3.60	1
T3980032	1993-May-30	49137.9410	0.9822	2.126	400.0	160.34	141.84	13.832	0.005	816.80	1.05	0.018	0.863	0.419	3.75	1
T3980033	1993-May-30	49137.9465	0.9832	2.154	400.0	163.34	139.85	14.027	0.008	898.62	1.35	0.008	0.872	0.417	3.98	1
T3980034	1993-May-30	49137.9554	0.9849	2.199	400.0	162.93	140.40	14.262	0.007	983.47	0.98	0.000	0.884	0.420	4.37	1
T3980035	1993-May-30	49137.9615	0.9860	2.229	400.0	162.92	143.42	14.281	0.008	1010.21	1.01	0.016	0.871	0.419	4.24	1
T3980036	1993-May-30	49137.9682	0.9873	2.261	400.0	162.69	143.57	13.988	0.005	764.05	0.83	0.001	0.907	0.408	4.45	1

Table A.5 cont.: HV 982 differential photometry – V.

Frame	Date	HJD −2400000.0	Orbital Phase	X	T	Row	Col	$m_{\rm raw}$	$\sigma_{m_{\rm raw}}$	sky	CHI	Sharp	$V-C$	$C-C$	Seeing (FWHM)	ILCA
T3980037	1993-May-30	49138.0028	0.9938	2.407	400.0	163.74	142.24	14.118	0.007	727.32	1.27	−0.004	0.894	0.425	5.08	1
T3980038	1993-May-30	49138.0475	0.0021	2.516	400.0	158.71	144.07	14.926	0.013	703.45	1.18	0.002	0.751	0.425	7.17	0
T4070002	1993-Jun-25	49163.8432	0.8371	1.987	400.0	163.43	138.20	13.171	0.003	280.10	1.32	0.000	0.223	0.427	4.29	1
T4070003	1993-Jun-25	49163.8524	0.8388	2.034	400.0	162.50	139.50	13.399	0.003	280.98	0.93	0.000	0.219	0.435	4.94	1
T4070004	1993-Jun-25	49163.8772	0.8435	2.162	400.0	164.61	140.92	13.362	0.003	297.06	1.15	0.002	0.224	0.431	4.68	1
T4070017	1993-Jun-28	49166.8138	0.3939	1.878	400.0	164.75	140.32	13.271	0.005	953.25	1.36	0.017	0.554	0.437	3.29	1
T4070018	1993-Jun-28	49166.8277	0.3965	1.949	400.0	165.81	140.17	13.358	0.004	979.92	1.13	0.010	0.591	0.437	3.42	1
T4070019	1993-Jun-28	49166.8340	0.3977	1.982	400.0	162.16	140.79	13.339	0.005	992.91	1.36	0.015	0.611	0.429	3.20	1
T4070020	1993-Jun-28	49166.8408	0.3989	2.017	400.0	163.14	140.57	13.374	0.004	1006.29	1.21	0.013	0.625	0.436	3.31	1
T4070021	1993-Jun-28	49166.8478	0.4002	2.053	400.0	161.62	141.55	13.476	0.005	1022.21	1.31	0.016	0.657	0.434	3.40	1
T4070022	1993-Jun-28	49166.8667	0.4038	2.150	400.0	164.05	139.18	13.714	0.006	1232.74	1.15	0.023	0.694	0.438	3.36	1
T4070023	1993-Jun-28	49166.8732	0.4050	2.183	400.0	162.90	143.43	13.688	0.006	1196.12	1.36	0.008	0.724	0.434	3.30	1
T4070024	1993-Jun-28	49166.8791	0.4061	2.212	400.0	162.94	142.71	13.757	0.007	1348.35	1.28	0.042	0.738	0.444	2.86	1
T4070025	1993-Jun-28	49166.8849	0.4072	2.240	400.0	163.57	142.94	14.730	0.017	2011.96	1.30	0.039	0.804	0.408	3.04	1
T4070026	1993-Jun-28	49166.8930	0.4087	2.279	400.0	161.60	142.24	13.858	0.008	1299.67	1.46	0.019	0.811	0.433	3.16	1
T4070027	1993-Jun-28	49166.8989	0.4098	2.306	400.0	162.89	143.44	14.545	0.011	1652.81	1.06	0.010	0.804	0.441	3.30	1
T4070028	1993-Jun-28	49166.9047	0.4109	2.331	400.0	161.96	142.47	13.849	0.006	1265.95	1.14	0.015	0.834	0.435	3.26	1
T4070029	1993-Jun-28	49166.9120	0.4123	2.362	400.0	162.05	142.94	14.621	0.012	1560.56	1.11	−0.007	0.847	0.436	3.48	1
T3990027	1993-Jun-29	49168.1918	0.6522	1.712	400.0	161.90	140.58	12.690	0.004	160.72	1.80	0.013	0.209	0.426	2.96	1
T3990028	1993-Jun-29	49168.1973	0.6532	1.687	400.0	161.18	139.74	12.638	0.003	160.60	1.78	0.006	0.204	0.429	2.90	1
T3990029	1993-Jun-29	49168.2030	0.6542	1.662	400.0	163.69	141.32	12.701	0.003	160.50	1.43	0.003	0.202	0.433	3.05	1
T3990030	1993-Jun-29	49168.2123	0.6560	1.622	400.0	165.28	139.60	12.599	0.004	158.37	2.07	0.019	0.206	0.427	2.77	1
T3990031	1993-Jun-29	49168.2179	0.6571	1.599	400.0	164.12	141.34	12.637	0.003	158.83	1.72	0.026	0.207	0.432	2.92	1
T3990032	1993-Jun-29	49168.2234	0.6581	1.577	400.0	163.82	141.69	12.648	0.003	161.71	1.80	0.015	0.208	0.430	2.96	1
T3990033	1993-Jun-29	49168.2334	0.6600	1.538	400.0	163.15	141.37	12.626	0.003	162.32	1.68	0.013	0.198	0.431	2.93	1
T3990034	1993-Jun-29	49168.2388	0.6610	1.518	400.0	163.10	141.82	12.580	0.003	158.53	1.86	0.021	0.199	0.436	2.76	1
T3990035	1993-Jun-29	49168.2441	0.6620	1.499	400.0	163.05	141.48	12.581	0.003	160.71	1.79	0.014	0.201	0.429	2.78	1
T3990036	1993-Jun-29	49168.2496	0.6630	1.479	400.0	162.93	141.40	12.561	0.004	158.39	2.08	0.018	0.204	0.427	2.69	1
T4080001	1993-Jun-29	49168.2631	0.6655	1.434	400.0	162.32	141.54	12.631	0.004	155.76	2.05	0.009	0.207	0.427	2.83	1
T4080002	1993-Jun-29	49168.2686	0.6665	1.416	400.0	162.12	141.51	12.692	0.003	157.17	1.52	0.009	0.204	0.426	3.19	1
T4080003	1993-Jun-29	49168.2740	0.6676	1.399	400.0	161.85	141.72	12.527	0.004	154.15	2.04	0.017	0.201	0.428	2.74	1
T4080004	1993-Jun-29	49168.2795	0.6686	1.383	400.0	161.63	141.85	12.543	0.003	156.00	1.91	0.011	0.204	0.426	2.72	1
T4080005	1993-Jun-29	49168.2849	0.6696	1.367	400.0	161.56	141.59	12.548	0.003	169.07	1.88	0.013	0.206	0.425	2.68	1
T4080006	1993-Jun-29	49168.2905	0.6707	1.352	400.0	161.28	141.99	12.522	0.004	225.65	2.08	0.018	0.209	0.424	2.73	1
T4080007	1993-Jun-29	49168.2962	0.6717	1.336	400.0	161.21	141.94	12.506	0.004	434.28	1.82	0.015	0.202	0.432	2.62	1
T4090007	1993-Jul-02	49170.9098	0.1616	2.396	400.0	161.54	141.98	12.749	0.005	3266.79	1.46	0.041	0.223	0.425	2.20	1
T4090009	1993-Jul-02	49170.9258	0.1646	2.449	400.0	161.65	141.71	12.773	0.005	3370.35	1.57	0.040	0.220	0.431	2.30	1
T4090010	1993-Jul-02	49170.9328	0.1659	2.469	400.0	161.10	141.19	12.784	0.005	3412.51	1.42	0.004	0.219	0.431	2.47	1
T4220008	1993-Jul-22	49190.8303	0.8953	2.292	400.0	160.43	144.28	13.491	0.003	185.86	1.05	0.000	0.216	0.433	4.94	1

Table A.5 cont.: HV 982 differential photometry – V.

Frame	Date	HJD −2400000.0	Orbital Phase	X	T	Row	Col	$m_{\rm raw}$	$\sigma_{m_{\rm raw}}$	sky	CHI	Sharp	$V-C$	$C-C$	Seeing (FWHM)	ILCA
T4220009	1993-Jul-22	49190.8359	0.8964	2.317	400.0	159.70	143.88	13.397	0.003	185.44	0.98	−0.001	0.226	0.423	4.71	1
T4220010	1993-Jul-22	49190.8429	0.8977	2.347	400.0	159.25	143.65	13.573	0.004	183.67	1.26	0.001	0.233	0.424	4.75	1
T4220011	1993-Jul-22	49190.8484	0.8987	2.369	400.0	159.18	143.76	13.634	0.004	181.39	1.07	0.003	0.228	0.420	4.52	1
T4220012	1993-Jul-22	49190.8539	0.8998	2.391	400.0	158.42	144.46	14.663	0.007	173.15	1.10	0.010	0.236	0.437	4.65	1
T4220013	1993-Jul-22	49190.9009	0.9086	2.514	400.0	157.29	142.98	13.938	0.006	178.72	1.46	0.000	0.231	0.427	5.82	1
T4220014	1993-Jul-22	49190.9088	0.9100	2.522	400.0	159.36	144.05	13.751	0.004	181.97	1.18	−0.001	0.223	0.428	5.60	1
T4220018	1993-Jul-22	49190.9343	0.9148	2.522	400.0	157.30	143.62	13.930	0.005	171.71	1.28	−0.003	0.226	0.430	5.50	1
T4220019	1993-Jul-22	49190.9458	0.9170	2.508	400.0	157.94	143.34	13.674	0.003	166.08	0.97	0.002	0.238	0.423	5.37	1
T4220020	1993-Jul-22	49190.9516	0.9181	2.498	400.0	157.32	143.45	13.782	0.004	152.34	1.21	0.004	0.223	0.429	5.64	1
T4220024	1993-Jul-22	49190.9677	0.9211	2.460	400.0	158.27	142.71	13.605	0.004	151.28	1.16	−0.001	0.233	0.430	4.98	1
T4220025	1993-Jul-22	49190.9735	0.9222	2.443	400.0	158.08	142.37	13.607	0.004	149.73	1.19	0.001	0.226	0.427	4.99	1
T4220026	1993-Jul-22	49190.9791	0.9232	2.426	400.0	158.16	142.96	13.732	0.004	151.99	1.06	−0.002	0.243	0.419	4.96	1
T4220028	1993-Jul-22	49190.9997	0.9271	2.348	400.0	158.21	141.90	14.153	0.005	158.41	1.10	0.001	0.253	0.434	6.95	0
T4220029	1993-Jul-22	49191.0077	0.9286	2.313	400.0	155.80	142.75	14.091	0.005	160.69	1.25	−0.003	0.255	0.424	6.74	0
T4230007	1993-Jul-23	49191.8451	0.0855	2.367	400.0	162.31	144.14	13.906	0.005	236.87	1.18	−0.001	0.208	0.432	6.79	0
T4230008	1993-Jul-23	49191.8511	0.0867	2.390	400.0	164.98	142.36	13.786	0.004	235.73	1.13	−0.001	0.211	0.419	6.31	0
T4230009	1993-Jul-23	49191.8571	0.0878	2.412	400.0	163.46	142.36	13.834	0.004	232.09	1.04	−0.004	0.207	0.426	6.52	0
T4230010	1993-Jul-23	49191.8630	0.0889	2.432	400.0	163.75	142.74	13.799	0.005	227.63	1.29	0.001	0.212	0.429	6.41	0
T4230011	1993-Jul-23	49191.8686	0.0899	2.450	400.0	163.88	143.21	13.993	0.004	221.84	1.08	0.001	0.222	0.434	7.03	0
T4230015	1993-Jul-23	49191.8899	0.0939	2.501	400.0	163.17	143.29	13.993	0.004	215.34	1.07	−0.003	0.202	0.438	6.73	0
T4230016	1993-Jul-23	49191.8979	0.0954	2.513	400.0	162.47	145.14	14.876	0.010	204.68	1.37	0.000	0.205	0.472	6.82	0
T4240018	1993-Jul-24	49193.0447	0.3104	2.106	400.0	161.84	142.79	12.911	0.003	163.09	1.44	0.028	0.227	0.417	3.25	1
T4240019	1993-Jul-24	49193.0518	0.3117	2.070	400.0	161.59	142.84	12.832	0.003	160.33	1.56	0.022	0.219	0.427	2.92	1
T4240020	1993-Jul-24	49193.0598	0.3132	2.028	400.0	161.44	142.80	12.772	0.003	154.32	1.66	0.031	0.218	0.420	2.69	1
T4240024	1993-Jul-24	49193.0809	0.3172	1.919	400.0	161.71	142.24	12.940	0.003	156.69	1.34	0.020	0.220	0.422	3.49	1
T4240026	1993-Jul-24	49193.1031	0.3213	1.809	400.0	160.52	143.62	12.918	0.003	161.62	1.18	0.007	0.222	0.424	3.37	1
T4240028	1993-Jul-24	49193.1130	0.3232	1.761	400.0	160.23	143.80	12.783	0.003	157.74	1.66	0.033	0.220	0.421	2.99	1
T4240031	1993-Jul-24	49193.1421	0.3286	1.631	400.0	158.20	143.45	12.716	0.004	154.32	1.80	0.039	0.223	0.421	2.74	1
T4240033	1993-Jul-24	49193.1512	0.3303	1.593	400.0	158.62	144.30	12.768	0.003	156.17	1.55	0.028	0.224	0.417	3.02	1
T4250001	1993-Jul-24	49193.1884	0.3373	1.455	400.0	157.73	144.40	12.660	0.004	151.87	1.98	0.050	0.225	0.422	2.54	1
T4250002	1993-Jul-24	49193.1941	0.3384	1.436	400.0	156.98	144.40	12.681	0.003	149.98	1.73	0.036	0.230	0.421	2.77	1
T4250005	1993-Jul-24	49193.2198	0.3432	1.359	400.0	167.71	144.16	12.759	0.004	149.17	1.74	0.016	0.219	0.427	3.17	1
T4250007	1993-Jul-24	49193.2299	0.3451	1.331	400.0	163.05	144.64	12.702	0.003	146.81	1.64	0.034	0.231	0.418	2.88	1
T4250011	1993-Jul-24	49193.2619	0.3511	1.256	400.0	161.07	143.55	12.693	0.003	138.06	1.62	0.031	0.230	0.420	2.97	1
T4250013	1993-Jul-24	49193.2711	0.3528	1.238	400.0	161.53	144.32	12.635	0.004	136.58	2.27	0.049	0.227	0.419	2.60	1
T4250015	1993-Jul-24	49193.2807	0.3546	1.220	400.0	160.78	143.84	12.640	0.003	175.93	1.72	0.040	0.226	0.419	2.54	1
T4250017	1993-Jul-24	49193.2899	0.3563	1.204	400.0	161.58	145.02	12.570	0.004	549.58	1.82	0.039	0.232	0.419	2.33	1
T4250018	1993-Jul-24	49193.2961	0.3575	1.194	400.0	161.20	144.41	12.628	0.004	1872.89	1.40	0.030	0.245	0.419	2.46	1
T4270004	1993-Jul-27	49196.0333	0.8705	2.123	400.0	163.20	142.95	13.003	0.004	522.87	1.67	0.014	0.290	0.382	3.41	0

Table A.5 cont.: HV 982 differential photometry – V.

Frame	Date	HJD −2400000.0	Orbital Phase	X	T	Row	Col	$m_{\rm raw}$	$\sigma_{m_{\rm raw}}$	sky	CHI	Sharp	$V-C$	$C-C$	Seeing (FWHM)	ILCA
T4270007	1993-Jul-27	49196.0633	0.8762	1.967	400.0	162.18	143.24	12.865	0.003	458.51	1.17	0.014	0.244	0.412	3.14	1
T4270009	1993-Jul-27	49196.0735	0.8781	1.915	400.0	162.19	142.89	12.803	0.004	424.77	1.78	0.049	0.235	0.414	2.98	1
T4270012	1993-Jul-27	49196.0997	0.8830	1.786	400.0	161.57	143.42	12.846	0.003	312.52	1.38	0.006	0.240	0.413	3.20	1
T4270014	1993-Jul-27	49196.1106	0.8850	1.734	400.0	160.14	143.40	12.842	0.004	251.82	1.78	0.037	0.247	0.415	3.05	1
T4270017	1993-Jul-27	49196.1358	0.8897	1.623	400.0	160.12	142.77	12.710	0.003	159.97	1.58	0.029	0.244	0.413	2.79	1
T4270019	1993-Jul-27	49196.1450	0.8915	1.585	400.0	160.35	143.38	12.697	0.004	159.67	1.93	0.025	0.242	0.411	2.74	1
T4270022	1993-Jul-27	49196.1693	0.8960	1.493	400.0	159.14	143.14	12.605	0.005	154.30	2.37	0.058	0.247	0.408	2.38	1
T4270026	1993-Jul-27	49196.1979	0.9014	1.399	400.0	158.41	143.04	12.657	0.004	156.57	2.15	0.034	0.244	0.418	2.74	1
T4270030	1993-Jul-27	49196.2317	0.9077	1.306	400.0	157.60	144.19	12.582	0.006	145.78	2.80	0.066	0.244	0.416	2.21	1
T4270032	1993-Jul-27	49196.2413	0.9095	1.283	400.0	160.35	143.10	12.548	0.005	141.56	2.42	0.049	0.243	0.407	2.31	1
T4270036	1993-Jul-27	49196.2687	0.9147	1.227	400.0	159.64	143.96	12.583	0.004	134.88	2.13	0.052	0.248	0.414	2.30	1
T4270037	1993-Jul-27	49196.2748	0.9158	1.216	400.0	159.61	143.35	12.557	0.006	143.19	2.72	0.076	0.247	0.413	2.10	1
T4280002	1993-Jul-27	49196.2901	0.9187	1.191	400.0	159.76	143.19	12.548	0.004	669.57	2.03	0.047	0.252	0.414	2.25	1
T4280003	1993-Jul-27	49196.2966	0.9199	1.181	400.0	159.72	143.69	12.560	0.005	2505.74	1.72	0.039	0.257	0.415	2.38	1
T4280007	1993-Aug-15	49214.8395	0.3954	2.519	400.0	163.31	141.66	13.440	0.004	159.61	1.51	0.027	0.572	0.422	3.19	1
T4280008	1993-Aug-15	49214.8460	0.3966	2.524	400.0	164.48	140.93	13.336	0.004	152.56	1.45	0.036	0.593	0.417	2.81	1
T4280009	1993-Aug-15	49214.8518	0.3977	2.527	400.0	164.31	140.99	13.343	0.005	151.26	1.89	0.025	0.600	0.424	2.90	1
T4280013	1993-Aug-15	49214.8838	0.4037	2.502	400.0	164.47	140.84	13.462	0.005	148.99	1.63	0.039	0.706	0.431	2.97	1
T4280014	1993-Aug-15	49214.8900	0.4049	2.490	400.0	163.69	140.66	13.545	0.004	148.95	1.47	0.019	0.733	0.421	3.16	1
T4280015	1993-Aug-15	49214.8980	0.4064	2.471	400.0	164.68	140.78	13.670	0.004	159.74	1.28	0.027	0.759	0.416	3.56	1
S1250025	1993-Aug-16	49215.9887	0.6108	2.071	400.0	164.21	142.66	15.721	0.019	212.20	1.46	0.015	0.184	0.440	3.66	1
S1250026	1993-Aug-16	49216.0010	0.6131	2.007	400.0	163.17	142.44	14.742	0.008	171.62	1.28	−0.004	0.202	0.427	4.13	1
S1250027	1993-Aug-16	49216.0080	0.6144	1.971	400.0	163.23	142.85	13.935	0.005	221.19	1.32	−0.005	0.211	0.435	3.81	1
S1250028	1993-Aug-16	49216.0187	0.6165	1.916	400.0	162.93	142.32	13.713	0.006	545.18	1.40	−0.004	0.198	0.424	4.06	1
S1250029	1993-Aug-16	49216.0250	0.6176	1.884	400.0	161.75	141.95	13.855	0.011	1149.98	2.06	−0.023	0.194	0.420	4.01	1
S1250030	1993-Aug-16	49216.0312	0.6188	1.853	400.0	162.93	142.42	14.058	0.024	2384.84	2.90	−0.043	0.152	0.468	4.26	0
S1630012	1993-Sep-11	49242.0130	0.4886	0.000	400.0	166.48	139.92	15.979	0.014	135.38	1.07	−0.005	0.274	0.438	0.00	1
S1630013	1993-Sep-11	49242.0324	0.4922	0.000	400.0	167.14	140.24	14.636	0.006	153.79	1.06	−0.003	0.235	0.430	0.00	1
S1630014	1993-Sep-11	49242.0392	0.4935	0.000	400.0	165.09	139.83	14.275	0.005	154.86	1.01	0.017	0.237	0.420	3.51	1
T4410027	1993-Sep-14	49244.8534	0.0210	2.342	400.0	158.63	141.56	13.710	0.004	173.93	1.06	0.000	0.532	0.423	4.81	1
T4410028	1993-Sep-14	49244.8628	0.0227	2.302	400.0	158.23	140.79	13.896	0.005	167.74	1.24	0.000	0.505	0.416	5.48	1
T4410029	1993-Sep-14	49244.8687	0.0239	2.274	400.0	159.18	141.73	13.941	0.004	168.02	1.16	−0.001	0.489	0.421	5.72	1
T4410030	1993-Sep-14	49244.8753	0.0251	2.243	400.0	158.02	141.73	13.867	0.004	169.88	1.20	0.002	0.481	0.426	5.48	1
T4410031	1993-Sep-14	49244.8809	0.0262	2.216	400.0	157.85	141.17	13.713	0.004	170.14	1.27	0.000	0.469	0.422	4.92	1
T4410032	1993-Sep-14	49244.8867	0.0272	2.187	400.0	157.41	141.92	13.689	0.004	172.32	1.24	−0.002	0.462	0.423	4.99	1
T4410033	1993-Sep-14	49244.8932	0.0284	2.155	400.0	158.01	141.73	13.613	0.005	172.42	1.42	0.002	0.446	0.412	4.75	1
T4410034	1993-Sep-14	49244.9042	0.0305	2.098	400.0	157.48	141.16	13.509	0.003	168.22	1.08	0.002	0.425	0.411	4.63	1
T4410035	1993-Sep-14	49244.9099	0.0316	2.068	400.0	157.86	141.12	13.537	0.004	169.59	1.18	−0.002	0.418	0.415	4.72	1
T4410037	1993-Sep-14	49244.9218	0.0338	2.007	400.0	157.37	140.14	13.705	0.004	165.10	1.04	0.000	0.387	0.420	5.32	1

Table A.5 cont.: HV 982 differential photometry – V.

Frame	Date	HJD −2400000.0	Orbital Phase	X	T	Row	Col	$m_{\rm raw}$	$\sigma_{m_{\rm raw}}$	sky	CHI	Sharp	$V-C$	$C-C$	Seeing (FWHM)	ILCA
T4420001	1993-Sep-14	49244.9403	0.0373	1.912	400.0	165.02	142.76	13.785	0.004	162.62	1.26	0.002	0.348	0.433	5.78	1
T4420003	1993-Sep-14	49244.9499	0.0391	1.863	400.0	165.21	141.65	13.666	0.004	164.95	1.30	0.001	0.358	0.414	5.41	1
T4420006	1993-Sep-14	49244.9657	0.0420	1.786	400.0	165.56	142.28	13.736	0.004	158.75	1.04	0.002	0.322	0.415	5.92	1
T4420007	1993-Sep-14	49244.9714	0.0431	1.759	400.0	163.87	141.66	13.741	0.005	166.43	1.36	−0.001	0.315	0.413	6.18	0
T4420009	1993-Sep-14	49244.9807	0.0448	1.716	400.0	165.19	141.27	13.519	0.004	160.58	1.28	0.001	0.310	0.423	5.28	1
T4420011	1993-Sep-14	49244.9901	0.0466	1.674	400.0	165.62	141.12	13.721	0.004	159.41	1.33	−0.002	0.297	0.419	5.95	1
T4420013	1993-Sep-14	49244.9997	0.0484	1.632	400.0	165.34	141.18	13.549	0.003	158.67	1.11	−0.001	0.286	0.417	5.44	1
T4420015	1993-Sep-14	49245.0089	0.0501	1.595	400.0	163.80	140.48	13.479	0.003	162.37	1.03	0.006	0.278	0.417	5.28	1
T4420017	1993-Sep-14	49245.0182	0.0519	1.557	400.0	164.45	140.82	13.307	0.003	163.94	1.22	0.004	0.267	0.414	4.80	1
T4420019	1993-Sep-14	49245.0284	0.0538	1.519	400.0	164.56	141.00	13.268	0.004	163.78	1.32	0.001	0.260	0.418	4.73	1
T4420021	1993-Sep-14	49245.0374	0.0555	1.486	400.0	165.10	140.92	13.207	0.003	165.19	1.10	0.001	0.253	0.413	4.61	1
T4420023	1993-Sep-14	49245.0467	0.0572	1.454	400.0	165.01	141.70	13.063	0.003	157.85	1.31	0.002	0.242	0.417	4.15	1
T4420025	1993-Sep-14	49245.0600	0.0597	1.411	400.0	162.55	139.85	13.289	0.003	160.51	1.12	0.001	0.238	0.413	4.82	1
T4420027	1993-Sep-14	49245.0713	0.0618	1.377	400.0	164.24	143.86	13.276	0.003	163.34	1.00	0.000	0.231	0.425	4.81	1
T4420029	1993-Sep-14	49245.0828	0.0640	1.345	400.0	161.63	143.37	13.419	0.003	167.40	1.06	−0.002	0.231	0.424	5.40	1
T4420031	1993-Sep-14	49245.0927	0.0659	1.319	400.0	164.16	143.69	13.350	0.004	169.51	1.51	0.005	0.227	0.425	5.37	1
T4420034	1993-Sep-14	49245.1192	0.0708	1.258	400.0	164.06	144.19	13.387	0.008	179.88	3.57	−0.053	0.234	0.423	4.18	1
T4430001	1993-Sep-14	49245.1540	0.0773	1.194	400.0	163.83	143.45	13.266	0.003	176.93	1.11	0.000	0.224	0.425	5.03	1
T4430004	1993-Sep-14	49245.1806	0.0823	1.158	400.0	164.45	143.63	12.939	0.003	179.23	1.22	0.012	0.227	0.426	3.94	1
T4430007	1993-Sep-14	49245.2073	0.0873	1.131	400.0	166.30	143.36	13.087	0.003	171.46	1.05	0.005	0.226	0.422	4.41	1
T4440036	1993-Sep-16	49246.9299	0.4102	1.937	400.0	161.12	143.26	13.562	0.006	190.43	1.79	0.050	0.826	0.424	3.13	1
T4460006	1993-Sep-16	49246.9982	0.4230	1.616	400.0	163.41	144.71	13.652	0.005	169.92	1.43	0.011	0.854	0.429	3.57	1
T4460012	1993-Sep-16	49247.0791	0.4382	1.340	400.0	163.55	142.17	13.117	0.004	180.70	1.52	0.019	0.589	0.423	2.98	1
T4460018	1993-Sep-16	49247.1647	0.4542	1.171	400.0	163.03	142.83	12.725	0.003	172.97	1.59	0.015	0.382	0.426	2.56	1
T4460025	1993-Sep-16	49247.2328	0.4670	1.112	400.0	163.45	143.66	12.770	0.003	384.14	1.34	0.015	0.267	0.425	3.04	1
S1640033	1993-Sep-17	49247.9366	0.5989	1.889	400.0	163.16	141.21	12.909	0.002	186.14	0.92	0.011	0.220	0.424	3.27	1
S1640034	1993-Sep-17	49247.9422	0.5999	1.861	400.0	163.27	141.70	12.920	0.003	184.35	1.47	0.010	0.216	0.425	3.37	1
S1640035	1993-Sep-17	49247.9477	0.6010	1.834	400.0	163.39	141.13	12.883	0.003	181.45	1.21	0.014	0.211	0.432	3.25	1
T5940008	1994-Mar-14	49425.9174	0.9582	1.231	400.0	161.35	144.69	14.856	0.008	159.47	1.24	0.012	0.552	0.426	4.66	1
T5940018	1994-Mar-14	49426.0840	0.9894	1.784	400.0	162.26	142.86	14.494	0.008	188.27	1.39	0.004	0.936	0.424	3.89	1
T5940024	1994-Mar-14	49426.1522	0.0022	2.130	400.0	162.02	143.11	15.065	0.010	188.40	1.25	−0.006	0.782	0.431	5.88	1
T5990003	1994-Mar-16	49428.1892	0.3840	2.333	400.0	164.74	145.14	13.235	0.004	230.29	1.35	0.030	0.421	0.417	2.96	1
T5990004	1994-Mar-16	49428.1949	0.3851	2.357	400.0	164.23	144.94	12.929	0.004	234.22	1.81	0.035	0.441	0.420	2.58	1
T5990005	1994-Mar-16	49428.2013	0.3863	2.383	400.0	163.75	143.51	12.995	0.004	246.16	1.77	0.044	0.449	0.424	2.68	1
T5990006	1994-Mar-16	49428.2069	0.3873	2.404	400.0	163.80	144.15	13.000	0.004	258.40	1.62	0.033	0.475	0.427	2.66	1
T5990007	1994-Mar-16	49428.2124	0.3883	2.423	400.0	163.55	143.88	13.925	0.005	248.06	1.26	0.046	0.488	0.422	2.77	1
T5990008	1994-Mar-16	49428.2182	0.3894	2.442	400.0	162.51	144.15	13.692	0.006	292.88	1.64	0.037	0.504	0.422	2.87	1
T5990009	1994-Mar-16	49428.2237	0.3905	2.458	400.0	162.29	144.79	14.014	0.007	415.02	1.49	0.021	0.534	0.426	2.98	1
T5990010	1994-Mar-16	49428.2294	0.3915	2.473	400.0	162.60	144.17	14.186	0.007	999.24	1.06	0.027	0.528	0.427	2.88	1

Table A.5 cont.: HV 982 differential photometry – V.

Frame	Date	HJD −2400000.0	Orbital Phase	X	T	Row	Col	$m_{\rm raw}$	$\sigma_{m_{\rm raw}}$	sky	CHI	Sharp	$V-C$	$C-C$	Seeing (FWHM)	ILCA
T5990032	1994-Mar-22	49433.9769	0.4688	1.438	400.0	162.61	142.01	12.846	0.003	493.06	1.20	0.005	0.273	0.425	3.25	1
T5990035	1994-Mar-22	49434.0007	0.4732	1.521	400.0	162.53	142.59	13.047	0.003	478.80	1.26	0.009	0.245	0.420	3.92	1
T5990038	1994-Mar-22	49434.0247	0.4777	1.616	400.0	162.98	141.97	13.077	0.003	431.09	1.25	0.003	0.237	0.420	4.19	1
T6000003	1994-Mar-22	49434.0548	0.4834	1.749	400.0	164.30	140.93	12.815	0.003	259.29	1.21	0.016	0.229	0.418	3.13	1
T6000007	1994-Mar-22	49434.0856	0.4892	1.899	400.0	164.38	141.39	13.102	0.003	215.77	1.17	0.011	0.227	0.418	3.45	1
T6000010	1994-Mar-22	49434.1098	0.4937	2.024	400.0	163.82	141.33	13.091	0.003	258.53	1.32	0.000	0.216	0.424	4.08	1
T6000013	1994-Mar-22	49434.1344	0.4983	2.150	400.0	163.83	140.72	12.998	0.003	233.50	1.35	0.005	0.230	0.418	3.63	1
T6000016	1994-Mar-22	49434.1617	0.5034	2.284	400.0	162.20	141.03	13.079	0.003	234.72	1.20	0.003	0.224	0.420	4.05	1
T6000019	1994-Mar-22	49434.1882	0.5084	2.395	400.0	163.35	140.59	13.192	0.003	225.13	1.31	0.005	0.211	0.414	4.20	1
T6000022	1994-Mar-22	49434.2149	0.5134	2.478	400.0	161.53	141.29	13.141	0.003	229.38	1.34	0.004	0.242	0.419	4.09	1
T4760008	1994-Jun-08	49511.8388	0.0626	1.732	400.0	163.13	142.46	12.664	0.003	229.23	1.74	0.034	0.223	0.423	2.78	1
T4760011	1994-Jun-08	49511.8635	0.0672	1.851	400.0	163.17	142.47	12.860	0.003	175.96	1.35	0.016	0.236	0.421	3.13	1
T4760014	1994-Jun-08	49511.8875	0.0717	1.973	400.0	163.59	142.43	12.731	0.004	176.22	2.05	0.021	0.232	0.427	2.70	1
T4760017	1994-Jun-08	49511.9366	0.0809	2.224	400.0	161.22	142.27	13.177	0.003	188.62	1.31	0.020	0.239	0.417	3.03	1
T4760019	1994-Jun-08	49512.0009	0.0930	2.474	400.0	160.64	141.39	13.144	0.003	193.90	1.39	−0.003	0.222	0.420	3.89	1
T4760022	1994-Jun-08	49512.0249	0.0975	2.518	400.0	159.66	141.22	13.424	0.004	180.95	1.25	−0.002	0.226	0.423	4.05	1
T4760025	1994-Jun-08	49512.0699	0.1059	2.502	400.0	159.21	140.12	13.644	0.004	185.90	1.24	−0.001	0.243	0.415	5.34	1
T4760028	1994-Jun-08	49512.0959	0.1108	2.438	400.0	165.32	145.16	13.240	0.004	188.35	1.43	0.003	0.226	0.418	4.38	1
T4760031	1994-Jun-08	49512.1217	0.1156	2.342	400.0	164.18	144.35	13.246	0.003	195.15	1.12	0.000	0.243	0.420	4.33	1
T4760034	1994-Jun-08	49512.1456	0.1201	2.233	400.0	164.79	145.19	13.046	0.003	210.22	1.39	0.014	0.217	0.435	3.95	1
T4770002	1994-Jun-08	49512.1743	0.1255	2.088	400.0	164.02	143.90	13.230	0.003	204.59	1.22	0.002	0.233	0.412	4.42	1
T4770005	1994-Jun-08	49512.2002	0.1303	1.954	400.0	163.26	144.62	13.223	0.003	188.80	1.14	−0.001	0.226	0.417	4.60	1
T4770008	1994-Jun-08	49512.2188	0.1338	1.860	400.0	161.96	145.18	13.743	0.004	180.10	1.28	0.000	0.216	0.434	6.19	0
T4770014	1994-Jun-08	49512.2825	0.1458	1.572	400.0	159.83	145.79	12.849	0.003	220.26	1.40	0.013	0.223	0.423	3.54	1
T4770023	1994-Jun-14	49517.8117	0.1821	1.684	400.0	163.16	142.46	14.905	0.008	283.90	1.01	−0.027	0.213	0.442	3.61	1
T4790008	1994-Jul-29	49562.8886	0.6310	2.521	400.0	164.93	142.04	13.469	0.003	170.79	1.16	0.024	0.222	0.425	2.88	1
T4790014	1994-Jul-29	49562.9522	0.6429	2.452	400.0	164.14	140.88	12.779	0.003	149.89	1.35	0.012	0.206	0.422	2.93	1
T4790020	1994-Jul-29	49563.1487	0.6797	1.552	400.0	163.38	143.45	12.579	0.003	345.56	1.47	0.037	0.221	0.432	2.30	1
T4790033	1994-Jul-30	49563.9182	0.8239	2.517	400.0	161.01	140.48	13.094	0.004	151.35	1.52	0.012	0.211	0.425	3.86	1
T6400002	1994-Jul-30	49564.1491	0.8672	1.540	400.0	162.42	143.12	12.609	0.003	246.91	1.61	0.036	0.233	0.418	2.65	1
T6400005	1994-Jul-30	49564.1723	0.8716	1.456	400.0	161.51	143.20	12.607	0.004	236.75	2.08	0.046	0.232	0.419	2.63	1
T6400008	1994-Jul-30	49564.1957	0.8760	1.383	400.0	161.36	143.23	12.622	0.004	233.56	2.19	0.039	0.227	0.420	2.60	1
T6380002	1994-Aug-26	49591.0498	0.9093	1.643	400.0	163.76	144.82	12.748	0.003	458.68	1.52	0.026	0.231	0.418	3.04	1
T4880015	1994-Sep-02	49598.0070	0.2133	1.749	400.0	163.50	144.35	13.127	0.003	153.49	1.34	0.009	0.216	0.423	4.22	1
T4880019	1994-Sep-02	49598.0456	0.2205	1.581	400.0	162.28	143.77	13.155	0.003	154.80	1.17	0.002	0.222	0.414	4.57	1
T4880023	1994-Sep-02	49598.0847	0.2278	1.439	400.0	161.78	144.02	13.127	0.003	150.25	1.30	0.001	0.216	0.418	4.64	1
T4880027	1994-Sep-02	49598.1235	0.2351	1.326	400.0	161.09	144.46	13.480	0.003	151.76	1.18	0.000	0.210	0.421	5.66	1
T4880031	1994-Sep-02	49598.1648	0.2429	1.233	400.0	165.31	142.71	13.055	0.003	151.12	1.26	0.002	0.211	0.417	4.69	1
T4880035	1994-Sep-02	49598.2083	0.2510	1.165	400.0	164.60	143.55	13.043	0.003	151.01	1.49	0.007	0.222	0.412	4.54	1

Table A.5 cont.: HV 982 differential photometry – V.

Frame	Date	HJD −2400000.0	Orbital Phase	X	T	Row	Col	$m_{\rm raw}$	$\sigma_{m_{\rm raw}}$	sky	CHI	Sharp	$V-C$	$C-C$	Seeing (FWHM)	ILCA
T5610002	1994-Sep-03	49598.8613	0.3734	2.429	400.0	162.38	143.64	13.234	0.003	161.39	1.30	0.020	0.330	0.421	3.67	1
T5610005	1994-Sep-03	49598.8860	0.3780	2.335	400.0	162.21	143.90	13.387	0.004	155.23	1.35	0.007	0.361	0.416	4.13	1
T5610007	1994-Sep-03	49598.9063	0.3818	2.242	400.0	162.34	143.93	13.272	0.004	150.14	1.44	0.019	0.403	0.413	3.74	1
T5610010	1994-Sep-03	49598.9300	0.3863	2.124	400.0	161.57	142.83	14.875	0.007	102.52	1.17	0.006	0.466	0.404	4.10	1
T5610012	1994-Sep-03	49598.9465	0.3894	2.038	400.0	161.15	144.48	13.673	0.005	149.93	1.40	0.003	0.494	0.411	4.71	1
T5610014	1994-Sep-03	49599.1566	0.4288	1.244	400.0	163.72	144.48	15.111	0.010	140.85	1.38	0.043	0.760	0.435	3.40	1
T5610015	1994-Sep-03	49599.1625	0.4299	1.233	400.0	163.29	144.01	14.767	0.009	144.68	1.42	0.049	0.750	0.414	3.28	1
T5610016	1994-Sep-03	49599.1680	0.4309	1.222	400.0	163.20	143.98	13.637	0.005	153.30	1.68	0.053	0.727	0.417	3.08	1
T5610017	1994-Sep-03	49599.1740	0.4320	1.212	400.0	163.09	144.12	13.583	0.004	153.41	1.45	0.023	0.699	0.414	3.29	1
T5610019	1994-Sep-03	49599.1834	0.4338	1.196	400.0	162.92	144.25	14.153	0.006	148.91	1.38	0.044	0.679	0.415	3.22	1
T5610021	1994-Sep-03	49599.1923	0.4354	1.183	400.0	163.49	144.43	14.063	0.005	155.61	1.15	0.012	0.653	0.422	3.88	1
T5610023	1994-Sep-03	49599.2015	0.4372	1.170	400.0	163.04	144.92	13.207	0.004	156.92	1.46	0.016	0.614	0.419	3.60	1
T6460001	1994-Sep-04	49600.1967	0.6237	1.173	400.0	162.46	144.44	12.501	0.003	143.26	1.64	0.018	0.218	0.418	2.54	1
T5640033	1994-Oct-02	49628.0817	0.8502	1.235	400.0	163.85	142.01	12.897	0.003	202.31	1.24	0.007	0.224	0.418	3.79	1
T5690001	1994-Oct-02	49628.1342	0.8601	1.155	400.0	162.65	142.40	12.920	0.003	133.47	1.58	0.016	0.233	0.414	4.01	1
T5690022	1994-Oct-05	49631.0763	0.4115	1.230	400.0	163.88	142.83	14.003	0.007	154.47	1.76	0.058	0.836	0.416	2.99	1
T5690023	1994-Oct-05	49631.0819	0.4126	1.220	400.0	163.77	143.14	13.835	0.006	154.90	1.83	0.052	0.859	0.417	2.83	1
T5690024	1994-Oct-05	49631.0880	0.4137	1.209	400.0	163.90	142.78	13.789	0.008	153.58	2.33	0.074	0.861	0.426	2.88	1
T5690025	1994-Oct-05	49631.0935	0.4147	1.200	400.0	163.54	142.90	13.936	0.006	155.64	1.52	0.032	0.893	0.418	3.39	1
T5690026	1994-Oct-05	49631.0990	0.4158	1.192	400.0	163.93	143.21	13.966	0.005	155.75	1.40	0.024	0.897	0.425	3.41	1
T5690027	1994-Oct-05	49631.1046	0.4168	1.183	400.0	163.60	143.41	14.101	0.006	153.95	1.56	0.028	0.912	0.417	3.17	1
T5690028	1994-Oct-05	49631.1100	0.4179	1.175	400.0	163.50	143.10	14.465	0.008	151.74	1.67	0.057	0.916	0.428	2.91	1
T5690029	1994-Oct-05	49631.1155	0.4189	1.168	400.0	164.03	143.38	14.487	0.010	151.47	2.02	0.104	0.893	0.428	2.79	1
T5690030	1994-Oct-05	49631.1210	0.4199	1.161	400.0	163.73	143.35	14.597	0.008	150.86	1.40	0.034	0.916	0.420	2.70	1
T5690031	1994-Oct-05	49631.1265	0.4209	1.155	400.0	164.39	143.60	14.358	0.007	151.02	1.53	0.051	0.895	0.420	2.74	1
T5690032	1994-Oct-05	49631.1319	0.4219	1.149	400.0	163.89	143.61	14.393	0.007	153.09	1.44	0.059	0.874	0.428	2.59	1
T5690033	1994-Oct-05	49631.1374	0.4230	1.143	400.0	164.05	143.62	14.246	0.009	154.75	2.16	0.101	0.868	0.422	2.54	1
T5690034	1994-Oct-05	49631.1428	0.4240	1.138	400.0	164.04	143.97	14.154	0.008	156.43	1.88	0.078	0.842	0.426	2.65	1
T5690035	1994-Oct-05	49631.1483	0.4250	1.133	400.0	164.38	143.53	14.247	0.007	155.79	1.58	0.043	0.836	0.418	2.37	1
T5690036	1994-Oct-05	49631.1538	0.4260	1.129	400.0	164.01	143.81	14.222	0.008	154.43	1.92	0.081	0.800	0.430	2.45	1
T6050022	1994-Dec-26	49712.9940	0.7655	1.105	400.0	163.97	143.40	12.760	0.003	151.58	1.47	0.022	0.231	0.429	3.59	1
T6050025	1994-Dec-26	49713.0092	0.7684	1.107	400.0	164.53	143.71	12.895	0.004	146.55	1.79	0.003	0.220	0.435	4.00	1

Table A.6: HV 982 differential photometry – I.

Frame	Date	HJD −2400000.0	Orbital Phase	X	T	Row	Col	$m_{\rm raw}$	$\sigma_{m_{\rm raw}}$	sky	CHI	Sharp	$V-C$	$C-C$	Seeing (FWHM)	ILCA
T3870003	1993-Mar-26	49072.8926	0.7900	1.247	200.0	154.62	135.59	14.514	0.007	249.46	1.28	0.022	0.444	0.248	3.53	1

Table A.6 cont.: HV 982 differential photometry – I.

Frame	Date	HJD −2400000.0	Orbital Phase	X	T	Row	Col	$m_{\rm raw}$	$\sigma_{m_{\rm raw}}$	sky	CHI	Sharp	$V-C$	$C-C$	Seeing (FWHM)	ILCA
T3870004	1993-Mar-26	49072.9014	0.7917	1.265	200.0	163.93	141.42	14.325	0.006	206.91	1.25	0.017	0.435	0.254	3.71	1
T3870005	1993-Mar-26	49072.9224	0.7956	1.314	200.0	162.82	142.93	14.509	0.006	215.85	1.13	−0.002	0.431	0.259	4.36	1
T3870006	1993-Mar-26	49072.9309	0.7972	1.336	200.0	163.66	143.30	14.661	0.007	220.68	1.16	0.013	0.436	0.281	4.97	1
T3870007	1993-Mar-26	49072.9376	0.7985	1.354	200.0	162.29	142.64	14.830	0.008	229.40	1.18	−0.004	0.430	0.259	5.51	0
T3870008	1993-Mar-26	49072.9435	0.7996	1.371	200.0	164.06	140.93	14.965	0.010	244.68	1.22	−0.007	0.407	0.264	5.20	0
T3870009	1993-Mar-26	49072.9472	0.8003	1.382	200.0	163.05	141.74	14.941	0.010	252.00	1.24	−0.003	0.462	0.250	4.86	1
T3870010	1993-Mar-26	49072.9538	0.8015	1.401	200.0	163.16	141.39	14.797	0.008	253.96	1.11	0.003	0.429	0.277	4.73	1
T3870011	1993-Mar-26	49072.9586	0.8024	1.416	200.0	164.70	141.29	14.645	0.006	263.54	0.85	0.001	0.439	0.258	4.98	1
T3870012	1993-Mar-26	49072.9646	0.8035	1.435	200.0	163.94	141.80	14.690	0.007	262.42	1.12	0.002	0.416	0.271	5.05	0
T3870013	1993-Mar-26	49072.9698	0.8045	1.453	200.0	161.83	141.08	14.571	0.008	263.52	1.27	0.003	0.413	0.274	4.70	1
T3870014	1993-Mar-26	49072.9757	0.8056	1.473	200.0	163.64	140.44	14.756	0.009	268.24	1.55	−0.034	0.428	0.243	4.41	1
T3870015	1993-Mar-26	49072.9817	0.8067	1.494	200.0	164.60	141.99	14.786	0.007	275.16	1.00	0.006	0.415	0.283	5.27	0
T3870016	1993-Mar-26	49072.9857	0.8075	1.508	200.0	162.66	141.87	14.662	0.008	276.57	1.19	0.005	0.435	0.258	4.89	1
T3870017	1993-Mar-26	49072.9905	0.8084	1.526	200.0	164.10	142.17	14.718	0.009	279.97	1.25	0.007	0.419	0.286	4.92	1
T3870018	1993-Mar-26	49072.9944	0.8091	1.541	200.0	165.28	141.26	14.698	0.008	280.04	1.22	0.005	0.421	0.268	4.83	1
T3870019	1993-Mar-26	49072.9996	0.8101	1.561	200.0	162.67	141.37	14.625	0.008	284.82	1.19	0.002	0.440	0.266	4.59	1
T3870020	1993-Mar-26	49073.0034	0.8108	1.576	200.0	163.74	142.17	14.679	0.010	292.03	1.48	0.004	0.450	0.274	4.83	1
T3870021	1993-Mar-26	49073.0082	0.8117	1.596	200.0	164.98	141.68	14.651	0.008	302.39	1.15	0.016	0.438	0.255	4.74	1
T3870022	1993-Mar-26	49073.0135	0.8127	1.618	200.0	165.21	141.32	14.625	0.007	293.31	1.07	0.013	0.425	0.262	4.55	1
T3870023	1993-Mar-26	49073.0181	0.8136	1.637	200.0	165.12	140.90	14.849	0.009	300.08	1.17	−0.002	0.423	0.260	5.25	0
T3870024	1993-Mar-26	49073.0319	0.8161	1.702	700.0	165.74	142.07	13.568	0.005	1088.89	1.06	−0.001	0.410	0.269	5.93	0
T3870025	1993-Mar-26	49073.0468	0.8189	1.771	700.0	165.41	141.79	13.761	0.005	1069.46	1.03	0.000	0.408	0.266	6.68	0
T3990011	1993-Jun-29	49167.9635	0.6094	2.513	100.0	161.19	143.38	14.788	0.010	327.29	1.41	0.078	0.450	0.240	2.32	1
T3990022	1993-Jun-29	49168.1401	0.6425	1.968	100.0	160.56	141.25	14.860	0.010	231.13	1.49	0.076	0.431	0.243	2.78	1
T3990023	1993-Jun-29	49168.1436	0.6431	1.950	100.0	159.99	142.52	14.831	0.010	227.56	1.51	0.089	0.428	0.246	2.68	1
T3990024	1993-Jun-29	49168.1458	0.6435	1.939	100.0	159.47	142.05	14.843	0.010	216.15	1.44	0.096	0.445	0.246	2.64	1
T4080013	1993-Jul-01	49169.8851	0.9695	2.278	200.0	161.37	144.25	14.395	0.008	1007.68	1.07	0.077	0.904	0.245	1.88	1
T4080014	1993-Jul-01	49169.8889	0.9702	2.296	200.0	160.79	144.43	14.451	0.009	1003.94	1.14	0.048	0.917	0.226	2.29	1
T4080017	1993-Jul-01	49169.9326	0.9784	2.460	200.0	160.59	142.91	14.627	0.011	1050.69	1.33	0.078	1.048	0.245	2.08	1
T4080018	1993-Jul-01	49169.9375	0.9794	2.473	200.0	160.67	143.27	14.613	0.013	1056.24	1.57	0.080	1.065	0.230	1.92	1
T4080021	1993-Jul-01	49169.9765	0.9867	2.527	200.0	159.06	142.44	14.693	0.010	1078.54	1.15	0.091	1.130	0.231	2.08	1
T4080022	1993-Jul-01	49169.9804	0.9874	2.527	200.0	160.24	142.27	14.739	0.013	1100.89	1.32	0.070	1.137	0.242	2.35	1
T4080025	1993-Jul-01	49170.0288	0.9965	2.451	100.0	158.85	141.00	15.434	0.016	535.01	1.26	0.084	1.123	0.247	2.32	1
T4080026	1993-Jul-01	49170.0353	0.9977	2.431	100.0	160.16	141.47	15.477	0.018	534.12	1.34	0.070	1.109	0.231	2.61	1
T4080029	1993-Jul-01	49170.0704	0.0043	2.291	100.0	157.64	140.92	15.310	0.012	502.85	1.07	0.059	0.986	0.246	2.35	1
T4080030	1993-Jul-01	49170.0730	0.0047	2.280	100.0	158.52	141.16	15.305	0.013	505.77	1.12	0.063	0.970	0.229	2.39	1
T4080033	1993-Jul-01	49170.1100	0.0117	2.096	100.0	157.38	140.79	15.133	0.010	409.91	1.13	0.049	0.869	0.229	2.26	1
T4080034	1993-Jul-01	49170.1120	0.0121	2.085	100.0	157.27	141.20	15.231	0.011	402.11	1.05	0.006	0.866	0.249	3.02	1
T4080035	1993-Jul-01	49170.1154	0.0127	2.068	100.0	157.96	140.79	15.128	0.013	394.55	1.37	0.105	0.877	0.239	2.31	1

Table A.6 cont.: HV 982 differential photometry – I.

Frame	Date	HJD −2400000.0	Orbital Phase	X	T	Row	Col	$m_{\rm raw}$	$\sigma_{m_{\rm raw}}$	sky	CHI	Sharp	$V-C$	$C-C$	Seeing (FWHM)	ILCA
T4060019	1993-Jul-01	49170.1612	0.0213	1.834	100.0	156.55	142.71	14.960	0.013	301.53	1.76	0.141	0.735	0.250	2.26	1
T4060020	1993-Jul-01	49170.1644	0.0219	1.819	100.0	155.98	140.99	15.018	0.011	296.79	1.38	0.119	0.748	0.230	2.56	1
T4060023	1993-Jul-01	49170.1978	0.0281	1.664	100.0	159.00	142.23	14.915	0.014	229.49	2.06	0.142	0.675	0.246	2.45	1
T4060024	1993-Jul-01	49170.1998	0.0285	1.655	100.0	158.61	142.23	14.849	0.015	220.94	2.28	0.161	0.667	0.248	2.24	1
T4060025	1993-Jul-01	49170.2021	0.0289	1.645	100.0	158.56	142.39	14.869	0.015	221.23	2.28	0.162	0.669	0.245	2.23	1
T4060026	1993-Jul-01	49170.2044	0.0294	1.636	100.0	158.74	142.12	14.826	0.014	218.55	2.15	0.136	0.656	0.239	2.19	1
T4060027	1993-Jul-01	49170.2672	0.0411	1.405	100.0	164.10	140.51	14.736	0.018	95.75	3.29	0.209	0.572	0.237	2.32	1
T4060043	1993-Jul-02	49170.8329	0.1472	2.033	500.0	*	*	*	*	*	*	*	*	*	*	0
T4060044	1993-Jul-02	49170.8402	0.1485	2.070	400.0	162.24	144.82	13.147	0.006	2757.51	1.51	0.038	0.443	0.237	2.09	1
T4060045	1993-Jul-02	49170.8465	0.1497	2.102	300.0	161.84	144.53	13.470	0.007	2078.82	1.46	0.019	0.436	0.234	2.21	1
T4090001	1993-Jul-02	49170.8516	0.1507	2.127	200.0	162.10	144.01	13.873	0.008	1421.29	1.36	0.047	0.439	0.232	1.96	1
T4090002	1993-Jul-02	49170.8610	0.1524	2.174	150.0	161.60	144.23	14.204	0.011	1041.88	1.59	0.114	0.418	0.248	1.74	1
T4090003	1993-Jul-02	49170.8660	0.1534	2.199	200.0	161.38	144.64	13.864	0.008	1479.40	1.23	0.046	0.439	0.240	1.77	1
T4090008	1993-Jul-02	49170.9181	0.1632	2.424	200.0	160.05	143.21	13.965	0.010	1514.60	1.59	0.086	0.431	0.233	2.08	1
T4100027	1993-Jul-04	49172.8958	0.5338	2.361	200.0	159.07	144.56	14.114	0.008	1712.23	1.09	0.031	0.436	0.278	3.20	1
T4100028	1993-Jul-04	49172.9067	0.5359	2.404	300.0	159.65	144.90	13.896	0.008	2650.42	1.02	0.014	0.441	0.266	3.82	1
T4100029	1993-Jul-04	49172.9152	0.5375	2.433	300.0	158.77	145.38	14.015	0.009	2624.82	1.04	−0.005	0.444	0.272	4.20	1
T4100030	1993-Jul-04	49172.9208	0.5385	2.450	300.0	158.63	145.39	13.942	0.008	2614.27	1.06	0.015	0.445	0.269	3.95	1
T4220007	1993-Jul-22	49190.8257	0.8945	2.268	200.0	158.47	145.46	14.494	0.009	529.78	1.24	0.015	0.418	0.256	4.31	1
T4220015	1993-Jul-22	49190.9138	0.9110	2.525	200.0	157.37	143.99	14.856	0.009	390.36	1.05	0.004	0.421	0.251	5.31	0
T4220016	1993-Jul-22	49190.9259	0.9133	2.527	200.0	155.90	143.45	15.151	0.011	400.66	1.00	0.006	0.457	0.246	5.55	0
T4220017	1993-Jul-22	49190.9295	0.9139	2.525	200.0	156.31	143.70	15.232	0.014	395.51	1.30	0.001	0.418	0.279	5.52	0
T4220021	1993-Jul-22	49190.9565	0.9190	2.489	200.0	154.44	143.50	14.904	0.010	365.81	1.23	0.000	0.426	0.278	5.26	0
T4220022	1993-Jul-22	49190.9598	0.9196	2.482	200.0	157.77	143.81	14.850	0.012	363.95	1.49	0.006	0.430	0.250	4.94	1
T4220023	1993-Jul-22	49190.9633	0.9203	2.473	200.0	157.44	144.24	14.709	0.007	356.95	1.00	−0.007	0.428	0.266	4.46	1
T4220030	1993-Jul-22	49191.0193	0.9308	2.262	200.0	154.87	141.25	14.836	0.008	254.96	1.03	−0.001	0.485	0.264	4.91	1
T4220031	1993-Jul-22	49191.0237	0.9316	2.241	200.0	157.47	142.90	15.185	0.010	258.23	1.04	−0.003	0.493	0.256	5.82	0
T4230012	1993-Jul-23	49191.8757	0.0913	2.469	200.0	161.18	144.09	15.153	0.013	428.77	1.21	0.004	0.372	0.299	6.60	0
T4230013	1993-Jul-23	49191.8792	0.0919	2.477	200.0	160.44	143.21	15.050	0.012	438.79	1.20	0.026	0.401	0.275	6.14	0
T4230014	1993-Jul-23	49191.8829	0.0926	2.486	200.0	161.84	142.86	15.112	0.011	440.17	1.01	0.001	0.391	0.264	6.66	0
T4240021	1993-Jul-24	49193.0657	0.3143	1.999	200.0	*	*	*	*	*	*	*	*	0.248	2.88	1
T4240022	1993-Jul-24	49193.0708	0.3153	1.973	200.0	159.54	143.62	14.192	0.006	330.65	1.27	0.047	0.423	0.242	3.35	1
T4240023	1993-Jul-24	49193.0757	0.3162	1.948	200.0	159.20	142.48	14.132	0.007	312.38	1.49	0.044	0.435	0.231	3.13	1
T4240027	1993-Jul-24	49193.1081	0.3223	1.786	200.0	158.42	142.69	14.200	0.005	354.32	1.03	0.027	0.439	0.244	3.42	1
T4240029	1993-Jul-24	49193.1175	0.3240	1.742	200.0	158.27	143.05	13.984	0.008	311.45	1.98	0.086	0.437	0.244	2.59	1
T4240032	1993-Jul-24	49193.1467	0.3295	1.613	200.0	157.36	142.61	14.023	0.007	296.98	1.59	0.058	0.452	0.223	2.79	1
T4240034	1993-Jul-24	49193.1565	0.3313	1.574	200.0	157.40	143.71	13.969	0.008	300.64	1.87	0.080	0.441	0.232	2.67	1
T4250003	1993-Jul-24	49193.1986	0.3392	1.423	200.0	157.23	144.33	13.972	0.009	232.45	2.31	0.082	0.446	0.238	2.70	1
T4250006	1993-Jul-24	49193.2254	0.3442	1.344	200.0	161.38	143.56	14.047	0.006	222.30	1.38	0.046	0.453	0.224	2.84	1

Table A.6 cont.: HV 982 differential photometry – I.

Frame	Date	HJD −2400000.0	Orbital Phase	X	T	Row	Col	$m_{\rm raw}$	$\sigma_{m_{\rm raw}}$	sky	CHI	Sharp	$V-C$	$C-C$	Seeing (FWHM)	ILCA
T4250008	1993-Jul-24	49193.2352	0.3461	1.319	200.0	162.27	144.79	14.039	0.007	218.44	1.75	0.043	0.445	0.242	2.83	1
T4250009	1993-Jul-24	49193.2388	0.3468	1.310	200.0	160.51	142.47	14.130	0.006	209.51	1.51	0.064	0.449	0.229	3.26	1
T4250012	1993-Jul-24	49193.2666	0.3520	1.247	200.0	161.73	144.04	14.056	0.007	206.29	1.59	0.048	0.438	0.241	2.96	1
T4250014	1993-Jul-24	49193.2756	0.3537	1.230	200.0	160.88	144.10	14.023	0.009	197.41	2.18	0.076	0.466	0.233	2.83	1
T4250016	1993-Jul-24	49193.2854	0.3555	1.212	200.0	161.15	143.72	13.966	0.007	446.41	1.67	0.055	0.454	0.225	2.55	1
T4270005	1993-Jul-27	49196.0410	0.8720	2.085	200.0	161.03	142.33	14.181	0.006	460.67	1.22	0.036	0.445	0.239	3.04	1
T4270008	1993-Jul-27	49196.0682	0.8771	1.944	200.0	161.55	142.75	14.124	0.007	451.76	1.48	0.043	0.439	0.239	2.87	1
T4270010	1993-Jul-27	49196.0792	0.8791	1.888	200.0	159.67	142.52	14.100	0.007	430.86	1.45	0.045	0.431	0.239	2.84	1
T4270013	1993-Jul-27	49196.1061	0.8842	1.757	200.0	159.85	142.82	14.100	0.007	371.58	1.42	0.057	0.436	0.242	2.96	1
T4270015	1993-Jul-27	49196.1161	0.8861	1.711	200.0	159.70	143.40	14.067	0.007	361.15	1.50	0.062	0.441	0.242	2.80	1
T4270018	1993-Jul-27	49196.1402	0.8906	1.606	200.0	159.43	142.03	14.014	0.008	280.09	2.03	0.087	0.431	0.235	2.64	1
T4270020	1993-Jul-27	49196.1496	0.8923	1.569	200.0	159.78	142.49	14.034	0.008	280.73	1.94	0.091	0.437	0.242	2.66	1
T4270024	1993-Jul-27	49196.1832	0.8986	1.446	200.0	157.58	142.92	13.982	0.009	271.04	2.24	0.092	0.425	0.240	2.56	1
T4270028	1993-Jul-27	49196.2114	0.9039	1.360	200.0	157.52	142.75	14.029	0.007	213.28	1.74	0.061	0.418	0.253	2.84	1
T4270031	1993-Jul-27	49196.2368	0.9087	1.295	200.0	159.99	143.41	13.940	0.009	207.69	2.38	0.079	0.427	0.241	2.40	1
T4270033	1993-Jul-27	49196.2458	0.9104	1.274	200.0	160.07	143.57	13.913	0.008	218.60	2.03	0.082	0.431	0.232	2.23	1
T4270035	1993-Jul-27	49196.2643	0.9138	1.236	200.0	159.37	143.68	13.930	0.009	222.23	2.32	0.113	0.445	0.229	2.27	1
T4280001	1993-Jul-27	49196.2795	0.9167	1.208	200.0	159.78	144.10	13.932	0.011	220.48	2.78	0.123	0.444	0.229	2.28	1
T4280010	1993-Aug-15	49214.8567	0.3986	2.527	200.0	162.55	142.11	14.594	0.010	444.69	1.43	0.061	0.849	0.223	2.95	1
T4280011	1993-Aug-15	49214.8603	0.3993	2.527	200.0	161.95	141.41	14.530	0.010	431.65	1.55	0.071	0.853	0.243	2.64	1
T4280016	1993-Aug-15	49214.9028	0.4073	2.460	200.0	162.67	140.13	14.707	0.009	458.15	1.19	0.051	0.977	0.233	2.87	1
T4280017	1993-Aug-15	49214.9062	0.4079	2.450	200.0	161.98	140.46	14.764	0.009	477.91	1.14	0.047	1.013	0.220	3.02	1
T4280020	1993-Aug-15	49214.9468	0.4155	2.294	200.0	160.56	140.24	14.898	0.012	494.96	1.37	0.046	1.114	0.255	3.05	1
T4280021	1993-Aug-15	49214.9507	0.4163	2.276	200.0	161.18	140.73	14.962	0.010	509.78	1.06	0.004	1.110	0.243	3.43	1
T4280022	1993-Aug-15	49214.9600	0.4180	2.232	200.0	169.82	137.13	14.869	0.011	400.71	1.34	0.081	1.108	0.256	3.08	1
T4280023	1993-Aug-15	49214.9662	0.4192	2.202	200.0	161.07	143.82	14.991	0.010	381.01	1.13	0.064	1.124	0.253	3.46	1
T4280026	1993-Aug-15	49215.0013	0.4257	2.022	200.0	162.00	143.41	14.721	0.010	304.10	1.43	0.072	1.030	0.249	3.07	1
T4280027	1993-Aug-15	49215.0049	0.4264	2.003	200.0	162.60	143.55	14.696	0.010	304.78	1.56	0.083	0.999	0.248	3.07	1
T4280028	1993-Aug-15	49215.0086	0.4271	1.984	200.0	160.93	143.59	14.737	0.009	290.89	1.29	0.052	0.997	0.244	3.29	1
T4280029	1993-Aug-15	49215.0120	0.4278	1.966	200.0	162.12	143.56	14.715	0.010	293.12	1.44	0.051	0.967	0.251	3.23	1
T4280032	1993-Aug-15	49215.0455	0.4340	1.799	200.0	160.47	143.18	14.623	0.009	319.22	1.44	0.036	0.875	0.249	3.26	1
T4280033	1993-Aug-15	49215.0493	0.4347	1.780	200.0	160.51	142.43	14.528	0.009	323.17	1.57	0.073	0.847	0.247	3.08	1
T4280034	1993-Aug-15	49215.0526	0.4354	1.765	200.0	160.57	143.38	14.493	0.010	312.71	1.65	0.074	0.852	0.237	2.94	1
T4280035	1993-Aug-15	49215.0561	0.4360	1.748	200.0	160.08	143.20	14.416	0.011	331.96	2.03	0.104	0.842	0.238	2.78	1
S1250001	1993-Aug-15	49215.1080	0.4458	1.529	200.0	158.06	143.88	14.314	0.007	412.92	1.26	0.032	0.697	0.237	3.05	1
S1250002	1993-Aug-15	49215.1113	0.4464	1.517	200.0	158.71	143.21	14.300	0.006	417.36	1.17	0.029	0.685	0.247	3.04	1
S1250004	1993-Aug-15	49215.1299	0.4499	1.451	200.0	158.53	144.04	14.233	0.007	410.23	1.30	0.040	0.645	0.237	2.92	1
S1250005	1993-Aug-15	49215.1334	0.4505	1.440	200.0	158.80	143.97	14.248	0.006	388.80	1.18	0.043	0.636	0.254	3.05	1
S1250006	1993-Aug-15	49215.1371	0.4512	1.428	200.0	158.38	144.66	14.180	0.006	403.39	1.19	0.027	0.630	0.237	2.86	1

Table A.6 cont.: HV 982 differential photometry – I.

Frame	Date	HJD −2400000.0	Orbital Phase	X	T	Row	Col	$m_{\rm raw}$	$\sigma_{m_{\rm raw}}$	sky	CHI	Sharp	$V-C$	$C-C$	Seeing (FWHM)	ILCA
S1250008	1993-Aug-15	49215.1553	0.4546	1.372	200.0	157.62	143.46	14.130	0.006	444.27	1.23	0.046	0.580	0.247	2.93	1
S1250010	1993-Aug-15	49215.1785	0.4590	1.310	200.0	156.94	144.12	14.108	0.006	400.01	1.26	0.051	0.551	0.235	2.98	1
S1250011	1993-Aug-15	49215.1821	0.4596	1.301	200.0	157.94	145.10	14.077	0.009	389.57	1.87	0.089	0.536	0.246	2.90	1
S1250013	1993-Aug-15	49215.2004	0.4631	1.260	200.0	157.06	144.69	14.037	0.007	378.99	1.55	0.057	0.516	0.246	2.82	1
S1250014	1993-Aug-15	49215.2038	0.4637	1.253	200.0	156.15	144.92	14.129	0.006	396.12	1.25	0.020	0.511	0.253	3.54	1
S1250016	1993-Aug-15	49215.2267	0.4680	1.210	200.0	163.13	146.13	14.006	0.008	393.96	1.91	0.080	0.473	0.248	2.84	1
S1250017	1993-Aug-15	49215.2301	0.4686	1.204	200.0	164.69	143.23	13.953	0.006	386.66	1.44	0.034	0.496	0.244	2.55	1
S1250020	1993-Aug-15	49215.2663	0.4754	1.154	200.0	163.38	144.03	14.012	0.006	348.60	1.43	0.040	0.431	0.247	3.30	1
S1250021	1993-Aug-15	49215.2696	0.4760	1.150	200.0	163.12	143.95	13.966	0.009	370.70	2.04	0.091	0.453	0.243	2.82	1
S1290003	1993-Aug-18	49218.1000	0.0066	1.528	200.0	163.94	139.05	15.209	0.012	346.55	1.11	0.004	0.891	0.231	5.61	0
S1290005	1993-Aug-18	49218.1232	0.0109	1.446	200.0	165.05	141.73	15.066	0.009	317.93	1.02	−0.003	0.831	0.234	5.45	0
S1290007	1993-Aug-18	49218.1487	0.0157	1.368	200.0	166.41	140.95	15.268	0.013	287.17	1.39	0.004	0.779	0.246	6.63	0
S1290009	1993-Aug-18	49218.1690	0.0195	1.313	200.0	163.51	143.14	15.170	0.009	281.46	0.93	0.008	0.714	0.276	6.75	0
S1290011	1993-Aug-18	49218.1954	0.0244	1.253	200.0	164.77	140.68	14.952	0.009	288.26	1.13	0.011	0.686	0.227	5.90	0
S1290013	1993-Aug-18	49218.2188	0.0288	1.209	200.0	165.29	140.34	14.927	0.010	294.16	1.26	0.003	0.630	0.225	5.60	0
S1290015	1993-Aug-18	49218.2471	0.0341	1.167	200.0	160.35	142.28	14.938	0.009	318.63	1.10	−0.007	0.571	0.250	6.01	0
S1330003	1993-Aug-20	49220.0855	0.3787	1.563	200.0	163.35	140.79	15.250	0.012	255.84	1.30	0.089	0.572	0.243	3.05	1
S1330005	1993-Aug-20	49220.1061	0.3826	1.486	200.0	162.04	141.18	15.008	0.014	247.87	1.78	0.106	0.625	0.214	2.79	1
T0810012	1993-Sep-07	49237.9461	0.7264	1.982	200.0	163.11	141.79	13.889	0.009	224.61	2.44	0.095	0.426	0.233	2.39	1
T0810017	1993-Sep-07	49238.0084	0.7380	1.679	200.0	163.00	139.55	13.876	0.011	217.42	2.88	0.111	0.437	0.239	2.43	1
T0810022	1993-Sep-07	49238.0686	0.7493	1.446	200.0	162.06	139.07	13.765	0.012	272.59	3.31	0.115	0.432	0.236	2.10	1
S1620004	1993-Sep-08	49238.8652	0.8986	2.363	200.0	159.63	141.88	13.900	0.009	350.79	2.22	0.084	0.443	0.247	2.34	1
S1620006	1993-Sep-08	49238.8896	0.9032	2.255	200.0	159.97	143.05	13.991	0.008	296.00	1.90	0.077	0.452	0.237	2.63	1
S1620008	1993-Sep-08	49238.9105	0.9071	2.152	200.0	161.97	142.63	13.995	0.007	292.43	1.66	0.071	0.448	0.242	2.65	1
S1620010	1993-Sep-08	49238.9293	0.9106	2.055	200.0	157.09	140.60	13.955	0.006	288.03	1.56	0.057	0.443	0.235	2.48	1
S1620012	1993-Sep-08	49238.9502	0.9145	1.947	200.0	162.80	142.92	13.969	0.007	262.29	1.75	0.065	0.456	0.232	2.66	1
S1620014	1993-Sep-08	49238.9684	0.9179	1.855	200.0	159.79	141.57	13.984	0.008	259.78	1.95	0.076	0.461	0.236	2.55	1
S1620016	1993-Sep-08	49238.9878	0.9216	1.761	200.0	161.23	141.96	13.863	0.010	238.73	2.68	0.136	0.463	0.237	2.08	1
S1620018	1993-Sep-08	49239.0140	0.9265	1.643	200.0	161.44	143.21	13.925	0.009	251.85	2.40	0.099	0.482	0.229	2.33	1
S1620020	1993-Sep-08	49239.0329	0.9300	1.566	200.0	166.97	138.25	13.877	0.012	253.86	3.05	0.124	0.495	0.237	2.11	1
S1620022	1993-Sep-08	49239.0543	0.9341	1.486	200.0	164.34	137.81	13.977	0.009	241.81	2.42	0.095	0.512	0.259	2.48	1
S1620024	1993-Sep-08	49239.0733	0.9376	1.422	200.0	163.96	140.78	14.017	0.009	269.97	2.28	0.082	0.554	0.236	2.59	1
S1620026	1993-Sep-08	49239.0915	0.9410	1.367	200.0	163.24	140.59	14.070	0.008	278.43	1.98	0.076	0.573	0.244	2.56	1
S1620028	1993-Sep-08	49239.1100	0.9445	1.317	200.0	162.54	141.96	14.155	0.006	294.63	1.36	0.045	0.615	0.236	2.86	1
S1620030	1993-Sep-08	49239.1282	0.9479	1.274	200.0	162.62	141.87	14.099	0.008	294.22	1.86	0.077	0.645	0.246	2.45	1
S1620032	1993-Sep-08	49239.1462	0.9513	1.237	200.0	161.83	142.60	14.111	0.010	280.81	2.26	0.096	0.686	0.235	2.33	1
S1630002	1993-Sep-08	49239.1726	0.9562	1.191	200.0	161.69	142.58	14.171	0.007	284.80	1.60	0.066	0.740	0.221	2.40	1
S1630003	1993-Sep-08	49239.1773	0.9571	1.184	200.0	162.62	143.44	14.192	0.011	287.30	2.34	0.102	0.739	0.239	2.34	1
S1630005	1993-Sep-08	49239.1957	0.9606	1.160	200.0	164.98	142.74	14.240	0.009	274.99	1.85	0.081	0.766	0.246	2.53	1

Table A.6 cont.: HV 982 differential photometry – I.

Frame	Date	HJD −2400000.0	Orbital Phase	X	T	Row	Col	$m_{\rm raw}$	$\sigma_{m_{\rm raw}}$	sky	CHI	Sharp	$V-C$	$C-C$	Seeing (FWHM)	ILCA
S1630015	1993-Sep-11	49242.0457	0.4947	0.000	200.0	162.32	138.82	18.128	0.011	338.09	1.09	0.050	0.074	*	3.97	0
S1630016	1993-Sep-11	49242.0644	0.4982	0.000	200.0	161.83	138.04	17.264	0.054	284.91	1.14	0.089	0.550	0.291	0.00	0
T4410036	1993-Sep-14	49244.9168	0.0329	2.035	200.0	157.07	141.30	14.822	0.008	324.69	1.07	0.003	0.584	0.260	4.93	1
T4410038	1993-Sep-14	49244.9311	0.0356	1.961	200.0	156.25	140.13	15.085	0.012	339.27	1.36	0.025	0.575	0.249	5.92	0
T4420002	1993-Sep-14	49244.9454	0.0382	1.888	200.0	163.68	139.68	14.953	0.011	287.37	1.36	0.006	0.552	0.249	5.49	0
T4420004	1993-Sep-14	49244.9580	0.0406	1.825	200.0	164.19	141.15	14.985	0.009	266.00	1.03	0.002	0.526	0.257	5.71	0
T4420005	1993-Sep-14	49244.9612	0.0412	1.810	200.0	164.44	141.73	14.962	0.010	293.35	1.17	0.003	0.530	0.274	5.72	0
T4420008	1993-Sep-14	49244.9760	0.0440	1.739	200.0	163.22	140.90	14.906	0.008	238.04	1.08	−0.006	0.486	0.272	5.50	0
T4420010	1993-Sep-14	49244.9855	0.0457	1.696	200.0	164.59	141.09	15.053	0.010	238.16	1.20	−0.002	0.496	0.265	5.96	0
T4420012	1993-Sep-14	49244.9953	0.0476	1.653	200.0	162.53	140.66	14.811	0.009	220.04	1.27	0.001	0.469	0.259	5.43	0
T4420014	1993-Sep-14	49245.0041	0.0492	1.616	200.0	163.71	141.41	14.689	0.008	222.60	1.27	0.019	0.474	0.256	5.05	0
T4420016	1993-Sep-14	49245.0138	0.0511	1.576	200.0	162.51	141.48	14.704	0.008	216.27	1.22	0.010	0.475	0.253	4.91	1
T4420018	1993-Sep-14	49245.0227	0.0527	1.541	200.0	164.43	141.29	16.220	0.008	241.02	1.37	0.011	0.489	0.225	4.39	1
T4420020	1993-Sep-14	49245.0331	0.0547	1.503	200.0	163.76	140.83	14.450	0.008	212.92	1.43	0.023	0.447	0.256	4.22	1
T4420022	1993-Sep-14	49245.0421	0.0564	1.471	200.0	163.44	140.28	14.380	0.007	230.64	1.39	0.024	0.457	0.242	4.07	1
T4420024	1993-Sep-14	49245.0512	0.0581	1.440	200.0	164.27	139.09	14.383	0.006	206.45	1.16	0.013	0.449	0.248	4.13	1
T4420026	1993-Sep-14	49245.0661	0.0609	1.393	200.0	163.10	143.16	15.944	0.007	208.53	1.32	0.025	0.453	0.144	4.20	0
T4420028	1993-Sep-14	49245.0762	0.0628	1.364	200.0	164.09	141.88	14.575	0.006	225.53	1.05	0.004	0.434	0.261	4.82	1
T4420030	1993-Sep-14	49245.0882	0.0650	1.331	200.0	163.37	142.90	14.417	0.006	222.42	1.19	0.003	0.449	0.255	4.22	1
T4420032	1993-Sep-14	49245.0972	0.0667	1.309	200.0	163.60	143.18	14.353	0.007	229.89	1.28	0.031	0.433	0.257	4.12	1
T4420035	1993-Sep-14	49245.1258	0.0720	1.245	200.0	164.21	143.24	14.377	0.007	210.48	1.30	0.029	0.428	0.256	4.23	1
T4430002	1993-Sep-14	49245.1585	0.0782	1.188	200.0	164.27	143.90	14.471	0.006	244.03	1.12	0.008	0.425	0.257	4.53	1
T4430005	1993-Sep-14	49245.1866	0.0834	1.151	200.0	165.00	143.50	14.336	0.006	258.90	1.25	0.017	0.444	0.257	3.96	1
T4430008	1993-Sep-14	49245.2124	0.0883	1.127	200.0	162.03	143.17	14.315	0.006	245.17	1.09	0.019	0.459	0.244	4.00	1
T4440035	1993-Sep-16	49246.9254	0.4093	1.962	200.0	159.03	142.22	14.816	0.010	333.05	1.40	0.076	1.037	0.246	3.08	1
T4460005	1993-Sep-16	49246.9936	0.4221	1.637	200.0	162.49	143.88	15.096	0.012	259.10	1.42	0.040	1.087	0.248	4.06	1
T4460011	1993-Sep-16	49247.0747	0.4373	1.353	200.0	163.27	142.37	14.449	0.007	237.81	1.32	0.036	0.839	0.239	3.00	1
T4460017	1993-Sep-16	49247.1531	0.4520	1.188	200.0	162.67	143.45	14.181	0.007	294.06	1.53	0.065	0.644	0.240	2.75	1
T4460024	1993-Sep-16	49247.2280	0.4661	1.114	200.0	163.39	144.03	13.995	0.008	402.20	1.78	0.073	0.512	0.235	2.59	1
S1880020	1993-Nov-22	49313.9636	0.9745	1.197	200.0	167.59	142.95	15.047	0.010	509.40	1.01	0.031	0.971	0.248	3.72	1
S1880025	1993-Nov-22	49314.0408	0.9889	1.116	200.0	161.99	144.16	14.912	0.011	280.09	1.43	0.072	1.156	0.233	3.22	1
T5780020	1994-Feb-23	49406.9481	0.4027	1.194	200.0	161.74	144.39	14.961	0.010	386.23	1.19	−0.005	0.908	0.261	4.65	1
T5940017	1994-Mar-14	49426.0786	0.9884	1.756	200.0	161.10	144.76	15.150	0.011	400.04	1.03	0.021	1.137	0.254	4.17	1
T5940023	1994-Mar-14	49426.1468	0.0012	2.100	200.0	160.47	144.95	15.977	0.022	378.71	1.14	−0.003	1.027	0.256	5.53	0
T5990031	1994-Mar-22	49433.9723	0.4679	1.422	200.0	161.85	142.60	14.271	0.006	383.74	1.13	0.031	0.470	0.257	3.71	1
T5990034	1994-Mar-22	49433.9961	0.4724	1.503	200.0	162.26	143.30	14.396	0.006	423.63	1.03	0.009	0.466	0.261	4.18	1
T5990037	1994-Mar-22	49434.0200	0.4769	1.595	200.0	161.99	142.71	14.362	0.007	428.54	1.25	0.003	0.435	0.262	4.17	1
T6000002	1994-Mar-22	49434.0493	0.4824	1.722	200.0	162.69	143.92	13.986	0.007	363.88	1.68	0.053	0.436	0.253	2.83	1
T6000006	1994-Mar-22	49434.0811	0.4883	1.875	200.0	162.52	143.32	14.242	0.007	329.16	1.35	0.049	0.458	0.243	3.06	1

Table A.6 cont.: HV 982 differential photometry – I.

Frame	Date	HJD −2400000.0	Orbital Phase	X	T	Row	Col	$m_{\rm raw}$	$\sigma_{m_{\rm raw}}$	sky	CHI	Sharp	$V-C$	$C-C$	Seeing (FWHM)	ILCA
T6000009	1994-Mar-22	49434.1054	0.4929	1.999	200.0	162.49	142.50	14.134	0.005	416.48	1.07	0.025	0.433	0.244	3.51	1
T6000012	1994-Mar-22	49434.1298	0.4975	2.125	200.0	162.99	142.66	14.299	0.006	437.04	1.04	0.014	0.450	0.243	3.91	1
T6000015	1994-Mar-22	49434.1573	0.5026	2.261	200.0	160.68	142.77	14.312	0.007	435.82	1.26	0.018	0.424	0.261	4.00	1
T6000018	1994-Mar-22	49434.1809	0.5070	2.365	200.0	161.42	142.79	14.512	0.010	471.38	1.40	0.010	0.412	0.264	4.69	1
T6000021	1994-Mar-22	49434.2106	0.5126	2.466	200.0	158.49	141.82	14.427	0.007	428.20	1.11	0.009	0.435	0.255	4.36	1
T4760009	1994-Jun-08	49511.8439	0.0636	1.754	200.0	161.80	144.37	13.962	0.008	344.27	2.00	0.088	0.446	0.239	2.56	1
T4760012	1994-Jun-08	49511.8678	0.0680	1.871	200.0	161.33	144.66	14.426	0.008	329.77	1.43	0.069	0.442	0.266	3.16	1
T4760015	1994-Jun-08	49511.8922	0.0726	1.995	200.0	161.85	143.45	14.115	0.006	337.77	1.34	0.041	0.470	0.230	2.68	1
T4760018	1994-Jun-08	49511.9928	0.0915	2.451	200.0	158.09	143.27	14.963	0.009	321.97	1.11	0.024	0.451	0.243	3.17	1
T4760020	1994-Jun-08	49512.0051	0.0938	2.483	200.0	157.88	141.92	14.586	0.007	332.50	1.14	0.028	0.463	0.239	3.67	1
T4760023	1994-Jun-08	49512.0563	0.1034	2.521	200.0	156.99	141.07	14.239	0.006	399.73	1.04	0.023	0.423	0.245	3.41	1
T4760026	1994-Jun-08	49512.0745	0.1068	2.495	200.0	156.24	140.51	14.501	0.006	388.50	1.00	0.006	0.436	0.243	4.50	1
T4760029	1994-Jun-08	49512.1021	0.1120	2.419	200.0	161.77	144.85	14.469	0.008	432.35	1.17	0.004	0.462	0.257	4.45	1
T4760032	1994-Jun-08	49512.1262	0.1165	2.324	200.0	162.50	144.79	14.383	0.008	384.96	1.29	0.009	0.451	0.240	4.07	1
T4760035	1994-Jun-08	49512.1512	0.1212	2.207	200.0	163.01	143.99	14.370	0.006	353.78	1.09	0.011	0.443	0.243	3.95	1
T4770003	1994-Jun-08	49512.1790	0.1264	2.066	200.0	161.72	142.96	14.492	0.008	383.78	1.20	0.004	0.422	0.245	4.50	1
T4770006	1994-Jun-08	49512.2050	0.1312	1.931	200.0	161.38	144.33	14.495	0.007	352.91	1.11	0.005	0.431	0.249	4.43	1
T4770009	1994-Jun-08	49512.2232	0.1347	1.840	200.0	159.76	144.82	14.885	0.009	339.53	1.07	−0.002	0.368	0.267	6.09	0
T4770015	1994-Jun-08	49512.2867	0.1466	1.557	200.0	158.42	145.39	14.160	0.006	411.99	1.27	0.028	0.438	0.248	3.36	1
T4770024	1994-Jun-14	49517.8172	0.1831	1.707	200.0	162.14	143.36	15.488	0.015	454.62	1.14	0.022	0.434	0.241	3.35	1
T4790009	1994-Jul-29	49562.8935	0.6319	2.524	200.0	161.28	141.82	14.831	0.007	461.10	0.91	−0.010	0.445	0.259	2.84	1
T4790015	1994-Jul-29	49562.9564	0.6437	2.441	200.0	162.12	140.91	13.975	0.008	395.13	1.96	0.069	0.443	0.230	2.63	1
T4790021	1994-Jul-29	49563.1530	0.6805	1.537	200.0	162.53	144.59	13.880	0.008	455.26	1.81	0.043	0.463	0.229	2.25	1
T4790034	1994-Jul-30	49563.9260	0.8254	2.507	200.0	160.36	141.59	14.273	0.007	392.96	1.28	−0.007	0.456	0.234	3.89	1
T6400003	1994-Jul-30	49564.1534	0.8680	1.525	200.0	161.15	143.14	13.951	0.008	263.33	1.89	0.057	0.454	0.232	2.66	1
T6400006	1994-Jul-30	49564.1768	0.8724	1.443	200.0	160.85	142.62	13.962	0.007	269.19	1.67	0.041	0.461	0.236	2.80	1
T6400009	1994-Jul-30	49564.2000	0.8768	1.371	200.0	160.85	142.90	13.933	0.008	245.57	2.01	0.086	0.451	0.234	2.69	1
T6380003	1994-Aug-26	49591.0548	0.9102	1.623	200.0	162.40	144.31	14.170	0.007	392.72	1.46	0.040	0.458	0.251	3.47	1
T4880016	1994-Sep-02	49598.0115	0.2141	1.730	200.0	162.06	144.59	14.413	0.006	286.35	1.04	−0.003	0.434	0.251	4.50	1
T4880020	1994-Sep-02	49598.0501	0.2214	1.565	200.0	161.15	143.81	14.455	0.007	287.20	1.22	0.001	0.387	0.253	5.26	0
T4880024	1994-Sep-02	49598.0892	0.2287	1.426	200.0	159.41	143.85	14.545	0.006	260.94	0.93	0.003	0.417	0.245	5.37	0
T4880028	1994-Sep-02	49598.1287	0.2361	1.313	200.0	160.02	143.55	14.496	0.006	266.74	1.12	0.000	0.411	0.247	4.94	1
T4880032	1994-Sep-02	49598.1693	0.2437	1.226	200.0	164.72	142.60	14.460	0.008	267.04	1.42	−0.005	0.425	0.250	5.20	0
T4880036	1994-Sep-02	49598.2127	0.2518	1.160	200.0	163.79	143.75	14.394	0.006	261.31	1.13	0.007	0.407	0.253	4.79	1
T5610003	1994-Sep-03	49598.8666	0.3744	2.412	200.0	159.83	143.74	14.508	0.008	444.27	1.25	0.022	0.534	0.244	4.10	1
T5610008	1994-Sep-03	49598.9107	0.3827	2.222	200.0	160.02	143.35	14.682	0.009	309.99	1.36	0.016	0.625	0.221	4.02	1
T5610013	1994-Sep-03	49598.9508	0.3902	2.018	200.0	159.20	143.94	15.269	0.012	278.29	1.14	0.009	0.723	0.263	4.76	1
T5610018	1994-Sep-03	49599.1784	0.4328	1.205	200.0	162.33	144.00	15.143	0.012	309.06	1.30	0.051	0.878	0.259	3.49	1
T5610020	1994-Sep-03	49599.1878	0.4346	1.190	200.0	162.84	143.98	15.614	0.016	310.30	1.23	0.046	0.850	0.261	3.31	1

Table A.6 cont.: HV 982 differential photometry – I.

Frame	Date	HJD −2400000.0	Orbital Phase	X	T	Row	Col	$m_{\rm raw}$	$\sigma_{m_{\rm raw}}$	sky	CHI	Sharp	$V-C$	$C-C$	Seeing (FWHM)	ILCA
T5610022	1994-Sep-03	49599.1970	0.4363	1.177	200.0	162.29	144.45	14.546	0.008	293.06	1.28	0.044	0.842	0.251	3.45	1
T6460002	1994-Sep-04	49600.2013	0.6246	1.167	200.0	162.24	144.06	13.772	0.007	287.09	2.02	0.065	0.448	0.231	2.23	1
T5640034	1994-Oct-02	49628.0864	0.8511	1.227	200.0	163.32	141.98	14.243	0.006	247.95	1.13	0.003	0.434	0.243	4.44	1
T5690002	1994-Oct-02	49628.1387	0.8609	1.151	200.0	162.29	142.53	14.405	0.006	174.19	1.19	0.000	0.445	0.240	4.55	1
T6020006	1994-Dec-25	49712.0173	0.5825	1.108	200.0	163.10	144.04	14.173	0.007	196.73	1.54	0.045	0.424	0.264	3.53	1
T6020007	1994-Dec-25	49712.0201	0.5830	1.109	200.0	163.59	143.76	14.131	0.008	201.29	1.84	0.058	0.423	0.256	3.33	1
T6040006	1994-Dec-25	49712.0998	0.5979	1.176	400.0	164.14	144.44	13.421	0.005	483.73	1.70	0.035	0.415	0.270	3.51	1
T6040007	1994-Dec-25	49712.1049	0.5989	1.183	400.0	164.60	144.68	13.496	0.006	519.56	1.67	0.033	0.400	0.278	3.86	1
T6050023	1994-Dec-26	49712.9991	0.7665	1.105	400.0	163.76	144.34	13.515	0.004	428.02	1.27	0.013	0.433	0.276	4.29	1
T6050024	1994-Dec-26	49713.0041	0.7674	1.106	400.0	164.22	145.09	13.616	0.005	406.61	1.42	0.027	0.417	0.285	4.42	1
T6080007	1994-Dec-30	49717.0002	0.5164	1.107	200.0	164.99	145.77	14.957	0.009	221.24	1.14	0.006	0.377	0.294	7.13	0
T6080013	1994-Dec-30	49717.0606	0.5277	1.145	200.0	166.97	145.28	15.343	0.009	181.50	0.98	−0.006	0.340	0.315	7.72	0
T6080018	1994-Dec-30	49717.1251	0.5398	1.239	200.0	165.94	144.42	15.603	0.013	263.27	1.06	−0.006	0.365	0.332	8.23	0

A.2 HV 1620 differential photometry

Table A.7: HV 1620 differential photometry – u.

Frame	Date	HJD −2400000.0	Orbital Phase	X	T	Row	Col	$m_{\rm raw}$	$\sigma_{m_{\rm raw}}$	sky	CHI	Sharp	$V-C$	$C-C$	Seeing (FWHM)	ILCA
T3830011	1993-Mar-10	49057.0535	0.3970	2.198	600.0	178.95	274.24	15.752	0.013	139.49	1.10	0.006	1.120	−0.593	4.00	0
T3840010	1993-Mar-12	49058.9457	0.9188	1.890	600.0	178.56	270.97	16.423	0.019	40.73	1.31	0.011	1.173	−0.557	6.97	0
T3840012	1993-Mar-12	49058.9988	0.9334	2.077	600.0	176.85	272.80	16.355	0.016	53.30	1.05	0.005	1.216	−0.598	6.37	0
T3840013	1993-Mar-12	49059.0202	0.9393	2.139	600.0	176.03	276.78	15.683	0.011	55.72	1.14	−0.001	1.225	−0.581	3.76	0
T3960003	1993-May-23	49130.8894	0.7576	2.225	1200.0	177.41	268.86	14.376	0.005	46.71	1.21	0.005	0.833	−0.475	2.60	1
T4260026	1993-Jul-27	49195.8711	0.6766	1.845	1200.0	174.06	271.46	14.820	0.006	85.65	1.02	−0.003	0.848	−0.463	5.28	1
T4270001	1993-Jul-27	49195.9693	0.7037	1.499	1200.0	174.41	272.87	14.479	0.005	67.20	0.95	−0.004	0.814	−0.448	4.82	1
S1300006	1993-Aug-19	49218.9479	0.0402	1.384	1200.0	173.62	275.95	14.469	0.005	17.59	1.04	−0.001	1.228	−0.464	3.83	1
S1330007	1993-Aug-20	49220.1325	0.3668	1.140	1200.0	168.49	271.17	15.394	0.008	21.63	1.05	0.010	0.833	−0.457	3.79	1
T4430019	1993-Sep-15	49245.8864	0.4686	1.354	1200.0	171.48	274.62	15.689	0.011	15.87	1.26	0.012	1.007	−0.441	6.27	1
T4430022	1993-Sep-15	49245.9109	0.4754	1.301	1200.0	171.51	274.08	15.382	0.007	16.08	0.96	−0.008	1.048	−0.451	6.72	1
T4430025	1993-Sep-15	49245.9347	0.4819	1.257	1200.0	172.00	273.83	15.272	0.007	15.84	1.05	0.002	1.099	−0.475	6.32	1
T4430028	1993-Sep-15	49245.9584	0.4885	1.221	1200.0	172.32	273.03	14.933	0.006	13.18	0.99	0.000	1.092	−0.450	5.02	1
T4430031	1993-Sep-15	49245.9822	0.4950	1.191	1200.0	171.31	272.47	15.145	0.007	13.66	1.17	0.004	1.133	−0.441	5.25	1
T4430034	1993-Sep-15	49246.0074	0.5020	1.167	1200.0	170.56	271.47	15.154	0.006	12.08	1.03	0.000	1.141	−0.463	5.04	1
T4430037	1993-Sep-15	49246.0316	0.5087	1.151	1200.0	170.42	270.89	14.924	0.006	11.96	1.09	−0.001	1.132	−0.456	5.22	1
T4440003	1993-Sep-15	49246.0651	0.5179	1.140	1200.0	170.55	269.48	14.900	0.006	13.24	1.01	−0.002	1.131	−0.461	4.75	1

Table A.7 cont.: HV 1620 differential photometry – u.

Frame	Date	HJD −2400000.0	Orbital Phase	X	T	Row	Col	$m_{\rm raw}$	$\sigma_{m_{\rm raw}}$	sky	CHI	Sharp	$V-C$	$C-C$	Seeing (FWHM)	ILCA
T4440006	1993-Sep-15	49246.0908	0.5250	1.139	1200.0	170.49	268.52	14.788	0.006	14.05	1.14	−0.007	1.101	−0.461	4.88	1
T4440009	1993-Sep-15	49246.1347	0.5371	1.156	1200.0	170.36	266.36	14.654	0.006	44.89	1.29	0.002	1.058	−0.453	4.36	1
T4440012	1993-Sep-15	49246.1623	0.5447	1.177	1200.0	169.59	265.83	14.840	0.005	29.78	0.98	−0.005	1.030	−0.446	4.38	1
T4440015	1993-Sep-15	49246.1862	0.5513	1.203	1200.0	169.60	265.45	14.839	0.006	23.17	1.18	0.002	1.007	−0.461	4.05	1
T4440018	1993-Sep-15	49246.2255	0.5621	1.261	1200.0	169.71	266.79	14.648	0.005	27.19	1.04	−0.015	0.982	−0.446	3.08	1
T5440002	1994-Jan-19	49372.0365	0.2551	1.698	1200.0	174.15	270.53	15.259	0.008	22.19	1.14	−0.003	0.807	−0.450	6.97	1
T5780002	1994-Feb-22	49405.9073	0.5952	1.571	1200.0	168.63	265.74	15.011	0.008	134.10	1.02	−0.009	0.922	−0.455	5.90	1
T5780028	1994-Feb-23	49407.0738	0.9168	2.153	1200.0	176.68	269.52	14.950	0.008	149.33	1.11	−0.007	0.936	−0.441	4.30	1
T5820013	1994-Mar-12	49423.9338	0.5661	1.844	1200.0	175.32	268.94	14.573	0.005	18.42	1.11	−0.009	0.958	−0.454	3.31	1
T5820016	1994-Mar-12	49424.1608	0.6287	2.121	1200.0	175.52	270.10	14.652	0.005	18.59	0.95	−0.009	0.881	−0.461	3.82	1
T5960011	1994-Mar-17	49428.9493	0.9491	1.952	1200.0	174.89	269.49	15.503	0.009	15.88	1.23	−0.002	1.081	−0.470	6.56	1
T5960017	1994-Mar-17	49429.0333	0.9723	2.191	1200.0	178.78	274.45	16.535	0.020	15.94	1.45	−0.003	1.255	−0.469	4.99	1
T5960030	1994-Mar-21	49432.8899	0.0358	1.770	1200.0	175.95	265.39	14.452	0.006	61.46	1.35	−0.015	0.302	0.594	2.59	0
T5960036	1994-Mar-21	49432.9413	0.0499	1.962	1200.0	177.62	266.70	14.613	0.006	51.09	1.18	0.014	1.168	−0.457	3.16	1
T5980006	1994-Mar-21	49432.9948	0.0647	2.132	1200.0	179.08	269.31	14.769	0.006	24.08	1.11	0.016	1.035	−0.463	3.37	1
T5980009	1994-Mar-21	49433.0195	0.0715	2.186	1200.0	178.48	270.16	14.887	0.005	19.08	0.93	0.012	1.005	−0.459	4.03	1
T5980015	1994-Mar-21	49433.0616	0.0831	2.226	1200.0	175.02	274.01	14.987	0.006	18.93	1.03	0.004	0.936	−0.464	5.13	1
T5980021	1994-Mar-21	49433.1132	0.0973	2.176	1200.0	178.39	271.91	14.853	0.006	18.54	1.03	−0.003	0.912	−0.470	4.37	1
T5980027	1994-Mar-21	49433.1680	0.1124	2.025	1200.0	178.02	273.92	14.709	0.006	17.45	1.12	0.010	0.912	−0.462	4.13	1
T6220008	1994-Mar-21	49433.2145	0.1253	1.855	1200.0	177.24	275.01	14.647	0.005	28.38	1.12	0.002	0.899	−0.452	4.38	1
T5470010	1994-Mar-24	49435.8933	0.8640	1.813	1200.0	176.43	265.56	14.542	0.006	184.64	1.04	0.004	0.883	−0.466	4.02	1
T5470013	1994-Mar-24	49435.9168	0.8704	1.902	1200.0	176.20	265.49	14.617	0.005	187.13	0.90	−0.014	0.900	−0.462	4.00	1
T5470019	1994-Mar-24	49435.9660	0.8840	2.073	1200.0	178.09	267.91	14.967	0.007	193.81	0.98	−0.006	0.912	−0.443	4.45	1
T5470025	1994-Mar-24	49436.0155	0.8977	2.193	1200.0	178.20	271.04	15.063	0.009	185.96	1.19	−0.001	0.950	−0.463	4.71	1
T5470031	1994-Mar-24	49436.0578	0.9093	2.226	1200.0	179.34	272.72	15.291	0.009	156.50	1.01	−0.001	0.962	−0.457	5.27	1
T5470037	1994-Mar-24	49436.1175	0.9258	2.149	1200.0	177.26	274.50	15.572	0.008	68.34	0.82	0.010	0.961	−0.485	6.97	0
T5060010	1994-Apr-06	49448.9147	0.4547	2.020	1200.0	176.84	269.72	14.591	0.004	20.93	0.86	−0.004	0.998	−0.455	3.32	1
T5060012	1994-Apr-06	49448.9408	0.4619	2.103	1200.0	178.17	271.08	14.687	0.005	19.86	0.94	−0.010	1.018	−0.447	3.39	1
T5060020	1994-Apr-06	49448.9985	0.4778	2.216	1200.0	178.20	275.10	15.411	0.008	17.02	1.18	−0.003	1.069	−0.451	4.41	1
T5060027	1994-Apr-06	49449.0752	0.4989	2.165	1200.0	176.89	277.54	16.202	0.016	38.85	1.19	−0.006	1.117	−0.456	8.01	1
T5300004	1994-May-16	49488.8640	0.4709	2.177	1200.0	178.53	268.77	15.247	0.007	28.31	1.00	0.003	1.053	−0.468	5.56	1
T5300007	1994-May-16	49488.9007	0.4810	2.223	1200.0	178.96	270.75	15.152	0.007	23.75	1.19	−0.002	1.090	−0.457	4.72	1
T5300010	1994-May-16	49488.9345	0.4903	2.216	1200.0	178.93	272.54	15.191	0.007	20.00	1.09	−0.001	1.114	−0.464	4.75	1
T5300013	1994-May-16	49488.9675	0.4994	2.165	1200.0	178.34	273.30	15.121	0.007	21.72	1.10	0.002	1.133	−0.457	4.70	1
T5300016	1994-May-16	49489.0016	0.5088	2.076	1200.0	178.62	275.11	15.136	0.006	21.55	0.96	0.000	1.145	−0.452	4.90	1
T5300019	1994-May-16	49489.0349	0.5180	1.963	1200.0	177.78	275.16	14.761	0.005	20.59	0.89	0.002	1.124	−0.447	3.77	1
T5300022	1994-May-16	49489.0643	0.5261	1.854	1200.0	177.88	275.61	14.663	0.004	21.16	0.90	−0.007	1.114	−0.461	3.86	1
T5300026	1994-May-16	49489.1058	0.5376	1.698	1200.0	177.29	276.60	14.551	0.004	20.66	0.94	−0.010	1.058	−0.457	4.07	1
T5300030	1994-May-16	49489.1564	0.5515	1.525	1200.0	177.52	278.89	14.949	0.007	24.75	1.20	0.000	*	*	5.86	0

Table A.7 cont.: HV 1620 differential photometry – u.

Frame	Date	HJD −2400000.0	Orbital Phase	X	T	Row	Col	$m_{\rm raw}$	$\sigma_{m_{\rm raw}}$	sky	CHI	Sharp	$V-C$	$C-C$	Seeing (FWHM)	ILCA
T5300034	1994-May-16	49489.1986	0.5632	1.404	1200.0	170.51	274.33	14.400	0.005	23.24	1.15	−0.001	0.975	−0.457	4.36	1
T5440024	1994-Jun-10	49514.1389	0.4406	1.384	1200.0	172.71	275.18	14.251	0.004	12.84	0.92	−0.002	0.948	−0.451	3.96	1
T4580013	1994-Jun-12	49515.8014	0.8990	2.195	1200.0	177.90	270.56	15.337	0.007	17.31	0.99	−0.001	0.959	−0.461	5.34	1
T4580016	1994-Jun-12	49515.8853	0.9221	2.184	1200.0	178.42	275.57	15.120	0.007	14.43	1.04	0.002	0.943	−0.461	5.24	1
T4580022	1994-Jun-12	49515.9325	0.9352	2.064	1200.0	178.51	274.82	14.989	0.007	13.73	1.27	−0.005	0.997	−0.460	4.86	1
T4580028	1994-Jun-12	49515.9748	0.9468	1.917	1200.0	177.91	276.15	14.970	0.006	12.10	1.04	−0.002	1.062	−0.464	4.97	1
T4580034	1994-Jun-12	49516.0252	0.9607	1.727	1200.0	173.61	275.23	14.806	0.004	11.03	0.81	0.003	1.146	−0.458	4.34	1
T4590003	1994-Jun-12	49516.0776	0.9752	1.544	1200.0	173.54	276.39	14.615	0.005	11.08	1.01	−0.003	1.259	−0.453	3.66	1
T4590009	1994-Jun-12	49516.1202	0.9869	1.419	1200.0	173.37	276.78	14.526	0.006	10.27	1.25	0.015	1.355	−0.445	3.26	1
T4590015	1994-Jun-12	49516.1740	0.0018	1.294	1200.0	172.49	273.10	14.622	0.005	10.97	1.11	−0.001	1.425	−0.455	3.64	1
T4590021	1994-Jun-12	49516.2223	0.0151	1.215	1200.0	172.02	271.69	14.705	0.006	11.93	1.19	−0.001	1.410	−0.459	4.05	1
T4590027	1994-Jun-12	49516.2643	0.0267	1.169	1200.0	171.24	271.63	15.703	0.009	11.77	1.06	−0.007	1.331	−0.451	4.09	1
T4810010	1994-Jul-30	49564.0160	0.1944	1.354	1200.0	173.02	274.30	13.878	0.004	8.53	1.08	−0.023	0.813	−0.460	3.03	1
T4810018	1994-Jul-30	49564.2523	0.2596	1.149	1200.0	169.39	270.75	13.771	0.004	29.74	1.12	−0.010	0.769	−0.451	3.07	1
T4810021	1994-Jul-30	49564.2739	0.2656	1.162	1200.0	169.36	269.46	13.836	0.003	38.15	0.84	−0.001	0.774	−0.458	3.19	1
T4810033	1994-Jul-31	49564.8152	0.4148	2.013	1200.0	174.08	274.64	14.558	0.004	14.12	0.92	−0.001	0.918	−0.462	3.79	1
T6360001	1994-Jul-31	49564.8638	0.4282	1.834	1200.0	173.40	275.89	14.355	0.004	10.32	0.91	0.009	0.931	−0.456	3.48	1
T6360007	1994-Jul-31	49564.9155	0.4425	1.643	1200.0	173.18	277.18	15.760	0.011	8.11	1.33	−0.001	0.889	−0.461	3.67	1
T6370007	1994-Aug-01	49565.8060	0.6880	2.035	1200.0	176.21	273.27	14.894	0.005	15.19	0.96	−0.002	0.834	−0.472	5.22	1
T6370010	1994-Aug-01	49565.8298	0.6946	1.952	1200.0	175.60	274.68	15.318	0.020	13.79	1.46	−0.007	0.821	−0.458	4.72	1
T6370013	1994-Aug-01	49565.8530	0.7010	1.865	1200.0	175.82	275.55	16.565	0.019	12.17	1.41	0.001	0.805	−0.420	5.37	0
T4780004	1994-Aug-25	49589.8245	0.3113	1.725	1200.0	175.34	274.24	14.434	0.005	37.80	1.12	−0.014	0.828	−0.465	4.32	1
T4780010	1994-Aug-25	49589.8720	0.3243	1.559	1200.0	175.15	276.64	14.092	0.004	31.99	1.11	−0.010	0.819	−0.463	3.47	1
T4780016	1994-Aug-25	49589.9194	0.3374	1.417	1200.0	174.72	277.48	14.290	0.004	27.36	0.91	−0.003	0.819	−0.460	4.43	1
T4780019	1994-Aug-25	49590.0392	0.3704	1.193	1200.0	172.56	271.26	13.827	0.003	83.74	0.90	−0.004	0.840	−0.456	3.46	1
T4780025	1994-Aug-25	49590.0895	0.3843	1.151	1200.0	171.64	269.71	13.743	0.003	90.47	0.96	−0.014	0.857	−0.464	3.14	1
T4780032	1994-Aug-25	49590.1482	0.4005	1.139	1200.0	171.68	267.20	13.761	0.003	97.96	0.97	0.006	0.864	−0.457	3.18	1
T4850002	1994-Aug-25	49590.1943	0.4132	1.156	1200.0	170.71	264.79	13.823	0.003	96.94	1.02	0.006	0.887	−0.451	3.28	1
T4850006	1994-Aug-25	49590.2340	0.4242	1.191	1200.0	170.11	270.57	13.833	0.003	94.80	0.93	−0.028	0.905	−0.455	3.23	1
T4850019	1994-Aug-31	49595.8183	0.9641	1.687	1200.0	174.71	274.69	14.364	0.005	19.77	1.26	−0.005	1.182	−0.461	3.01	1
T4850024	1994-Aug-31	49596.0772	0.0355	1.149	1200.0	170.91	273.36	14.548	0.004	11.19	0.89	−0.005	1.257	−0.459	4.51	1
T4850027	1994-Aug-31	49596.1096	0.0444	1.139	1200.0	170.78	271.59	14.419	0.005	11.53	1.04	−0.009	1.181	−0.456	4.04	1
T4850030	1994-Aug-31	49596.1451	0.0542	1.142	1200.0	171.10	269.52	15.417	0.024	14.13	0.95	0.072	1.101	−0.437	3.98	1
T4850033	1994-Aug-31	49596.1721	0.0616	1.153	1200.0	170.26	267.82	14.300	0.004	14.24	0.85	0.000	1.044	−0.461	4.25	1
T4850036	1994-Aug-31	49596.2051	0.0707	1.178	1200.0	171.88	271.28	13.980	0.004	15.35	1.03	−0.014	0.982	−0.461	3.43	1
T7370026	1995-Apr-12	49820.0719	0.8031	2.137	1200.0	178.86	272.21	14.392	0.006	162.68	1.19	−0.021	0.836	−0.476	3.67	1
T7370031	1995-Apr-12	49820.1293	0.8190	1.955	1200.0	177.40	271.95	15.084	0.010	80.80	1.53	−0.026	0.830	−0.438	3.63	1
T7370036	1995-Apr-12	49820.1875	0.8350	1.736	1200.0	177.19	273.52	14.232	0.007	16.96	1.88	−0.062	0.842	−0.455	3.07	1
T7430009	1995-May-08	49846.2074	0.0101	1.440	1200.0	175.01	274.33	14.978	0.007	26.11	1.11	−0.004	1.418	−0.458	5.05	1

Table A.7 cont.: HV 1620 differential photometry – u.

Frame	Date	HJD −2400000.0	Orbital Phase	X	T	Row	Col	$m_{\rm raw}$	$\sigma_{m_{\rm raw}}$	sky	CHI	Sharp	$V-C$	$C-C$	Seeing (FWHM)	ILCA
T7430013	1995-May-08	49846.2470	0.0210	1.340	1200.0	173.89	274.88	14.726	0.006	23.16	1.13	−0.003	1.371	−0.453	4.51	1
T7210017	1995-May-10	49848.0451	0.5169	1.987	1200.0	174.25	272.89	15.097	0.008	82.78	1.23	0.039	1.137	−0.459	3.87	1
T7210021	1995-May-10	49848.0849	0.5278	1.839	1200.0	173.98	274.39	14.796	0.007	45.26	1.30	−0.016	1.096	−0.452	4.23	1
T7210025	1995-May-10	49848.1296	0.5402	1.673	1200.0	173.54	275.67	15.069	0.007	17.60	1.15	0.001	1.050	−0.456	4.36	1
T7210029	1995-May-10	49848.1631	0.5494	1.557	1200.0	173.68	277.00	15.678	0.010	15.38	1.17	−0.023	1.012	−0.444	3.66	1

Table A.8: HV 1620 differential photometry – v.

Frame	Date	HJD −2400000.0	Orbital Phase	X	T	Row	Col	$m_{\rm raw}$	$\sigma_{m_{\rm raw}}$	sky	CHI	Sharp	$V-C$	$C-C$	Seeing (FWHM)	ILCA
T3840014	1993-Mar-12	49059.0290	0.9418	2.160	600.0	176.40	276.79	15.819	0.015	66.68	1.46	0.062	2.767	−1.227	3.47	1
T3960004	1993-May-23	49130.9051	0.7620	2.223	1200.0	172.84	268.68	14.465	0.007	43.48	1.55	0.058	2.545	−1.220	2.83	1
T4260031	1993-Jul-27	49195.9087	0.6870	1.704	1200.0	171.63	268.76	14.762	0.007	87.63	1.27	−0.006	2.498	−1.178	4.54	0
T4270002	1993-Jul-27	49195.9845	0.7079	1.455	1200.0	172.06	270.38	14.599	0.005	72.87	1.04	−0.001	2.504	−1.192	4.05	1
T5440003	1994-Jan-19	49372.0536	0.2599	1.762	1200.0	170.43	269.70	15.357	0.010	27.73	1.39	0.000	2.494	−1.206	6.43	1
T5780004	1994-Feb-22	49405.9477	0.6063	1.713	1200.0	172.03	266.76	15.065	0.009	151.32	1.23	0.005	2.581	−1.189	5.51	1
T5780029	1994-Feb-23	49407.0921	0.9219	2.190	1200.0	174.73	268.84	15.527	0.012	178.45	1.15	0.024	2.621	−1.211	3.48	1
T5820014	1994-Mar-12	49424.1270	0.6194	2.194	1200.0	171.57	268.41	14.934	0.009	19.84	1.55	0.060	2.594	−1.213	3.54	1
T5820017	1994-Mar-12	49424.1761	0.6329	2.077	1200.0	172.09	266.14	14.597	0.008	21.72	1.75	0.029	2.587	−1.220	3.43	1
T5960013	1994-Mar-17	49428.9681	0.9543	2.018	1200.0	172.58	269.41	15.846	0.010	20.45	1.09	0.006	2.799	−1.214	5.40	1
T5960033	1994-Mar-21	49432.9168	0.0432	1.871	1200.0	174.40	265.96	14.573	0.011	70.53	2.17	0.081	2.897	−1.225	2.59	1
T5980018	1994-Mar-21	49433.0874	0.0902	2.214	1200.0	175.05	270.45	14.742	0.008	20.85	1.59	0.021	2.605	−1.219	3.60	1
T5470016	1994-Mar-24	49435.9418	0.8773	1.993	1200.0	174.34	266.99	14.945	0.010	212.94	1.29	−0.001	2.587	−1.186	4.57	1
T5470034	1994-Mar-24	49436.0823	0.9161	2.211	1200.0	173.12	272.46	15.479	0.015	178.77	1.41	0.001	2.648	−1.200	5.51	1
T5060017	1994-Apr-06	49448.9739	0.4710	2.182	1200.0	173.91	272.80	15.193	0.012	23.79	1.85	0.068	2.748	−1.210	3.65	1
T5300006	1994-May-16	49488.8824	0.4760	2.207	1200.0	174.86	268.92	15.216	0.008	34.16	1.23	−0.005	2.753	−1.217	4.90	1
T5300015	1994-May-16	49488.9861	0.5046	2.120	1200.0	173.87	271.57	15.151	0.013	25.73	2.01	−0.072	2.810	−1.215	4.54	1
T5300025	1994-May-16	49489.0901	0.5332	1.756	1200.0	174.93	273.93	14.959	0.007	24.18	1.21	0.013	2.791	−1.212	4.43	1
T5440027	1994-Jun-10	49514.1619	0.4469	1.330	1200.0	170.68	272.99	15.178	0.007	19.24	1.11	0.012	2.677	−1.215	4.33	1
T4580012	1994-Jun-12	49515.8611	0.9155	2.217	1200.0	174.61	272.50	15.080	0.007	22.89	1.20	0.012	2.637	−1.216	4.81	1
T4580031	1994-Jun-12	49516.0013	0.9541	1.817	1200.0	170.32	271.78	15.051	0.007	19.31	1.18	0.003	2.781	−1.218	4.58	1
T4590012	1994-Jun-12	49516.1443	0.9936	1.358	1200.0	170.97	274.40	14.912	0.009	19.69	1.76	0.049	3.062	−1.216	3.45	1
T4810011	1994-Jul-30	49564.0306	0.1984	1.321	1200.0	170.65	271.68	14.171	0.006	15.43	1.59	0.015	2.520	−1.216	2.90	1
T4810036	1994-Jul-31	49564.8387	0.4213	1.929	1200.0	170.00	272.49	14.671	0.008	18.37	1.69	0.033	2.626	−1.214	3.67	1
T4780007	1994-Aug-25	49589.8482	0.3178	1.639	1200.0	172.66	273.14	14.399	0.006	40.78	1.45	0.021	2.529	−1.215	3.64	1
T4780022	1994-Aug-25	49590.0637	0.3772	1.169	1200.0	170.42	268.75	14.097	0.006	93.34	1.41	0.033	2.576	−1.213	3.04	1
T4850003	1994-Aug-25	49590.2109	0.4178	1.168	1200.0	168.95	270.95	14.207	0.006	94.64	1.36	0.031	2.619	−1.210	3.35	1

Table A.8 cont.: HV 1620 differential photometry – v.

Frame	Date	HJD −2400000.0	Orbital Phase	X	T	Row	Col	$m_{\rm raw}$	$\sigma_{m_{\rm raw}}$	sky	CHI	Sharp	$V-C$	$C-C$	Seeing (FWHM)	ILCA
T4850020	1994-Aug-31	49595.8338	0.9683	1.632	1200.0	171.52	272.34	14.580	0.008	19.48	1.74	0.051	2.887	−1.217	3.17	1
T4850025	1994-Aug-31	49596.0918	0.0395	1.143	1200.0	169.80	270.76	14.872	0.007	16.63	1.32	0.021	2.912	−1.215	4.27	1
T4850034	1994-Aug-31	49596.1868	0.0657	1.162	1200.0	168.82	266.10	14.471	0.006	20.48	1.40	0.029	2.715	−1.216	3.64	1
T6410003	1994-Aug-31	49596.2515	0.0835	1.235	1200.0	169.69	269.48	14.726	0.007	105.01	1.22	0.030	2.630	−1.213	3.93	1
T7370027	1995-Apr-12	49820.0875	0.8074	2.094	1200.0	174.76	269.14	14.416	0.006	185.45	1.27	0.006	2.528	−1.211	3.01	1
T7370032	1995-Apr-12	49820.1454	0.8234	1.895	1200.0	174.71	270.10	14.633	0.007	76.65	1.45	0.034	2.535	−1.214	2.94	1
T6300002	1995-Apr-12	49820.2134	0.8421	1.642	1200.0	174.57	271.28	14.337	0.007	19.39	1.81	0.032	2.566	−1.215	3.01	1
T7430010	1995-May-08	49846.2224	0.0142	1.399	1200.0	172.88	271.56	14.972	0.008	27.73	1.44	0.016	3.065	−1.215	4.00	1
T7210008	1995-May-10	49847.9398	0.4878	2.224	1200.0	171.03	267.28	16.716	0.029	44.44	1.60	0.026	2.759	−1.219	4.66	1
T7210009	1995-May-10	49847.9569	0.4926	2.211	1200.0	171.16	269.17	15.121	0.009	136.43	1.20	0.003	2.813	−1.197	4.36	1
T7210012	1995-May-10	49847.9963	0.5034	2.138	1200.0	170.93	270.19	15.371	0.010	130.25	1.11	−0.006	2.822	−1.201	5.00	1
T7210018	1995-May-10	49848.0606	0.5211	1.931	1200.0	170.78	270.71	14.984	0.007	93.32	1.02	0.005	2.812	−1.214	4.32	1

Table A.9: HV 1620 differential photometry – b.

Frame	Date	HJD −2400000.0	Orbital Phase	X	T	Row	Col	$m_{\rm raw}$	$\sigma_{m_{\rm raw}}$	sky	CHI	Sharp	$V-C$	$C-C$	Seeing (FWHM)	ILCA
T3830012	1993-Mar-10	49057.0644	0.4000	2.213	600.0	169.10	276.57	15.186	0.012	343.10	1.24	0.053	2.757	−0.754	3.29	1
T3830014	1993-Mar-10	49057.0828	0.4051	2.228	600.0	171.61	272.51	15.188	0.013	340.86	1.36	0.021	2.746	−0.743	3.49	1
T3840018	1993-Mar-12	49059.0759	0.9547	2.228	600.0	176.00	275.02	15.215	0.012	138.33	1.49	0.023	2.922	−0.756	3.41	1
T3960005	1993-May-23	49130.9204	0.7662	2.210	1200.0	173.66	270.17	13.855	0.006	54.37	1.78	0.043	2.700	−0.766	2.71	1
T4260036	1993-Jul-27	49195.9499	0.6984	1.561	1200.0	174.34	270.95	14.163	0.005	155.23	1.11	0.003	2.660	−0.748	4.37	1
T4270003	1993-Jul-27	49195.9999	0.7122	1.412	1200.0	175.35	270.79	14.089	0.004	139.28	1.06	−0.004	2.660	−0.741	4.08	1
T5440004	1994-Jan-19	49372.0705	0.2645	1.825	1200.0	171.96	268.97	14.812	0.007	50.26	1.24	−0.001	2.635	−0.749	6.54	0
T5780003	1994-Feb-22	49405.9297	0.6014	1.648	1200.0	170.65	268.39	14.689	0.032	272.72	4.93	−0.237	2.720	−0.755	5.22	0
T5820015	1994-Mar-12	49424.1443	0.6241	2.162	1200.0	172.15	270.18	14.193	0.007	45.43	1.68	0.039	2.749	−0.759	3.37	1
T5820020	1994-Mar-12	49424.2070	0.6414	1.974	1200.0	173.20	267.34	14.022	0.005	64.97	1.43	0.036	2.715	−0.757	3.50	1
T5980003	1994-Mar-21	49432.9708	0.0581	2.063	1200.0	175.94	269.33	14.147	0.008	109.60	1.99	0.070	2.936	−0.760	2.91	1
T5980024	1994-Mar-21	49433.1403	0.1048	2.111	1200.0	175.52	269.71	14.550	0.005	38.39	1.11	0.002	2.756	−0.758	5.04	0
T5470022	1994-Mar-24	49435.9918	0.8911	2.145	1200.0	175.69	271.04	14.326	0.005	413.97	0.92	0.008	2.745	−0.754	3.97	1
T6210003	1994-Mar-24	49436.1509	0.9350	2.054	1200.0	175.61	266.77	14.797	0.007	69.70	1.15	−0.007	2.814	−0.755	6.19	0
T5060024	1994-Apr-06	49449.0250	0.4851	2.226	1200.0	175.54	276.72	14.738	0.007	66.82	1.31	0.003	2.961	−0.750	4.39	1
T5300009	1994-May-16	49488.9193	0.4861	2.225	1200.0	175.61	271.87	14.481	0.006	52.18	1.27	0.016	2.972	−0.756	4.15	1
T5300018	1994-May-16	49489.0200	0.5139	2.016	1200.0	175.68	272.30	14.499	0.006	48.34	1.21	0.011	2.990	−0.759	4.37	1
T5300029	1994-May-16	49489.1316	0.5447	1.606	1200.0	177.68	274.12	14.660	0.006	46.97	1.28	0.000	2.875	−0.753	5.51	0
T4580019	1994-Jun-12	49515.9089	0.9287	2.132	1200.0	176.05	274.19	14.404	0.006	48.18	1.33	−0.002	2.811	−0.757	4.55	1
T4580037	1994-Jun-12	49516.0494	0.9674	1.639	1200.0	172.90	273.60	14.273	0.006	44.74	1.56	0.039	3.019	−0.755	3.56	1

Table A.9 cont.: HV 1620 differential photometry – b.

Frame	Date	HJD −2400000.0	Orbital Phase	X	T	Row	Col	$m_{\rm raw}$	$\sigma_{m_{\rm raw}}$	sky	CHI	Sharp	$V-C$	$C-C$	Seeing (FWHM)	ILCA
T4590018	1994-Jun-12	49516.1985	0.0085	1.250	1200.0	173.34	271.30	14.476	0.007	46.38	1.63	0.053	3.245	−0.752	3.40	1
T4810012	1994-Jul-30	49564.0457	0.2026	1.291	1200.0	173.62	272.87	13.637	0.006	32.35	1.88	0.028	2.681	−0.758	2.70	1
T6360004	1994-Jul-31	49564.8912	0.4358	1.731	1200.0	172.34	274.54	13.950	0.006	33.54	1.86	0.033	2.806	−0.761	2.97	1
T4780013	1994-Aug-25	49589.8960	0.3310	1.483	1200.0	174.58	275.02	13.866	0.005	48.77	1.39	0.014	2.684	−0.763	3.60	1
T4780029	1994-Aug-25	49590.1146	0.3913	1.141	1200.0	172.16	268.59	13.693	0.005	169.34	1.42	0.021	2.738	−0.757	3.08	1
T4850007	1994-Aug-25	49590.2488	0.4282	1.208	1200.0	171.49	271.23	13.793	0.005	183.63	1.27	0.016	2.793	−0.759	3.16	1
T4850021	1994-Aug-31	49595.8488	0.9725	1.581	1200.0	173.26	273.19	14.317	0.006	33.64	1.39	0.023	3.065	−0.759	3.61	1
T4850028	1994-Aug-31	49596.1243	0.0484	1.138	1200.0	173.15	270.96	14.527	0.007	24.99	1.64	0.036	2.985	−0.764	3.92	1
T4850037	1994-Aug-31	49596.2217	0.0753	1.195	1200.0	172.52	273.20	14.373	0.006	46.50	1.51	0.052	2.841	−0.764	3.21	1
T6410004	1994-Aug-31	49596.2666	0.0877	1.259	1200.0	173.43	271.38	13.945	0.013	5203.6	1.22	−0.017	2.739	−0.755	3.50	1
T7370028	1995-Apr-12	49820.1022	0.8115	2.049	1200.0	176.06	270.43	13.705	0.004	343.66	1.17	0.003	2.680	−0.755	2.85	1
T7370033	1995-Apr-12	49820.1601	0.8274	1.839	1200.0	175.57	270.99	13.977	0.005	95.01	1.50	0.018	2.707	−0.757	2.84	1
T6300003	1995-Apr-12	49820.2281	0.8462	1.592	1200.0	176.39	272.37	14.320	0.006	36.47	1.52	0.037	2.744	−0.762	3.18	1
T7430014	1995-May-08	49846.2617	0.0251	1.309	1200.0	174.99	273.64	14.370	0.006	73.31	1.32	0.019	3.143	−0.751	3.91	1
T7210010	1995-May-10	49847.9718	0.4966	2.190	1200.0	171.66	271.28	14.588	0.007	286.26	1.05	0.020	2.971	−0.753	3.90	1
T7210013	1995-May-10	49848.0112	0.5075	2.097	1200.0	172.57	271.16	14.448	0.006	247.15	1.10	0.012	2.975	−0.750	3.97	1
T7210022	1995-May-10	49848.0998	0.5320	1.783	1200.0	172.69	272.63	14.552	0.007	97.13	1.31	0.014	2.954	−0.756	3.63	1

Table A.10: HV 1620 differential photometry – y.

Frame	Date	HJD −2400000.0	Orbital Phase	X	T	Row	Col	$m_{\rm raw}$	$\sigma_{m_{\rm raw}}$	sky	CHI	Sharp	$V-C$	$C-C$	Seeing (FWHM)	ILCA
T3830015	1993-Mar-10	49057.0934	0.4080	2.231	400.0	172.48	272.19	14.997	0.012	639.35	1.13	0.019	2.860	−0.395	3.56	1
T3840019	1993-Mar-12	49059.0931	0.9594	2.230	400.0	173.27	277.13	14.609	0.009	236.06	1.51	0.073	3.120	−0.407	2.56	1
T3960002	1993-May-23	49130.8764	0.7540	2.219	700.0	173.29	272.46	13.486	0.006	128.77	2.09	0.065	2.810	−0.396	2.29	1
T3960010	1993-May-23	49130.9775	0.7819	2.092	700.0	175.18	272.54	13.551	0.006	117.50	1.94	0.039	2.835	−0.405	2.81	1
T0810026	1993-Sep-07	49238.1117	0.3247	1.139	700.0	171.90	272.89	13.246	0.006	152.31	1.93	0.039	2.809	−0.406	2.02	1
T5440005	1994-Jan-19	49372.0844	0.2684	1.874	700.0	173.58	270.51	14.553	0.007	123.14	1.33	−0.003	2.769	−0.396	6.43	0
T5780005	1994-Feb-22	49405.9684	0.6120	1.786	700.0	175.97	273.86	14.394	0.007	400.66	1.14	−0.007	2.845	−0.401	5.98	0
T5820018	1994-Mar-12	49424.1908	0.6369	2.033	700.0	173.42	269.84	13.708	0.005	148.06	1.53	0.018	2.868	−0.406	3.49	1
T5820021	1994-Mar-12	49424.2202	0.6451	1.929	700.0	174.01	270.11	13.714	0.005	272.73	1.36	0.014	2.842	−0.410	3.64	1
T5980012	1994-Mar-21	49433.0407	0.0773	2.214	700.0	176.96	274.72	13.768	0.007	119.92	2.08	0.075	2.936	−0.408	2.85	1
T5980030	1994-Mar-21	49433.1889	0.1182	1.954	700.0	174.80	275.60	13.806	0.005	117.05	1.41	0.028	2.898	−0.410	3.72	1
T5470028	1994-Mar-24	49436.0370	0.9036	2.218	700.0	175.00	275.25	14.063	0.006	605.68	1.17	0.014	2.880	−0.398	4.30	1
T6210006	1994-Mar-24	49436.1727	0.9410	1.983	700.0	178.59	269.45	14.456	0.005	131.34	1.04	−0.005	2.943	−0.401	6.29	0
T5060030	1994-Apr-06	49449.0991	0.5055	2.108	700.0	176.94	276.79	14.820	0.009	300.40	1.17	0.005	3.057	−0.394	6.77	0
T5300012	1994-May-16	49488.9555	0.4961	2.190	700.0	175.21	275.48	14.333	0.006	129.67	1.37	0.008	3.095	−0.407	4.64	1

Table A.10 cont.: HV 1620 differential photometry – y.

Frame	Date	HJD −2400000.0	Orbital Phase	X	T	Row	Col	$m_{\rm raw}$	$\sigma_{m_{\rm raw}}$	sky	CHI	Sharp	$V-C$	$C-C$	Seeing (FWHM)	ILCA
T5300021	1994-May-16	49489.0521	0.5228	1.903	700.0	176.93	275.97	14.029	0.006	117.58	1.54	0.036	3.114	−0.408	3.68	1
T5300033	1994-May-16	49489.1823	0.5587	1.451	700.0	178.61	280.55	14.221	0.006	125.86	1.44	0.004	2.957	−0.408	4.60	1
T4580025	1994-Jun-12	49515.9539	0.9411	1.996	700.0	177.01	276.93	14.155	0.005	97.05	1.33	0.018	2.975	−0.406	4.51	1
T4590006	1994-Jun-12	49516.0984	0.9809	1.483	700.0	174.86	276.83	13.968	0.008	97.99	2.19	0.074	3.243	−0.404	3.06	1
T4590024	1994-Jun-12	49516.2435	0.0209	1.190	700.0	174.24	272.72	14.112	0.006	89.92	1.46	0.031	3.296	−0.404	3.42	1
T4810013	1994-Jul-30	49564.0574	0.2058	1.271	700.0	174.63	275.43	13.448	0.004	59.94	1.57	0.039	2.812	−0.409	2.69	1
T4780035	1994-Aug-25	49590.1698	0.4065	1.144	700.0	174.17	269.83	13.509	0.004	259.38	1.37	0.033	2.883	−0.405	3.13	1
T4850008	1994-Aug-25	49590.2607	0.4315	1.223	700.0	172.48	274.80	13.531	0.004	335.63	1.27	0.014	2.907	−0.400	3.04	1
T4850022	1994-Aug-31	49595.8611	0.9759	1.544	700.0	175.34	276.23	14.022	0.006	68.17	1.77	0.036	3.196	−0.409	3.40	1
T4850031	1994-Aug-31	49596.1571	0.0575	1.145	700.0	173.23	272.80	13.930	0.005	71.45	1.38	0.026	3.044	−0.410	3.86	1
T6410002	1994-Aug-31	49596.2384	0.0799	1.215	700.0	174.09	275.53	14.378	0.008	93.60	1.75	0.074	2.950	−0.414	3.18	1
T7370029	1995-Apr-12	49820.1142	0.8148	2.012	700.0	175.88	273.06	13.697	0.005	500.50	1.21	0.022	2.811	−0.401	2.79	1
T7370034	1995-Apr-12	49820.1721	0.8307	1.798	700.0	176.62	273.44	13.676	0.005	117.67	1.62	0.048	2.834	−0.400	2.74	1
T6300001	1995-Apr-12	49820.2011	0.8387	1.690	700.0	177.21	274.35	13.462	0.006	94.03	2.15	0.046	2.832	−0.401	2.51	1
T6300005	1995-Apr-12	49820.2442	0.8506	1.542	700.0	178.80	275.24	13.979	0.007	128.08	1.79	0.018	2.867	−0.409	2.87	1

Table A.11: HV 1620 differential photometry – V.

Frame	Date	HJD −2400000.0	Orbital Phase	X	T	Row	Col	$m_{\rm raw}$	$\sigma_{m_{\rm raw}}$	sky	CHI	Sharp	$V-C$	$C-C$	Seeing (FWHM)	ILCA
T2770016	1992-Nov-04	48930.9747	0.6301	1.144	100.0	174.44	272.41	14.204	0.006	110.78	1.50	0.054	1.052	−0.051	3.16	1
T2770017	1992-Nov-04	48930.9888	0.6340	1.150	400.0	174.75	273.35	12.672	0.003	875.10	1.43	0.023	1.031	−0.053	3.29	1
T2770018	1992-Nov-04	48931.0027	0.6379	1.159	400.0	173.70	273.88	12.635	0.003	433.37	1.34	0.015	1.028	−0.054	3.10	1
T2770019	1992-Nov-04	48931.0092	0.6397	1.163	400.0	174.43	273.96	12.691	0.003	426.92	1.56	0.019	1.027	−0.056	3.30	1
T2770020	1992-Nov-04	48931.0167	0.6417	1.170	400.0	174.00	273.49	13.117	0.003	421.07	1.12	0.005	1.021	−0.061	4.45	1
T2770021	1992-Nov-04	48931.0267	0.6445	1.179	400.0	174.46	273.46	12.861	0.003	414.03	1.34	0.014	1.020	−0.055	3.78	1
T2770022	1992-Nov-04	48931.0390	0.6479	1.191	400.0	174.42	273.90	12.900	0.003	396.40	1.32	0.007	1.016	−0.058	3.93	1
T2770023	1992-Nov-04	48931.0473	0.6502	1.201	400.0	174.15	272.50	12.779	0.003	376.28	1.55	0.016	1.017	−0.054	3.53	1
T2770024	1992-Nov-04	48931.0552	0.6523	1.211	400.0	175.12	273.45	12.732	0.003	359.50	1.27	0.026	1.013	−0.053	3.28	1
T2770025	1992-Nov-04	48931.0631	0.6545	1.222	400.0	174.92	272.55	12.698	0.003	334.51	1.37	0.028	1.011	−0.053	3.19	1
T2770026	1992-Nov-04	48931.0770	0.6584	1.242	400.0	175.17	272.96	12.821	0.003	270.61	1.34	0.012	0.995	−0.053	3.68	1
T2770027	1992-Nov-04	48931.0839	0.6603	1.254	400.0	174.16	273.68	12.707	0.003	230.55	1.57	0.033	1.008	−0.050	3.19	1
T2770028	1992-Nov-04	48931.0911	0.6622	1.266	400.0	173.63	272.83	12.813	0.003	176.15	1.51	0.027	1.004	−0.046	3.26	1
T2680002	1992-Nov-04	48931.0987	0.6643	1.280	400.0	174.42	273.08	12.837	0.003	140.68	1.66	0.030	0.995	−0.048	3.25	1
T2680001	1992-Nov-04	48931.0987	0.6643	1.280	400.0	174.42	273.08	12.837	0.003	140.68	1.66	0.030	0.995	−0.048	3.25	1
T2770029	1992-Nov-04	48931.0987	0.6643	1.280	400.0	174.42	273.08	12.837	0.003	140.68	1.66	0.030	0.995	−0.048	3.25	1
T2680003	1992-Nov-04	48931.1151	0.6689	1.312	400.0	175.08	273.01	13.206	0.004	91.22	1.51	0.040	0.991	−0.046	3.53	1

Table A.11 cont.: HV 1620 differential photometry – V.

Frame	Date	HJD −2400000.0	Orbital Phase	X	T	Row	Col	$m_{\rm raw}$	$\sigma_{m_{\rm raw}}$	sky	CHI	Sharp	$V-C$	$C-C$	Seeing (FWHM)	ILCA
T2680004	1992-Nov-04	48931.1257	0.6718	1.335	400.0	175.85	273.56	12.868	0.004	132.58	1.92	0.012	0.992	−0.048	3.79	1
T2680005	1992-Nov-04	48931.1325	0.6737	1.350	400.0	174.95	273.87	12.858	0.003	136.20	1.59	0.028	0.992	−0.047	3.72	1
T2680006	1992-Nov-04	48931.1395	0.6756	1.367	400.0	176.66	274.76	12.995	0.003	141.15	1.42	0.014	0.997	−0.056	4.16	1
T2680007	1992-Nov-04	48931.1464	0.6775	1.384	400.0	174.66	274.13	13.040	0.003	144.59	1.26	0.009	0.988	−0.051	4.36	1
T2680008	1992-Nov-04	48931.1539	0.6796	1.403	400.0	173.53	273.90	13.055	0.003	150.80	1.30	0.007	0.989	−0.057	4.40	1
T2680009	1992-Nov-04	48931.1599	0.6812	1.419	400.0	175.71	273.72	12.992	0.003	173.27	1.18	0.007	0.982	−0.051	4.19	1
T2680010	1992-Nov-04	48931.1672	0.6832	1.439	400.0	172.45	272.74	12.908	0.004	282.27	1.55	0.021	0.985	−0.052	3.82	1
T2680011	1992-Nov-04	48931.1757	0.6856	1.463	400.0	174.45	274.11	12.909	0.003	929.56	1.19	0.014	0.978	−0.053	3.89	1
T2680025	1992-Nov-05	48931.9114	0.8884	1.142	400.0	175.29	272.67	12.552	0.004	557.92	1.84	0.052	1.071	−0.057	2.73	1
T2680026	1992-Nov-05	48931.9181	0.8903	1.140	400.0	174.32	273.22	12.589	0.004	553.77	1.79	0.052	1.072	−0.053	2.78	1
T2680027	1992-Nov-05	48931.9239	0.8919	1.139	400.0	174.73	270.85	12.617	0.003	551.00	1.67	0.050	1.073	−0.053	3.07	1
T2680028	1992-Nov-05	48931.9332	0.8945	1.138	400.0	173.63	271.75	12.548	0.004	548.13	2.13	0.065	1.080	−0.055	2.65	1
T2680029	1992-Nov-05	48931.9399	0.8963	1.138	400.0	173.46	272.19	12.570	0.004	552.79	2.04	0.055	1.076	−0.053	2.70	1
T2680030	1992-Nov-05	48931.9470	0.8983	1.138	400.0	174.21	272.22	12.602	0.004	549.24	2.16	0.067	1.077	−0.053	2.79	1
T2680031	1992-Nov-05	48931.9531	0.8999	1.139	400.0	173.43	271.35	12.624	0.005	549.55	2.52	0.078	1.082	−0.053	2.87	1
T2680032	1992-Nov-05	48931.9734	0.9055	1.144	400.0	173.76	270.69	12.654	0.005	535.42	2.22	0.071	1.082	−0.051	2.83	1
T2680033	1992-Nov-05	48931.9797	0.9073	1.147	400.0	173.21	270.69	12.619	0.005	530.58	2.21	0.068	1.086	−0.050	2.77	1
T0030001	1992-Nov-05	48931.9870	0.9093	1.151	400.0	173.38	269.66	12.792	0.004	535.73	1.96	0.046	1.080	−0.050	3.34	1
T0030002	1992-Nov-05	48931.9946	0.9114	1.155	400.0	173.62	270.86	12.826	0.004	534.10	1.88	0.045	1.089	−0.049	3.43	1
T0030003	1992-Nov-05	48932.0009	0.9131	1.159	400.0	172.60	271.19	12.838	0.004	530.79	1.72	0.037	1.084	−0.050	3.43	1
T0030004	1992-Nov-05	48932.0078	0.9150	1.165	400.0	174.48	270.45	12.879	0.005	520.56	1.92	0.043	1.089	−0.050	3.57	1
T0030005	1992-Nov-05	48932.0144	0.9169	1.170	400.0	175.43	269.07	12.901	0.004	515.05	1.73	0.034	1.089	−0.051	3.65	1
T0030006	1992-Nov-05	48932.0209	0.9186	1.176	400.0	173.65	269.30	12.885	0.004	512.71	1.85	0.042	1.096	−0.050	3.53	1
T0030007	1992-Nov-05	48932.0277	0.9205	1.182	400.0	174.02	268.67	12.864	0.005	509.38	1.97	0.046	1.097	−0.049	3.46	1
T0030008	1992-Nov-05	48932.0400	0.9239	1.196	400.0	173.01	269.29	13.085	0.004	504.64	1.43	0.011	1.092	−0.053	4.41	1
T0030009	1992-Nov-05	48932.0459	0.9255	1.203	400.0	174.03	269.69	13.104	0.004	496.10	1.40	0.014	1.104	−0.053	4.28	1
T0030010	1992-Nov-05	48932.0518	0.9272	1.210	400.0	173.04	269.22	13.014	0.004	484.71	1.54	0.022	1.104	−0.051	4.05	1
T0030011	1992-Nov-05	48932.0588	0.9291	1.220	400.0	173.20	268.92	13.119	0.005	466.52	1.82	0.024	1.098	−0.050	4.37	1
T0030012	1992-Nov-05	48932.0758	0.9338	1.245	400.0	173.66	270.85	13.523	0.003	116.64	1.08	0.031	1.139	−0.055	2.96	1
T0030013	1992-Nov-05	48932.0840	0.9360	1.259	400.0	174.22	269.86	13.496	0.004	98.11	1.33	0.046	1.144	−0.053	2.78	1
T0030014	1992-Nov-05	48932.0896	0.9376	1.268	400.0	174.55	270.52	12.733	0.003	335.59	1.62	0.041	1.152	−0.057	2.85	1
T0030015	1992-Nov-05	48932.0958	0.9393	1.280	400.0	172.95	270.26	12.752	0.005	298.32	2.18	0.066	1.157	−0.053	2.83	1
T0030016	1992-Nov-05	48932.1018	0.9410	1.291	400.0	174.40	270.16	12.757	0.004	256.02	1.67	0.049	1.161	−0.057	2.82	1
T0030017	1992-Nov-05	48932.1079	0.9426	1.303	400.0	174.58	270.81	12.831	0.004	201.45	1.92	0.043	1.162	−0.051	2.88	1
T0030018	1992-Nov-05	48932.1139	0.9443	1.316	400.0	172.64	270.17	12.896	0.005	153.53	2.24	0.070	1.172	−0.054	2.73	1
T0030019	1992-Nov-05	48932.1201	0.9460	1.329	400.0	175.43	268.76	12.885	0.004	145.09	1.76	0.045	1.180	−0.051	2.90	1
T0030020	1992-Nov-05	48932.1262	0.9477	1.342	400.0	173.46	270.17	12.919	0.004	141.27	2.05	0.063	1.191	−0.049	2.92	1
T0030021	1992-Nov-05	48932.1320	0.9493	1.356	400.0	174.49	269.51	13.026	0.004	137.80	1.87	0.050	1.203	−0.052	2.92	1
T0030022	1992-Nov-05	48932.1379	0.9509	1.370	400.0	175.92	270.12	13.175	0.004	130.15	1.76	0.045	1.209	−0.056	3.28	1

Table A.11 cont.: HV 1620 differential photometry – V.

Frame	Date	HJD −2400000.0	Orbital Phase	X	T	Row	Col	$m_{\rm raw}$	$\sigma_{m_{\rm raw}}$	sky	CHI	Sharp	$V-C$	$C-C$	Seeing (FWHM)	ILCA
T0030023	1992-Nov-05	48932.1462	0.9532	1.390	400.0	173.16	269.88	13.140	0.004	151.52	1.79	0.063	1.221	−0.053	3.04	1
T0030024	1992-Nov-05	48932.1530	0.9551	1.408	400.0	173.02	270.10	13.134	0.004	181.04	1.77	0.022	1.227	−0.054	3.95	1
T0030025	1992-Nov-05	48932.1593	0.9568	1.425	400.0	173.37	270.72	13.187	0.004	219.82	1.51	0.020	1.236	−0.055	3.96	1
T0030026	1992-Nov-05	48932.1654	0.9585	1.442	400.0	173.02	270.63	13.076	0.004	323.67	1.56	0.035	1.255	−0.054	3.65	1
T0030027	1992-Nov-05	48932.1713	0.9601	1.458	400.0	172.67	270.24	13.010	0.005	670.14	2.11	0.056	1.258	−0.052	3.28	1
T0030028	1992-Nov-05	48932.1774	0.9618	1.476	400.0	172.51	269.47	13.055	0.005	1921.8	1.46	0.037	1.265	−0.056	3.33	1
T0360021	1992-Nov-28	48954.9288	0.2356	1.154	400.0	176.29	267.82	12.748	0.002	134.38	1.21	0.010	0.963	−0.052	3.70	1
T0360022	1992-Nov-28	48954.9545	0.2427	1.173	400.0	175.64	268.28	13.155	0.003	125.99	1.30	0.011	0.957	−0.052	4.14	1
T0360023	1992-Nov-28	48954.9734	0.2479	1.192	400.0	175.29	268.32	13.514	0.004	118.52	1.22	0.017	0.962	−0.049	3.50	1
T0360025	1992-Nov-28	48955.0029	0.2560	1.231	400.0	183.23	274.82	14.230	0.005	115.47	1.22	0.018	0.956	−0.047	3.34	1
T0360026	1992-Nov-28	48955.0343	0.2647	1.284	400.0	173.53	266.77	14.362	0.006	111.98	1.39	0.047	0.976	−0.058	3.53	1
T0360027	1992-Nov-28	48955.1378	0.2932	1.551	400.0	174.04	267.12	13.148	0.003	170.15	1.34	0.027	0.966	−0.063	3.58	1
T0360028	1992-Nov-28	48955.1449	0.2952	1.574	400.0	174.67	267.25	13.443	0.004	295.18	1.33	0.013	0.961	−0.050	4.08	1
T3630017	1993-Jan-30	49017.9988	0.6275	1.670	400.0	171.87	270.87	13.110	0.003	139.14	1.40	0.010	1.065	−0.050	4.24	1
T3630019	1993-Jan-30	49018.0211	0.6336	1.752	400.0	172.51	271.78	13.067	0.003	140.53	1.16	0.005	1.059	−0.057	3.98	1
T3630021	1993-Jan-30	49018.0530	0.6424	1.873	400.0	178.37	271.64	13.534	0.004	105.89	1.39	0.006	1.045	−0.054	4.49	1
T3630023	1993-Jan-30	49018.0867	0.6517	1.998	400.0	176.43	271.87	13.953	0.005	77.27	1.35	0.003	1.029	−0.046	5.30	0
T3630025	1993-Jan-30	49018.0972	0.6546	2.034	400.0	175.59	273.40	13.342	0.004	128.42	1.30	0.005	1.015	−0.046	6.12	0
T3630027	1993-Jan-30	49018.1279	0.6631	2.128	400.0	173.59	271.42	13.508	0.004	135.46	1.22	0.005	0.995	−0.046	7.07	0
T3630029	1993-Jan-30	49018.1507	0.6694	2.181	400.0	173.57	271.42	13.259	0.003	136.76	1.23	0.000	0.998	−0.044	5.73	0
T3630031	1993-Jan-30	49018.1696	0.6746	2.212	400.0	172.84	272.74	13.608	0.004	199.12	1.08	0.000	0.992	−0.047	5.91	0
T3720002	1993-Feb-18	49036.9014	0.8399	1.515	400.0	174.53	269.11	12.732	0.003	144.40	1.77	0.030	1.024	−0.054	3.04	1
T3720003	1993-Feb-18	49036.9198	0.8450	1.575	400.0	173.45	269.93	12.745	0.004	154.82	1.90	0.042	1.027	−0.052	2.90	1
T3720004	1993-Feb-18	49036.9385	0.8502	1.639	400.0	173.99	269.29	12.842	0.004	169.82	1.75	0.033	1.029	−0.057	3.39	1
T3720005	1993-Feb-18	49036.9816	0.8621	1.798	400.0	173.57	270.05	13.119	0.003	189.34	1.39	0.010	1.050	−0.065	4.12	1
T3720006	1993-Feb-18	49037.0270	0.8746	1.969	400.0	172.68	271.62	12.757	0.004	169.55	2.07	0.027	1.062	−0.049	3.07	1
T3720007	1993-Feb-18	49037.0475	0.8802	2.041	400.0	171.95	271.75	13.023	0.004	166.63	1.90	0.040	1.066	−0.052	3.94	1
T3720008	1993-Feb-18	49037.0653	0.8852	2.097	400.0	172.25	271.52	12.755	0.003	172.56	1.41	0.025	1.074	−0.054	2.96	1
T3720009	1993-Feb-18	49037.0880	0.8914	2.158	400.0	172.17	272.42	12.721	0.004	168.18	2.05	0.022	1.075	−0.054	2.83	1
T3720010	1993-Feb-18	49037.1082	0.8970	2.198	400.0	170.92	272.82	12.763	0.003	167.27	1.62	0.019	1.081	−0.044	2.90	1
T3720011	1993-Feb-18	49037.1139	0.8986	2.206	400.0	171.60	272.71	12.752	0.004	165.11	1.83	0.011	1.078	−0.047	2.80	1
T3720012	1993-Feb-18	49037.1506	0.9087	2.231	400.0	174.48	271.47	12.775	0.003	162.30	1.57	0.025	1.096	−0.057	2.69	1
T3720013	1993-Feb-18	49037.1594	0.9111	2.228	400.0	174.70	272.29	12.719	0.005	173.93	2.33	0.055	1.102	−0.057	2.45	1
T3720014	1993-Feb-18	49037.1809	0.9171	2.208	400.0	174.76	272.59	12.791	0.004	200.38	1.77	0.021	1.102	−0.058	2.72	1
T3720015	1993-Feb-18	49037.1867	0.9186	2.200	400.0	174.21	272.60	12.854	0.003	227.35	1.41	0.016	1.110	−0.053	3.06	1
T3720016	1993-Feb-18	49037.1922	0.9201	2.191	400.0	174.32	272.54	12.836	0.004	306.57	1.75	0.017	1.103	−0.055	3.02	1
T3830009	1993-Mar-10	49057.0201	0.3878	2.123	400.0	174.10	275.28	13.141	0.003	2166.3	0.89	0.004	1.031	−0.046	3.13	1
T3830010	1993-Mar-10	49057.0308	0.3908	2.151	400.0	173.18	273.34	13.126	0.004	2181.8	1.05	0.019	1.035	−0.059	3.10	1
T3830013	1993-Mar-10	49057.0742	0.4027	2.223	400.0	172.52	273.12	12.965	0.005	1846.3	1.67	−0.004	1.043	−0.043	4.31	1

Table A.11 cont.: HV 1620 differential photometry – V.

Frame	Date	HJD −2400000.0	Orbital Phase	X	T	Row	Col	$m_{\rm raw}$	$\sigma_{m_{\rm raw}}$	sky	CHI	Sharp	$V-C$	$C-C$	Seeing (FWHM)	ILCA
T3830017	1993-Mar-10	49057.1103	0.4127	2.220	400.0	175.21	276.83	13.550	0.007	2135.1	1.19	0.005	1.060	−0.057	4.83	1
T3830019	1993-Mar-10	49057.1267	0.4172	2.208	400.0	175.12	270.92	13.482	0.006	2387.1	1.09	0.003	1.048	−0.046	4.06	1
T3830020	1993-Mar-10	49057.1404	0.4210	2.186	400.0	169.76	273.53	13.415	0.005	2285.2	1.06	0.007	1.075	−0.045	3.92	1
T3840007	1993-Mar-12	49058.9036	0.9072	1.729	400.0	177.30	273.35	12.665	0.004	450.04	1.87	0.042	1.094	−0.055	2.62	1
T3840008	1993-Mar-12	49058.9229	0.9125	1.802	400.0	176.91	272.87	12.743	0.004	556.82	1.76	0.038	1.092	−0.054	3.00	1
T3840009	1993-Mar-12	49058.9307	0.9147	1.832	400.0	175.32	273.79	12.772	0.004	593.51	1.76	0.029	1.093	−0.057	2.81	1
T3840011	1993-Mar-12	49058.9874	0.9303	2.039	400.0	173.84	273.10	12.719	0.004	737.84	1.96	0.050	1.125	−0.057	2.52	1
T3840015	1993-Mar-12	49059.0376	0.9441	2.178	400.0	172.50	273.66	12.918	0.005	802.26	1.87	0.060	1.184	−0.057	2.89	1
T3840016	1993-Mar-12	49059.0549	0.9489	2.207	400.0	175.59	275.11	12.788	0.004	822.27	1.44	0.026	1.193	−0.053	2.56	1
T3840017	1993-Mar-12	49059.0647	0.9516	2.219	400.0	174.86	275.02	12.806	0.004	825.35	1.69	0.026	1.214	−0.053	2.68	1
T3840021	1993-Mar-12	49059.1195	0.9667	2.211	400.0	174.61	275.87	12.891	0.004	818.58	1.77	0.025	1.305	−0.051	2.65	1
T3840022	1993-Mar-12	49059.1296	0.9695	2.196	400.0	174.94	274.57	12.867	0.004	809.09	1.60	0.033	1.326	−0.056	2.45	1
T3840023	1993-Mar-12	49059.1368	0.9715	2.183	400.0	175.03	273.07	12.907	0.005	805.74	1.93	0.049	1.336	−0.049	2.61	1
T3840024	1993-Mar-12	49059.1422	0.9730	2.172	400.0	175.19	273.62	12.980	0.004	801.79	1.52	0.018	1.344	−0.053	3.14	1
T3840025	1993-Mar-12	49059.1482	0.9746	2.158	400.0	175.49	273.18	12.898	0.005	795.35	1.95	0.039	1.355	−0.058	2.48	1
T3840026	1993-Mar-12	49059.1539	0.9762	2.145	400.0	174.62	272.96	13.025	0.005	793.23	1.65	0.044	1.364	−0.051	2.86	1
T3840027	1993-Mar-12	49059.1605	0.9780	2.128	400.0	174.00	272.64	13.131	0.004	792.78	1.41	0.020	1.384	−0.049	3.19	1
T3840028	1993-Mar-12	49059.1669	0.9798	2.110	400.0	174.15	273.01	12.993	0.004	785.40	1.42	0.027	1.391	−0.049	2.82	1
T3840029	1993-Mar-12	49059.1751	0.9820	2.086	400.0	173.59	271.96	13.001	0.005	771.47	1.75	0.034	1.416	−0.053	2.80	1
T3840030	1993-Mar-12	49059.1809	0.9836	2.068	400.0	173.22	274.69	12.969	0.004	762.98	1.34	0.019	1.424	−0.055	2.63	1
T3840031	1993-Mar-12	49059.1870	0.9853	2.048	400.0	172.83	274.17	12.990	0.004	754.85	1.65	0.036	1.442	−0.053	2.55	1
T3840032	1993-Mar-12	49059.1940	0.9872	2.024	400.0	172.81	273.84	12.890	0.005	743.47	1.72	0.027	1.427	−0.059	2.09	1
T3840033	1993-Mar-12	49059.2002	0.9890	2.003	400.0	172.99	273.69	13.034	0.005	739.50	1.82	0.052	1.463	−0.055	2.77	1
T3760001	1993-Mar-28	49075.0467	0.3587	2.231	400.0	173.79	271.98	12.711	0.003	155.28	1.72	0.006	1.012	−0.053	3.17	1
T3760002	1993-Mar-28	49075.0578	0.3618	2.228	400.0	174.02	271.72	12.723	0.004	158.86	1.82	0.003	1.014	−0.051	3.13	1
T3760003	1993-Mar-28	49075.0644	0.3636	2.223	400.0	174.65	272.27	12.726	0.002	159.15	1.18	0.011	1.016	−0.053	3.05	1
T3760004	1993-Mar-28	49075.0721	0.3657	2.217	100.0	173.06	272.44	14.283	0.008	41.19	1.88	0.023	1.036	−0.063	3.57	1
T3760005	1993-Mar-28	49075.0736	0.3661	2.215	100.0	173.76	272.46	14.301	0.007	40.96	1.62	0.020	1.034	−0.053	3.67	1
T3760006	1993-Mar-28	49075.0752	0.3666	2.213	100.0	174.52	272.53	14.378	0.006	41.06	1.46	0.019	1.024	−0.063	4.03	1
T3760007	1993-Mar-28	49075.0767	0.3670	2.211	100.0	172.14	272.58	14.302	0.008	41.38	2.08	0.030	1.044	−0.053	3.54	1
T3760008	1993-Mar-28	49075.0806	0.3681	2.206	100.0	172.26	272.89	14.409	0.008	41.35	1.95	0.022	1.034	−0.047	3.74	1
T3760009	1993-Mar-28	49075.0821	0.3685	2.204	100.0	173.10	271.97	14.283	0.007	40.85	1.76	0.049	1.040	−0.048	3.45	1
T3760010	1993-Mar-28	49075.0837	0.3689	2.201	100.0	173.42	271.69	14.277	0.007	39.96	1.68	0.019	1.045	−0.046	3.67	1
T3760011	1993-Mar-28	49075.0852	0.3693	2.199	100.0	174.71	273.03	14.259	0.007	41.20	1.84	0.040	1.038	−0.057	3.55	1
T3760012	1993-Mar-28	49075.0889	0.3704	2.193	100.0	173.48	272.35	14.416	0.007	40.17	1.66	0.018	1.041	−0.052	3.78	1
T3760013	1993-Mar-28	49075.0905	0.3708	2.190	100.0	172.79	272.53	14.366	0.008	39.73	1.84	0.053	1.039	−0.054	3.63	1
T3760014	1993-Mar-28	49075.0920	0.3712	2.187	100.0	173.19	273.14	14.423	0.006	40.59	1.38	0.017	1.034	−0.058	3.87	1
T3760015	1993-Mar-28	49075.0936	0.3716	2.184	100.0	172.48	272.40	14.460	0.006	40.38	1.44	0.023	1.034	−0.056	4.00	1
T3760016	1993-Mar-28	49075.0988	0.3731	2.173	100.0	172.44	272.41	14.348	0.007	39.93	1.70	0.004	1.022	−0.055	3.92	1

Table A.11 cont.: HV 1620 differential photometry – V.

Frame	Date	HJD −2400000.0	Orbital Phase	X	T	Row	Col	$m_{\rm raw}$	$\sigma_{m_{\rm raw}}$	sky	CHI	Sharp	$V-C$	$C-C$	Seeing (FWHM)	ILCA
T3760017	1993-Mar-28	49075.1004	0.3735	2.170	100.0	171.70	273.48	14.325	0.007	39.13	1.59	0.017	1.043	−0.054	4.01	1
T3760018	1993-Mar-28	49075.1019	0.3740	2.167	100.0	174.08	272.42	14.302	0.007	38.41	1.78	0.052	1.047	−0.058	3.71	1
T3760019	1993-Mar-28	49075.1035	0.3744	2.163	100.0	172.90	272.29	14.335	0.007	38.51	1.61	0.019	1.058	−0.072	4.08	0
T3760020	1993-Mar-28	49075.1089	0.3759	2.149	400.0	173.03	272.34	12.828	0.003	159.30	1.57	0.001	1.028	−0.055	3.90	1
T3760021	1993-Mar-28	49075.1151	0.3776	2.134	400.0	173.40	272.92	12.783	0.004	159.59	1.73	−0.010	1.031	−0.051	3.80	1
T3760022	1993-Mar-28	49075.1212	0.3793	2.117	400.0	172.82	273.03	12.728	0.003	157.16	1.68	−0.009	1.031	−0.054	3.70	1
T3760023	1993-Mar-28	49075.2218	0.4070	1.761	400.0	174.27	272.17	12.624	0.004	151.27	1.95	0.009	1.066	−0.057	3.07	1
T3760024	1993-Mar-28	49075.2296	0.4091	1.731	400.0	173.66	271.90	12.654	0.004	176.78	1.83	0.004	1.065	−0.054	3.13	1
T3760025	1993-Mar-28	49075.2359	0.4109	1.708	400.0	175.26	272.37	12.753	0.003	304.60	1.60	0.011	1.066	−0.053	3.39	1
T3760026	1993-Mar-28	49075.2419	0.4125	1.686	400.0	174.92	271.52	12.726	0.003	825.84	1.30	0.006	1.063	−0.055	3.39	1
T3910001	1993-Apr-14	49092.0424	0.0454	2.188	400.0	176.15	274.22	13.154	0.004	299.12	1.54	0.014	1.305	−0.056	3.80	1
T3910002	1993-Apr-14	49092.0504	0.0476	2.174	400.0	176.84	274.31	13.226	0.004	314.30	1.60	0.011	1.287	−0.067	4.08	1
T3910003	1993-Apr-14	49092.0564	0.0492	2.161	400.0	176.14	269.74	13.233	0.003	320.49	1.23	0.005	1.275	−0.054	3.93	1
T3910004	1993-Apr-14	49092.0626	0.0509	2.147	400.0	175.46	269.56	13.135	0.003	310.51	1.33	0.021	1.264	−0.059	3.51	1
T3910005	1993-Apr-14	49092.0695	0.0528	2.129	400.0	175.19	270.19	13.145	0.004	288.40	1.45	0.031	1.241	−0.053	3.42	1
T3910006	1993-Apr-14	49092.0764	0.0547	2.111	400.0	175.52	270.52	13.454	0.005	265.86	1.65	0.020	1.230	−0.052	3.76	1
T3910007	1993-Apr-14	49092.0822	0.0564	2.094	400.0	175.52	270.58	13.539	0.004	244.79	1.36	0.015	1.229	−0.051	3.68	1
T3910008	1993-Apr-14	49092.0902	0.0585	2.070	400.0	175.36	270.52	13.569	0.004	207.76	1.34	0.020	1.217	−0.048	3.49	1
T3910009	1993-Apr-14	49092.0958	0.0601	2.052	400.0	175.13	270.61	13.596	0.006	188.42	1.78	0.035	1.207	−0.044	3.31	1
T3910010	1993-Apr-14	49092.1016	0.0617	2.033	400.0	176.32	270.43	13.731	0.005	169.58	1.55	0.035	1.187	−0.052	3.40	1
T3910015	1993-Apr-15	49092.8619	0.2713	1.915	400.0	174.26	273.10	13.290	0.005	183.12	1.73	0.072	0.971	−0.058	2.54	1
T3910016	1993-Apr-15	49092.8697	0.2735	1.943	400.0	171.05	274.72	13.373	0.005	191.50	1.79	0.051	0.971	−0.054	2.81	1
T3910017	1993-Apr-15	49092.8828	0.2771	1.991	400.0	171.58	274.85	14.064	0.005	194.76	1.31	0.052	0.982	−0.060	3.05	1
T3910018	1993-Apr-15	49092.8908	0.2793	2.018	400.0	172.33	274.53	13.219	0.005	208.82	2.09	0.066	0.974	−0.055	2.70	1
T3910019	1993-Apr-15	49092.8970	0.2810	2.039	400.0	177.25	271.45	12.690	0.004	212.19	1.98	0.059	0.979	−0.061	3.00	1
T3910020	1993-Apr-15	49092.9070	0.2838	2.071	400.0	175.28	270.98	12.668	0.004	214.34	2.09	0.049	0.978	−0.059	2.98	1
T3910021	1993-Apr-15	49092.9131	0.2855	2.090	400.0	176.39	271.57	12.751	0.004	213.49	1.80	0.044	0.967	−0.059	3.07	1
T3910022	1993-Apr-15	49092.9190	0.2871	2.107	400.0	174.46	272.06	12.741	0.004	209.92	1.78	0.043	0.978	−0.063	3.01	1
T3910023	1993-Apr-15	49092.9246	0.2886	2.122	400.0	174.57	271.80	12.716	0.004	200.50	1.88	0.043	0.973	−0.060	2.91	1
T3910024	1993-Apr-15	49092.9319	0.2906	2.141	400.0	176.27	272.43	12.782	0.003	201.00	1.48	0.039	0.969	−0.057	3.04	1
T3910025	1993-Apr-15	49093.0329	0.3185	2.199	400.0	172.87	272.28	13.690	0.004	189.79	1.23	0.030	0.980	−0.052	3.54	1
T3910026	1993-Apr-15	49093.0413	0.3208	2.186	400.0	174.11	272.14	12.743	0.003	207.56	1.48	0.033	0.986	−0.053	3.25	1
T3910027	1993-Apr-15	49093.0472	0.3225	2.175	400.0	174.21	272.58	13.100	0.004	206.22	1.56	0.038	0.989	−0.054	3.38	1
T3930003	1993-Apr-17	49094.8501	0.8196	1.890	400.0	174.42	274.52	13.856	0.006	189.17	1.53	0.032	1.018	−0.054	3.48	1
T3930004	1993-Apr-17	49094.8574	0.8216	1.918	400.0	172.67	272.70	13.427	0.004	194.89	1.28	0.020	1.002	−0.048	3.37	1
T3930005	1993-Apr-17	49094.8632	0.8232	1.939	400.0	172.46	272.61	13.541	0.004	199.19	1.41	0.017	1.001	−0.052	3.95	1
T3930006	1993-Apr-17	49094.8692	0.8249	1.961	400.0	172.66	273.54	13.671	0.005	197.31	1.39	0.013	0.991	−0.053	4.63	1
T3930007	1993-Apr-17	49094.8753	0.8266	1.983	400.0	172.85	273.33	13.773	0.004	198.71	1.16	0.002	1.010	−0.065	4.78	1
T3930008	1993-Apr-17	49094.8808	0.8281	2.002	400.0	172.54	273.25	13.629	0.005	201.09	1.48	0.002	1.005	−0.052	4.79	1

Table A.11 cont.: HV 1620 differential photometry – V.

Frame	Date	HJD −2400000.0	Orbital Phase	X	T	Row	Col	$m_{\rm raw}$	$\sigma_{m_{\rm raw}}$	sky	CHI	Sharp	$V-C$	$C-C$	Seeing (FWHM)	ILCA
T3930009	1993-Apr-17	49094.8868	0.8297	2.023	400.0	172.55	273.01	13.736	0.004	197.75	1.29	0.010	1.005	−0.051	4.29	1
T3930010	1993-Apr-17	49094.8930	0.8314	2.044	400.0	172.01	274.08	14.021	0.005	196.92	1.33	0.007	1.008	−0.058	4.75	1
T3930011	1993-Apr-17	49094.8993	0.8332	2.064	400.0	171.30	274.48	14.156	0.006	190.12	1.50	0.019	1.029	−0.057	4.17	1
T3930012	1993-Apr-17	49094.9811	0.8557	2.224	400.0	172.58	275.16	14.671	0.007	209.06	1.21	0.004	1.025	−0.055	5.22	0
T3930013	1993-Apr-17	49095.0065	0.8627	2.221	400.0	172.24	275.26	13.461	0.004	215.11	1.42	0.004	1.020	−0.053	5.31	0
T3930014	1993-Apr-17	49095.0155	0.8652	2.214	400.0	170.93	274.01	13.244	0.005	204.83	1.73	−0.003	1.035	−0.054	4.90	1
T3930015	1993-Apr-17	49095.0212	0.8668	2.208	400.0	173.35	274.97	13.179	0.003	200.81	1.27	0.004	1.035	−0.057	4.72	1
T3930016	1993-Apr-17	49095.0272	0.8684	2.200	400.0	174.93	270.28	13.069	0.003	198.85	1.35	0.005	1.051	−0.051	4.42	1
T3930017	1993-Apr-17	49095.0367	0.8711	2.184	400.0	173.96	269.86	13.373	0.003	192.57	1.18	0.005	1.059	−0.055	4.29	1
T3930020	1993-Apr-18	49095.8298	0.0898	1.824	400.0	174.93	272.57	13.050	0.003	179.40	1.29	0.002	1.069	−0.052	4.41	1
T3930021	1993-Apr-18	49095.8413	0.0929	1.868	400.0	175.43	272.81	13.145	0.003	175.72	1.36	0.002	1.049	−0.044	4.63	1
T3930022	1993-Apr-18	49095.8472	0.0946	1.890	400.0	174.85	273.36	12.924	0.003	171.59	1.33	0.007	1.068	−0.055	3.98	1
T3930023	1993-Apr-18	49095.8534	0.0963	1.913	400.0	172.98	270.31	12.939	0.003	169.52	1.28	0.005	1.062	−0.051	4.07	1
T3930024	1993-Apr-18	49095.8592	0.0979	1.935	400.0	173.03	270.52	12.962	0.003	171.24	1.34	0.009	1.058	−0.049	4.06	1
T3930025	1993-Apr-18	49095.8651	0.0995	1.956	400.0	172.57	270.39	12.946	0.003	173.89	1.23	0.011	1.059	−0.049	3.98	1
T3930026	1993-Apr-18	49095.8710	0.1011	1.977	400.0	172.55	269.67	12.866	0.003	170.42	1.50	0.012	1.059	−0.050	3.64	1
T3930027	1993-Apr-18	49095.8767	0.1027	1.997	400.0	172.44	270.07	13.017	0.003	170.49	1.33	0.007	1.056	−0.048	4.12	1
T3930028	1993-Apr-18	49095.8822	0.1042	2.016	400.0	172.69	269.88	12.860	0.003	169.56	1.42	0.013	1.056	−0.052	3.61	1
T3930029	1993-Apr-18	49095.8881	0.1058	2.036	400.0	172.82	270.33	12.851	0.002	169.69	1.16	0.009	1.053	−0.049	3.69	1
T3930031	1993-Apr-18	49095.9788	0.1308	2.224	400.0	174.29	273.43	13.077	0.004	203.47	1.50	0.019	1.035	−0.052	4.09	1
T3930032	1993-Apr-18	49095.9886	0.1336	2.226	400.0	173.88	273.68	13.043	0.003	208.49	1.32	0.015	1.032	−0.058	4.00	1
T3930033	1993-Apr-18	49095.9954	0.1354	2.225	400.0	173.76	273.85	13.597	0.005	214.32	1.55	0.012	1.030	−0.058	4.55	1
T0010007	1993-Apr-21	49099.0012	0.9643	2.217	400.0	172.35	273.69	13.645	0.005	205.10	1.58	0.004	1.279	−0.052	5.07	0
T0010008	1993-Apr-21	49099.0086	0.9663	2.210	400.0	170.77	272.76	13.441	0.004	211.34	1.44	0.012	1.293	−0.051	4.47	1
T0010009	1993-Apr-21	49099.0254	0.9710	2.185	400.0	173.27	273.83	13.427	0.004	218.35	1.34	0.005	1.317	−0.056	4.44	1
T0010010	1993-Apr-21	49099.0408	0.9752	2.154	400.0	173.38	274.22	13.565	0.004	224.79	1.30	0.000	1.352	−0.052	4.85	1
T0010011	1993-Apr-21	49099.0526	0.9785	2.125	400.0	173.35	273.29	13.965	0.005	226.45	1.35	0.010	1.376	−0.068	4.99	0
T3960011	1993-May-23	49130.9963	0.7871	2.035	400.0	174.38	269.27	12.540	0.003	232.52	1.53	−0.005	0.985	−0.049	3.13	1
T3960012	1993-May-23	49131.0017	0.7886	2.016	400.0	174.89	269.69	12.467	0.004	229.69	1.95	0.000	0.988	−0.054	2.88	1
T3960013	1993-May-23	49131.0085	0.7905	1.993	400.0	174.33	269.56	12.475	0.003	229.50	1.88	−0.001	0.983	−0.054	2.95	1
T3960014	1993-May-23	49131.0142	0.7920	1.973	400.0	174.88	270.15	12.414	0.004	228.14	2.19	−0.004	0.983	−0.051	2.70	1
T3960015	1993-May-23	49131.0197	0.7935	1.953	400.0	174.76	270.00	12.489	0.003	234.74	1.93	−0.012	0.986	−0.055	3.03	1
T3960016	1993-May-23	49131.2624	0.8605	1.236	400.0	175.21	272.78	12.412	0.003	159.57	1.86	0.010	1.044	−0.056	2.99	1
T3960017	1993-May-23	49131.2685	0.8622	1.227	400.0	174.01	271.86	12.380	0.004	159.92	2.11	0.017	1.049	−0.055	2.82	1
T3960018	1993-May-23	49131.2740	0.8637	1.219	400.0	173.20	273.69	12.425	0.003	177.88	1.96	0.005	1.043	−0.056	3.05	1
T3960019	1993-May-23	49131.2794	0.8652	1.212	400.0	174.53	273.36	12.485	0.003	250.58	1.55	0.024	1.045	−0.055	3.14	1
T3960020	1993-May-23	49131.2848	0.8666	1.205	400.0	174.60	272.60	12.416	0.003	520.12	1.70	0.013	1.046	−0.057	2.90	1
T3960021	1993-May-23	49131.2907	0.8683	1.198	400.0	174.28	273.15	12.463	0.003	1697.6	1.46	0.020	1.045	−0.053	3.13	1
T4250023	1993-Jul-26	49195.1164	0.4685	1.199	400.0	174.29	274.90	13.481	0.004	126.90	1.32	0.000	1.164	−0.056	5.93	0

Table A.11 cont.: HV 1620 differential photometry – V.

Frame	Date	HJD −2400000.0	Orbital Phase	X	T	Row	Col	$m_{\rm raw}$	$\sigma_{m_{\rm raw}}$	sky	CHI	Sharp	$V-C$	$C-C$	Seeing (FWHM)	ILCA
T4250024	1993-Jul-26	49195.1352	0.4737	1.179	400.0	174.84	275.15	13.669	0.004	130.44	1.14	−0.002	1.182	−0.052	6.54	0
T4250025	1993-Jul-26	49195.1450	0.4764	1.170	400.0	174.87	273.78	13.546	0.004	130.54	1.30	−0.005	1.199	−0.051	6.02	0
T4250026	1993-Jul-26	49195.1509	0.4781	1.165	400.0	173.89	273.04	13.646	0.004	132.48	1.14	−0.005	1.201	−0.054	6.45	0
T4250030	1993-Jul-26	49195.1705	0.4834	1.152	400.0	172.72	273.66	13.661	0.005	129.23	1.43	−0.010	1.222	−0.049	6.23	0
T4250031	1993-Jul-26	49195.1763	0.4850	1.149	400.0	174.76	273.52	13.588	0.004	129.51	1.18	0.002	1.226	−0.048	5.99	0
T4250032	1993-Jul-26	49195.1834	0.4870	1.146	400.0	173.23	272.77	13.357	0.003	131.60	1.28	0.000	1.239	−0.052	5.34	0
T4260002	1993-Jul-26	49195.2054	0.4931	1.140	400.0	173.80	273.24	13.306	0.004	132.43	1.36	−0.001	1.262	−0.045	4.93	1
T4260004	1993-Jul-26	49195.2162	0.4961	1.138	400.0	174.10	272.16	13.338	0.004	130.85	1.32	−0.002	1.280	−0.047	5.12	0
T4260006	1993-Jul-26	49195.2292	0.4997	1.139	400.0	174.13	272.30	13.274	0.004	129.87	1.48	−0.003	1.283	−0.045	4.86	1
T4260008	1993-Jul-26	49195.2429	0.5034	1.141	400.0	171.65	271.91	13.370	0.004	130.76	1.32	0.001	1.274	−0.043	5.00	1
T4260011	1993-Jul-26	49195.2737	0.5119	1.154	400.0	173.69	271.41	13.107	0.004	132.50	1.46	0.002	1.289	−0.047	4.36	1
T4260012	1993-Jul-26	49195.2799	0.5136	1.158	400.0	172.67	271.02	13.255	0.004	150.57	1.53	0.001	1.284	−0.050	4.66	1
T4260021	1993-Jul-27	49195.8383	0.6676	1.973	400.0	173.54	270.50	13.147	0.003	555.20	1.11	0.004	0.982	−0.043	4.56	1
T4260024	1993-Jul-27	49195.8544	0.6720	1.914	400.0	173.42	270.50	13.041	0.004	542.94	1.40	0.008	0.975	−0.044	4.28	1
T4260027	1993-Jul-27	49195.8822	0.6797	1.809	400.0	173.77	271.04	12.935	0.004	510.60	1.48	0.011	0.976	−0.039	4.09	0
T4260029	1993-Jul-27	49195.8932	0.6827	1.768	400.0	173.81	270.32	12.903	0.003	506.81	1.33	0.012	0.974	−0.046	3.97	1
T4260032	1993-Jul-27	49195.9224	0.6908	1.660	400.0	175.00	271.87	13.001	0.004	480.18	1.38	0.001	0.972	−0.044	4.49	1
T4260034	1993-Jul-27	49195.9347	0.6942	1.617	400.0	174.95	271.62	12.919	0.003	466.39	1.45	0.009	0.963	−0.045	4.17	1
S1300004	1993-Aug-19	49218.9273	0.0345	1.443	400.0	182.79	263.01	17.937	0.016	92.57	1.38	0.049	*	*	3.65	0
S1300005	1993-Aug-19	49218.9374	0.0373	1.416	400.0	175.45	274.01	13.015	0.004	144.56	1.81	0.017	1.369	−0.053	3.39	1
S1300008	1993-Aug-19	49218.9746	0.0475	1.326	400.0	177.11	275.72	12.970	0.004	136.17	1.73	0.022	1.289	−0.051	3.53	1
S1300009	1993-Aug-19	49218.9937	0.0528	1.287	400.0	175.55	274.36	14.546	0.008	133.17	1.44	0.036	1.250	−0.052	3.70	1
S1330006	1993-Aug-20	49220.1220	0.3639	1.143	400.0	174.49	274.37	14.158	0.007	154.95	1.67	0.085	1.028	−0.059	2.84	1
T0780003	1993-Sep-06	49236.9023	0.9912	1.379	400.0	173.21	270.44	13.143	0.004	121.21	1.70	0.030	1.479	−0.063	3.41	1
T0780004	1993-Sep-06	49236.9175	0.9954	1.343	400.0	172.48	272.48	13.178	0.005	120.42	1.96	0.035	1.498	−0.059	3.51	1
T0780005	1993-Sep-06	49236.9235	0.9970	1.330	400.0	172.27	272.12	13.105	0.005	119.38	1.97	0.037	1.501	−0.058	3.20	1
T0780006	1993-Sep-06	49236.9318	0.9993	1.312	400.0	172.92	272.10	13.080	0.005	120.16	2.07	0.049	1.511	−0.059	3.14	1
T0780007	1993-Sep-06	49236.9376	0.0010	1.300	400.0	172.49	273.25	13.083	0.004	119.81	1.86	0.044	1.510	−0.059	3.10	1
T0780008	1993-Sep-06	49236.9461	0.0033	1.284	400.0	172.56	272.47	13.020	0.004	119.14	1.97	0.047	1.521	−0.058	2.92	1
T0780009	1993-Sep-06	49236.9518	0.0049	1.273	400.0	172.59	272.09	12.975	0.005	117.67	2.33	0.054	1.513	−0.056	2.75	1
T0780010	1993-Sep-06	49236.9589	0.0068	1.261	400.0	172.52	272.32	13.033	0.005	119.13	2.07	0.043	1.515	−0.052	2.99	1
T0780011	1993-Sep-06	49236.9651	0.0085	1.250	400.0	171.86	272.62	12.994	0.005	118.72	2.13	0.046	1.514	−0.058	2.88	1
T0780012	1993-Sep-06	49236.9716	0.0103	1.240	400.0	172.08	272.05	12.884	0.006	119.60	2.77	0.060	1.510	−0.060	2.47	1
T0780013	1993-Sep-06	49236.9793	0.0124	1.228	400.0	175.46	271.59	12.904	0.005	133.28	2.46	0.057	1.503	−0.056	2.50	1
T0780014	1993-Sep-06	49236.9871	0.0146	1.217	400.0	173.62	270.86	12.949	0.005	161.95	2.34	0.060	1.504	−0.055	2.79	1
T0780015	1993-Sep-06	49236.9948	0.0167	1.207	400.0	175.04	270.62	12.909	0.006	193.98	2.72	0.061	1.489	−0.056	2.54	1
T0780016	1993-Sep-06	49237.0060	0.0198	1.194	400.0	173.49	271.46	12.924	0.005	238.88	2.28	0.048	1.482	−0.058	2.62	1
T0780017	1993-Sep-06	49237.0151	0.0223	1.184	400.0	175.15	271.31	12.912	0.005	269.93	2.35	0.063	1.469	−0.059	2.78	1
T0780018	1993-Sep-06	49237.0221	0.0243	1.177	400.0	173.29	271.04	12.849	0.005	288.86	2.37	0.052	1.450	−0.051	2.59	1

Table A.11 cont.: HV 1620 differential photometry – V.

Frame	Date	HJD −2400000.0	Orbital Phase	X	T	Row	Col	$m_{\rm raw}$	$\sigma_{m_{\rm raw}}$	sky	CHI	Sharp	$V-C$	$C-C$	Seeing (FWHM)	ILCA
T0780019	1993-Sep-06	49237.0278	0.0258	1.172	400.0	173.84	273.58	12.852	0.005	301.75	2.31	0.051	1.448	−0.062	2.66	1
T0780020	1993-Sep-06	49237.0341	0.0276	1.167	400.0	175.25	271.28	12.834	0.005	314.93	2.16	0.054	1.426	−0.064	2.61	1
T0780021	1993-Sep-06	49237.0415	0.0296	1.161	400.0	172.28	270.21	12.809	0.005	328.55	2.14	0.054	1.418	−0.058	2.55	1
T0780022	1993-Sep-06	49237.0505	0.0321	1.155	400.0	174.71	271.70	12.774	0.005	341.13	2.30	0.062	1.397	−0.056	2.46	1
T0780023	1993-Sep-06	49237.0564	0.0337	1.152	400.0	170.67	271.98	12.908	0.004	352.31	1.93	0.044	1.390	−0.054	2.96	1
T0780024	1993-Sep-06	49237.0662	0.0364	1.147	400.0	174.47	272.19	12.852	0.005	358.66	2.12	0.045	1.365	−0.052	2.84	1
T0780025	1993-Sep-06	49237.0722	0.0381	1.144	400.0	174.65	271.31	12.818	0.004	368.09	2.04	0.043	1.354	−0.055	2.89	1
T0780026	1993-Sep-06	49237.0804	0.0403	1.142	400.0	174.60	271.50	12.754	0.005	373.33	2.26	0.065	1.339	−0.056	2.52	1
T0780027	1993-Sep-06	49237.0876	0.0423	1.140	400.0	174.56	271.15	12.733	0.005	379.99	2.28	0.057	1.327	−0.055	2.56	1
T0780028	1993-Sep-06	49237.0932	0.0438	1.139	400.0	176.30	272.21	12.763	0.004	384.75	1.95	0.048	1.309	−0.060	2.76	1
T0780029	1993-Sep-06	49237.0997	0.0456	1.139	400.0	175.31	270.40	12.721	0.004	387.70	2.10	0.060	1.297	−0.055	2.64	1
T0780030	1993-Sep-06	49237.1069	0.0476	1.138	400.0	173.59	271.52	12.734	0.004	387.36	2.12	0.048	1.290	−0.056	2.74	1
T0780031	1993-Sep-06	49237.1127	0.0492	1.139	400.0	172.76	273.66	12.703	0.005	393.01	2.19	0.043	1.271	−0.056	2.78	1
T0780032	1993-Sep-06	49237.1189	0.0509	1.139	400.0	174.73	271.17	12.624	0.005	389.21	2.22	0.056	1.261	−0.059	2.40	1
T0780033	1993-Sep-06	49237.1250	0.0526	1.140	400.0	170.41	273.94	12.653	0.004	394.17	2.10	0.044	1.253	−0.058	2.60	1
T0780034	1993-Sep-06	49237.1323	0.0546	1.142	400.0	174.73	270.91	12.684	0.004	398.75	1.83	0.047	1.239	−0.056	2.78	1
T0800001	1993-Sep-06	49237.1427	0.0575	1.146	400.0	173.42	270.62	12.692	0.004	396.80	2.08	0.049	1.213	−0.051	2.82	1
T0800002	1993-Sep-06	49237.1488	0.0592	1.149	400.0	170.49	272.48	12.655	0.004	396.50	2.06	0.040	1.202	−0.053	2.79	1
T0800003	1993-Sep-06	49237.1547	0.0608	1.152	400.0	171.98	270.64	12.622	0.004	395.14	2.02	0.052	1.191	−0.052	2.62	1
T0800004	1993-Sep-06	49237.1605	0.0624	1.155	400.0	172.49	271.77	12.637	0.004	395.47	2.00	0.044	1.182	−0.055	2.70	1
T0800005	1993-Sep-06	49237.1662	0.0640	1.159	400.0	172.78	271.09	12.700	0.004	396.07	2.01	0.049	1.169	−0.051	2.93	1
T0800006	1993-Sep-06	49237.1729	0.0658	1.164	400.0	172.79	271.42	12.663	0.004	389.21	2.14	0.043	1.162	−0.054	2.78	1
T0800007	1993-Sep-06	49237.1785	0.0674	1.168	400.0	172.73	272.33	12.696	0.005	381.95	2.18	0.058	1.155	−0.054	2.76	1
T0800008	1993-Sep-06	49237.1840	0.0689	1.173	400.0	172.86	271.78	12.671	0.005	390.03	2.21	0.058	1.143	−0.056	2.49	1
T0800009	1993-Sep-06	49237.1924	0.0712	1.181	400.0	171.95	271.31	12.649	0.004	485.21	1.90	0.023	1.128	−0.051	2.70	1
T0800010	1993-Sep-06	49237.1980	0.0727	1.186	400.0	170.24	271.73	12.668	0.004	477.98	1.88	0.040	1.121	−0.050	2.74	1
T0800012	1993-Sep-06	49237.2270	0.0808	1.222	400.0	173.04	271.85	12.611	0.004	405.92	2.18	0.056	1.095	−0.057	2.80	1
T0800013	1993-Sep-06	49237.2331	0.0824	1.231	400.0	172.08	271.02	12.614	0.004	407.83	1.90	0.050	1.090	−0.055	2.77	1
T0800014	1993-Sep-06	49237.2388	0.0840	1.239	400.0	171.83	270.62	12.613	0.004	423.36	2.13	0.049	1.079	−0.055	2.83	1
T0810024	1993-Sep-07	49238.0964	0.3205	1.139	400.0	173.18	272.20	12.174	0.006	283.62	3.60	−0.027	0.978	−0.064	2.57	0
T0810025	1993-Sep-07	49238.1035	0.3224	1.138	400.0	172.56	272.17	12.188	0.006	287.73	3.19	−0.016	0.963	−0.054	2.30	0
T0810027	1993-Sep-07	49238.1189	0.3267	1.140	400.0	173.88	271.05	12.179	0.006	297.23	3.22	−0.015	0.970	−0.064	2.24	0
T0810028	1993-Sep-07	49238.1249	0.3284	1.141	400.0	172.40	271.09	12.216	0.004	297.00	2.47	−0.006	0.974	−0.060	2.32	0
T0810029	1993-Sep-07	49238.1312	0.3301	1.143	400.0	175.94	272.73	12.204	0.004	299.42	1.78	0.023	0.978	−0.062	2.02	0
T0810030	1993-Sep-07	49238.1375	0.3318	1.145	400.0	174.30	272.80	12.213	0.017	302.12	8.87	−0.200	0.945	−0.058	2.36	0
T0810031	1993-Sep-07	49238.1431	0.3333	1.147	400.0	173.83	273.11	12.200	0.018	302.32	9.18	−0.158	0.948	−0.056	2.35	0
T0810032	1993-Sep-07	49238.1486	0.3349	1.150	400.0	172.32	271.84	12.213	0.008	305.69	3.66	−0.025	0.971	−0.061	2.16	0
T0810033	1993-Sep-07	49238.1553	0.3367	1.154	400.0	174.16	272.20	12.195	0.017	309.48	8.83	−0.173	0.940	−0.072	2.32	0
T0810034	1993-Sep-07	49238.1609	0.3383	1.157	400.0	174.33	272.01	12.234	0.008	314.48	4.13	−0.046	0.979	−0.055	2.43	0

Table A.11 cont.: HV 1620 differential photometry – V.

Frame	Date	HJD −2400000.0	Orbital Phase	X	T	Row	Col	$m_{\rm raw}$	$\sigma_{m_{\rm raw}}$	sky	CHI	Sharp	$V-C$	$C-C$	Seeing (FWHM)	ILCA
T0810035	1993-Sep-07	49238.1668	0.3399	1.161	400.0	172.21	271.12	12.208	0.006	315.59	3.19	−0.020	0.968	−0.054	2.14	0
T0810036	1993-Sep-07	49238.1728	0.3415	1.166	400.0	*	*	*	*	*	*	*	*	*	*	0
S1600002	1993-Sep-07	49238.1869	0.3454	1.178	400.0	174.50	273.09	12.234	0.018	313.77	8.76	−0.187	0.959	−0.066	2.26	0
S1600003	1993-Sep-07	49238.1929	0.3471	1.184	400.0	173.86	273.29	12.266	0.004	317.26	1.74	0.033	0.997	−0.065	1.96	0
S1600004	1993-Sep-07	49238.1989	0.3488	1.190	400.0	173.06	269.50	12.257	0.007	318.17	3.54	−0.022	0.993	−0.060	2.12	0
S1600005	1993-Sep-07	49238.2048	0.3504	1.197	400.0	173.76	270.56	12.282	0.006	319.66	2.95	−0.016	0.989	−0.064	2.17	0
S1600006	1993-Sep-07	49238.2114	0.3522	1.205	400.0	173.90	272.89	12.230	0.017	319.23	8.42	−0.183	0.963	−0.060	2.26	0
S1600007	1993-Sep-07	49238.2172	0.3538	1.212	400.0	172.87	272.33	12.287	0.006	322.68	3.01	−0.016	1.000	−0.053	2.42	0
S1600008	1993-Sep-07	49238.2230	0.3554	1.220	400.0	173.75	271.56	12.316	0.006	320.08	3.04	−0.008	0.995	−0.061	2.14	0
T4430017	1993-Sep-15	49245.8720	0.4647	1.392	400.0	174.48	274.30	13.336	0.004	159.73	1.39	−0.001	1.165	−0.052	5.05	0
T4430020	1993-Sep-15	49245.8975	0.4717	1.332	400.0	174.38	274.02	13.582	0.004	163.88	1.40	−0.001	1.195	−0.051	4.77	1
T4430023	1993-Sep-15	49245.9212	0.4782	1.284	400.0	174.60	274.17	13.671	0.004	158.15	1.37	0.001	1.217	−0.055	5.53	0
T4430026	1993-Sep-15	49245.9450	0.4848	1.243	400.0	173.72	273.92	13.480	0.004	151.73	1.22	0.004	1.244	−0.052	4.85	1
T4430029	1993-Sep-15	49245.9686	0.4913	1.209	400.0	174.40	273.15	13.486	0.005	133.82	1.62	0.004	1.273	−0.050	4.37	1
T4430032	1993-Sep-15	49245.9923	0.4978	1.182	400.0	174.78	273.78	13.411	0.004	132.35	1.54	0.014	1.289	−0.049	4.04	1
T4430035	1993-Sep-15	49246.0177	0.5048	1.160	400.0	174.83	272.18	13.477	0.004	133.76	1.44	0.018	1.291	−0.042	4.15	1
T4440001	1993-Sep-15	49246.0482	0.5132	1.144	400.0	174.77	271.12	13.234	0.004	151.13	1.45	0.013	1.290	−0.054	4.08	1
T4440004	1993-Sep-15	49246.0759	0.5209	1.139	400.0	174.74	271.25	13.342	0.004	155.16	1.43	0.017	1.270	−0.051	4.01	1
T4440007	1993-Sep-15	49246.1210	0.5333	1.147	400.0	173.50	269.56	12.972	0.004	170.00	1.60	0.027	1.229	−0.052	3.34	1
T4440010	1993-Sep-15	49246.1468	0.5404	1.163	400.0	173.01	269.42	13.062	0.005	151.31	1.96	0.035	1.209	−0.053	3.33	1
T4440013	1993-Sep-15	49246.1725	0.5475	1.186	400.0	173.58	269.29	13.405	0.004	125.58	1.52	0.028	1.181	−0.051	3.31	1
T4440016	1993-Sep-15	49246.2057	0.5567	1.227	400.0	173.12	269.50	13.560	0.003	104.29	1.13	0.011	1.149	−0.057	3.70	1
T4440019	1993-Sep-15	49246.2358	0.5650	1.276	400.0	172.67	270.12	13.119	0.004	223.22	1.65	0.025	1.145	−0.060	2.63	1
T5440007	1994-Jan-19	49372.0957	0.2715	1.914	400.0	174.43	269.42	15.203	0.010	172.74	1.22	−0.003	0.950	−0.061	6.19	0
T5820008	1994-Mar-12	49423.9029	0.5575	1.722	400.0	174.84	272.81	12.508	0.004	215.78	2.27	0.029	1.154	−0.059	2.50	1
T5820009	1994-Mar-12	49423.9090	0.5592	1.744	400.0	174.57	272.92	12.566	0.004	223.54	2.20	0.027	1.146	−0.052	2.32	1
T5820036	1994-Mar-15	49426.9592	0.4003	1.963	400.0	174.41	272.70	13.056	0.003	218.83	1.24	0.002	1.040	−0.053	4.73	1
T5960008	1994-Mar-17	49428.9113	0.9386	1.804	400.0	174.37	273.78	13.316	0.004	200.16	1.36	0.000	1.124	−0.054	5.24	0
T5960029	1994-Mar-21	49432.8797	0.0329	1.726	400.0	176.03	270.34	12.655	0.004	403.23	2.04	0.030	1.379	−0.059	2.32	1
T5960032	1994-Mar-21	49432.9064	0.0403	1.826	400.0	175.84	270.49	12.703	0.004	420.00	1.98	0.041	1.326	−0.051	2.57	1
T5960035	1994-Mar-21	49432.9310	0.0471	1.919	400.0	175.99	270.41	12.656	0.005	424.06	2.32	0.052	1.277	−0.052	2.36	1
T5980002	1994-Mar-21	49432.9604	0.0552	2.024	400.0	176.09	271.02	12.687	0.005	404.98	2.56	0.051	1.222	−0.048	2.58	1
T5980005	1994-Mar-21	49432.9842	0.0618	2.099	400.0	177.70	272.46	12.833	0.004	316.41	1.98	0.052	1.182	−0.049	2.59	1
T5980008	1994-Mar-21	49433.0088	0.0685	2.162	400.0	176.27	272.77	12.663	0.006	250.25	2.88	0.058	1.139	−0.048	2.54	1
T5980011	1994-Mar-21	49433.0334	0.0753	2.205	400.0	178.26	273.39	12.888	0.003	200.24	1.61	0.039	1.112	−0.051	3.16	1
T5980014	1994-Mar-21	49433.0511	0.0802	2.222	400.0	176.85	275.28	12.694	0.004	217.39	2.10	0.053	1.101	−0.049	2.66	1
T5980017	1994-Mar-21	49433.0770	0.0873	2.223	400.0	177.16	273.64	12.743	0.004	225.65	1.86	0.043	1.080	−0.056	2.99	1
T5980020	1994-Mar-21	49433.1015	0.0941	2.199	400.0	176.39	273.84	12.869	0.003	223.67	1.27	0.017	1.064	−0.057	3.44	1
T5980023	1994-Mar-21	49433.1268	0.1011	2.150	400.0	177.46	272.54	12.901	0.003	202.55	1.56	0.017	1.047	−0.050	3.70	1

Table A.11 cont.: HV 1620 differential photometry – V.

Frame	Date	HJD −2400000.0	Orbital Phase	X	T	Row	Col	$m_{\rm raw}$	$\sigma_{m_{\rm raw}}$	sky	CHI	Sharp	$V-C$	$C-C$	Seeing (FWHM)	ILCA
T5980026	1994-Mar-21	49433.1567	0.1093	2.067	400.0	175.92	273.76	12.899	0.005	189.71	2.44	−0.019	1.056	−0.057	4.25	1
T5980029	1994-Mar-21	49433.1815	0.1162	1.983	400.0	175.76	274.36	12.851	0.003	198.00	1.40	−0.003	1.055	−0.061	4.10	1
T5980033	1994-Mar-21	49433.2034	0.1222	1.903	400.0	175.71	273.37	12.784	0.003	200.07	1.38	−0.005	1.047	−0.060	4.03	1
T5470008	1994-Mar-24	49435.8759	0.8592	1.742	400.0	176.02	270.41	12.662	0.003	979.65	1.26	0.011	1.032	−0.054	3.47	1
T5470011	1994-Mar-24	49435.9034	0.8668	1.846	400.0	176.08	270.21	12.683	0.003	1020.1	1.40	0.013	1.035	−0.053	3.22	1
T5470014	1994-Mar-24	49435.9272	0.8733	1.935	400.0	175.85	270.74	12.891	0.003	1065.3	1.23	0.020	1.040	−0.051	3.67	1
T5470017	1994-Mar-24	49435.9520	0.8801	2.023	400.0	176.95	271.17	12.939	0.003	1126.7	1.11	0.009	1.051	−0.057	3.85	1
T5470020	1994-Mar-24	49435.9778	0.8873	2.104	400.0	177.27	272.90	12.891	0.003	1185.6	1.13	0.022	1.050	−0.050	3.28	1
T5470023	1994-Mar-24	49436.0022	0.8940	2.165	400.0	175.66	273.36	12.970	0.004	1191.6	1.43	0.022	1.062	−0.053	3.70	1
T5470026	1994-Mar-24	49436.0259	0.9005	2.206	400.0	176.61	274.20	13.032	0.004	1204.6	1.44	0.015	1.061	−0.049	4.07	1
T5470030	1994-Mar-24	49436.0476	0.9065	2.224	400.0	174.99	275.55	13.163	0.004	1196.0	1.20	0.007	1.063	−0.048	4.57	1
T5470033	1994-Mar-24	49436.0721	0.9133	2.221	400.0	174.16	274.81	13.227	0.004	1121.1	1.13	0.001	1.060	−0.051	4.87	1
T5470036	1994-Mar-24	49436.1069	0.9229	2.175	400.0	175.80	274.57	13.377	0.004	942.36	1.03	−0.005	1.065	−0.056	5.51	0
T6210002	1994-Mar-24	49436.1404	0.9321	2.092	400.0	177.86	268.73	13.423	0.004	419.96	1.32	0.004	1.092	−0.063	5.67	0
T6210005	1994-Mar-24	49436.1653	0.9390	2.012	400.0	174.60	269.68	13.347	0.004	214.87	1.26	−0.001	1.110	−0.056	5.54	0
T6210008	1994-Mar-24	49436.1842	0.9442	1.944	400.0	178.81	268.85	13.517	0.004	223.47	1.16	−0.004	1.136	−0.059	5.95	0
T5060008	1994-Apr-06	49448.8967	0.4497	1.951	400.0	175.45	273.73	12.880	0.004	238.30	2.02	0.048	1.123	−0.045	2.64	1
T5060011	1994-Apr-06	49448.9260	0.4578	2.053	400.0	176.28	274.34	12.603	0.006	270.18	2.81	0.075	1.155	−0.052	2.29	1
T5060014	1994-Apr-06	49448.9552	0.4659	2.137	300.0	176.04	275.75	13.165	0.006	223.86	2.25	0.060	1.182	−0.052	2.75	1
T5060016	1994-Apr-06	49448.9636	0.4682	2.157	300.0	175.69	276.22	13.610	0.006	219.42	1.81	0.054	1.191	−0.039	2.96	0
T5060019	1994-Apr-06	49448.9880	0.4749	2.202	400.0	176.12	277.70	13.284	0.004	244.61	1.62	0.029	1.203	−0.042	3.37	1
T5060023	1994-Apr-06	49449.0144	0.4822	2.225	400.0	175.51	277.61	13.803	0.006	281.86	1.70	0.043	1.223	−0.036	3.51	0
T5060025	1994-Apr-06	49449.0353	0.4879	2.223	400.0	176.11	277.30	13.526	0.005	297.72	1.60	0.014	1.245	−0.044	4.23	1
T5060028	1994-Apr-06	49449.0875	0.5023	2.140	400.0	175.72	277.90	14.072	0.006	332.32	1.33	0.000	1.249	−0.050	5.66	0
T5060031	1994-Apr-06	49449.1064	0.5076	2.089	400.0	177.71	275.58	13.489	0.005	380.72	1.39	−0.001	1.262	−0.052	5.22	0
T5300002	1994-May-16	49488.8498	0.4670	2.143	400.0	176.79	271.46	13.246	0.004	272.90	1.34	0.002	1.164	−0.046	4.88	1
T5300024	1994-May-16	49489.0797	0.5304	1.801	400.0	178.52	275.36	13.121	0.004	214.35	1.71	0.013	1.241	−0.057	4.07	1
T5300028	1994-May-16	49489.1195	0.5414	1.654	400.0	178.35	275.74	13.110	0.003	211.42	1.24	0.007	1.193	−0.055	4.44	1
T5300032	1994-May-16	49489.1749	0.5566	1.473	400.0	178.24	278.17	13.004	0.004	228.10	1.63	0.012	1.144	−0.055	4.25	1
T5300036	1994-May-16	49489.2123	0.5670	1.373	400.0	173.75	274.24	12.896	0.004	211.75	1.61	0.003	1.106	−0.049	4.23	1
T5440022	1994-Jun-10	49514.1259	0.4370	1.422	400.0	175.39	274.41	12.872	0.003	147.65	1.56	0.020	1.104	−0.063	3.26	1
T5440025	1994-Jun-10	49514.1489	0.4433	1.364	400.0	175.16	274.54	12.673	0.003	153.36	1.65	0.025	1.116	−0.056	3.22	1
T5440028	1994-Jun-10	49514.1719	0.4497	1.312	400.0	175.45	275.86	13.520	0.005	145.12	1.75	0.038	1.142	−0.064	3.06	1
T4580008	1994-Jun-12	49515.7880	0.8953	2.168	400.0	175.65	273.33	13.060	0.003	185.57	1.26	0.004	1.062	−0.056	4.64	1
T4580010	1994-Jun-12	49515.8478	0.9118	2.226	400.0	176.65	275.70	13.145	0.003	192.91	1.23	0.008	1.083	−0.061	4.40	1
T4580014	1994-Jun-12	49515.8717	0.9184	2.208	400.0	176.17	275.14	13.103	0.003	192.71	1.33	0.008	1.087	−0.058	4.46	1
T4580017	1994-Jun-12	49515.8956	0.9250	2.167	400.0	176.38	276.12	13.099	0.003	178.51	1.26	−0.003	1.089	−0.058	4.50	1
T4580020	1994-Jun-12	49515.9191	0.9315	2.109	400.0	176.37	274.95	12.967	0.003	168.60	1.29	0.008	1.112	−0.057	4.02	1
T4580023	1994-Jun-12	49515.9433	0.9381	2.034	400.0	176.70	274.96	13.043	0.004	188.60	1.49	0.012	1.140	−0.060	4.13	1

Table A.11 cont.: HV 1620 differential photometry – V.

Frame	Date	HJD −2400000.0	Orbital Phase	X	T	Row	Col	$m_{\rm raw}$	$\sigma_{m_{\rm raw}}$	sky	CHI	Sharp	$V-C$	$C-C$	Seeing (FWHM)	ILCA
T4580026	1994-Jun-12	49515.9612	0.9431	1.972	400.0	176.27	275.69	13.044	0.004	179.49	1.56	0.012	1.161	−0.061	4.15	1
T4580029	1994-Jun-12	49515.9855	0.9498	1.882	400.0	177.56	276.34	13.163	0.004	174.39	1.64	0.006	1.187	−0.053	4.36	1
T4580032	1994-Jun-12	49516.0117	0.9570	1.783	400.0	173.09	274.04	13.018	0.004	152.74	1.68	0.016	1.228	−0.049	3.91	1
T4580035	1994-Jun-12	49516.0355	0.9636	1.695	400.0	173.87	274.23	12.928	0.004	151.74	1.68	0.011	1.280	−0.062	3.53	1
T4590001	1994-Jun-12	49516.0631	0.9712	1.597	400.0	174.38	274.86	12.966	0.004	174.41	1.83	0.020	1.328	−0.057	3.24	1
T4590004	1994-Jun-12	49516.0877	0.9780	1.517	400.0	174.07	275.64	12.882	0.005	181.79	2.50	0.060	1.372	−0.053	2.90	1
T4590007	1994-Jun-12	49516.1057	0.9829	1.463	400.0	175.57	275.94	12.874	0.005	194.90	2.60	0.048	1.412	−0.059	2.77	1
T4590010	1994-Jun-12	49516.1306	0.9898	1.395	400.0	175.35	276.44	12.840	0.005	191.95	2.18	0.053	1.447	−0.054	2.64	1
T4590013	1994-Jun-12	49516.1559	0.9968	1.335	400.0	174.68	274.49	12.959	0.004	185.48	1.90	0.053	1.486	−0.060	2.92	1
T4590016	1994-Jun-12	49516.1846	0.0047	1.277	400.0	175.85	273.25	13.036	0.005	174.14	2.13	0.048	1.499	−0.055	3.12	1
T4590019	1994-Jun-12	49516.2087	0.0113	1.237	400.0	175.73	272.59	13.057	0.004	168.40	1.87	0.029	1.493	−0.053	3.14	1
T4590022	1994-Jun-12	49516.2327	0.0179	1.204	400.0	174.88	271.92	13.005	0.005	167.68	2.17	0.044	1.474	−0.055	3.16	1
T4590025	1994-Jun-12	49516.2507	0.0229	1.183	400.0	174.89	271.77	12.997	0.004	165.21	1.92	0.040	1.450	−0.059	3.19	1
T4810008	1994-Jul-30	49564.0013	0.1904	1.393	400.0	175.69	273.95	12.354	0.003	102.67	1.85	0.020	0.982	−0.059	2.71	1
T4810014	1994-Jul-30	49564.2272	0.2527	1.140	400.0	173.67	273.86	12.367	0.003	194.17	1.81	0.028	0.943	−0.049	2.69	1
T4810016	1994-Jul-30	49564.2393	0.2560	1.143	300.0	172.49	273.11	12.604	0.003	145.93	1.78	0.027	0.945	−0.048	2.43	1
T4810019	1994-Jul-30	49564.2618	0.2622	1.153	300.0	173.01	272.55	12.611	0.005	143.51	2.63	0.055	0.947	−0.055	2.37	1
T4810022	1994-Jul-30	49564.2834	0.2682	1.168	300.0	172.47	272.19	12.691	0.005	237.88	2.26	0.050	0.943	−0.049	2.47	1
T4810031	1994-Jul-31	49564.8021	0.4112	2.062	400.0	172.09	274.26	12.779	0.003	138.65	1.62	0.014	1.050	−0.053	3.72	1
T4810034	1994-Jul-31	49564.8252	0.4176	1.983	400.0	172.76	274.55	12.704	0.003	127.31	1.58	0.009	1.060	−0.053	3.17	1
T4810037	1994-Jul-31	49564.8487	0.4241	1.897	400.0	172.75	275.09	12.595	0.003	130.24	1.81	0.028	1.064	−0.052	2.86	1
T6360002	1994-Jul-31	49564.8777	0.4320	1.788	400.0	173.33	275.74	12.482	0.004	116.26	2.36	0.023	1.081	−0.057	2.58	1
T6360005	1994-Jul-31	49564.9013	0.4386	1.700	400.0	173.66	275.77	12.523	0.004	114.48	2.05	0.026	1.088	−0.054	2.64	1
T6370005	1994-Aug-01	49565.7909	0.6839	2.088	400.0	174.15	274.00	12.987	0.003	187.60	1.33	−0.002	0.972	−0.051	4.76	1
T6370008	1994-Aug-01	49565.8163	0.6909	2.005	400.0	174.93	273.50	13.568	0.004	140.30	1.41	0.002	0.968	−0.053	5.26	0
T6370011	1994-Aug-01	49565.8399	0.6974	1.920	400.0	175.40	273.66	13.492	0.004	137.74	1.32	0.005	0.983	−0.062	4.60	1
T6370014	1994-Aug-01	49565.8642	0.7041	1.828	400.0	175.26	274.36	15.081	0.009	196.65	1.13	−0.002	0.974	−0.057	4.37	1
T4780002	1994-Aug-25	49589.8081	0.3067	1.792	400.0	174.53	272.82	12.654	0.002	223.01	1.25	0.005	0.964	−0.053	3.74	1
T4780005	1994-Aug-25	49589.8348	0.3141	1.693	400.0	175.72	274.39	12.642	0.003	178.99	1.54	0.013	0.971	−0.054	3.66	1
T4780008	1994-Aug-25	49589.8583	0.3206	1.609	400.0	176.86	275.40	12.472	0.003	163.68	1.59	0.013	0.977	−0.048	2.99	1
T4780011	1994-Aug-25	49589.8822	0.3272	1.531	400.0	175.47	276.03	12.431	0.002	150.50	1.42	0.010	0.977	−0.055	2.98	1
T4780014	1994-Aug-25	49589.9061	0.3338	1.458	400.0	176.63	276.23	12.599	0.003	159.09	1.59	0.013	0.979	−0.053	3.45	1
T4780017	1994-Aug-25	49590.0249	0.3665	1.212	400.0	175.90	272.26	12.425	0.002	457.85	1.18	0.010	1.013	−0.055	3.21	1
T4780020	1994-Aug-25	49590.0498	0.3734	1.183	400.0	174.79	271.53	12.437	0.003	469.44	1.62	0.019	1.016	−0.057	3.08	1
T4780023	1994-Aug-25	49590.0740	0.3801	1.162	400.0	175.26	270.93	12.388	0.003	480.42	1.41	0.009	1.029	−0.055	2.97	1
T4780026	1994-Aug-25	49590.0997	0.3871	1.147	400.0	175.54	271.24	12.435	0.003	480.49	1.59	0.014	1.027	−0.055	3.01	1
T4780028	1994-Aug-25	49590.1276	0.3948	1.139	350.0	175.60	269.78	12.480	0.003	427.57	1.73	0.013	1.040	−0.052	2.64	1
T4780033	1994-Aug-25	49590.1583	0.4033	1.140	350.0	176.02	269.02	12.592	0.003	433.70	1.70	0.025	1.042	−0.053	3.07	1
T4780036	1994-Aug-25	49590.1769	0.4084	1.146	350.0	174.40	268.47	12.567	0.003	436.53	1.65	0.028	1.044	−0.053	2.90	1

Table A.11 cont.: HV 1620 differential photometry – V.

Frame	Date	HJD −2400000.0	Orbital Phase	X	T	Row	Col	$m_{\rm raw}$	$\sigma_{m_{\rm raw}}$	sky	CHI	Sharp	$V-C$	$C-C$	Seeing (FWHM)	ILCA
T4850004	1994-Aug-25	49590.2208	0.4205	1.176	350.0	173.29	274.39	12.596	0.003	424.90	1.72	0.029	1.058	−0.050	3.19	1
T4850009	1994-Aug-25	49590.2677	0.4335	1.232	350.0	173.52	273.59	12.670	0.003	1432.7	1.27	0.013	1.067	−0.054	3.21	1
T4300024	1995-Feb-12	49760.9066	0.4880	1.476	400.0	174.81	273.64	12.532	0.004	743.98	1.80	0.033	1.248	−0.053	2.56	1
T4300027	1995-Feb-12	49760.9218	0.4922	1.523	400.0	174.34	274.29	12.666	0.004	765.99	1.89	0.032	1.258	−0.048	2.94	1

Table A.12: HV 1620 differential photometry – I.

Frame	Date	HJD −2400000.0	Orbital Phase	X	T	Row	Col	$m_{\rm raw}$	$\sigma_{m_{\rm raw}}$	sky	CHI	Sharp	$V-C$	$C-C$	Seeing (FWHM)	ILCA
T3830016	1993-Mar-10	49057.1003	0.4099	2.230	100.0	169.83	274.61	15.226	0.013	654.14	1.02	−0.015	3.174	0.143	3.59	1
T3840020	1993-Mar-12	49059.1011	0.9616	2.228	100.0	171.24	274.40	14.858	0.010	288.20	1.40	0.046	3.385	0.154	2.66	1
T3960006	1993-May-23	49130.9383	0.7711	2.186	700.0	172.12	271.53	12.315	0.003	1539.41	1.34	−0.010	3.062	0.165	2.72	1
T3960007	1993-May-23	49130.9519	0.7749	2.161	300.0	172.94	272.11	13.116	0.005	600.87	1.54	0.004	3.081	0.146	2.05	1
T3960008	1993-May-23	49130.9570	0.7763	2.150	200.0	172.65	271.88	13.595	0.006	408.16	1.69	0.025	3.097	0.146	2.18	1
T3960009	1993-May-23	49130.9611	0.7774	2.140	100.0	173.07	272.02	14.415	0.010	204.04	2.10	0.101	3.128	0.141	2.41	1
T4250027	1993-Jul-26	49195.1551	0.4792	1.163	100.0	173.67	272.69	15.352	0.008	104.32	0.98	0.010	3.334	0.162	5.08	0
T4250028	1993-Jul-26	49195.1596	0.4805	1.159	300.0	174.26	273.39	14.250	0.007	307.58	1.32	0.006	3.309	0.158	5.35	0
T4250029	1993-Jul-26	49195.1644	0.4818	1.156	300.0	173.24	273.92	14.527	0.007	318.14	1.16	−0.010	3.305	0.168	6.25	0
T4250033	1993-Jul-26	49195.1888	0.4885	1.144	300.0	172.68	271.84	14.168	0.006	340.98	1.11	−0.002	3.352	0.158	5.13	0
T4250034	1993-Jul-26	49195.1934	0.4898	1.142	300.0	174.21	273.14	13.989	0.005	325.56	1.11	0.006	3.357	0.154	4.47	1
T4260001	1993-Jul-26	49195.2001	0.4916	1.141	300.0	173.83	272.94	14.017	0.006	318.89	1.36	0.001	3.367	0.150	4.71	1
T4260003	1993-Jul-26	49195.2105	0.4945	1.139	300.0	173.04	273.18	14.092	0.006	338.72	1.31	0.008	3.369	0.152	4.80	1
T4260005	1993-Jul-26	49195.2235	0.4981	1.138	300.0	172.87	272.58	13.962	0.005	357.58	1.24	0.009	3.380	0.149	4.39	1
T4260007	1993-Jul-26	49195.2344	0.5011	1.139	300.0	174.22	272.16	13.857	0.005	354.99	1.30	0.012	3.383	0.150	4.07	1
T4260009	1993-Jul-26	49195.2545	0.5066	1.145	300.0	172.89	272.03	14.696	0.009	365.22	1.20	−0.004	3.398	0.150	4.07	1
T4260010	1993-Jul-26	49195.2656	0.5097	1.150	300.0	172.31	272.01	13.816	0.005	328.83	1.24	0.001	3.381	0.149	3.68	1
T4260022	1993-Jul-27	49195.8430	0.6689	1.958	100.0	170.20	268.96	15.081	0.010	245.12	1.23	0.016	3.143	0.155	4.36	1
T4260023	1993-Jul-27	49195.8470	0.6700	1.942	300.0	171.18	269.92	13.836	0.005	731.03	0.96	−0.001	3.091	0.156	4.47	1
T4260025	1993-Jul-27	49195.8609	0.6738	1.890	300.0	171.50	270.28	13.716	0.004	676.41	0.98	0.010	3.087	0.155	4.21	1
T4260028	1993-Jul-27	49195.8874	0.6811	1.790	300.0	173.01	270.45	13.703	0.005	654.24	1.28	0.008	3.088	0.157	4.24	1
T4260030	1993-Jul-27	49195.8985	0.6842	1.749	300.0	173.21	269.97	13.796	0.005	674.18	1.13	0.007	3.077	0.155	4.57	1
T4260033	1993-Jul-27	49195.9288	0.6926	1.638	300.0	174.24	271.36	13.788	0.004	619.69	0.92	0.005	3.092	0.156	4.53	1
T4260035	1993-Jul-27	49195.9400	0.6957	1.599	300.0	175.13	271.01	13.704	0.005	595.27	1.17	0.003	3.092	0.156	4.25	1
S1300007	1993-Aug-19	49218.9618	0.0440	1.355	300.0	175.91	275.82	13.693	0.006	413.98	1.64	0.031	3.385	0.148	3.06	1
S1300010	1993-Aug-19	49219.0116	0.0577	1.256	300.0	175.47	274.45	13.924	0.005	354.20	1.26	0.017	3.309	0.148	3.33	1
S1330008	1993-Aug-20	49220.1429	0.3697	1.139	300.0	177.53	273.85	13.531	0.004	301.33	1.23	0.025	3.121	0.149	2.58	1
T4430018	1993-Sep-15	49245.8771	0.4661	1.381	200.0	172.83	273.44	15.466	0.012	250.37	1.04	−0.003	3.297	0.165	6.24	0

Table A.12 cont.: HV 1620 differential photometry – I.

Frame	Date	HJD −2400000.0	Orbital Phase	X	T	Row	Col	$m_{\rm raw}$	$\sigma_{m_{\rm raw}}$	sky	CHI	Sharp	$V-C$	$C-C$	Seeing (FWHM)	ILCA
T4430021	1993-Sep-15	49245.9019	0.4729	1.323	200.0	172.70	273.41	14.944	0.010	257.31	1.22	0.003	3.298	0.153	4.80	1
T4430024	1993-Sep-15	49245.9256	0.4794	1.276	200.0	174.78	272.68	14.773	0.009	264.53	1.25	−0.002	3.319	0.159	5.50	0
T4430027	1993-Sep-15	49245.9493	0.4860	1.237	200.0	173.28	272.13	14.600	0.007	264.02	1.07	0.007	3.386	0.152	4.34	1
T4430030	1993-Sep-15	49245.9731	0.4925	1.204	200.0	173.23	272.98	14.773	0.008	249.29	1.17	−0.002	3.367	0.157	4.51	1
T4430033	1993-Sep-15	49245.9969	0.4991	1.178	200.0	173.66	272.28	15.048	0.008	190.25	1.06	−0.003	3.398	0.148	4.39	1
T4430036	1993-Sep-15	49246.0221	0.5060	1.158	200.0	174.05	272.41	14.889	0.007	176.76	1.06	−0.008	3.396	0.151	4.89	1
T4440002	1993-Sep-15	49246.0551	0.5151	1.142	200.0	173.84	271.99	14.527	0.007	177.73	1.28	0.012	3.395	0.146	3.69	1
T4440005	1993-Sep-15	49246.0816	0.5224	1.138	200.0	171.56	271.36	14.569	0.006	178.01	1.13	0.010	3.365	0.150	3.94	1
T4440008	1993-Sep-15	49246.1257	0.5346	1.149	200.0	174.86	270.05	14.322	0.006	215.65	1.30	0.036	3.337	0.147	3.32	1
T4440011	1993-Sep-15	49246.1532	0.5422	1.167	200.0	173.13	269.78	14.424	0.006	222.27	1.20	0.012	3.323	0.150	3.55	1
T4440014	1993-Sep-15	49246.1770	0.5487	1.190	200.0	172.74	269.30	14.710	0.007	190.57	1.10	0.049	3.299	0.150	3.60	1
T4440017	1993-Sep-15	49246.2163	0.5596	1.242	200.0	173.14	271.62	14.361	0.009	148.13	1.95	0.084	3.280	0.143	2.66	1
T4440020	1993-Sep-15	49246.2405	0.5663	1.284	200.0	171.69	270.45	14.385	0.008	879.14	1.19	0.002	3.227	0.145	2.69	1
T5440006	1994-Jan-19	49372.0909	0.2701	1.895	200.0	173.98	270.95	15.730	0.017	345.71	1.06	−0.003	3.116	0.165	6.15	0
T5780006	1994-Feb-22	49405.9768	0.6143	1.815	200.0	173.09	273.18	15.115	0.016	965.50	1.13	0.009	3.111	0.166	5.70	0
T5820010	1994-Mar-12	49423.9145	0.5607	1.763	200.0	174.88	274.45	13.833	0.006	333.37	1.65	0.058	3.251	0.140	2.72	1
T5820011	1994-Mar-12	49423.9178	0.5617	1.776	200.0	175.05	274.45	14.544	0.009	331.38	1.52	0.064	3.238	0.140	2.67	1
T5820012	1994-Mar-12	49423.9238	0.5633	1.798	200.0	173.91	274.86	14.087	0.010	341.74	2.16	0.089	3.250	0.152	2.82	1
T5820022	1994-Mar-12	49424.2268	0.6469	1.908	200.0	172.88	269.21	13.843	0.008	3290.27	1.06	0.001	3.111	0.145	3.21	1
T5960009	1994-Mar-17	49428.9160	0.9399	1.820	200.0	173.18	275.19	14.676	0.008	349.23	1.06	0.000	3.225	0.159	5.80	0
T5960010	1994-Mar-17	49428.9201	0.9411	1.836	200.0	172.58	273.92	14.666	0.008	342.37	1.12	0.000	3.226	0.150	5.47	0
T5960012	1994-Mar-17	49428.9586	0.9517	1.979	200.0	173.87	274.67	14.541	0.008	372.72	1.30	0.010	3.302	0.148	4.78	1
T5960014	1994-Mar-17	49428.9771	0.9568	2.042	200.0	173.54	276.11	15.525	0.015	324.13	1.23	−0.005	3.312	0.172	5.18	0
T5960016	1994-Mar-17	49429.0207	0.9688	2.164	200.0	174.35	277.93	14.850	0.010	358.92	1.26	0.002	3.373	0.161	5.89	0
T5960018	1994-Mar-17	49429.1334	0.9999	2.160	200.0	176.72	277.28	15.182	0.011	273.38	1.10	0.001	3.454	0.168	6.84	0
T5960019	1994-Mar-17	49429.1466	0.0035	2.128	200.0	173.84	273.52	15.543	0.013	264.87	1.10	−0.007	3.506	0.162	5.98	0
T5960028	1994-Mar-21	49432.8751	0.0317	1.707	200.0	174.51	271.96	13.825	0.008	297.20	2.02	0.031	3.427	0.142	2.29	1
T5960031	1994-Mar-21	49432.8989	0.0382	1.796	200.0	175.38	272.13	13.861	0.007	326.67	1.70	0.054	3.409	0.144	2.27	1
T5960034	1994-Mar-21	49432.9258	0.0457	1.898	200.0	174.86	271.49	13.857	0.006	346.90	1.60	0.048	3.376	0.145	2.20	1
T5980001	1994-Mar-21	49432.9541	0.0535	2.001	200.0	174.91	272.33	13.921	0.009	372.05	2.24	0.067	3.345	0.145	2.51	1
T5980004	1994-Mar-21	49432.9798	0.0605	2.085	200.0	175.85	273.22	13.998	0.008	379.45	1.95	0.070	3.294	0.145	2.60	1
T5980007	1994-Mar-21	49433.0042	0.0673	2.151	200.0	174.53	274.25	13.893	0.007	390.36	1.83	0.051	3.265	0.144	2.58	1
T5980010	1994-Mar-21	49433.0288	0.0741	2.198	200.0	176.67	273.40	14.031	0.007	384.95	1.48	0.044	3.229	0.148	3.10	1
T5980013	1994-Mar-21	49433.0467	0.0790	2.219	200.0	174.89	275.14	13.874	0.008	370.52	1.91	0.076	3.224	0.154	2.66	1
T5980016	1994-Mar-21	49433.0725	0.0861	2.225	200.0	172.86	274.00	13.900	0.006	375.10	1.40	0.028	3.189	0.146	2.99	1
T5980019	1994-Mar-21	49433.0967	0.0928	2.206	200.0	173.95	273.03	13.984	0.007	350.33	1.57	0.004	3.187	0.143	3.48	1
T5980022	1994-Mar-21	49433.1223	0.0998	2.161	200.0	173.67	272.86	13.955	0.005	324.47	1.29	0.027	3.176	0.145	3.42	1
T5980025	1994-Mar-21	49433.1523	0.1081	2.082	200.0	172.61	273.06	13.843	0.005	348.18	1.16	0.008	3.177	0.144	3.41	1
T5980028	1994-Mar-21	49433.1771	0.1150	2.000	200.0	174.17	272.76	13.838	0.006	346.02	1.53	−0.009	3.175	0.140	3.46	1

Table A.12 cont.: HV 1620 differential photometry – I.

Frame	Date	HJD −2400000.0	Orbital Phase	X	T	Row	Col	$m_{\rm raw}$	$\sigma_{m_{\rm raw}}$	sky	CHI	Sharp	$V-C$	$C-C$	Seeing (FWHM)	ILCA
T5980031	1994-Mar-21	49433.1954	0.1200	1.934	200.0	174.41	273.90	13.857	0.005	355.09	1.21	0.001	3.178	0.137	3.54	1
T5470009	1994-Mar-24	49435.8827	0.8610	1.766	200.0	175.05	272.14	13.935	0.006	576.79	1.36	0.032	3.165	0.144	3.08	1
T5470012	1994-Mar-24	49435.9079	0.8680	1.861	200.0	174.35	272.11	13.879	0.007	593.35	1.59	0.001	3.163	0.144	2.78	1
T5470015	1994-Mar-24	49435.9317	0.8746	1.950	200.0	173.90	272.11	14.059	0.006	583.16	1.22	0.010	3.173	0.145	3.45	1
T5470018	1994-Mar-24	49435.9569	0.8815	2.038	200.0	173.35	273.15	14.097	0.008	618.33	1.42	0.018	3.167	0.149	3.57	1
T5470021	1994-Mar-24	49435.9828	0.8886	2.117	200.0	175.19	274.32	14.157	0.005	669.00	0.95	−0.004	3.171	0.144	3.39	1
T5470024	1994-Mar-24	49436.0065	0.8952	2.174	200.0	173.42	273.83	14.146	0.007	623.44	1.16	0.014	3.189	0.151	3.65	1
T5470027	1994-Mar-24	49436.0303	0.9017	2.211	200.0	173.34	275.12	14.123	0.007	623.46	1.30	0.015	3.166	0.147	3.75	1
T5470029	1994-Mar-24	49436.0432	0.9053	2.222	200.0	172.24	275.48	14.259	0.006	636.48	0.94	0.002	3.179	0.148	4.09	1
T5470032	1994-Mar-24	49436.0671	0.9119	2.224	200.0	173.11	276.00	14.474	0.009	606.72	1.21	−0.002	3.182	0.159	4.97	1
T5470035	1994-Mar-24	49436.0921	0.9188	2.201	200.0	174.69	275.08	14.732	0.010	616.39	1.15	−0.007	3.187	0.159	5.74	0
T6210001	1994-Mar-24	49436.1346	0.9305	2.109	200.0	177.21	270.96	14.854	0.010	551.98	1.03	−0.004	3.217	0.159	6.20	0
T6210004	1994-Mar-24	49436.1606	0.9377	2.029	200.0	174.14	268.04	14.610	0.008	433.35	1.10	−0.001	3.216	0.149	5.76	0
T6210007	1994-Mar-24	49436.1793	0.9428	1.964	200.0	177.78	267.04	14.601	0.007	423.08	1.01	−0.003	3.248	0.150	5.68	0
T5060009	1994-Apr-06	49448.9029	0.4514	1.972	200.0	173.57	273.51	13.981	0.006	396.35	1.51	0.055	3.248	0.145	2.56	1
T5060013	1994-Apr-06	49448.9505	0.4645	2.124	200.0	174.37	276.85	14.052	0.006	423.76	1.37	0.048	3.287	0.152	2.87	1
T5060015	1994-Apr-06	49448.9595	0.4670	2.147	200.0	173.71	277.12	14.432	0.010	427.61	1.65	0.055	3.295	0.152	3.19	1
T5060018	1994-Apr-06	49448.9830	0.4735	2.194	200.0	172.96	278.47	14.514	0.007	334.58	1.12	0.022	3.316	0.148	3.83	1
T5060022	1994-Apr-06	49449.0099	0.4809	2.223	200.0	173.35	278.00	14.428	0.007	407.38	1.13	0.013	3.337	0.158	3.84	1
T5060026	1994-Apr-06	49449.0397	0.4891	2.220	200.0	174.24	278.55	15.777	0.019	368.60	1.09	0.019	3.356	0.162	4.68	1
T5060029	1994-Apr-06	49449.0922	0.5036	2.130	200.0	176.86	275.42	14.914	0.010	492.66	1.01	0.000	3.266	0.175	6.48	0
T5060032	1994-Apr-06	49449.1113	0.5089	2.075	200.0	174.13	275.47	14.627	0.010	564.48	1.29	−0.002	3.326	0.162	5.66	0
T5300003	1994-May-16	49488.8546	0.4683	2.154	200.0	174.35	272.69	14.264	0.006	416.12	1.12	0.002	3.275	0.154	4.17	1
T5300005	1994-May-16	49488.8732	0.4734	2.191	200.0	172.70	273.70	14.274	0.007	414.95	1.32	0.009	3.286	0.142	4.25	1
T5300008	1994-May-16	49488.9101	0.4836	2.226	200.0	173.86	274.96	14.191	0.006	452.03	1.12	0.007	3.332	0.154	3.81	1
T5300011	1994-May-16	49488.9484	0.4942	2.203	200.0	175.09	274.34	14.283	0.007	444.57	1.20	0.012	3.389	0.150	3.88	1
T5300014	1994-May-16	49488.9766	0.5020	2.149	200.0	175.57	274.29	14.345	0.007	438.33	1.11	0.016	3.382	0.153	4.13	1
T5300017	1994-May-16	49489.0106	0.5113	2.053	200.0	173.57	274.81	14.673	0.008	448.73	1.11	0.004	3.374	0.155	4.76	1
T5300020	1994-May-16	49489.0455	0.5209	1.931	200.0	175.40	273.79	14.204	0.006	405.63	1.15	0.022	3.375	0.146	3.54	1
T5300023	1994-May-16	49489.0736	0.5287	1.825	200.0	177.73	274.81	14.120	0.006	371.73	1.18	0.009	3.353	0.152	3.56	1
T5300027	1994-May-16	49489.1149	0.5401	1.672	200.0	178.56	276.42	14.110	0.006	323.50	1.23	0.019	3.324	0.148	3.72	1
T5300031	1994-May-16	49489.1704	0.5554	1.488	200.0	177.39	277.70	14.229	0.006	325.41	1.26	0.009	3.257	0.149	4.23	1
T5300035	1994-May-16	49489.2080	0.5658	1.385	200.0	173.08	274.13	13.964	0.005	301.66	1.32	0.020	3.237	0.146	3.47	1
T5440023	1994-Jun-10	49514.1301	0.4382	1.412	200.0	175.63	274.14	13.929	0.006	210.00	1.62	0.027	3.211	0.147	3.18	1
T5440026	1994-Jun-10	49514.1530	0.4445	1.355	200.0	175.21	274.39	14.080	0.006	208.84	1.35	0.016	3.226	0.145	3.83	1
T5440029	1994-Jun-10	49514.1820	0.4525	1.293	200.0	174.44	275.79	14.743	0.011	204.12	1.70	0.087	3.275	0.145	2.96	1
T4580009	1994-Jun-12	49515.7924	0.8965	2.176	200.0	172.48	275.27	14.157	0.005	245.76	1.17	−0.007	3.172	0.148	4.24	1
T4580011	1994-Jun-12	49515.8521	0.9130	2.224	200.0	174.07	275.40	14.128	0.005	248.20	1.22	0.004	3.180	0.149	4.04	1
T4580015	1994-Jun-12	49515.8762	0.9197	2.202	200.0	174.49	276.51	14.242	0.006	229.16	1.28	−0.002	3.193	0.150	4.33	1

Table A.12 cont.: HV 1620 differential photometry – I.

Frame	Date	HJD −2400000.0	Orbital Phase	X	T	Row	Col	$m_{\rm raw}$	$\sigma_{m_{\rm raw}}$	sky	CHI	Sharp	$V-C$	$C-C$	Seeing (FWHM)	ILCA
T4580018	1994-Jun-12	49515.8999	0.9262	2.159	200.0	174.88	275.39	14.099	0.006	224.88	1.38	−0.001	3.209	0.152	3.78	1
T4580021	1994-Jun-12	49515.9236	0.9327	2.097	200.0	174.92	275.12	14.198	0.006	217.10	1.21	0.001	3.233	0.155	4.25	1
T4580024	1994-Jun-12	49515.9477	0.9394	2.021	200.0	175.63	275.03	14.249	0.006	220.57	1.23	0.008	3.261	0.150	3.97	1
T4580027	1994-Jun-12	49515.9655	0.9443	1.958	200.0	175.91	274.70	14.155	0.006	218.25	1.27	0.013	3.273	0.155	3.78	1
T4580030	1994-Jun-12	49515.9923	0.9517	1.858	200.0	171.71	273.67	14.317	0.006	196.39	1.32	0.007	3.305	0.146	4.18	1
T4580033	1994-Jun-12	49516.0162	0.9582	1.768	200.0	173.15	273.82	14.231	0.005	185.30	1.08	−0.004	3.341	0.144	3.90	1
T4580036	1994-Jun-12	49516.0402	0.9649	1.679	200.0	173.16	273.95	14.053	0.008	152.03	1.99	0.055	3.379	0.150	3.10	1
T4590002	1994-Jun-12	49516.0685	0.9727	1.580	200.0	173.76	274.64	14.061	0.007	172.69	1.75	0.041	3.418	0.145	2.88	1
T4590005	1994-Jun-12	49516.0923	0.9792	1.504	200.0	173.92	275.13	14.028	0.007	181.65	1.79	0.056	3.458	0.147	2.76	1
T4590008	1994-Jun-12	49516.1112	0.9844	1.449	200.0	173.58	275.15	14.133	0.008	191.25	1.90	0.050	3.488	0.144	2.85	1
T4590011	1994-Jun-12	49516.1350	0.9910	1.385	200.0	173.58	275.59	14.033	0.009	206.07	2.20	0.056	3.506	0.148	2.44	1
T4590014	1994-Jun-12	49516.1650	0.9993	1.316	200.0	174.76	272.58	14.145	0.008	204.50	1.91	0.063	3.545	0.143	2.76	1
T4590017	1994-Jun-12	49516.1894	0.0060	1.269	200.0	174.57	271.96	14.194	0.008	195.16	1.90	0.068	3.555	0.147	2.80	1
T4590020	1994-Jun-12	49516.2132	0.0126	1.230	200.0	173.99	271.86	14.288	0.006	171.00	1.32	0.046	3.558	0.145	3.19	1
T4590023	1994-Jun-12	49516.2372	0.0192	1.198	200.0	175.88	271.11	14.217	0.006	162.88	1.26	0.049	3.528	0.151	3.12	1
T4590026	1994-Jun-12	49516.2552	0.0242	1.179	200.0	174.67	272.09	14.381	0.006	162.82	1.29	0.034	3.521	0.150	3.34	1
T4810009	1994-Jul-30	49564.0072	0.1920	1.379	200.0	174.55	273.30	13.605	0.005	225.61	1.65	0.035	3.108	0.136	2.47	1
T4810015	1994-Jul-30	49564.2336	0.2544	1.141	200.0	173.71	273.84	13.548	0.006	176.68	2.03	0.053	3.067	0.142	2.37	1
T4810017	1994-Jul-30	49564.2433	0.2571	1.144	150.0	172.40	273.87	13.895	0.009	134.28	2.61	0.090	3.072	0.140	2.39	1
T4810020	1994-Jul-30	49564.2654	0.2632	1.155	150.0	172.98	272.18	13.958	0.009	124.44	2.56	0.083	3.085	0.144	2.37	1
T4810023	1994-Jul-30	49564.2869	0.2691	1.171	150.0	171.38	272.19	14.042	0.007	532.91	1.51	0.064	3.065	0.146	2.72	1
T4810032	1994-Jul-31	49564.8063	0.4124	2.049	200.0	169.74	274.62	13.886	0.006	414.95	1.44	0.011	3.156	0.148	3.27	1
T4810035	1994-Jul-31	49564.8297	0.4188	1.969	200.0	170.28	274.85	13.872	0.005	389.01	1.11	0.005	3.160	0.147	3.43	1
T4810038	1994-Jul-31	49564.8532	0.4253	1.882	200.0	170.79	274.55	13.746	0.006	398.77	1.77	0.048	3.170	0.140	2.66	1
T6360003	1994-Jul-31	49564.8821	0.4333	1.773	200.0	171.47	274.96	13.720	0.006	316.80	1.70	0.034	3.172	0.143	2.52	1
T6360006	1994-Jul-31	49564.9063	0.4399	1.683	150.0	172.53	275.97	14.160	0.006	221.69	1.50	0.056	3.211	0.146	2.74	1
T6370006	1994-Aug-01	49565.7971	0.6856	2.070	200.0	172.01	273.20	14.017	0.006	372.81	1.27	0.002	3.104	0.145	4.04	1
T6370009	1994-Aug-01	49565.8206	0.6921	1.991	200.0	173.59	272.17	14.730	0.008	362.91	1.09	0.006	3.098	0.147	5.18	0
T6370012	1994-Aug-01	49565.8441	0.6985	1.906	200.0	172.79	273.82	14.797	0.008	282.80	1.12	0.009	3.102	0.144	3.85	1
T4780003	1994-Aug-25	49589.8152	0.3087	1.767	200.0	171.92	272.30	13.746	0.005	415.82	1.16	0.001	3.083	0.145	3.37	1
T4780006	1994-Aug-25	49589.8392	0.3153	1.678	200.0	174.57	274.03	13.720	0.006	385.23	1.58	0.018	3.086	0.146	3.22	1
T4780009	1994-Aug-25	49589.8629	0.3218	1.595	200.0	175.14	275.06	13.632	0.006	359.91	1.76	0.038	3.087	0.144	2.80	1
T4780012	1994-Aug-25	49589.8867	0.3284	1.518	200.0	175.75	275.37	13.736	0.006	306.64	1.75	0.042	3.108	0.143	3.09	1
T4780015	1994-Aug-25	49589.9105	0.3350	1.447	200.0	176.11	276.45	13.932	0.006	294.98	1.38	0.024	3.109	0.143	3.86	1
T4780018	1994-Aug-25	49590.0299	0.3679	1.206	200.0	175.27	271.92	13.566	0.006	318.01	1.72	0.046	3.125	0.145	2.72	1
T4780021	1994-Aug-25	49590.0545	0.3747	1.179	200.0	175.17	271.57	13.585	0.005	311.67	1.51	0.024	3.126	0.145	2.76	1
T4780024	1994-Aug-25	49590.0803	0.3818	1.158	200.0	176.43	271.94	13.599	0.006	316.19	1.71	0.027	3.129	0.143	2.52	1
T4780027	1994-Aug-25	49590.1047	0.3885	1.145	200.0	174.59	270.72	13.554	0.006	314.56	1.86	0.013	3.130	0.141	2.40	1
T4780030	1994-Aug-25	49590.1339	0.3966	1.138	175.0	174.21	269.89	13.730	0.008	267.15	2.25	0.046	3.136	0.148	2.40	1

Table A.12 cont.: HV 1620 differential photometry – I.

Frame	Date	HJD −2400000.0	Orbital Phase	X	T	Row	Col	$m_{\rm raw}$	$\sigma_{m_{\rm raw}}$	sky	CHI	Sharp	$V-C$	$C-C$	Seeing (FWHM)	ILCA
T4780034	1994-Aug-25	49590.1622	0.4044	1.141	175.0	175.57	269.12	13.783	0.005	293.56	1.41	0.023	3.161	0.144	2.61	1
T4850001	1994-Aug-25	49590.1819	0.4098	1.148	175.0	175.05	269.14	13.772	0.007	310.37	1.84	0.046	3.159	0.147	2.56	1
T4850005	1994-Aug-25	49590.2250	0.4217	1.179	175.0	173.46	273.66	13.790	0.007	296.51	1.80	0.045	3.177	0.143	2.72	1
T4850010	1994-Aug-25	49590.2719	0.4346	1.238	175.0	172.80	274.92	13.813	0.009	3662.50	1.25	−0.029	3.164	0.147	2.63	1
T4850018	1994-Aug-31	49595.8094	0.9616	1.727	200.0	172.68	273.15	13.797	0.006	545.10	1.39	0.022	3.322	0.147	2.61	1
T4850023	1994-Aug-31	49596.0676	0.0328	1.155	200.0	175.12	275.30	14.052	0.007	185.97	1.81	0.037	3.457	0.146	3.22	1
T4850026	1994-Aug-31	49596.1008	0.0420	1.141	200.0	174.90	274.37	14.073	0.007	207.44	1.62	0.019	3.406	0.148	3.52	1
T4850029	1994-Aug-31	49596.1333	0.0509	1.139	200.0	175.91	273.11	14.507	0.009	128.16	1.77	0.064	3.356	0.143	3.23	1
T4850032	1994-Aug-31	49596.1630	0.0591	1.147	200.0	173.99	271.81	14.033	0.006	196.77	1.43	0.027	3.310	0.143	3.43	1
T4850035	1994-Aug-31	49596.1960	0.0682	1.168	200.0	173.12	271.09	13.780	0.007	200.49	1.86	0.053	3.262	0.147	2.93	1
T6410001	1994-Aug-31	49596.2314	0.0780	1.204	200.0	174.56	275.52	14.952	0.011	347.83	1.41	0.045	3.218	0.141	2.95	1
T4300025	1995-Feb-12	49760.9117	0.4894	1.492	400.0	173.42	275.68	13.085	0.005	702.25	1.62	0.033	3.335	0.145	2.81	1
T4300026	1995-Feb-12	49760.9167	0.4908	1.507	400.0	173.21	275.78	13.132	0.004	714.38	1.36	0.010	3.345	0.147	3.00	1
T7370025	1995-Apr-12	49820.0615	0.8002	2.166	200.0	172.39	273.64	13.507	0.005	572.67	1.42	0.025	3.048	0.151	2.51	1
T7370030	1995-Apr-12	49820.1202	0.8164	1.994	200.0	175.00	271.34	13.949	0.007	699.46	1.44	0.034	3.081	0.146	2.54	1
T7370035	1995-Apr-12	49820.1781	0.8324	1.779	200.0	176.00	272.39	13.622	0.007	383.26	2.13	0.038	3.092	0.152	2.43	1
T6300004	1995-Apr-12	49820.2379	0.8489	1.565	200.0	177.83	273.00	14.300	0.007	381.64	1.24	0.017	3.131	0.143	3.22	1

A.3 HV 2241 differential photometry

Table A.13: HV 2241 differential photometry – u.

Frame	Date	HJD −2400000.0	Orbital Phase	X	T	Row	Col	$m_{\rm raw}$	$\sigma_{m_{\rm raw}}$	sky	CHI	Sharp	$V-C$	$C-C$	Seeing (FWHM)	ILCA
T4100001	1993-Jul-03	49172.0992	0.6102	2.117	1200.0	105.14	446.99	13.635	0.004	834.32	1.00	0.019	−0.188	0.048	3.12	1
T4100002	1993-Jul-03	49172.1194	0.6149	1.988	1200.0	106.07	447.58	13.570	0.004	785.95	1.04	0.007	−0.203	0.051	3.36	1
T4100003	1993-Jul-03	49172.1339	0.6182	1.900	1200.0	107.31	448.14	13.536	0.003	744.62	0.81	0.015	−0.195	0.027	3.46	1
T5910009	1994-Mar-16	49427.9321	0.5221	1.329	1200.0	107.78	452.82	13.381	0.003	20.53	1.12	0.012	0.071	0.042	3.78	1
T5910014	1994-Mar-16	49427.9723	0.5313	1.463	1200.0	107.21	453.86	13.299	0.003	19.34	1.40	0.004	0.029	0.040	3.38	1
T5910034	1994-Mar-20	49431.9219	0.4408	1.331	1200.0	110.40	451.33	13.298	0.003	41.68	1.26	0.007	0.008	0.025	3.46	1
T5970003	1994-Mar-20	49431.9709	0.4521	1.500	1200.0	109.56	452.11	13.432	0.004	26.35	1.52	−0.006	0.041	0.022	3.60	1
T5970009	1994-Mar-20	49432.0127	0.4617	1.690	1200.0	108.84	452.63	13.519	0.006	22.61	2.20	−0.001	0.098	0.023	2.95	1
T5970015	1994-Mar-20	49432.0488	0.4700	1.887	1200.0	108.20	451.81	13.737	0.005	24.50	1.59	0.003	0.139	0.027	3.37	1
T5970021	1994-Mar-20	49432.0911	0.4798	2.151	1200.0	106.06	451.14	14.232	0.005	22.75	1.21	0.007	0.169	0.043	4.16	1
T5970027	1994-Mar-20	49432.1321	0.4892	2.418	1200.0	104.45	449.46	14.291	0.005	19.02	1.36	0.011	0.190	0.034	3.59	1
T5970033	1994-Mar-20	49432.1722	0.4984	2.647	1200.0	99.67	452.91	14.933	0.008	19.21	1.16	−0.006	0.158	0.016	4.22	1
T6220001	1994-Mar-20	49432.2197	0.5094	2.802	1200.0	101.03	450.49	14.963	0.006	28.64	1.07	−0.008	0.119	0.030	4.96	1

Table A.13 cont.: HV 2241 differential photometry – u.

Frame	Date	HJD −2400000.0	Orbital Phase	X	T	Row	Col	$m_{\rm raw}$	$\sigma_{m_{\rm raw}}$	sky	CHI	Sharp	$V-C$	$C-C$	Seeing (FWHM)	ILCA
T5050009	1994-Apr-07	49449.9247	0.5864	1.512	1200.0	107.87	456.19	13.515	0.004	56.24	1.31	−0.001	−0.185	0.032	4.38	1
T5050015	1994-Apr-07	49449.9726	0.5974	1.736	1200.0	107.09	456.00	13.799	0.004	33.32	1.24	−0.010	−0.196	0.021	5.33	1
T5050021	1994-Apr-07	49450.0173	0.6077	1.993	1200.0	103.18	456.60	14.316	0.005	28.09	1.17	0.000	−0.210	0.032	6.66	1
T5050028	1994-Apr-07	49450.0732	0.6206	2.355	1200.0	102.94	454.55	14.425	0.004	24.36	0.93	0.003	−0.245	0.032	6.17	1
T5050034	1994-Apr-07	49450.1268	0.6329	2.665	1200.0	100.80	451.26	15.029	0.007	21.27	1.00	−0.005	−0.238	0.027	7.25	1
T5090010	1994-Apr-09	49451.8291	0.0249	1.234	1200.0	108.44	452.54	13.290	0.003	23.09	1.15	0.011	0.334	0.030	2.78	1
T5090014	1994-Apr-09	49451.8659	0.0334	1.327	1200.0	107.89	453.42	13.479	0.004	19.89	1.44	0.023	0.233	0.025	3.55	1
T5090018	1994-Apr-09	49451.9033	0.0420	1.450	1200.0	107.60	453.73	13.393	0.004	18.75	1.49	0.012	0.146	0.020	3.33	1
T5090022	1994-Apr-09	49451.9357	0.0495	1.582	1200.0	107.25	454.23	13.489	0.003	17.76	1.12	0.024	0.070	0.024	3.64	1
T5090026	1994-Apr-09	49451.9729	0.0580	1.766	1200.0	106.41	453.91	13.726	0.003	19.84	1.08	0.007	−0.004	0.019	4.12	1
T5090030	1994-Apr-09	49452.0148	0.0677	2.011	1200.0	105.92	453.61	13.416	0.004	18.42	1.62	0.026	−0.074	0.027	2.83	1
T5090034	1994-Apr-09	49452.0522	0.0763	2.253	1200.0	104.27	453.13	13.648	0.004	20.59	1.30	0.026	−0.120	0.020	3.33	1
T6280009	1994-Apr-09	49452.1079	0.0891	2.598	1200.0	101.78	451.39	13.908	0.004	25.11	1.31	0.020	−0.155	0.030	3.44	1
T6280013	1994-Apr-09	49452.1464	0.0980	2.761	1200.0	100.87	449.48	14.205	0.004	24.62	1.07	0.008	−0.171	0.008	3.86	1
T6280017	1994-Apr-09	49452.1806	0.1059	2.814	1200.0	100.04	448.54	14.285	0.005	22.71	1.14	−0.012	−0.191	−0.003	3.50	0
T6260003	1994-Apr-09	49452.2253	0.1162	2.731	1200.0	100.00	446.26	14.401	0.006	26.51	1.16	0.003	−0.203	0.004	4.33	1
T4870009	1994-Aug-27	49591.9667	0.2951	2.012	1200.0	106.35	449.48	16.368	0.017	8.81	1.45	0.037	−0.313	0.032	3.86	1
T4870026	1994-Sep-04	49599.8323	0.1063	2.698	1200.0	102.15	448.99	14.443	0.004	13.67	0.99	0.002	−0.195	0.023	5.03	1
T4870029	1994-Sep-04	49599.8655	0.1140	2.524	1200.0	102.89	447.66	14.326	0.005	13.04	1.11	−0.002	−0.205	0.032	5.25	1
T4870032	1994-Sep-04	49599.9011	0.1222	2.297	1200.0	105.27	447.89	14.250	0.019	13.33	5.55	−0.017	−0.227	0.026	3.73	1
T4870035	1994-Sep-04	49599.9284	0.1284	2.117	1200.0	106.88	447.85	13.682	0.004	12.76	1.20	0.004	−0.220	0.026	3.66	1
T5620001	1994-Sep-04	49599.9639	0.1366	1.895	1200.0	108.29	447.86	13.557	0.004	13.20	1.33	−0.003	−0.236	0.032	3.74	1
T5620004	1994-Sep-04	49600.0001	0.1450	1.696	1200.0	109.84	448.48	13.465	0.003	12.70	1.27	0.002	−0.237	0.023	3.92	1
T5620007	1994-Sep-04	49600.0278	0.1513	1.565	1200.0	110.77	448.75	13.307	0.003	12.73	1.24	−0.014	−0.252	0.021	3.80	1
T5660003	1994-Oct-01	49626.9571	0.3525	1.551	1200.0	108.29	446.56	13.458	0.003	54.55	0.98	0.003	−0.215	0.014	4.12	1
T5660021	1994-Oct-03	49628.9701	0.8160	1.476	1200.0	107.57	448.42	14.273	0.005	15.73	1.28	−0.001	−0.216	0.025	3.80	1
T5660028	1994-Oct-03	49629.1493	0.8573	1.098	1200.0	109.43	450.86	13.644	0.003	20.43	1.11	−0.012	−0.152	0.017	3.88	1
T5680008	1994-Oct-05	49630.9437	0.2705	1.562	1200.0	107.76	449.08	12.963	0.003	11.68	1.43	−0.019	−0.297	0.022	3.01	1
T5680012	1994-Oct-05	49630.9800	0.2788	1.419	1200.0	108.86	449.38	12.853	0.003	11.56	1.32	−0.026	−0.289	0.024	2.94	1
T5680016	1994-Oct-05	49631.0163	0.2872	1.306	1200.0	109.57	450.14	12.807	0.002	12.49	1.14	−0.015	−0.296	0.036	2.91	1
T5680021	1994-Oct-05	49631.0484	0.2946	1.228	1200.0	109.88	450.58	13.199	0.003	20.33	1.31	−0.010	−0.287	0.026	2.76	1
T4890009	1994-Nov-01	49657.8763	0.4724	1.534	1200.0	110.40	448.46	13.650	0.003	28.07	1.12	0.006	0.155	0.029	4.12	1
T4890012	1994-Nov-01	49657.9098	0.4801	1.406	1200.0	111.24	448.97	13.589	0.003	21.99	1.19	0.003	0.186	0.032	4.16	1
T4890015	1994-Nov-01	49657.9432	0.4878	1.304	1200.0	112.40	449.39	13.568	0.003	19.80	1.06	−0.001	0.201	0.031	4.32	1
T4890018	1994-Nov-01	49657.9716	0.4943	1.234	1200.0	112.48	449.92	13.475	0.004	18.35	1.30	−0.001	0.200	0.022	4.39	1
T4890021	1994-Nov-01	49658.0051	0.5020	1.171	1200.0	112.96	450.23	13.543	0.003	18.57	1.13	0.000	0.176	0.026	4.72	1
T4890024	1994-Nov-01	49658.0415	0.5104	1.123	1200.0	113.03	450.78	13.581	0.003	17.00	1.15	0.000	0.136	0.024	4.57	1
T4890027	1994-Nov-01	49658.0706	0.5171	1.098	1200.0	113.02	451.73	13.499	0.003	15.84	1.15	0.002	0.097	0.032	5.05	1
T4890031	1994-Nov-01	49658.1058	0.5252	1.084	1200.0	112.97	452.80	13.366	0.004	21.33	1.36	0.004	0.053	0.040	5.03	1

Table A.13 cont.: HV 2241 differential photometry – u.

Frame	Date	HJD −2400000.0	Orbital Phase	X	T	Row	Col	$m_{\rm raw}$	$\sigma_{m_{\rm raw}}$	sky	CHI	Sharp	$V-C$	$C-C$	Seeing (FWHM)	ILCA
T4890034	1994-Nov-01	49658.1393	0.5329	1.086	1200.0	112.83	453.87	13.343	0.003	22.40	1.02	0.003	0.015	0.035	5.30	1
T4890037	1994-Nov-01	49658.1693	0.5398	1.100	1200.0	113.28	454.58	12.876	0.004	102.10	1.76	0.027	−0.018	0.029	3.07	1
T4900009	1994-Nov-02	49658.8832	0.7042	1.494	1200.0	107.40	448.44	13.615	0.003	28.23	1.05	−0.005	−0.287	0.039	5.01	1
T4900016	1994-Nov-02	49659.0855	0.7508	1.089	1200.0	109.64	449.89	14.055	0.004	20.50	0.96	−0.001	−0.278	0.036	6.03	1
T4900034	1994-Nov-03	49659.8862	0.9352	1.472	1200.0	108.14	449.37	15.010	0.008	16.48	1.34	0.020	0.164	0.025	4.18	1
T4910001	1994-Nov-03	49659.9314	0.9456	1.321	1200.0	109.79	449.99	13.934	0.004	13.67	1.21	0.000	0.274	0.023	4.03	1
T4910005	1994-Nov-03	49659.9679	0.9540	1.230	1200.0	109.71	449.50	14.111	0.004	12.57	1.15	−0.003	0.361	0.034	4.29	1
T4910008	1994-Nov-03	49660.0080	0.9633	1.158	1200.0	109.99	449.43	14.482	0.006	11.89	1.33	−0.005	0.472	0.038	4.35	1
T4910019	1994-Nov-03	49660.1398	0.9936	1.088	1200.0	110.16	452.92	14.367	0.005	20.48	1.16	−0.001	0.666	0.030	5.88	1
T4910021	1994-Nov-03	49660.1578	0.9978	1.097	1200.0	109.29	453.63	14.509	0.006	37.23	1.26	0.002	0.642	0.019	6.21	1
T4910032	1994-Nov-04	49660.9534	0.1810	1.257	1200.0	108.64	446.99	14.193	0.005	19.56	1.20	−0.005	−0.258	0.006	7.95	1
T4910034	1994-Nov-04	49660.9725	0.1853	1.215	1200.0	108.59	446.55	14.269	0.005	19.51	1.27	−0.006	−0.286	0.028	8.09	1
T4910037	1994-Nov-04	49661.0055	0.1929	1.157	1200.0	107.98	446.99	14.147	0.004	17.23	0.95	−0.001	−0.278	0.027	7.83	1
T4920003	1994-Nov-04	49661.0527	0.2038	1.105	1200.0	107.36	447.08	14.078	0.004	16.63	0.93	−0.002	−0.293	0.027	8.36	1
T4920006	1994-Nov-04	49661.0800	0.2101	1.089	1200.0	108.11	448.30	13.958	0.004	16.08	1.09	0.001	−0.291	0.027	8.04	1
T4920009	1994-Nov-04	49661.1134	0.2178	1.083	1200.0	107.49	449.08	13.854	0.004	16.79	1.07	0.002	−0.287	0.019	7.91	1
T4920012	1994-Nov-04	49661.1465	0.2254	1.092	1200.0	107.75	449.79	13.879	0.004	20.32	1.10	0.002	−0.297	0.036	7.64	1
T6070025	1994-Dec-28	49715.0570	0.6396	1.145	1200.0	110.64	453.38	13.048	0.003	44.34	1.12	−0.001	−0.220	0.024	4.20	1
T6070028	1994-Dec-28	49715.0916	0.6476	1.200	1200.0	110.23	454.30	13.064	0.002	29.14	0.87	0.002	−0.218	0.019	4.19	1
T6070031	1994-Dec-28	49715.1256	0.6554	1.274	1200.0	110.09	455.29	13.177	0.003	36.68	1.07	−0.001	−0.233	0.023	4.33	1
T6090009	1995-Jan-01	49718.9720	0.5412	1.086	1200.0	110.54	450.59	13.495	0.002	19.43	0.68	−0.001	−0.002	0.039	5.25	1
T6090012	1995-Jan-01	49719.0057	0.5489	1.103	1200.0	110.15	451.86	13.569	0.002	18.59	0.84	0.001	−0.031	0.028	5.70	1
T6090015	1995-Jan-01	49719.0395	0.5567	1.136	1200.0	109.59	452.87	14.117	0.003	19.48	0.74	−0.001	−0.069	0.048	7.89	1
T6090018	1995-Jan-01	49719.0681	0.5633	1.178	1200.0	110.12	454.04	13.917	0.003	14.92	0.77	−0.001	−0.087	0.039	7.01	1
T6090021	1995-Jan-01	49719.1034	0.5714	1.248	1200.0	109.63	455.50	14.321	0.003	14.30	0.79	0.000	−0.116	0.066	7.69	0
T6090035	1995-Jan-03	49720.9337	0.9929	1.084	1200.0	109.01	451.87	14.036	0.003	29.09	0.89	0.003	0.684	0.022	4.50	1
T6100002	1995-Jan-03	49720.9720	0.0017	1.088	1200.0	108.71	452.86	13.862	0.003	28.01	0.92	0.002	0.619	0.028	4.07	1
T6100005	1995-Jan-03	49721.0050	0.0093	1.107	1200.0	108.20	453.21	14.033	0.005	22.53	1.28	−0.020	0.534	0.034	5.64	1
T6100008	1995-Jan-03	49721.0323	0.0156	1.134	1200.0	109.08	454.31	13.537	0.003	18.79	0.93	−0.001	0.444	0.033	3.52	1
T6100011	1995-Jan-03	49721.0652	0.0232	1.182	1200.0	108.54	455.35	13.596	0.003	16.39	0.92	0.004	0.365	0.025	3.83	1
T6100015	1995-Jan-03	49721.1000	0.0312	1.252	1200.0	108.04	455.65	13.646	0.003	22.45	0.85	−0.002	0.260	0.023	4.11	1
T6100018	1995-Jan-03	49721.1269	0.0374	1.322	1200.0	107.91	456.33	13.701	0.003	29.38	0.87	−0.001	0.190	0.027	4.43	1
T6880003	1995-Feb-11	49760.1318	0.0192	1.784	1200.0	105.99	453.11	14.102	0.003	17.35	0.89	−0.001	0.397	0.031	3.71	1
T7020010	1995-Mar-02	49778.9876	0.3612	1.382	1200.0	109.19	452.74	13.015	0.003	15.89	1.33	−0.010	−0.217	0.024	3.08	1
T7020014	1995-Mar-02	49779.0283	0.3706	1.533	1200.0	108.72	452.76	13.582	0.004	13.71	1.25	−0.028	−0.210	0.022	3.41	1
T7020018	1995-Mar-02	49779.0666	0.3794	1.713	1200.0	107.27	453.36	15.198	0.006	9.06	0.99	−0.008	−0.194	0.029	3.62	1

Table A.14: HV 2241 differential photometry – v.

Frame	Date	HJD −2400000.0	Orbital Phase	X	T	Row	Col	$m_{\rm raw}$	$\sigma_{m_{\rm raw}}$	sky	CHI	Sharp	$V-C$	$C-C$	Seeing (FWHM)	ILCA
T4100004	1993-Jul-03	49172.1490	0.6217	1.813	1200.0	107.10	448.36	13.614	0.005	701.45	1.20	0.012	−0.242	0.136	3.04	1
T4100005	1993-Jul-03	49172.1660	0.6256	1.722	1200.0	107.65	449.20	13.602	0.005	650.67	1.28	0.015	−0.241	0.137	3.06	1
T4100006	1993-Jul-03	49172.1814	0.6291	1.645	1200.0	108.34	449.82	13.506	0.004	603.32	1.19	0.016	−0.246	0.125	2.94	1
T5910012	1994-Mar-16	49427.9539	0.5271	1.397	1200.0	106.18	450.87	13.619	0.004	22.50	1.22	0.016	0.013	0.140	3.29	1
T5910037	1994-Mar-20	49431.9435	0.4458	1.399	1200.0	107.97	448.97	13.652	0.004	36.83	1.44	0.021	−0.006	0.128	3.21	1
T5970018	1994-Mar-20	49432.0701	0.4749	2.017	1200.0	106.48	448.45	14.248	0.005	24.53	1.18	0.008	0.131	0.139	4.03	1
T5970036	1994-Mar-20	49432.1955	0.5038	2.744	1200.0	102.18	450.06	14.662	0.005	21.46	1.03	−0.006	0.106	0.140	4.57	1
T5050012	1994-Apr-07	49449.9513	0.5925	1.629	1200.0	105.29	453.49	13.878	0.004	37.49	1.28	−0.003	−0.235	0.129	4.56	1
T5050024	1994-Apr-07	49450.0409	0.6132	2.144	1200.0	104.01	452.33	14.215	0.005	26.95	1.39	0.001	−0.267	0.140	5.49	1
T5090012	1994-Apr-09	49451.8472	0.0291	1.277	1200.0	106.41	450.58	13.649	0.004	20.34	1.26	0.019	0.215	0.135	2.77	1
T5090024	1994-Apr-09	49451.9543	0.0537	1.670	1200.0	105.60	451.08	13.789	0.003	21.24	1.07	0.017	−0.012	0.141	3.61	1
T5090036	1994-Apr-09	49452.0713	0.0807	2.378	1200.0	104.15	450.27	13.729	0.004	21.87	1.27	0.009	−0.182	0.116	3.26	1
T6280019	1994-Apr-09	49452.2003	0.1104	2.798	1200.0	101.23	446.18	13.890	0.005	25.02	1.59	−0.018	−0.266	0.118	3.34	1
T6260001	1994-Apr-09	49452.2003	0.1104	2.798	1200.0	101.23	446.18	13.890	0.005	25.02	1.60	−0.017	−0.266	0.118	3.34	1
T4870027	1994-Sep-04	49599.8470	0.1097	2.627	1200.0	103.64	448.22	14.423	0.004	19.11	0.97	0.001	−0.239	0.134	5.17	1
T4870036	1994-Sep-04	49599.9434	0.1319	2.021	1200.0	106.94	448.07	13.656	0.004	18.29	1.31	0.005	−0.282	0.141	3.36	1
T5660005	1994-Oct-01	49626.9796	0.3577	1.460	1200.0	103.59	447.09	14.136	0.003	38.55	0.83	0.002	−0.260	0.120	4.13	1
T5660022	1994-Oct-03	49628.9850	0.8194	1.421	1200.0	106.05	448.42	15.141	0.009	18.81	1.54	0.022	−0.186	0.084	3.76	0
T5680010	1994-Oct-05	49630.9619	0.2747	1.486	1200.0	106.72	449.49	13.202	0.004	15.54	1.85	−0.008	−0.340	0.179	2.77	0
T4890010	1994-Nov-01	49657.8917	0.4759	1.472	1200.0	108.97	448.48	13.837	0.004	23.43	1.37	0.011	0.152	0.135	3.53	1
T4890019	1994-Nov-01	49657.9865	0.4977	1.204	1200.0	110.67	449.13	13.843	0.004	19.50	1.19	0.016	0.164	0.137	3.98	1
T4890028	1994-Nov-01	49658.0854	0.5205	1.090	1200.0	110.86	450.76	13.735	0.003	17.65	1.05	0.008	0.035	0.132	4.39	1
T4900010	1994-Nov-02	49658.8981	0.7077	1.438	1200.0	106.36	448.00	13.935	0.004	23.76	1.15	0.004	−0.337	0.147	4.94	1
T4900017	1994-Nov-02	49659.1002	0.7542	1.084	1200.0	107.07	449.48	14.517	0.005	22.70	1.19	0.006	−0.302	0.117	5.20	1
T4900036	1994-Nov-03	49659.9084	0.9403	1.392	1200.0	107.17	449.46	14.242	0.005	18.57	1.30	0.016	0.154	0.124	3.87	1
T4910035	1994-Nov-04	49660.9873	0.1888	1.187	1200.0	106.05	445.79	14.246	0.004	21.55	0.87	−0.006	−0.332	0.138	7.15	1
T4920007	1994-Nov-04	49661.0953	0.2136	1.084	1200.0	106.36	447.48	14.233	0.005	18.98	1.20	−0.001	−0.324	0.117	7.22	1
T6070026	1994-Dec-28	49715.0725	0.6432	1.167	1200.0	108.04	451.47	13.355	0.002	34.78	0.90	−0.005	−0.266	0.125	3.72	1
T6090010	1995-Jan-01	49718.9870	0.5446	1.092	1200.0	107.95	449.54	13.880	0.003	19.42	0.91	0.005	−0.038	0.127	5.10	1
T6090019	1995-Jan-01	49719.0836	0.5669	1.206	1200.0	107.68	452.45	14.546	0.004	15.52	0.83	0.004	−0.141	0.169	7.88	0
T6090036	1995-Jan-03	49720.9485	0.9963	1.083	1200.0	106.27	450.90	14.462	0.005	23.30	1.13	0.005	0.571	0.139	4.65	1
T6100009	1995-Jan-03	49721.0472	0.0190	1.154	1200.0	106.60	452.60	13.877	0.003	19.66	0.81	0.003	0.317	0.142	3.46	1
T6880005	1995-Feb-11	49760.1501	0.0234	1.888	1200.0	105.25	450.40	14.304	0.004	18.07	1.02	−0.003	0.270	0.148	3.57	1
T7020011	1995-Mar-02	49779.0031	0.3648	1.435	1200.0	107.48	449.96	14.303	0.003	16.91	0.79	−0.007	−0.252	0.136	3.35	1

Table A.15: HV 2241 differential photometry – b.

Frame	Date	HJD −2400000.0	Orbital Phase	X	T	Row	Col	$m_{\rm raw}$	$\sigma_{m_{\rm raw}}$	sky	CHI	Sharp	$V-C$	$C-C$	Seeing (FWHM)	ILCA
T4100007	1993-Jul-03	49172.1960	0.6325	1.577	1200.0	111.07	452.68	12.964	0.004	1036.8	1.35	0.033	−0.266	0.127	2.84	1
T4100008	1993-Jul-03	49172.2177	0.6375	1.486	1200.0	112.04	453.30	12.954	0.004	912.65	1.43	0.043	−0.271	0.127	2.94	1
T4100009	1993-Jul-03	49172.2329	0.6410	1.429	1200.0	112.33	453.52	12.952	0.003	826.95	1.17	0.022	−0.287	0.136	2.99	1
T5910017	1994-Mar-16	49427.9937	0.5362	1.550	1200.0	108.30	451.92	13.061	0.004	44.74	1.61	0.036	−0.033	0.117	2.72	1
T5970006	1994-Mar-20	49431.9916	0.4569	1.589	1200.0	110.29	450.73	13.264	0.006	41.51	2.47	−0.054	0.022	0.105	3.44	1
T5970024	1994-Mar-20	49432.1116	0.4845	2.285	1200.0	109.02	448.64	13.698	0.005	44.45	1.78	0.006	0.163	0.114	3.64	1
T5050018	1994-Apr-07	49449.9938	0.6023	1.852	1200.0	108.96	453.09	13.345	0.003	57.92	1.18	0.000	−0.254	0.113	4.72	1
T5050030	1994-Apr-07	49450.0922	0.6250	2.476	1200.0	107.84	451.68	13.883	0.004	58.48	1.12	0.000	−0.274	0.110	5.86	1
T5050036	1994-Apr-07	49450.1467	0.6375	2.745	1200.0	105.46	450.14	14.287	0.005	51.58	1.19	0.005	−0.300	0.100	6.30	1
T5090016	1994-Apr-09	49451.8846	0.0377	1.385	1200.0	108.22	452.33	13.218	0.003	45.07	1.29	0.020	0.115	0.108	3.14	1
T5090028	1994-Apr-09	49451.9948	0.0631	1.890	1200.0	108.75	451.71	13.003	0.003	56.76	1.38	0.018	−0.097	0.107	2.76	1
T6280011	1994-Apr-09	49452.1268	0.0935	2.689	1200.0	106.10	449.56	13.197	0.003	75.40	1.41	0.033	−0.205	0.088	3.35	1
T6260005	1994-Apr-09	49452.2446	0.1206	2.648	1200.0	105.30	446.60	13.298	0.004	240.36	1.36	0.006	−0.251	0.092	3.99	1
T4870030	1994-Sep-04	49599.8805	0.1174	2.432	1200.0	108.06	450.13	13.537	0.004	31.20	1.26	0.002	−0.245	0.119	4.54	1
T5620002	1994-Sep-04	49599.9789	0.1401	1.809	1200.0	111.15	450.51	13.080	0.003	30.77	1.33	−0.001	−0.275	0.110	3.43	1
T5660029	1994-Oct-03	49629.1642	0.8607	1.090	1200.0	108.92	451.66	14.169	0.005	35.11	1.31	0.006	−0.202	0.093	3.78	1
T5680014	1994-Oct-05	49630.9981	0.2830	1.359	1200.0	109.70	451.72	12.687	0.002	28.84	1.26	−0.022	−0.329	0.107	2.70	1
T4890013	1994-Nov-01	49657.9247	0.4835	1.357	1200.0	112.41	451.14	13.496	0.003	43.62	1.19	0.006	0.165	0.114	4.13	1
T4890022	1994-Nov-01	49658.0234	0.5063	1.144	1200.0	112.73	451.05	13.390	0.003	37.01	1.10	0.011	0.130	0.112	4.12	1
T4890032	1994-Nov-01	49658.1211	0.5287	1.083	1200.0	112.62	453.28	13.213	0.003	40.92	1.25	0.004	0.009	0.114	4.14	1
T4900011	1994-Nov-02	49658.9134	0.7112	1.385	1200.0	109.38	450.11	13.397	0.003	38.05	1.18	−0.005	−0.326	0.117	4.48	1
T4900018	1994-Nov-02	49659.1152	0.7577	1.083	1200.0	109.09	451.41	15.470	0.008	35.03	1.00	0.000	−0.335	0.126	5.46	1
T4910003	1994-Nov-03	49659.9497	0.9498	1.272	1200.0	110.08	451.77	13.908	0.004	31.20	1.29	0.012	0.246	0.112	4.05	1
T4920001	1994-Nov-04	49661.0336	0.1994	1.122	1200.0	106.96	447.26	13.996	0.004	36.13	1.17	−0.001	−0.335	0.113	7.95	1
T4920010	1994-Nov-04	49661.1283	0.2212	1.085	1200.0	107.43	449.90	13.882	0.003	35.84	0.98	−0.007	−0.338	0.111	7.67	1
T6070029	1994-Dec-28	49715.1071	0.6512	1.231	1200.0	110.17	453.53	12.942	0.002	43.05	0.85	−0.006	−0.279	0.105	3.70	1
T6090013	1995-Jan-01	49719.0213	0.5525	1.116	1200.0	109.45	451.46	13.683	0.003	28.05	0.85	0.001	−0.077	0.110	6.14	1
T6100003	1995-Jan-03	49720.9869	0.0051	1.094	1200.0	107.99	453.67	13.867	0.003	34.02	1.04	0.000	0.482	0.118	4.45	1
T6100013	1995-Jan-03	49721.0817	0.0270	1.213	1200.0	108.12	454.54	13.420	0.002	32.63	0.85	0.002	0.221	0.112	3.51	1
T6880007	1995-Feb-11	49760.1685	0.0277	2.000	1200.0	107.72	450.69	13.843	0.003	32.90	0.94	0.003	0.223	0.124	3.84	1
T7020015	1995-Mar-02	49779.0437	0.3742	1.602	1200.0	109.42	450.95	13.698	0.004	34.18	1.30	−0.042	−0.239	0.095	3.08	1

Table A.16: HV 2241 differential photometry – y.

Frame	Date	HJD −2400000.0	Orbital Phase	X	T	Row	Col	$m_{\rm raw}$	$\sigma_{m_{\rm raw}}$	sky	CHI	Sharp	$V-C$	$C-C$	Seeing (FWHM)	ILCA
T4100010	1993-Jul-03	49172.2466	0.6442	1.386	700.0	113.97	457.42	12.677	0.005	883.78	2.06	0.051	−0.333	0.142	2.90	1

Table A.16 cont.: HV 2241 differential photometry – y.

Frame	Date	HJD −2400000.0	Orbital Phase	X	T	Row	Col	$m_{\rm raw}$	$\sigma_{m_{\rm raw}}$	sky	CHI	Sharp	$V-C$	$C-C$	Seeing (FWHM)	ILCA
T4100011	1993-Jul-03	49172.2557	0.6463	1.356	700.0	113.91	457.72	12.751	0.006	751.07	2.57	0.068	−0.341	0.148	2.85	1
T4100012	1993-Jul-03	49172.2661	0.6486	1.326	700.0	113.84	457.17	12.845	0.004	585.99	1.73	0.046	−0.353	0.141	2.53	1
T5970012	1994-Mar-20	49432.0308	0.4659	1.779	700.0	112.54	451.96	12.990	0.006	116.32	2.46	−0.049	0.046	0.124	3.07	1
T5970030	1994-Mar-20	49432.1533	0.4941	2.541	700.0	107.70	454.71	13.672	0.004	125.62	1.27	−0.005	0.107	0.141	4.52	1
T5050026	1994-Apr-07	49450.0563	0.6167	2.238	700.0	109.25	455.86	13.321	0.003	175.04	1.02	0.000	−0.302	0.121	5.56	1
T5050032	1994-Apr-07	49450.1108	0.6292	2.579	700.0	109.08	454.14	13.460	0.003	184.53	1.05	−0.001	−0.310	0.113	5.78	1
T5050038	1994-Apr-07	49450.1622	0.6411	2.786	700.0	107.86	452.66	13.963	0.004	179.30	0.96	−0.002	−0.341	0.122	7.56	1
T5090020	1994-Apr-09	49451.9202	0.0459	1.512	700.0	109.60	454.65	12.857	0.003	122.66	1.43	0.032	−0.005	0.130	2.92	1
T5090032	1994-Apr-09	49452.0360	0.0726	2.141	700.0	110.17	453.55	12.758	0.003	162.91	1.30	0.028	−0.189	0.130	3.06	1
T6280015	1994-Apr-09	49452.1638	0.1020	2.799	700.0	108.59	451.26	12.952	0.002	214.18	1.08	0.010	−0.258	0.108	3.81	1
T6260007	1994-Apr-09	49452.2601	0.1242	2.573	700.0	108.29	450.45	12.770	0.005	5231.5	1.16	−0.007	−0.317	0.130	3.64	1
T4870033	1994-Sep-04	49599.9131	0.1249	2.224	700.0	111.62	453.86	12.811	0.002	66.92	1.06	0.011	−0.319	0.135	3.19	1
T5620005	1994-Sep-04	49600.0122	0.1477	1.640	700.0	113.11	454.58	12.818	0.002	62.85	1.06	0.007	−0.341	0.132	3.41	1
T5680019	1994-Oct-05	49631.0333	0.2911	1.264	700.0	111.02	455.50	12.504	0.003	66.07	1.40	−0.035	−0.372	0.125	2.61	1
T4890016	1994-Nov-01	49657.9553	0.4906	1.274	700.0	113.72	454.87	13.185	0.003	86.03	1.35	0.018	0.147	0.125	3.99	1
T4890025	1994-Nov-01	49658.0543	0.5134	1.111	700.0	113.58	455.40	13.242	0.004	72.84	1.45	0.002	0.053	0.131	4.69	1
T4890035	1994-Nov-01	49658.1515	0.5357	1.090	700.0	113.53	456.72	13.069	0.003	81.47	1.23	0.001	−0.071	0.128	4.75	1
T4900012	1994-Nov-02	49658.9257	0.7140	1.349	700.0	110.13	453.41	12.793	0.002	87.43	1.16	0.010	−0.376	0.143	3.97	1
T4900019	1994-Nov-02	49659.1329	0.7617	1.085	700.0	110.44	454.39	14.831	0.007	75.42	1.17	0.001	−0.356	0.134	5.43	1
T4910006	1994-Nov-03	49659.9798	0.9568	1.208	700.0	110.49	454.15	15.131	0.009	58.83	1.28	0.018	0.265	0.116	3.65	1
T4920004	1994-Nov-04	49661.0646	0.2066	1.097	700.0	109.21	451.66	13.388	0.002	59.92	0.82	0.003	−0.377	0.127	6.86	1
T4920013	1994-Nov-04	49661.1585	0.2282	1.098	700.0	108.21	452.74	13.571	0.003	87.00	0.90	−0.002	−0.390	0.129	7.30	1
T6070032	1994-Dec-28	49715.1383	0.6584	1.305	700.0	111.61	456.76	13.012	0.002	159.25	0.89	0.000	−0.327	0.137	4.89	1
T6090016	1995-Jan-01	49719.0521	0.5596	1.151	700.0	111.78	454.81	13.485	0.003	55.97	1.08	−0.002	−0.151	0.139	6.68	1
T6100006	1995-Jan-03	49721.0173	0.0121	1.117	700.0	109.65	456.46	13.270	0.003	54.15	1.20	0.006	0.330	0.129	3.30	1
T6100016	1995-Jan-03	49721.1119	0.0339	1.279	700.0	109.48	457.33	13.234	0.002	62.23	0.93	0.001	0.100	0.130	3.84	1
T6100019	1995-Jan-03	49721.1390	0.0402	1.355	700.0	109.00	457.92	13.341	0.002	113.20	0.87	0.001	0.043	0.122	4.52	1
T6880009	1995-Feb-11	49760.1837	0.0312	2.091	700.0	110.53	453.36	13.446	0.003	125.49	0.99	0.006	0.122	0.137	3.88	1
T7020020	1995-Mar-02	49779.0806	0.3827	1.783	700.0	111.53	452.77	14.743	0.005	75.05	0.87	−0.030	−0.266	0.169	3.40	0

Table A.17: HV 2241 differential photometry – V.

Frame	Date	HJD −2400000.0	Orbital Phase	X	T	Row	Col	$m_{\rm raw}$	$\sigma_{m_{\rm raw}}$	sky	CHI	Sharp	$V-C$	$C-C$	Seeing (FWHM)	ILCA
T8300012	1995-Feb-05	49753.9786	0.6023	1.185	200.0	112.08	452.67	13.803	0.003	−111.7	0.97	0.005	−0.286	0.130	2.80	1
T8300013	1995-Feb-05	49753.9827	0.6032	1.193	200.0	113.27	451.01	12.246	0.002	56.87	1.53	−0.006	−0.289	0.135	2.79	1
T7050005	1995-Mar-07	49784.1056	0.5398	2.008	400.0	111.73	454.35	12.262	0.002	107.92	1.09	0.006	−0.097	0.132	3.87	1
T7050008	1995-Mar-07	49784.1209	0.5433	2.105	400.0	111.15	452.53	12.299	0.002	112.16	0.95	0.002	−0.111	0.134	4.17	1

Table A.18: HV 2241 differential photometry – I.

Frame	Date	HJD −2400000.0	Orbital Phase	X	T	Row	Col	$m_{\rm raw}$	$\sigma_{m_{\rm raw}}$	sky	CHI	Sharp	$V-C$	$C-C$	Seeing (FWHM)	ILCA
T4100013	1993-Jul-03	49172.2728	0.6502	1.309	200.0	114.06	456.63	13.137	0.003	448.62	1.26	0.024	−0.390	0.095	2.43	1
T4100014	1993-Jul-03	49172.2761	0.6509	1.300	200.0	113.26	456.78	13.208	0.004	421.96	1.33	0.026	−0.394	0.090	2.51	1
T4100015	1993-Jul-03	49172.2792	0.6517	1.292	200.0	113.87	456.71	13.247	0.004	413.67	1.40	−0.003	−0.395	0.099	2.45	1
T5910007	1994-Mar-16	49427.9183	0.5189	1.286	200.0	109.66	451.65	13.027	0.003	228.08	1.25	0.000	−0.016	0.099	2.85	1
T5910008	1994-Mar-16	49427.9230	0.5200	1.299	200.0	109.39	451.80	13.106	0.003	234.80	1.09	0.000	−0.016	0.089	3.07	1
T5910010	1994-Mar-16	49427.9414	0.5242	1.351	200.0	109.00	452.80	13.009	0.003	229.85	1.26	0.001	−0.038	0.092	2.73	1
T5910011	1994-Mar-16	49427.9447	0.5249	1.361	200.0	110.20	452.17	12.968	0.004	242.35	1.61	0.031	−0.040	0.089	2.59	1
T5910013	1994-Mar-16	49427.9630	0.5292	1.422	200.0	109.85	452.20	12.924	0.003	251.76	1.41	0.032	−0.065	0.091	2.41	1
T5910015	1994-Mar-16	49427.9813	0.5334	1.491	200.0	110.30	452.75	13.095	0.003	237.49	1.13	0.022	−0.090	0.090	3.24	1
T5910016	1994-Mar-16	49427.9845	0.5341	1.503	200.0	110.09	452.40	12.970	0.003	241.49	1.42	0.024	−0.091	0.086	2.67	1
T5910018	1994-Mar-16	49428.0031	0.5384	1.583	200.0	109.75	452.16	12.903	0.004	262.04	1.77	0.034	−0.110	0.093	2.30	1
T5910019	1994-Mar-16	49428.0066	0.5392	1.598	200.0	109.41	452.02	13.862	0.009	278.06	2.30	0.080	−0.114	0.084	2.52	1
T5910030	1994-Mar-20	49431.9021	0.4362	1.273	200.0	112.17	451.03	12.882	0.004	247.14	1.66	−0.015	−0.120	0.076	2.57	1
T5910031	1994-Mar-20	49431.9053	0.4370	1.281	200.0	112.31	451.16	12.893	0.003	252.52	1.38	−0.004	−0.114	0.066	2.48	1
T5910032	1994-Mar-20	49431.9090	0.4378	1.290	200.0	111.82	450.68	12.895	0.003	249.02	1.50	0.001	−0.111	0.070	2.45	1
T5910033	1994-Mar-20	49431.9124	0.4386	1.299	200.0	111.69	450.76	12.926	0.003	256.61	1.23	−0.009	−0.110	0.070	2.67	1
T5910035	1994-Mar-20	49431.9310	0.4429	1.353	200.0	112.41	450.81	12.992	0.004	262.63	1.49	0.022	−0.082	0.073	2.64	1
T5910036	1994-Mar-20	49431.9343	0.4436	1.363	200.0	111.86	450.51	13.020	0.003	259.93	1.30	0.013	−0.073	0.069	2.69	1
T5970001	1994-Mar-20	49431.9581	0.4491	1.444	200.0	112.49	451.61	13.045	0.004	260.50	1.77	−0.038	−0.081	0.083	3.25	1
T5970002	1994-Mar-20	49431.9617	0.4500	1.457	200.0	112.53	450.48	13.037	0.004	268.57	1.79	−0.034	−0.073	0.076	3.21	1
T5970004	1994-Mar-20	49431.9797	0.4541	1.528	200.0	112.51	451.60	12.992	0.006	280.42	2.45	−0.045	−0.056	0.077	2.99	1
T5970005	1994-Mar-20	49431.9827	0.4548	1.541	200.0	113.10	450.53	13.057	0.005	283.58	2.17	−0.023	−0.046	0.086	3.12	1
T5970007	1994-Mar-20	49432.0007	0.4589	1.621	200.0	112.67	450.74	13.007	0.006	317.39	2.63	−0.058	−0.032	0.087	2.91	1
T5970008	1994-Mar-20	49432.0038	0.4597	1.636	200.0	112.67	450.60	13.007	0.006	331.78	2.46	−0.054	−0.021	0.085	2.85	1
T5970010	1994-Mar-20	49432.0217	0.4638	1.725	200.0	113.33	450.19	12.988	0.006	348.54	2.37	−0.059	−0.001	0.086	2.67	1
T5970011	1994-Mar-20	49432.0247	0.4645	1.741	200.0	113.37	450.28	13.009	0.005	343.88	2.12	−0.040	0.007	0.085	2.82	1
T5970013	1994-Mar-20	49432.0368	0.4673	1.807	200.0	113.14	449.62	13.074	0.004	379.53	1.69	−0.036	0.024	0.085	2.82	1
T5970014	1994-Mar-20	49432.0399	0.4680	1.824	200.0	113.14	450.01	13.112	0.004	390.88	1.69	−0.027	0.032	0.088	3.00	1
T5970016	1994-Mar-20	49432.0579	0.4721	1.929	200.0	112.50	450.47	13.281	0.004	359.30	1.34	−0.016	0.054	0.087	3.34	1
T5970017	1994-Mar-20	49432.0611	0.4729	1.949	200.0	113.52	449.24	13.250	0.004	351.50	1.44	−0.016	0.058	0.086	3.11	1
T5970019	1994-Mar-20	49432.0792	0.4770	2.061	200.0	113.82	449.82	13.283	0.004	362.55	1.37	−0.012	0.078	0.086	3.21	1
T5970020	1994-Mar-20	49432.0823	0.4777	2.082	200.0	113.06	449.05	13.297	0.004	353.08	1.42	−0.013	0.071	0.095	3.22	1
T5970022	1994-Mar-20	49432.0998	0.4818	2.196	200.0	113.18	449.55	13.286	0.004	353.65	1.26	−0.025	0.087	0.103	3.11	1
T5970023	1994-Mar-20	49432.1028	0.4825	2.215	200.0	113.43	447.98	13.450	0.004	356.98	1.14	0.006	0.093	0.095	3.42	1
T5970025	1994-Mar-20	49432.1204	0.4865	2.330	200.0	113.07	448.51	13.271	0.003	355.89	1.06	−0.008	0.109	0.091	2.84	1
T5970026	1994-Mar-20	49432.1234	0.4872	2.350	200.0	113.28	447.64	13.320	0.004	367.46	1.34	−0.015	0.102	0.099	3.08	1
T5970028	1994-Mar-20	49432.1439	0.4919	2.480	200.0	109.84	453.21	13.497	0.005	350.61	1.52	−0.011	0.087	0.094	4.24	1
T5970029	1994-Mar-20	49432.1472	0.4927	2.500	200.0	109.93	452.83	13.714	0.004	369.52	1.06	0.000	0.095	0.091	4.72	1

Table A.18 cont.: HV 2241 differential photometry – I.

Frame	Date	HJD −2400000.0	Orbital Phase	X	T	Row	Col	$m_{\rm raw}$	$\sigma_{m_{\rm raw}}$	sky	CHI	Sharp	$V-C$	$C-C$	Seeing (FWHM)	ILCA
T5970031	1994-Mar-20	49432.1594	0.4955	2.571	200.0	108.86	453.17	13.657	0.005	326.77	1.46	−0.009	0.072	0.090	4.15	1
T5970032	1994-Mar-20	49432.1629	0.4963	2.590	200.0	109.20	453.13	13.778	0.006	307.73	1.47	−0.013	0.066	0.097	4.27	1
T5970034	1994-Mar-20	49432.1825	0.5008	2.686	200.0	112.57	452.95	13.604	0.005	397.21	1.49	−0.004	0.047	0.090	4.00	1
T5970035	1994-Mar-20	49432.1864	0.5017	2.703	200.0	111.62	452.98	13.610	0.005	393.42	1.58	−0.014	0.050	0.098	4.01	1
T5970037	1994-Mar-20	49432.2049	0.5060	2.768	200.0	112.09	451.73	13.679	0.004	426.40	1.14	0.000	0.031	0.085	4.31	1
T5970038	1994-Mar-20	49432.2081	0.5067	2.776	200.0	111.53	452.52	13.682	0.005	426.24	1.24	0.001	0.045	0.094	4.25	1
T6220002	1994-Mar-20	49432.2286	0.5114	2.811	200.0	113.18	451.01	13.654	0.005	800.57	1.20	0.001	−0.008	0.087	4.31	1
T5050007	1994-Apr-07	49449.9080	0.5825	1.440	200.0	108.97	454.68	12.989	0.002	249.41	0.99	0.006	−0.291	0.092	3.28	1
T5050008	1994-Apr-07	49449.9139	0.5839	1.462	200.0	109.47	455.25	12.956	0.002	243.94	1.05	−0.012	−0.294	0.085	3.34	1
T5050010	1994-Apr-07	49449.9345	0.5886	1.545	200.0	110.10	455.80	13.203	0.003	251.80	1.22	0.007	−0.298	0.080	4.14	1
T5050011	1994-Apr-07	49449.9407	0.5901	1.572	200.0	110.34	455.65	13.160	0.003	247.89	1.08	−0.002	−0.310	0.090	3.90	1
T5050013	1994-Apr-07	49449.9604	0.5946	1.664	200.0	110.68	456.27	12.983	0.003	259.75	1.40	0.017	−0.319	0.093	3.64	1
T5050014	1994-Apr-07	49449.9636	0.5953	1.679	200.0	110.43	454.94	13.229	0.004	266.66	1.31	0.008	−0.307	0.080	4.26	1
T5050016	1994-Apr-07	49449.9816	0.5995	1.773	200.0	110.35	453.46	13.542	0.004	265.57	1.21	−0.002	−0.290	0.058	5.45	1
T5050017	1994-Apr-07	49449.9848	0.6002	1.790	200.0	111.09	454.24	13.339	0.004	258.88	1.35	0.002	−0.316	0.078	4.84	1
T5050019	1994-Apr-07	49450.0028	0.6044	1.893	200.0	109.58	455.45	13.451	0.020	275.42	6.90	−0.125	−0.307	0.074	4.39	1
T5050020	1994-Apr-07	49450.0070	0.6053	1.919	200.0	108.74	455.46	13.236	0.004	281.43	1.29	0.004	−0.310	0.085	4.52	1
T5050022	1994-Apr-07	49450.0285	0.6103	2.051	200.0	108.36	454.49	13.487	0.004	301.91	1.16	0.005	−0.318	0.061	5.21	1
T5050023	1994-Apr-07	49450.0316	0.6110	2.071	200.0	111.60	454.05	13.347	0.003	299.39	1.17	0.006	−0.320	0.074	4.81	1
T5050025	1994-Apr-07	49450.0501	0.6153	2.191	200.0	109.76	452.14	13.208	0.003	349.86	0.96	0.005	−0.335	0.076	4.36	1
T5050027	1994-Apr-07	49450.0629	0.6182	2.275	200.0	111.82	453.30	13.453	0.004	416.09	1.23	−0.002	−0.332	0.067	5.18	1
T5050029	1994-Apr-07	49450.0829	0.6228	2.406	200.0	111.16	453.64	13.481	0.004	399.77	1.11	0.000	−0.332	0.070	5.16	1
T5050031	1994-Apr-07	49450.1035	0.6276	2.532	200.0	110.90	451.88	13.803	0.004	349.89	1.08	0.003	−0.341	0.054	5.31	1
T5050033	1994-Apr-07	49450.1175	0.6308	2.610	200.0	109.36	452.92	13.713	0.004	451.99	1.09	0.005	−0.341	0.082	5.84	1
T5050035	1994-Apr-07	49450.1369	0.6353	2.701	200.0	110.22	450.05	13.915	0.005	419.76	1.05	−0.003	−0.343	0.043	6.18	0
T5050037	1994-Apr-07	49450.1558	0.6396	2.767	200.0	109.54	450.75	13.678	0.005	500.07	1.30	0.001	−0.377	0.066	5.85	1
T6280001	1994-Apr-07	49450.1689	0.6426	2.797	200.0	113.21	449.40	14.115	0.006	485.14	1.18	−0.002	−0.362	0.063	6.81	1
T5090009	1994-Apr-09	49451.8200	0.0228	1.211	200.0	109.58	452.31	13.119	0.004	315.33	1.53	0.036	0.206	0.075	2.31	1
T5090011	1994-Apr-09	49451.8382	0.0270	1.250	200.0	109.89	453.18	13.063	0.004	322.30	1.56	0.018	0.153	0.081	2.36	1
T5090013	1994-Apr-09	49451.8563	0.0312	1.295	200.0	110.03	452.61	13.081	0.004	311.58	1.78	0.036	0.114	0.080	2.47	1
T5090015	1994-Apr-09	49451.8752	0.0355	1.349	200.0	109.77	452.55	13.194	0.004	291.72	1.57	0.043	0.072	0.080	3.05	1
T5090017	1994-Apr-09	49451.8937	0.0398	1.409	200.0	109.76	452.87	13.072	0.004	285.36	1.41	0.039	0.026	0.078	2.83	1
T5090019	1994-Apr-09	49451.9132	0.0443	1.480	200.0	110.21	452.28	13.002	0.004	281.62	1.71	0.045	−0.023	0.079	2.64	1
T5090021	1994-Apr-09	49451.9265	0.0473	1.534	200.0	110.21	452.66	13.071	0.003	289.04	1.09	0.032	−0.036	0.070	3.00	1
T5090023	1994-Apr-09	49451.9453	0.0517	1.617	200.0	110.36	452.36	13.018	0.003	311.71	1.33	0.031	−0.078	0.078	2.88	1
T5090025	1994-Apr-09	49451.9637	0.0559	1.708	200.0	110.48	452.63	13.169	0.005	341.16	2.02	0.052	−0.085	0.075	3.44	1
T5090027	1994-Apr-09	49451.9834	0.0605	1.813	200.0	110.81	452.96	13.217	0.005	341.55	1.62	0.037	−0.128	0.074	3.77	1
T5090029	1994-Apr-09	49452.0047	0.0654	1.938	200.0	111.60	452.24	12.846	0.003	305.11	1.54	0.035	−0.171	0.070	2.47	1
T5090031	1994-Apr-09	49452.0292	0.0710	2.091	200.0	111.26	451.33	12.845	0.003	347.02	1.47	−0.004	−0.204	0.071	2.73	1

Table A.18 cont.: HV 2241 differential photometry – I.

Frame	Date	HJD −2400000.0	Orbital Phase	X	T	Row	Col	$m_{\rm raw}$	$\sigma_{m_{\rm raw}}$	sky	CHI	Sharp	$V-C$	$C-C$	Seeing (FWHM)	ILCA
T5090033	1994-Apr-09	49452.0429	0.0742	2.180	200.0	111.26	452.07	12.846	0.003	401.74	1.35	0.023	−0.217	0.085	2.74	1
T5090035	1994-Apr-09	49452.0621	0.0786	2.306	200.0	111.43	450.91	12.910	0.003	437.95	1.28	0.020	−0.232	0.078	3.02	1
T6280007	1994-Apr-09	49452.0820	0.0832	2.435	200.0	111.42	451.98	12.853	0.003	450.09	1.35	0.040	−0.249	0.084	2.59	1
T6280010	1994-Apr-09	49452.1177	0.0914	2.638	200.0	111.23	449.86	12.838	0.004	566.22	1.46	0.002	−0.258	0.065	2.74	1
T6280012	1994-Apr-09	49452.1363	0.0957	2.721	200.0	109.99	451.22	13.063	0.005	504.00	1.72	0.034	−0.275	0.072	3.45	1
T6280014	1994-Apr-09	49452.1572	0.1005	2.785	200.0	111.25	449.68	13.029	0.005	550.15	2.07	0.037	−0.276	0.063	3.47	1
T6280016	1994-Apr-09	49452.1712	0.1037	2.808	200.0	111.18	450.94	12.711	0.005	550.13	2.27	−0.062	−0.312	0.066	2.90	1
T6280018	1994-Apr-09	49452.1908	0.1082	2.812	200.0	110.27	450.51	12.868	0.003	563.14	1.23	0.002	−0.316	0.069	3.31	1
T6260002	1994-Apr-09	49452.2154	0.1139	2.769	200.0	110.57	449.98	12.997	0.003	487.60	1.21	−0.002	−0.323	0.080	3.73	1
T6260004	1994-Apr-09	49452.2355	0.1185	2.699	200.0	110.97	450.37	12.879	0.003	549.70	1.24	−0.010	−0.353	0.089	3.43	1
T6260006	1994-Apr-09	49452.2536	0.1227	2.613	200.0	110.84	450.85	12.905	0.005	5854.2	1.00	0.005	−0.327	0.064	3.51	1
T4870008	1994-Aug-27	49591.9568	0.2928	2.087	200.0	113.49	455.81	15.128	0.014	615.70	1.21	0.042	−0.412	0.075	3.09	1
T4870010	1994-Aug-27	49591.9825	0.2987	1.919	800.0	113.49	456.19	12.766	0.003	2264.9	0.99	0.001	−0.396	0.081	3.06	1
T4870011	1994-Aug-27	49591.9961	0.3018	1.839	800.0	112.79	456.34	13.124	0.004	2226.0	1.08	−0.010	−0.392	0.081	3.27	1
T4870012	1994-Aug-27	49592.0063	0.3042	1.782	800.0	112.64	456.34	12.305	0.002	2355.9	1.01	0.012	−0.404	0.097	3.06	1
T4870013	1994-Aug-27	49592.0161	0.3064	1.732	600.0	113.10	456.29	14.072	0.008	1819.3	1.13	0.022	−0.387	0.078	3.27	1
T4870014	1994-Aug-27	49592.1167	0.3296	1.326	600.0	113.59	457.21	12.484	0.002	1567.9	0.94	−0.004	−0.376	0.087	2.82	1
T4870015	1994-Aug-27	49592.1254	0.3316	1.302	600.0	113.49	457.46	13.970	0.009	2350.9	1.18	−0.008	−0.368	0.117	2.88	0
T4870016	1994-Aug-27	49592.1336	0.3335	1.280	600.0	113.16	457.16	11.865	0.002	1053.3	1.15	−0.011	−0.360	0.086	2.82	1
T4870017	1994-Aug-27	49592.1450	0.3361	1.252	600.0	113.87	456.53	12.413	0.002	1442.9	1.02	0.008	−0.359	0.083	3.23	1
T4870018	1994-Aug-27	49592.1555	0.3385	1.230	400.0	112.93	456.58	12.961	0.003	1150.6	1.11	0.000	−0.360	0.083	3.53	1
T4870019	1994-Aug-27	49592.1613	0.3399	1.217	400.0	113.91	457.33	12.820	0.003	885.40	0.98	−0.010	−0.375	0.091	3.71	1
T4870020	1994-Aug-27	49592.1722	0.3424	1.196	400.0	113.80	457.47	12.534	0.002	846.27	0.98	0.002	−0.356	0.084	3.41	1
T4870021	1994-Aug-27	49592.1806	0.3443	1.181	400.0	113.64	457.69	13.178	0.005	1240.5	1.34	0.018	−0.349	0.091	3.61	1
T4870022	1994-Aug-27	49592.1863	0.3456	1.172	400.0	114.70	457.04	13.975	0.007	1738.8	0.98	0.002	−0.403	0.091	3.84	1
T4870023	1994-Aug-27	49592.2136	0.3519	1.133	400.0	113.11	455.86	14.261	0.009	1945.8	0.94	−0.003	−0.382	0.109	4.07	1
T4870024	1994-Sep-04	49599.8228	0.1041	2.744	200.0	111.92	453.26	13.133	0.004	542.50	1.39	0.033	−0.293	0.098	3.43	1
T4870028	1994-Sep-04	49599.8561	0.1118	2.589	200.0	112.21	453.14	13.353	0.004	418.37	1.39	0.003	−0.304	0.095	4.43	1
T4870031	1994-Sep-04	49599.8897	0.1195	2.385	200.0	111.41	453.29	13.431	0.004	380.86	1.17	0.003	−0.325	0.101	4.64	1
T4870034	1994-Sep-04	49599.9192	0.1263	2.190	200.0	113.01	454.11	12.866	0.003	352.30	1.26	0.009	−0.340	0.095	2.96	1
T4870037	1994-Sep-04	49599.9526	0.1340	1.975	200.0	113.10	454.68	12.840	0.003	273.18	1.19	−0.003	−0.343	0.093	2.90	1
T5620003	1994-Sep-04	49599.9911	0.1429	1.753	200.0	113.54	454.55	12.910	0.003	226.62	1.14	0.004	−0.345	0.079	3.16	1
T5620006	1994-Sep-04	49600.0183	0.1491	1.616	200.0	113.43	454.86	12.845	0.002	220.26	1.11	0.009	−0.355	0.087	2.92	1
T5660002	1994-Oct-01	49626.9480	0.3504	1.600	200.0	110.25	453.72	13.779	0.004	242.19	1.03	0.001	−0.332	0.077	3.44	1
T5660004	1994-Oct-01	49626.9698	0.3554	1.506	200.0	107.98	453.42	12.904	0.002	217.82	1.10	0.007	−0.328	0.077	3.46	1
T5660006	1994-Oct-01	49626.9904	0.3601	1.428	200.0	108.73	454.84	13.974	0.005	188.25	1.26	0.011	−0.338	0.071	3.63	1
T5660019	1994-Oct-03	49628.9552	0.8126	1.544	200.0	110.68	454.47	14.472	0.006	233.11	1.16	0.038	−0.329	0.067	3.06	1
T5660020	1994-Oct-03	49628.9610	0.8139	1.520	200.0	110.95	454.01	14.189	0.006	221.11	1.28	0.041	−0.347	0.086	3.17	1
T5660023	1994-Oct-03	49629.0350	0.8310	1.276	200.0	109.61	454.17	15.371	0.010	163.39	1.10	0.019	−0.343	0.080	3.31	1

Table A.18 cont.: HV 2241 differential photometry – I.

Frame	Date	HJD −2400000.0	Orbital Phase	X	T	Row	Col	$m_{\rm raw}$	$\sigma_{m_{\rm raw}}$	sky	CHI	Sharp	$V-C$	$C-C$	Seeing (FWHM)	ILCA
T5660024	1994-Oct-03	49629.0388	0.8318	1.266	200.0	110.63	454.40	15.319	0.011	172.35	1.28	0.030	−0.355	0.065	3.01	1
T5660025	1994-Oct-03	49629.1344	0.8538	1.111	200.0	109.51	453.65	14.742	0.009	142.85	1.54	0.040	−0.283	0.070	3.12	1
T5660027	1994-Oct-03	49629.1402	0.8552	1.106	200.0	109.67	454.20	13.872	0.005	161.69	1.42	0.032	−0.284	0.074	3.20	1
T5680007	1994-Oct-05	49630.9244	0.2660	1.660	200.0	109.90	454.91	13.301	0.004	253.14	1.53	0.009	−0.448	0.104	3.20	1
T5680009	1994-Oct-05	49630.9529	0.2726	1.531	200.0	112.00	455.66	12.524	0.003	219.53	1.51	−0.030	−0.411	0.080	2.45	1
T5680011	1994-Oct-05	49630.9711	0.2768	1.458	200.0	110.75	455.67	12.566	0.003	190.62	1.44	−0.028	−0.404	0.079	2.48	1
T5680013	1994-Oct-05	49630.9890	0.2809	1.394	200.0	111.29	455.59	12.531	0.003	209.42	1.55	−0.037	−0.405	0.086	2.43	1
T5680015	1994-Oct-05	49631.0071	0.2851	1.337	200.0	111.71	455.30	12.594	0.003	185.67	1.43	−0.019	−0.404	0.079	2.64	1
T5680018	1994-Oct-05	49631.0271	0.2897	1.282	200.0	111.20	454.40	12.599	0.002	182.76	1.11	−0.020	−0.405	0.081	2.66	1
T5680020	1994-Oct-05	49631.0394	0.2925	1.252	200.0	111.27	455.39	12.905	0.002	202.48	1.01	−0.006	−0.402	0.077	2.34	1
T5680022	1994-Oct-05	49631.0574	0.2967	1.213	200.0	110.57	455.88	12.995	0.003	186.30	1.46	−0.019	−0.402	0.075	2.44	1
T4890008	1994-Nov-01	49657.8671	0.4703	1.582	200.0	112.31	453.54	13.296	0.004	377.86	1.33	0.012	0.057	0.089	3.56	1
T4890011	1994-Nov-01	49657.9007	0.4780	1.445	200.0	113.48	454.48	13.254	0.003	295.73	0.98	0.013	0.096	0.086	3.30	1
T4890014	1994-Nov-01	49657.9341	0.4857	1.335	200.0	113.87	454.52	13.415	0.004	288.48	1.25	0.015	0.114	0.085	3.83	1
T4890017	1994-Nov-01	49657.9625	0.4922	1.259	200.0	113.53	454.78	13.341	0.004	280.97	1.32	0.018	0.128	0.083	3.70	1
T4890020	1994-Nov-01	49657.9958	0.4999	1.190	200.0	113.71	454.05	13.494	0.004	220.14	1.33	0.017	0.109	0.080	4.09	1
T4890023	1994-Nov-01	49658.0324	0.5083	1.135	200.0	113.72	454.15	13.370	0.004	211.30	1.55	0.030	0.071	0.079	3.93	1
T4890026	1994-Nov-01	49658.0608	0.5149	1.106	200.0	113.23	454.43	13.424	0.005	205.12	1.56	0.014	0.034	0.075	4.05	1
T4890029	1994-Nov-01	49658.0945	0.5226	1.087	200.0	112.83	455.67	13.272	0.004	193.38	1.52	0.019	−0.022	0.083	4.21	1
T4890033	1994-Nov-01	49658.1302	0.5308	1.084	200.0	112.21	456.48	13.192	0.004	207.62	1.34	0.014	−0.069	0.081	3.97	1
T4890036	1994-Nov-01	49658.1600	0.5377	1.093	200.0	113.92	455.51	12.865	0.003	248.59	1.42	0.023	−0.104	0.086	2.59	1
T4890038	1994-Nov-01	49658.1787	0.5420	1.106	200.0	114.15	456.47	12.815	0.004	2160.5	1.37	0.037	−0.111	0.077	2.44	1
T4900008	1994-Nov-02	49658.8742	0.7022	1.539	200.0	109.51	454.25	12.946	0.003	298.61	1.40	0.017	−0.403	0.099	3.60	1
T4900013	1994-Nov-02	49658.9318	0.7154	1.333	200.0	110.39	453.64	13.018	0.003	348.45	1.19	0.017	−0.407	0.100	3.87	1
T4900015	1994-Nov-02	49659.0760	0.7486	1.094	200.0	109.58	452.89	14.220	0.005	222.88	1.15	0.001	−0.398	0.072	5.34	1
T4900020	1994-Nov-02	49659.1591	0.7678	1.095	200.0	109.97	454.01	14.375	0.007	286.41	1.25	0.013	−0.399	0.091	4.74	1
T4900032	1994-Nov-03	49659.8660	0.9306	1.563	200.0	110.66	454.92	14.550	0.009	393.10	1.36	0.062	−0.015	0.060	2.98	1
T4900033	1994-Nov-03	49659.8771	0.9331	1.516	200.0	110.61	455.05	14.394	0.006	290.96	1.09	0.022	0.001	0.072	3.61	1
T4900035	1994-Nov-03	49659.8967	0.9376	1.440	200.0	111.14	455.37	14.427	0.006	261.95	1.18	0.035	0.031	0.076	3.36	1
T4900037	1994-Nov-03	49659.9204	0.9431	1.360	200.0	111.69	455.07	13.329	0.003	257.18	1.10	0.018	0.082	0.076	3.06	1
T4910002	1994-Nov-03	49659.9407	0.9478	1.301	200.0	111.79	455.75	13.843	0.005	223.52	1.35	0.027	0.114	0.082	3.56	1
T4910004	1994-Nov-03	49659.9587	0.9519	1.255	200.0	111.97	454.65	13.658	0.004	213.75	1.32	0.034	0.167	0.085	3.56	1
T4910007	1994-Nov-03	49659.9989	0.9611	1.175	200.0	110.22	453.85	13.951	0.005	165.04	1.42	0.032	0.267	0.083	3.50	1
T4910009	1994-Nov-03	49660.0541	0.9739	1.107	200.0	110.18	453.67	14.955	0.010	177.09	1.39	0.044	0.402	0.076	3.94	1
T4910010	1994-Nov-03	49660.0585	0.9749	1.104	200.0	110.33	453.99	14.284	0.006	171.64	1.36	0.038	0.386	0.081	3.92	1
T4910012	1994-Nov-03	49660.1045	0.9855	1.084	200.0	109.78	454.45	14.958	0.009	155.73	1.25	0.023	0.450	0.069	4.53	1
T4910013	1994-Nov-03	49660.1083	0.9863	1.083	200.0	109.93	454.21	15.267	0.010	157.15	1.23	0.014	0.471	0.072	4.51	1
T4910014	1994-Nov-03	49660.1120	0.9872	1.083	200.0	111.12	453.91	15.143	0.010	162.66	1.28	0.032	0.462	0.057	4.25	1
T4910015	1994-Nov-03	49660.1203	0.9891	1.083	200.0	109.85	455.37	15.060	0.010	187.62	1.30	0.000	0.457	0.078	4.71	1

Table A.18 cont.: HV 2241 differential photometry – I.

Frame	Date	HJD −2400000.0	Orbital Phase	X	T	Row	Col	$m_{\rm raw}$	$\sigma_{m_{\rm raw}}$	sky	CHI	Sharp	$V-C$	$C-C$	Seeing (FWHM)	ILCA
T4910016	1994-Nov-03	49660.1237	0.9899	1.083	200.0	109.44	454.80	14.563	0.008	180.56	1.51	0.025	0.478	0.077	4.39	1
T4910017	1994-Nov-03	49660.1270	0.9907	1.084	200.0	109.75	454.75	14.270	0.006	162.12	1.29	0.002	0.461	0.070	5.05	1
T4910018	1994-Nov-03	49660.1302	0.9914	1.084	200.0	110.19	454.64	14.009	0.005	156.15	1.35	0.013	0.461	0.069	4.32	1
T4910020	1994-Nov-03	49660.1488	0.9957	1.091	200.0	110.89	454.34	14.122	0.006	181.81	1.39	0.006	0.451	0.068	4.60	1
T4910022	1994-Nov-03	49660.1668	0.9998	1.101	200.0	110.17	456.85	14.262	0.006	532.05	1.03	−0.005	0.428	0.065	5.30	1
T4910031	1994-Nov-04	49660.9416	0.1782	1.291	200.0	108.93	453.30	13.840	0.004	204.90	1.09	−0.002	−0.374	0.058	6.92	1
T4910033	1994-Nov-04	49660.9633	0.1832	1.238	200.0	109.70	451.52	13.725	0.004	165.24	1.14	0.002	−0.395	0.058	6.66	1
T4910036	1994-Nov-04	49660.9963	0.1908	1.175	200.0	109.22	451.77	14.026	0.005	181.32	1.18	0.001	−0.398	0.072	7.10	1
T4920002	1994-Nov-04	49661.0434	0.2017	1.114	200.0	108.11	449.91	13.806	0.004	177.35	1.04	−0.002	−0.409	0.056	7.09	1
T4920005	1994-Nov-04	49661.0709	0.2080	1.094	200.0	108.34	450.57	13.543	0.003	151.96	1.02	0.002	−0.394	0.060	6.13	1
T4920008	1994-Nov-04	49661.1043	0.2157	1.083	200.0	107.89	452.15	13.893	0.004	117.30	1.01	0.002	−0.401	0.046	7.14	0
T4920011	1994-Nov-04	49661.1374	0.2233	1.087	200.0	108.61	450.94	13.516	0.003	166.69	1.12	0.005	−0.409	0.064	6.08	1
T4920014	1994-Nov-04	49661.1646	0.2296	1.102	200.0	110.73	451.73	13.853	0.005	243.46	1.26	0.001	−0.396	0.051	6.95	1
T6340003	1994-Dec-24	49711.1248	0.7341	1.242	200.0	112.00	452.12	13.136	0.002	221.51	0.69	0.001	−0.391	0.075	4.60	1
T6340004	1994-Dec-24	49711.1282	0.7349	1.250	200.0	111.47	452.51	13.212	0.002	213.47	0.89	−0.007	−0.404	0.087	4.79	1
T6340005	1994-Dec-24	49711.1314	0.7357	1.257	200.0	111.55	452.32	13.262	0.002	224.27	0.77	−0.001	−0.393	0.079	5.01	1
T6340006	1994-Dec-24	49711.1346	0.7364	1.265	200.0	111.44	452.43	13.319	0.002	241.46	0.78	0.000	−0.397	0.094	5.25	1
T6340007	1994-Dec-24	49711.1378	0.7371	1.273	200.0	110.95	453.11	13.263	0.002	272.54	0.77	0.001	−0.398	0.089	5.28	1
T6340008	1994-Dec-24	49711.1410	0.7379	1.281	200.0	112.01	453.07	13.378	0.003	331.48	0.85	0.000	−0.398	0.087	5.42	1
T6340009	1994-Dec-24	49711.1442	0.7386	1.289	200.0	111.32	452.93	13.389	0.003	413.05	0.92	−0.002	−0.384	0.090	5.68	1
T6340010	1994-Dec-24	49711.1478	0.7394	1.298	200.0	110.57	452.07	13.458	0.002	581.39	0.66	0.000	−0.396	0.104	5.87	1
T6340011	1994-Dec-24	49711.1510	0.7402	1.307	200.0	110.42	452.29	13.395	0.003	866.02	0.75	−0.002	−0.381	0.097	5.42	1
T6070022	1994-Dec-28	49715.0290	0.6332	1.111	200.0	110.21	453.43	12.939	0.003	174.29	1.16	−0.019	−0.335	0.073	3.46	1
T6070024	1994-Dec-28	49715.0439	0.6366	1.126	200.0	111.07	453.68	12.859	0.003	181.31	1.20	−0.016	−0.334	0.078	3.44	1
T6070027	1994-Dec-28	49715.0819	0.6454	1.179	200.0	111.20	454.83	12.807	0.003	201.05	1.36	−0.011	−0.358	0.078	3.27	1
T6070030	1994-Dec-28	49715.1165	0.6533	1.248	200.0	112.07	454.98	12.977	0.004	210.43	1.56	−0.013	−0.349	0.079	3.62	1
T6070033	1994-Dec-28	49715.1447	0.6598	1.320	200.0	111.39	455.94	13.109	0.002	1032.3	0.58	0.001	−0.353	0.086	4.51	1
T6090008	1995-Jan-01	49718.9623	0.5389	1.083	200.0	111.18	452.52	13.491	0.003	233.56	0.83	−0.002	−0.087	0.088	4.57	1
T6090011	1995-Jan-01	49718.9967	0.5468	1.096	200.0	109.54	453.35	13.358	0.003	233.95	0.97	−0.003	−0.132	0.082	4.51	1
T6090014	1995-Jan-01	49719.0304	0.5546	1.124	200.0	110.94	454.72	13.720	0.003	213.50	0.92	0.000	−0.160	0.078	6.10	1
T6090017	1995-Jan-01	49719.0591	0.5612	1.160	200.0	111.83	454.49	13.607	0.002	197.41	0.70	−0.001	−0.189	0.081	5.83	1
T6090020	1995-Jan-01	49719.0934	0.5691	1.221	200.0	110.52	455.02	14.197	0.004	183.55	0.88	0.000	−0.193	0.100	7.80	1
T6090034	1995-Jan-03	49720.9247	0.9908	1.086	200.0	108.99	454.58	13.819	0.004	268.22	1.03	−0.002	0.458	0.086	3.40	1
T6090037	1995-Jan-03	49720.9577	0.9984	1.084	200.0	108.75	455.05	13.966	0.004	239.52	0.88	0.003	0.424	0.085	4.79	1
T6100004	1995-Jan-03	49720.9959	0.0072	1.099	200.0	108.41	455.57	13.857	0.003	211.72	0.81	0.002	0.360	0.083	4.79	1
T6100007	1995-Jan-03	49721.0233	0.0135	1.122	200.0	109.45	454.92	13.412	0.003	185.49	1.19	−0.007	0.285	0.089	2.93	1
T6100010	1995-Jan-03	49721.0562	0.0211	1.164	200.0	109.27	455.63	13.334	0.003	186.48	1.23	−0.002	0.193	0.098	3.02	1
T6100014	1995-Jan-03	49721.0907	0.0291	1.227	200.0	109.03	455.56	13.403	0.003	209.96	1.02	−0.006	0.113	0.089	3.56	1
T6100017	1995-Jan-03	49721.1180	0.0353	1.292	200.0	108.63	456.14	13.356	0.003	206.07	1.00	−0.012	0.055	0.087	3.53	1

Table A.18 cont.: HV 2241 differential photometry – I.

Frame	Date	HJD −2400000.0	Orbital Phase	X	T	Row	Col	$m_{\rm raw}$	$\sigma_{m_{\rm raw}}$	sky	CHI	Sharp	$V-C$	$C-C$	Seeing (FWHM)	ILCA
T6100020	1995-Jan-03	49721.1452	0.0416	1.372	200.0	109.19	457.02	13.418	0.003	593.16	0.87	0.003	0.002	0.086	3.94	1
T8300010	1995-Feb-05	49753.9534	0.5965	1.146	200.0	109.47	450.30	12.710	0.003	151.88	1.63	−0.014	−0.300	0.083	2.77	1
T8300011	1995-Feb-05	49753.9726	0.6009	1.175	200.0	115.71	439.34	14.455	0.017	155.38	0.95	−0.028	−0.197	0.039	3.12	0
T8300014	1995-Feb-05	49753.9924	0.6055	1.211	200.0	110.13	450.08	13.179	0.002	173.21	0.84	−0.001	−0.310	0.083	4.24	1
T8300019	1995-Feb-05	49754.1043	0.6313	1.558	200.0	110.40	453.65	13.263	0.003	176.55	1.14	0.004	−0.329	0.078	4.87	1
T8300020	1995-Feb-05	49754.1126	0.6332	1.595	200.0	109.60	453.62	13.318	0.003	184.87	0.92	0.001	−0.332	0.089	5.45	1
T8300022	1995-Feb-05	49754.1179	0.6344	1.619	200.0	108.73	453.55	13.213	0.003	185.74	1.02	0.004	−0.333	0.085	4.84	1
T8300023	1995-Feb-05	49754.1214	0.6352	1.636	200.0	109.01	452.61	13.211	0.004	187.39	1.40	0.007	−0.337	0.090	4.29	1
T8300024	1995-Feb-05	49754.1270	0.6365	1.663	200.0	109.15	454.27	13.250	0.003	206.16	1.10	0.003	−0.342	0.090	4.54	1
T6880002	1995-Feb-11	49760.1221	0.0170	1.721	200.0	110.97	450.85	13.424	0.004	234.17	1.18	−0.027	0.231	0.087	3.24	1
T6880004	1995-Feb-11	49760.1410	0.0213	1.824	200.0	110.46	451.69	13.371	0.003	248.88	0.94	−0.002	0.194	0.088	2.85	1
T6880006	1995-Feb-11	49760.1591	0.0255	1.931	200.0	111.31	450.96	13.452	0.003	292.07	0.91	−0.008	0.149	0.092	3.33	1
T6880008	1995-Feb-11	49760.1776	0.0298	2.045	200.0	111.00	450.86	13.495	0.003	275.05	0.97	−0.006	0.104	0.076	3.39	1
T7020009	1995-Mar-02	49778.9780	0.3590	1.345	200.0	110.93	451.60	12.943	0.003	189.01	1.50	−0.035	−0.336	0.081	2.59	1
T7020013	1995-Mar-02	49779.0185	0.3684	1.486	200.0	111.85	451.38	12.974	0.004	185.35	1.56	−0.060	−0.324	0.083	2.74	1
T7020017	1995-Mar-02	49779.0570	0.3772	1.655	200.0	112.10	451.48	13.375	0.004	213.20	1.50	−0.060	−0.308	0.071	2.72	1
T7020022	1995-Mar-02	49779.1027	0.3878	1.904	200.0	112.37	449.93	17.734	0.062	207.73	0.90	0.068	−0.213	0.038	3.83	0
T7050006	1995-Mar-07	49784.1108	0.5410	2.040	400.0	112.27	452.63	12.664	0.003	419.12	1.46	0.008	−0.120	0.087	4.30	1
T7050007	1995-Mar-07	49784.1158	0.5421	2.072	400.0	112.66	452.82	12.712	0.002	433.26	1.10	0.005	−0.131	0.094	4.30	1

Appendix B

Synthetic Aperture Photometry for Photometric Calibration

This appendix presents various tables and figures related to the reduction and analysis of the data obtained for the photometric calibration of the MJUO *uvbyVI* photometric system for both standard stars and programme stars.

Figures B.1 to B.8 present night-by-night composite images of the individual flat-fielded images of the Standard star observations obtained for the calibration of the MJUO photometric system to the standard systems. Useful observations were secured on eight nights: for *VI*, 1994-Dec-26 (JDP), 1995-Feb-12 (JDP), 1995-Sep-02 (ACG), 1995-Sep-03 (ACG) & 1995-Oct-23 (ACG); for *uvby* 1995-Sep-18 (JDP & MZZ), 1995-Sep-19 (JDP & MZZ) & 1995-Oct-10 (WT & MZZ) – the bracketed initials after each observation date indicate the observer(s) for each night: JDP, the author; ACG, Alan Gilmore; WT, William Tobin; and MZZ, Mohd Zambri Zainuddin. Tables B.1 to B.8 give the adopted Synthetic Aperture Photometry of Standard stars extracted from the individual standard star images. Figures B.9 to B.11 present plots of various properties of the images and the extracted photometry against Airmass while figures B.12 to B.18 present plots of the residuals between the catalogue photometry and the transformed photometry for the standard stars as a function of *Universal Time Coordinated* (UTC), Airmass, colour, magnitude, Hour Angle and Declination.

Figures B.19 to B.32 present representative image and MIDAS perspective-plots of the 100×100-pixel regions centered on the Optimum-Target-Position adopted for the given nights for the three programme stars, HV 982, HV 1620 and HV 2241. The figures include the 'raw' flat-fielded images and the profile-fitted cleaned images[1]. The smoothness of the profile-fitted cleaned image is indicative of the success of the profile-fitting routine. In theory, one would want that the cleaned image be perfectly smooth, (apart from noise) indicating that all objects in the image have been well accounted for.

B.1 Raw Images

The following eight composite images are useful for gaining an immediate feeling for the photometric quality of the individual nights and also allows identification of obviously problematic images, e.g. standards with cosmic rays within in the synthetic photometry aperture. For each individual image of the composites, the 61×61-pixel region is centered on the Optimum-Target-Position adopted for the given night. Also shown are circles representing the adopted 24″ aperture used to calculate the synthetic aperture photometry throughtout this thesis. The filter through which each individual image was acquired is noted in the bottom left of each individual image. The sky background value reported by DAOPHOT II for each individual image has been subtracted for the purposes of display.

[1]The 'cleaned images' have had the profiles of all successfully fitted stars subtracted (DAOPHOT II routine SUBSTAR).

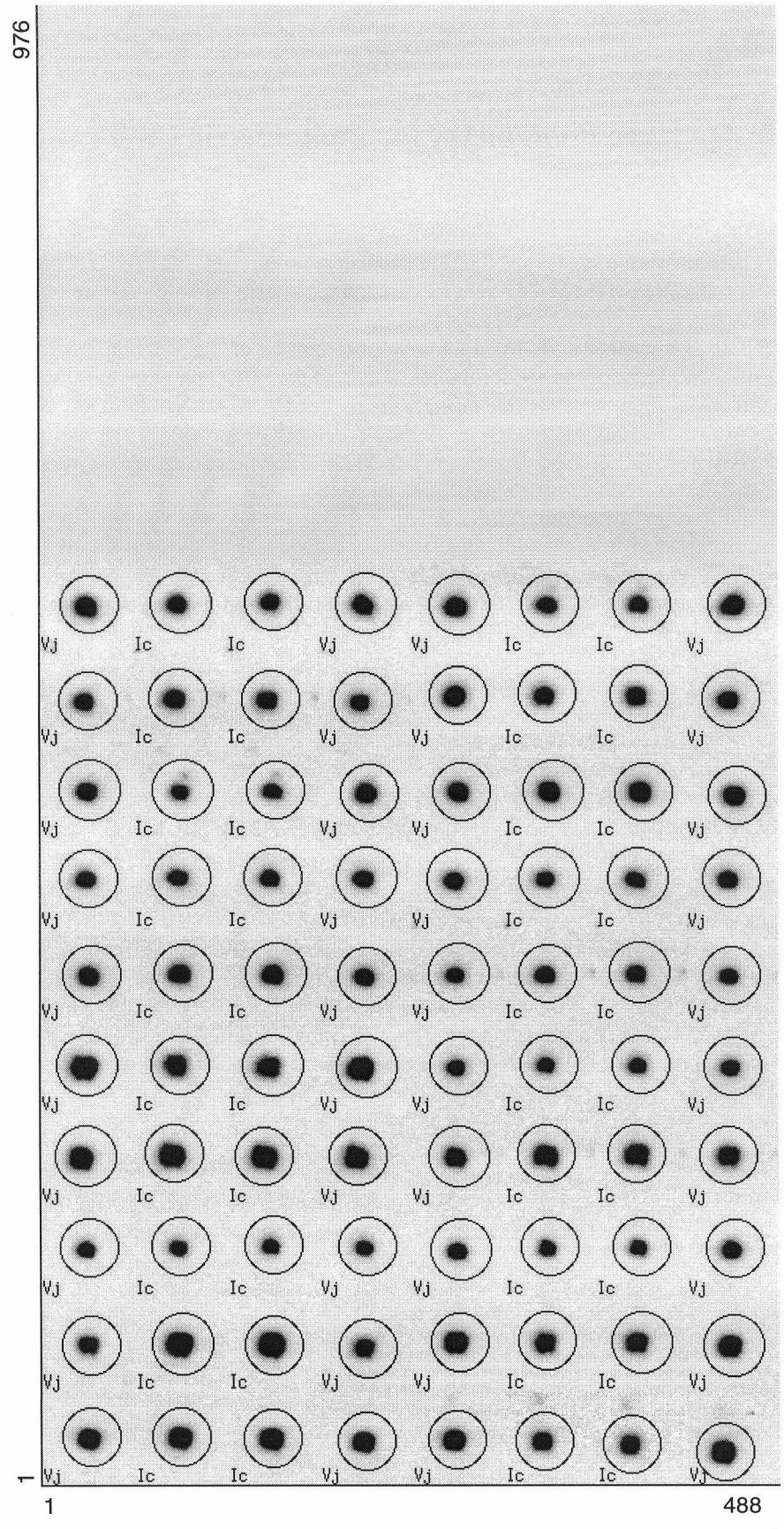

Figure B.1: Standard star image cut outs – 1994-Dec-26. This image is a montage of flat-fielded images of the standard star observations. For each image the 61×61-pixel region centered on the Optimum-Target-Position, which for this night was $(Row, Col) = (163, 142)$ is shown. The circles represent $24''$ apertures and are placed at the centroid used to calculate each aperture magnitude.

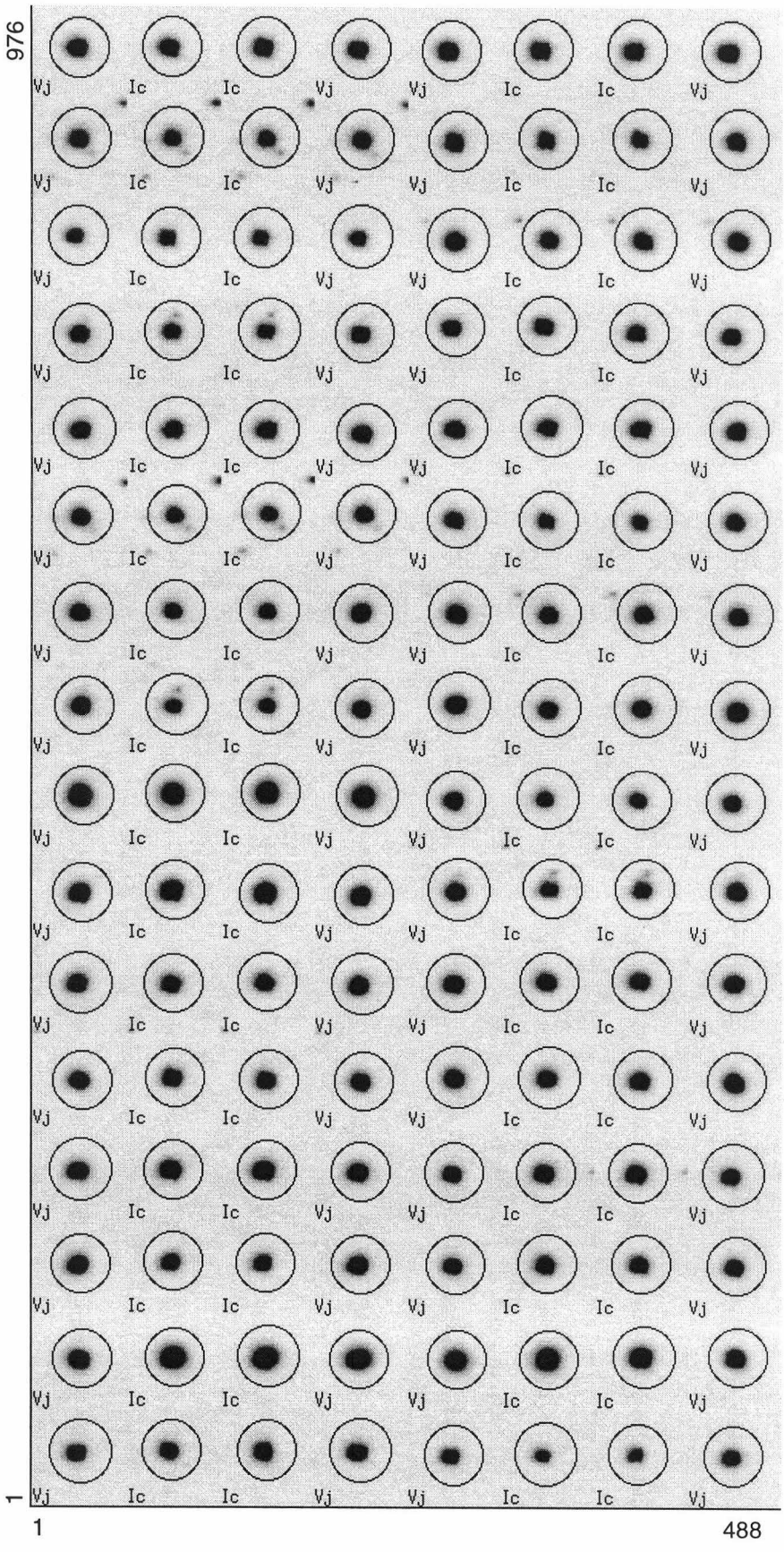

Figure B.2: Standard star image cut outs – 1995-Feb-12. This image is a montage of flat-fielded images of the standard star observations. For each image the 61×61-pixel region centered on the Optimum-Target-Position, which for this night was $(Row, Col) = (174, 271)$ is shown.

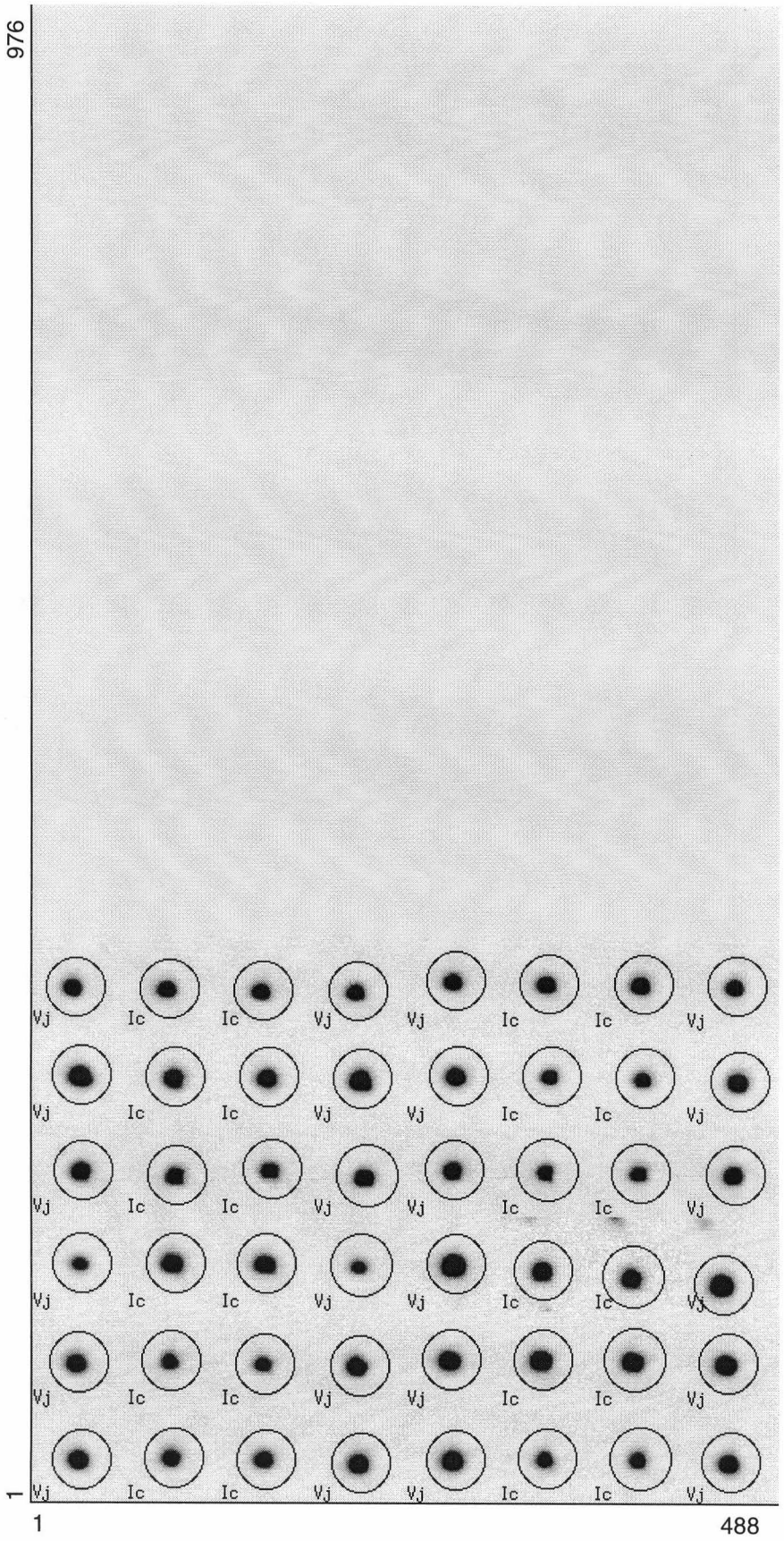

Figure B.3: Standard star image cut outs – 1995-Sep-02. This image is a montage of flat-fielded images of the standard star observations. For each image the 61×61-pixel region centered on the Optimum-Target-Position, which for this night was $(Row, Col) = (110, 452)$ is shown.

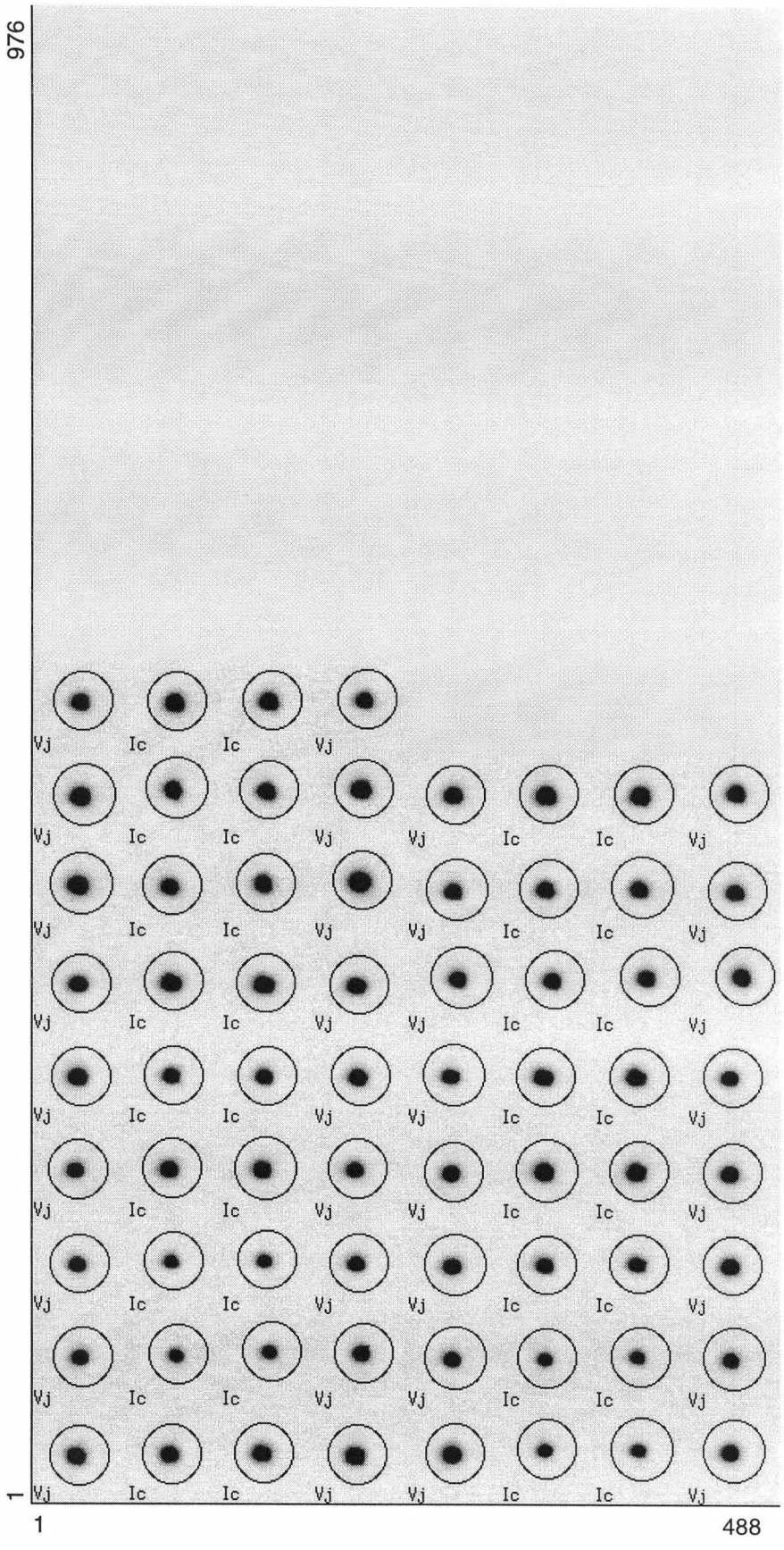

Figure B.4: Standard star image cut outs – 1995-Sep-03. This image is a montage of flat-fielded images of the standard star observations. For each image the 61×61-pixel region centered on the Optimum-Target-Position, which for this night was $(Row, Col) = (110, 452)$ is shown.

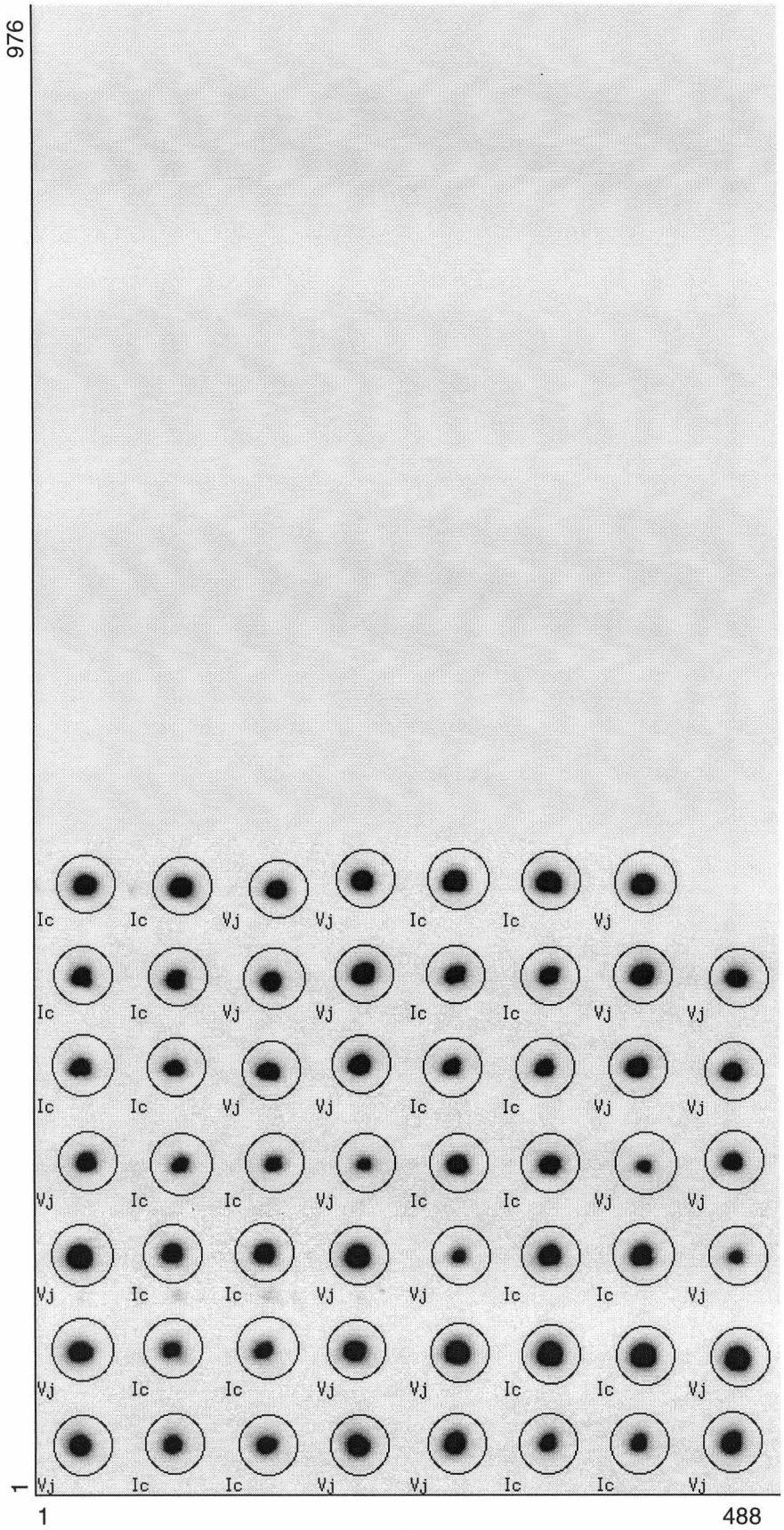

Figure B.5: Standard star image cut outs – 1995-Oct-23. This image is a montage of flat-fielded images of the standard star observations. For each image the 61×61-pixel region centered on the Optimum-Target-Position, which for this night was $(Row, Col) = (163, 142)$ is shown. **There is one extra frame in this image, as compared to table B.5, corresponding to the I exposure T8980004 which has no corresponding V exposure (frame number 27, i.e. row 4, column 3 counting from the bottom left).**

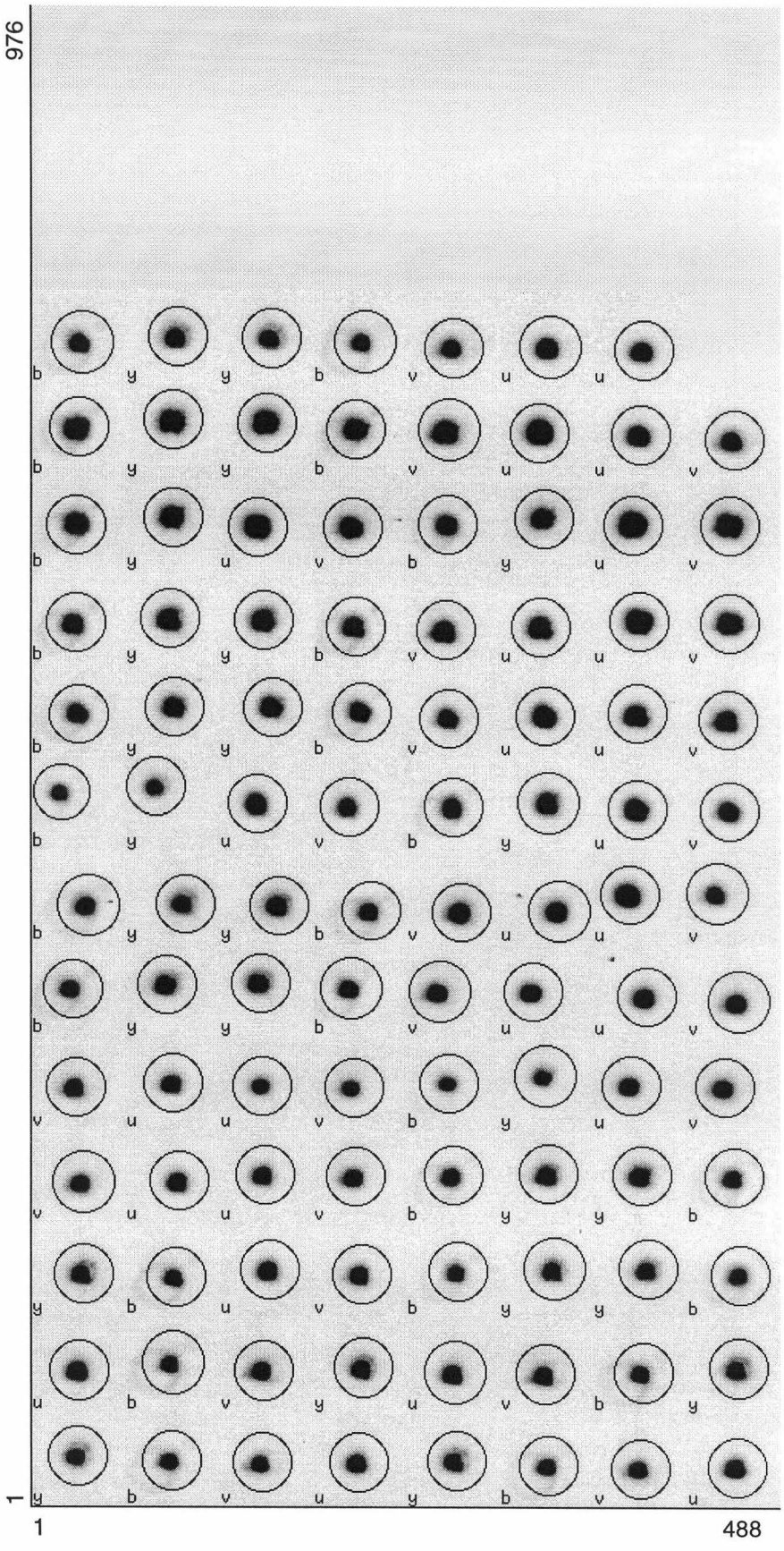

Figure B.6: Standard star image cut outs – 1995-Sep-18. This image is a montage of flat-fielded images of the standard star observations. For each image the 61×61-pixel region centered on the Optimum-Target-Position, which for this night was $(Row, Col) = (110, 452)$ is shown. There is one extra frame in this image, as compared to table B.6 corresponding to the saturated exposure T8880029 (frame number 102, i.e. row 13, column 6 counting from the bottom left). In order to fit into the image, the aperture for frame number 57 (i.e. row 7, column 1) is only $22.2''$ in diameter.

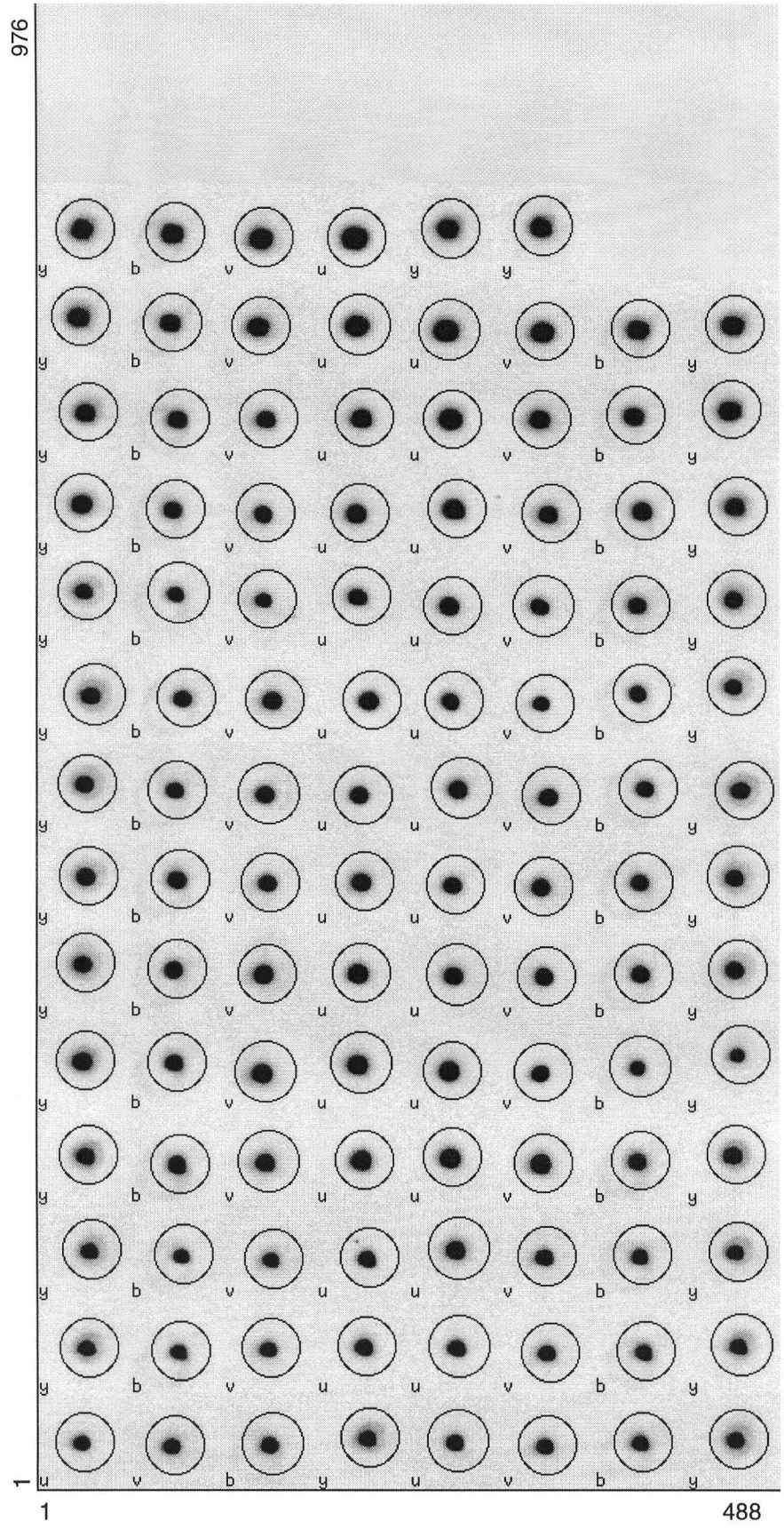

Figure B.7: Standard star image cut outs – 1995-Sep-19. This image is a montage of flat-fielded images of the standard star observations. For each image the 61×61-pixel region centered on the Optimum-Target-Position, which for this night was $(Row, Col) = (163, 142)$ is shown.

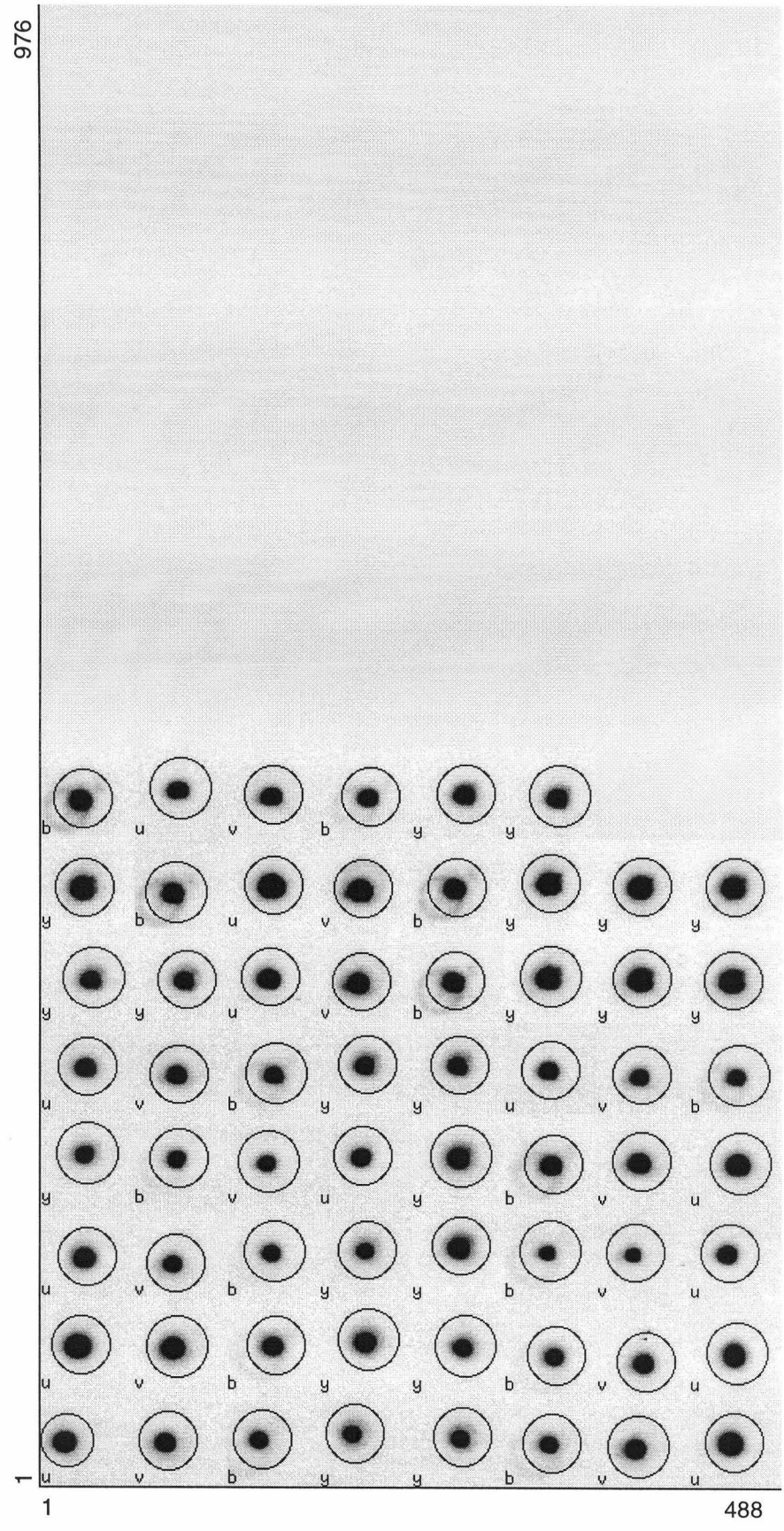

Figure B.8: Standard star image cut outs – 1995-Oct-25. This image is a montage of flat-fielded images of the standard star observations. For each image the 61×61-pixel region centered on the Optimum-Target-Position, which for this night was $(Row, Col) = (163, 142)$ is shown. In order to fit into the image, the aperture for frame number 1 (i.e. row 1, column 1) is only $21.0''$ in diameter.

B.2 Raw calibration photometry

The following eight tables list, night by night, the adopted synthetic aperture photometry for the standard star observations. Each table lists the following columns:

1. **Star** The standard star observed. Taken from the catalogues of Kilkenny and Menzies (1989), Menzies et al. (1989), Menzies, Marang and Westerhuys (1990), Landolt (1983; 1992), Graham (1982) and Bessell (1995) for *VI* and Kilkenny and Laing (1992), Kilkenny (1977; 1977a; 1977b), Cousins (1987), Kilkenny and Hill (1975), Graham (1972), Graham and Slettebak (1973) Bessell and Wickramasinghe (1978) for *uvby*.

2. **Frame** The computer magnetic tape file name of the image. The first four characters, usually a letter followed by three digits identifies the physical tape, the last four digits identifies the specific image on the tape.

3. **HJD−2400000.0)** The (modified) Heliocentric Julian Day number of mid-exposure. The begining and finishing times of each exposure are recorded in the image header at the time the image file is first created by the PM3000 CCD system.[2] At the time the image is read from tape to disk back in Christchurch, a correction for the known drift behaviour of the PM3000 clock is applied, the mid time of the exposure is calculated, the appropriate heliocentric correction is calculated and the heliocentric Julian Day number is added to the image header information (see section 2.3.6).

4. **Filter** The filter used for the observation.

5. **X** The airmass (see appendix A).

6. **T** The exposure duration in seconds.

7. **Row** and **Col** The MIDAS position of the stellar centroid of the target reported by the DAOPHOT II profile fitting photometry.

8. $\mathbf{m}_{\mathrm{raw}}$ The magnitude of target reported by the DAOPHOT II synthetic aperture photometry routine (`Photometry`) [mag].

9. $\sigma_{\mathbf{m}_{\mathrm{raw}}}$ The standard error on magnitude reported by the DAOPHOT II synthetic aperture photometry routine [mag].

10. **sky** The background sky level reported by the DAOPHOT II synthetic aperture photometry routine [ADU].

11. $\sigma_{\mathbf{m}_{\mathrm{sky}}}$ The standard error of the **sky** value reported by the DAOPHOT II synthetic aperture photometry routine [ADU].

12. **skew** The 'skewness of the sky values about the mean' (Stetson, 1994a).

13. **Seeing (FWHM)** The seeing, in terms of the 'mean' Full Width at Half Maximum [arcsec] (see appendix A).

[2] Exposure begining and finishing times are recorded provided the `expose` and `readout` commands are used to obtain the exposure. If instead `obs` is used, the start time and exposure duration (in deci-secs) are recorded in the header. Either way it is possible to compute the precise moment of mid-exposure.

B.2.1 Raw VI calibration photometry

Table B.1: Standard star VI photometry – 1994-Dec-26. These are from a 24″ synthetic aperture.

Star	Frame	HJD −2400000.0	Filter	X	T	Row	Col	$m_{\rm raw}$	$\sigma_{m_{\rm raw}}$	sky	$\sigma_{\rm sky}$	sky skew	Seeing (FWHM)
THPEb	T6040033	49712.9204	V	1.211	60.0	163.938	141.821	11.851	0.002	23.471	5.660	0.100	3.181
THPEb	T6040034	49712.9216	I	1.215	60.0	162.348	142.202	11.754	0.002	63.687	6.210	0.030	3.631
THPEb	T6040035	49712.9227	I	1.219	60.0	161.387	141.263	11.758	0.002	60.401	6.110	0.000	3.698
THPEb	T6040036	49712.9238	V	1.223	60.0	161.912	139.307	11.857	0.002	18.708	5.600	0.000	3.248
THPEC	T6050001	49712.9318	V	1.256	400.0	160.734	140.192	11.877	0.002	114.007	7.810	0.110	3.581
THPEC	T6050002	49712.9369	I	1.277	400.0	157.802	139.369	12.670	0.006	360.835	11.660	0.070	4.389
THPEC	T6050003	49712.9420	I	1.298	400.0	155.109	137.117	12.659	0.006	360.847	11.330	0.140	4.641
THPEC	T6050004	49712.9470	V	1.321	400.0	156.177	132.391	11.882	0.002	97.057	7.620	0.130	4.481
THPEE	T6050005	49712.9520	V	1.342	60.0	163.746	140.442	12.770	0.004	8.868	5.260	0.050	3.914
THPEE	T6050006	49712.9532	I	1.348	60.0	162.674	140.500	11.519	0.002	48.351	5.890	0.010	4.808
THPEE	T6050007	49712.9543	I	1.354	60.0	161.974	140.440	11.520	0.002	47.664	6.100	0.000	4.826
THPEE	T6050008	49712.9555	V	1.359	60.0	162.618	138.445	12.777	0.004	8.877	5.460	0.000	4.284
DM−38222	T6050010	49712.9617	V	1.421	10.0	162.681	142.192	11.998	0.002	2.675	4.970	0.100	4.241
DM−38222	T6050011	49712.9623	I	1.425	10.0	159.867	143.406	12.621	0.003	9.974	5.190	0.030	4.802
DM−38222	T6050012	49712.9628	I	1.428	10.0	161.502	142.180	12.623	0.003	9.873	5.240	0.060	5.283
DM−38222	T6050013	49712.9634	V	1.432	10.0	161.638	140.063	12.002	0.002	1.669	5.140	0.130	4.124
DM−441028	T6050014	49712.9754	V	1.063	10.0	162.968	142.878	12.302	0.002	1.504	5.000	0.000	2.151
DM−441028	T6050015	49712.9760	I	1.064	10.0	162.273	143.861	12.493	0.003	5.928	5.210	0.000	2.170
DM−441028	T6050016	49712.9765	I	1.065	10.0	162.012	145.060	12.498	0.003	5.933	5.090	0.000	1.966
DM−441028	T6050017	49712.9771	V	1.066	10.0	162.960	143.945	12.296	0.002	0.722	5.080	0.000	2.077
DM−261339	T6050018	49712.9823	V	1.122	25.0	163.752	141.883	11.799	0.002	7.953	5.340	0.020	1.917
DM−261339	T6050019	49712.9831	I	1.123	25.0	162.262	143.741	12.614	0.003	19.770	5.470	0.000	2.564
DM−261339	T6050020	49712.9838	I	1.125	25.0	161.933	144.189	12.616	0.003	19.943	5.400	0.000	2.194
DM−261339	T6050021	49712.9845	V	1.126	25.0	162.963	143.050	11.797	0.002	7.069	5.340	0.070	2.120
E2−b	T6050026	49713.0193	V	1.078	25.0	160.708	143.003	12.071	0.002	3.542	5.200	0.140	4.697
E2−b	T6050027	49713.0200	I	1.080	25.0	158.360	145.497	11.931	0.002	18.866	5.450	0.100	5.227
E2−b	T6050028	49713.0208	I	1.081	25.0	156.458	143.389	11.940	0.002	19.221	5.370	0.010	4.851
E2−b	T6050029	49713.0215	V	1.082	25.0	157.193	143.198	12.080	0.002	3.021	5.270	0.070	4.524
E2−L	T6050030	49713.0249	V	1.090	60.0	162.612	143.038	12.546	0.003	10.544	5.300	0.030	4.494
E2−L	T6050031	49713.0260	I	1.092	60.0	160.313	145.150	12.290	0.003	51.844	6.360	0.000	5.104
E2−L	T6050032	49713.0271	I	1.095	60.0	159.461	145.028	12.280	0.003	52.510	6.230	0.040	5.073
E2−L	T6050033	49713.0283	V	1.097	60.0	159.468	144.158	12.556	0.003	10.861	5.260	0.000	4.586
DM−261339	T6050034	49713.0411	V	1.326	25.0	161.520	141.664	11.837	0.002	8.971	5.260	0.000	4.820
DM−261339	T6050035	49713.0418	I	1.330	25.0	161.937	142.305	12.637	0.003	26.095	5.710	0.010	5.517
DM−261339	T6050036	49713.0425	I	1.333	25.0	161.553	142.152	12.639	0.003	26.540	5.540	0.000	5.708
DM−261339	T6050037	49713.0433	V	1.337	25.0	162.667	140.578	11.834	0.002	8.939	5.310	0.030	4.894

Table B.1 cont.: Standard star VI photometry – 1994-Dec-26.

Star	Frame	HJD −2400000.0	Filter	X	T	Row	Col	$m_{\rm raw}$	$\sigma_{m_{\rm raw}}$	sky	$\sigma_{\rm sky}$	sky skew	Seeing (FWHM)
DM−441028	T6060002	49713.0489	V	1.273	10.0	163.135	141.744	12.333	0.002	3.390	5.060	0.050	2.638
DM−441028	T6060003	49713.0495	I	1.276	10.0	161.960	143.318	12.511	0.003	10.411	5.170	0.020	2.305
DM−441028	T6060004	49713.0500	I	1.278	10.0	161.992	143.181	12.510	0.003	10.252	5.230	0.040	2.312
DM−441028	T6060005	49713.0506	V	1.281	10.0	162.248	141.840	12.326	0.002	2.544	5.010	0.140	2.805
E2−b	T6060010	49713.0861	V	1.278	25.0	165.109	140.926	12.107	0.002	9.872	5.150	0.040	3.261
E2−b	T6060011	49713.0869	I	1.281	25.0	163.837	142.332	11.948	0.002	23.585	5.490	0.020	3.267
E2−b	T6060012	49713.0876	I	1.284	25.0	163.888	141.787	11.944	0.002	23.331	5.370	0.090	3.218
E2−b	T6060013	49713.0883	V	1.288	25.0	163.249	140.278	12.110	0.002	9.655	5.220	0.000	2.798
E2−L	T6060014	49713.0917	V	1.304	60.0	162.653	141.822	12.574	0.003	23.956	5.370	0.050	2.823
E2−L	T6060015	49713.0929	I	1.310	60.0	161.226	141.983	12.297	0.003	54.906	6.040	0.000	3.070
E2−L	T6060016	49713.0940	I	1.315	60.0	160.859	142.685	12.298	0.003	54.959	5.990	0.000	2.983
E2−L	T6060017	49713.0951	V	1.320	60.0	161.168	141.214	12.576	0.003	23.998	5.390	0.010	3.094
DM−243988	T6060018	49713.1028	V	1.134	10.0	163.286	144.311	12.257	0.002	2.794	5.010	0.000	2.577
DM−243988	T6060019	49713.1034	I	1.135	10.0	162.779	145.320	12.363	0.003	6.735	5.130	0.000	2.743
DM−243988	T6060020	49713.1039	I	1.136	10.0	162.190	144.961	12.368	0.003	6.842	5.160	0.000	2.601
DM−243988	T6060021	49713.1045	V	1.138	10.0	162.769	144.804	12.257	0.002	2.024	5.040	0.070	3.002
E355	T6060022	49713.1076	V	1.040	10.0	161.703	143.874	12.135	0.002	2.610	5.190	0.050	2.737
E355	T6060023	49713.1082	I	1.041	10.0	161.696	144.906	12.557	0.003	6.178	5.420	0.010	2.786
E355	T6060024	49713.1087	I	1.042	10.0	159.778	144.749	12.552	0.003	5.643	5.380	0.080	3.507
E355	T6060025	49713.1093	V	1.043	10.0	160.751	145.150	12.139	0.002	1.860	5.180	0.000	2.768
DM−314800	T6060026	49713.1154	V	1.035	10.0	164.016	141.682	11.995	0.002	2.164	5.230	0.090	2.694
DM−314800	T6060027	49713.1160	I	1.035	10.0	163.964	141.677	12.747	0.004	6.333	5.770	0.090	2.577
DM−314800	T6060028	49713.1165	I	1.036	10.0	163.838	142.107	12.753	0.004	6.157	5.810	0.130	3.316
DM−314800	T6060029	49713.1171	V	1.036	10.0	164.936	140.230	11.993	0.002	1.548	5.260	0.130	3.150
E2−b	T6060030	49713.1215	V	1.464	25.0	165.037	141.149	12.137	0.002	11.556	5.170	0.000	3.310
E2−b	T6060031	49713.1223	I	1.469	25.0	164.640	141.790	11.962	0.002	26.255	5.420	0.030	3.273
E2−b	T6060032	49713.1230	I	1.473	25.0	164.138	141.299	11.959	0.002	24.933	5.520	0.100	3.538
E2−b	T6060033	49713.1237	V	1.478	25.0	165.108	139.189	12.146	0.002	11.439	5.320	0.000	3.766
E2−L	T6060034	49713.1288	V	1.514	60.0	162.642	140.093	12.609	0.003	33.856	5.650	0.060	3.341
E2−L	T6060035	49713.1299	I	1.523	60.0	161.069	141.976	12.306	0.003	68.868	6.460	0.110	3.520
E2−L	T6060036	49713.1311	I	1.530	60.0	160.738	141.164	12.308	0.003	73.174	6.320	0.020	3.205
E2−L	T6060037	49713.1322	V	1.539	60.0	161.007	140.088	12.614	0.003	38.056	5.710	0.090	3.218
DM−243988	T6070001	49713.1401	V	1.247	10.0	162.715	144.149	12.277	0.002	4.922	5.140	0.080	4.179
DM−243988	T6070002	49713.1407	I	1.250	10.0	161.178	144.726	12.371	0.003	10.739	5.240	0.100	3.150
DM−243988	T6070003	49713.1412	I	1.252	10.0	161.220	144.764	12.379	0.003	11.772	5.330	0.000	3.501
DM−243988	T6070004	49713.1418	V	1.254	10.0	161.267	142.170	12.279	0.002	5.633	5.090	0.000	3.316
E355	T6070005	49713.1442	V	1.106	10.0	163.780	142.993	12.150	0.002	7.875	5.390	0.000	3.643
E355	T6070006	49713.1448	I	1.107	10.0	162.651	143.783	12.555	0.003	14.297	5.450	0.090	3.458
E355	T6070007	49713.1453	I	1.108	10.0	162.654	145.324	12.558	0.003	14.831	5.520	0.050	3.150

Table B.1 cont.: Standard star VI photometry – 1994-Dec-26.

Star	Frame	HJD −2400000.0	Filter	X	T	Row	Col	$m_{\rm raw}$	$\sigma_{m_{\rm raw}}$	sky	$\sigma_{\rm sky}$	sky skew	Seeing (FWHM)
E355	T6070008	49713.1459	V	1.110	10.0	162.705	143.824	12.145	0.002	8.742	5.380	0.070	3.236
DM−314800	T6070009	49713.1510	V	1.082	10.0	163.836	142.728	12.004	0.002	16.626	5.580	0.060	3.520
DM−314800	T6070010	49713.1516	I	1.083	10.0	163.161	144.205	12.762	0.004	28.285	6.220	0.100	3.877
DM−314800	T6070011	49713.1521	I	1.084	10.0	163.161	144.211	12.751	0.004	29.785	6.160	0.180	3.489
DM−314800	T6070012	49713.1527	V	1.085	10.0	164.977	144.086	11.998	0.002	19.860	5.520	0.120	3.698

Table B.2: Standard star VI photometry – 1995-Feb-12. These are from a $24''$ synthetic aperture.

Star	Frame	HJD −2400000.0	Filter	X	T	Row	Col	$m_{\rm raw}$	$\sigma_{m_{\rm raw}}$	sky	$\sigma_{\rm sky}$	sky skew	Seeing (FWHM)
DM−441028	T4300008	49760.8762	V	1.138	10.0	173.647	273.949	12.280	0.003	27.041	5.680	0.020	2.466
DM−441028	T4300009	49760.8768	I	1.140	10.0	172.191	275.286	12.468	0.003	39.620	5.970	0.020	2.355
DM−441028	T4300010	49760.8773	I	1.141	10.0	172.709	275.115	12.459	0.003	36.776	5.960	0.030	3.187
DM−441028	T4300011	49760.8779	V	1.143	10.0	172.698	274.685	12.279	0.003	22.396	5.540	0.050	2.940
DM−261339	T4300012	49760.8825	V	1.220	10.0	172.697	272.208	12.781	0.004	21.673	5.680	0.000	2.681
DM−261339	T4300013	49760.8831	I	1.222	10.0	171.651	272.796	13.597	0.008	23.825	5.720	0.000	3.341
DM−261339	T4300014	49760.8836	I	1.224	10.0	171.019	273.327	13.591	0.007	22.954	5.630	0.000	3.637
DM−261339	T4300015	49760.8842	V	1.226	10.0	172.285	272.183	12.780	0.004	19.883	5.460	0.030	3.070
E2−b	T4300016	49760.8889	V	1.083	25.0	174.945	272.077	12.049	0.002	34.878	5.940	0.010	3.242
E2−b	T4300017	49760.8896	I	1.085	25.0	173.798	272.957	11.917	0.002	37.620	5.850	0.060	4.524
E2−b	T4300018	49760.8903	I	1.086	25.0	173.620	273.688	11.913	0.002	37.528	5.840	0.000	4.457
E2−b	T4300019	49760.8911	V	1.088	25.0	172.221	272.357	12.053	0.002	34.517	5.710	0.010	4.346
E2−L	T4300020	49760.8951	V	1.097	60.0	175.282	271.897	12.521	0.003	81.168	6.550	0.010	4.863
E2−L	T4300021	49760.8963	I	1.100	60.0	174.075	272.441	12.259	0.003	81.979	6.650	0.000	5.301
E2−L	T4300022	49760.8974	I	1.102	60.0	174.660	273.522	12.256	0.003	79.824	6.580	0.050	4.709
E2−L	T4300023	49760.8986	V	1.105	60.0	174.804	274.110	12.509	0.003	79.601	6.710	0.000	3.914
DM−261339	T4300028	49760.9318	V	1.479	25.0	174.141	273.047	11.819	0.002	47.710	6.110	0.030	2.570
DM−261339	T4300029	49760.9325	I	1.485	25.0	173.189	274.824	12.620	0.004	41.596	6.030	0.000	2.946
DM−261339	T4300030	49760.9332	I	1.490	25.0	171.981	274.304	12.615	0.003	41.144	5.770	0.000	2.743
DM−261339	T4300031	49760.9340	V	1.496	25.0	173.172	273.151	11.826	0.002	47.493	6.110	0.000	2.620
DM−441028	T4300032	49760.9376	V	1.382	10.0	173.877	273.166	12.310	0.003	11.510	5.530	0.000	2.607
DM−441028	T4300033	49760.9382	I	1.385	10.0	173.185	273.939	12.487	0.003	10.901	5.700	0.000	2.965
DM−441028	T4300034	49760.9388	I	1.388	10.0	173.254	274.210	12.485	0.003	10.824	5.550	0.000	2.792
DM−441028	T4300035	49760.9393	V	1.391	10.0	174.231	272.977	12.303	0.003	10.666	5.430	0.100	2.577
E2−b	T8220001	49760.9486	V	1.260	25.0	173.877	272.751	12.074	0.002	38.528	5.720	0.000	2.891
E2−b	T8220002	49760.9494	I	1.263	25.0	172.755	273.337	11.922	0.002	36.985	6.000	0.000	2.953
E2−b	T8220003	49760.9501	I	1.266	25.0	172.719	273.202	11.922	0.002	36.842	5.780	0.030	3.051

Table B.2 cont.: Standard star VI photometry – 1995-Feb-12.

Star	Frame	HJD −2400000.0	Filter	X	T	Row	Col	$m_{\rm raw}$	$\sigma_{m_{\rm raw}}$	sky	$\sigma_{\rm sky}$	sky skew	Seeing (FWHM)
E2−b	T8220004	49760.9508	V	1.269	25.0	172.953	272.144	12.078	0.002	38.235	5.740	0.020	2.860
E2−L	T8220005	49760.9553	V	1.290	60.0	173.140	271.739	12.538	0.004	92.489	6.760	0.000	2.916
E2−L	T8220006	49760.9565	I	1.295	60.0	172.076	272.152	12.272	0.003	88.641	6.670	0.000	2.996
E2−L	T8220007	49760.9576	I	1.300	60.0	171.102	272.100	12.264	0.003	88.302	6.630	0.090	3.070
E2−L	T8220008	49760.9587	V	1.305	60.0	171.655	270.950	12.536	0.003	93.167	6.540	0.070	2.823
DM−243988	T8220009	49760.9669	V	1.126	10.0	175.134	270.260	12.256	0.002	20.561	5.500	0.030	2.663
DM−243988	T8220010	49760.9675	I	1.127	10.0	174.226	272.285	12.373	0.003	20.509	5.310	0.030	3.113
DM−243988	T8220011	49760.9680	I	1.128	10.0	174.103	271.054	12.369	0.003	20.725	5.500	0.000	2.724
DM−243988	T8220012	49760.9686	V	1.129	10.0	174.970	270.155	12.252	0.002	19.454	5.570	0.000	2.768
E3−W	T8220013	49760.9722	V	1.037	25.0	174.732	272.734	12.027	0.002	34.373	5.770	0.060	2.761
E3−W	T8220014	49760.9730	I	1.038	25.0	173.849	272.855	12.381	0.003	32.319	6.010	0.070	2.792
E3−W	T8220015	49760.9737	I	1.039	25.0	174.042	272.078	12.370	0.003	32.158	5.950	0.090	3.082
E3−W	T8220016	49760.9745	V	1.040	25.0	174.090	270.853	12.031	0.002	34.397	5.930	0.040	2.860
E355	T8220017	49760.9785	V	1.044	10.0	173.662	272.911	12.101	0.002	12.585	5.510	0.100	2.614
E355	T8220018	49760.9791	I	1.044	10.0	173.106	272.890	12.536	0.003	12.682	5.530	0.000	3.224
E355	T8220019	49760.9797	I	1.045	10.0	172.856	274.233	12.532	0.003	12.219	5.640	0.050	3.008
E355	T8220020	49760.9802	V	1.046	10.0	173.759	272.708	12.105	0.002	13.188	5.520	0.040	2.866
E3−W	T8220025	49761.0116	V	1.106	25.0	174.287	273.934	12.044	0.002	36.282	5.850	0.000	2.681
E3−W	T8220026	49761.0124	I	1.107	25.0	173.800	275.311	12.385	0.003	33.700	6.010	0.050	3.033
E3−W	T8220027	49761.0131	I	1.109	25.0	173.277	276.226	12.388	0.003	33.173	5.900	0.010	2.965
E3−W	T8220028	49761.0138	V	1.111	25.0	173.976	275.030	12.039	0.002	35.766	5.840	0.030	2.552
E2−b	T8220029	49761.0163	V	1.672	25.0	175.187	271.200	12.145	0.002	46.699	5.990	0.060	3.076
E2−b	T8220030	49761.0170	I	1.679	25.0	174.156	273.111	11.952	0.002	42.525	5.920	0.050	3.631
E2−b	T8220031	49761.0177	I	1.685	25.0	173.679	271.372	11.955	0.002	42.494	5.740	0.090	3.557
E2−b	T8220032	49761.0185	V	1.692	25.0	174.734	270.066	12.150	0.002	47.089	5.980	0.060	2.829
DM−314800	T8220033	49761.0265	V	1.095	10.0	175.879	273.691	11.973	0.002	17.402	5.620	0.060	2.324
DM−314800	T8220034	49761.0271	I	1.096	10.0	175.690	275.291	12.742	0.004	16.687	6.080	0.040	2.718
DM−314800	T8220035	49761.0277	I	1.097	10.0	175.222	274.928	12.733	0.004	16.140	5.840	0.090	3.014
DM−314800	T8220036	49761.0282	V	1.098	10.0	175.939	274.326	11.976	0.002	16.628	5.700	0.090	2.429
DM−308345	T8230005	49761.0412	V	1.034	25.0	175.671	273.291	11.582	0.002	31.539	5.830	0.040	3.187
DM−308345	T8230006	49761.0420	I	1.034	25.0	174.168	275.198	11.839	0.002	28.965	5.630	0.010	3.544
DM−308345	T8230007	49761.0427	I	1.033	25.0	174.674	276.191	11.836	0.002	28.937	5.610	0.000	3.489
DM−308345	T8230008	49761.0434	V	1.033	25.0	176.669	273.856	11.583	0.002	31.825	5.760	0.030	2.983
E355	T8230013	49761.0778	V	1.328	10.0	174.120	271.244	12.156	0.002	14.594	5.650	0.020	3.292
E355	T8230014	49761.0784	I	1.331	10.0	172.947	272.707	12.551	0.003	14.357	5.570	0.040	2.447
E355	T8230015	49761.0790	I	1.333	10.0	172.804	272.198	12.557	0.003	14.249	5.490	0.020	2.447
E355	T8230016	49761.0795	V	1.336	10.0	173.023	270.794	12.161	0.002	13.795	5.500	0.000	2.577
DM−314800	T8230017	49761.0855	V	1.287	10.0	175.801	272.267	12.000	0.002	15.924	5.700	0.090	2.946
DM−314800	T8230018	49761.0861	I	1.290	10.0	174.672	272.718	12.745	0.004	16.720	5.730	0.120	2.435

Table B.2 cont.: Standard star VI photometry – 1995-Feb-12.

Star	Frame	HJD −2400000.0	Filter	X	T	Row	Col	$m_{\rm raw}$	$\sigma_{m_{\rm raw}}$	sky	$\sigma_{\rm sky}$	sky skew	Seeing (FWHM)
DM−314800	T8230019	49761.0866	*I*	1.292	10.0	174.212	273.174	12.748	0.004	16.314	5.950	0.170	2.749
DM−314800	T8230020	49761.0872	*V*	1.295	10.0	175.164	271.072	12.003	0.002	15.544	5.540	0.040	2.694
DM−308345	T8230021	49761.0922	*V*	1.036	25.0	175.831	274.771	11.578	0.002	26.781	5.570	0.000	2.909
DM−308345	T8230022	49761.0929	*I*	1.036	25.0	175.148	271.765	11.832	0.002	27.613	5.580	0.010	2.139
DM−308345	T8230023	49761.0937	*I*	1.037	25.0	174.920	272.773	11.827	0.002	27.578	5.800	0.000	2.256
DM−308345	T8230024	49761.0944	*V*	1.037	25.0	175.881	270.883	11.578	0.002	25.523	5.560	0.020	3.008
E4−T	T8230025	49761.0977	*V*	1.052	10.0	174.904	272.267	12.053	0.002	7.939	5.290	0.000	2.835
E4−T	T8230026	49761.0983	*I*	1.053	10.0	174.135	273.757	12.322	0.003	9.922	5.330	0.010	2.706
E4−T	T8230027	49761.0988	*I*	1.054	10.0	174.226	273.813	12.322	0.002	9.783	5.160	0.000	2.620
E4−T	T8230028	49761.0993	*V*	1.055	10.0	174.159	272.423	12.048	0.002	7.113	5.300	0.090	3.600
E545	T8230029	49761.1134	*V*	1.006	10.0	175.879	272.830	12.065	0.002	4.042	5.290	0.050	2.953
E545	T8230030	49761.1140	*I*	1.005	10.0	174.988	272.829	12.360	0.003	6.834	5.390	0.000	2.312
E545	T8230031	49761.1145	*I*	1.005	10.0	175.814	273.235	12.355	0.003	5.817	5.340	0.110	2.589
E545	T8230032	49761.1151	*V*	1.005	10.0	176.652	271.920	12.062	0.002	3.627	5.310	0.000	2.361
E5−y	T8230033	49761.1185	*V*	1.004	60.0	175.184	273.854	12.345	0.003	36.177	6.070	0.070	2.663
E5−y	T8230034	49761.1197	*I*	1.003	60.0	175.019	275.284	12.748	0.004	53.662	6.430	0.080	2.774
E5−y	T8230035	49761.1208	*I*	1.003	60.0	175.257	276.667	12.752	0.004	53.466	6.390	0.020	2.515
E5−y	T8230036	49761.1220	*V*	1.003	60.0	176.218	276.233	12.341	0.003	32.778	5.860	0.090	2.540
DM−073477	T8260001	49761.1302	*V*	1.252	10.0	174.268	272.899	12.152	0.002	3.489	5.160	0.000	2.139
DM−073477	T8260002	49761.1308	*I*	1.251	10.0	173.185	272.250	12.853	0.004	7.895	5.250	0.100	2.182
DM−073477	T8260003	49761.1314	*I*	1.250	10.0	173.282	272.114	12.856	0.004	8.110	5.210	0.020	2.034
DM−073477	T8260004	49761.1319	*V*	1.250	10.0	174.105	272.169	12.152	0.002	2.918	5.240	0.000	2.120
E3−W	T8260005	49761.1348	*V*	1.721	25.0	175.752	269.883	12.146	0.002	13.580	5.470	0.000	2.466
E3−W	T8260006	49761.1355	*I*	1.728	25.0	174.685	270.728	12.432	0.003	34.360	5.950	0.050	2.811
E3−W	T8260007	49761.1362	*I*	1.735	25.0	174.288	270.349	12.435	0.003	33.738	6.000	0.060	3.051
E3−W	T8260008	49761.1370	*V*	1.742	25.0	175.658	268.105	12.144	0.002	10.753	5.530	0.100	2.583
E355	T8260009	49761.1401	*V*	1.761	10.0	175.233	271.258	12.229	0.002	1.565	5.160	0.000	2.860
E355	T8260010	49761.1407	*I*	1.767	10.0	174.809	272.902	12.592	0.003	11.311	5.560	0.030	2.823
E355	T8260011	49761.1412	*I*	1.773	10.0	174.049	272.028	12.577	0.003	10.636	5.570	0.150	3.242
E355	T8260012	49761.1418	*V*	1.778	10.0	175.286	270.838	12.233	0.002	0.597	5.110	0.000	2.663
DM−314800	T8260013	49761.1470	*V*	1.735	10.0	175.091	271.231	12.077	0.002	0.682	5.330	0.090	2.102
DM−314800	T8260014	49761.1476	*I*	1.741	10.0	173.184	273.052	12.791	0.004	12.089	5.860	0.090	2.583
DM−314800	T8260015	49761.1481	*I*	1.747	10.0	173.758	273.682	12.791	0.004	12.000	5.730	0.070	2.348
DM−314800	T8260016	49761.1487	*V*	1.753	10.0	174.792	272.007	12.082	0.002	−0.469	5.360	0.130	2.244
E4−T	T8260017	49761.1524	*V*	1.176	10.0	172.845	276.235	12.078	0.002	−1.267	4.960	0.000	1.855
E4−T	T8260018	49761.1530	*I*	1.178	10.0	172.061	277.285	12.330	0.003	5.688	5.190	0.010	1.991
E4−T	T8260019	49761.1536	*I*	1.180	10.0	171.228	273.175	12.334	0.003	6.089	5.320	0.010	2.028
E4−T	T8260020	49761.1541	*V*	1.182	10.0	171.943	271.785	12.073	0.002	−1.619	5.070	0.030	1.812
DM−308345	T8260021	49761.1603	*V*	1.153	10.0	171.836	273.159	12.599	0.003	−1.141	5.110	0.000	1.751

Table B.2 cont.: Standard star VI photometry – 1995-Feb-12.

Star	Frame	HJD −2400000.0	Filter	X	T	Row	Col	$m_{\rm raw}$	$\sigma_{m_{\rm raw}}$	sky	$\sigma_{\rm sky}$	sky skew	Seeing (FWHM)
DM−308345	T8260022	49761.1609	I	1.155	10.0	170.963	272.125	12.842	0.004	6.879	5.300	0.000	2.478
DM−308345	T8260023	49761.1614	I	1.156	10.0	170.013	272.269	12.841	0.004	7.280	5.160	0.000	2.268
DM−308345	T8260024	49761.1620	V	1.158	10.0	172.693	272.743	12.601	0.003	−1.000	5.040	0.000	2.034
E545	T8260025	49761.1639	V	1.008	10.0	174.945	270.736	12.067	0.002	−1.063	5.230	0.000	2.459
E545	T8260026	49761.1646	I	1.008	10.0	175.224	272.038	12.350	0.003	4.500	5.270	0.140	2.219
E545	T8260027	49761.1651	I	1.009	10.0	174.928	271.752	12.363	0.003	4.775	5.180	0.060	2.607
E545	T8260028	49761.1656	V	1.009	10.0	176.046	271.774	12.061	0.002	−2.352	5.060	0.110	2.583
E5−y	T8260029	49761.1691	V	1.011	60.0	174.164	274.251	12.339	0.003	6.585	5.480	0.170	2.700
E5−y	T8260030	49761.1703	I	1.011	60.0	173.283	274.968	12.737	0.004	48.303	6.170	0.160	2.589
E5−y	T8260031	49761.1714	I	1.012	60.0	173.840	275.152	12.740	0.004	49.003	6.320	0.120	2.620
E5−y	T8260032	49761.1725	V	1.013	60.0	174.980	274.275	12.347	0.003	7.189	5.420	0.060	2.626
DM−073477	T8260033	49761.1780	V	1.228	10.0	174.882	273.072	12.058	0.002	−1.320	5.150	0.000	2.083
DM−073477	T8260034	49761.1786	I	1.229	10.0	173.276	275.005	12.714	0.003	8.689	5.300	0.010	2.595
DM−073477	T8260035	49761.1791	I	1.229	10.0	173.234	275.321	12.697	0.003	7.720	5.290	0.080	2.176
DM−073477	T8260036	49761.1797	V	1.229	10.0	175.186	274.769	12.014	0.002	−2.485	4.990	0.170	1.948
E4−T	T6810001	49761.1830	V	1.291	10.0	173.288	271.282	12.095	0.002	−1.127	5.050	0.000	2.281
E4−T	T6810002	49761.1836	I	1.293	10.0	172.150	272.170	12.347	0.003	11.553	5.410	0.000	2.398
E4−T	T6810003	49761.1842	I	1.296	10.0	172.160	272.126	12.342	0.003	11.586	5.290	0.000	2.361
E4−T	T6810004	49761.1847	V	1.298	10.0	172.802	271.158	12.095	0.002	−1.184	5.010	0.000	2.213
E4−T	T6810005	49761.1883	V	1.315	10.0	171.029	270.160	12.098	0.002	0.077	5.170	0.000	2.546
E4−T	T6810006	49761.1889	I	1.317	10.0	169.856	271.107	12.341	0.003	14.934	5.440	0.000	2.817
E4−T	T6810007	49761.1894	I	1.320	10.0	170.045	270.876	12.344	0.003	15.189	5.290	0.050	2.589
E4−T	T6810008	49761.1900	V	1.323	10.0	170.283	269.944	12.097	0.002	0.374	5.100	0.000	2.626

Table B.3: Standard star VI photometry – 1995-Sep-02. These are from a $24''$ synthetic aperture.

Star	Frame	HJD −2400000.0	Filter	X	T	Row	Col	$m_{\rm raw}$	$\sigma_{m_{\rm raw}}$	sky	$\sigma_{\rm sky}$	sky skew	Seeing (FWHM)
E902	T8730009	49962.9701	V	1.004	10.0	110.819	448.235	12.347	0.002	4.511	4.560	0.190	3.322
E902	T8730010	49962.9708	I	1.004	10.0	109.677	449.305	12.829	0.003	7.443	4.740	0.020	3.359
E902	T8730011	49962.9713	I	1.004	10.0	108.777	448.352	12.830	0.004	7.006	4.830	0.000	3.396
E902	T8730012	49962.9718	V	1.004	10.0	110.199	445.986	12.356	0.002	4.904	4.610	0.000	3.594
FEIGE110	T8730013	49962.9872	V	1.402	25.0	110.657	448.218	12.351	0.002	14.541	4.890	0.070	3.852
FEIGE110	T8730014	49962.9880	I	1.399	25.0	109.718	449.087	13.083	0.004	21.330	4.870	0.040	3.113
FEIGE110	T8730015	49962.9887	I	1.397	25.0	109.708	448.867	13.087	0.004	21.406	5.010	0.000	3.310
FEIGE110	T8730016	49962.9894	V	1.394	25.0	108.088	446.879	12.348	0.002	14.170	4.940	0.050	3.267
DM−3515910	T8730017	49962.9977	V	1.085	10.0	109.101	448.743	12.427	0.003	2.860	4.590	0.000	3.193

Table B.3 cont.: Standard star VI photometry – 1995-Sep-02.

Star	Frame	HJD −2400000.0	Filter	X	T	Row	Col	$m_{\rm raw}$	$\sigma_{m_{\rm raw}}$	sky	$\sigma_{\rm sky}$	sky skew	Seeing (FWHM)
DM−3515910	T8730018	49962.9983	I	1.084	10.0	108.283	450.154	13.168	0.004	4.873	4.450	0.000	3.470
DM−3515910	T8730019	49962.9989	I	1.083	10.0	107.865	448.286	13.165	0.004	4.605	4.560	0.000	2.990
DM−3515910	T8730020	49962.9994	V	1.082	10.0	108.643	447.158	12.423	0.002	1.803	4.520	0.070	3.236
THPEb	T8730021	49963.0216	V	1.070	60.0	108.234	451.051	11.960	0.002	20.775	4.970	0.000	3.131
THPEb	T8730022	49963.0228	I	1.068	60.0	107.178	451.277	11.927	0.002	38.873	5.250	0.000	3.064
THPEb	T8730023	49963.0239	I	1.066	60.0	106.022	450.687	11.921	0.002	38.909	5.280	0.000	2.897
THPEb	T8730024	49963.0251	V	1.064	60.0	106.101	448.777	11.957	0.002	20.480	4.960	0.010	3.045
THPEE	T8730025	49963.0526	V	1.027	25.0	110.920	451.241	13.669	0.007	4.999	4.670	0.020	3.957
THPEE	T8730026	49963.0534	I	1.026	25.0	110.621	451.217	12.431	0.003	15.610	4.820	0.000	3.809
THPEE	T8730027	49963.0541	I	1.025	25.0	109.183	451.144	12.429	0.003	15.668	4.840	0.020	3.464
THPEE	T8730028	49963.0548	V	1.025	25.0	109.787	449.684	13.675	0.007	4.812	4.540	0.000	3.575
THPEC	T8730029	49963.0612	V	1.018	400.0	110.862	451.023	11.812	0.002	109.783	7.240	0.100	4.161
THPEC	T8730030	49963.0663	I	1.014	400.0	107.227	447.242	12.623	0.005	313.038	9.990	0.050	4.229
THPEC	T8730031	49963.0714	I	1.011	400.0	104.943	442.768	12.600	0.006	329.648	10.540	0.110	4.185
THPEC	T8730032	49963.0765	V	1.008	400.0	103.075	438.300	11.814	0.002	82.632	6.360	0.010	3.828
E902	T8740001	49963.1450	V	1.510	10.0	111.997	450.037	12.366	0.002	−4.158	4.640	0.070	2.928
E902	T8740002	49963.1456	I	1.515	10.0	112.113	447.293	12.829	0.003	−0.197	4.690	0.160	3.335
E902	T8740003	49963.1462	I	1.518	10.0	112.862	451.215	12.835	0.003	0.455	4.710	0.010	2.940
E902	T8740004	49963.1467	V	1.522	10.0	113.815	446.674	12.369	0.002	−4.386	4.780	0.000	2.872
DM−3515910	T8740005	49963.1574	V	1.106	10.0	110.194	450.994	12.435	0.003	−4.057	4.620	0.000	2.872
DM−3515910	T8740006	49963.1580	I	1.108	10.0	109.849	450.695	13.170	0.004	0.754	4.650	0.000	3.298
DM−3515910	T8740007	49963.1586	I	1.109	10.0	109.851	449.084	13.173	0.005	1.002	4.670	0.000	2.928
DM−3515910	T8740008	49963.1591	V	1.110	10.0	110.909	448.345	12.432	0.002	−4.331	4.480	0.000	3.064
DM−38222	T8740009	49963.1670	V	1.039	10.0	111.164	451.019	11.926	0.002	−4.409	4.460	0.130	3.544
DM−38222	T8740010	49963.1676	I	1.040	10.0	111.055	449.868	12.575	0.003	1.275	4.600	0.000	3.643
DM−38222	T8740011	49963.1681	I	1.041	10.0	110.935	450.060	12.571	0.003	1.362	4.650	0.000	3.292
DM−38222	T8740012	49963.1687	V	1.042	10.0	110.956	448.908	11.927	0.002	−4.172	4.340	0.040	3.366
DM−38222	T8740017	49963.2170	V	1.140	10.0	113.048	451.020	11.942	0.002	−3.955	4.510	0.130	2.848
DM−38222	T8740018	49963.2176	I	1.142	10.0	113.181	451.242	12.569	0.003	2.771	4.470	0.120	2.096
DM−38222	T8740019	49963.2182	I	1.143	10.0	113.199	449.791	12.575	0.003	3.436	4.580	0.000	2.133
DM−38222	T8740020	49963.2187	V	1.145	10.0	114.279	447.859	11.944	0.002	−4.436	4.470	0.140	2.885
E1−S	T8740021	49963.2266	V	1.080	10.0	106.984	447.047	12.387	0.002	−3.386	4.430	0.000	2.607
E1−S	T8740022	49963.2272	I	1.082	10.0	106.942	446.169	12.146	0.002	3.601	4.790	0.000	2.114
E1−S	T8740023	49963.2277	I	1.083	10.0	107.273	445.019	12.141	0.002	2.646	4.700	0.120	1.966
E1−S	T8740024	49963.2283	V	1.084	10.0	108.091	444.776	12.383	0.002	−4.378	4.450	0.120	2.509
E1−v	T8740025	49963.2360	V	1.099	25.0	110.965	451.852	12.142	0.002	−1.415	4.390	0.000	2.312
E1−v	T8740026	49963.2368	I	1.100	25.0	111.016	450.199	11.917	0.002	13.948	4.740	0.120	2.090
E1−v	T8740027	49963.2375	I	1.102	25.0	111.815	449.972	11.917	0.002	14.917	4.870	0.080	2.139
E1−v	T8740028	49963.2383	V	1.104	25.0	112.129	448.724	12.143	0.002	−1.204	4.620	0.000	2.373

Table B.4: Standard star VI photometry – 1995-Sep-03. These are from a $24''$ synthetic aperture.

Star	Frame	HJD −2400000.0	Filter	X	T	Row	Col	$m_{\rm raw}$	$\sigma_{m_{\rm raw}}$	sky	$\sigma_{\rm sky}$	sky skew	Seeing (FWHM)
E902	T8750004	49963.8513	V	1.104	10.0	108.661	451.095	12.414	0.003	9.976	4.860	0.000	2.268
E902	T8750005	49963.8519	I	1.102	10.0	108.056	452.255	12.837	0.004	10.705	4.890	0.160	2.916
E902	T8750006	49963.8525	I	1.101	10.0	106.944	452.986	12.843	0.004	10.852	5.050	0.130	3.119
E902	T8750007	49963.8530	V	1.100	10.0	106.953	451.779	12.404	0.003	8.700	4.890	0.130	2.786
DM−3515910	T8750008	49963.8651	V	1.790	10.0	109.772	452.984	12.533	0.003	11.026	4.890	0.030	3.131
DM−3515910	T8750009	49963.8657	I	1.783	10.0	109.260	455.753	13.185	0.005	11.879	4.710	0.110	2.330
DM−3515910	T8750010	49963.8662	I	1.777	10.0	109.668	455.980	13.186	0.005	11.913	4.690	0.070	2.238
DM−3515910	T8750011	49963.8668	V	1.771	10.0	108.634	454.777	12.533	0.003	10.036	4.670	0.010	2.700
FEIGE110	T8750012	49963.8729	V	2.737	25.0	110.897	453.202	12.668	0.003	38.070	5.320	0.000	2.527
FEIGE110	T8750013	49963.8736	I	2.713	25.0	112.165	454.695	13.243	0.005	46.632	5.400	0.010	2.330
FEIGE110	T8750014	49963.8743	I	2.692	25.0	112.020	457.007	13.222	0.005	46.072	5.440	0.030	2.552
FEIGE110	T8750015	49963.8751	V	2.671	25.0	111.267	456.168	12.590	0.003	37.265	5.220	0.100	2.761
DM−3515910	T8750020	49963.9098	V	1.408	10.0	109.862	452.735	12.471	0.003	6.915	4.660	0.080	2.096
DM−3515910	T8750021	49963.9104	I	1.404	10.0	109.220	452.877	13.182	0.005	7.620	4.600	0.000	1.991
DM−3515910	T8750022	49963.9109	I	1.401	10.0	108.848	454.248	13.176	0.005	7.708	4.640	0.000	1.929
DM−3515910	T8750023	49963.9115	V	1.398	10.0	108.844	452.694	12.480	0.003	6.595	4.610	0.020	1.972
FEIGE110	T8750024	49963.9166	V	1.887	25.0	109.254	453.069	12.433	0.003	29.219	5.130	0.050	2.133
FEIGE110	T8750025	49963.9174	I	1.877	25.0	109.103	455.126	13.110	0.005	31.963	5.020	0.000	2.059
FEIGE110	T8750026	49963.9181	I	1.869	25.0	108.947	455.849	13.101	0.005	31.176	5.310	0.120	2.065
FEIGE110	T8750027	49963.9188	V	1.860	25.0	108.049	454.080	12.419	0.003	28.115	5.220	0.070	2.250
DM−38222	T8750028	49963.9236	V	1.541	10.0	109.878	452.801	12.004	0.002	6.982	4.540	0.030	1.935
DM−38222	T8750029	49963.9242	I	1.536	10.0	109.226	453.254	12.600	0.003	7.814	4.650	0.000	2.046
DM−38222	T8750030	49963.9247	I	1.532	10.0	108.296	454.192	12.594	0.003	7.211	4.670	0.100	2.040
DM−38222	T8750031	49963.9253	V	1.528	10.0	108.182	453.205	12.004	0.002	6.007	4.590	0.120	2.164
E1−S	T8750032	49963.9297	V	1.607	10.0	107.978	452.936	12.472	0.003	7.053	4.580	0.000	1.972
E1−S	T8750033	49963.9303	I	1.602	10.0	107.962	453.834	12.179	0.002	8.810	4.550	0.000	2.059
E1−S	T8750034	49963.9308	I	1.598	10.0	107.751	453.686	12.182	0.002	8.602	4.670	0.000	1.892
E1−S	T8750035	49963.9314	V	1.594	10.0	107.029	453.770	12.472	0.003	6.156	4.630	0.040	1.997
E1−v	T8760001	49963.9392	V	1.536	25.0	109.043	451.773	12.207	0.002	19.371	5.100	0.000	2.003
E1−v	T8760002	49963.9400	I	1.530	25.0	108.873	452.846	11.947	0.002	24.273	5.090	0.030	1.966
E1−v	T8760003	49963.9407	I	1.525	25.0	108.046	452.948	11.947	0.002	24.143	5.010	0.000	1.929
E1−v	T8760004	49963.9414	V	1.520	25.0	107.919	452.038	12.207	0.002	18.116	4.900	0.120	2.096
DM−38222	T8760009	49963.9663	V	1.283	10.0	109.707	452.297	11.971	0.002	4.978	4.660	0.030	2.201
DM−38222	T8760010	49963.9669	I	1.281	10.0	109.262	453.257	12.588	0.003	6.790	4.660	0.000	1.800
DM−38222	T8760011	49963.9674	I	1.278	10.0	108.898	453.042	12.587	0.003	6.293	4.580	0.050	1.868
DM−38222	T8760012	49963.9680	V	1.276	10.0	109.261	452.815	11.965	0.002	3.902	4.560	0.110	1.917
E1−S	T8760013	49963.9710	V	1.343	10.0	108.772	453.750	12.427	0.003	4.564	4.640	0.000	1.935
E1−S	T8760014	49963.9716	I	1.340	10.0	108.171	453.324	12.154	0.002	5.972	4.550	0.100	1.781

Table B.4 cont.: Standard star VI photometry – 1995-Sep-03.

Star	Frame	HJD −2400000.0	Filter	X	T	Row	Col	$m_{\rm raw}$	$\sigma_{m_{\rm raw}}$	sky	$\sigma_{\rm sky}$	sky skew	Seeing (FWHM)
E1−S	T8760015	49963.9721	I	1.337	10.0	107.696	453.246	12.164	0.002	5.797	4.490	0.090	2.016
E1−S	T8760016	49963.9727	V	1.335	10.0	107.842	453.275	12.424	0.002	3.738	4.540	0.110	2.065
E1−v	T8770002	49963.9980	V	1.227	25.0	109.911	452.273	12.166	0.002	17.727	4.850	0.000	2.127
E1−v	T8770003	49963.9988	I	1.224	25.0	109.096	453.697	11.923	0.002	24.316	4.980	0.040	2.120
E1−v	T8770004	49963.9995	I	1.221	25.0	108.313	452.704	11.928	0.002	24.442	4.940	0.000	2.065
E1−v	T8770005	49964.0002	V	1.219	25.0	108.034	452.097	12.167	0.002	16.998	4.750	0.000	2.219
DM−441028	T8770006	49964.0362	V	1.399	10.0	113.667	456.789	12.346	0.002	6.890	4.570	0.000	2.046
DM−441028	T8770007	49964.0368	I	1.396	10.0	114.063	456.200	12.492	0.003	10.025	4.620	0.000	2.040
DM−441028	T8770008	49964.0373	I	1.393	10.0	114.910	458.023	12.486	0.003	9.262	4.510	0.040	1.917
DM−441028	T8770009	49964.0379	V	1.390	10.0	115.674	459.310	12.342	0.002	6.031	4.390	0.070	2.379
DM−261339	T8770010	49964.0459	V	1.723	25.0	109.805	456.859	11.888	0.002	28.026	4.930	0.030	2.558
DM−261339	T8770011	49964.0467	I	1.715	25.0	108.047	456.139	12.629	0.003	32.452	5.040	0.010	2.324
DM−261339	T8770012	49964.0474	I	1.707	25.0	108.019	458.017	12.625	0.003	31.212	5.070	0.080	3.057
DM−261339	T8770013	49964.0482	V	1.699	25.0	110.258	459.841	11.878	0.002	26.798	4.980	0.050	3.255
DM−441028	T8770018	49964.0929	V	1.161	10.0	110.695	453.854	12.309	0.002	3.976	4.460	0.020	1.935
DM−441028	T8770019	49964.0935	I	1.159	10.0	109.702	455.221	12.478	0.003	8.858	4.600	0.000	2.096
DM−441028	T8770020	49964.0940	I	1.157	10.0	109.886	455.832	12.470	0.003	8.189	4.510	0.040	1.831
DM−441028	T8770021	49964.0946	V	1.156	10.0	111.287	453.974	12.302	0.002	2.639	4.450	0.170	1.899
DM−231339	T8770022	49964.0992	V	1.321	25.0	111.651	453.775	11.818	0.002	15.203	4.850	0.040	2.521
DM−231339	T8770023	49964.1000	I	1.317	25.0	110.650	458.671	12.593	0.003	26.997	4.990	0.050	3.033
DM−231339	T8770024	49964.1007	I	1.313	25.0	110.184	457.800	12.598	0.003	27.124	4.850	0.050	2.595
DM−231339	T8770025	49964.1014	V	1.310	25.0	111.077	459.052	11.813	0.002	14.241	4.830	0.050	2.225
E2−b	T8770026	49964.1083	V	1.217	25.0	110.298	455.292	12.091	0.002	7.913	4.680	0.110	2.133
E2−b	T8770027	49964.1091	I	1.214	25.0	109.984	455.894	11.918	0.002	24.298	4.820	0.060	2.416
E2−b	T8770028	49964.1098	I	1.212	25.0	110.840	455.931	11.917	0.002	23.429	5.050	0.050	2.392
E2−b	T8770029	49964.1105	V	1.209	25.0	112.101	457.293	12.089	0.002	6.698	4.640	0.140	2.287
E2−L	T8770030	49964.1254	V	1.160	60.0	111.041	455.067	12.557	0.003	10.047	4.650	0.000	2.546
E2−L	T8770031	49964.1266	I	1.157	60.0	111.158	454.887	12.264	0.002	52.151	5.530	0.000	2.583
E2−L	T8770032	49964.1277	I	1.153	60.0	111.815	456.123	12.261	0.002	52.467	5.410	0.030	2.139
E2−L	T8770033	49964.1289	V	1.150	60.0	113.032	456.993	12.542	0.003	9.364	4.620	0.000	2.238

Table B.5: Standard star VI photometry – 1995-Oct-23. These are from a $24''$ synthetic aperture.

Star	Frame	HJD −2400000.0	Filter	X	T	Row	Col	$m_{\rm raw}$	$\sigma_{m_{\rm raw}}$	sky	$\sigma_{\rm sky}$	sky skew	Seeing (FWHM)
E902	T8960003	50013.8977	V	1.087	10.0	108.814	452.293	12.408	0.003	−0.361	4.720	0.110	1
E902	T8960004	50013.8983	I	1.088	10.0	108.102	453.088	12.873	0.004	4.854	5.090	0.050	2

Table B.5 cont.: Standard star VI photometry – 1995-Oct-23.

Star	Frame	HJD −2400000.0	Filter	X	T	Row	Col	$m_{\rm raw}$	$\sigma_{m_{\rm raw}}$	sky	$\sigma_{\rm sky}$	sky skew	Seeing (FWHM)
E902	T8960005	50013.8989	I	1.089	10.0	108.083	452.355	12.875	0.004	4.853	5.050	0.060	3
E902	T8960006	50013.8995	V	1.090	10.0	107.294	452.158	12.430	0.003	−0.067	4.910	0.000	4
FEIGE110	T8960007	50013.9143	V	1.282	25.0	109.836	453.403	12.404	0.003	2.950	4.790	0.000	5
FEIGE110	T8960008	50013.9152	I	1.282	25.0	109.277	453.375	13.121	0.005	21.022	5.290	0.050	6
FEIGE110	T8960009	50013.9159	I	1.282	25.0	108.307	453.343	13.129	0.005	20.824	5.320	0.000	7
FEIGE110	T8960010	50013.9167	V	1.282	25.0	108.256	453.883	12.403	0.003	1.960	4.810	0.000	8
DM−3515910	T8960011	50013.9224	V	1.015	10.0	109.039	451.647	12.470	0.003	−2.379	4.580	0.020	9
DM−3515910	T8960012	50013.9230	I	1.015	10.0	107.194	452.845	13.206	0.005	2.574	4.890	0.010	10
DM−3515910	T8960013	50013.9236	I	1.015	10.0	107.556	452.755	13.201	0.005	2.276	4.780	0.090	11
DM−3515910	T8960014	50013.9242	V	1.015	10.0	104.878	451.953	12.486	0.003	−2.555	4.700	0.010	12
THPEb	T8960015	50013.9337	V	1.009	60.0	111.748	450.307	11.922	0.002	3.890	4.880	0.000	13
THPEb	T8960016	50013.9349	I	1.009	60.0	111.298	449.299	11.830	0.002	37.229	5.450	0.000	14
THPEb	T8960017	50013.9361	I	1.008	60.0	111.805	448.204	11.829	0.002	38.298	5.590	0.000	15
THPEb	T8960018	50013.9376	V	1.007	60.0	113.004	446.738	11.923	0.002	3.676	4.730	0.000	16
THPEC	T8960020	50013.9598	V	1.001	400.0	108.729	451.901	11.865	0.002	88.756	6.950	0.120	17
THPEC	T8960021	50013.9650	I	1.001	400.0	107.185	453.438	12.638	0.005	242.771	9.600	0.160	18
THPEC	T8960022	50013.9701	I	1.002	400.0	106.334	453.876	12.656	0.005	236.321	9.380	0.080	19
THPEC	T8960023	50013.9752	V	1.003	400.0	107.150	452.088	11.863	0.002	59.674	6.340	0.130	20
TPHEE	T8960024	50013.9814	V	1.004	25.0	113.064	452.204	13.712	0.007	4.025	4.670	0.000	21
TPHEE	T8960025	50013.9822	I	1.005	25.0	111.301	452.238	12.460	0.003	14.972	4.960	0.050	22
TPHEE	T8960026	50013.9830	I	1.005	25.0	110.833	452.866	12.460	0.003	14.465	5.010	0.040	23
TPHEE	T8960027	50013.9837	V	1.005	25.0	111.770	451.990	13.718	0.007	3.804	4.640	0.000	24
DM−3515910	T8980002	50014.0229	V	1.122	10.0	112.953	451.818	12.480	0.003	0.976	4.570	0.000	25
DM−3515910	T8980003	50014.0235	I	1.124	10.0	112.812	449.821	13.203	0.005	5.012	4.680	0.000	26
TPHEE	T8980007	50014.0876	V	1.170	25.0	111.743	451.059	13.694	0.007	4.180	4.660	0.100	27
TPHEE	T8980008	50014.0884	I	1.173	25.0	111.844	451.110	12.465	0.003	14.421	4.840	0.070	28
TPHEE	T8980009	50014.0891	I	1.175	25.0	111.250	450.835	12.466	0.003	13.973	4.700	0.110	29
TPHEE	T8980010	50014.0899	V	1.177	25.0	112.831	450.627	13.690	0.007	3.638	4.650	0.150	30
DM−441028	T8980011	50014.1059	V	1.009	10.0	110.239	452.858	12.311	0.002	−0.300	4.480	0.130	31
DM−441028	T8980012	50014.1065	I	1.010	10.0	109.711	452.788	12.501	0.003	3.513	4.570	0.000	32
DM−441028	T8980013	50014.1071	I	1.010	10.0	110.120	452.011	12.486	0.003	2.479	4.520	0.180	33
DM−441028	T8980014	50014.1077	V	1.010	10.0	110.677	450.143	12.321	0.002	−0.323	4.560	0.000	34
DM−261339	T8980015	50014.1141	V	1.060	25.0	109.146	453.746	11.810	0.002	5.897	4.790	0.150	35
DM−261339	T8980016	50014.1149	I	1.060	25.0	108.316	452.350	12.612	0.003	12.767	4.860	0.140	36
DM−261339	T8980017	50014.1157	I	1.061	25.0	108.186	451.758	12.621	0.003	13.013	4.820	0.000	37
DM−261339	T8980018	50014.1164	V	1.061	25.0	108.235	452.070	11.810	0.002	5.739	4.790	0.140	38
DM−441028	T8980023	50014.1519	V	1.061	10.0	110.136	449.922	12.327	0.002	−0.102	4.440	0.000	39
DM−441028	T8980024	50014.1525	I	1.063	10.0	110.244	450.779	12.501	0.003	3.832	4.620	0.070	40
DM−441028	T8980025	50014.1531	I	1.063	10.0	111.206	450.071	12.508	0.003	3.795	4.460	0.000	41

Table B.5 cont.: Standard star VI photometry – 1995-Oct-23.

Star	Frame	HJD −2400000.0	Filter	X	T	Row	Col	$m_{\rm raw}$	$\sigma_{m_{\rm raw}}$	sky	$\sigma_{\rm sky}$	sky skew	Seeing (FWHM)
DM−441028	T8980026	50014.1537	V	1.064	10.0	112.791	448.671	12.325	0.002	−1.379	4.440	0.140	42
DM−261339	T8980027	50014.1591	V	1.121	25.0	111.202	452.335	11.828	0.002	5.736	4.750	0.110	43
DM−261339	T8980028	50014.1600	I	1.123	25.0	110.237	451.873	12.627	0.003	13.338	4.890	0.040	44
DM−261339	T8980029	50014.1607	I	1.125	25.0	111.288	451.148	12.628	0.003	13.449	4.990	0.000	45
DM−261339	T8980030	50014.1615	V	1.126	25.0	111.334	451.997	11.826	0.002	6.145	4.690	0.050	46
E2−L	T8980031	50014.1703	V	1.038	60.0	112.873	450.302	12.565	0.003	8.041	4.780	0.000	47
E2−L	T8980032	50014.1715	I	1.040	60.0	112.342	450.237	12.291	0.002	33.287	5.300	0.050	48
E2−L	T8980033	50014.1727	I	1.041	60.0	113.878	448.945	12.297	0.002	32.271	5.240	0.020	49
E2−L	T8980034	50014.1738	V	1.043	60.0	115.985	447.280	12.563	0.003	8.853	4.810	0.080	50
E2−b	T8990001	50014.1805	V	1.052	25.0	111.948	453.920	12.104	0.002	5.800	4.650	0.000	51
E2−b	T8990002	50014.1813	I	1.053	25.0	111.756	453.953	11.945	0.002	19.998	5.150	0.060	52
E2−b	T8990003	50014.1820	I	1.054	25.0	111.853	453.232	11.945	0.002	22.003	5.160	0.060	53
E2−b	T8990004	50014.1828	V	1.056	25.0	112.891	451.621	12.108	0.002	8.691	4.850	0.000	54

B.2.2 Raw *uvby* calibration photometry

Table B.6: Standard star *uvby* photometry – 1995-Sep-18. These are from a 24″ synthetic aperture.

Star	Frame	HJD −2400000.0	Filter	X	T	Row	Col	m_{raw}	$\sigma_{m_{\mathrm{raw}}}$	sky	σ_{sky}	sky skew	Seeing (FWHM)
E704	T6950020	49978.8233	y	1.033	5.0	108.113	452.928	12.044	0.002	−1.372	4.660	0.150	1.670
E704	T6950021	49978.8238	b	1.034	10.0	107.816	450.095	12.156	0.002	−1.337	4.680	0.110	1.985
E704	T6950022	49978.8245	v	1.035	20.0	106.159	448.738	11.963	0.002	−2.224	4.680	0.140	1.794
E704	T6950023	49978.8254	u	1.036	45.0	107.964	448.854	11.742	0.002	−1.245	4.640	0.000	2.194
E704	T6950024	49978.8270	y	1.038	5.0	110.845	449.925	12.046	0.002	−1.235	4.700	0.000	1.689
E704	T6950025	49978.8276	b	1.039	10.0	110.198	447.012	12.156	0.002	−2.424	4.500	0.140	1.997
E704	T6950026	49978.8283	v	1.040	20.0	108.757	445.205	11.963	0.002	−2.333	4.690	0.110	2.059
E704	T6950027	49978.8291	u	1.041	45.0	110.810	446.208	11.742	0.002	−2.097	4.570	0.040	2.379
E710	T6950028	49978.8394	u	1.056	60.0	109.063	447.104	11.720	0.002	−2.065	4.650	0.000	2.657
E710	T6950029	49978.8351	b	1.049	20.0	108.681	451.742	12.033	0.002	−1.797	4.770	0.040	1.831
E710	T6950030	49978.8360	v	1.050	45.0	106.884	447.156	11.695	0.002	−2.037	4.670	0.010	2.157
E710	T6950031	49978.8408	y	1.058	10.0	111.146	448.861	12.012	0.002	−1.370	4.510	0.000	2.201
E710	T6950032	49978.8435	u	1.063	60.0	109.845	445.693	11.717	0.002	−2.100	4.670	0.000	2.385
E710	T6950033	49978.8445	v	1.064	45.0	108.223	444.896	11.708	0.002	−2.378	4.630	0.000	2.009
E710	T6950034	49978.8454	b	1.066	20.0	110.729	446.069	12.044	0.002	−2.421	4.660	0.020	1.818
E710	T6950035	49978.8460	y	1.067	10.0	112.124	448.779	11.909	0.002	−2.024	4.720	0.000	1.800
E710	T6950036	49978.8465	y	1.068	10.0	112.240	448.299	11.905	0.002	−2.371	4.740	0.000	2.022
E710	T6950037	49978.8472	b	1.069	20.0	110.837	446.249	12.041	0.002	−3.079	4.590	0.100	1.726
E713	T8850002	49978.8657	u	1.112	90.0	111.020	450.949	12.347	0.002	0.809	4.550	0.000	3.329
E713	T8850003	49978.8669	v	1.114	45.0	109.770	448.271	12.351	0.002	0.122	4.730	0.080	2.897
E713	T8850004	49978.8677	b	1.116	20.0	112.276	449.692	12.637	0.003	0.656	4.660	0.000	2.589
E713	T8850005	49978.8683	y	1.118	10.0	113.864	451.757	12.488	0.003	0.987	4.520	0.000	3.033
E713	T8850006	49978.8688	y	1.119	10.0	114.152	451.845	12.489	0.003	0.955	4.730	0.020	2.922
E713	T8850007	49978.8695	b	1.121	20.0	112.872	448.281	12.632	0.003	0.220	4.660	0.030	2.983
E713	T8850008	49978.8704	v	1.123	45.0	111.759	446.786	12.365	0.002	0.350	4.420	0.000	2.737
E713	T8850009	49978.8717	u	1.126	90.0	113.152	447.680	12.367	0.002	0.608	4.650	0.010	3.144
E751	T8850010	49978.8758	u	1.162	45.0	107.743	452.165	12.378	0.002	0.137	4.480	0.060	2.977
E751	T8850011	49978.8766	v	1.164	20.0	106.043	450.730	12.318	0.002	−0.053	4.410	0.080	2.903
E751	T8850012	49978.8772	b	1.166	10.0	108.876	452.089	12.381	0.002	0.218	4.700	0.000	2.879
E751	T8850013	49978.8777	y	1.167	5.0	110.039	452.744	12.215	0.002	0.331	4.600	0.030	2.737
E751	T8850014	49978.8782	y	1.169	5.0	110.110	452.152	12.217	0.002	0.685	4.650	0.000	2.953
E751	T8850015	49978.8788	b	1.171	10.0	109.227	450.899	12.377	0.002	−0.333	4.710	0.110	2.755
E751	T8850016	49978.8794	v	1.173	20.0	107.227	448.084	12.334	0.002	−0.217	4.540	0.000	2.761
E751	T8850017	49978.8803	u	1.176	45.0	109.138	450.684	12.390	0.002	−0.304	4.540	0.100	3.162
E103	T8850022	49978.9617	u	1.197	90.0	106.230	449.222	12.985	0.004	−0.455	4.500	0.000	3.107
E103	T8850023	49978.9629	v	1.194	45.0	104.664	448.095	12.758	0.003	−1.033	4.470	0.060	2.946

Table B.6 cont.: Standard star $uvby$ photometry – 1995-Sep-18.

Star	Frame	HJD −2400000.0	Filter	X	T	Row	Col	$m_{\rm raw}$	$\sigma_{m_{\rm raw}}$	sky	$\sigma_{\rm sky}$	sky skew	Seeing (FWHM)
E103	T8850024	49978.9637	b	1.191	20.0	106.293	451.254	12.951	0.004	−1.085	4.600	0.030	2.651
E103	T8850025	49978.9643	y	1.189	10.0	107.845	455.768	12.803	0.003	−1.187	4.530	0.090	2.601
E103	T8850026	49978.9684	u	1.175	180.0	103.150	449.917	12.202	0.002	−0.440	4.560	0.140	2.983
E103	T8850027	49978.9704	v	1.170	90.0	103.204	448.765	11.992	0.002	−0.349	4.560	0.000	2.663
E103	T8850028	49978.9716	b	1.166	40.0	104.815	451.172	12.186	0.002	−0.308	4.500	0.000	2.466
E103	T8850029	49978.9724	y	1.164	20.0	105.241	454.032	12.036	0.002	−0.418	4.540	0.140	2.860
E103	T8850030	49978.9730	y	1.162	20.0	104.997	455.205	12.038	0.002	−0.089	4.530	0.000	2.601
E103	T8850031	49978.9739	b	1.160	40.0	102.884	451.723	12.183	0.002	−0.893	4.560	0.050	2.632
E103	T8850032	49978.9751	v	1.156	90.0	99.980	449.718	11.975	0.002	−1.414	4.630	0.140	2.768
E103	T8850033	49978.9772	u	1.149	180.0	100.090	449.873	12.188	0.002	−0.396	4.600	0.000	3.187
E803	T8860001	49978.9941	u	1.160	90.0	112.815	446.928	11.878	0.002	−3.407	4.560	0.150	2.940
E803	T8860002	49978.9953	v	1.164	45.0	111.949	443.742	11.762	0.002	−3.357	4.580	0.120	2.595
E803	T8860003	49978.9961	b	1.166	20.0	114.789	444.928	12.007	0.002	−3.227	4.720	0.070	2.577
E803	T8860004	49978.9967	y	1.167	10.0	116.683	446.312	11.901	0.002	−2.916	4.630	0.020	2.108
E803	T8860005	49978.9972	y	1.169	10.0	116.831	445.289	11.898	0.002	−3.360	4.680	0.120	2.601
E803	T8860006	49978.9979	b	1.171	20.0	116.158	441.907	12.015	0.002	−3.280	4.730	0.000	2.336
E803	T8860007	49978.9988	v	1.174	45.0	114.113	441.187	11.773	0.002	−3.466	4.530	0.000	3.070
E803	T8860008	49979.0000	u	1.178	90.0	116.780	441.936	11.906	0.002	−3.180	4.590	0.000	3.279
DM−11162	T8860009	49979.0183	u	1.265	360.0	101.871	453.098	11.418	0.001	−0.533	4.450	0.000	3.735
DM−11162	T8860010	49979.0219	v	1.257	180.0	97.676	453.792	12.609	0.003	−1.496	4.540	0.000	3.150
DM−11162	T8860011	49979.0238	b	1.253	80.0	97.911	457.741	12.987	0.004	−2.575	4.470	0.050	2.866
DM−11162	T8860012	49979.0250	y	1.250	40.0	98.269	461.731	12.850	0.003	−1.525	4.610	0.000	2.681
DM−11162	T8860013	49979.0347	u	1.231	180.0	103.186	450.925	12.147	0.002	−3.308	4.450	0.110	3.631
DM−11162	T8860014	49979.0373	v	1.226	180.0	101.781	449.033	12.583	0.003	−3.782	4.580	0.260	3.224
DM−11162	T8860015	49979.0397	b	1.223	150.0	109.042	448.799	12.301	0.002	−1.350	4.650	0.000	3.347
DM−11162	T8860016	49979.0415	y	1.220	80.0	109.963	451.748	12.097	0.002	0.903	4.500	0.000	3.125
DM−261339	T8860017	49979.0521	u	1.356	180.0	107.017	447.870	11.925	0.002	−2.237	4.540	0.000	3.785
DM−261339	T8860018	49979.0547	v	1.342	180.0	106.322	446.994	12.481	0.003	−2.011	4.600	0.000	3.532
DM−261339	T8860019	49979.0570	b	1.330	150.0	109.209	448.258	12.310	0.002	−0.146	4.600	0.050	3.248
DM−261339	T8860020	49979.0588	y	1.322	80.0	110.288	452.878	12.274	0.002	0.801	4.620	0.000	3.427
DM−261339	T8860021	49979.0602	y	1.315	80.0	112.833	453.162	12.273	0.002	0.764	4.660	0.000	3.396
DM−261339	T8860022	49979.0621	b	1.305	150.0	109.863	450.329	12.299	0.002	−0.038	4.570	0.010	3.329
DM−261339	T8860023	49979.0645	v	1.293	180.0	106.259	446.236	12.459	0.003	−2.266	4.590	0.000	3.267
DM−261339	T8860024	49979.0671	u	1.281	180.0	108.039	447.960	11.862	0.002	−2.862	4.520	0.040	3.809
E103	T8860029	49979.1385	u	1.021	180.0	107.055	449.715	12.058	0.002	−3.451	4.460	0.000	4.241
E103	T8860030	49979.1405	v	1.022	90.0	104.859	446.240	11.896	0.002	−4.019	4.450	0.000	3.403
E103	T8860031	49979.1418	b	1.024	40.0	106.717	447.083	12.120	0.002	−4.089	4.500	0.000	3.230
E103	T8860032	49979.1426	y	1.024	20.0	107.148	449.823	11.987	0.002	−4.138	4.360	0.040	3.668
E103	T8860033	49979.1433	y	1.025	20.0	107.283	449.307	11.991	0.002	−4.143	4.550	0.070	3.433

Table B.6 cont.: Standard star *uvby* photometry – 1995-Sep-18.

Star	Frame	HJD −2400000.0	Filter	X	T	Row	Col	$m_{\rm raw}$	$\sigma_{m_{\rm raw}}$	sky	$\sigma_{\rm sky}$	sky skew	Seeing (FWHM)
E103	T8860034	49979.1441	*b*	1.026	40.0	105.743	445.143	12.120	0.002	−4.216	4.520	0.000	3.415
E103	T8860035	49979.1454	*v*	1.027	90.0	103.756	442.965	11.903	0.002	−4.150	4.460	0.000	3.631
E103	T8860036	49979.1475	*u*	1.030	180.0	105.187	445.293	12.064	0.002	−3.987	4.440	0.000	4.284
E302	T8880001	49979.1503	*u*	1.302	45.0	108.262	449.153	11.757	0.002	−5.134	4.470	0.000	4.518
E302	T8880002	49979.1511	*v*	1.298	20.0	106.252	448.318	12.093	0.002	−5.359	4.600	0.000	4.395
E302	T8880003	49979.1517	*b*	1.295	10.0	107.188	450.092	12.279	0.002	−5.656	4.520	0.040	5.178
E302	T8880004	49979.1523	*y*	1.293	5.0	109.002	455.180	12.205	0.002	−5.027	4.520	0.000	4.512
E302	T8880005	49979.1567	*u*	1.274	45.0	103.007	449.240	11.740	0.002	−5.140	4.430	0.000	4.851
E302	T8880006	49979.1576	*v*	1.270	20.0	103.946	449.082	12.078	0.002	−5.836	4.520	0.070	3.883
E302	T8880007	49979.1582	*b*	1.268	10.0	105.244	450.795	12.272	0.002	−6.301	4.450	0.130	3.587
E302	T8880008	49979.1587	*y*	1.265	5.0	106.788	455.093	12.204	0.002	−5.524	4.530	0.000	3.137
E301	T8880010	49979.1710	*u*	1.220	45.0	104.435	451.411	11.471	0.001	0.817	4.270	0.000	5.153
E301	T8880011	49979.1718	*v*	1.218	20.0	106.187	451.420	11.810	0.002	−0.327	4.430	0.200	4.691
E301	T8880012	49979.1724	*b*	1.215	10.0	109.045	453.457	12.027	0.002	0.709	4.700	0.000	4.974
E301	T8880013	49979.1730	*y*	1.213	5.0	109.326	457.762	11.965	0.002	0.850	4.410	0.000	4.346
E301	T8880014	49979.1735	*y*	1.212	5.0	109.199	456.369	11.963	0.002	0.823	4.330	0.000	4.660
E301	T8880015	49979.1741	*b*	1.209	10.0	106.394	452.260	12.010	0.002	−0.324	4.500	0.170	4.204
E301	T8880016	49979.1748	*v*	1.207	20.0	105.647	451.573	11.800	0.002	−0.128	4.720	0.110	4.506
E301	T8880017	49979.1757	*u*	1.203	45.0	104.428	450.472	11.450	0.001	0.570	4.480	0.000	4.623
E301	T8880022	49979.2381	*u*	1.053	45.0	109.281	449.246	11.324	0.001	30.116	5.140	0.000	2.515
E301	T8880023	49979.2389	*v*	1.052	20.0	108.673	446.094	11.727	0.002	19.900	4.820	0.030	2.490
E301	T8880024	49979.2396	*b*	1.051	10.0	110.741	446.781	11.968	0.002	20.800	5.210	0.000	2.503
E301	T8880025	49979.2401	*y*	1.050	5.0	112.270	450.682	11.924	0.002	8.849	4.630	0.000	2.213
E301	T8880026	49979.2406	*y*	1.049	5.0	112.230	450.178	11.922	0.002	9.625	4.600	0.020	1.880
E301	T8880027	49979.2413	*b*	1.048	10.0	111.662	447.893	11.967	0.002	29.299	5.290	0.030	1.985
E301	T8880028	49979.2420	*v*	1.047	20.0	109.264	444.295	11.722	0.002	38.535	5.310	0.010	2.170
E301	T8880030	49979.2452	*u*	1.043	30.0	110.948	442.910	11.748	0.002	104.999	6.410	0.000	2.669

Table B.7: Standard star *uvby* photometry – 1995-Sep-19. These are from a 24″ synthetic aperture.

Star	Frame	HJD −2400000.0	Filter	X	T	Row	Col	$m_{\rm raw}$	$\sigma_{m_{\rm raw}}$	sky	$\sigma_{\rm sky}$	sky skew	Seeing (FWHM)
E751	T8870006	49979.8094	*u*	1.033	45.0	161.819	141.153	12.224	0.002	10.271	5.190	0.000	1.954
E751	T8870007	49979.8103	*v*	1.034	20.0	159.886	139.096	12.220	0.002	2.893	5.110	0.000	2.330
E751	T8870008	49979.8109	*b*	1.035	10.0	162.734	139.830	12.300	0.002	1.991	5.000	0.000	2.441
E751	T8870009	49979.8115	*y*	1.036	5.0	166.144	144.085	12.149	0.002	−0.846	4.790	0.060	2.065
E751	T8870011	49979.8217	*u*	1.050	45.0	162.829	141.662	12.233	0.002	0.791	4.920	0.070	2.176

Table B.7 cont.: Standard star $uvby$ photometry – 1995-Sep-19.

Star	Frame	HJD −2400000.0	Filter	X	T	Row	Col	$m_{\rm raw}$	$\sigma_{m_{\rm raw}}$	sky	$\sigma_{\rm sky}$	sky skew	Seeing (FWHM)
E751	T8870012	49979.8225	v	1.051	20.0	161.105	138.974	12.219	0.002	−0.089	4.810	0.070	2.139
E751	T8870013	49979.8231	b	1.052	10.0	163.171	140.991	12.304	0.002	−0.222	4.820	0.070	2.231
E751	T8870014	49979.8237	y	1.053	5.0	164.891	142.918	12.155	0.002	−0.278	4.820	0.090	2.133
E751	T8870015	49979.8254	y	1.055	5.0	165.208	141.289	12.161	0.002	0.183	4.840	0.060	2.059
E751	T8870016	49979.8260	b	1.056	10.0	164.197	139.038	12.309	0.002	−0.582	4.930	0.040	2.139
E751	T8870017	49979.8268	v	1.058	20.0	162.171	140.741	12.216	0.002	−1.533	4.970	0.160	2.262
E751	T8870018	49979.8277	u	1.059	45.0	164.099	141.916	12.242	0.002	−0.621	4.960	0.020	2.632
E713	T8890001	49979.8320	u	1.052	90.0	164.033	141.677	12.254	0.002	0.018	4.940	0.060	2.521
E713	T8890002	49979.8333	v	1.054	45.0	162.758	138.250	12.293	0.002	−0.199	5.060	0.000	2.490
E713	T8890003	49979.8342	b	1.055	25.0	165.265	138.916	12.334	0.002	−0.064	4.910	0.020	2.275
E713	T8890004	49979.8348	y	1.056	12.0	166.782	142.841	12.242	0.002	0.310	4.910	0.020	2.182
E713	T8890005	49979.8354	y	1.057	12.0	167.151	142.829	12.251	0.002	0.465	4.950	0.000	2.102
E713	T8890006	49979.8362	b	1.059	25.0	166.186	139.680	12.334	0.002	−0.089	4.950	0.030	1.991
E713	T8890007	49979.8371	v	1.060	45.0	164.147	137.078	12.303	0.002	−0.092	5.110	0.030	2.053
E713	T8890008	49979.8384	u	1.062	90.0	166.158	137.802	12.256	0.002	−0.107	4.990	0.030	2.348
E704	T8890009	49979.8538	u	1.087	45.0	163.847	143.866	11.758	0.002	−1.309	5.010	0.000	2.392
E704	T8890010	49979.8547	v	1.089	20.0	161.155	138.988	11.975	0.002	−2.076	5.090	0.080	2.182
E704	T8890011	49979.8553	b	1.090	10.0	163.293	139.727	12.163	0.002	−2.405	4.740	0.150	2.034
E704	T8890012	49979.8559	y	1.091	5.0	165.048	142.316	12.053	0.002	−1.662	4.810	0.060	1.695
E704	T8890013	49979.8564	y	1.092	5.0	165.082	142.879	12.058	0.002	−1.365	4.820	0.000	2.120
E704	T8890014	49979.8570	b	1.094	10.0	164.064	137.156	12.169	0.002	−2.017	4.910	0.040	2.774
E704	T8890015	49979.8577	v	1.095	20.0	160.811	138.895	11.984	0.002	−2.294	4.910	0.000	2.540
E704	T8890016	49979.8586	u	1.097	45.0	162.877	140.226	11.769	0.002	−2.075	5.010	0.060	2.872
E710	T8890017	49979.8675	u	1.119	60.0	160.268	142.131	11.735	0.002	−1.281	4.980	0.090	2.768
E710	T8890018	49979.8686	v	1.121	45.0	159.210	138.296	11.721	0.002	−1.053	4.990	0.010	2.872
E710	T8890019	49979.8694	b	1.123	20.0	161.932	139.903	12.050	0.002	−1.232	4.930	0.000	2.379
E710	T8890020	49979.8701	y	1.125	10.0	163.756	143.997	11.904	0.002	−1.258	4.930	0.120	2.182
E710	T8890021	49979.8706	y	1.126	10.0	162.916	144.292	11.909	0.002	−1.060	4.990	0.020	2.299
E710	T8890022	49979.8714	b	1.128	20.0	161.918	143.258	12.052	0.002	−1.597	4.810	0.030	2.176
E710	T8890023	49979.8723	v	1.131	45.0	158.767	136.701	11.720	0.002	−2.400	4.910	0.140	2.620
E710	T8890024	49979.8734	u	1.134	60.0	160.664	142.680	11.753	0.002	−2.190	4.820	0.040	2.811
DM−38222	T8890025	49979.8883	u	1.477	180.0	160.107	138.256	11.481	0.001	−0.534	5.000	0.000	2.959
DM−38222	T8890026	49979.8903	v	1.465	90.0	159.070	136.831	12.445	0.003	−1.985	4.980	0.050	3.033
DM−38222	T8890027	49979.8915	b	1.457	40.0	161.961	140.750	12.853	0.003	−2.712	4.620	0.060	2.835
DM−38222	T8890028	49979.8923	y	1.452	20.0	166.706	149.240	12.845	0.004	−2.029	4.810	0.000	2.546
DM−38222	T8890029	49979.8949	y	1.435	40.0	163.147	146.766	12.092	0.002	−0.227	4.850	0.000	2.749
DM−38222	T8890030	49979.8961	b	1.427	80.0	161.707	143.166	12.094	0.002	−1.263	4.880	0.000	2.885
DM−38222	T8890031	49979.8981	v	1.413	180.0	159.823	140.252	11.670	0.002	−1.469	4.970	0.140	2.891
DM−38222	T8890032	49979.9013	u	1.394	180.0	160.967	141.120	11.411	0.001	−2.080	4.970	0.100	2.681

Table B.7 cont.: Standard star *uvby* photometry – 1995-Sep-19.

Star	Frame	HJD −2400000.0	Filter	X	T	Row	Col	$m_{\rm raw}$	$\sigma_{m_{\rm raw}}$	sky	$\sigma_{\rm sky}$	sky skew	Seeing (FWHM)
DM−38222	T8900002	49979.9691	u	1.120	100.0	162.842	139.861	11.846	0.002	1.120	4.770	0.100	2.589
DM−38222	T8900003	49979.9708	v	1.116	100.0	161.242	139.227	12.187	0.002	1.420	4.940	0.020	2.977
DM−38222	T8900004	49979.9722	b	1.112	80.0	163.995	141.116	12.005	0.002	1.662	4.580	0.000	2.712
DM−38222	T8900005	49979.9734	y	1.110	40.0	165.023	144.082	12.026	0.002	1.899	4.690	0.100	2.663
DM−38222	T8900006	49979.9743	y	1.108	40.0	165.230	142.790	12.017	0.002	1.665	4.810	0.120	2.731
DM−38222	T8900007	49979.9756	b	1.105	80.0	163.908	140.911	12.004	0.002	1.398	4.640	0.050	2.817
DM−38222	T8900008	49979.9771	v	1.101	100.0	162.132	139.084	12.184	0.002	0.951	4.880	0.000	2.755
DM−38222	T8900009	49979.9788	u	1.097	100.0	162.876	139.933	11.825	0.002	−0.018	4.720	0.110	2.749
E103	T8900010	49979.9840	u	1.124	180.0	161.935	138.127	12.040	0.002	0.579	4.900	0.000	2.509
E103	T8900011	49979.9860	v	1.119	90.0	159.232	137.034	11.864	0.002	−0.120	4.860	0.040	2.614
E103	T8900012	49979.9873	b	1.117	40.0	163.637	140.153	12.082	0.002	−0.911	4.810	0.110	2.552
E103	T8900013	49979.9881	y	1.115	20.0	164.758	143.750	11.961	0.002	−0.070	4.680	0.000	2.441
E103	T8900014	49979.9888	y	1.113	20.0	164.141	143.211	11.960	0.002	−0.226	4.660	0.000	2.527
E103	T8900015	49979.9896	b	1.111	40.0	162.277	139.249	12.084	0.002	−0.536	4.630	0.010	2.521
E103	T8900016	49979.9909	v	1.108	90.0	160.755	136.779	11.868	0.002	−0.414	4.810	0.000	2.601
E103	T8900017	49979.9930	u	1.103	180.0	161.706	136.333	12.018	0.002	−0.286	4.820	0.090	2.626
E803	T8900018	49980.0060	u	1.205	90.0	165.644	140.678	11.792	0.002	−1.164	4.830	0.000	2.749
E803	T8900019	49980.0072	v	1.209	45.0	164.156	135.778	11.682	0.002	−1.441	4.710	0.000	2.706
E803	T8900020	49980.0080	b	1.212	20.0	166.957	141.282	11.935	0.002	−1.811	4.790	0.080	2.527
E803	T8900021	49980.0087	y	1.214	10.0	168.648	140.286	11.841	0.002	−1.141	4.700	0.000	2.601
E803	T8900022	49980.0093	y	1.216	10.0	168.649	140.783	11.838	0.002	−1.727	4.850	0.050	2.490
E803	T8900023	49980.0100	b	1.218	20.0	167.745	139.095	11.936	0.002	−2.246	4.690	0.080	2.533
E803	T8900024	49980.0109	v	1.222	45.0	165.273	137.857	11.691	0.002	−1.908	4.700	0.040	2.761
E803	T8900025	49980.0122	u	1.227	90.0	167.894	137.855	11.814	0.002	−1.731	4.830	0.070	2.805
DM−11162	T8900026	49980.0278	u	1.239	180.0	160.838	138.043	12.000	0.002	−0.659	4.940	0.000	2.459
DM−11162	T8900027	49980.0303	v	1.234	180.0	159.679	136.354	12.476	0.003	−0.156	4.860	0.000	2.681
DM−11162	T8900028	49980.0327	b	1.230	150.0	162.637	143.259	12.199	0.002	0.795	4.730	0.010	2.521
DM−11162	T8900029	49980.0345	y	1.227	80.0	164.133	148.143	12.009	0.002	3.579	4.860	0.000	2.299
DM−11162	T8900030	49980.0358	y	1.225	80.0	163.920	148.263	12.012	0.002	3.725	4.760	0.000	2.102
DM−11162	T8900031	49980.0377	b	1.222	150.0	163.008	146.701	12.194	0.002	0.990	4.720	0.000	2.299
DM−11162	T8900032	49980.0402	v	1.218	180.0	159.760	142.970	12.466	0.003	−0.394	4.760	0.040	2.416
DM−11162	T8900033	49980.0428	u	1.215	180.0	160.682	145.095	11.976	0.002	−1.193	4.800	0.090	2.724
DM−261339	T8910002	49980.0516	u	1.345	180.0	159.907	139.216	11.735	0.002	2.511	4.800	0.000	2.632
DM−261339	T8910003	49980.0541	v	1.331	180.0	158.790	138.872	12.328	0.002	2.402	4.650	0.030	3.174
DM−261339	T8910004	49980.0565	b	1.319	150.0	161.711	140.180	12.196	0.002	4.334	4.710	0.080	2.694
DM−261339	T8910005	49980.0583	y	1.311	80.0	163.863	144.250	12.187	0.002	5.990	4.730	0.000	2.657
DM−261339	T8910006	49980.0597	y	1.304	80.0	162.086	144.740	12.185	0.002	5.259	4.690	0.080	3.292
DM−261339	T8910007	49980.0615	b	1.295	150.0	160.972	141.190	12.190	0.002	4.937	4.710	0.000	2.712
DM−261339	T8910008	49980.0640	v	1.283	180.0	159.214	138.911	12.312	0.002	1.799	4.890	0.160	2.934

Table B.7 cont.: Standard star *uvby* photometry – 1995-Sep-19.

Star	Frame	HJD −2400000.0	Filter	X	T	Row	Col	$m_{\rm raw}$	$\sigma_{m_{\rm raw}}$	sky	$\sigma_{\rm sky}$	sky skew	Seeing (FWHM)
DM−261339	T8910009	49980.0666	u	1.272	180.0	159.802	138.972	11.690	0.002	2.131	4.860	0.080	2.768
DM−38222	T8910014	49980.1353	u	1.062	100.0	162.797	142.185	11.849	0.002	1.517	4.800	0.000	3.156
DM−38222	T8910015	49980.1369	v	1.064	100.0	163.880	139.148	12.202	0.002	0.841	4.580	0.150	2.755
DM−38222	T8910016	49980.1384	b	1.067	80.0	165.046	141.151	12.036	0.002	1.713	4.890	0.090	2.780
DM−38222	T8910017	49980.1396	y	1.069	40.0	164.883	144.251	12.049	0.002	3.134	4.790	0.050	2.564
DM−38222	T8910018	49980.1405	y	1.070	40.0	165.008	144.016	12.046	0.002	2.717	4.680	0.160	2.398
DM−38222	T8910019	49980.1417	b	1.073	80.0	164.091	139.788	12.038	0.002	1.504	4.630	0.180	2.422
DM−38222	T8910020	49980.1433	v	1.076	100.0	161.193	139.921	12.231	0.002	1.564	4.650	0.000	2.552
DM−38222	T8910021	49980.1450	u	1.079	100.0	163.071	140.870	11.892	0.002	1.142	4.880	0.030	2.835
E302	T8910022	49980.1453	u	1.312	45.0	160.263	140.326	11.724	0.002	0.871	4.830	0.000	3.366
E302	T8910023	49980.1462	v	1.308	20.0	158.177	140.305	12.067	0.002	0.086	4.590	0.050	3.088
E302	T8910024	49980.1468	b	1.305	10.0	159.240	142.702	12.264	0.002	−0.173	4.550	0.150	3.008
E302	T8910025	49980.1474	y	1.303	5.0	161.028	146.722	12.187	0.002	0.343	4.590	0.030	3.624
E302	T8910026	49980.1479	y	1.301	5.0	159.984	145.953	12.182	0.002	−0.153	4.500	0.050	3.359
E302	T8910027	49980.1485	b	1.298	10.0	158.927	142.297	12.264	0.002	−0.056	4.500	0.020	3.039
E302	T8910028	49980.1492	v	1.295	20.0	155.812	140.057	12.072	0.002	−0.220	4.710	0.000	3.248
E302	T8910029	49980.1501	u	1.290	45.0	159.815	140.870	11.720	0.002	−0.005	4.710	0.000	3.470
E301	T8910030	49980.1533	u	1.280	45.0	157.694	137.975	11.493	0.001	−0.048	4.820	0.000	3.594
E301	T8910031	49980.1542	v	1.276	20.0	160.019	137.151	11.842	0.002	−0.423	4.590	0.000	3.403
E301	T8910032	49980.1548	b	1.274	10.0	162.094	138.767	12.063	0.002	−0.476	4.490	0.000	3.403
E301	T8910033	49980.1553	y	1.271	5.0	162.894	142.097	12.027	0.002	−0.414	4.650	0.000	3.310
E301	T8910034	49980.1559	y	1.269	5.0	162.788	142.299	12.192	0.002	−0.977	4.640	0.080	3.384
E301	T8910035	49980.1565	b	1.267	10.0	160.892	139.886	12.075	0.002	−1.277	4.580	0.120	3.174
E301	T8910036	49980.1572	v	1.264	20.0	158.135	136.873	11.849	0.002	−1.065	4.740	0.010	3.359
E301	T8910037	49980.1581	u	1.260	45.0	158.098	137.223	11.521	0.001	−1.218	4.770	0.060	3.846
E301	T6650001	49980.1603	y	1.251	5.0	158.791	143.302	12.095	0.002	−1.061	4.610	0.120	2.996
E301	T6650002	49980.1608	y	1.249	5.0	159.104	144.823	12.075	0.002	−1.392	4.490	0.150	3.150

Table B.8: Standard star *uvby* photometry – 1995-Oct-25. These are from a 24″ synthetic aperture.

Star	Frame	HJD −2400000.0	Filter	X	T	Row	Col	$m_{\rm raw}$	$\sigma_{m_{\rm raw}}$	sky	$\sigma_{\rm sky}$	sky skew	Seeing (FWHM)
DM−38222	T9000019	50015.8656	u	1.131	200.0	148.283	139.702	11.077	0.001	−1.998	5.280	0.070	2.805
DM−38222	T9000020	50015.8585	v	1.151	180.0	153.151	139.717	11.520	0.001	5.070	5.360	0.000	2.724
DM−38222	T9000021	50015.8605	b	1.146	80.0	153.690	141.285	11.990	0.002	0.844	5.390	0.000	2.589
DM−38222	T9000022	50015.8617	y	1.142	40.0	154.075	145.281	12.005	0.002	−2.146	5.090	0.110	2.459
DM−38222	T9000024	50015.8757	y	1.106	40.0	164.228	142.800	12.000	0.002	2.931	5.090	0.020	2.410

Table B.8 cont.: Standard star $uvby$ photometry – 1995-Oct-25.

Star	Frame	HJD −2400000.0	Filter	X	T	Row	Col	$m_{\rm raw}$	$\sigma_{m_{\rm raw}}$	sky	$\sigma_{\rm sky}$	sky skew	Seeing (FWHM)
DM−38222	T9000025	50015.8772	b	1.102	80.0	161.915	139.026	11.977	0.002	2.026	5.020	0.030	2.435
DM−38222	T9000026	50015.8796	v	1.096	180.0	158.024	136.674	11.501	0.001	2.868	5.160	0.000	2.854
DM−38222	T9000027	50015.8829	u	1.089	200.0	159.727	140.189	11.049	0.001	1.942	5.070	0.040	3.236
DM−38222	T9000028	50015.8859	u	1.083	200.0	156.950	140.864	11.044	0.001	1.915	5.060	0.000	3.501
DM−38222	T9000029	50015.8892	v	1.076	180.0	158.677	140.029	11.496	0.001	2.033	5.180	0.000	3.409
DM−38222	T9000030	50015.8919	b	1.072	80.0	162.867	141.151	11.973	0.002	0.924	4.980	0.000	3.181
DM−38222	T9000031	50015.8932	y	1.069	40.0	162.902	144.668	12.000	0.002	1.071	5.060	0.030	3.501
E902	T9000032	50015.8960	y	1.095	40.0	165.936	140.744	12.398	0.003	−0.247	5.150	0.070	3.162
E902	T9000033	50015.8974	b	1.098	80.0	165.171	134.932	12.474	0.003	−0.039	4.940	0.010	3.359
E902	T9000034	50015.8998	v	1.104	180.0	163.261	130.727	12.078	0.002	0.731	4.960	0.000	3.224
E902	T9000035	50015.9043	u	1.116	360.0	161.818	136.672	11.932	0.002	2.411	5.130	0.000	4.148
E902	T9010001	50015.9114	u	1.133	360.0	160.976	137.832	11.934	0.002	1.772	5.200	0.120	3.563
E902	T9010002	50015.9152	v	1.143	180.0	157.872	134.037	12.085	0.002	0.664	5.020	0.000	2.632
E902	T9010003	50015.9180	b	1.150	80.0	161.701	141.685	12.462	0.003	−0.442	4.870	0.150	3.162
E902	T9010004	50015.9194	y	1.154	40.0	162.284	143.301	12.393	0.003	0.035	4.940	0.090	2.607
FEIGE110	T9010005	50015.9307	y	1.292	240.0	163.226	145.787	11.459	0.001	15.743	5.120	0.000	2.688
FEIGE110	T9010006	50015.9341	b	1.296	200.0	160.681	142.675	12.368	0.003	2.057	5.000	0.060	1.942
FEIGE110	T9010007	50015.9375	v	1.300	250.0	156.035	141.765	12.490	0.003	1.014	4.940	0.000	2.194
FEIGE110	T9010008	50015.9419	u	1.307	250.0	157.019	141.857	11.969	0.002	0.157	4.920	0.030	2.854
FEIGE110	T9010013	50016.0145	y	1.586	100.0	160.708	144.969	12.472	0.003	4.479	5.070	0.000	3.230
FEIGE110	T9010014	50016.0170	b	1.605	200.0	159.848	142.087	12.466	0.003	1.271	5.140	0.070	3.218
FEIGE110	T9010015	50016.0206	v	1.632	250.0	157.986	139.709	12.634	0.003	−0.267	5.050	0.000	3.094
FEIGE110	T9010016	50016.0246	u	1.663	250.0	159.277	143.863	12.250	0.002	−1.139	5.040	0.000	3.378
DM−3515910	T9010017	50016.0368	y	1.180	100.0	162.802	143.734	11.515	0.001	2.661	5.030	0.000	2.872
DM−3515910	T9010018	50016.0393	b	1.189	200.0	163.156	138.947	11.479	0.001	0.730	5.210	0.110	2.774
DM−3515910	T9010019	50016.0431	v	1.203	250.0	160.170	140.853	11.638	0.002	−0.277	5.220	0.000	3.329
DM−3515910	T9010020	50016.0468	u	1.216	250.0	163.873	139.821	11.276	0.001	−1.202	4.990	0.050	3.489
E103	T9010021	50016.0585	u	1.046	180.0	161.152	141.005	11.982	0.002	−3.140	4.870	0.010	3.187
E103	T9010022	50016.0609	v	1.049	90.0	160.090	136.330	11.822	0.002	−3.586	4.900	0.000	2.768
E103	T9010023	50016.0623	b	1.051	40.0	162.778	136.808	12.063	0.002	−3.833	4.820	0.090	2.761
E103	T9010024	50016.0637	y	1.053	20.0	161.880	143.258	11.942	0.002	−3.067	4.780	0.000	2.503
E103	T9010025	50016.0646	y	1.055	20.0	162.077	143.325	11.943	0.002	−3.026	4.780	0.000	2.435
E175	T9010026	50016.0717	u	1.050	180.0	160.983	140.298	12.110	0.002	−3.304	5.080	0.030	2.885
E175	T9010027	50016.0739	v	1.053	90.0	160.276	136.754	12.075	0.002	−4.116	5.160	0.000	2.355
E175	T9010028	50016.0753	b	1.055	40.0	162.883	136.791	12.217	0.002	−4.024	5.010	0.000	2.466
E175	T9010029	50016.0763	y	1.056	20.0	164.669	138.695	11.986	0.002	−3.640	4.710	0.030	2.392
E175	T9010030	50016.0772	y	1.058	20.0	164.942	138.253	11.984	0.002	−4.278	4.740	0.120	2.422
E204	T9010031	50016.0880	u	1.003	90.0	159.192	139.690	11.374	0.001	−4.159	5.130	0.000	2.885
E204	T9010032	50016.0895	v	1.002	45.0	157.676	137.112	11.145	0.001	−4.315	5.080	0.000	2.657

Table B.8 cont.: Standard star $uvby$ photometry – 1995-Oct-25.

Star	Frame	HJD −2400000.0	Filter	X	T	Row	Col	$m_{\rm raw}$	$\sigma_{m_{\rm raw}}$	sky	$\sigma_{\rm sky}$	sky skew	Seeing (FWHM)
E204	T9010033	50016.0906	b	1.002	20.0	159.280	137.927	11.372	0.001	−4.160	5.120	0.000	2.336
E204	T9010034	50016.0915	y	1.002	10.0	160.660	140.911	11.225	0.001	−4.104	5.060	0.030	2.589
E204	T9010035	50016.0923	y	1.001	10.0	159.873	139.862	11.225	0.001	−3.984	4.870	0.030	2.509
E204	T9020001	50016.0945	y	1.001	10.0	158.924	139.246	11.226	0.001	−3.795	4.990	0.060	2.780
E204	T9020002	50016.0955	y	1.001	10.0	158.896	138.065	11.223	0.001	−4.609	5.070	0.190	2.478
E204	T9020003	50016.0964	b	1.001	20.0	157.754	134.950	11.372	0.001	−4.015	4.970	0.000	2.601
E302	T9020008	50016.1661	u	1.019	90.0	161.310	140.018	10.685	0.001	−4.412	4.990	0.000	3.347
E302	T9020009	50016.1676	v	1.018	45.0	158.884	137.838	10.986	0.001	−5.196	5.000	0.050	3.094
E302	T9020010	50016.1689	b	1.017	20.0	160.070	139.153	11.371	0.001	−5.056	4.960	0.000	2.620
E302	T9020011	50016.1698	y	1.016	10.0	160.856	142.231	11.318	0.001	−5.151	5.080	0.050	2.392
E302	T9020012	50016.1707	y	1.016	10.0	159.896	139.872	11.320	0.001	−5.037	4.740	0.000	3.051
E302	T9020013	50016.1716	y	1.015	10.0	160.220	140.294	11.320	0.001	−5.062	4.950	0.000	2.737
E302	T9020014	50016.1725	b	1.014	20.0	158.010	135.714	11.366	0.001	−5.147	4.960	0.040	2.657
E103	T9020016	50016.1830	u	1.477	180.0	160.710	142.787	12.276	0.002	18.252	5.250	0.000	3.458
E103	T9020017	50016.1852	v	1.491	90.0	161.031	138.832	11.990	0.002	18.194	5.200	0.000	3.064
E103	T9020018	50016.1866	b	1.499	40.0	163.725	138.123	12.172	0.002	19.908	5.240	0.040	3.002
E103	T9020019	50016.1876	y	1.506	20.0	166.231	140.201	12.014	0.002	11.511	5.220	0.030	2.977
E103	T9020020	50016.1884	y	1.511	20.0	166.673	138.758	12.018	0.002	13.586	5.160	0.000	2.891

B.3 Correlations between the transformation coefficients and the properties

The following three figures plot the catalogue V magnitude and either the $(b-y)$ colour (for the $uvby$ photometry) or the $(V-I)$ colour (for the VI photometry) of the standard stars and the UTC and measured seeing for each observation against the Airmass in any effort to identify systematic effects in the transformed photometry. Each figure presents graphs for two filters (u and v in figure B.9, b and y in figure B.10 and V and I in figure B.11). Observations from the different nights are indicated by different symbols in different colours. No systematic effects are evident in these plots.

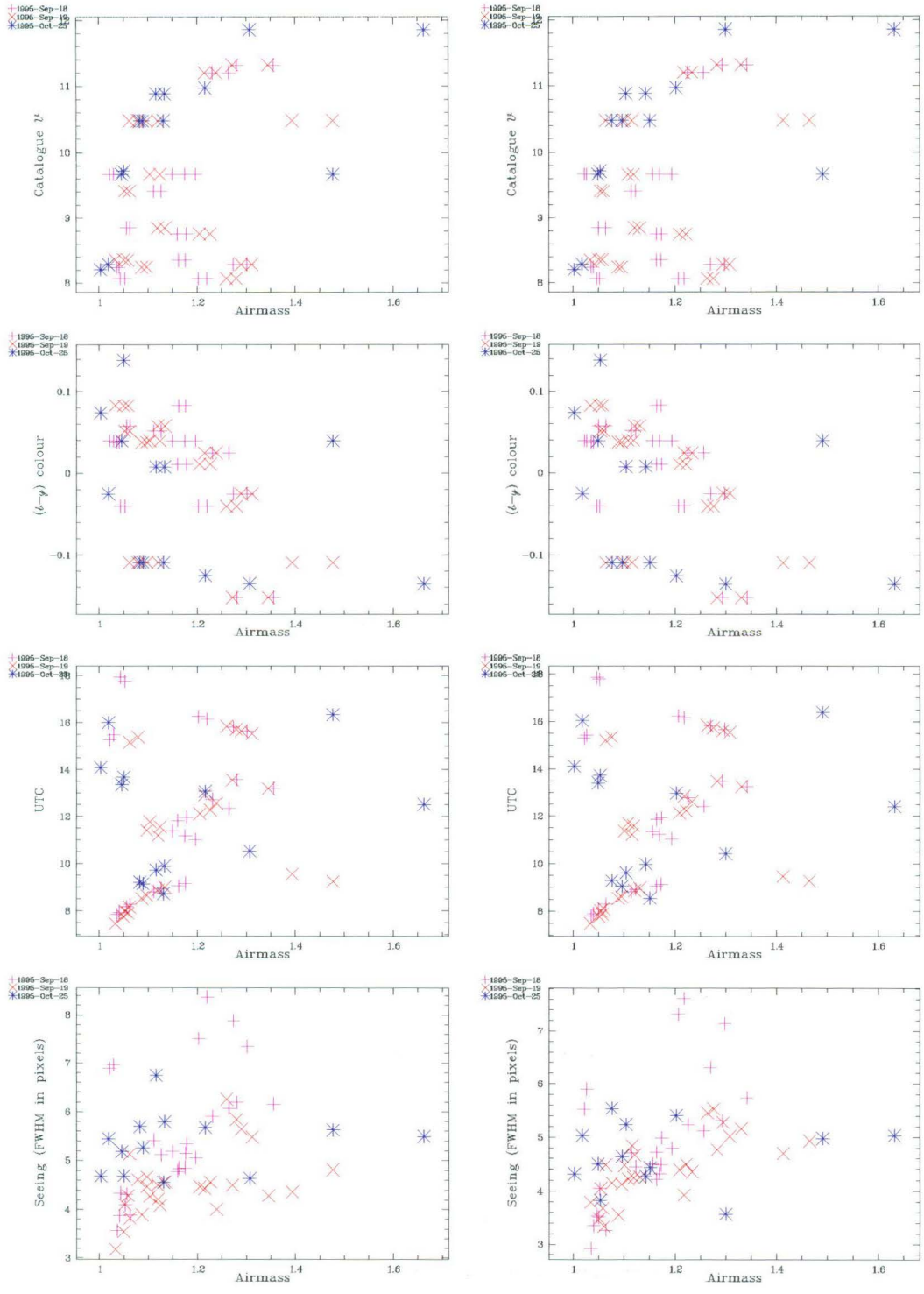

Figure B.9: Various properties of the u (left) and v (right) standard star observations plotted against Airmass in order to identify any systematic effects.

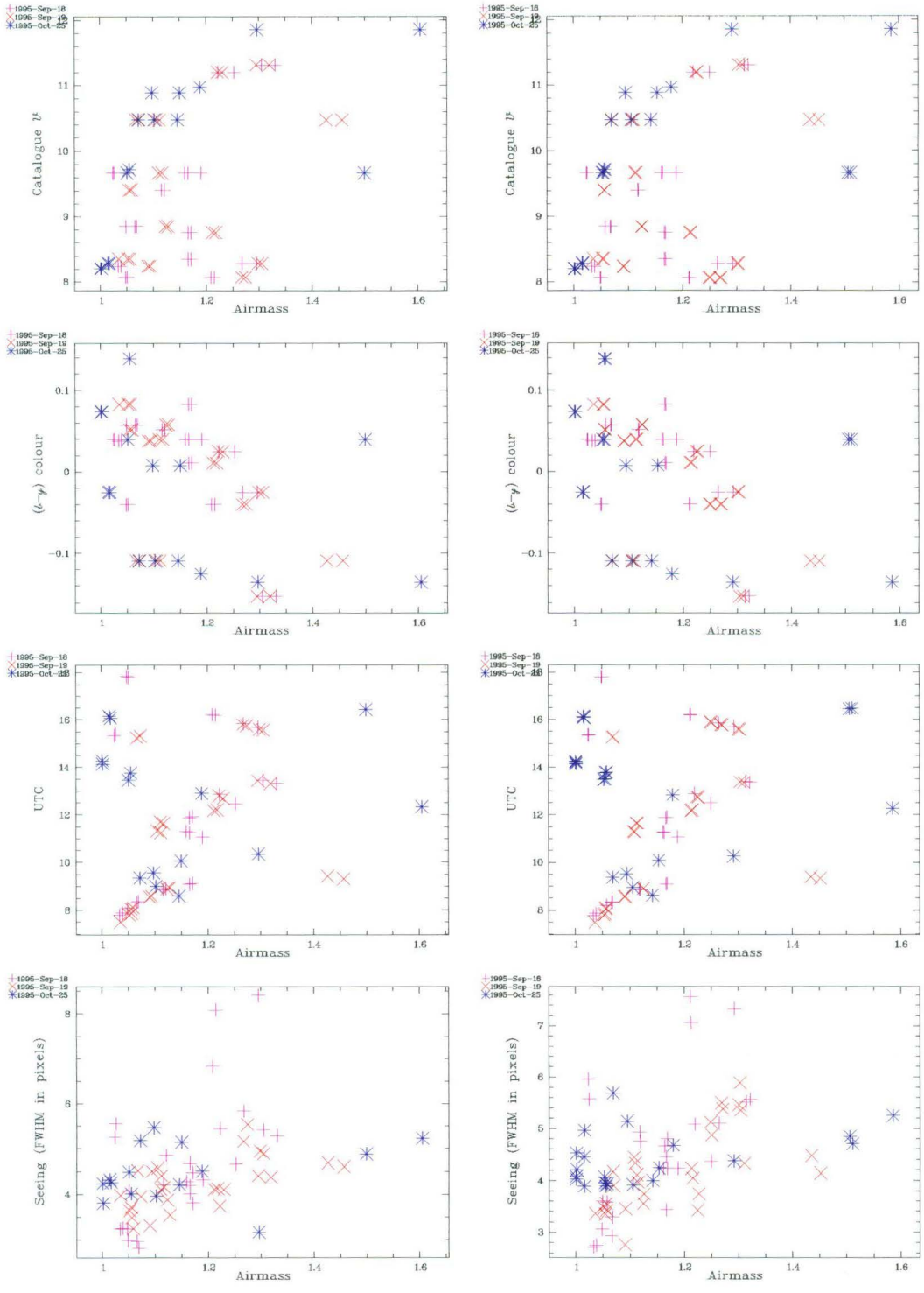

Figure B.10: Various properties of the b (left) and y (right) standard star observations plotted against Airmass in order to identify any systematic effects.

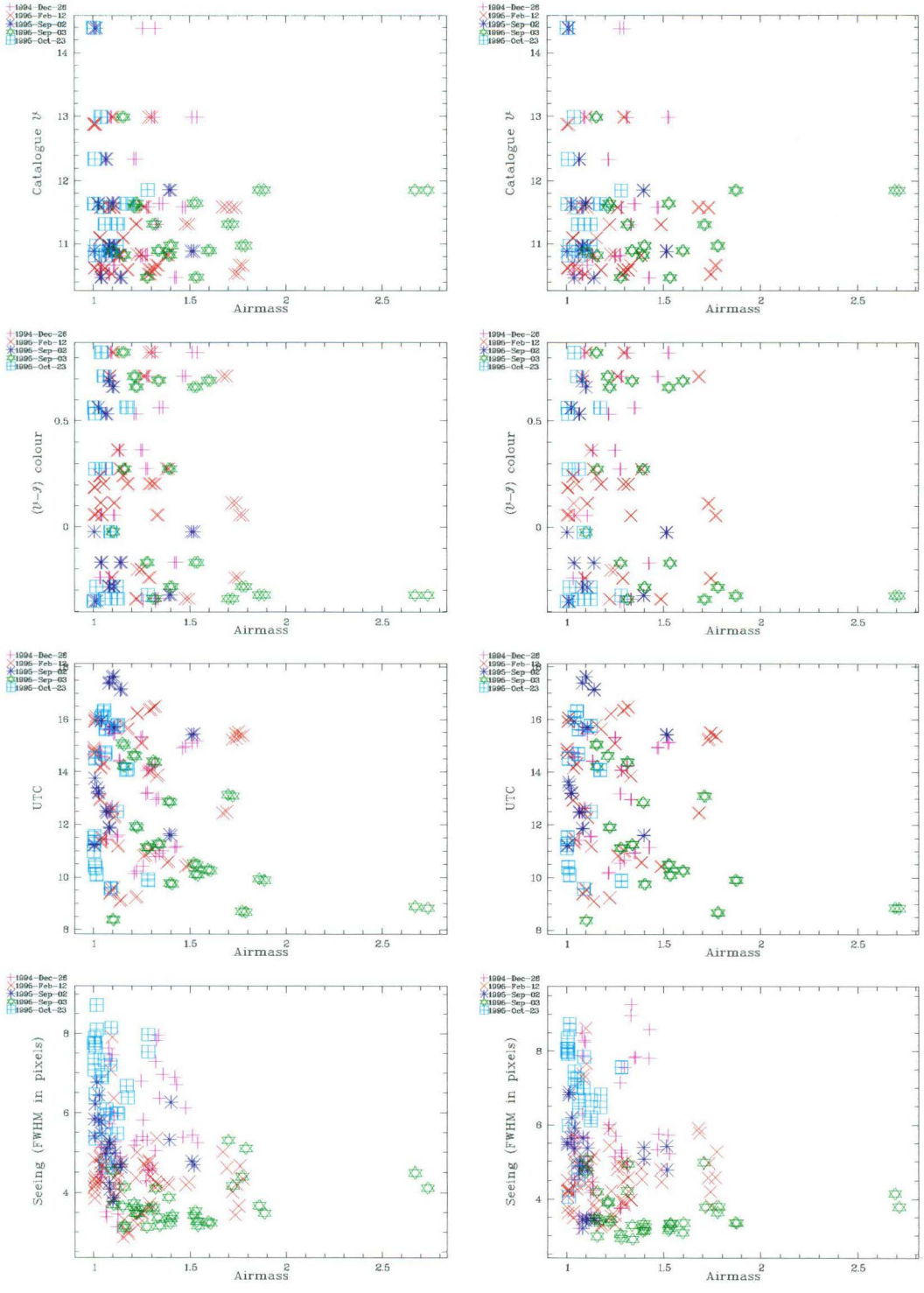

Figure B.11: Various properties of the V (left) and I (right) standard star observations plotted against Airmass in order to identify any systematic effects.

B.4 Transformation residuals

Residuals between the $(V-I)$, V, I, $(u-b)$, $(v-b)$, $(b-y)$ and y catalogue photometry and the transformed photometry for the standard stars as a function of *Universal Time Coordinated* (UTC), Airmass, colour, magnitude, Hour Angle and Declination are presented in the following seven figures. Observations from the different nights are indicated by different symbols in different colours. Circled points indicate observations excluded from the final transformation coefficient determinations (see tables 5.3 and 5.6). All graphs have the vertical scale to ease direct comparison between the different magnitudes and colours.

B.4.1 Transformation residuals for VI

The lower precision of the $(V-I)$ and I photometry as compared to the V photometry is clearly seen in the residuals. No significant trends are evident, although there is perhaps the hint of a non-linear dependance of the the $(V-I)$ colour on $(V-I)$ (lower most panels in figure B.12).

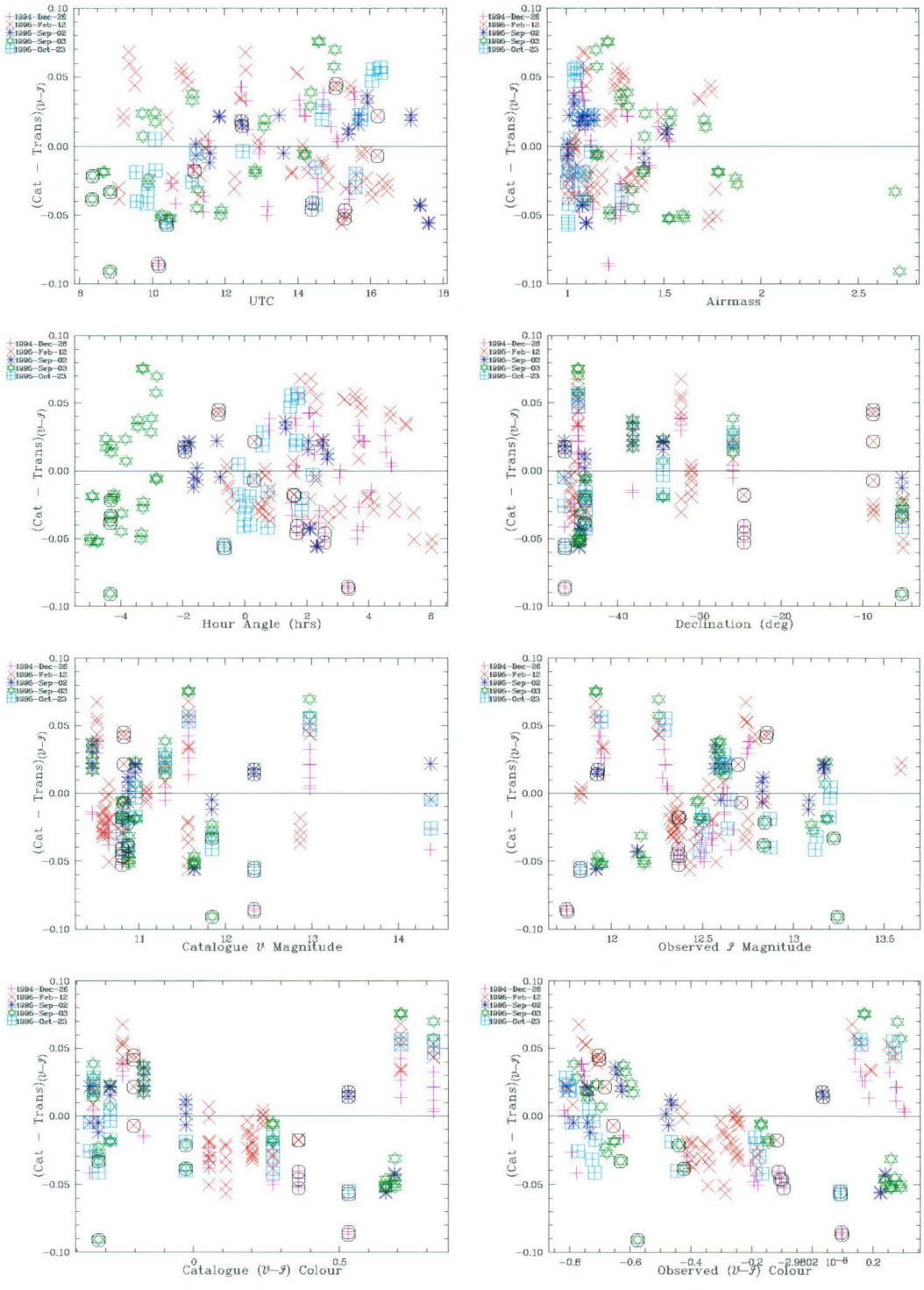

Figure B.12: Residuals between the transformed $V - I$ colours and the catalogue $V - I$ colours plotted against relevant properties. Circled points indicate those observations excluded from the final determinations of the transformation equation coefficients.

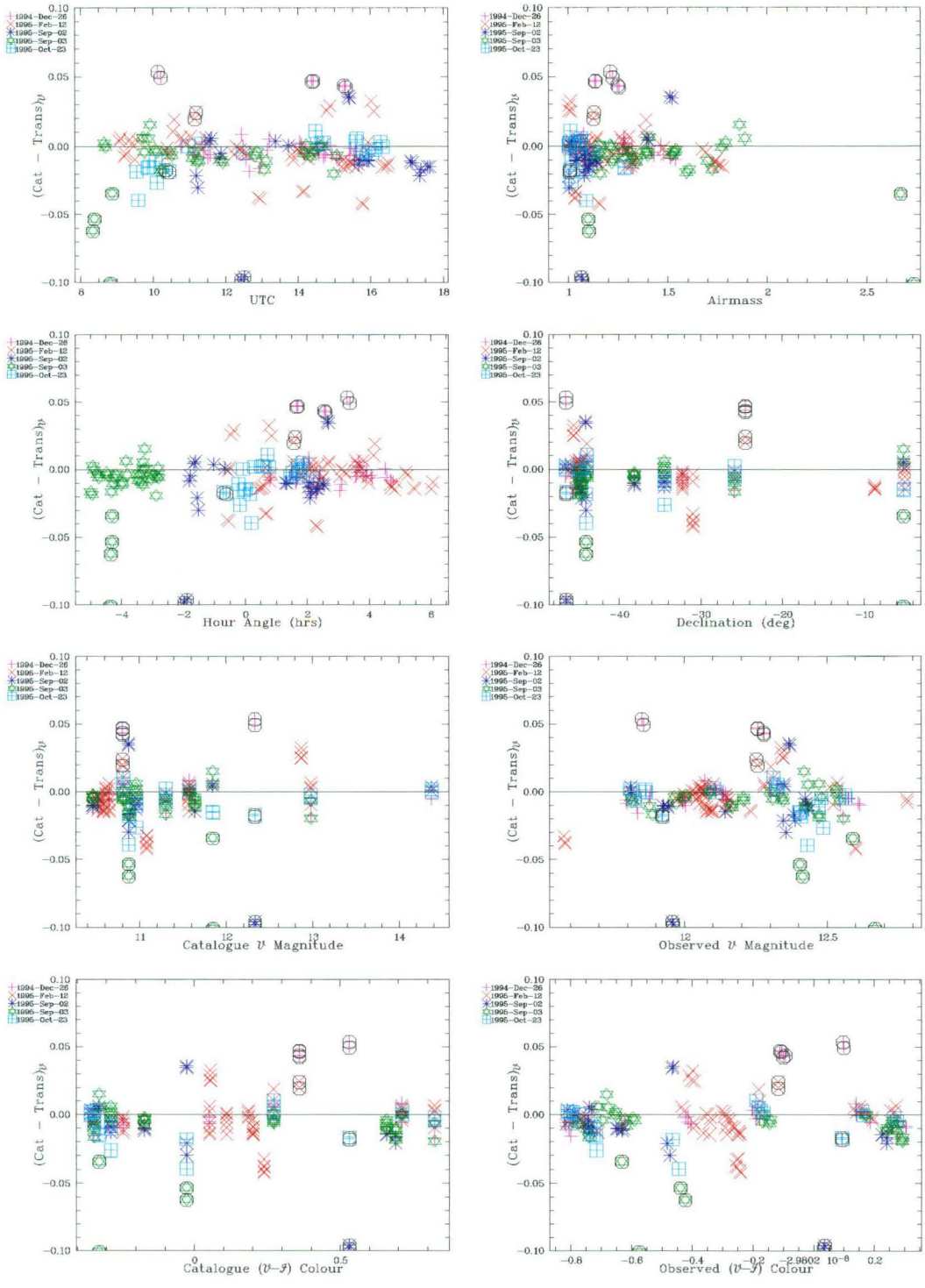

Figure B.13: Residuals between the transformed V magnitudes and the catalogue V magnitudes plotted against relevant properties. Circled points indicate those observations excluded from the final determinations of the transformation equation coefficients.

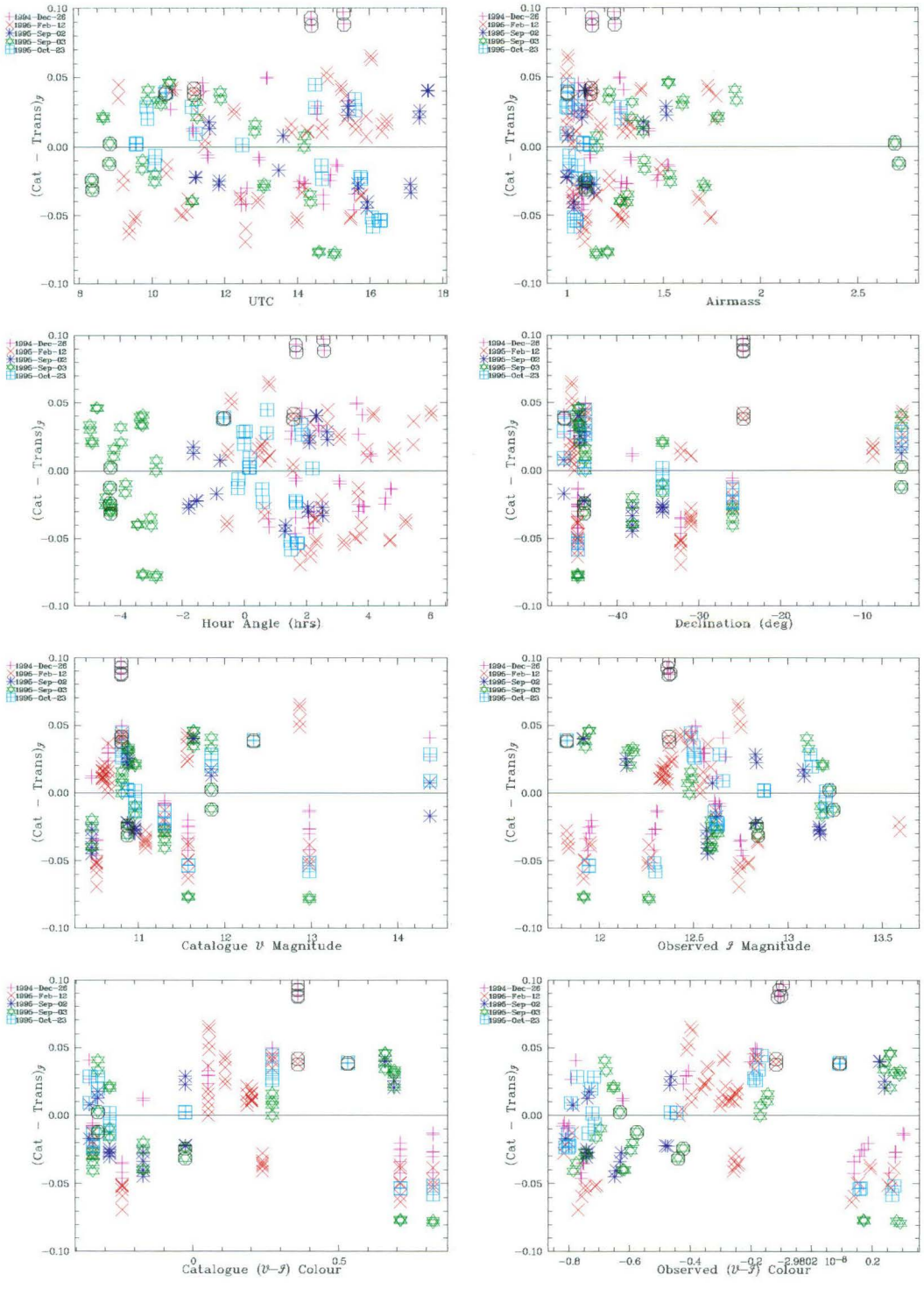

Figure B.14: Residuals between the transformed I magnitudes and the catalogue I magnitudes plotted against relevant properties. Circled points indicate those observations excluded from the final determinations of the transformation equation coefficients.

B.4.2 Transformation residuals for $uvby$

The generally higher quality of the $uvby$ photometry, as compared to the VI photometry, is immediately evident in the much lower scatter for all transformations except for the y transformation for which the scatter is 'only' of the same order as that for the V transformation. No significant trends are obvious in the $uvby$ residuals.

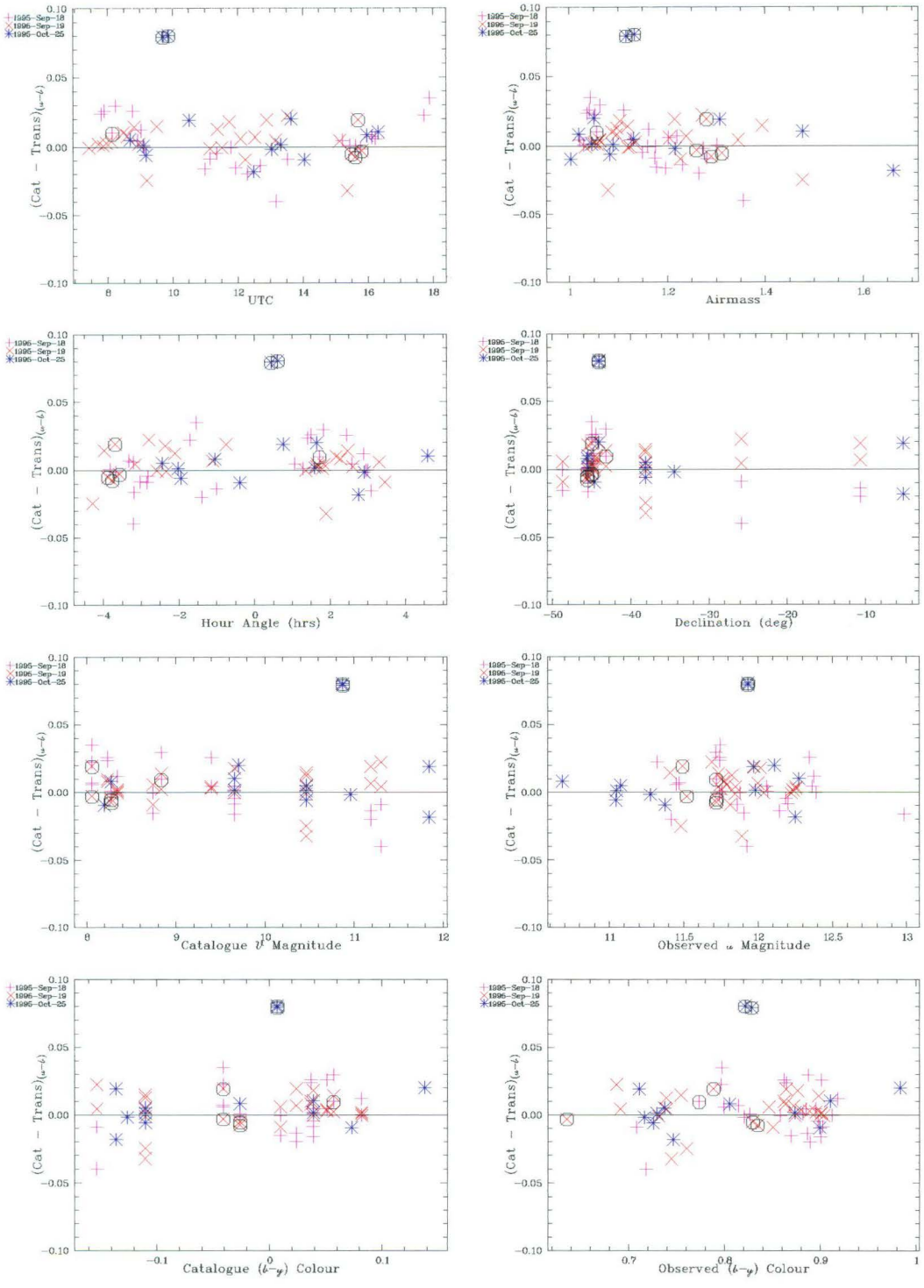

Figure B.15: Residuals between the transformed $u - b$ colours and the catalogue $u - b$ colours plotted against relevant properties. Circled points indicate those observations excluded from the final determinations of the transformation equation coefficients.

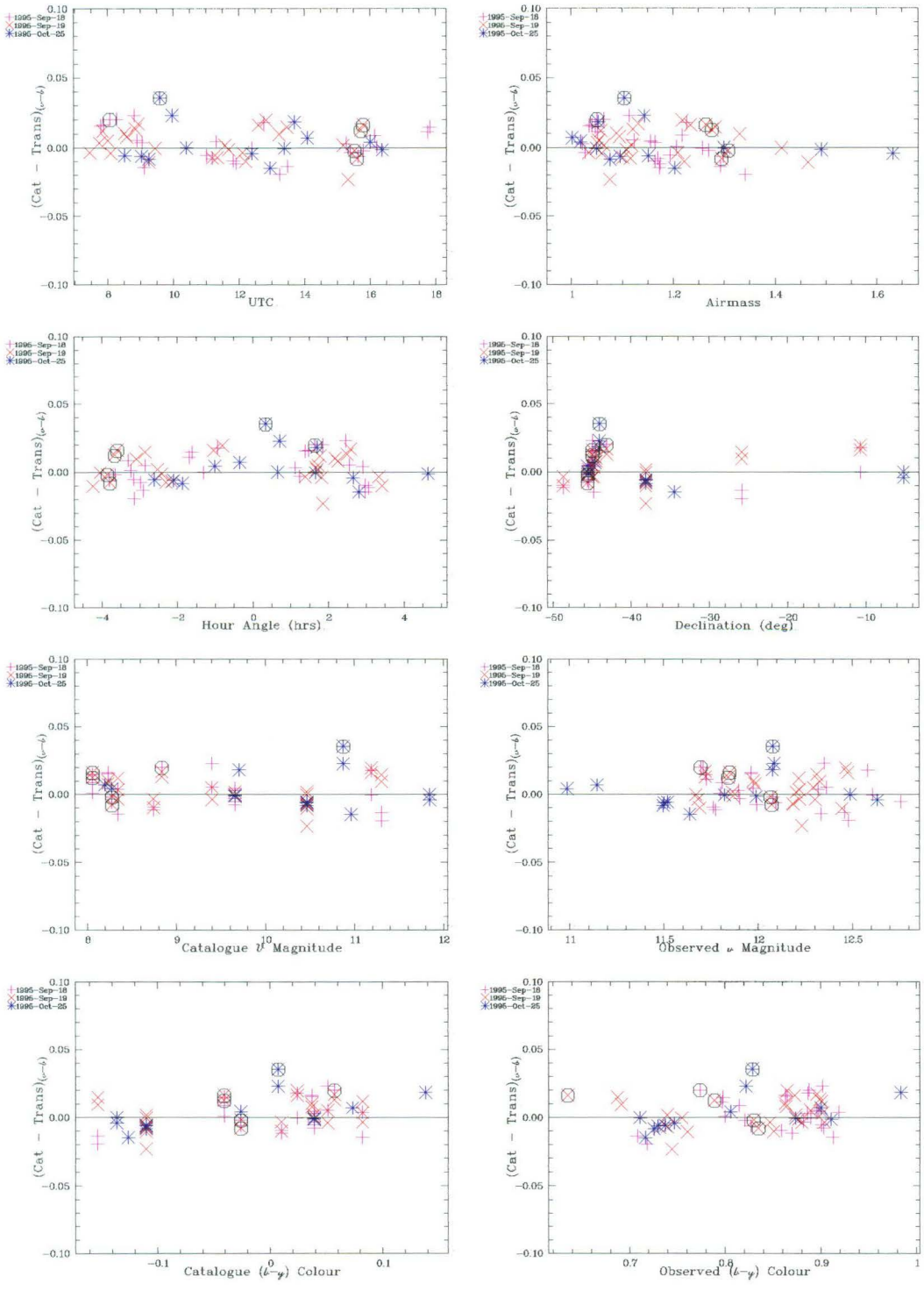

Figure B.16: Residuals between the transformed $v - b$ colours and the catalogue $v - b$ colours plotted against relevant properties. Circled points indicate those observations excluded from the final determinations of the transformation equation coefficients.

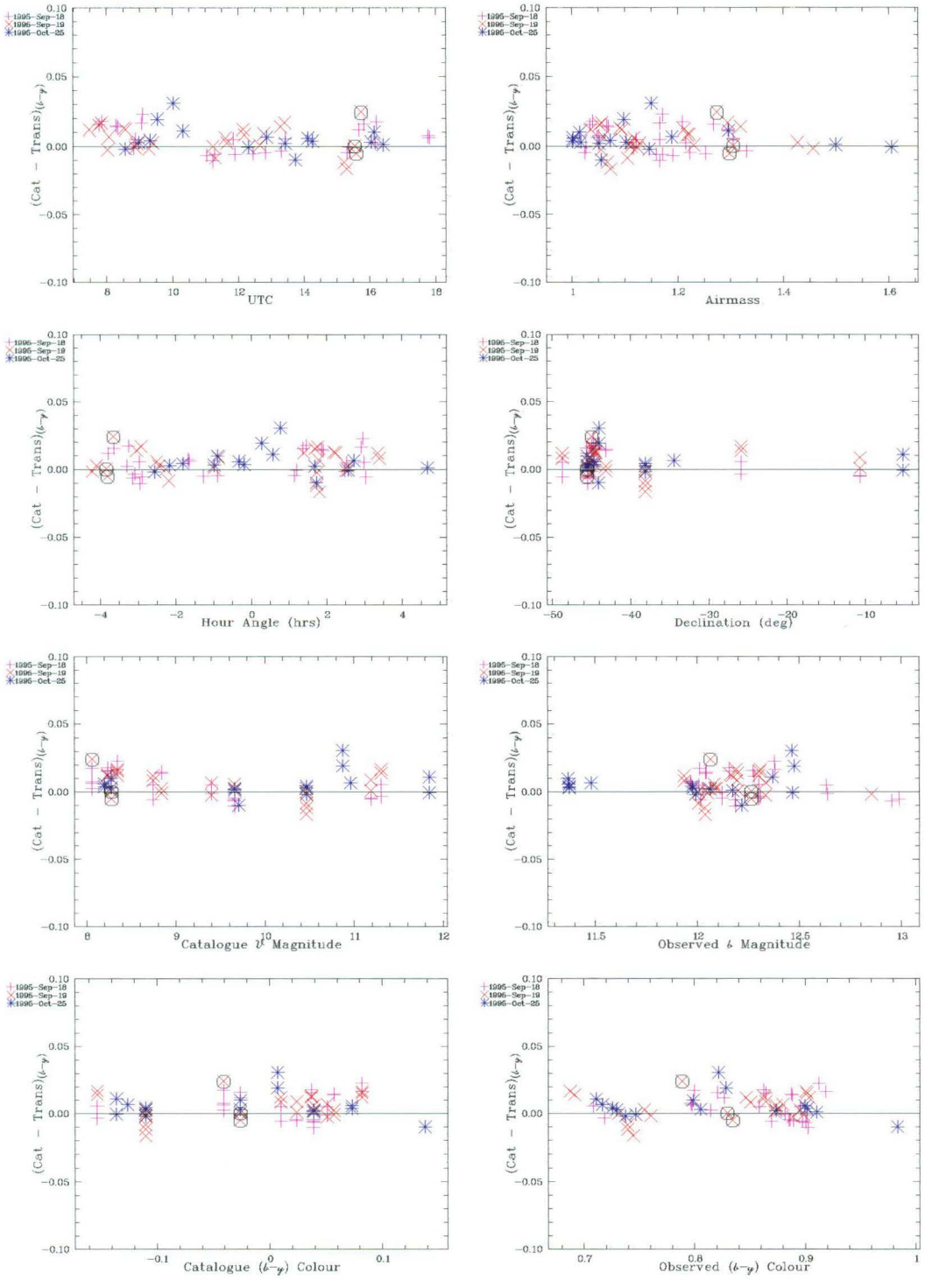

Figure B.17: Residuals between the transformed $b - y$ colours and the catalogue $b - y$ colours plotted against relevant properties. Circled points indicate those observations excluded from the final determinations of the transformation equation coefficients.

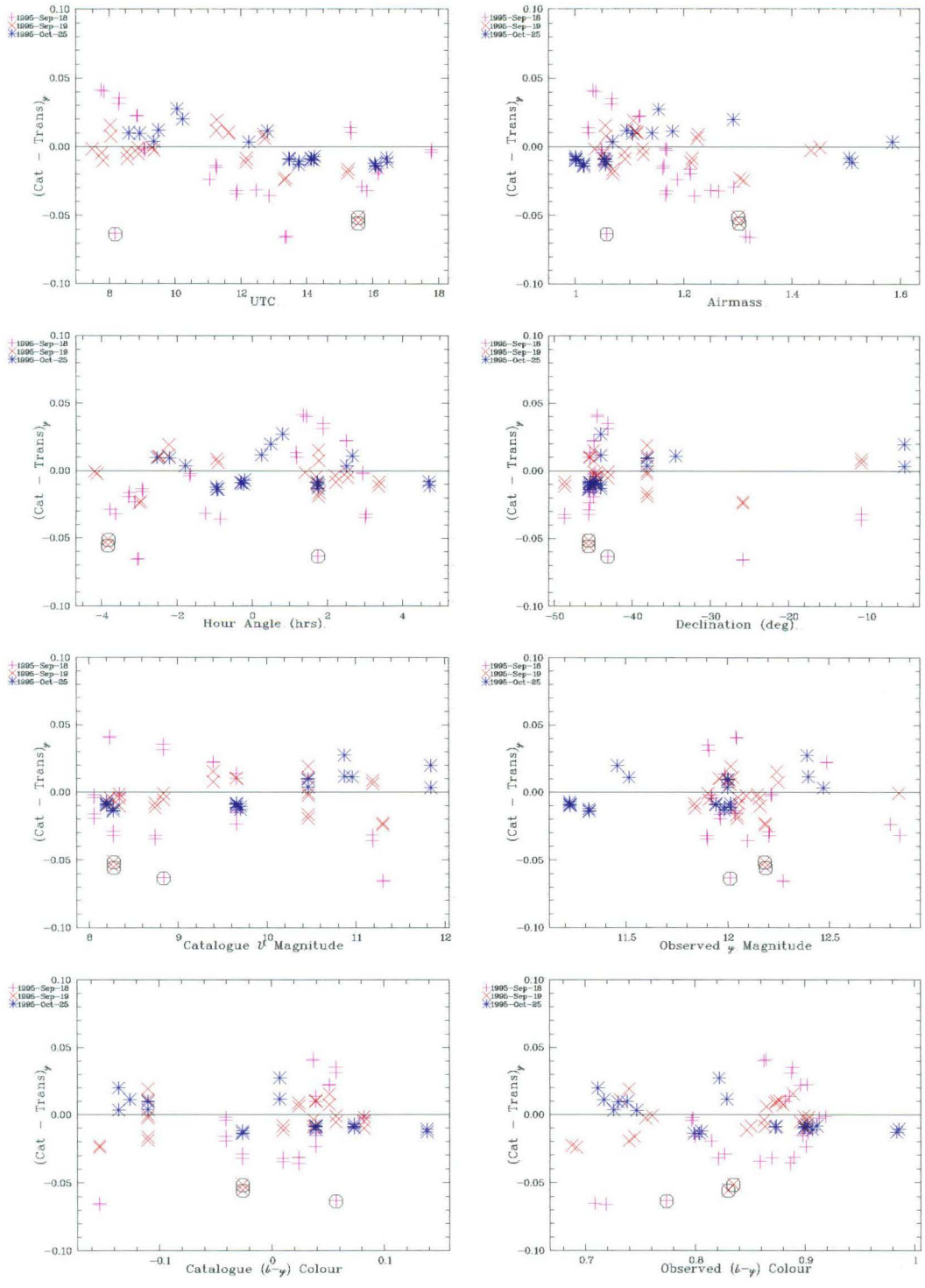

Figure B.18: Residuals between the transformed y magnitudes and the catalogue $y = V$ magnitudes plotted against relevant properties. Circled points indicate those observations excluded from the final determinations of the transformation equation coefficients.

B.5 HV 982 reductions - Representative raw and cleaned images

Representative images and MIDAS perspective-plots of HV 982 are presented in the following six figures. The 100×100-pixel regions centered on the Optimum-Target-Position adopted for the given nights for both the raw flat-fielded frames and the cleaned frames which have had the successfully fitted stars subtracted. The images have six circles centered on the stellar centroids reported by DAOPHOT II overplotted. The circles correspond to the smallest (12.10 pixels = 15.″0), the adopted (19.36 pixels = 24.″0) and the next larger (20.16 pixels = 25.″0) and the largest (30.24 pixels = 37.″5 apertures for which synthetic aperture photometry was extracted and finally the inner and outer radii of the sky annulus (at 35.0 pixels = 56.″8 and 45.0 pixels = 73.″0). The flatness of the subtracted images and perspective-plots is indicative of the success of the fitting procedure. Figures in all six colours (*uvbyVI*) are provided for this the most crowded of the three programme star fields.

HV 982, V, 1994-Dec-26

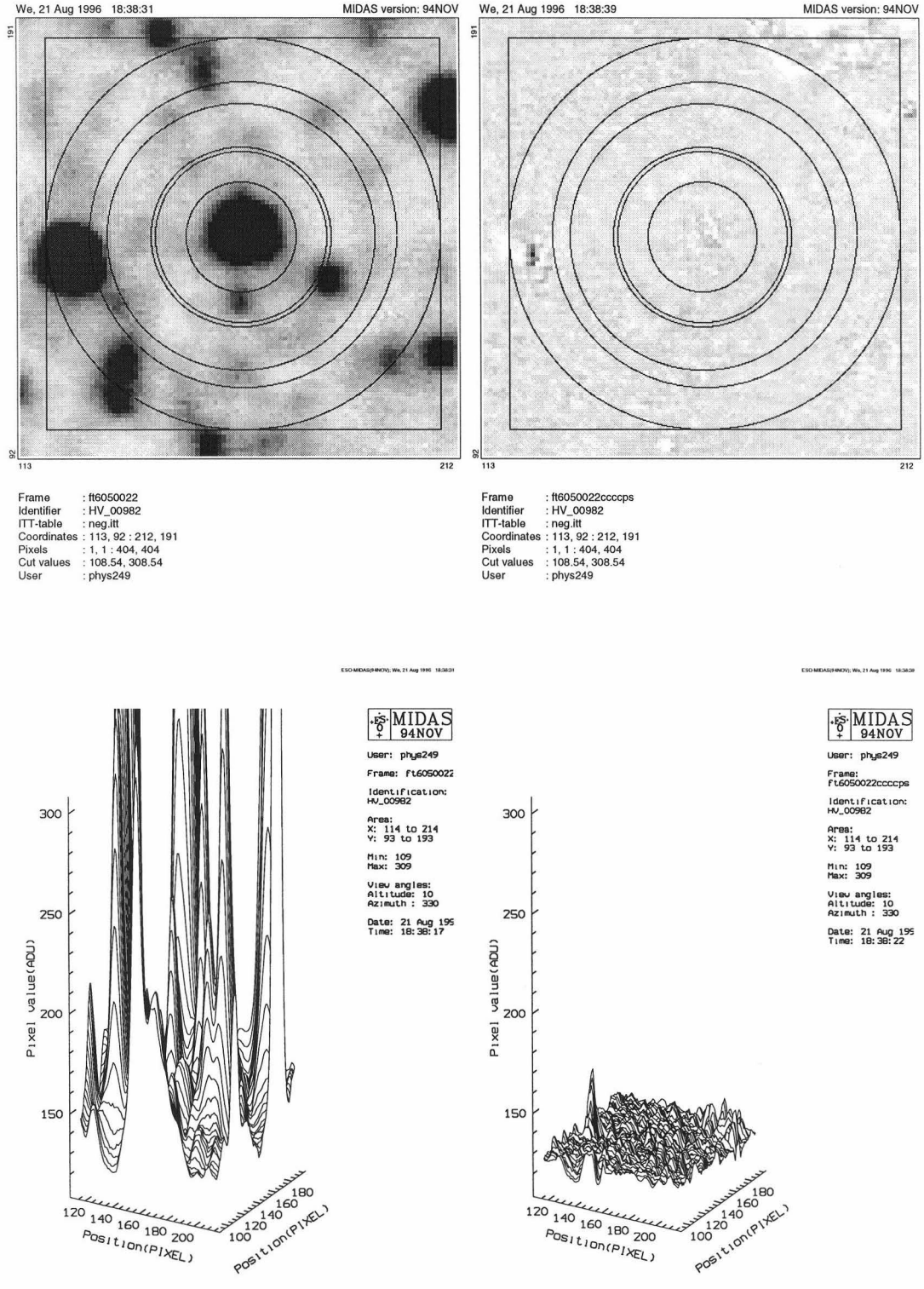

Figure B.19: Image and perspective plot views of T6050022, raw and cleaned. This is the first V frame of HV 982 from the night of 1994-Dec-26.

HV 982, *I*, 1994-Dec-26

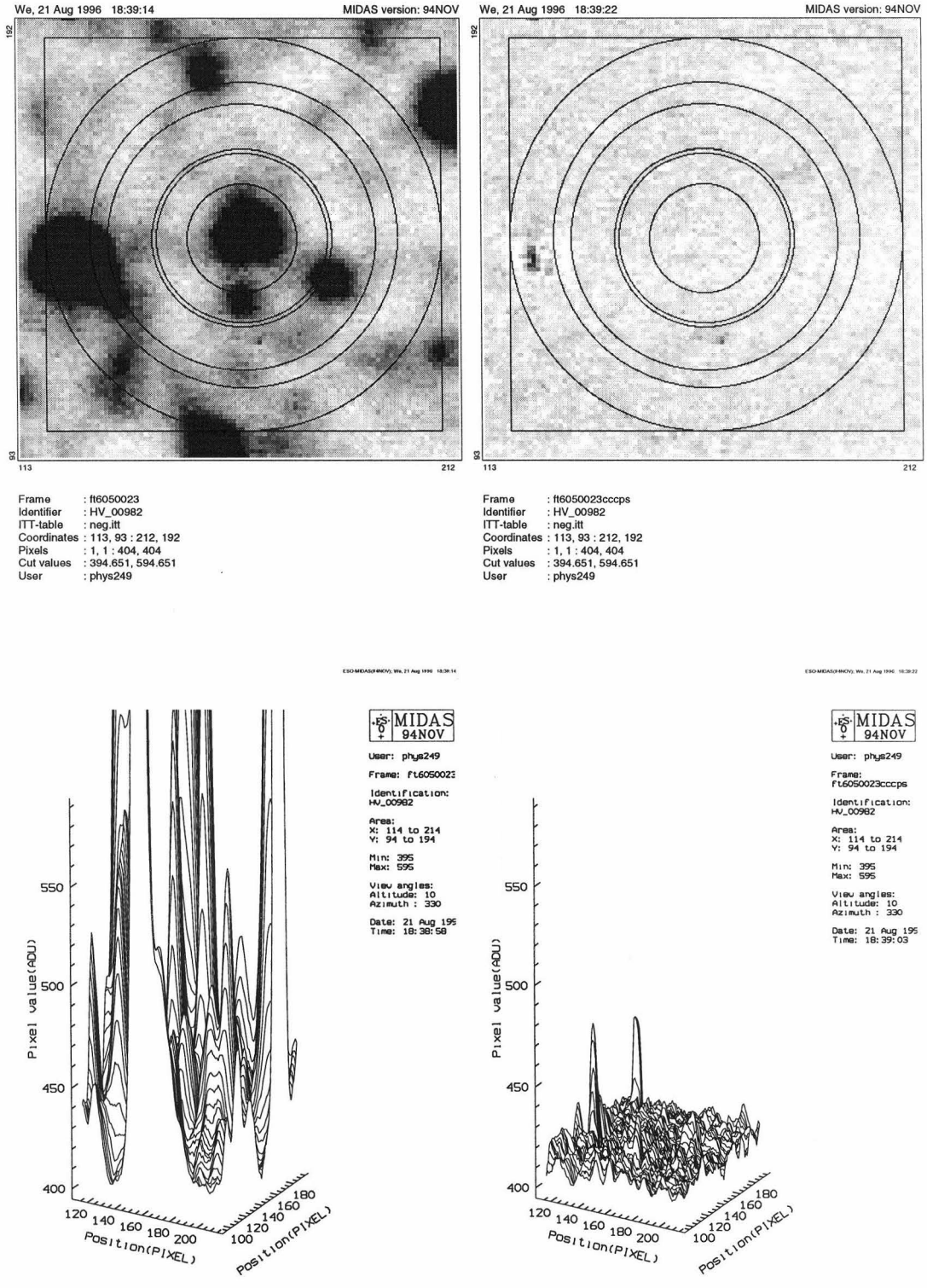

Figure B.20: Image and perspective plot views of T6050023, raw and cleaned. This is the first *I* frame of HV 982 from the night of 1994-Dec-26.

HV 982, u, 1995-Sep-18

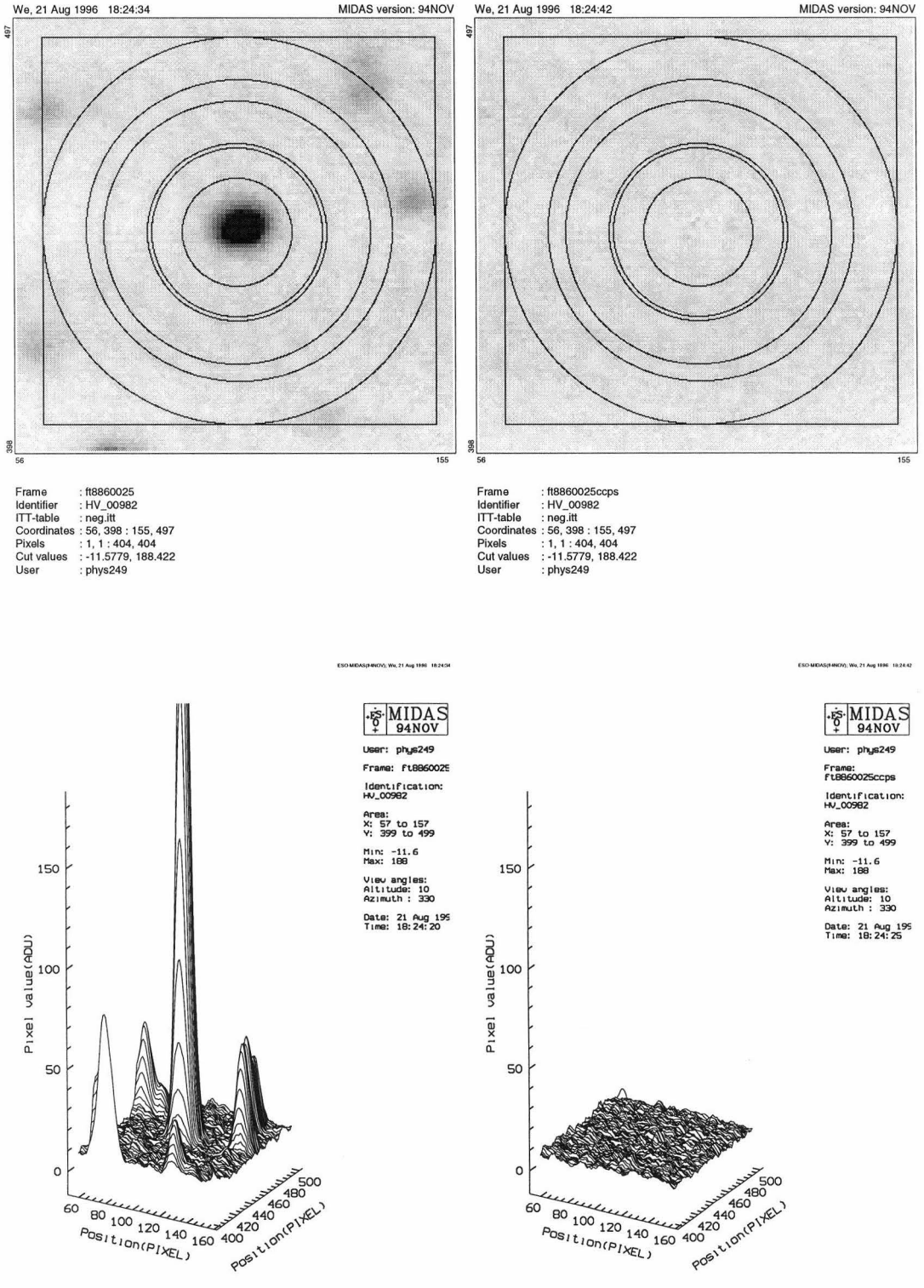

Figure B.21: Image and perspective plot views of T8860025, raw and cleaned. This is the u frame of HV 982 from the night of 1995-Sep-18.

HV 982, v, 1995-Sep-18

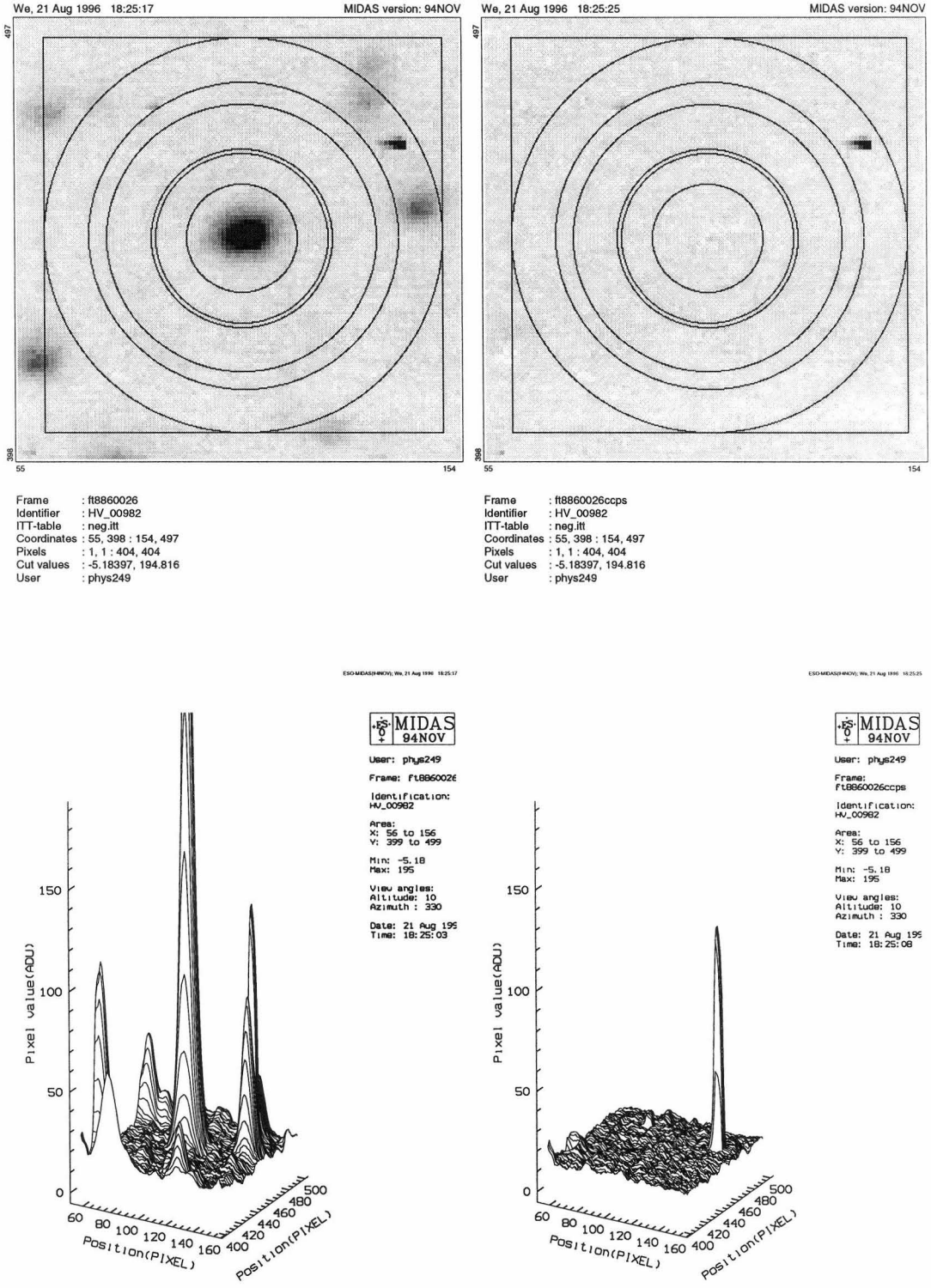

Figure B.22: Image and perspective plot views of T8860026, raw and cleaned. This is the v frame of HV 982 from the night of 1995-Sep-18. The cosmic ray in the sky annulus does not significantly alter the reported sky value.

HV 982, *b*, 1995-Sep-18

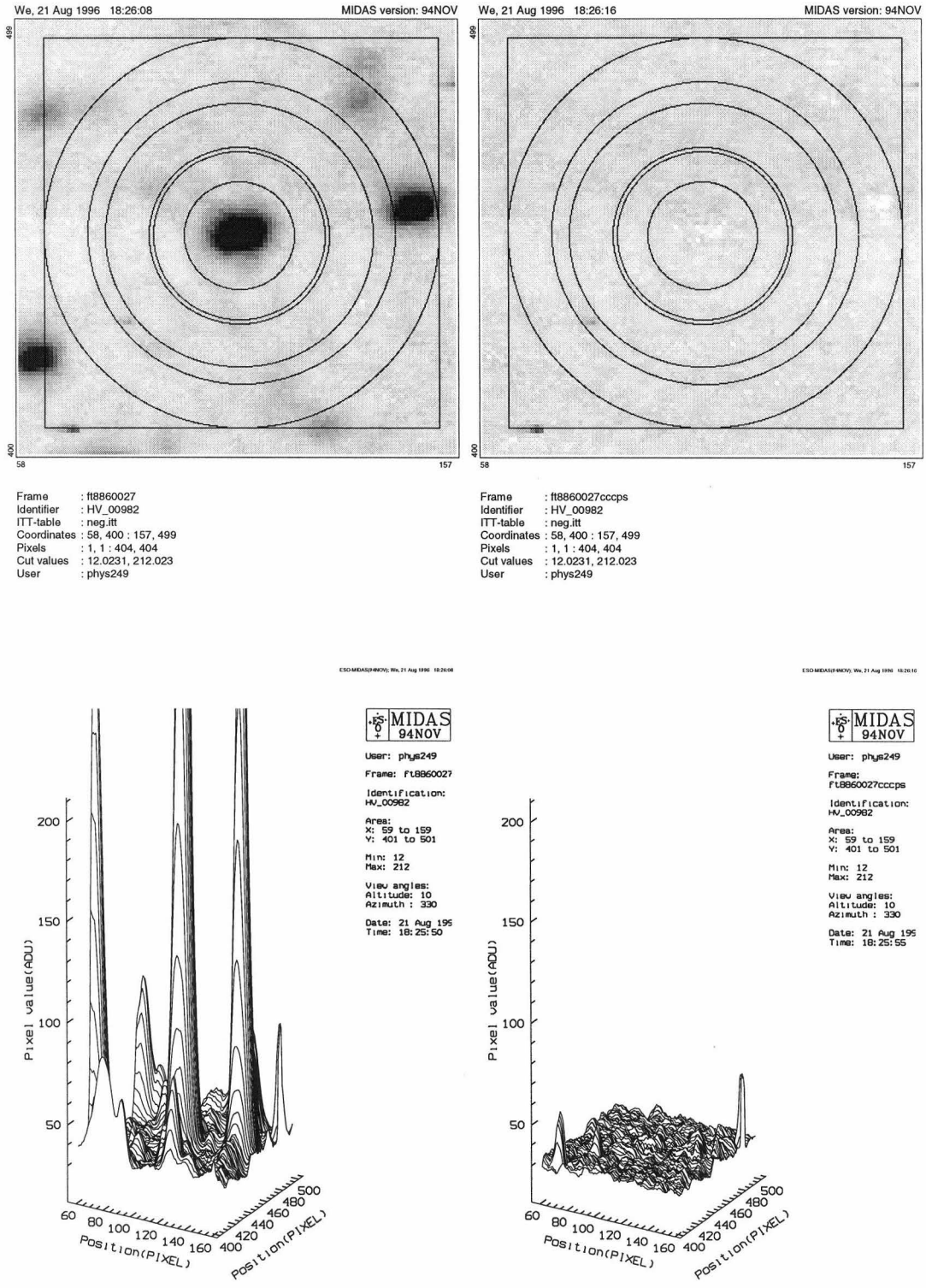

Figure B.23: Image and perspective plot views of T8860027, raw and cleaned. This is the *b* frame of HV 982 from the night of 1995-Sep-18.

HV 982, y, 1995-Sep-18

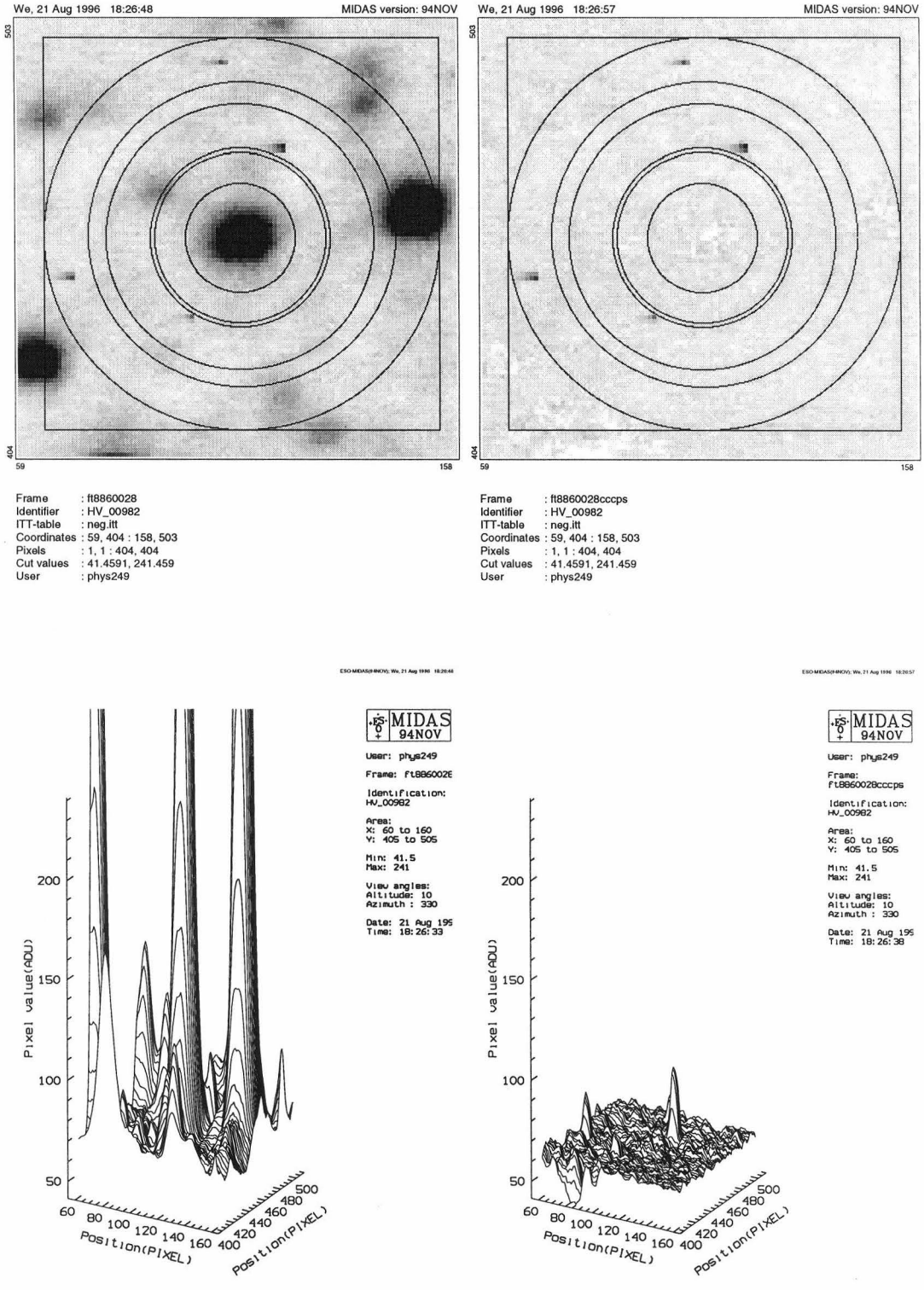

Figure B.24: Image and perspective plot views of T8860028, raw and cleaned. This is the y frame of HV 982 from the night of 1995-Sep-18. The cosmic ray just outside the 25.″0 aperture does not contribute to the measured magnitude for smaller apertures (including the adopted 24.″0 photometry) and the cosmic rays in the sky annulus do not significantly affect the sky measurement.

B.6 HV 1620 reductions - Representative raw and cleaned images

Representative V and I images and MIDAS perspective-plots of HV 1620 are presented in the following two figures. Figures for *uvby* are not presented in this less crowded, as compared with HV 982, field. The 100×100-pixel regions centered on the Optimum-Target-Position adopted for the given nights for both the raw flat-fielded frames and the cleaned frames which have had the successfully fitted stars subtracted. The images have six circles also centered on Optimum-Target-Position. The circles correspond to the smallest (12.10 pixels = 15.″0), the adopted (19.36 pixels = 24.″0) and the next larger (20.16 pixels = 25.″0) and the largest (30.24 pixels = 37.″5 apertures for which synthetic aperture photometry was extracted and finally the inner and outer radii of the sky annulus (at 35.0 pixels = 56.″8 and 45.0 pixels = 73.″0). The stellar centroids maybe offsett from the Optimum-Target-Position, however the final synthetic aperture photometry was calculated with the apertures centered at the stellar centroids determined during the cleaning procedure. The indicated circles thus do not correspond exactly to the apertures used to determine the photometry, but given the small deviations of the stellar centroids from the Optimum-Target-Position, the difference is in most cases negligible, at least for the larger apertures. The flatness of the subtracted images and perspective-plots is indicative of the success of the fitting procedure. The perspective-plots of the cleaned images are shown at a 100× greater vertical scale compared to the perspective-plots of the raw frames. The following four figures present image and perspective-plots for the *VI* observations of 1995-Sep-02 which have been excluded from the determinations of the standard system photometry for HV 1620. The strong gradient across the first I image (figure B.28) is thought to be due to contamination by the fluorescent lights inside the telescope dome being accidentally switched on during the exposure. No problem is obvious for the second HV 1620 I image for that nigth (figure B.29) but the 0.5 mag systematic error in the transformed I magnitude for this image can not possible be a random error. Similarly there are no obvious problems for either of the V images (figures B.27 and B.30).

HV 1620, V, 1994-Dec-26

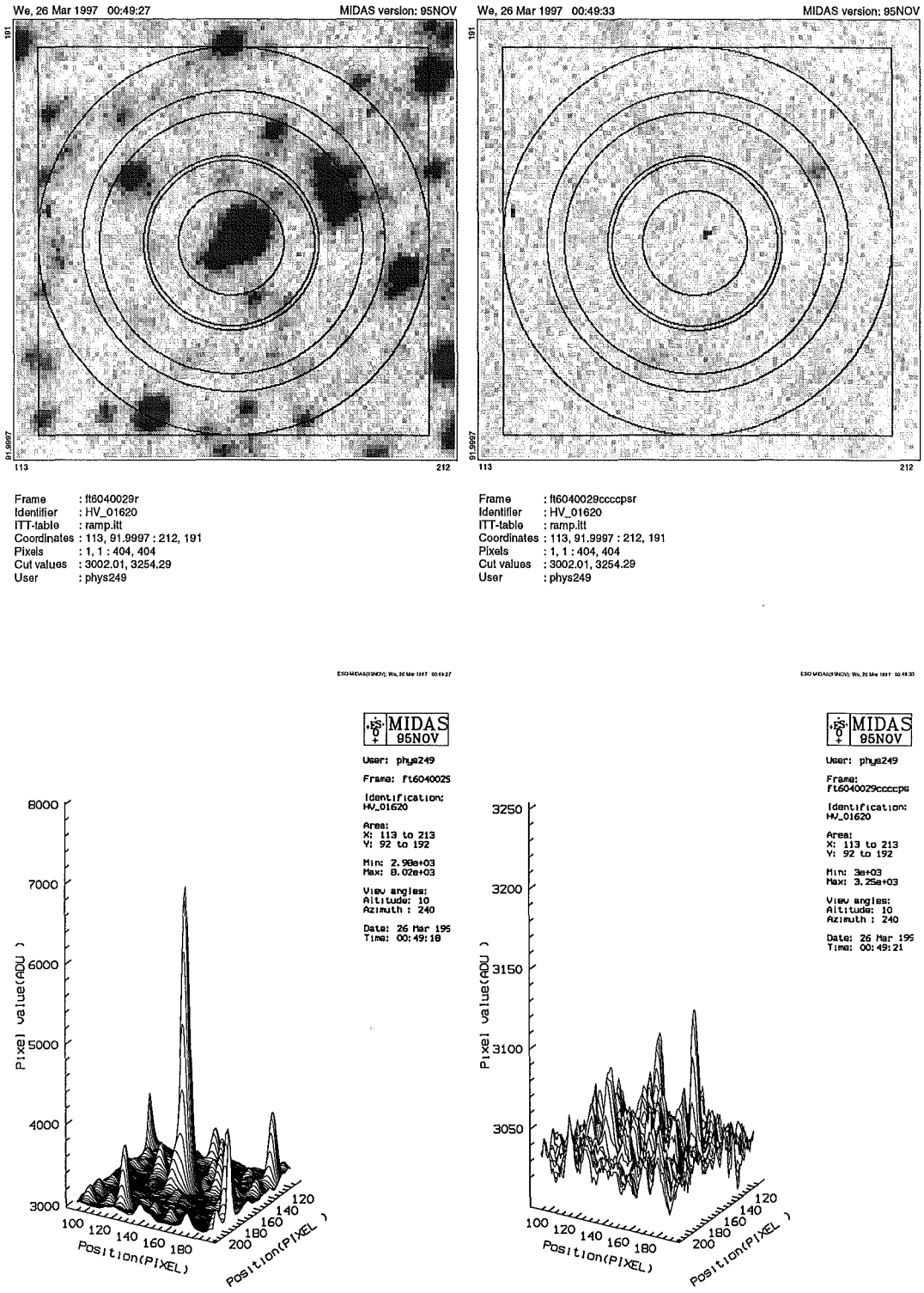

Figure B.25: Image and perspective plot views of T6040029, raw and cleaned. This is first V frame of HV 1620 from the night of 1994-Dec-26.

HV 1620, *I*, 1994-Dec-26

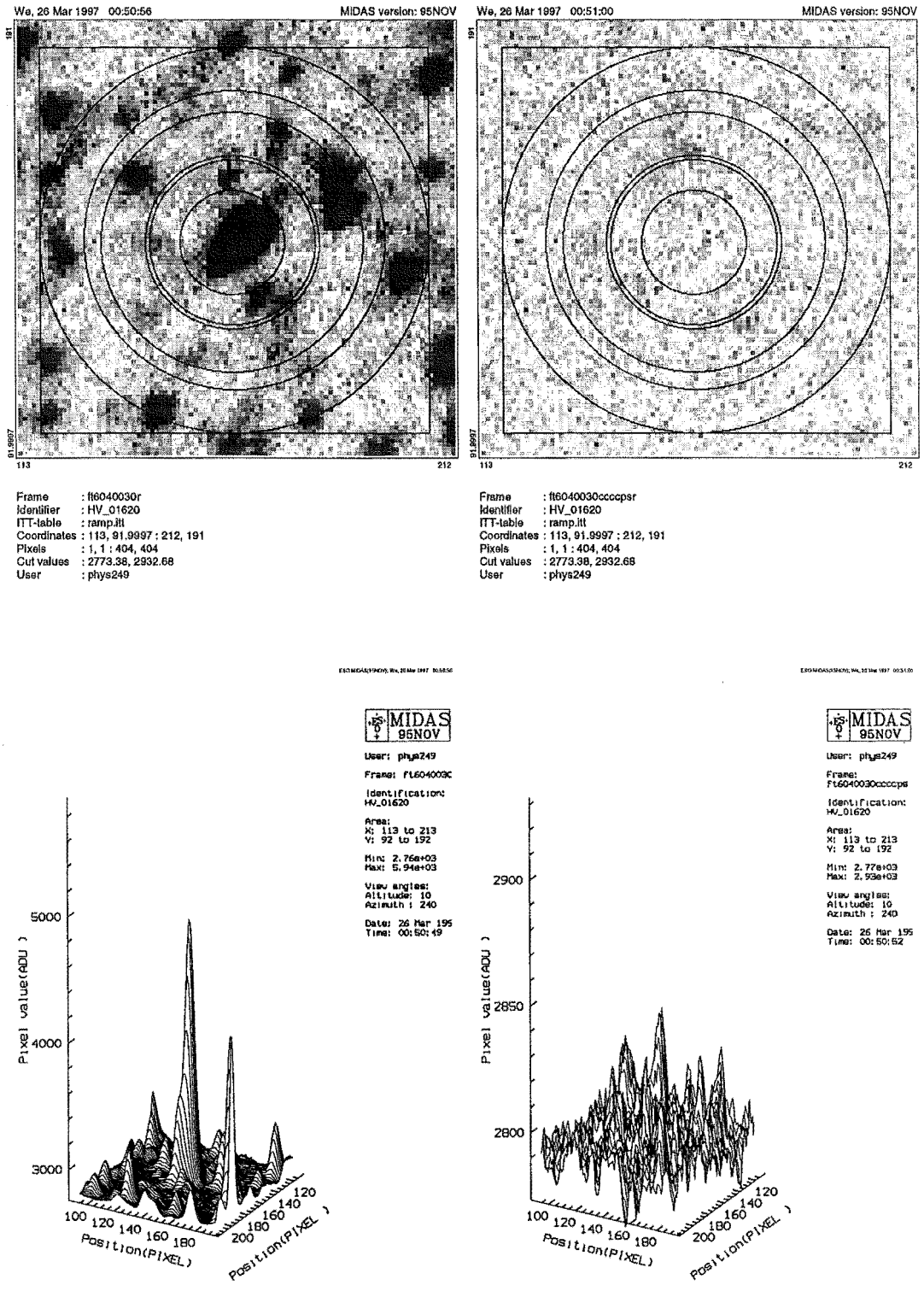

Figure B.26: Image and perspective plot views of T6040030, raw and cleaned. This is first *I* frame of HV 1620 from the night of 1994-Dec-26.

HV 1620, V, 1995-Sep-02

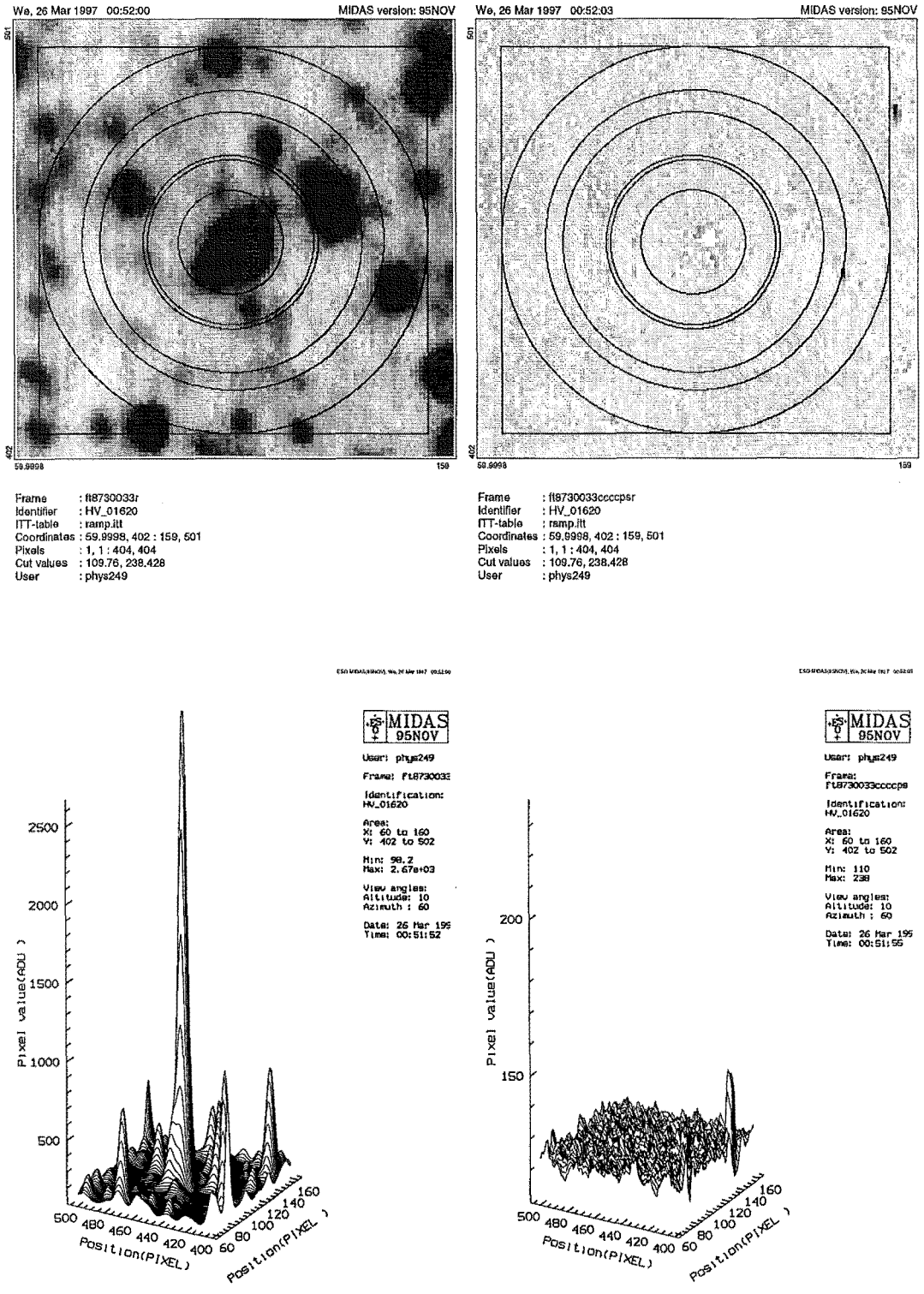

Figure B.27: Image and perspective plot views of T8730033, raw and cleaned. This is first V frame of HV 1620 from the night of 1995-Sep-02.

HV 1620, *I*, 1995-Sep-02

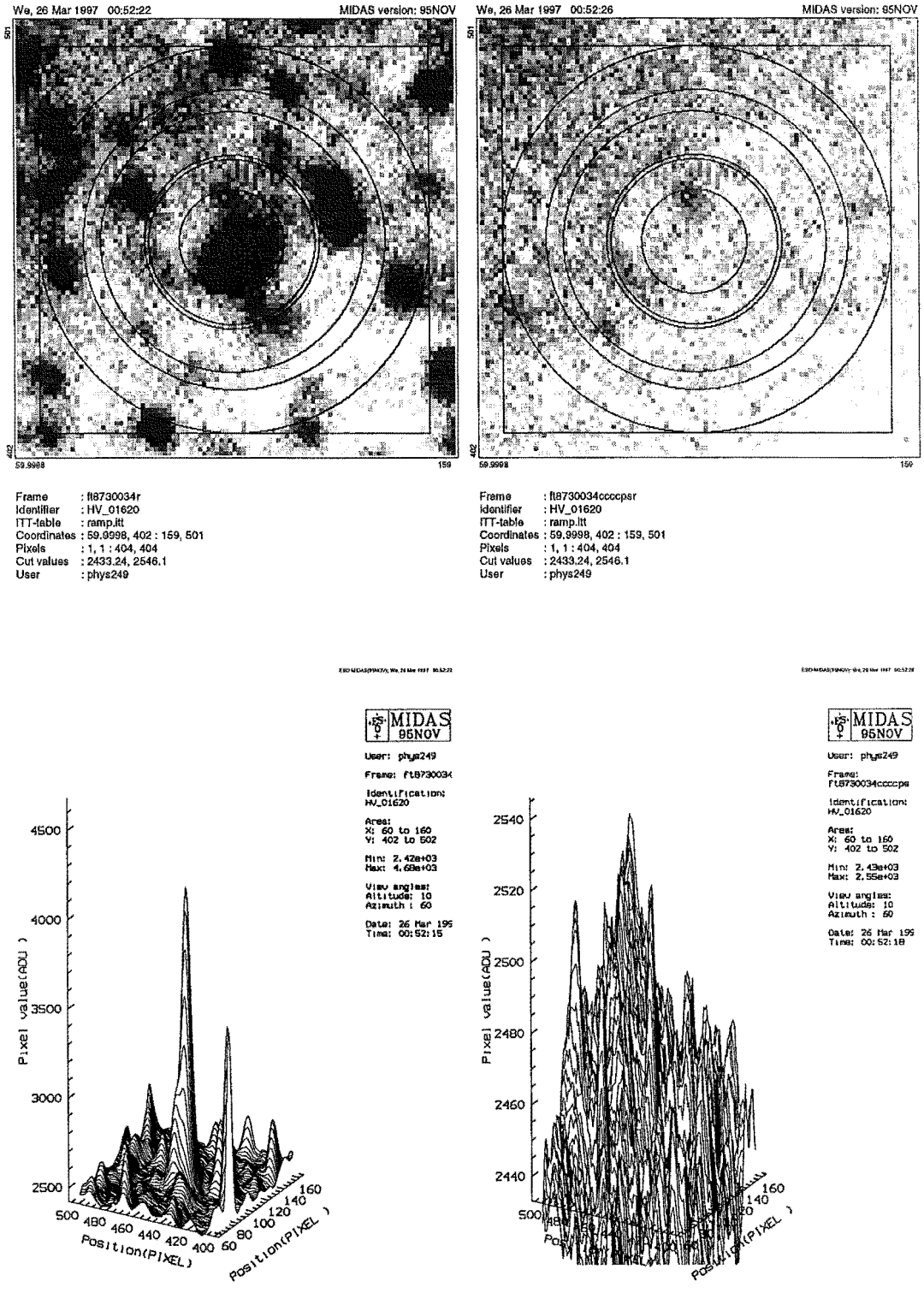

Figure B.28: Image and perspective plot views of T8730034, raw and cleaned. This is first *I* frame of HV 1620 from the night of 1995-Sep-02.

HV 1620, *I*, 1995-Sep-02

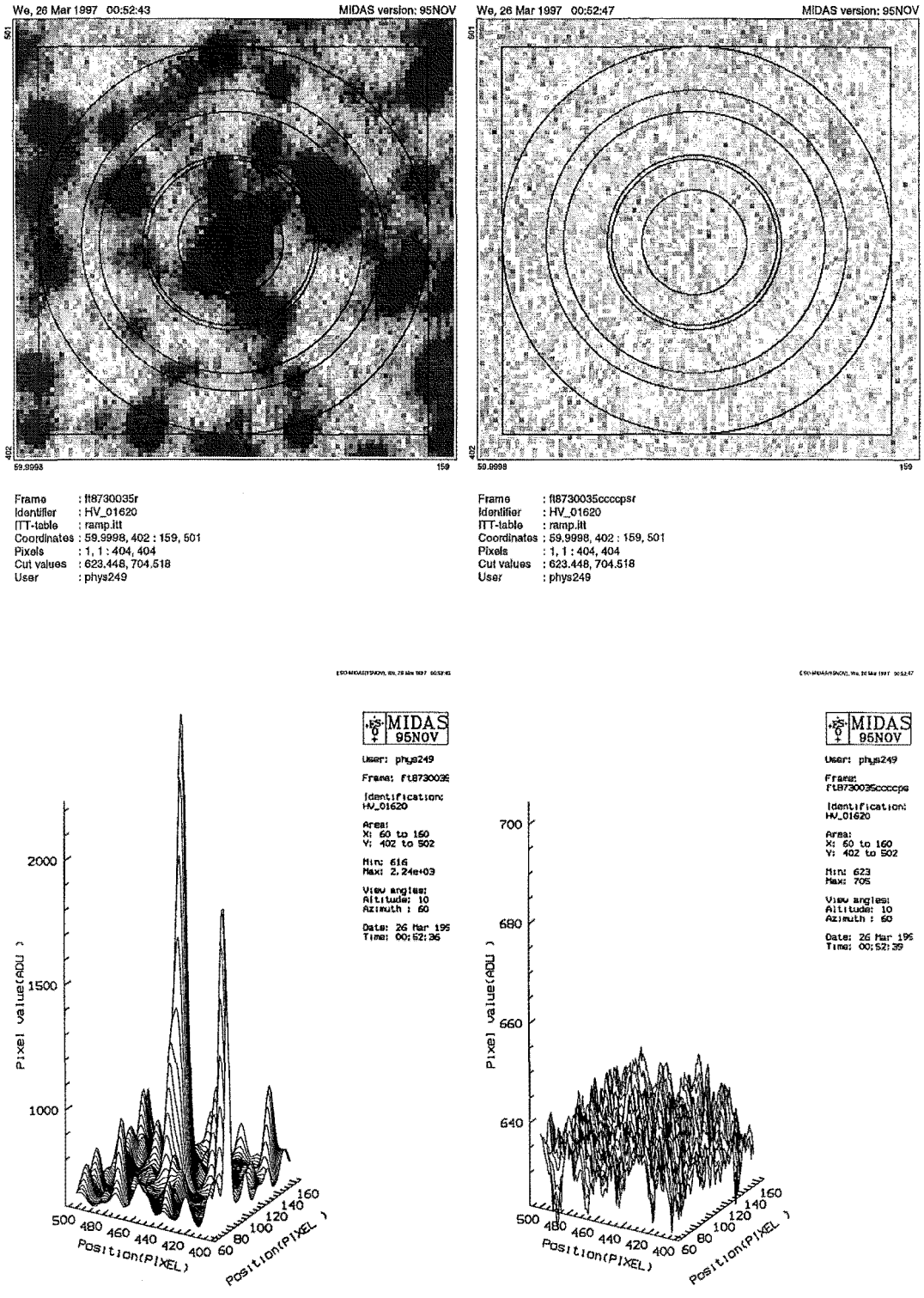

Figure B.29: Image and perspective plot views of T8730035, raw and cleaned. This is second *I* frame of HV 1620 from the night of 1995-Sep-02.

HV 1620, *V*, 1995-Sep-02

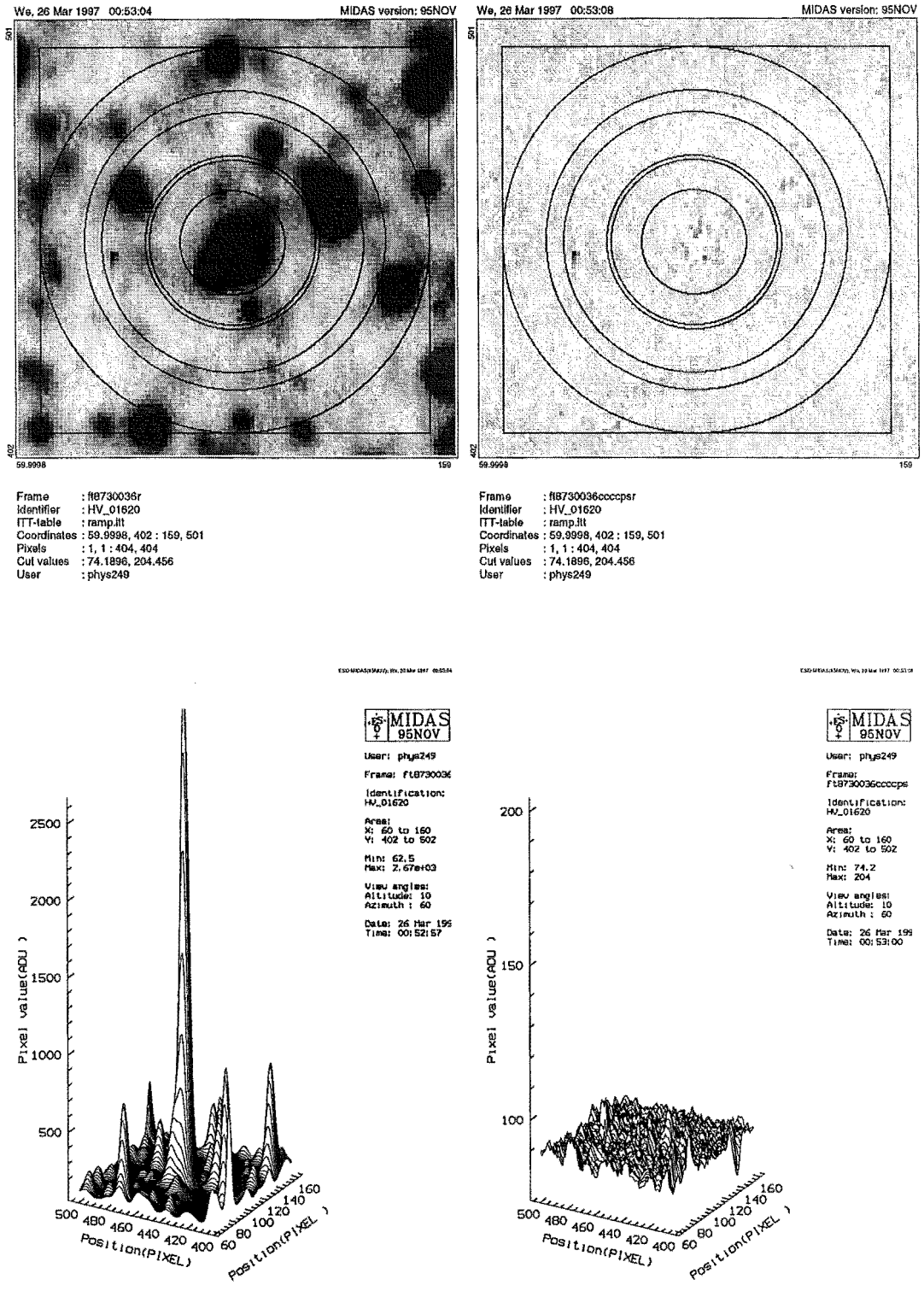

Figure B.30: Image and perspective plot views of T8730036, raw and cleaned. This is second *V* frame of HV 1620 from the night of 1995-Sep-02.

B.7 HV 2241 reductions - Representative raw and cleaned images

Representative V and I images and MIDAS perspective-plots of HV 2241 are presented in the following two figures. Figures for *uvby* are not presented in this, the least crowded of the fields of the three observed programme stars. The 100×100-pixel regions centered on the Optimum-Target-Position adopted for the given night for both the raw flat-fielded frames and the cleaned frames which have had the successfully fitted stars subtracted. The images have six circles centered on Optimum-Target-Position. The circles correspond to the smallest (12.10 pixels = 15.″0), the adopted (19.36 pixels = 24.″0) and the next larger (20.16 pixels = 25.″0) and the largest (30.24 pixels = 37.″5 apertures for which synthetic aperture photometry was extracted and finally the inner and outer radii of the sky annulus (at 35.0 pixels = 56.″8 and 45.0 pixels = 73.″0). The stellar centroids maybe offsett from the Optimum-Target-Position, however the final synthetic aperture photometry was calculated with the apertures centered at the stellar centroids determined during the cleaning procedure. The indicated circles thus do not correspond exactly to the apertures used to determine the photometry, but given the small deviations of the stellar centroids from the Optimum-Target-Position, the difference is in most cases negligible, at least for the larger apertures. The flatness of the subtracted images and perspective-plots is indicative of the success of the fitting procedure. The perspective-plots of the cleaned images are shown at a 100× greater vertical scale compared to the perspective-plots of the raw frames.

The apparently poor fit to HV 2241 (evidenced by the obvious residual remaining after the PSF subtraction) should not significantly affect the extracted synthetic aperture photometry since the main purpose of the PSF fitting and subtraction procedure is to account for the (generally) much fainter field stars near enough that light from their profile wings affects either the aperture summation or the sky calculation. For the fainter stars any systematic error in the fitted PSF is clearly below the noise level in the image (otherwise similar subtraction 'pimples', as Stetson calls them, would be apparent for these stars also).

HV 2241, V, 1995-Sep-02

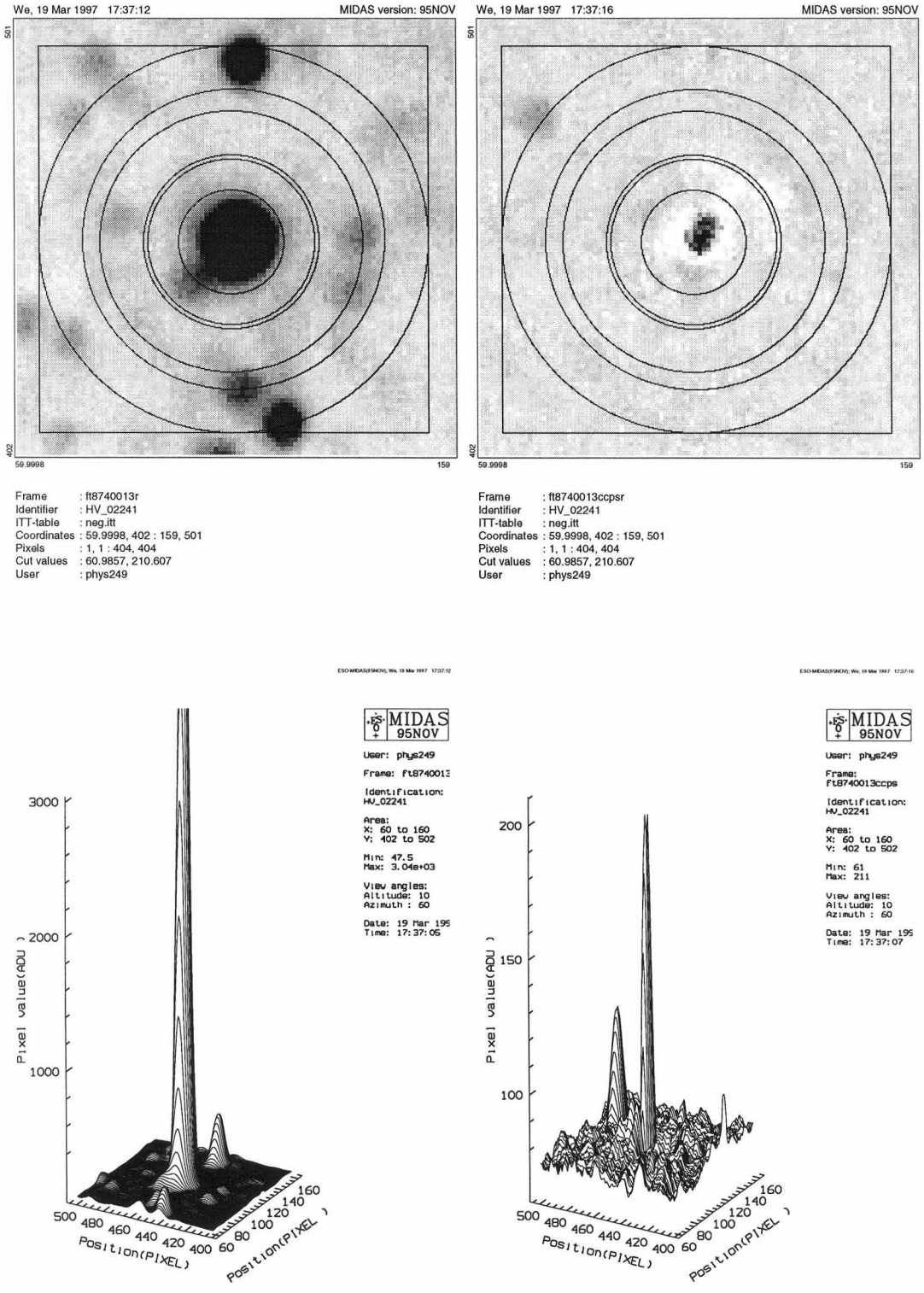

Figure B.31: Image and perspective plot views of T8740013, raw and cleaned. This is first V frame of HV 2241 from the night of 1995-Sep-02.

HV 2241, *I*, 1995-Sep-02

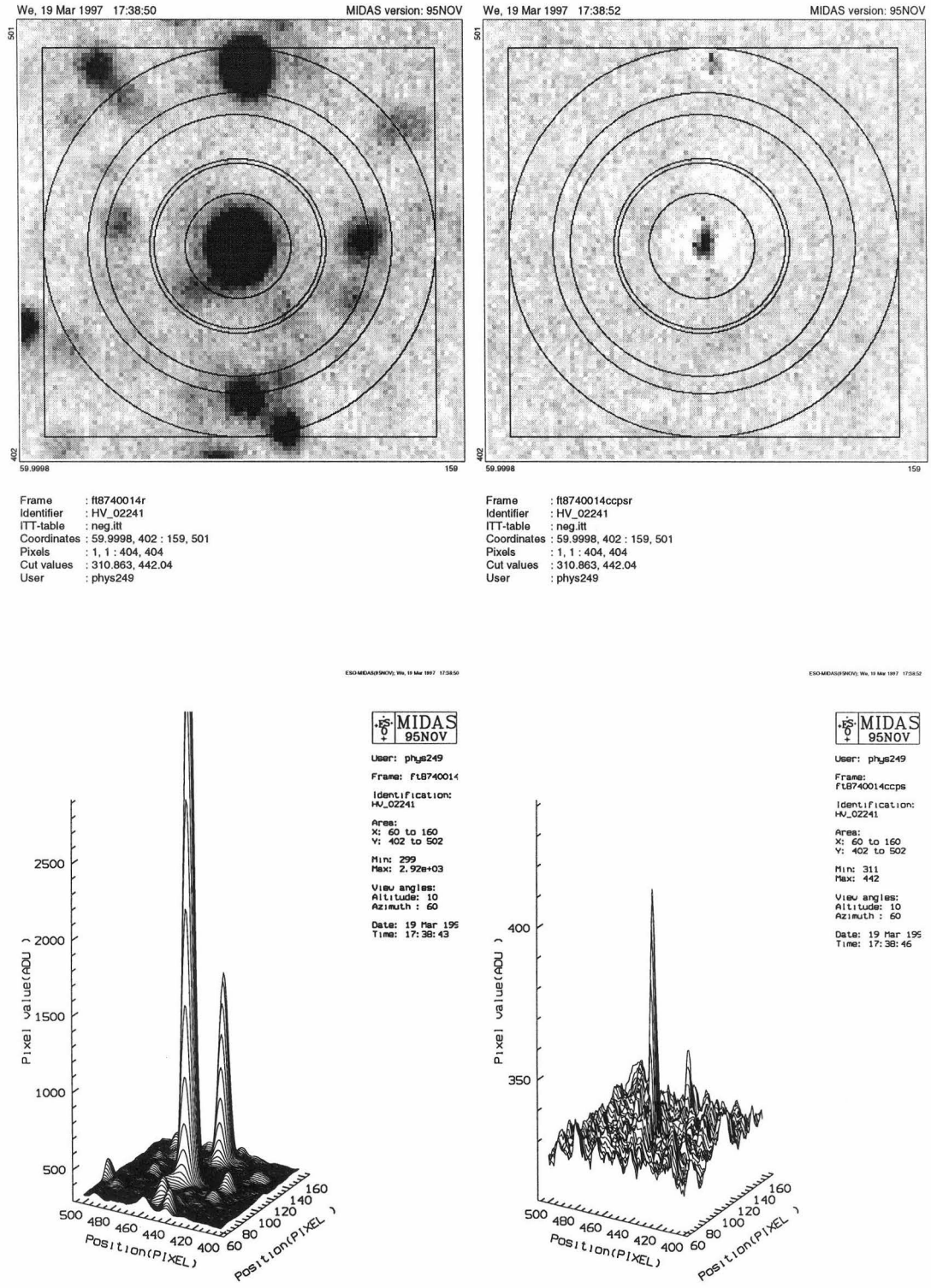

Figure B.32: Image and perspective plot views of T8740014, raw and cleaned. This is first *I* frame of HV 2241 from the night of 1995-Sep-02.

Appendix C

Tinkering with the Wilson and Devinney Synthetic Light Curve Program

A number of alterations have been made to the *WD95* program obtained directly from Wilson in 1995:

- Incorporation of Milone's atmosphere subroutine (which I call `ATMK93`) (Milone, 1996). In the current version of the software (`WD95K93jdp`) there are essentially 3 options for calculation of the atmosphere intensities, blackbodies, Wilson's original Carbon-Gingerich approximations (which are the two options available in the original version of the program), and Kurucz models (made available via the `ATMK93` subroutine).
- A derivative of `LC` (`SS` for Stellar Surface) to permit plotting of the 3-dimensional figures incorporating the grid points used to calculate the models (e.g. figure 5.7).
- A derivative of `LC` (`KF` for Kurucz Flux) which calculates the observed light as a function of wavelength at a given phase, as against `LC` which of course calculates the observed light as a function of phase for a (number of) given wavelength(s). This is used for generation of the spectral flux distributions which can be compared with the observed flux distribution as measured by calibrated photometry and spectrophotometry (see below, section C.1).

In addition to this I have written a suite of software which wraps around the *WD95* program. A major aspect of this is the development of a much more user-friendly format for the I/O file. Input parameters for both `LC` and `DC`, as well as the various derivatives thereof, are taken from the same input file. In addition, this file can be automatically updated with the results of a `DC` iteration. A log of the input parameters and various output results is also maintained.

C.1 Spectral flux distributions

In order to compare the observed flux distributions of the binaries with those of theoretical models it is desirable to compute the theoretical flux distributions as appropriate for binary stars of the characteristics of a given *WD95* solution. In order to do this a certain amount of tinkering with the *WD95* program was necessary. The solution employed was a modification of `LC`, hereafter referred to as `KF`, to compute the observed light for a range of wavelengths at a given phase.

The major problem to be overcome is the setting of the relative flux levels between different wavelengths. In the original versions of the *WD95* program, which permit simultaneous solution of multiple bandpass light curves, the overall flux levels between bandpasses are nonetheless independent. The key to resolving the problem is as follows.

In `LC` the monochromatic luminosity of the system at each wavelength is in fact determined via the user-supplied parameters `L1` (the luminosities of the primary component) and, in certain modes of operation, `L2` – namely setting `IPB` equal to 1). The normal emergent intensities for each wavelength at the pole of each star are then scaled in such a way as to be consistent with these input luminosities and the input effective temperatures. All other calculations are simply made relative to the polar intensities.

Therefore, the appropriate scaling in order to preserve the relative flux levels for each wavelength at which the spectral flux density is to be calculated is simply to scale the polar intensity to the appropriate value for the model atmosphere with the 'observed' polar temperature.

The *WD95* has two internal parameters which specify the polar normal emergent intensities, `SBRH` and `SBRC` (Surface-BRightness-Hot and Surface-BRightness-Cool).

These parameters are first calculated in arbitary units, in subroutine `LUM`:

$$\mathtt{SBR} = \frac{\mathtt{RATPOL} \times \mathtt{XLUM}}{4 \times \mathtt{SUM} \times \mathtt{DELTH} \times \mathtt{DARKIN}} \tag{C.1}$$

where SBR is either SBRH or SBRC depending on which component of the binary is being considered, RATPOL is the ratio of the Stellar-Model-Flux (SMF) to the BlackBody-Flux (BBF) at the pole of the star, XLUM is either L1 or L2 again depending on which component of the binary is being considered, SUM is the integrated flux over the stellar surface, DELTH is a factor arising from the integration over the surface and DARKIN is the correction factor (hereafter LD) from SMF to Stellar-Model-normal-emergent-Intensity (SMI) at the pole – in the notation of section D.4.1, SMF is F_λ, SMI is $I_\lambda(1)$ and LD is given by the multiplicative factor of $I_\lambda(1)$ in equations D.18, D.19, D.20 and D.21, depending on which limb-darkening law is being used.

When the *WD95* control integer IPB is set to 1 the above is used to calculate both SBRH and SBRC, but if IPB is set to 0 then above is only used to calculate SBRH and SBRC is derived from SBRH and the input effective temperatures as folows. First, for convenience, rewriting RATPOL as $\mathrm{SMF_P/BBF_P}$ and DARKIN as $\mathrm{LD_P}$ then,

$$\mathrm{SBRH} = \frac{\left(\frac{\mathrm{SMF_{P,1}}}{\mathrm{BBF_{P,1}}}\right) \times \mathrm{L1}}{4 \times \mathrm{SUM_1} \times \mathrm{DELTH} \times \mathrm{LD_{P,1}}}. \tag{C.2}$$

From the *WD95* computer program, SBRC is calculated by,

$$\mathrm{SBRC} = \frac{\mathrm{RATCH} \times \mathrm{SBRH} \times \mathrm{DHFAC} \times \left[\exp\left(\frac{\mathrm{XLUMP}}{\mathrm{TPOLH}}\right) - 1.\right]}{\mathrm{DCFAC} \times \left[\exp\left(\frac{\mathrm{XLUMP}}{\mathrm{TPOLC}}\right) - 1.\right]} \tag{C.3}$$

where RATCH is the ratio of the Stellar-to-Blackbody flux ratio at the pole of the cool star to the Stellar-to-Blackbody flux ratio at the pole of the hot star (i.e. $(\mathrm{SMF_{P,2}/BBF_{P,2}})/(\mathrm{SMF_{P,1}/BBF_{P,1}})$), DHFAC and DCFAC are the polar flux-to-intensity limb-darkening correction factors for the hot and the cool stars respectively (i.e. $\mathrm{LD_{P,1}}$ and $\mathrm{LD_{P,2}}$), XLUMP is equal to $hc/\lambda kT$ and therefore the exponential factors give the ratio of the blackbody fluxes for blackbodies at temperatures of TPOLH and TPOLC, the effective temperatures of the atmospheres of the two stars at their poles (i.e. $\mathrm{BBF_{P,2}/BBF_{P,1}}$). So rewriting equation C.3 we obtain,

$$\mathrm{SBRC} = \frac{\left(\frac{\mathrm{SMF_{P,2}}}{\mathrm{BBF_{P,2}}}\right)}{\left(\frac{\mathrm{SMF_{P,1}}}{\mathrm{BBF_{P,1}}}\right)} \times \frac{\left(\frac{\mathrm{SMF_{P,1}}}{\mathrm{BBF_{P,1}}}\right) \times \mathrm{L1}}{4 \times \mathrm{SUM_1} \times \mathrm{DELTH} \times \mathrm{LD_{P,1}}} \times \frac{\mathrm{LD_{P,1}} \times \mathrm{BBF_{P,2}}}{\mathrm{LD_{P,2}} \times \mathrm{BBF_{P,1}}} \tag{C.4}$$

Now since SMI = SMF/LD, if SBRH is set to be equal to $\mathrm{SMI_{P,1}}$ then from equation C.2 it is obvious that,

$$\frac{\mathrm{L1}}{4 \times \mathrm{BBF_{P,1}} \times \mathrm{SUM_1} \times \mathrm{DELTH} \times \mathrm{LD_{P,1}}} = 1 \tag{C.5}$$

and thus

$$\mathrm{SBRC} = \frac{\left(\frac{\mathrm{SMF_{P,2}}}{\mathrm{BBF_{P,2}}}\right)}{\left(\frac{\mathrm{SMF_{P,1}}}{\mathrm{BBF_{P,1}}}\right)} \times \mathrm{SMI_{P,1}} \times 1. \times \frac{\mathrm{LD_{P,1}} \times \mathrm{BBF_{P,2}}}{\mathrm{LD_{P,2}} \times \mathrm{BBF_{P,1}}} = \frac{\frac{\mathrm{SMF_{P,2}}}{\mathrm{LD_{P,2}}}}{\frac{\mathrm{SMF_{P,1}}}{\mathrm{LD_{P,1}}}} \times \mathrm{SMI_{P,1}} = \frac{\mathrm{SMI_{P,2}}}{\mathrm{SMI_{P,1}}} \times \mathrm{SMI_{P,1}} = \mathrm{SMI_{P,2}} \tag{C.6}$$

as one would hope!

As indicated in the above equations, the basic calculation of the lights and the luminosities from the two model stars of the *WD95* model relies, in the first instance, on a blackbody approximation. To improve upon this a subroutine must be provided which calculates the ratio of the 'real' Stellar-Flux (i.e. the Stellar-Model-Flux) to the BlackBody-Flux.

The standard version of the program (*WD95*) has an option for using approximation polynomials, which are fits to the Carbon and Gingerich (1969) fluxes via the subroutine ATM. A version of the program obtainable from E.F. Milone (*WD93K93*) has a modified version of the ATM subroutine – which will be referred to here after as *ATMK93* – which interpolates in user-supplied data files based on the Kurucz Models (Kurucz, 1993). In June of 1995 the MJUO MCEB group obtained a copy of *WD95* directly from Wilson and in early 1996 a copy of *WD93K93* from Milone. The *ATMK93* subroutine was integrated into the *WD95* program – giving a new version *WD95K93* – in such a way that both of the above two methods are retained (control parameters IFAT1 and IFAT2 can be set to either 0 for blackbodies, 1 for the Wilson Approximation or 2 for the Milone/Kurucz adaptation).

However, since the use of *ATMK93* to compute spectral fluxes would have required the computation of a data file for each wavelength of interest (perhaps 1221 wavelenghts if one wished to compute flux distributions at each of the Kurucz model wavelengths), and since the *WD95* program itself was designed for only 17 descrete wavelengths anyway, another ATM subroutine was written to perform the necessary

calculations for an arbitrary number of wavelengths. The new version of the ATM – *ATMKMFULL* – requires three input files, the first of which lists the wavelengths and record number of the wavelengths, the second of which lists the effective temperature and gravity of each of the Kurucz models, and finally the actual limb-darkening Kurucz models which list the normal emergent intensities and fractional limb-darkening coefficients at each of the wavelengths listed in the first file, for each of the models listed in the second. While the first two files are trivial in size, the third is some 50 Mbytes for the usual 410 Kurucz atmosphere models.

For a given input effective temperature and wavelength, along with the mean effective gravity of the star, the subroutine computes the Kurucz-Model-Flux to BlackBody-Flux ratio and the limb-darkening coefficients.

As a test of the new program, I constructed a *WD95* model binary system consisting of two stars whose effective temperatures and mean gravities were equal to those of the Kurucz (1993) 'Vega' model (namely CDROM13/FLUXES/FVEGA.PCK with $T_{\rm eff} = 9\,550$ K and $\log[g] = 3.95$). The Surface potentials (Ω_1 & Ω_2) were set to 30.000 so that the radii of the stars would be small compared with their separation, i.e. the system would be well detached, and hence tidal distortions and variations of the local effective surface gravity and effective temperature would be insignificant for the model stars, therefore reasonably approximating single, isolated stars. After adjusting the Major-Semi-Axis so that the mean radii of the two components was equal to the observed radius of Vega, $2.76\,\mathcal{R}_\odot$ (Code et al., 1976), the orbital period was adjusted so as to give the desired $\log[g]$. The orbital eccentricity was set to zero and the orbital inclination to 90° so that at mid eclipse, the total light would be from just one of the stars, i.e. what one would expect to recieve from Vega itself. The remaining parameters were set as appropriate – the full *WD95* parameter set for the model is given below.

Figure C.1 plots the spectral flux distribution obtained from the modified *WD95* program. Also shown is the FVEGA spectral flux multiplied by $\pi\mathcal{R}^2_{\rm Vega}$, the projected surface area of Vega (in units of the solar radius to be consistent with the output from the *WD95* program). The excellent agreement is self-evident lending confidence that the modified program is at least computing spectral flux densities of the correct form. Furthermore, scaling the FVEGA spectral flux so that the monochromatic flux at $\lambda 555.6$ nm is equal to that observed at Earth (i.e. 3.46×10^{-9} erg s^{-1} cm^{-2} Å^{-1}, Mégessier 1995), the mean distance modulus obtained from individual synthetic *uvbyVI* photometric magnitudes is -0.53 mag, in good agreement with the observed distance modulus of -0.50 ± 0.17 mag (Code et al., 1976).

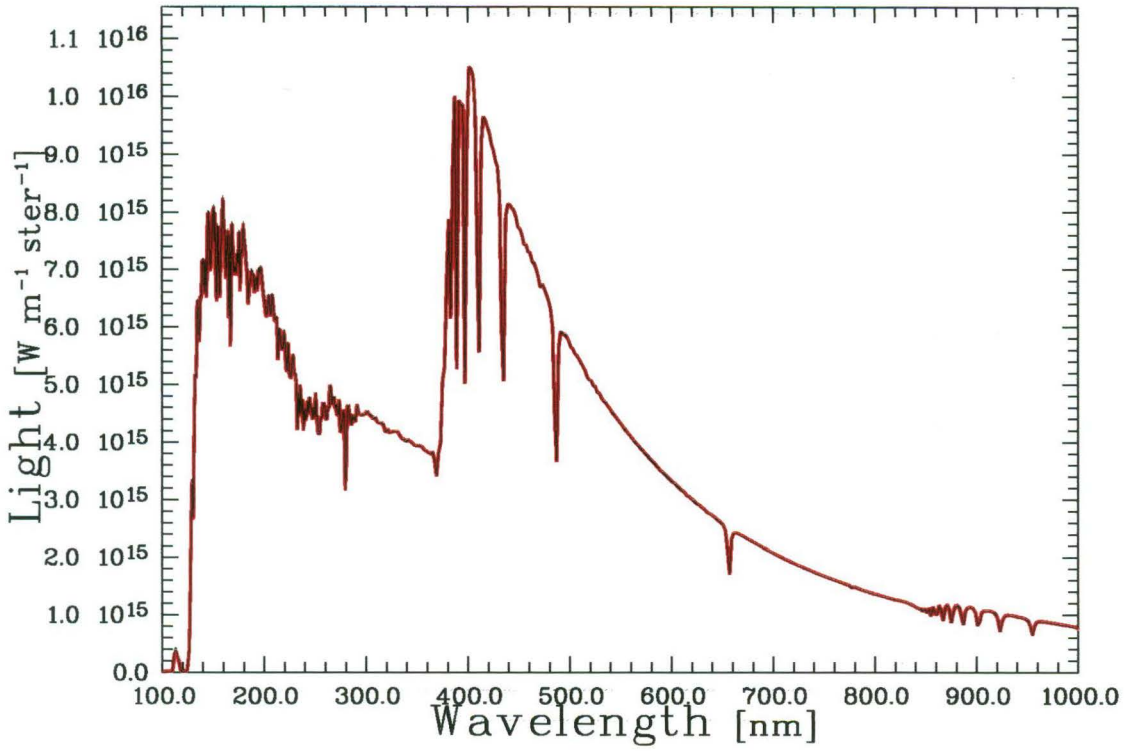

Figure C.1: Theoretical spectral flux densities for Vega. More precisely, plotted is the total light emitted in the direction of an observer, but (somehow) measured *at the surface* of Vega. Two spectra are shown. The thin black line is that obtained from the *WD95* LC derivative KF for a well-detached binary system with two components of the mass, radius and effective surface gravity of Vega at mid eclipse as seen an inclination of 90° (i.e. only one of the Vega-like stars is visible). The thick (red) line is that obtained simply by multiplying the Kurucz theoretical stellar atmosphere for Vega (CDROM13/FLUXES/FVEGA.PCK, $T_{\rm eff} = 9\,550$ and $\log[g] = 3.95$; Kurucz, 1993) by the projected visible area of Vega in units of the solar radius so as to be consistent with the KF output, i.e. $\pi\mathcal{R}^2_{\rm Vega}/\mathcal{R}^2_\odot = \pi\times 2.76^2$ (Code et al., 1976).

***WD* IO file C.1**: Parameter set for a *WD95* model binary star consisting of two stars with the $T_{\rm eff} = 9\,550$ and $\log[g] = 3.95$ of the Kurucz (1993) CDROM13/FLUXES/FVEGA.PCK Vega model and the observed radius of Vega ($2.76\mathcal{R}_{\odot}$, Code, 1976).

```
Parameter File for dcjob and lcjob for : Vega : Two stars of Vega R and Log[g]
=========================================
 MODE = 02     IPB =  0     IPB 0/1 Couple/Decouple L & T
IFAT1 =  2  IFAT2 =  2     Atmospheres 0=BlackBody 1=Wilson's Approx' 2=Kurucz Models
   N1 = 30     N2 = 30     Grid Points
  N1L = 15    N2L = 15     Grid Points (Course Grid)
 MREF =  1   NREF =  1     Reflection Effect
ICOR1 =  0  ICOR2 =  0     Proximity Effect Corrections 1) apply 0) don't
 ISYM =  1     LD =  2     Asym/symetrical deriv's & LD model

Period = 37.32690   E(MJD) =    0.000
     SMAxis =  80.052   (C)  (Scaled SMAxis : *******)
        ECC =   0.0000  (C)
  Long Peri =  90.000   (C)
 Phase Off' =   0.0000  (C)
Inclination =  90.000   (C)
      M2/M1 =   1.00000 (C)
         T1 =   0.9550  (C)      T2 =   0.9550 (C)                      Star#1    Star#2
       POT1 =  30.0000  (C)    POT2 =  30.0000 (C)            M/Msun     2.21      2.21
         F1 =   1.000   (C)      F2 =   1.000  (C)      (Mean R)/Rsun    2.46      2.46
         g1 =   1.000   (C)      g2 =   1.000  (C)               Mbol    0.47      0.47
         A1 =   1.000   (C)      A2 =   1.000  (C)       Log[g] (cgs)    3.95      3.95

Light Curves  Number of light curves = 01
============
Name   WL      L1      L2     x1    x2    y1    y2   3rdL  N Sigma   PHN    Zero  Factor
               (C)     (C)    (C)   (C)                 (C)
umj  0.3512  1.0000  1.0000 0.598 0.598 0.241 0.241 0.0000 0 0.1000 .2500  1.995 1.0000

Observed and Model Magnitudes                        Phase of IUE observation :  0.0000
Name      M1L      M1SA     SF1      M2L     M2SA     SF2      M1A2L   M1A2A    M1st    Arat
umj     2.748  19.4742213.653    2.748  19.4742213.653    1.995  18.721   0.000   0.000
Mean Scale Factor : 2213.653

   LDC Guide file :/astro/jdp/mceb/dat/im05k2MJUO.ldc.guide.uonly

LC plots start at : -0.20  finish at :  1.20   step : 0.0025

Radial Velocity Curves
======================
IFVC1 = 0 IFVC2 = 0
THE = .0000  VUNIT = 100.000  VGAMMA = 0.0000 (C)
Name   WL      L1      L2     x1    x2    y1    y2   Sigma

Bolometic LDCs  x1 = 0.000 y1 = 0.000
                x2 = 0.000 y2 = 0.000

Pritchards Weighting Factors
                Start Finish  Weight
1st Phase Range  0.000  0.200  1.000
2nd Phase Range  0.500  0.700  1.000
Number of points to Bin together outside above ranges = 01

Printing
========
ifder = 1   ifm = 1   ifr = 1 ifrad = 0

SPOTS : Number on... Star#1 :   0, Star#2 :   0
=====
 KSPA = 1  NSPA =   1  KSPB = 0  NSPB =   0 ISMV1 = 0 ISMV2 = 0 (Moving Spots)
STAR XLAT (C,C)   XLONG (C,C)  RADSP (C,C)  TEMSP (C,C)

Scratch Pad
===========
K0 = 0 KDISK = 0
```

Appendix D

Synthetic photometry and other related quantities

Synthetic photometry and limb-darkening coefficients derived from theoretical stellar atmosphere models (Kurucz, 1993), hereafter the Kurucz models, have been used extensively throughout this research. The use of synthetic photometry is an integral component of the EROS analysis procedure ($M_{\mathrm{Kurucz},\bar{\lambda}}$), for the investigation of the effects of metallicity on observables such as $(b-y)$ and c_1, e.g. see figure 5.3, in the absolute flux calibration of the standard photometric systems (section 5.5.1), and in the flux fitting procedure (section 5.6). Tabulations of limb-darkeing coefficents have been used for all light curve analysis.

D.1 Intensity, flux, light and luminosity

As pointed out by Wilson (1992b; 1993a) there is often a misinterpretation of the meanings of the quantities of light, luminosity, flux and intensity. This is often not helped by textbooks which only serve to confuse the matter, usually simply for want of providing the appropriate units of the quantity concerned.

- The *spectral intensity* ($\mathcal{I}$) from any source is the amount of energy radiated into a unit area per unit time interval, per unit frequency/wavelength interval, per unit surface area of the radiator. It therefore has units of $[\mathrm{W\,m^{-2}\,m^{-1}\,srad^{-1}}]$ in the wavelength domain or equivalently $[\mathrm{W\,m^{-2}hz^{-1}\,srad^{-1}}]$ in the frequency domain. (For convenience in the following I will consider only the wavelength domain.) For a blackbody at temperature T, the spectral intensity or *Spectral Radiance* (Sterken and Manfroid (1992), pg 120), is given by

$$\mathcal{I}_{BB}(\lambda) = \frac{2hc^2}{\lambda^5}\left[\frac{1}{\exp\left[\frac{hc}{\lambda kT}\right]-1}\right] \quad [\mathrm{W\,m^{-2}\,m^{-1}\,srad^{-1}}]. \tag{D.1}$$

- The *spectral flux* ($\mathcal{F}$) from any source is the total amount of energy radiated per unit time interval, per unit wavelength interval, per unit surface area of the radiator. It therefore has units of $[\mathrm{W\,m^{-2}\,m^{-1}}]$. It is the integral of the spectral intensity over solid angle, i.e.

$$\begin{aligned}\mathcal{F}(\lambda) &= \int_0^{2\pi} \mathcal{I}(\lambda)\cdot\cos[\phi]\cdot d\Omega \quad [\mathrm{W\,m^{-2}\,m^{-1}}], \\ &= \int_0^{\pi}\int_0^{\frac{\pi}{2}} \mathcal{I}(\lambda)\cdot\cos[\phi]\cdot\sin[\phi]\cdot d\phi\cdot d\theta.\end{aligned} \tag{D.2}$$

  For a blackbody where the *spectral intensity* is independant of emergent angle (ϕ) the integration results in a factor of π and so for a blackbody the flux is numerically equal to the intensity times π, i.e.

$$\mathcal{F}_{BB}(\lambda) = \frac{2\pi hc^2}{\lambda^5}\left[\frac{1}{\exp\left[\frac{hc}{\lambda kT}\right]-1}\right] \quad [\mathrm{W\,m^{-2}\,m^{-1}}]. \tag{D.3}$$

  The *astrophysical flux* ($\mathcal{F}_{\mathrm{A}}$) which is commonly tabulated (for example the Kurucz Stellar Atmosphere Models, Kurucz, 1979) is related to the physical flux by $\mathcal{F} = \pi\times\mathcal{F}_{\mathrm{A}}$

- The *light* ($\mathcal{L}$) which has units of $[\mathrm{W\,m^{-1}\,srad^{-1}}]$ is calculated, at least in the context of the *WD* program, by integrating the intensity over the surface of the visible surface of the star.

$$\mathcal{L}(\lambda) = \int_{\substack{\mathrm{Visible}\\ \mathrm{Surface}}} \mathcal{I}(\lambda)\cdot\cos[\phi]\cdot dS \quad [\mathrm{W\,m^{-1}\,srad^{-1}}]. \tag{D.4}$$

  Light is in general a function of orbital phase and of the orbital inclination. For a spherical star whose atmosphere is that of a perfect blackbody, the light is given by πR^2 times the blackbody intensity

(R being the radius of the star), or equivalently, R^2 times the blackbody flux. The observed light is obtained by multiplying the above defined light by $d^2 d\Omega$ where d is the distance between the observer and the star and $d\Omega$ is the angle at the star subtended by the observer's detector.

- The *Luminosity* (L) is the total light emitted by the star into all space and has units [W m^{-1}]. It is the integral of the light over a sphere centered on the star, i.e.

$$\begin{aligned} L(\lambda) &= \int_0^{4\pi} \mathcal{L}(\lambda) \cdot d\Omega \quad [\mathrm{W\,m^{-1}}], \\ &= 2 \int_0^{\pi} \int_0^{\frac{\pi}{2}} \mathcal{L}(\lambda) \cdot \sin[\phi] \cdot d\phi \cdot d\theta. \end{aligned} \tag{D.5}$$

  This is of course equivalent to the more standard definition of luminosity, namely that the luminosity is equal to the integral over the stellar surface of flux at the surface the star, i.e.

$$\begin{aligned} L(\lambda) &= \int_{\mathrm{A}} \mathcal{F}(\lambda) \cdot dS \quad [\mathrm{W\,m^{-1}}], \\ &= 2 \int_0^{\pi} \int_0^{\frac{\pi}{2}} \mathcal{F}(\lambda) \cdot R^2 \cdot \sin[\phi] \cdot d\phi \cdot d\theta. \end{aligned} \tag{D.6}$$

  For a spherical star whose atmosphere is that of a perfect blackbody, the luminosity is given by 4π times the light, $4\pi R^2$ times the spectral flux, or equivalently $4\pi^2 R^2$ times the blackbody spectral intensity.

Note that all of the above quantities are monochromatic. Bolometric luminosities, for example, are simply determined by integrating over λ from zero to infinity.

D.2 The Kurucz Theoretical Stellar Atmosphere Models

All computations involving theoretical stellar atmosphere models have been made with the Kurucz theoretical stellar atmosphere models (Kurucz, 1993). These were obtained directly from R.L. Kurucz on CDROM (`CDROM13`, `CDROM16` and `CDROM17`). Almost all of the calculations have used the `CDROM16` intensities tabulated for 17 values of emergent angle ($\mu = 1.0$ to $\mu = 0.01$)[1] at each of 1221 wavelengths (λ90.9 nm to λ160 μm) for (usually[2]) 410 combinations of $T_{\rm eff}$/log[g] ($3\,500 \leq T_{\rm eff} \leq 50\,000$ K, $0.0 \leq \log[g] \leq 5.0$) at abundances ranging from $[M/H] = +1.0$ to $[M/H] = -1.0$. These tabulations were computed from the microturbulance= 2 km s^{-1} model grids of `CDROM13` using the ATLAS9 program. Where calibration has been reqiured (e.g. see section C.1), the flux distribution for Vega (`CDROM13/FLUXES/FVEGA.PCK`) has generally been employed. This particular model has $T_{\rm eff} = 9550$ K and $\log[g] = 3.95$ and thus corresponds to the $[M/H] = -0.5$, $E(B-V) = 0.000$ model described in Castelli and Kurucz (1994).

D.3 Synthetic photometry

Synthetic photometry for standard *uvby* and *UBVRI* and non-standard MJUO *uvbyVI* and EROS $B_{\rm E}/R_{\rm E}$ bandpasses (see appendix F) has been calculated by convolving the spectral response functions of the bandpasses with the Kurucz stellar atmosphere model spectral flux densities to obtain the bandpass integrated fluxes (i.e. $\mathcal{F}_{\bar{\lambda}}$), i.e.

$$\mathcal{F}_{\bar{\lambda}}(T_{\rm eff}, \log[g]) = \pi \frac{\int_0^{\infty} S_{\bar{\lambda}}(\lambda) \cdot \mathcal{F}_{\rm A}(\lambda, T_{\rm eff}, \log[g]) \cdot d\lambda}{\int_0^{\infty} S_{\bar{\lambda}}(\lambda) \cdot d\lambda}, \tag{D.7}$$

where where $S_{\bar{\lambda}}(\lambda)$ is the spectral response of the bandpass denoted by $\bar{\lambda}$ and $\mathcal{F}_{\rm A}(\lambda, T_{\rm eff}, \log[g])$ is the *astrophysical* spectral flux density for a model atmosphere with effective temperature $T_{\rm eff}$ and effective gravity $\log[g]$ (c.f. equation 7.10). The $\mathcal{F}_{\rm A}$ can either be taken directly from `CDROM13/FLUXES` or alternatively are derived from the `CDROM16` intensities ($\mathcal{I}$) according to,

$$\mathcal{F}_{\rm A}(\lambda, T_{\rm eff}, \log[g]) \equiv 2 \int_0^1 \mathcal{I}(\lambda, T_{\rm eff}, \log[g], \mu) \cdot \mu \cdot d\mu. \tag{D.8}$$

[1] $\mu = \cos[\theta]$ where θ is the emergent angle, i.e. the angle between the line of sight and the normal to the stellar atmosphere surface. Also see section D.4.

[2] Some of the Kurucz models have only 409 $T_{\rm eff}$/log[g] combinations, presumably due to convergence problems, see Kurucz (1993)

Table D.1: Adopted standard system *uvby* (Crawford et al., 1972) and *UBVRI* (Johnson, 1965) photometry for Vega for the calibration of the standard system synthetic photometry. Note $m_y = m_V$ has been adopted.

	mag		mag
V	0.03	m_u	1.442
$B-V$	0.00	m_v	0.195
$U-B$	0.00	m_b	0.034
$V-R$	−0.04	m_y	0.030
$V-I$	−0.06	m_U	0.03
$b-y$	0.004	m_B	0.03
$\mathrm{m_1}$	0.157	m_V	0.03
$\mathrm{c_1}$	1.089	m_R	0.09
		m_I	0.07

All integrations have been computed numerically employing a simple trapezium formula. Bandpass responses at the 1221 wavelengths of the Kurucz models were interpolated between the tabulated response functions using a cubic spline routine. Obviously, response functions were set to zero for all wavelengths shorter and longer than the tabulated minimum and maximum wavelengths for each bandpass.

Now the luminosity (L) of a star of radius $\mathcal{R}$ is given by,

$$L_{\mathrm{Bol}} = 4\pi\mathcal{R}^2\mathcal{F}_{\mathrm{Bol}} = 4\pi\mathcal{R}^2\sigma T_{\mathrm{eff}}^4, \tag{D.9}$$

where $\sigma = 5.67051\times10^{-5}\,\mathrm{erg\,cm^{-2}\,K^{-4}\,s^{-1}}$ is the Stefan-Boltzman constant (Lang, 1992), and $\mathcal{F}_{\mathrm{Bol}}$ is the integrated bolometric flux, obtained from the integral in equation D.7 with $S(\lambda) \equiv 1.0$. The relative error in $\mathcal{F}_{\mathrm{Bol}}$ due to the numerical integration, or equivalently in a stellar bolometric luminosity, is given by,

$$\frac{\Delta\mathcal{F}_{\mathrm{Bol}}}{\mathcal{F}_{\mathrm{Bol}}} = \frac{\Delta L_{\mathrm{Bol}}}{L_{\mathrm{Bol}}} \approx 4\frac{\Delta T_{\mathrm{eff}}}{T_{\mathrm{eff}}} = 4\frac{(\mathcal{F}_{\mathrm{Bol}}/\sigma)^{\frac{1}{4}} - T_{\mathrm{eff}}}{T_{\mathrm{eff}}} \tag{D.10}$$

where T_{eff} is of course the effective temperature of the model. In practice, the error in the bolometric luminosity, resulting from the simple trapezium numerical integration scheme, is typically 1.2 percent with a maximum error of 2.7 percent. There is a systematic tendency to overestimate the luminosity. A more sophisticated numerical integration scheme may reduce the systematic error, and should be investigated.

Calibration of the synthetic photometry, for the standard *uvby* and *UBVRI* systems at least, was achieved by adopting the standard system photometry of Vega (see table D.1) and setting zero points ($c_{\bar{\lambda}}$) according to,

$$m_{\bar{\lambda}} = -2.5\log_{10}[\mathcal{F}_{\bar{\lambda},Vega}] + c_{\bar{\lambda}} \tag{D.11}$$

D.4 Computation of the Limb-Darkening Coefficients

The variation of emergent intensity across the stellar surface, commonly called Limb-Darkening, is well known and understood. For eclipsing binaries, limb-darkening plays an integral rôle in determining the exact shape of the light curve during eclipse phases. Neglecting the effects of variation of local effective gravity (and hence local effective temperature and thus local effective radiant flux intensity) across the surface, which is not unreasonable for well detached systems, in the absence of limb-darkening, the light curve during the eclipses would have straight sides and a flat bottoms (if the eclipses are total, i.e. one component smaller than the other). The limb-darkening thus results in the curvature of the light curve during eclipses.

Modern computer codes for analysis of eclipsing binary light curves, i.e. in the current context the *WD95* program, allow for the contribution of limb-darkening to the form of the light curve. In the case of the *WD95* program, analytical approximations are employed to model the actual limb-darkening effect. The standard *WD95* program provides for two options, the 'Linear' and the 'Logarithmic' approximations.[3] The possible options are purposely restricted since appropriate tabulations of the so-called limb-darkening coefficients (LDCs – see below for the definition of LDCs) for alternative approximations must be made readily available to potential users before it is worth incorporating the alternative approximations into the synthetic light curve codes.

[3]Actually there is a third undocumented option, the 'Square Root' approximation (Díaz-Cordovés and Giménez, 1992). Indeed, it would not be terribly difficult to modify the program to accomodate almost any other formalism.

The only star for which effects of limb-darkening can be directly measured is the Sun, e.g. Allen (1976). Eclipsing binaries can be used to investigate limb-darkening, but for this purpose, data of exceptional quality is required. Correlations between the effects of limb-darkening and other physical processes (e.g. gravity darkening) must also be carefully accounted for so that in general it is more practical to use theoretical stellar atmosphere models to 'fix' the limb-darkening and thus remove the limb-darkening from the usually already long list of binary star model parameters being solved for in the light curve analysis.

The theoretical atmosphere models show that limb-darkening is a function of both the effective temperature ($T_{\rm eff}$) and the effective gravity ($\log[g]$) of the atmosphere as well as the photometric bandpass ($\bar{\lambda}$) being considered. The traditional formulation of the analytic approximations is the specification of the emergent intensity (I) as a function of the emergent angle (or more precisely $\mu = \cos[\theta]$ where θ is the emergent angle, i.e. the angle between the line of sight and the normal to the stellar atmosphere surface). For example, the logarithmic law is usually defined as,

$$\hat{\mathcal{I}}(\mu) = \mathcal{I}(\mu = 1)\,(1 - x(1-\mu) - y\mu\ln[\mu])\,, \tag{D.12}$$

where $\mathcal{I}(\mu = 1)$ is the actual model normal emergent intensity, $\hat{\mathcal{I}}(\mu)$ is the approximation and x and y are the LDCs. The simplist approach to dealing with the observational range of $T_{\rm eff}$, $\log[g]$ and λs is to interpolate within tabulations of the LDCs for grids of $T_{\rm eff}$ and $\log[g]$ for each $\bar{\lambda}$ of interest.

Al-Naimiy (1978) tabulated LDCs for the linear approximation based on the Carbon and Gingerich (1969) stellar atmosphere models, and since then many authors (e.g. Eade and Rucinski, 1985; Claret and Giménez, 1990; Díaz-Cordovés and Giménez, 1992; Van Hamme,1993) have published various updates on these providing tabulations for an ever increasing variety of approximations based on ever increasingly physical and accurate stellar atmosphere models. Most recently, the virtues and merits of the several approximations suggested by various authors over the years have been systematically investigated by Díaz-Cordovés and Giménez (1995).

LDCs have been derived from the Kurucz models rather than adopting one or other of the tabulations to be found in the literature because LDCs appropriate for non-Solar metallicity atmosphere models are more appropriate for the stars in the Magellanic Clouds whereas, although never stated implicitly, the tablulations in the literature are for Solar metallicity. Moreover, for the non-standard EROS $B_{\rm E}/R_{\rm E}$ bandpasses, no truely appropriate tabulations are readily available. In any case, it is arguable that the 'hands on' experience gained from the calculation of the LDCs is far more valuable as a learning experience than adopting a priori some published tabulations. Furthermore, the need to calculate LDCs was the original reason for becoming involved with calculating astrophysically useful data from the Kurucz atmosphere models and lead to the synthetic photometry calculations.

The following two sections detail the derivation of LDCs for the slightly simpler case of considering monochromatic wavelengths and the more general case of 'real' bandpasses (i.e. heterochromatic LDCs). The formulation of the derivations are again specifically relevant to the Kurucz stellar atmosphere models which are provided over a $T_{\rm eff}/\log[g]$ grid (see section D.2).

D.4.1 Monochromatic LDCs

We use the following notation: approximate quantities, as derived from the various approximations are denoted by symbols with 'hats' e.g. $\hat{\mathcal{I}}$ or $\hat{\mathcal{F}}$ for the intensity and flux respectively as against the corresponding quantites obtained directly from the models without hats, i.e. $\mathcal{I}$ and $\mathcal{F}$.

The LDCs for the various most widely-used approximations are defined by the following equations. For the Linear approximation,

$$\hat{\mathcal{I}}_\lambda(\mu) = \mathcal{I}_\lambda(1) \cdot (1 - x_\lambda\,(1-\mu))\,. \tag{D.13}$$

For the Quadratic approximation,

$$\hat{\mathcal{I}}_\lambda(\mu) = \mathcal{I}_\lambda(1) \cdot \left(1 - x_\lambda(1-\mu) - y_\lambda(1-\mu)^2\right)\,. \tag{D.14}$$

For the Logarithmic approximation,

$$\hat{\mathcal{I}}_\lambda(\mu) = \mathcal{I}_\lambda(1) \cdot (1 - x_\lambda(1-\mu) - y_\lambda\mu\ln[\mu])\,. \tag{D.15}$$

And for the Square Root approximation,

$$\hat{\mathcal{I}}_\lambda(\mu) = \mathcal{I}_\lambda(1) \cdot (1 - x_\lambda(1-\mu) - y_\lambda(1-\sqrt{\mu}))\,. \tag{D.16}$$

A number of different approaches can be taken in determining the LDCs. Giménez and co-workers prefer LDCs derived from chi-squared minimisation considerations (Claret and Giménez, 1990; Díaz-Cordovés and Giménez, 1992; Díaz-Cordovés et al., 1995) arguing that for the purposes of use with eclipsing binary codes the most important consideration is that the approximation represent the actual limb-darkening profile as best as is possible. This method has been adopted for the calculation of LDCs for use in the current work. The actual calculations were made employing a *Numerical Recipes* (Press et al., 1980) chi-squared minimisation algorithm (`LFIT`) with the requirement that the normal emergent intensity (i.e. $\mathcal{I}(1)$) be correctly predicted.

A number of other authors, (e.g. Wade and Rucinski, 1985; Van Hamme, 1993) prefer to reduce the problem to one of linear algebra by imposing either one or two 'more physical' constraints on the approximations. Full derivations of the LDC equations following the methods of both Wade and Rucinski and Van Hamme are given below, a) for completeness and b) because some of the derivations are useful even for the chi-squared minimisation approach.

Both Wade and Rucinski and Van Hamme impose as their first constraint perhaps the most obvious physical constaraint on the limb-darkening approximations, namely that they predict the same Flux[4] ($\mathcal{F}_\lambda$) as does the model atmosphere. The flux is given by,

$$\mathcal{F}_\lambda \equiv 2\int_0^1 \mathcal{I}_\lambda(\mu)\cdot d\mu = 2\int_0^1 \hat{\mathcal{I}}_\lambda(\mu)\cdot d\mu. \tag{D.17}$$

This constraint implies for the linear case defined by (D.13),

$$\begin{aligned}\mathcal{F}_\lambda &= 2\int_0^1 \mathcal{I}_\lambda(1)\cdot(1-x_\lambda(1-\mu))\cdot\mu\cdot d\mu,\\ &= 2\mathcal{I}_\lambda(1)\left[\frac{\mu^2}{2}-x_\lambda\mu^2\left(\frac{1}{2}-\frac{\mu}{3}\right)\right]_0^1,\\ &= \mathcal{I}_\lambda(1)\left(1-\frac{x_\lambda}{3}\right).\end{aligned} \tag{D.18}$$

For the quadratic case defined by (D.14),

$$\begin{aligned}\mathcal{F}_\lambda &= 2\int_0^1 \mathcal{I}_\lambda(1)\cdot\left(1-x_\lambda(1-\mu)-y_\lambda(1-\mu)^2\right)\cdot\mu\cdot d\mu,\\ &= 2\mathcal{I}_\lambda(1)\left[\frac{\mu^2}{2}-x_\lambda\mu^2\left(\frac{1}{2}-\frac{\mu}{3}\right)-y_\lambda\mu^2\left(\frac{1}{2}-\frac{2\mu}{3}+\frac{\mu^2}{4}\right)\right]_0^1,\\ &= \mathcal{I}_\lambda(1)\left(1-\frac{x_\lambda}{3}-\frac{y_\lambda}{6}\right).\end{aligned} \tag{D.19}$$

For the logarithmic case defined by (D.15),

$$\begin{aligned}\mathcal{F}_\lambda &= 2\int_0^1 \mathcal{I}_\lambda(1)\cdot(1-x_\lambda(1-\mu)-y_\lambda\mu\ln[\mu])\cdot\mu\cdot d\mu,\\ &= 2\mathcal{I}_\lambda(1)\left[\frac{\mu^2}{2}-x_\lambda\mu^2\left(\frac{1}{2}-\frac{\mu}{3}\right)-y_\lambda\mu^3\left(\frac{\ln[\mu]}{3}-\frac{1}{9}\right)\right]_0^1,\\ &= \mathcal{I}_\lambda(1)\left(1-\frac{x_\lambda}{3}+\frac{2y_\lambda}{9}\right).\end{aligned} \tag{D.20}$$

And for the square root case defined by (D.16),

$$\begin{aligned}\mathcal{F}_\lambda &= 2\int_0^1 \mathcal{I}_\lambda(1)\cdot(1-x_\lambda(1-\mu)-y_\lambda(1-\sqrt{\mu}))\cdot\mu\cdot d\mu,\\ &= 2\mathcal{I}_\lambda(1)\left[\frac{\mu^2}{2}-x_\lambda\mu^2\left(\frac{1}{2}-\frac{\mu}{3}\right)-y_\lambda\mu^2\left(\frac{1}{2}-\frac{2\sqrt{\mu}}{5}\right)\right]_0^1,\\ &= \mathcal{I}_\lambda(1)\left(1-\frac{x_\lambda}{3}-\frac{y_\lambda}{5}\right).\end{aligned} \tag{D.21}$$

[4]For the purposes of the calculation of the LDCs we can neglect the distinction between physical and astrophysical flux since it simply results in a factor of π in the flux which cancels out in the final calculation of the LDCs.

For the linear case, (D.18) is all that is required to solve for the LDC x_λ,

$$x_\lambda = 3\left(1 - \frac{\mathcal{F}_\lambda}{\mathcal{I}_\lambda(1)}\right). \tag{D.22}$$

For the other approximations a second constraint is required. The second constraint applied by Van Hamme is that the limb-darkening approximations have the same mean intensity, $\bar{\mathcal{I}}_\lambda$ as the model atmospheres, i.e.

$$\bar{\mathcal{I}}_\lambda \equiv \int_0^1 \mathcal{I}_\lambda(\mu)\cdot d\mu = \int_0^1 \hat{\mathcal{I}}_\lambda(\mu)\cdot d\mu. \tag{D.23}$$

This leads to the following expressions. For the quadratic case,

$$\begin{aligned}
\bar{\mathcal{I}}_\lambda &= \int_0^1 \mathcal{I}_\lambda(1)\cdot\left(1 - x_\lambda(1-\mu) - y_\lambda(1-\mu)^2\right)\cdot d\mu,\\
&= \mathcal{I}_\lambda(1)\left[\mu - x_\lambda\mu\left(1-\frac{\mu}{2}\right) - y_\lambda\mu\left(1-\mu+\frac{\mu^2}{3}\right)\right]_0^1,\\
&= \mathcal{I}_\lambda(1)\left(1 - \frac{x_\lambda}{2} - \frac{y_\lambda}{3}\right).
\end{aligned} \tag{D.24}$$

For the logarithmic case,

$$\begin{aligned}
\bar{\mathcal{I}}_\lambda &= \int_0^1 \mathcal{I}_\lambda(1)\cdot(1 - x_\lambda(1-\mu) - y_\lambda\mu\ln[\mu])\cdot d\mu,\\
&= \mathcal{I}_\lambda(1)\left[\mu - x_\lambda\mu\left(1-\frac{\mu}{2}\right) - y_\lambda\mu^2\left(\frac{\ln[\mu]}{2} - \frac{1}{4}\right)\right]_0^1,\\
&= \mathcal{I}_\lambda(1)\left(1 - \frac{x_\lambda}{2} + \frac{y_\lambda}{4}\right).
\end{aligned} \tag{D.25}$$

And for the square root case,

$$\begin{aligned}
\bar{\mathcal{I}}_\lambda &= \int_0^1 \mathcal{I}_\lambda(1)\cdot(1 - x_\lambda(1-\mu) - y_\lambda(1-\sqrt{\mu}))\cdot d\mu,\\
&= \mathcal{I}_\lambda(1)\left[\mu - x_\lambda\mu\left(1-\frac{\mu}{2}\right) - y_\lambda\mu\left(1-\mu+\frac{2\sqrt{\mu}}{3}\right)\right]_0^1,\\
&= \mathcal{I}_\lambda(1)\left(1 - \frac{x_\lambda}{2} - \frac{y_\lambda}{3}\right).
\end{aligned} \tag{D.26}$$

Wade and Rucinski on the other hand simply require that the approximations and models have the same values at $\mu = 0.1$, i.e.,

$$\hat{\mathcal{I}}_\lambda(0.1) = \mathcal{I}_\lambda(0.1). \tag{D.27}$$

This gives the following equations. For the quadratic case,

$$\begin{aligned}
\hat{\mathcal{I}}_\lambda(0.1) &= \mathcal{I}_\lambda(1)\cdot\left(1 - x_\lambda(1-0.1) - y_\lambda(1-0.1)^2\right),\\
&= \mathcal{I}_\lambda(1)\cdot(1 - 0.9x_\lambda - 0.81y_\lambda).
\end{aligned} \tag{D.28}$$

For the logarithmic case,

$$\begin{aligned}
\hat{\mathcal{I}}_\lambda(0.1) &= \mathcal{I}_\lambda(1)\cdot(1 - x_\lambda(1-0.1) - y_\lambda 0.1\ln[0.1]),\\
&= \mathcal{I}_\lambda(1)\cdot(1 - 0.9x_\lambda - 0.1\ln[0.1]y_\lambda).
\end{aligned} \tag{D.29}$$

And for the square root case,

$$\begin{aligned}
\hat{\mathcal{I}}_\lambda(0.1) &= \mathcal{I}_\lambda(1)\cdot\left(1 - x_\lambda(1-0.1) - y_\lambda(1-\sqrt{0.1})\right),\\
&= \mathcal{I}_\lambda(1)\cdot\left(1 - 0.9x_\lambda - (1-\sqrt{0.1})y_\lambda\right).
\end{aligned} \tag{D.30}$$

The above equations lead to the following relations for the LDCs. For Van Hamme, the quadratic case (D.19) and (D.24) give,

$$12\times(D.19) - 6\times(D.24) \Rightarrow 12 - 4x_\lambda - 12\frac{\mathcal{F}_\lambda}{\mathcal{I}_\lambda(1)} = 6 - 3x_\lambda - 4\frac{\bar{\mathcal{I}}_\lambda}{\mathcal{I}_\lambda(1)},$$

$$x_\lambda = 6 - 12\frac{\mathcal{F}_\lambda}{\mathcal{I}_\lambda(1)} + 6\frac{\bar{\mathcal{I}}_\lambda}{\mathcal{I}_\lambda(1)}, \tag{D.31}$$

and

$$y_\lambda = -6 + 18\frac{\mathcal{F}_\lambda}{\mathcal{I}_\lambda(1)} - 12\frac{\bar{\mathcal{I}}_\lambda}{\mathcal{I}_\lambda(1)}. \tag{D.32}$$

For the logarithmic case (D.20) and (D.25) give,

$$9 \times (D.20) - 8 \times (D.25) \Rightarrow 9 - 3x_\lambda - 9\frac{\mathcal{F}_\lambda}{\mathcal{I}_\lambda(1)} = 8 - 4x_\lambda - 8\frac{\bar{\mathcal{I}}_\lambda}{\mathcal{I}_\lambda(1)},$$

$$x_\lambda = -1 + 9\frac{\mathcal{F}_\lambda}{\mathcal{I}_\lambda(1)} - 8\frac{\bar{\mathcal{I}}_\lambda}{\mathcal{I}_\lambda(1)}, \tag{D.33}$$

and

$$y_\lambda = -6 + 18\frac{\mathcal{F}_\lambda}{\mathcal{I}_\lambda(1)} - 12\frac{\bar{\mathcal{I}}_\lambda}{\mathcal{I}_\lambda(1)}. \tag{D.34}$$

For the square root case (D.21) and (D.26) give,

$$30 \times (D.21) - 18 \times (D.26) \Rightarrow 30 - 10x_\lambda - 30\frac{\mathcal{F}_\lambda}{\mathcal{I}_\lambda(1)} = 18 - 9x_\lambda - 18\frac{\bar{\mathcal{I}}_\lambda}{\mathcal{I}_\lambda(1)},$$

$$x_\lambda = 12 - 30\frac{\mathcal{F}_\lambda}{\mathcal{I}_\lambda(1)} + 18\frac{\bar{\mathcal{I}}_\lambda}{\mathcal{I}_\lambda(1)}, \tag{D.35}$$

and

$$y_\lambda = -15 + 45\frac{\mathcal{F}_\lambda}{\mathcal{I}_\lambda(1)} - 30\frac{\bar{\mathcal{I}}_\lambda}{\mathcal{I}_\lambda(1)}. \tag{D.36}$$

For Wade & Rucinski, the quadratic case (D.19) and (D.28) give,

$$270 \times (D.19) - 100 \times (D.28) \Rightarrow 270 - 45y_\lambda - 270\frac{\mathcal{F}_\lambda}{\mathcal{I}_\lambda(1)} = 100 - 81y_\lambda - 100\frac{\mathcal{I}_\lambda(0.1)}{\mathcal{I}_\lambda(1)},$$

$$y_\lambda = \frac{270\mathcal{F}_\lambda - 170\mathcal{I}_\lambda(1) - 100\mathcal{I}_\lambda(0.1)}{36\mathcal{I}_\lambda(1)}, \tag{D.37}$$

and

$$x_\lambda = \frac{-243\mathcal{F}_\lambda + 193\mathcal{I}_\lambda(1) + 50\mathcal{I}_\lambda(0.1)}{36\mathcal{I}_\lambda(1)}. \tag{D.38}$$

For the logarithmic case (D.20) and (D.29) give,

$$270 \times (D.20) - 100 \times (D.29) \Rightarrow 270 + 60y_\lambda - 270\frac{\mathcal{F}_\lambda}{\mathcal{I}_\lambda(1)} = 100 - 10\ln[0.1]y_\lambda - 100\frac{\mathcal{I}_\lambda(0.1)}{\mathcal{I}_\lambda(1)},$$

$$y_\lambda = \frac{27\mathcal{F}_\lambda - 17\mathcal{I}_\lambda(1) - 10\mathcal{I}_\lambda(0.1)}{(6 + \ln[0.1])\,\mathcal{I}_\lambda(1)}, \tag{D.39}$$

and rearranging (D.20) we obtain,

$$x_\lambda = \frac{-3\mathcal{F}_\lambda + 3\mathcal{I}_\lambda(1)}{\mathcal{I}_\lambda(1)} + \frac{2}{3}y_\lambda. \tag{D.40}$$

For the square root case (D.21) and (D.30) give,

$$270 \times (D.21) - 100 \times (D.30) \Rightarrow 270 - 54y_\lambda - 270\frac{\mathcal{F}_\lambda}{\mathcal{I}_\lambda(1)} = 100 - \left(100 - \sqrt{1000}\right)y_\lambda - 100\frac{\mathcal{I}_\lambda(0.1)}{\mathcal{I}_\lambda(1)},$$

$$y_\lambda = \frac{135\mathcal{F}_\lambda - 85\mathcal{I}_\lambda(1) - 50\mathcal{I}_\lambda(0.1)}{\left(23 - \sqrt{250}\right)\mathcal{I}_\lambda(1)}, \tag{D.41}$$

and rearranging (D.21) we obtain,

$$x_\lambda = \frac{-3\mathcal{F}_\lambda + 3\mathcal{I}_\lambda(1)}{36\mathcal{I}_\lambda(1)} - \frac{3}{5}y_\lambda. \tag{D.42}$$

D.4.2 Heterochromatic LDCs

To compute heterochromatic, as against monochromatic, LDCs (i.e. LDCs applicable to bandpasses rather than at a single wavelength only), it is necessary to consider the following. Firstly for a bandpass defined by a response function $S(\lambda)$ we define a mean wavelength, $\bar{\lambda}$, by,

$$\bar{\lambda} = \frac{\int_0^\infty S(\lambda) \cdot \lambda \cdot d\lambda}{\int_0^\infty S(\lambda) \cdot d\lambda}, \tag{D.43}$$

then the heterochromatic intensity across a bandpass defined by the response function $S_{\bar{\lambda}}(\lambda)$, as a function of μ, i.e. $\mathcal{I}_{\bar{\lambda}}(\mu)$, is defined by the following integral,

$$\mathcal{I}_{\bar{\lambda}}(\mu) = \frac{\int_0^\infty S_{\bar{\lambda}}(\lambda) \cdot \mathcal{I}(\lambda, \mu) \cdot d\lambda}{\int_0^\infty S_{\bar{\lambda}}(\lambda) \cdot d\lambda}, \tag{D.44}$$

which can be approximated by the following summation

$$\begin{aligned} \mathcal{I}_{\bar{\lambda}}(\mu) &\approx \frac{\sum_{i=1}^\infty S_{\bar{\lambda}}(\lambda_i) \cdot \mathcal{I}(\lambda_i, \mu) \cdot \Delta\lambda_i}{\sum_{i=1}^\infty S_{\bar{\lambda}}(\lambda_i) \cdot \Delta\lambda_i}, \\ &= \frac{\sum_{i=1}^\infty S_{\bar{\lambda}}(\lambda_i) \cdot \mathcal{I}_i(\mu) \cdot \Delta\lambda_i}{\sum_{i=1}^\infty S_{\bar{\lambda}}(\lambda_i) \cdot \Delta\lambda_i}, \\ &\approx \frac{\sum_{i=1}^{1221} S_{\bar{\lambda}}(\lambda_i)\mathcal{I}_i(\mu)\Delta\lambda_i}{\sum_{i=1}^{1221} S_{\bar{\lambda}}(\lambda_i) \cdot \Delta\lambda_i}. \end{aligned} \tag{D.45}$$

Using this definition of the heterochromatic intensities we can derive heterochromatic LDCs using similar forms of the equations for the monochromatic LDCs. The appropriate integrated flux across a bandpass defined by the response function $S_{\bar{\lambda}}(\lambda)$ is given by,

$$\begin{aligned} \mathcal{F}_{\bar{\lambda}}(\mu) &= \frac{\int_0^\infty S_{\bar{\lambda}}(\lambda) \cdot \mathcal{F}(\lambda) \cdot d\lambda}{\int_0^\infty S_{\bar{\lambda}}(\lambda) \cdot d\lambda}, \\ &= 2\frac{\int_0^\infty S_{\bar{\lambda}}(\lambda) \int_0^1 \mathcal{I}(\lambda, \mu) \cdot \mu \cdot d\mu \cdot d\lambda}{\int_0^\infty S_{\bar{\lambda}}(\lambda) \cdot d\lambda}, \\ &= 2\frac{\int_0^\infty \int_0^1 S_{\bar{\lambda}}(\lambda) \cdot \mathcal{I}(\lambda, \mu) \cdot \mu \cdot d\mu \cdot d\lambda}{\int_0^\infty S_{\bar{\lambda}}(\lambda) \cdot d\lambda}. \end{aligned} \tag{D.46}$$

Numerically this can be approximated by the double summation,

$$\begin{aligned} \mathcal{F}_{\bar{\lambda}}(\mu) &\approx 2\frac{\sum_{i=1}^\infty \sum_{j=1}^\infty S_{\bar{\lambda}}(\lambda_i) \cdot \mathcal{I}(\lambda_i, \mu_j) \cdot \mu_j \cdot \Delta\mu_j \cdot \Delta\lambda_i}{\sum_{i=1}^\infty S_{\bar{\lambda}}(\lambda_i) \cdot \Delta\lambda_i}, \\ &\approx 2\frac{\sum_{i=1}^{1221} \sum_{j=1}^{17} S_{\bar{\lambda}}(\lambda_i) \cdot \mathcal{I}_i(\mu_j) \cdot \mu_j \cdot \Delta\mu_j \cdot \Delta\lambda_i}{\sum_{i=1}^{1221} S_{\bar{\lambda}}(\lambda_i) \cdot \Delta\lambda_i}. \end{aligned} \tag{D.47}$$

The *mean intensity* constraint then becomes,

$$\bar{\mathcal{I}}_{\bar{\lambda}} = \frac{\int_0^\infty \int_0^1 S_{\bar{\lambda}}(\lambda) \cdot \mathcal{I}(\lambda, \mu) \cdot d\mu \cdot d\lambda}{\int_0^\infty S_{\bar{\lambda}}(\lambda) \cdot d\lambda}, \tag{D.48}$$

which can be approximated by,

$$\begin{aligned} \bar{\mathcal{I}}_{\bar{\lambda}}(\mu) &\approx \frac{\sum_{i=1}^\infty \sum_{j=1}^\infty S_{\bar{\lambda}}(\lambda_i) \cdot \mathcal{I}(\lambda_i, \mu_j) \cdot \Delta\mu_j \cdot \Delta\lambda_i}{\sum_{i=1}^\infty S_{\bar{\lambda}}(\lambda_i) \cdot \Delta\lambda_i}, \\ &\approx \frac{\sum_{i=1}^{1221} \sum_{j=1}^{17} S_{\bar{\lambda}}(\lambda_i)\mathcal{I}_i(\mu_j) \cdot \Delta\mu_j \cdot \Delta\lambda_i}{\sum_{i=1}^{1221} S_{\bar{\lambda}}(\lambda_i) \cdot \Delta\lambda_i}, \end{aligned} \tag{D.49}$$

while the second constraint imposed by Wade and Rucinski simply becomes,

$$\bar{\mathcal{I}}_{\bar{\lambda}}(0.1) = \mathcal{I}_{\bar{\lambda}}(0.1). \tag{D.50}$$

With these definitions the heterochromatic LDCs are then given by equations (D.22) and (D.31) to (D.42) with the substitutions $x_\lambda \Rightarrow x_{\bar{\lambda}}$, $y_\lambda \Rightarrow y_{\bar{\lambda}}$, $\mathcal{F}_\lambda \Rightarrow \mathcal{F}_{\bar{\lambda}}$, $\mathcal{I}_\lambda \Rightarrow \mathcal{I}_{\bar{\lambda}}$, and $\hat{\mathcal{I}}_\lambda \Rightarrow \hat{\mathcal{I}}_{\bar{\lambda}}$.

D.4.3 Limb-Darkening Coefficients for the EROS B_E/R_E system.

Table D.2 tabulates the computed bolometric and EROS B_E/R_E system LDCs for the logarithmic approximation (equation D.15). These coefficients are determined according to the chi-squared minimization criterion (Díaz-Cordovés et al., 1995). Each row in the table gives the coeeficients for the effective temperature and gravity of the Kurucz stellar atmosphere model.

Table D.2: Bolometric, B_E and R_E Limb-Darkening Coefficients.

Model Number	$T_{\rm eff}$	log[g]	Bol' (x)	Bol' (y)	$B_{\rm E}$ (x)	$B_{\rm E}$ (y)	$R_{\rm E}$ (x)	$R_{\rm E}$ (y)
1	3500	0.00000	0.640	0.261	0.828	-0.199	0.849	0.049
2	3500	0.50000	0.635	0.264	0.844	-0.196	0.846	0.050
3	3500	1.00000	0.628	0.263	0.853	-0.192	0.832	0.040
4	3500	1.50000	0.623	0.264	0.860	-0.186	0.822	0.036
5	3500	2.00000	0.619	0.268	0.864	-0.173	0.812	0.036
6	3500	2.50000	0.616	0.277	0.869	-0.140	0.811	0.058
7	3500	3.00000	0.591	0.298	0.871	0.020	0.802	0.133
8	3500	3.50000	0.547	0.345	0.867	0.226	0.793	0.252
9	3500	4.00000	0.517	0.376	0.854	0.344	0.781	0.336
10	3500	4.50000	0.502	0.390	0.843	0.395	0.773	0.386
11	3500	5.00000	0.496	0.396	0.833	0.410	0.768	0.415
12	3750	0.00000	0.658	0.254	0.803	-0.228	0.833	0.106
13	3750	0.50000	0.655	0.249	0.820	-0.224	0.834	0.104
14	3750	1.00000	0.651	0.244	0.834	-0.214	0.831	0.095
15	3750	1.50000	0.644	0.236	0.842	-0.204	0.824	0.079
16	3750	2.00000	0.639	0.233	0.846	-0.190	0.815	0.064
17	3750	2.50000	0.634	0.231	0.848	-0.177	0.805	0.049
18	3750	3.00000	0.627	0.235	0.846	-0.145	0.795	0.050
19	3750	3.50000	0.605	0.273	0.845	0.018	0.788	0.157
20	3750	4.00000	0.567	0.339	0.838	0.245	0.777	0.316
21	3750	4.50000	0.535	0.384	0.825	0.376	0.763	0.419
22	3750	5.00000	0.517	0.403	0.813	0.429	0.751	0.467
23	4000	0.00000	0.659	0.246	0.794	-0.194	0.800	0.121
24	4000	0.50000	0.658	0.241	0.814	-0.187	0.805	0.129
25	4000	1.00000	0.657	0.237	0.831	-0.175	0.807	0.133
26	4000	1.50000	0.655	0.233	0.843	-0.162	0.807	0.132
27	4000	2.00000	0.651	0.226	0.849	-0.152	0.804	0.124
28	4000	2.50000	0.648	0.222	0.852	-0.144	0.800	0.115
29	4000	3.00000	0.645	0.219	0.851	-0.138	0.795	0.103
30	4000	3.50000	0.639	0.221	0.847	-0.118	0.789	0.101
31	4000	4.00000	0.619	0.262	0.840	0.011	0.778	0.193
32	4000	4.50000	0.585	0.333	0.829	0.223	0.761	0.344
33	4000	5.00000	0.553	0.387	0.815	0.366	0.741	0.449
34	4250	0.00000	0.652	0.237	0.786	-0.144	0.772	0.129
35	4250	0.50000	0.653	0.233	0.808	-0.127	0.777	0.141
36	4250	1.00000	0.654	0.226	0.827	-0.114	0.779	0.141
37	4250	1.50000	0.652	0.218	0.839	-0.101	0.778	0.140
38	4250	2.00000	0.651	0.214	0.848	-0.090	0.777	0.139
39	4250	2.50000	0.650	0.210	0.852	-0.087	0.775	0.134
40	4250	3.00000	0.648	0.207	0.853	-0.085	0.773	0.130
41	4250	3.50000	0.646	0.206	0.851	-0.082	0.771	0.126
42	4250	4.00000	0.643	0.209	0.847	-0.075	0.769	0.127
43	4250	4.50000	0.628	0.244	0.839	0.011	0.760	0.193
44	4250	5.00000	0.599	0.314	0.827	0.185	0.742	0.323
45	4500	0.00000	0.642	0.229	0.772	-0.105	0.750	0.154
46	4500	0.50000	0.645	0.227	0.797	-0.078	0.755	0.165
47	4500	1.00000	0.647	0.220	0.817	-0.055	0.758	0.167
48	4500	1.50000	0.650	0.216	0.834	-0.036	0.759	0.165
49	4500	2.00000	0.649	0.209	0.842	-0.027	0.757	0.160

Table D.2 cont.: Bolometric, B_E and R_E Limb-Darkening Coefficients.

Model Number	$T_{\rm eff}$	log[g]	Bol' (x)	Bol' (y)	$B_{\rm E}$ (x)	$B_{\rm E}$ (y)	$R_{\rm E}$ (x)	$R_{\rm E}$ (y)
50	4500	2.50000	0.649	0.204	0.848	-0.022	0.755	0.154
51	4500	3.00000	0.648	0.199	0.849	-0.023	0.753	0.149
52	4500	3.50000	0.647	0.196	0.849	-0.026	0.752	0.144
53	4500	4.00000	0.645	0.196	0.846	-0.027	0.750	0.141
54	4500	4.50000	0.643	0.199	0.843	-0.026	0.750	0.143
55	4500	5.00000	0.634	0.228	0.837	0.027	0.745	0.190
56	4750	0.00000	0.632	0.226	0.757	-0.072	0.729	0.190
57	4750	0.50000	0.637	0.221	0.783	-0.043	0.736	0.197
58	4750	1.00000	0.642	0.218	0.805	-0.014	0.740	0.198
59	4750	1.50000	0.644	0.214	0.821	0.011	0.741	0.197
60	4750	2.00000	0.646	0.212	0.832	0.030	0.741	0.195
61	4750	2.50000	0.648	0.207	0.839	0.038	0.740	0.188
62	4750	3.00000	0.648	0.202	0.842	0.039	0.739	0.181
63	4750	3.50000	0.648	0.198	0.843	0.036	0.738	0.175
64	4750	4.00000	0.647	0.195	0.843	0.032	0.737	0.170
65	4750	4.50000	0.646	0.195	0.840	0.028	0.736	0.167
66	4750	5.00000	0.644	0.198	0.837	0.028	0.736	0.169
67	5000	0.00000	0.619	0.219	0.741	-0.051	0.706	0.218
68	5000	0.50000	0.626	0.219	0.766	-0.013	0.714	0.229
69	5000	1.00000	0.633	0.216	0.789	0.021	0.719	0.228
70	5000	1.50000	0.638	0.217	0.807	0.053	0.722	0.229
71	5000	2.00000	0.642	0.217	0.819	0.077	0.723	0.228
72	5000	2.50000	0.645	0.213	0.827	0.088	0.723	0.221
73	5000	3.00000	0.647	0.210	0.832	0.094	0.723	0.215
74	5000	3.50000	0.648	0.206	0.834	0.094	0.723	0.208
75	5000	4.00000	0.649	0.203	0.835	0.090	0.724	0.203
76	5000	4.50000	0.649	0.201	0.835	0.087	0.724	0.199
77	5000	5.00000	0.648	0.202	0.833	0.084	0.724	0.198
78	5250	0.00000	0.610	0.211	0.731	-0.024	0.685	0.242
79	5250	0.50000	0.617	0.211	0.753	0.010	0.692	0.247
80	5250	1.00000	0.624	0.215	0.774	0.050	0.697	0.253
81	5250	1.50000	0.630	0.223	0.791	0.091	0.701	0.261
82	5250	2.00000	0.637	0.222	0.804	0.114	0.703	0.255
83	5250	2.50000	0.641	0.223	0.813	0.133	0.705	0.253
84	5250	3.00000	0.645	0.221	0.819	0.142	0.706	0.246
85	5250	3.50000	0.647	0.218	0.822	0.145	0.707	0.240
86	5250	4.00000	0.649	0.214	0.824	0.143	0.708	0.234
87	5250	4.50000	0.650	0.213	0.825	0.142	0.709	0.232
88	5250	5.00000	0.650	0.214	0.826	0.142	0.710	0.231
89	5500	0.00000	0.616	0.122	0.731	-0.116	0.675	0.161
90	5500	0.50000	0.610	0.215	0.744	0.048	0.671	0.277
91	5500	1.00000	0.616	0.221	0.761	0.086	0.675	0.282
92	5500	1.50000	0.623	0.227	0.776	0.121	0.679	0.284
93	5500	2.00000	0.630	0.235	0.789	0.155	0.682	0.287
94	5500	2.50000	0.636	0.236	0.798	0.174	0.686	0.283
95	5500	3.00000	0.641	0.233	0.805	0.183	0.688	0.274
96	5500	3.50000	0.645	0.230	0.808	0.188	0.689	0.268
97	5500	4.00000	0.648	0.226	0.811	0.188	0.690	0.261
98	5500	4.50000	0.649	0.225	0.813	0.188	0.692	0.259
99	5500	5.00000	0.650	0.227	0.814	0.193	0.694	0.262
100	5750	0.00000	0.623	0.110	0.737	-0.099	0.665	0.170
101	5750	0.50000	0.625	0.115	0.753	-0.065	0.669	0.174
102	5750	1.00000	0.616	0.231	0.757	0.122	0.661	0.304
103	5750	1.50000	0.622	0.234	0.768	0.150	0.663	0.302
104	5750	2.00000	0.628	0.236	0.778	0.172	0.666	0.296

Table D.2 cont.: Bolometric, B_E and R_E Limb-Darkening Coefficients.

Model Number	$T_{\rm eff}$	log[g]	Bol' (x)	Bol' (y)	$B_{\rm E}$ (x)	$B_{\rm E}$ (y)	$R_{\rm E}$ (x)	$R_{\rm E}$ (y)
105	5750	2.50000	0.633	0.242	0.785	0.198	0.668	0.298
106	5750	3.00000	0.638	0.243	0.791	0.212	0.670	0.294
107	5750	3.50000	0.643	0.242	0.794	0.221	0.671	0.289
108	5750	4.00000	0.646	0.237	0.797	0.223	0.673	0.282
109	5750	4.50000	0.648	0.237	0.799	0.227	0.674	0.282
110	5750	5.00000	0.649	0.237	0.800	0.230	0.677	0.282
111	6000	0.00000	0.633	0.107	0.743	-0.073	0.657	0.181
112	6000	0.50000	0.634	0.115	0.759	-0.039	0.661	0.182
113	6000	1.00000	0.636	0.121	0.771	-0.009	0.662	0.183
114	6000	1.50000	0.625	0.246	0.766	0.179	0.652	0.318
115	6000	2.00000	0.630	0.248	0.772	0.198	0.653	0.313
116	6000	2.50000	0.633	0.253	0.776	0.220	0.654	0.313
117	6000	3.00000	0.637	0.253	0.779	0.234	0.654	0.308
118	6000	3.50000	0.641	0.251	0.782	0.244	0.655	0.303
119	6000	4.00000	0.645	0.248	0.783	0.250	0.656	0.298
120	6000	4.50000	0.647	0.248	0.784	0.256	0.657	0.298
121	6000	5.00000	0.648	0.248	0.786	0.262	0.658	0.300
122	6250	0.50000	0.644	0.116	0.764	-0.017	0.653	0.193
123	6250	1.00000	0.645	0.128	0.776	0.022	0.655	0.193
124	6250	1.50000	0.646	0.135	0.783	0.049	0.655	0.193
125	6250	2.00000	0.634	0.262	0.770	0.224	0.644	0.330
126	6250	2.50000	0.636	0.263	0.771	0.239	0.643	0.324
127	6250	3.00000	0.639	0.263	0.771	0.252	0.642	0.319
128	6250	3.50000	0.642	0.260	0.772	0.261	0.642	0.313
129	6250	4.00000	0.644	0.256	0.772	0.267	0.641	0.307
130	6250	4.50000	0.646	0.255	0.771	0.275	0.641	0.308
131	6250	5.00000	0.648	0.256	0.771	0.283	0.641	0.310
132	6500	0.50000	0.654	0.116	0.765	-0.005	0.647	0.203
133	6500	1.00000	0.654	0.133	0.780	0.041	0.649	0.204
134	6500	1.50000	0.654	0.144	0.787	0.077	0.649	0.202
135	6500	2.00000	0.653	0.147	0.788	0.095	0.647	0.200
136	6500	2.50000	0.640	0.275	0.768	0.259	0.634	0.337
137	6500	3.00000	0.642	0.273	0.767	0.269	0.633	0.330
138	6500	3.50000	0.644	0.270	0.765	0.276	0.631	0.322
139	6500	4.00000	0.646	0.265	0.763	0.282	0.629	0.316
140	6500	4.50000	0.647	0.264	0.761	0.290	0.628	0.315
141	6500	5.00000	0.649	0.262	0.759	0.297	0.627	0.315
142	6750	0.50000	0.663	0.132	0.763	0.031	0.644	0.214
143	6750	1.00000	0.663	0.135	0.780	0.052	0.643	0.216
144	6750	1.50000	0.662	0.151	0.789	0.096	0.643	0.215
145	6750	2.00000	0.661	0.160	0.791	0.127	0.641	0.212
146	6750	2.50000	0.659	0.159	0.787	0.139	0.638	0.210
147	6750	3.00000	0.646	0.282	0.764	0.286	0.625	0.339
148	6750	3.50000	0.647	0.280	0.760	0.292	0.623	0.332
149	6750	4.00000	0.648	0.274	0.756	0.296	0.620	0.325
150	6750	4.50000	0.650	0.271	0.753	0.302	0.618	0.321
151	6750	5.00000	0.651	0.267	0.750	0.307	0.616	0.319
152	7000	0.50000	0.668	0.150	0.755	0.070	0.641	0.226
153	7000	1.00000	0.670	0.151	0.778	0.088	0.639	0.231
154	7000	1.50000	0.670	0.159	0.789	0.117	0.638	0.235
155	7000	2.00000	0.668	0.165	0.793	0.143	0.636	0.226
156	7000	2.50000	0.665	0.171	0.790	0.169	0.633	0.222
157	7000	3.00000	0.662	0.167	0.783	0.175	0.628	0.218
158	7000	3.50000	0.650	0.286	0.757	0.307	0.615	0.340
159	7000	4.00000	0.651	0.283	0.752	0.309	0.613	0.334

Table D.2 cont.: Bolometric, B_E and R_E Limb-Darkening Coefficients.

Model Number	$T_{\rm eff}$	log[g]	Bol' (x)	Bol' (y)	$B_{\rm E}$ (x)	$B_{\rm E}$ (y)	$R_{\rm E}$ (x)	$R_{\rm E}$ (y)
160	7000	4.50000	0.653	0.279	0.747	0.313	0.609	0.328
161	7000	5.00000	0.654	0.274	0.743	0.317	0.607	0.323
162	7250	0.50000	0.668	0.167	0.740	0.107	0.638	0.238
163	7250	1.00000	0.674	0.170	0.770	0.128	0.636	0.247
164	7250	1.50000	0.675	0.170	0.786	0.144	0.633	0.246
165	7250	2.00000	0.673	0.167	0.791	0.154	0.630	0.242
166	7250	2.50000	0.671	0.177	0.791	0.188	0.628	0.237
167	7250	3.00000	0.668	0.180	0.785	0.206	0.624	0.232
168	7250	3.50000	0.666	0.175	0.776	0.209	0.619	0.229
169	7250	4.00000	0.654	0.289	0.748	0.324	0.605	0.342
170	7250	4.50000	0.655	0.287	0.742	0.326	0.602	0.336
171	7250	5.00000	0.657	0.281	0.737	0.328	0.599	0.329
172	7500	0.50000	0.660	0.176	0.715	0.147	0.634	0.243
173	7500	1.00000	0.672	0.181	0.754	0.160	0.630	0.261
174	7500	1.50000	0.677	0.186	0.777	0.184	0.627	0.265
175	7500	2.00000	0.677	0.183	0.787	0.194	0.624	0.261
176	7500	2.50000	0.675	0.178	0.788	0.199	0.620	0.255
177	7500	3.00000	0.672	0.186	0.785	0.227	0.618	0.248
178	7500	3.50000	0.670	0.187	0.777	0.240	0.613	0.242
179	7500	4.00000	0.659	0.285	0.749	0.333	0.600	0.341
180	7500	4.50000	0.658	0.292	0.738	0.340	0.595	0.343
181	7500	5.00000	0.659	0.289	0.732	0.340	0.591	0.337
182	7750	1.00000	0.666	0.179	0.733	0.181	0.624	0.268
183	7750	1.50000	0.674	0.191	0.761	0.212	0.619	0.277
184	7750	2.00000	0.677	0.194	0.776	0.231	0.616	0.277
185	7750	2.50000	0.677	0.188	0.782	0.233	0.612	0.272
186	7750	3.00000	0.675	0.182	0.780	0.236	0.609	0.265
187	7750	3.50000	0.673	0.192	0.775	0.261	0.606	0.257
188	7750	4.00000	0.672	0.193	0.766	0.268	0.602	0.251
189	7750	4.50000	0.661	0.290	0.737	0.352	0.589	0.345
190	7750	5.00000	0.662	0.293	0.728	0.353	0.584	0.342
191	8000	1.00000	0.660	0.164	0.708	0.192	0.617	0.270
192	8000	1.50000	0.669	0.183	0.741	0.227	0.611	0.284
193	8000	2.00000	0.674	0.193	0.761	0.256	0.606	0.287
194	8000	2.50000	0.676	0.193	0.770	0.266	0.602	0.285
195	8000	3.00000	0.675	0.185	0.772	0.262	0.598	0.279
196	8000	3.50000	0.674	0.182	0.769	0.266	0.596	0.272
197	8000	4.00000	0.674	0.196	0.763	0.289	0.594	0.265
198	8000	4.50000	0.675	0.199	0.754	0.293	0.590	0.260
199	8000	5.00000	0.665	0.293	0.725	0.367	0.578	0.346
200	8250	1.00000	0.656	0.141	0.684	0.191	0.612	0.271
201	8250	1.50000	0.666	0.166	0.721	0.234	0.604	0.287
202	8250	2.00000	0.671	0.180	0.743	0.269	0.596	0.291
203	8250	2.50000	0.673	0.185	0.755	0.287	0.590	0.290
204	8250	3.00000	0.673	0.182	0.759	0.290	0.586	0.287
205	8250	3.50000	0.673	0.176	0.758	0.284	0.583	0.282
206	8250	4.00000	0.674	0.181	0.755	0.292	0.582	0.276
207	8250	4.50000	0.676	0.201	0.750	0.314	0.582	0.271
208	8250	5.00000	0.678	0.206	0.740	0.313	0.578	0.267
209	8500	1.00000	0.657	0.121	0.666	0.179	0.608	0.268
210	8500	1.50000	0.665	0.147	0.704	0.236	0.598	0.289
211	8500	2.00000	0.670	0.163	0.726	0.276	0.588	0.294
212	8500	2.50000	0.672	0.170	0.739	0.301	0.580	0.294
213	8500	3.00000	0.672	0.170	0.745	0.309	0.574	0.291
214	8500	3.50000	0.672	0.166	0.746	0.306	0.570	0.287

Table D.2 cont.: Bolometric, B_E and R_E Limb-Darkening Coefficients.

Model Number	$T_{\rm eff}$	log[g]	Bol' (x)	Bol' (y)	$B_{\rm E}$ (x)	$B_{\rm E}$ (y)	$R_{\rm E}$ (x)	$R_{\rm E}$ (y)
215	8500	4.00000	0.673	0.163	0.743	0.298	0.568	0.282
216	8500	4.50000	0.675	0.182	0.740	0.317	0.569	0.278
217	8500	5.00000	0.679	0.207	0.735	0.334	0.569	0.276
218	8750	1.50000	0.666	0.130	0.688	0.233	0.594	0.291
219	8750	2.00000	0.671	0.145	0.712	0.279	0.582	0.297
220	8750	2.50000	0.674	0.153	0.725	0.309	0.572	0.297
221	8750	3.00000	0.674	0.155	0.731	0.323	0.565	0.294
222	8750	3.50000	0.674	0.153	0.733	0.325	0.560	0.290
223	8750	4.00000	0.673	0.150	0.732	0.317	0.555	0.286
224	8750	4.50000	0.674	0.153	0.728	0.313	0.553	0.282
225	8750	5.00000	0.679	0.190	0.726	0.340	0.556	0.281
226	9000	1.50000	0.667	0.118	0.675	0.228	0.591	0.293
227	9000	2.00000	0.673	0.131	0.698	0.280	0.577	0.300
228	9000	2.50000	0.677	0.139	0.712	0.314	0.566	0.299
229	9000	3.00000	0.678	0.140	0.719	0.331	0.557	0.296
230	9000	3.50000	0.677	0.139	0.721	0.337	0.551	0.292
231	9000	4.00000	0.677	0.136	0.720	0.333	0.546	0.288
232	9000	4.50000	0.676	0.134	0.717	0.323	0.541	0.284
233	9000	5.00000	0.677	0.132	0.712	0.309	0.538	0.280
234	9250	2.00000	0.676	0.120	0.687	0.279	0.573	0.303
235	9250	2.50000	0.681	0.127	0.701	0.316	0.561	0.301
236	9250	3.00000	0.683	0.129	0.708	0.337	0.551	0.298
237	9250	3.50000	0.683	0.127	0.711	0.346	0.544	0.294
238	9250	4.00000	0.682	0.125	0.710	0.346	0.538	0.291
239	9250	4.50000	0.681	0.122	0.707	0.338	0.533	0.286
240	9250	5.00000	0.681	0.121	0.702	0.326	0.528	0.283
241	9500	2.00000	0.679	0.111	0.676	0.278	0.569	0.307
242	9500	2.50000	0.684	0.118	0.690	0.318	0.555	0.304
243	9500	3.00000	0.688	0.120	0.697	0.342	0.545	0.300
244	9500	3.50000	0.689	0.118	0.700	0.352	0.537	0.295
245	9500	4.00000	0.689	0.115	0.700	0.354	0.531	0.292
246	9500	4.50000	0.688	0.113	0.698	0.350	0.526	0.289
247	9500	5.00000	0.686	0.111	0.693	0.340	0.520	0.285
248	9750	2.00000	0.681	0.104	0.667	0.277	0.566	0.310
249	9750	2.50000	0.688	0.110	0.680	0.318	0.550	0.306
250	9750	3.00000	0.692	0.112	0.687	0.343	0.539	0.301
251	9750	3.50000	0.694	0.111	0.690	0.357	0.531	0.297
252	9750	4.00000	0.695	0.109	0.690	0.361	0.525	0.294
253	9750	4.50000	0.695	0.106	0.689	0.358	0.519	0.290
254	9750	5.00000	0.694	0.104	0.685	0.351	0.513	0.287
255	10000	2.00000	0.682	0.099	0.659	0.277	0.562	0.314
256	10000	2.50000	0.691	0.103	0.670	0.318	0.546	0.309
257	10000	3.00000	0.697	0.105	0.678	0.345	0.534	0.302
258	10000	3.50000	0.700	0.105	0.681	0.359	0.525	0.297
259	10000	4.00000	0.702	0.104	0.681	0.365	0.519	0.294
260	10000	4.50000	0.702	0.102	0.680	0.365	0.513	0.291
261	10000	5.00000	0.701	0.100	0.676	0.360	0.508	0.289
262	10500	2.00000	0.684	0.089	0.645	0.277	0.554	0.319
263	10500	2.50000	0.695	0.093	0.653	0.317	0.535	0.313
264	10500	3.00000	0.704	0.095	0.659	0.345	0.522	0.304
265	10500	3.50000	0.710	0.096	0.663	0.361	0.513	0.297
266	10500	4.00000	0.713	0.096	0.664	0.369	0.506	0.293
267	10500	4.50000	0.715	0.095	0.662	0.371	0.501	0.291
268	10500	5.00000	0.716	0.095	0.660	0.370	0.496	0.289
269	11000	2.50000	0.698	0.083	0.638	0.317	0.525	0.316

Table D.2 cont.: Bolometric, B_E and R_E Limb-Darkening Coefficients.

Model Number	$T_{\rm eff}$	log[g]	Bol' (x)	Bol' (y)	$B_{\rm E}$ (x)	$B_{\rm E}$ (y)	$R_{\rm E}$ (x)	$R_{\rm E}$ (y)
270	11000	3.00000	0.709	0.086	0.642	0.343	0.510	0.306
271	11000	3.50000	0.717	0.088	0.645	0.359	0.500	0.297
272	11000	4.00000	0.723	0.089	0.646	0.368	0.494	0.291
273	11000	4.50000	0.727	0.090	0.646	0.372	0.489	0.288
274	11000	5.00000	0.729	0.092	0.644	0.373	0.485	0.287
275	11500	2.50000	0.700	0.074	0.626	0.316	0.516	0.318
276	11500	3.00000	0.713	0.078	0.627	0.341	0.498	0.306
277	11500	3.50000	0.723	0.082	0.629	0.357	0.488	0.295
278	11500	4.00000	0.731	0.084	0.630	0.366	0.482	0.288
279	11500	4.50000	0.736	0.086	0.630	0.371	0.477	0.284
280	11500	5.00000	0.739	0.088	0.628	0.372	0.474	0.283
281	12000	2.50000	0.701	0.066	0.616	0.315	0.509	0.320
282	12000	3.00000	0.716	0.071	0.614	0.339	0.488	0.305
283	12000	3.50000	0.728	0.076	0.614	0.353	0.476	0.293
284	12000	4.00000	0.738	0.080	0.614	0.363	0.469	0.285
285	12000	4.50000	0.745	0.083	0.615	0.368	0.466	0.281
286	12000	5.00000	0.749	0.086	0.614	0.370	0.462	0.279
287	12500	2.50000	0.702	0.058	0.608	0.314	0.504	0.321
288	12500	3.00000	0.719	0.064	0.602	0.336	0.479	0.305
289	12500	3.50000	0.733	0.072	0.600	0.349	0.465	0.291
290	12500	4.00000	0.744	0.078	0.600	0.358	0.458	0.282
291	12500	4.50000	0.752	0.082	0.600	0.364	0.454	0.277
292	12500	5.00000	0.757	0.086	0.600	0.367	0.452	0.275
293	13000	2.50000	0.702	0.052	0.602	0.314	0.500	0.323
294	13000	3.00000	0.721	0.059	0.593	0.334	0.472	0.304
295	13000	3.50000	0.736	0.068	0.588	0.346	0.456	0.289
296	13000	4.00000	0.749	0.076	0.586	0.354	0.447	0.279
297	13000	4.50000	0.758	0.083	0.586	0.359	0.443	0.274
298	13000	5.00000	0.765	0.087	0.586	0.363	0.442	0.271
299	14000	2.00000	0.679	0.048	0.613	0.273	0.546	0.335
300	14000	2.50000	0.702	0.043	0.594	0.314	0.497	0.328
301	14000	3.00000	0.724	0.050	0.579	0.332	0.463	0.306
302	14000	3.50000	0.742	0.062	0.569	0.340	0.441	0.286
303	14000	4.00000	0.757	0.074	0.563	0.345	0.429	0.274
304	14000	4.50000	0.768	0.085	0.561	0.349	0.424	0.267
305	14000	5.00000	0.776	0.093	0.561	0.353	0.422	0.264
306	15000	2.50000	0.698	0.038	0.589	0.314	0.498	0.332
307	15000	3.00000	0.724	0.044	0.569	0.331	0.457	0.308
308	15000	3.50000	0.746	0.058	0.554	0.336	0.431	0.285
309	15000	4.00000	0.763	0.074	0.545	0.337	0.416	0.269
310	15000	4.50000	0.776	0.087	0.540	0.340	0.408	0.261
311	15000	5.00000	0.785	0.099	0.539	0.343	0.405	0.257
312	16000	2.50000	0.694	0.038	0.587	0.313	0.501	0.337
313	16000	3.00000	0.722	0.041	0.562	0.330	0.455	0.310
314	16000	3.50000	0.747	0.056	0.543	0.333	0.424	0.284
315	16000	4.00000	0.767	0.074	0.531	0.332	0.405	0.266
316	16000	4.50000	0.782	0.091	0.524	0.331	0.395	0.255
317	16000	5.00000	0.793	0.104	0.520	0.333	0.391	0.251
318	17000	2.50000	0.689	0.041	0.586	0.313	0.507	0.342
319	17000	3.00000	0.718	0.040	0.557	0.331	0.454	0.315
320	17000	3.50000	0.746	0.055	0.535	0.331	0.419	0.285
321	17000	4.00000	0.769	0.075	0.520	0.327	0.398	0.264
322	17000	4.50000	0.787	0.095	0.510	0.325	0.385	0.251
323	17000	5.00000	0.798	0.111	0.505	0.324	0.379	0.245
324	18000	2.50000	0.684	0.048	0.588	0.314	0.515	0.348

Table D.2 cont.: Bolometric, B_E and R_E Limb-Darkening Coefficients.

Model Number	$T_{\rm eff}$	log[g]	Bol' (x)	Bol' (y)	$B_{\rm E}$ (x)	$B_{\rm E}$ (y)	$R_{\rm E}$ (x)	$R_{\rm E}$ (y)
325	18000	3.00000	0.713	0.042	0.554	0.332	0.456	0.320
326	18000	3.50000	0.743	0.056	0.528	0.330	0.416	0.288
327	18000	4.00000	0.770	0.078	0.510	0.324	0.392	0.263
328	18000	4.50000	0.789	0.099	0.499	0.319	0.378	0.248
329	18000	5.00000	0.803	0.117	0.492	0.317	0.370	0.241
330	19000	2.50000	0.679	0.058	0.590	0.316	0.526	0.356
331	19000	3.00000	0.708	0.046	0.553	0.336	0.460	0.328
332	19000	3.50000	0.739	0.058	0.523	0.331	0.415	0.291
333	19000	4.00000	0.768	0.080	0.502	0.322	0.387	0.264
334	19000	4.50000	0.790	0.104	0.489	0.315	0.371	0.246
335	19000	5.00000	0.805	0.124	0.481	0.312	0.362	0.237
336	20000	3.00000	0.702	0.053	0.552	0.342	0.465	0.338
337	20000	3.50000	0.734	0.061	0.519	0.334	0.416	0.297
338	20000	4.00000	0.765	0.084	0.496	0.322	0.384	0.266
339	20000	4.50000	0.789	0.110	0.480	0.312	0.366	0.247
340	20000	5.00000	0.807	0.132	0.471	0.307	0.356	0.236
341	21000	3.00000	0.696	0.062	0.552	0.348	0.471	0.349
342	21000	3.50000	0.729	0.067	0.517	0.339	0.417	0.305
343	21000	4.00000	0.761	0.089	0.490	0.323	0.383	0.270
344	21000	4.50000	0.787	0.116	0.473	0.311	0.362	0.248
345	21000	5.00000	0.807	0.140	0.462	0.304	0.351	0.236
346	22000	3.00000	0.691	0.073	0.552	0.352	0.476	0.361
347	22000	3.50000	0.723	0.074	0.514	0.345	0.420	0.315
348	22000	4.00000	0.756	0.095	0.486	0.327	0.383	0.277
349	22000	4.50000	0.784	0.123	0.467	0.311	0.360	0.251
350	22000	5.00000	0.806	0.150	0.455	0.302	0.348	0.237
351	23000	3.00000	0.685	0.085	0.554	0.353	0.482	0.370
352	23000	3.50000	0.717	0.083	0.512	0.351	0.422	0.326
353	23000	4.00000	0.750	0.103	0.482	0.332	0.384	0.285
354	23000	4.50000	0.781	0.132	0.462	0.314	0.360	0.257
355	23000	5.00000	0.804	0.160	0.449	0.302	0.346	0.241
356	24000	3.00000	0.681	0.100	0.558	0.352	0.491	0.376
357	24000	3.50000	0.710	0.093	0.510	0.355	0.425	0.335
358	24000	4.00000	0.744	0.112	0.478	0.336	0.384	0.293
359	24000	4.50000	0.776	0.141	0.457	0.317	0.359	0.263
360	24000	5.00000	0.801	0.171	0.444	0.304	0.345	0.245
361	25000	3.00000	0.675	0.118	0.563	0.350	0.501	0.379
362	25000	3.50000	0.704	0.106	0.510	0.358	0.428	0.342
363	25000	4.00000	0.738	0.122	0.475	0.340	0.385	0.300
364	25000	4.50000	0.770	0.153	0.453	0.321	0.359	0.270
365	25000	5.00000	0.797	0.184	0.439	0.307	0.344	0.251
366	26000	3.00000	0.667	0.134	0.569	0.351	0.512	0.383
367	26000	3.50000	0.698	0.121	0.512	0.359	0.432	0.348
368	26000	4.00000	0.731	0.135	0.472	0.342	0.385	0.306
369	26000	4.50000	0.764	0.165	0.448	0.323	0.358	0.276
370	26000	5.00000	0.791	0.198	0.434	0.309	0.343	0.256
371	27000	3.50000	0.691	0.138	0.515	0.362	0.438	0.353
372	27000	4.00000	0.724	0.151	0.471	0.344	0.386	0.310
373	27000	4.50000	0.757	0.180	0.444	0.324	0.357	0.279
374	27000	5.00000	0.785	0.214	0.429	0.310	0.341	0.259
375	28000	3.50000	0.682	0.154	0.518	0.367	0.444	0.360
376	28000	4.00000	0.715	0.167	0.471	0.346	0.388	0.314
377	28000	4.50000	0.749	0.196	0.441	0.325	0.356	0.281
378	28000	5.00000	0.777	0.230	0.424	0.310	0.339	0.261
379	29000	3.50000	0.672	0.165	0.519	0.373	0.448	0.367

Table D.2 cont.: Bolometric, B_E and R_E Limb-Darkening Coefficients.

Model Number	$T_{\rm eff}$	log[g]	Bol' (x)	Bol' (y)	$B_{\rm E}$ (x)	$B_{\rm E}$ (y)	$R_{\rm E}$ (x)	$R_{\rm E}$ (y)
380	29000	4.00000	0.705	0.183	0.472	0.350	0.391	0.318
381	29000	4.50000	0.739	0.213	0.439	0.326	0.356	0.283
382	29000	5.00000	0.768	0.248	0.419	0.309	0.336	0.261
383	30000	3.50000	0.666	0.170	0.519	0.381	0.452	0.375
384	30000	4.00000	0.694	0.195	0.471	0.354	0.392	0.322
385	30000	4.50000	0.728	0.228	0.437	0.327	0.355	0.284
386	30000	5.00000	0.758	0.265	0.415	0.308	0.333	0.260
387	31000	3.50000	0.663	0.172	0.520	0.390	0.456	0.386
388	31000	4.00000	0.683	0.202	0.469	0.359	0.391	0.326
389	31000	4.50000	0.714	0.240	0.433	0.328	0.353	0.285
390	31000	5.00000	0.744	0.279	0.410	0.307	0.330	0.258
391	32000	4.00000	0.674	0.206	0.465	0.365	0.390	0.332
392	32000	4.50000	0.701	0.245	0.428	0.330	0.349	0.285
393	32000	5.00000	0.730	0.288	0.403	0.305	0.325	0.256
394	33000	4.00000	0.669	0.207	0.462	0.373	0.389	0.338
395	33000	4.50000	0.689	0.247	0.422	0.331	0.345	0.285
396	33000	5.00000	0.715	0.290	0.396	0.302	0.319	0.253
397	34000	4.00000	0.666	0.207	0.459	0.381	0.388	0.347
398	34000	4.50000	0.680	0.246	0.416	0.334	0.341	0.287
399	34000	5.00000	0.700	0.289	0.388	0.300	0.312	0.250
400	35000	4.00000	0.663	0.203	0.455	0.387	0.387	0.356
401	35000	4.50000	0.673	0.244	0.409	0.338	0.336	0.290
402	35000	5.00000	0.689	0.285	0.379	0.299	0.306	0.248
403	37500	4.50000	0.662	0.220	0.392	0.344	0.322	0.299
404	37500	5.00000	0.669	0.265	0.356	0.298	0.288	0.247
405	40000	4.50000	0.666	0.176	0.382	0.345	0.314	0.304
406	40000	5.00000	0.662	0.217	0.335	0.293	0.270	0.246
407	42500	5.00000	0.670	0.175	0.325	0.291	0.262	0.247
408	45000	5.00000	0.680	0.149	0.322	0.293	0.260	0.250
409	47500	5.00000	0.688	0.130	0.321	0.296	0.259	0.254
410	50000	5.00000	0.692	0.115	0.321	0.301	0.260	0.259

Appendix E

Guide to Analysis of EROS eclipsing binaries

This document describes the necessary steps to follow in order to enable the software for the analysis of EROS Eclipsing Binairies on the University of Canterbury's Computer Services Centre UNIX computer (CANTUA) running SunOS (Version 5.3) or on the UNIX Sparc server (NEWTON) of the Department of Physics and Astronomy, University of Canterbury. Also described is a simple procedure to follow to actually make use of the software, and an attempt to list the output generated by each procedure given below. This document should be used in conjunction with the 'Documentation of Eclipsing Binary Computer Model' by Wilson (Wilson, 1992b).

The analysis procedure is based on the synthetic light curve computer program of Wilson and Devinney, (e.g. Wilson and Devinney 1971, Wilson and Biermann 1976, Wilson and Sofia 1976, Wilson 1979, Wilson 1990, Wilson 1992a, Wilson 1992b, Wilson 1993, Wilson 1994 – hereafter the *WD95* program). The *WD95* program is comprised of essentially two FORTRAN executables, LC and DC. The former simply calculates the observables (namely the 'light' emitted by each component as well as the combined light, and the radial velocities of the indiviual components) of a binary system as a function of orbital phase, given the parameters of the system, i.e. the effective temperatures of the components, the period, the major semi-axis, the equipotentials that define the surfaces of the components etc. The latter optimises the parameters of the system in order to better fit a set of user-supplied photometric light curve and/or spectroscopic radial-velocity curve observations, by means of the technique of differential corrections.

Executables written by the author of this document simply provide for a slightly more user-friendly environment (in essence, simply a 'well' documented parameter file), based on the X11 application *Lucid Emacs* or *Xemacs* (hereafter generically *Emacs*) – although any other editor would presumably serve equally well – and a semi-automated interface to MIDAS and its graphical display and tabular data structure facilities. Essentially a combination of MIDAS command procedures (some times referred to as 'PRG's) and FORTRAN executables create appropriate input files for LC *and* DC from the (single) user-friendly parameter file, run as appropriate either LC or DC and then process the respective output from those executables, creating various ASCII and MIDAS data files, which are then displayed graphically, and in the case of DC 'updating' the parameter file by applying the parameter corrections as suggested by DC. A 'complete' record, including the input paramters, statistics relating to the quality of the model fit with respect to the observations and the resulting suggested corrections, is maintained throughout the analysis procedure in a log file.

E.1 Enabling the software

The appropriate software has been installed in subdirectories of `/astro/phys147/EROS/`. In order to run the software properly, first one must be a member of the `physastr` group, then several environment variables and MIDAS commands need to be defined. These are defined in the Unix script file...

```
/astro/phys147/EROS/.eros.cshrc
```

...and in the MIDAS command procedure...

```
/astro/phys147/EROS/prg/eroslogin.prg
```

To enable the software one should add the following line to one's `.cshrc`...

```
source /astro/phys147/EROS/.eros.cshrc
```

...and the following line to one's `login.prg` command procedure in one's midwork directory...

```
@@ EROSPRG:eroslogin.prg
```

Of course, the above needs only to be done ONCE, i.e. you do NOT have to perform the above each time you login, since `.cshrc` is sourced each time you login, assuming you are using a 'c-shell' (`csh`) or a 't-shell' (`tcsh`), and `login.prg` is sourced each time you commence a MIDAS session.

E.2 Detailed description of the analysis procedure

It is recomended that a unique subdirectory is created for each star analysed. For instance one might create an `EROS/` subdirectory in ones home directory, and then create subdirectories in `EROS/` for each star, e.g. `eros1066/`.

Once the steps described in section E.1 have been completed one is ready to commence the analysis. First, one needs to be in the appropriate directory. Then, set the environment variable `DISPLAY` if necessary, e.g.

```
UNIX$ setenv DISPLAY Hawking:0.0
```

Now, start an *Emacs* session with the following command...

```
UNIX$ ledclc
```

...if you forget this step, the command can in fact be issued from within the MIDAS session using the $ prefix. In addition to starting up the *Emacs* session, a template version of the DC/LC input/output file `dclcinput.dat` is copied into the current working directory. The model parameters are described in 'Documentation of Eclipsing Binary Computer Model' (Wilson, 1992b).

Next, start up a MIDAS session, e.g.

```
UNIX$ inmidas 40 -p
```

...and create a graphic window which you will make plenty of use of...

```
Midas 001> crea/grap 0 600,600,650,30
```

The above four steps MUST be carried out EVERY time you begin a session of analysis.

Before going any further, this is probably the best place to point out that limited help on the EROS analysis commands can be obtained by the MIDAS command `eros/help`, which will display the following help...

```
          EROS Eclipsing Binaries Analysis Software
          =========================================
New commands available...
eros/dattbls eros#star
eros/phase eros#star T0(HJD) period
eros/wilsonplot eros#star B-faint,B-bright,R-faint ,R-bright
eros/mid2lcvs4dc eros#star
eros/lcthenplot eros#star B-faint,B-bright,R-faint,R-bright
eros/dcthenplot eros#star B-faint,B-bright,R-faint,R-bright
eros/autodcthenplot MAX-ITER eros#star,B-faint,B-bright,R-faint,
                                                  R-bright [SCALE-SMAxis(Y/N)]
eros/lastdcthenplot eros#star B-faint,B-bright,R-faint,R-bright

eros/evoplot [table] [Y-col] [Y-range] [X-col] [X-range] [X-format]
eros/overplotevo table [X-col] [Y-col] [Lab-col] [Lab-format] [A/B/N] [A/B/N]
                                                                      [Y/N]
eros/ticksforevo
eros/mmerrors table [Mag1] [Mag2] [Mass1] [Mass2] [+uncert] [-uncert]
eros/wgmtplots Wil-table Gen-Table [X-axisP] [Y-axisP] [X-axisS] [Y-axisS]
                                                        [Plot-Errors(Y/N)]

eros/setxaxis X-start X-end
eros/setyaxis Y-start Y-end

  Brackets i.e.[ and ] imply OPTIONAL parameters which will not be prompted for
and so must be supplied on the command line if you wish to specify non-default
values.

'eros#star' means type 'eros' and then the catalogue number, e.g.\ eros1066
```

Now one is ready to begin the analysis. The following two steps must be performed only once for each target, unless for some reason the files created when the two commands are performed are somehow lost, or indeed if you wish for some reason to change the phasing of the data for instance. (In what follows eros1066 will be used by way of an example, obviously one will need to replace the star's name and the various parameters as appropriate for the particular star being analysed).

```
Midas 002> eros/dattbls eros1066
```

```
Midas 003> eros/phase eros1066 2448663.175 5.604
```

The appropriate values for Heliocentric Julian Date (HJD) of primary minimum and period should be taken from Grison et al. (1995). To see the light curves, type...

```
Midas 004> eros/wilsonplot eros1066 16.0,15.0,16.2,15.2
```

At this stage the above command is really just so you can be sure that the data has been phased appropriately, it is to a certain extent not 'required'.

Using the *Emacs* editor, iteratively edit the file `dclcinput.dat` appropriately and use the following command until an 'acceptable' approximate solution is obtained. Some hints for editing the `dclcinput.dat` file are given below.

```
Midas 005> eros/lcthenplot eros1066 16.0,15.0,16.2,15.2
```

Once an acceptable approximation has been obtained, use DC (see following command) until a final solution is obtained...

```
Midas 006> eros/dcthenplot eros1066 16.0,15.0,16.2,15.2
```

For `eros/dcthenplot`, if $B_{\rm Faint} = B_{\rm Bright} = R_{\rm Faint} = B_{\rm Bright} = 0.$ then the light curves will not be plotted. More to the point, the light curves will not be calculated, thus reducing the time to compute one iteration by a factor of perhaps a half. If you choose to operate in this manner, but at some point wish to see what the current solution looks like, simply run the `eros/lcthenplot` command. The following are some notes on editing the file `dclcinput.dat`.

1. This file is not input directly to either LC or DC. The actual input files required for LC and DC are created from this file. In the case of DC, in addition the files `dels4dc.dat` and `lcvs4dc.dat` are required to create the DC input file, but these are automatically created the first time one attemps run `eros/dcthenplot`.
2. The exact format of the file must be adhered to, otherwise the FORTRAN executables that atempt to process this file are liable to have problems. Thus it is recomended that one use *Emacs* in the **overwrite-mode** mode. Any mistakes should thus simply be re-typed. Do NOT use the delete/backspace key as this will destroy the format. Overwrite-mode is toggled by issuing the command overwrite-mode. This is done by typing `M-x` (here by `M-` the 'meta' key is implied. i.e. on the Sun and NCD X-terminals to type `M-x`, hold down the key directly to the left of the space bar, and then type x) which will give you the command prompt at the bottom of the window, now simply type `overwrite-mode<CR>`. Note that *Emacs* is **case sensitive**. In the information bar the current mode will be displayed. In general it should be `Fundamental ovwrt` if in `overwrite-mode`, otherwise it will simply say `Fundamental`.
3. After each iteration of `eros/dcthenplot`, `dclcinput.dat` will be updated. In order to view or edit this new version of `dclcinput.dat`, one must 'revert the buffer' first. This can be done either by selecting the `revert-buffer` menu command in the *Emacs* `file` menu, or by typing `M-x` (see above) which will give you the command prompt at the bottom of the window, now simply type `revert-buffer<CR>` and answer `yes` when prompted.
4. If `eros/dcthenplot` computes changes to the parameters that you do NOT wish to apply, then do NOT revert the buffer. Instead simply edit `dclcinput.dat` as it is. When you first try to do this, *Emacs* will warn you that the file on the disk has changed, and ask you if you really want to edit the buffer, to which you should answer `yes`, now edit as appropriate, then save the buffer (either `save` under the *Emacs* `file` menu or simply `C-x-s`, i.e. press and hold down the `control` key, and type `c` and then `s` while holding down the `control` key). Obviously if you do wish to apply the computed parameter corrections but forget to revert the buffer and then for some reason attempt the edit the buffer, again *Emacs* will warn you that the file on the disk has changed, and ask you if you really want to edit the buffer, to which you should of course answer `no`. You should then revert the buffer, and then edit the updated version.
5. After each successful iteration of `eros/dcthenplot` the input version of `dclcinput.dat` as well as the displayed information is written to a log file (`dclcinput.log`). So at any point you can return to an earlier version of `dclcinput.dat` by copying the appropriate portion of `dclcinput.log` to `dclcinput.dat`.

The above simple procedure forms the basis of the analysis. Once one has a reasonable grasp of the above, one can move on to applying it to the analysis philosophy and use it to determine the parameters of the components of the binary system.

The whole philosophy is to find the mass ratio (`M2/M1`) for which the light curve solution results in both components having a mass, radius and temperature consistent with the Geneva theoretical stellar evolution models (Schaerer et al., 1993). The procedure therefore, is to find the set of light curve solutions for a range of primary temperatures (`T1`) for each of a range of mass ratios. For instance one might find solutions for primary temperatures of 10000, 15000, 20000, 25000 and 30000 at mass ratios of 1.00, 0.75, and 0.50, i.e. fifteen individual solutions!

In general, at least initially, the appropriate mode[1] of operation is `mode=2`, i.e. detached binaries. Subsequent

[1]The mode is a control integer which specifies the morphological type of the binary, i.e. either well-detached, semi-detached, contact, double contact, etc. The *WD95* program in fact has seven options corresponding to various configurations, including those listed above.

analysis might indicate that some other mode is more appropriate (Wilson, 1992b), but this should perhaps be tested at least at each new mass ratio.

So to begin...

Set the mass ratio (M2/M1) parameter appropriately, (M2/M1=1.00 is probably as good a place to start as any), and insure that it is to be held fixed, i.e. the letter in the parentheses adjacent to it should at all times be a 'C'. Next set the primary temperature (T1) as appropriate and also make sure that it to is to be held fixed. In general, the following parameters should be optimised, Phase Off', Inclination, T2, POT1, POT2 and L1. The parameters to be optimised are specified by setting the letter in parentheses adjacent to the parameter or in the case of L1, L2, x1, y1 and 3rdL directly below) to 'V'. All other 'control characters' should be 'C's, unless you are dealing with an eccentric system in which case obviously the eccentricity (ECC) and the Longitude of Periastron (Long Peri) should also be optimised. In addition the axial rotation rates (F1 and F2) can be specified to be the appropriate values for synchronisation of the axial rotation rates to the orbital rotation rate at periastron by setting the control characters for F1 and F2 to 'E'.

E.2.1 For each value of the priamry temperature for a given mass ratio

Now simply iterate with the eros/dcthenplot command until an 'acceptable' solution for this particular value of mass ratio and primary temperature has been reached. The adopted convergence criterion is that the 'suggested parameter corrections' are all simultaneously less than their respective 'standard errors' or perhaps – even stronger – smaller by some, essentially arbitrary, factor. (This information is displayed (and logged) at the end of each iteration with
eros/dcthenplot).

Now life gets a little complicated... In *Emacs*, open (Open... under the *Emacs* file menu or C-x-f) the file dclcinput**ci**.dat. This file has the input parameters that just produced the suggested parameter corrections which are all less than their respective standard errors. Most of the parameters of the model are self-consistent in this file, but this is not in general the case for dclcinput.dat, which includes the most recent parameter corrections. The physical size of the system however will, in general, be incorrect, thus the major semi-axis (SMAxis) will need to be adjusted. The appropriately scaled SMAxis is listed on the same line as the SMAxis itself. The correct physical size of the system is determined by requiring that the 'observed' magnitudes of each component are, on average, equal to the distance and reddening corrected magnitudes of model stars of the same effective temperature and surface area. Simply type in the scaled value over the former value, save this file and now submit the following command...

```
Midas 007> eros/lastdcthenplot eros1066 16.0,15.0,16.2,15.2
```

This is exactly the same as the command eros/dcthenplot except the input parameters for DC are read from the file dclcinput**ci**.dat rather than dclcinput.dat. Once this iteration is complete, revert the buffer for dclcinput**ci**.dat (*Emacs* command in the file menu). This version of dclcinput**ci**.dat is the 'final result' (for that mass ratio and primary temperature), therefore this is the file you want to save, e.g. use the save as... function in the *Emacs* file menu or simply C-x-w. A 'descriptive' filename is probably the best policy, e.g. if this is the solution for M2/M1=1.00 and T1=1.5000 then perhaps dclcinput**ci**.dat.100.15000 would be a good convention. Having saved the file under its new name, you can 'kill' the buffer (Kill Buffer in the *Emacs* file menu or C-x k). A solution for a new primary temperature can now be found. Revert the dclcinput.dat file and edit to change the value of T1, and commence iterating again. Repeat for each value of T1.

When complete for each value of T1 there should be one dclcinputci.dat file for each value of T1 e.g.
dclcinputci.dat.100.10000, dclcinputci.dat.100.15000,
dclcinputci.dat.100.20000, dclcinputci.dat.100.25000
and dclcinputci.dat.100.30000 It is obviously useful to have these solutions printed on paper. For this purpose the following command may be of use...

```
Midas 008> $ a2psdclc dclcinputci.dat.100\* | lpr -Pphys809
```

...for instance to print out on the printer **phys809**. The output will look not unlike the example in figure E.1.

The solutions for each value of the primary temperature for a given mass ratio having been found, life gets even more complicated...

E.2.2 For each value of the mass ratio

The next step is to plot these light curve solutions on plots of the Geneva evolutionary models. The following command will produce the graphic shown in figure E.2.

```
Midas 009> eros/evoplots
```

A MIDAS table containing the parameters of the light curve solutions is now required. Assuming results files as above, then the following three commands would create an ASCII data file, a MIDAS table file containing all the data and then overplot the data on the plot of the Geneva models (e.g. figures E.3 and E.4)...

```
Midas 010> $ procbestdclcinputs dclcinputci.dat.100.\* eros1066wil100.dat
```

Printed by phys249 from cantua

Sep 11 1995 10:02 **dclcinputci.dat.100.20000** Page 1

```
Parameter File for dcjob and lcjob for : eros1066 16.0 15.0 16.2 15.2
==========================================
 MODE = 02     IPB = 0      IPB 0/1 Couple/Decouple L & T
IFAT1 = 0    IFAT2 = 0     Atmospheres 0) BlackBody 1) Model
   N1 = 15      N2 = 15    Grid Points
  N1L =  8     N2L =  8    Grid Points (Course Grid)
 MREF = 1     NREF = 1     Reflection Effect
ICOR1 = 0    ICOR2 = 0     Proximity Effect Corrections 1) apply 0) don't
 ISYM = 1       LD = 2     Asym/symetrical deriv's & LD model

Period =  5.60400   E(MJD) = 8663.175
     SMAxis =  32.510    (C)
        ECC =   0.2329   (V)
  Long Peri =  95.500    (V)
 Phase Off' =   0.1940   (V)
Inclination =  83.891    (V)
      M2/M1 =  1.00000   (C)
         T1 =  2.0000    (C)      T2 =   2.2121  (V)                    Star#1    Star#2
       POT1 =  7.4718    (V)    POT2 =   8.1787  (V)          M/Msun     7.36      7.36
         F1 =  1.000     (C)      F2 =   1.000   (C)   (Mean R)/Rsun     5.29      4.74
         g1 =  1.000     (C)      g2 =   1.000   (C)           Mbol     -4.22     -4.42
         A1 =  1.000     (C)      A2 =   1.000   (C)    Log[g] (cgs)     3.86      3.95

Light Curves  Number of light curves = 02
=============
Name   WL      L1      L2     x1    x2    y1    y2   3rdL  N Sigma   PHN    Zero  Factor
                (V)     (C)    (C)   (C)               (C)
Bold 0.4900  6.2849  6.0889 0.507 0.494 0.328 0.333 0.0000 0 0.0300 .0018 15.362 1.0000
Rold 0.6600  6.3966  6.0434 0.399 0.394 0.281 0.289 0.0000 0 0.0300 .0032 15.534 1.0000

Observed and Model Magnitudes
Name      M1L     M1SA    SF1       M2L     M2SA    SF2      M1A2L   M1A2A
Bold    16.115  16.182   1.031    16.149  16.225   1.036    15.379  15.450
Rold    16.267  16.201   0.970    16.329  16.264   0.971    15.545  15.480
Mean Scale Factor :    1.002

LC plots start at : -0.20  finish at :  1.20   step : 0.0025

Radial Velocity Curves
======================
IFVC1 = 0 IFVC2 = 0
THE = .0000  VUNIT = 100.000  VGAMMA = 0.0000 (C)
Name   WL      L1      L2     x1    x2    y1    y2   Sigma

Bolometic LDCs  x1 = 0.000 y1 = 0.000
                x2 = 0.000 y2 = 0.000

Pritchards Weighting Factors
                Start Finish  Weight
1st Phase Range  0.000  0.200  1.000
2nd Phase Range  0.500  0.700  1.000
Number of points to Bin together outside above ranges = 01

Printing
========
ifder = 1   ifm = 1   ifr = 1 ifrad = 0

NOTE : Spots NOT incorporated.
====   ===== ===
 KSPA = 0  NSPA = 0  KSPB = 0  NSPB = 0
ISMV1 = 0 ISMV2 = 0              Moving Spots

Scratch Pad
===========
K0 = 0 KDISK = 0
   Correlation Coefficients are...
   ===============================
 KEEP      10          11          14          16          20          23          24          26          26
  10    1.0000000  -0.7333499   0.0767093  -0.1026398   0.3507105   0.1120779   0.1877506  -0.1429510  -0.1236570
  11   -0.7333499   1.0000000  -0.2891210   0.0576194  -0.1591133  -0.0817624  -0.2192794   0.0112134  -0.0012318
  14    0.0767093  -0.2891210   1.0000000  -0.0883692   0.0517660   0.0742523  -0.0091393  -0.0720588  -0.0708830
  16   -0.1026398   0.0576194  -0.0883692   1.0000000  -0.3923150   0.3730957   0.5280480   0.2666178   0.2491837
  20    0.3507105  -0.1591133   0.0517660  -0.3923150   1.0000000  -0.0011986  -0.2390768  -0.6527798  -0.6108724
  23    0.1120779  -0.0817624   0.0742523   0.3730957  -0.0011986   1.0000000  -0.0215818  -0.5799123  -0.6054504
  24    0.1877506  -0.2192794  -0.0091393   0.5280480  -0.2390768  -0.0215818   1.0000000   0.6375793   0.6503194
  26   -0.1429510   0.0112134  -0.0720588   0.2666178  -0.6527798  -0.5799123   0.6375793   1.0000000   0.9955177
  26   -0.1236570  -0.0012318  -0.0708830   0.2491837  -0.6108724  -0.6054504   0.6503194   0.9955177   1.0000000
   Suggested Parameter Corections are...
   =====================================
  KEEP #10 P.C. IS :  0.00048 S.E. IS :  0.00497    E=ORBITAL ECCENTRICITY
  KEEP #11 P.C. IS : -0.00018 S.E. IS :  0.00241    PER=LONGITUDE OF PERIASTRON
  KEEP #14 P.C. IS :  0.00000 S.E. IS :  0.00011    PHASE SHIFT=PHASE OF PRIMARY CONJUNCTION
  KEEP #16 P.C. IS : -0.00441 S.E. IS :  0.04482    INCL=ORBITAL INCLINATION
  KEEP #20 P.C. IS :  0.00191 S.E. IS :  0.01212    T2=STAR 2 AVERAGE SURFACE TEMPERATURE
  KEEP #23 P.C. IS : -0.00938 S.E. IS :  0.03175    POT1=STAR 1 SURFACE POTENTIAL
  KEEP #24 P.C. IS :  0.00756 S.E. IS :  0.03118    POT2=STAR 2 SURFACE POTENTIAL
  KEEP #26 P.C. IS :  0.01194 S.E. IS :  0.05691    L1=STAR 1 RELATIVE MONOCHROMATIC LUMINOSITY
  KEEP #26 P.C. IS :  0.01243 S.E. IS :  0.05458    L1=STAR 1 RELATIVE MONOCHROMATIC LUMINOSITY
   Weighted sum of the squares of the residuals...
   ===============================================
  For CURRENT parameters : .513353683E-01
 For PREDICTED parameters : .513317734E-01
OMC stats for Bold curve :  mean =   0.0002 ;  sd =   0.0243 ;  min =  -0.1346 ;  max =   0.0681 (n = 0683)
OMC stats for Rold curve :  mean =   0.0000 ;  sd =   0.0175 ;  min =  -0.0773 ;  max =   0.0617 (n = 0724)
```

1

Figure E.1: An example of a `dclcinputci.dat` results file printed out using the `a2psdclc` command.

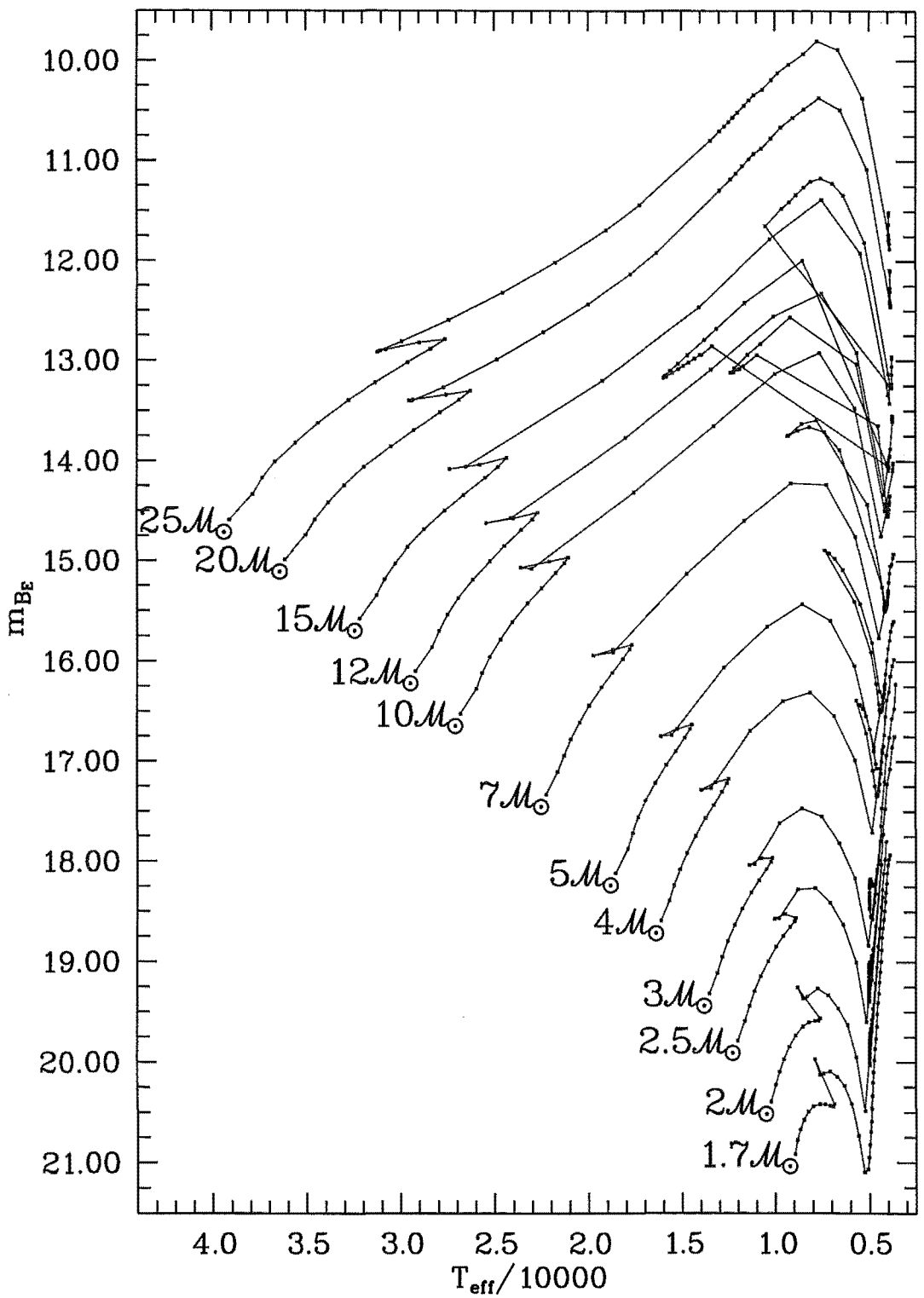

Figure E.2: Plot of $T_{\rm eff}/10\,000$ vs. $m_{B_{\rm E}}$ for theoretical evolutionary models for stars with metal abundances $Z = 0.008$ and ZAMS masses ranging from 1.7 to 25 $\mathcal{M}_\odot$ (Schaerer et al., 1993). Apparent magnitudes in the EROS $B_{\rm E}$ system ($m_{B_{\rm E}}$) have been calculated from surface fluxes derived from stellar atmosphere models (Kurucz, 1993) convolved with the spectral response function of the $B_{\rm E}$ bandpass, along with the adopted distance modulus of $(m - M)_0 = 18.35$ mag (Schmidt-Kaler, 1993), a total reddening of $E(B - V) = 0.08$ mag (Caldwell and Laney, 1991) and a ratio of interstellar extinction to colour excess of $\chi_{B_{\rm E}} = 2.47$ (Seaton, 1979).

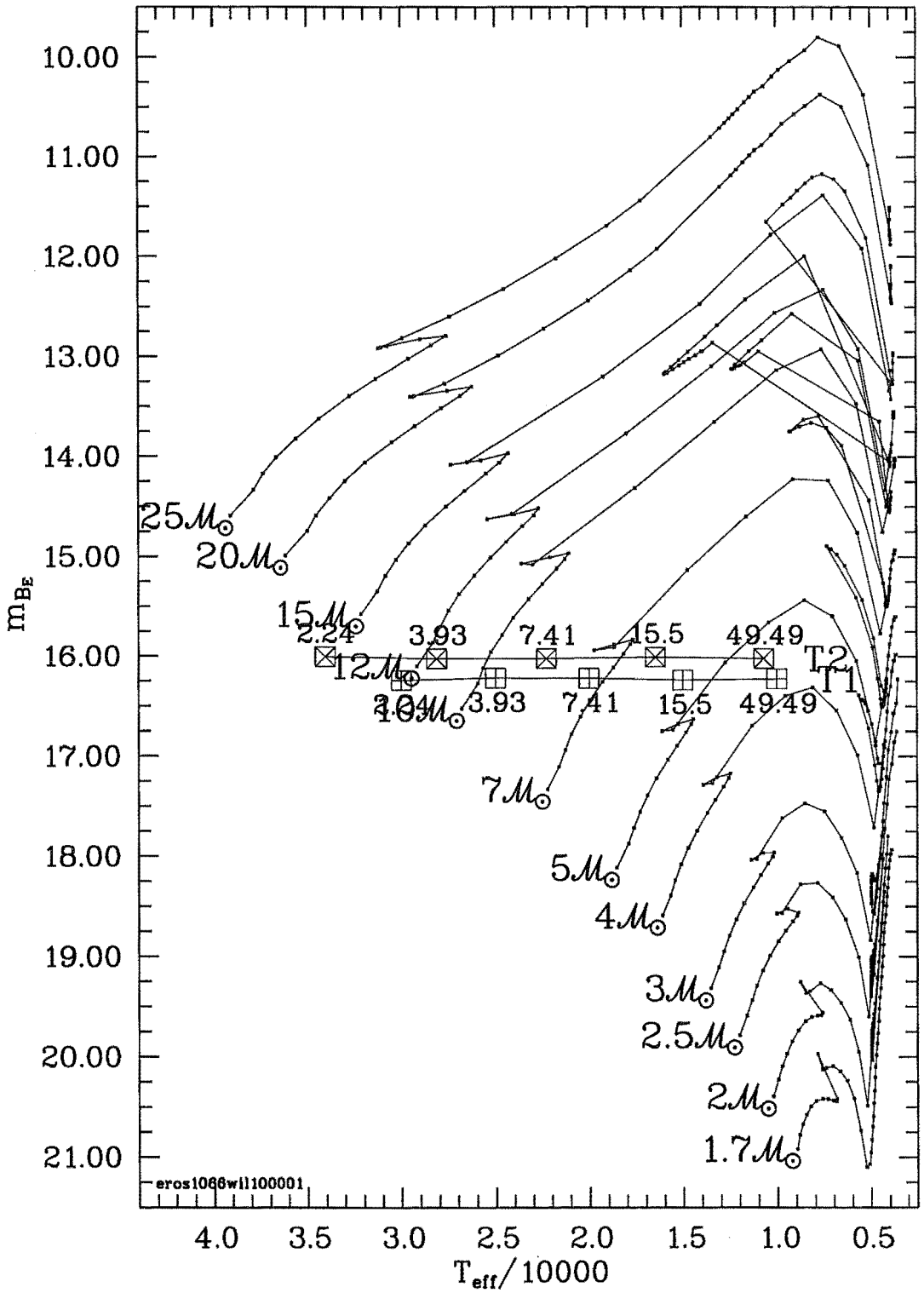

Figure E.3: Theoretical evolutionary models as for figure E.2 with *WD95* solutions overplotted. The *WD95* solutions are for $T_{\mathrm{eff},1}$ values ranging from 10 000 to 30 000 K at mass ratio equal to 1.00. Primary components are indicated by boxed + symbols, secondary components by boxed × symbols. The components are labelled by their masses (in solar units).

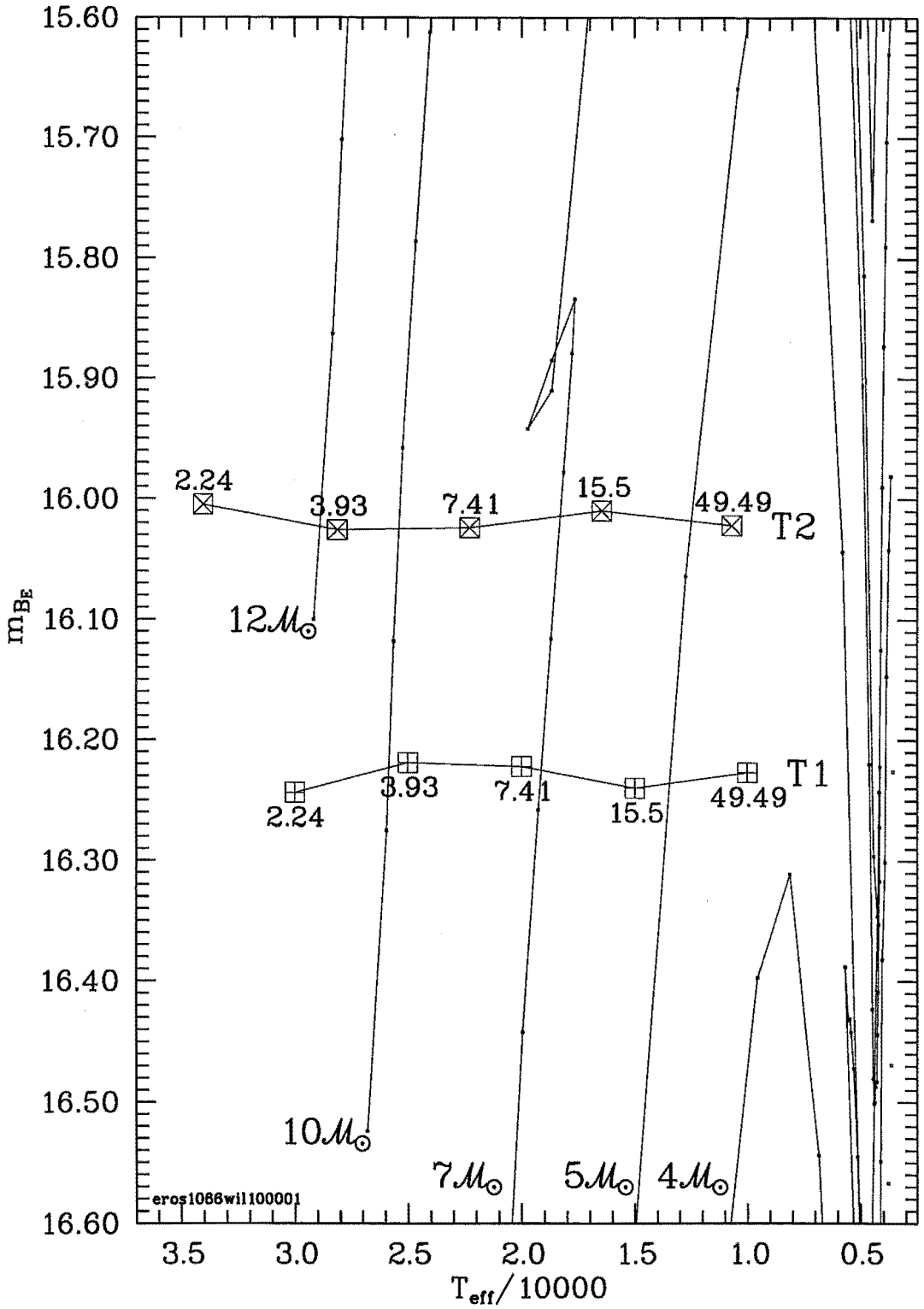

Figure E.4: Same as figure E.3 except with at enlarged vertical and horizontal scales to ease reading off the intersections between the *WD95* solution locii and the model evolutionary tracks. In this graph it is clear to see that as the effective temperature of the primary, and thus also that of the secondary, is reduced the system must necessarily be made bigger and thus more massive in order to produce the observed luminosity. As a result the mass of the *WD95* solution stars increases from left to right in this graph. For the evolution models on the other hand, as the mass is increased the temperature also increases, thus the evolution model masses increase from right to left. At some point the two will necessarily coincide, though not neccesarily at points corresponding to a single *WD95* solution. The intersections between the *WD95* solution locii and the evolution tracks give the temperatures at which the evolution model stars of the various masses have the same radii and temperatures, but not neccesarily the same masses as the *WD95* solution stars.

```
Midas 011> create/table eros1066wil100 125 8 eros1066wil100 EROSFMT:erosbestdclc
```

```
Midas 012> eros/overplotevo eros1066wil100
```

Consideration must now be given to the uncertainties in the stellar masses and temperatures due to uncertainties in the photometric zero-point (see section 7.1.6). The following command will compute columns in the MIDAS results table containing the mass and magnitude uncertainties...

```
Midas 013> eros/mmerrors eros1066wil100
```

It is also useful to replot these data on the Geneva models but at a somewhat larger scale so as to make reading off the temperatures of the Geneva models corresponding to light curve solutions as easy as possible. The following commands will achieve this...

```
Midas 014> eros/evoplots ?  ?  16.7,15.7 ?  3.5,0.5
```

```
Midas 015> eros/overplotevo eros1066wil100 ?  ?  ?  ?  B A Y
```

The following command is useful for increasing the number of tickmarks on the bottom and top axes in order to improve the accuracy of reading off the temperatures of the intersections of the Geneva models and the light curve solution locii.

```
Midas 016> eros/ticksforevo
```

The above sequence of commands will produce the graphic shown in figure E.5.

Old-fashioned graphical techniques are now required. The temperatures of the Geneva models corresponding to solutions of the light curves for both primary and secondary stars must be read-off. These are simply the temperatures corresponding to the intersections of the locii of the *WD95* models (labeled T1, T2, $T1^P$, $T2^P$, $T1^M$ and $T2^M$ in figure E.5) and the evolutionary tracks of the Geneva models. This data then needs to be put into an ASCII file suitable for MIDAS to create a table from. The following format is recomended:

```
01.00 10.0 2.640 2.679 2.580 2.660 2.679 2.600
01.00 07.0 1.900 1.980 1.820 1.920 2.000 1.840
01.00 05.0 1.280 1.360 1.120 1.290 1.380 1.170
```

The columns of the above file are as follows:

1. The mass ratio
2. The ZAMS mass of the Geneva Model
3. The temperature of intersection between the Geneva model and the T1 locii
4. The temperature of intersection between the Geneva model and the $T1^P$ locii
5. The temperature of intersection between the Geneva model and the $T1^M$ locii
6. The temperature of intersection between the Geneva model and the T2 locii
7. The temperature of intersection between the Geneva model and the $T2^P$ locii
8. The temperature of intersection between the Geneva model and the $T2^M$ locii

Use *Emacs* to create a file for the data. Save it, once again using a descriptive file name, e.g. `eros1066gen100.dat`. Given an appropriate file of the above format, the following command can be used to create the MIDAS table...

```
Midas 017> create/table eros1066gen100 8 8 eros1066gen100 EROSFMT:erosgenmt
```

The intersection of the *WD95* locii of solutions and the Geneva locii of solutions gives the primary and secondary effective temperatures for which the stars which are solutions to the *WD95* models are individually consistent with the Geneva evolutionary models, (even though the secondary as determined by the *WD95* program which corresponds to the Geneva-consistent primary will not in general be consistent with the Geneva models as well, and likewise for the primary corresponding to the Geneva-consistent secondary). The following command will produce a graphic not unlike that shown in figure E.6...

```
Midas 018> eros/wgmtplots eros1066wil100 eros1066gen100
```

Once again, it will be useful to replot figure E.6 but with redefined axes limits in order to make reading off the intersection points easier and to include the locii corresponding to the photometric uncertainties. The following command will produce a graphic not unlike that in figure E.7...

```
Midas 019> eros/wgmtplots eros1066wil100 eros1066gen100 1.6,2.4,0.1,0.01
                                                    5,10 1.8,2.6,0.1,0.01 5,10 Y
```

From this graph the temperatures and masses of the primary and secondary stars which would be consistent with both the photometric light curve and the Geneva evolutionary models can be read-off the upper and lower panels respectively. The temperature of the primary star that corresponds to the secondary temperature must now be found using the *WD95*

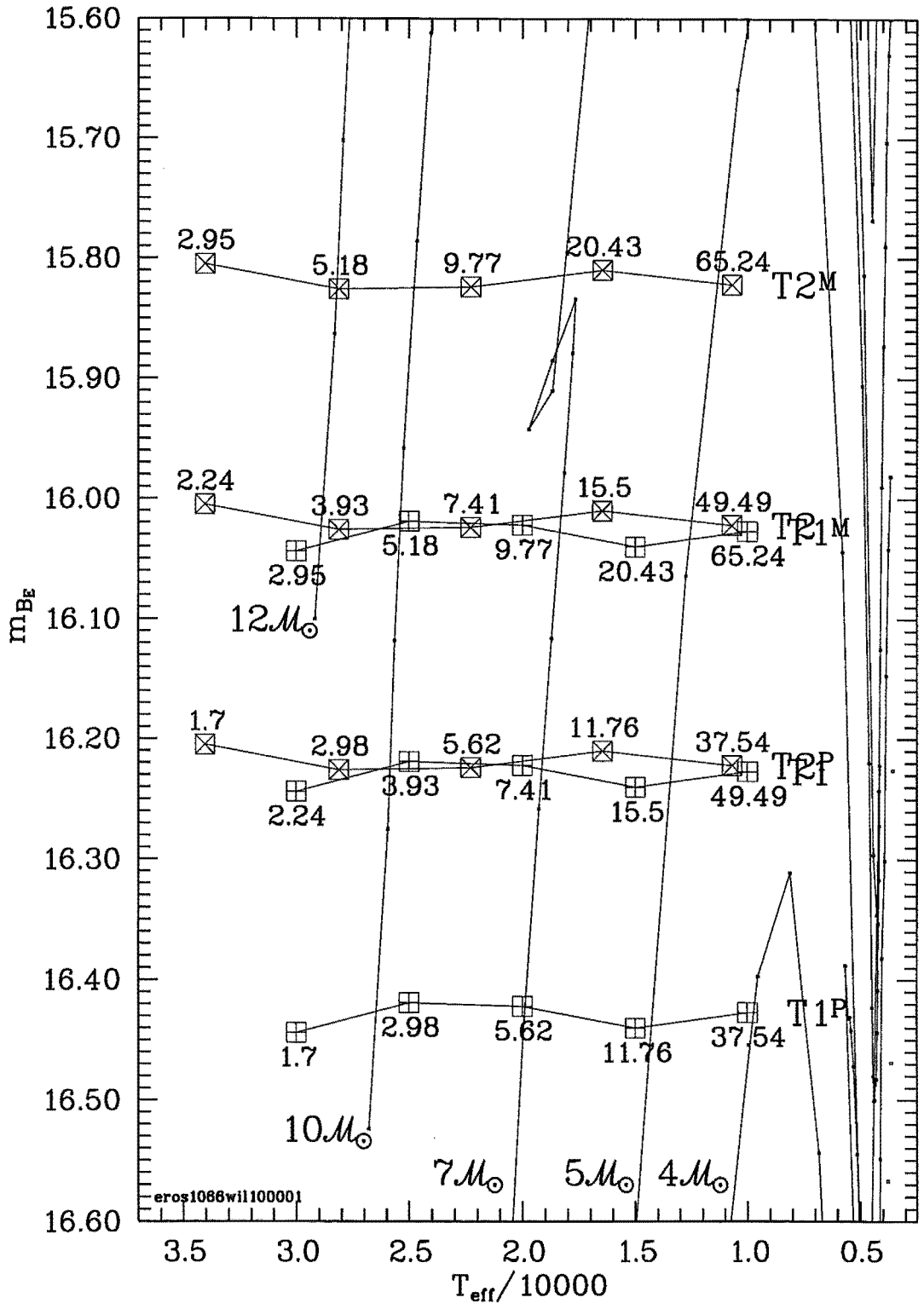

Figure E.5: Same as figure E.4 but with additional *WD95* locii corresponding to the possible solutions allowing for a ± 0.2 mag uncertainty in the photometry, distance modulus and reddening.

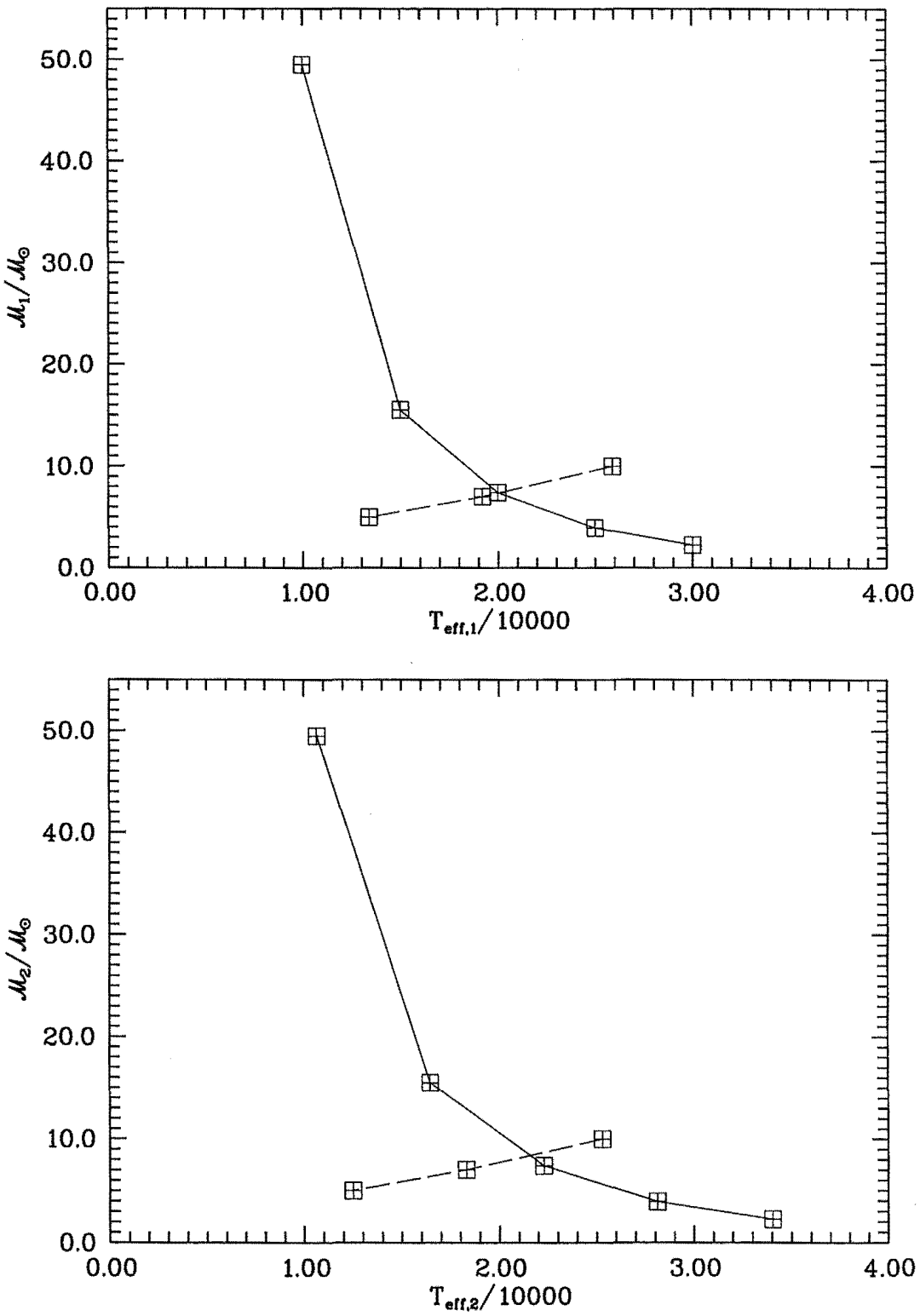

Figure E.6: $T_{\rm eff}/10\,000$ vs. $\mathcal{M}$ plots for the *WD95* solution locii (solid line) and the locii of points obtained from the intersections of the model evolution tracks and the *WD95* solution locii in the $T_{\rm eff}/m_{B_{\rm E}}$ plane, i.e. figure E.5 (dashed line). The upper panel pertains to the primary component and the lower panel to the secondary. The intersections of the two locii in the upper panel gives the effective temperature of the primary component at which a the *WD95* solution primary will have the radius, temperature and mass as the an evolution model star. Similarly the intersection in the lower panel gives the temperature of the secondary component for which the *WD95* solution secondary will have the same radius temperature, and mass as an evolution model star. In general howerver, the temperature and hence also the mass and radius, of the primary component corresponding to this particular secondary will not be the same as the temperature indicated by the intersection of the locii in the upper panel.

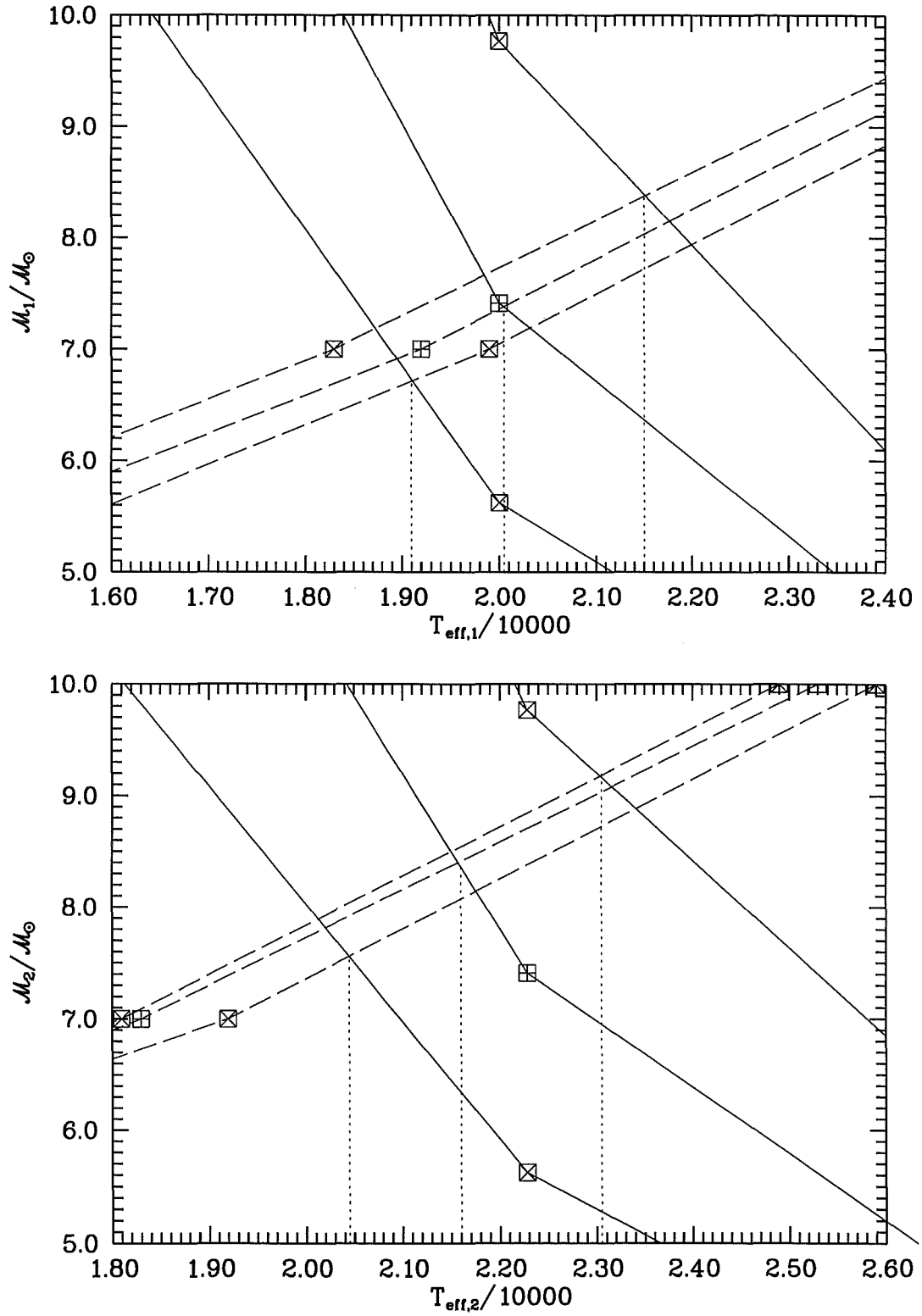

Figure E.7: Same as figure E.6 but with additional locii corresponding to the possible solutions allowing for a ± 0.2 mag uncertainty in the photometry, distance modulus and reddening. The effective temperature to adopt is indicated by the central dotted line. The range of acceptable effective temperature for each component is indicated by the other two dotted lines.

program. Edit `dclcinput.dat` to set the value of `T2` to that determined from the graph. In order to find the value of `T1` which corresponds to this value of `T2`, `T2` must be held constant while `T1` is allowed to vary, therefore the 'control character' for `T1` must be set to 'V', and for `T2` to 'C'. Now iterate with `eros/dcthenplot` until a solution is determined. Once convergence is reached, open the `dclcinputci.dat` file, adjust the major semi-axis so as to scale the system appropriately, and perform a final DC iteration with `eros/lastdcthenplot`. Revert the `dclcinputci.dat` buffer and the save the file under a new name. Maintaining the convention established earlier is the best policy, i.e. `dclcinputci.dat` appended by `100×M2/M1` appended by `10000×T1`. Also, don't forget to print the file (`a2psdclc`).

This essentially completes the requirements for this one value of the mass ratio. The solutions for a new mass ratio can now be found. Repeat the above procedure for each mass ratio.

Keep in mind that the object is to locate the mass ratio for which the masses, radii and temperatures of both of the stellar components – as determined by the *WD95* program solution for the photometric light curve – are both, simultaneously, consistent with the Geneva Models. Initially the primary-corresponding-to-the-Geneva-models-consistent-secondary will either be hotter or colder than the Geneva-models-consistent-primary. As the mass ratio is adjusted, eventually the point will be reached where this relationship is reversed. The point we are obviously after is that at which they are equal. Thus, once adjusting the mass ratio results in a reversal in the relationship between the the two temperatures of the primary ($T_{1,1}$ and $T_{1,2}$), the mass ratio for which they are equal can be determined graphically, see figure E.8.

E.2.3 Determining the mass ratio and primary temperature

Having found the Geneva-models-consistent-primary and the primary-corresponding-to-the-Geneva-models-consistent-secondary at a number of mass ratios, spanning the mass ratio at which the two primaries have the same temperature, these solution values of the mass ratio and primary temperature can be simply read from a graphic such as figure E.8, namely the intersection of the Geneva-models-consistent-primary-locus and the primary-corresponding-to-the-Geneva-models-consistent-secondary-locus.

A solution using these values of mass ratio and primary temperature should then be found (i.e. edit `dclcinput.dat`, iterate with `eros/dcthenplot`, edit `dclcinput`**`ci`**`.dat` and complete with `eros/lastdcthenplot`.

Alternatively, one may wish to adopt the implied mass ratio and fully re-apply the analysis procedure in order to determine the primary temperature, which should, of course, be the same, within the uncertainties, as that implied by the intersection in the RM–`T1` plane.

Either way, this is the solution to be adopted.

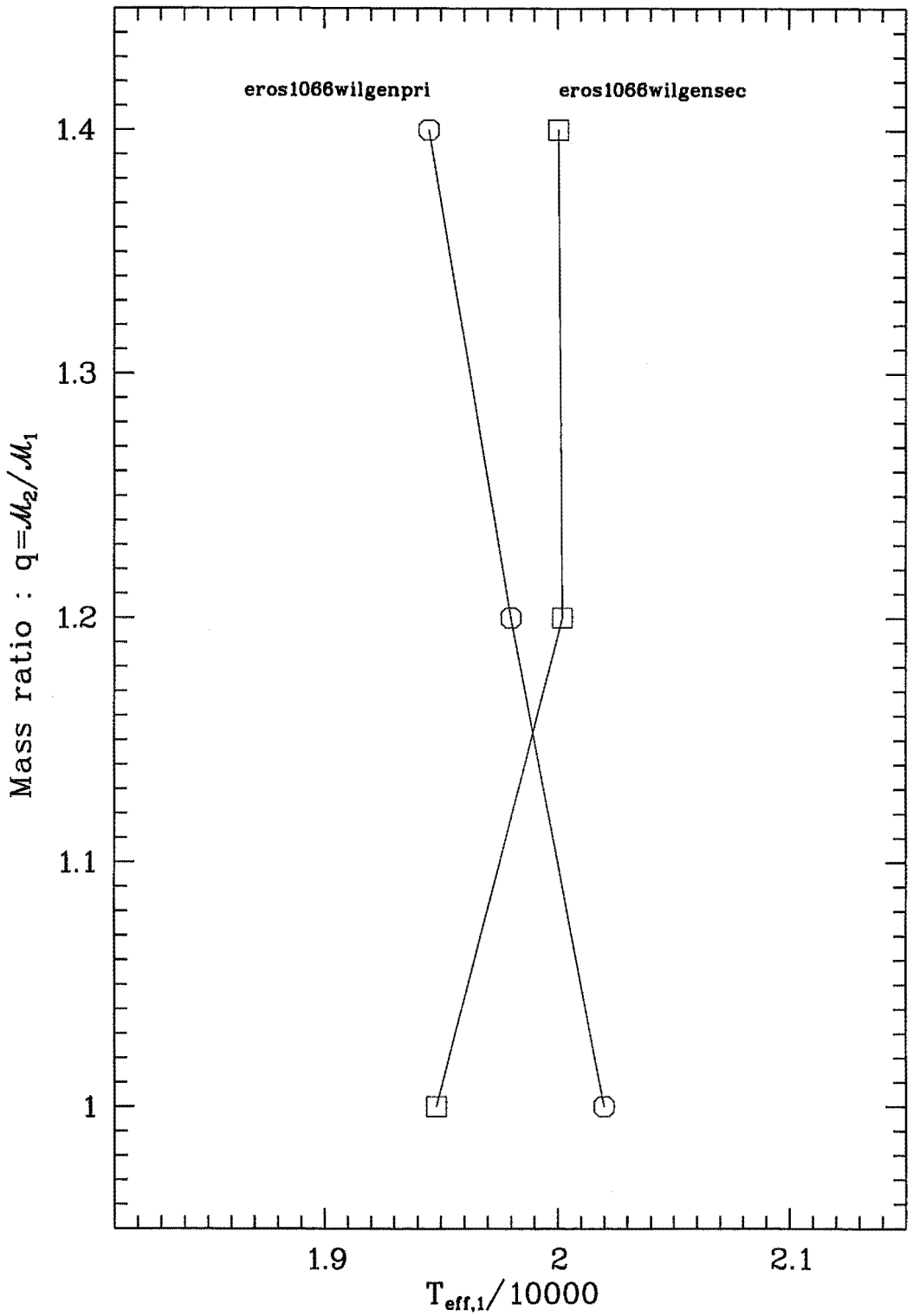

Figure E.8: The locii for the effective temperatures for the *WD95* primary components which match evolution model stars (circles) and the the effective temperatures of the *WD95* primary components which correspond to the *WD95* secondary components which match evolution model stars. The intersection of the two locii gives the solution mass ratio at which the two *WD95* primary components are indistinguishable.

Appendix F

Transmission and Response functions

Synthetic photometry derived from theoretical stellar atmosphere flux distributions (1993) and tabulated bandpass spectral response functions has been utilised throughout this research. This appendix tabulates the various filter transmission functions used.

The first section gives the transmission functions for the *uvbyI* filters of the MJUO *uvbyVI* photometric system as measured from transmission curves supplied by the manufacturer, Omega Optical Inc., Brattleboro, Vermont, USA, the V transmission function as measured by the author, and the typical quantum efficiency of an overcoated Thomson TH7882 CDA CCD as quoted by Photometrics. The second section tabulates the response functions for the 'standard' *uvby* (Schaifers and Voight, 1982a) and *UBVRI* (Bessell, 1990)[1] photometric systems adopted throughtout this research, a 'standard' atmosphere transmission function (Straižys, 1992) and the spectral reflectivity from an aluminised mirror. In the third section, the EROS $B_{\rm E}$ and $R_{\rm E}$ response functions, as provided by the EROS collaboration and the typical atmospheric transmission at La Silla observatory (Fluks and Thé, 1992) are tabulated. Table F.1 provides calculated mean wavelengths ($\bar{\lambda}$, also often labelled λ_0) and bandpass widths ($\Delta\lambda$) for all 17 bandpasses.

$$\bar{\lambda} = \frac{\int_0^\infty S(\lambda)\cdot\lambda\cdot d\lambda}{\int_0^\infty S(\lambda)\cdot d\lambda}, \tag{F.1}$$

$$\Delta\lambda \approx 2\sqrt{\frac{\int_0^\infty (\lambda-\bar{\lambda})^2\cdot S(\lambda)\cdot d\lambda}{\int_0^\infty S(\lambda)\cdot d\lambda}}. \tag{F.2}$$

Note that the effective wavelength for a bandpass with spectral intensity $\mathcal{I}_0(\lambda)$ incident upon it is,

$$\bar{\lambda} = \frac{\int_0^\infty \mathcal{I}_0(\lambda)\cdot S(\lambda)\cdot\lambda\cdot d\lambda}{\int_0^\infty \mathcal{I}_0(\lambda)\cdot S(\lambda)\cdot d\lambda}, \tag{F.3}$$

See, for example, Schaifers and Voight (1982a).

[1]Bessell's (1990) *UBVRI* system is an attempt the recreate the Johnson-Cousins *UBVRI* system.

Table F.1: Measured mean wavelengths ($\bar{\lambda}$) and bandpass widths ($\Delta\lambda$) for the standard Strömgren *uvby* Cousins *UBVRI*, the MJUO *uvbyVI* and EROS B_E/R_E photometric systems. For the standard systems, 'standard' values from the literature are also quoted (*uvby* pg. 329 and *UBV* pg. 211, *RI* pg. 310, (Straižys, 1992).)

Filter	$\bar{\lambda}$ [nm]	$\Delta\lambda$ [nm]	$\bar{\lambda}$ [nm]	$\Delta\lambda$ [nm]
		MJUO system		
u_{MJUO}	346.6	26.6		
v_{MJUO}	410.0	13.7		
b_{MJUO}	465.9	12.8		
y_{MJUO}	548.2	24.0		
V_{MJUO}	544.2	67.0		
I_{MJUO}	794.6	86.2		
		Standard Systems		
	Measured		Quoted	
u	346.5	24.5	350.0	30.0
v	410.8	17.9	411.0	19.0
b	466.8	17.3	467.0	18.0
y	545.9	19.6	547.0	23.0
U	360.5	43.9	360.0	~45.
B	441.3	71.8	440.0	~100.
V	551.2	72.4	550.5	~85.
R	658.5	129.5	660.0	~75.
I	806.0	92.5	810.0	~150.
		EROS system		
B_E	488.6	81.4		
R_E	668.2	115.6		

F.1 The MJUO $uvbyVI$ photometric system

Table F.2: The transmission function ($T_{u_{\rm MJUO}}$) of the MJUO u filter, as measured from transmission curves supplied by Omega Optical.

λ	$T_{u_{\rm MJUO}}$	λ	$T_{u_{\rm MJUO}}$	λ	$T_{u_{\rm MJUO}}$	λ	$T_{u_{\rm MJUO}}$	λ	$T_{u_{\rm MJUO}}$
310.00	0.0000	327.50	0.2600	345.00	0.4880	362.50	0.3500	380.00	0.0060
312.50	0.0080	330.00	0.3080	347.50	0.4900	365.00	0.2880	382.50	0.0010
315.00	0.0200	332.50	0.3600	350.00	0.4860	367.50	0.2200	385.00	0.0001
317.50	0.0500	335.00	0.4000	352.50	0.4800	370.00	0.1540	387.50	0.0000
320.00	0.0900	337.50	0.4350	355.00	0.4600	372.50	0.0950		
322.50	0.1450	340.00	0.4610	357.50	0.4300	375.00	0.0480		
325.00	0.2000	342.50	0.4780	360.00	0.3950	377.50	0.0200		

Table F.3: The transmission function ($T_{v_{\rm MJUO}}$) of the MJUO v filter, as measured from transmission curves supplied by Omega Optical.

λ	$T_{v_{\rm MJUO}}$	λ	$T_{v_{\rm MJUO}}$	λ	$T_{v_{\rm MJUO}}$	λ	$T_{v_{\rm MJUO}}$	λ	$T_{v_{\rm MJUO}}$
380.00	0.0000	395.00	0.0375	410.00	0.5093	425.00	0.0500	435.00	0.0031
385.00	0.0000	400.00	0.1937	415.00	0.4312	430.00	0.0125	445.00	0.0000
390.00	0.0062	405.00	0.4375	420.00	0.1750				

Table F.4: The transmission function ($T_{b_{\rm MJUO}}$) of the MJUO b filter, as measured from transmission curves supplied by Omega Optical.

λ	$T_{b_{\rm MJUO}}$	λ	$T_{b_{\rm MJUO}}$	λ	$T_{b_{\rm MJUO}}$	λ	$T_{b_{\rm MJUO}}$	λ	$T_{b_{\rm MJUO}}$
440.00	0.0000	455.00	0.1890	465.00	0.7468	475.00	0.2484	485.00	0.0203
445.00	0.0046	460.00	0.5796	470.00	0.6000	480.00	0.0718	505.00	0.0000
450.00	0.0343								

Table F.5: The transmission function ($T_{y_{\rm MJUO}}$) of the MJUO y filter, as measured from transmission curves supplied by Omega Optical.

λ	$T_{y_{\rm MJUO}}$	λ	$T_{y_{\rm MJUO}}$	λ	$T_{y_{\rm MJUO}}$	λ	$T_{y_{\rm MJUO}}$	λ	$T_{y_{\rm MJUO}}$
500.00	0.0000	530.00	0.1718	550.00	0.6125	565.00	0.1312	580.00	0.0265
515.00	0.0140	535.00	0.3203	555.00	0.4750	570.00	0.0843	585.00	0.0171
520.00	0.0343	540.00	0.5875	560.00	0.3031	575.00	0.0468	610.00	0.0000
525.00	0.0812	545.00	0.6843						

Table F.6: The transmission function ($T_{V_{\mathrm{MJUO}}}$) of the MJUO V filter, as measured from transmission curves generated on the Bausch & Lomb Spectragraph.

λ	$T_{V_{\mathrm{MJUO}}}$	λ	$T_{V_{\mathrm{MJUO}}}$	λ	$T_{V_{\mathrm{MJUO}}}$	λ	$T_{V_{\mathrm{MJUO}}}$	λ	$T_{V_{\mathrm{MJUO}}}$
477.00	0.0000	516.00	0.7900	559.00	0.6340	591.00	0.3058	624.00	0.0587
484.00	0.2360	527.00	0.7900	570.00	0.5371	602.00	0.2024	634.00	0.0212
494.00	0.6420	537.00	0.7680	581.00	0.4237	613.00	0.1215	677.00	0.0000
505.00	0.7550	548.00	0.7120						

Table F.7: The transmission function ($T_{I_{\mathrm{MJUO}}}$) of the MJUO I filter, as measured from transmission curves supplied by Omega Optical.

λ	$T_{I_{\mathrm{MJUO}}}$	λ	$T_{I_{\mathrm{MJUO}}}$	λ	$T_{I_{\mathrm{MJUO}}}$	λ	$T_{I_{\mathrm{MJUO}}}$	λ	$T_{I_{\mathrm{MJUO}}}$
690.00	0.0000	750.00	0.8125	800.00	0.8781	840.00	0.8437	880.00	0.1875
710.00	0.0750	760.00	0.8359	810.00	0.8687	850.00	0.8468	890.00	0.0750
720.00	0.2625	770.00	0.8500	820.00	0.8562	860.00	0.8015	900.00	0.0343
730.00	0.5468	780.00	0.8656	830.00	0.8437	870.00	0.4562	940.00	0.0000
740.00	0.7281	790.00	0.8812						

Table F.8: The quantum efficiency (QE) of an overcoated Thomson TH7882 CDA chip as claimed by Photometrics.

λ	QE	λ	QE	λ	QE	λ	QE	λ	QE
300.00	0.2210	460.00	0.1870	610.00	0.3740	760.00	0.2860	910.00	0.1130
310.00	0.2200	470.00	0.2000	620.00	0.3840	770.00	0.2850	920.00	0.1000
320.00	0.2180	480.00	0.2160	630.00	0.3920	780.00	0.2840	930.00	0.0840
330.00	0.2160	490.00	0.2350	640.00	0.3980	790.00	0.2780	940.00	0.0720
340.00	0.2150	500.00	0.2580	650.00	0.3950	800.00	0.2750	950.00	0.0680
350.00	0.2140	510.00	0.2700	660.00	0.3880	810.00	0.2700	960.00	0.0580
360.00	0.2100	520.00	0.2830	670.00	0.3810	820.00	0.2620	970.00	0.0500
370.00	0.2080	530.00	0.2960	680.00	0.3700	830.00	0.2540	980.00	0.0360
380.00	0.2050	540.00	0.3120	690.00	0.3500	840.00	0.2430	990.00	0.0300
390.00	0.2010	550.00	0.3280	700.00	0.3360	850.00	0.2290	1000.00	0.0240
400.00	0.1960	560.00	0.3350	710.00	0.3250	860.00	0.2160	1010.00	0.0220
410.00	0.1900	570.00	0.3450	720.00	0.3150	870.00	0.1900	1020.00	0.0170
420.00	0.1830	580.00	0.3500	730.00	0.3060	880.00	0.1740	1030.00	0.0130
430.00	0.1750	590.00	0.3600	740.00	0.2950	890.00	0.1480	1040.00	0.0090
440.00	0.1710	600.00	0.3650	750.00	0.2880	900.00	0.1280	1050.00	0.0050
450.00	0.1740								

F.2 Selected 'Standard' transmission and response functions

Table F.9: The transmission function (T_u) of the 'standard' Strömgren u filter, pg. 57 (Schaifers and Voight, 1982a). The response function of the 1P21 photomultiplier tube is included in the data.

λ	T_u	λ	T_u	λ	T_u	λ	T_u	λ	T_u
315.00	0.0000	330.00	0.2097	345.00	0.3439	360.00	0.2433	375.00	0.0211
317.50	0.0026	332.50	0.2499	347.50	0.3430	362.50	0.2038	377.50	0.0086
320.00	0.0296	335.00	0.2814	350.00	0.3337	365.00	0.1607	380.00	0.0039
322.50	0.0661	337.50	0.3126	352.50	0.3214	367.50	0.1129	382.50	0.0000
325.00	0.1104	340.00	0.3300	355.00	0.3043	370.00	0.0745		
327.50	0.1595	342.50	0.3392	357.50	0.2782	372.50	0.0455		

Table F.10: The transmission function (T_v) of the 'standard' Strömgren v filter, pg. 57 (Schaifers and Voight, 1982a). The response function of the 1P21 photomultiplier tube is included in the data.

λ	T_v	λ	T_v	λ	T_v	λ	T_v	λ	T_v
375.00	0.0000	390.00	0.0302	405.00	0.3992	420.00	0.2778	435.00	0.0192
377.50	0.0016	392.50	0.0478	407.50	0.4704	422.50	0.1776	437.50	0.0133
380.00	0.0035	395.00	0.0781	410.00	0.4898	425.00	0.1088	440.00	0.0068
382.50	0.0083	397.50	0.1297	412.50	0.4752	427.50	0.0654	442.50	0.0034
385.00	0.0146	400.00	0.2000	415.00	0.4300	430.00	0.0388	445.00	0.0000
387.50	0.0226	402.50	0.2988	417.50	0.3664	432.50	0.0259		

Table F.11: The transmission function (T_b) of the 'standard' Strömgren b filter, pg. 57 (Schaifers and Voight, 1982a). The response function of the 1P21 photomultiplier tube is included in the data.

λ	T_b	λ	T_b	λ	T_b	λ	T_b	λ	T_b
435.00	0.0000	450.00	0.0460	465.00	0.3992	480.00	0.0880	495.00	0.0067
437.50	0.0038	452.50	0.0728	467.50	0.4008	482.50	0.0544	497.50	0.0051
440.00	0.0091	455.00	0.1116	470.00	0.3806	485.00	0.0306	500.00	0.0028
442.50	0.0150	457.50	0.1780	472.50	0.3171	487.50	0.0194	502.50	0.0014
445.00	0.0216	460.00	0.2658	475.00	0.2283	490.00	0.0115	505.00	0.0000
447.50	0.0333	462.50	0.3535	477.50	0.1409	492.50	0.0092		

Table F.12: The transmission function (T_y) of the 'standard' Strömgren y filter, pg. 57 (Schaifers and Voight, 1982a). The response function of the 1P21 photomultiplier tube is included in the data.

λ	T_y	λ	T_y	λ	T_y	λ	T_y	λ	T_y
515.00	0.0000	530.00	0.0551	545.00	0.2013	560.00	0.0744	575.00	0.0029
517.50	0.0042	532.50	0.0790	547.50	0.2005	562.50	0.0433	577.50	0.0019
520.00	0.0102	535.00	0.1170	550.00	0.1984	565.00	0.0270	580.00	0.0014
522.50	0.0158	537.50	0.1584	552.50	0.1899	567.50	0.0172	582.50	0.0007
525.00	0.0228	540.00	0.1927	555.00	0.1590	570.00	0.0100	585.00	0.0000
527.50	0.0390	542.50	0.1998	557.50	0.1148	572.50	0.0057		

Table F.13: The transmission function (T_U) of the U filter of the 'standard' $UBVRI$ system (Column UX which includes extinction, Table 2, Bessell, 1990).

λ	T_U	λ	T_U	λ	T_U	λ	T_U	λ	T_U
300.00	0.000	325.00	0.423	350.00	0.905	375.00	0.989	400.00	0.238
305.00	0.016	330.00	0.560	355.00	0.943	380.00	0.916	405.00	0.114
310.00	0.068	335.00	0.673	360.00	0.981	385.00	0.804	410.00	0.051
315.00	0.167	340.00	0.772	365.00	0.993	390.00	0.625	415.00	0.019
320.00	0.287	345.00	0.841	370.00	1.000	395.00	0.423	420.00	0.000

Table F.14: The transmission function (T_B) of the B filter of the 'standard' $UBVRI$ system (Column B, Table 2, Bessell, 1990).

λ	T_B	λ	T_B	λ	T_B	λ	T_B	λ	T_B
360.00	0.000	410.00	0.978	450.00	0.853	490.00	0.424	530.00	0.095
370.00	0.030	420.00	1.000	460.00	0.740	500.00	0.325	540.00	0.043
380.00	0.134	430.00	0.978	470.00	0.640	510.00	0.235	550.00	0.009
390.00	0.567	440.00	0.935	480.00	0.536	520.00	0.150	560.00	0.000
400.00	0.920								

Table F.15: The transmission function (T_V) of the V filter of the 'standard' $UBVRI$ system (Column V, Table 2, Bessell, 1990).

λ	T_V	λ	T_V	λ	T_V	λ	T_V	λ	T_V
470.00	0.000	520.00	0.967	570.00	0.684	620.00	0.197	670.00	0.017
480.00	0.030	530.00	1.000	580.00	0.574	630.00	0.135	680.00	0.013
490.00	0.163	540.00	0.973	590.00	0.461	640.00	0.081	690.00	0.009
500.00	0.458	550.00	0.898	600.00	0.359	650.00	0.045	700.00	0.000
510.00	0.780	560.00	0.792	610.00	0.270	660.00	0.025		

Table F.16: The transmission function (T_R) of the R filter of the 'standard' $UBVRI$ system (Column R, Table 2, Bessell, 1990).

λ	T_R	λ	T_R	λ	T_R	λ	T_R	λ	T_R
550.00	0.00	600.00	1.00	650.00	0.86	700.00	0.61	750.00	0.35
560.00	0.23	610.00	0.98	660.00	0.81	710.00	0.56	800.00	0.14
570.00	0.74	620.00	0.96	670.00	0.78	720.00	0.51	850.00	0.03
580.00	0.91	630.00	0.93	680.00	0.72	730.00	0.46	900.00	0.00
590.00	0.98	640.00	0.90	690.00	0.67	740.00	0.40		

Table F.17: The transmission function (T_I) of the I filter of the 'standard' $UBVRI$ system (Column I, Table 2, Bessell, 1990).

λ	T_I	λ	T_I	λ	T_I	λ	T_I	λ	T_I
700.00	0.000	750.00	0.910	800.00	1.000	850.00	0.910	900.00	0.150
710.00	0.024	760.00	0.965	810.00	1.000	860.00	0.860	910.00	0.030
720.00	0.232	770.00	0.985	820.00	0.990	870.00	0.750	920.00	0.000
730.00	0.555	780.00	0.990	830.00	0.980	880.00	0.560		
740.00	0.785	790.00	0.995	840.00	0.950	890.00	0.330		

Table F.18: The transmission function (T_{Atm}) of a 'standard' atmosphere (Straižys, 1992) – the 'ozone concentration' is '$d = 3mm$'

λ	T_{Atm}	λ	T_{Atm}	λ	T_{Atm}	λ	T_{Atm}	λ	T_{Atm}
300.00	4.3618	465.00	0.3066	625.00	0.1675	785.00	0.0718	945.00	1.0505
305.00	2.9029	470.00	0.2951	630.00	0.1893	790.00	0.0788	950.00	0.8670
310.00	2.1425	475.00	0.2866	635.00	0.1663	795.00	0.0788	955.00	0.6491
315.00	1.5910	480.00	0.2781	640.00	0.1575	800.00	0.0846	960.00	0.4348
320.00	1.2857	485.00	0.2698	645.00	0.1512	805.00	0.0788	965.00	0.2980
325.00	1.1618	490.00	0.2614	650.00	0.1512	810.00	0.0846	970.00	0.1893
330.00	1.0534	495.00	0.2546	655.00	0.1388	815.00	0.1893	975.00	0.2698
335.00	0.9707	500.00	0.2491	660.00	0.1265	820.00	0.1701	980.00	0.1765
340.00	0.9113	505.00	0.2423	665.00	0.1217	825.00	0.1958	985.00	0.0905
345.00	0.8622	510.00	0.2369	670.00	0.1180	830.00	0.1893	990.00	0.0557
350.00	0.8151	515.00	0.2315	675.00	0.1144	835.00	0.1024	995.00	0.0557
355.00	0.7723	520.00	0.2261	680.00	0.1108	840.00	0.0788	1000.00	0.0443
360.00	0.7311	525.00	0.2221	685.00	0.1765	845.00	0.0672	1010.00	0.0443
365.00	0.6893	530.00	0.2181	690.00	0.2115	850.00	0.0614	1020.00	0.0443
370.00	0.6491	535.00	0.2141	695.00	0.1512	855.00	0.0614	1030.00	0.0443
375.00	0.6218	540.00	0.2102	700.00	0.1265	860.00	0.0557	1040.00	0.0443
380.00	0.5914	545.00	0.2075	705.00	0.1144	865.00	0.0557	1050.00	0.0557
385.00	0.5637	550.00	0.2062	710.00	0.1084	870.00	0.0614	1060.00	0.1024
390.00	0.5420	555.00	0.2036	715.00	0.1265	875.00	0.0672	1070.00	0.0905
395.00	0.5208	560.00	0.2010	720.00	0.1575	880.00	0.0788	1080.00	0.1512
400.00	0.5016	565.00	0.1997	725.00	0.1450	885.00	0.0964	1090.00	0.1765
405.00	0.4795	570.00	0.1971	730.00	0.1265	890.00	0.1765	1100.00	0.2288
410.00	0.4611	575.00	0.1958	735.00	0.1084	895.00	0.2698	1110.00	0.7311
415.00	0.4429	580.00	0.1932	740.00	0.0905	900.00	0.3567	1120.00	2.1347
420.00	0.4267	585.00	0.1919	745.00	0.0811	905.00	0.1765	1130.00	0.7745
425.00	0.4108	590.00	0.2155	750.00	0.0800	910.00	0.2980	1140.00	0.9680
430.00	0.3966	595.00	0.2102	755.00	0.0788	915.00	0.3123	1150.00	0.3567
435.00	0.3811	600.00	0.1893	760.00	0.9265	920.00	0.2423	1160.00	0.2023
440.00	0.3673	605.00	0.1816	765.00	0.6160	925.00	0.2155	1170.00	0.2023
445.00	0.3537	610.00	0.1790	770.00	0.1060	930.00	0.5729	1180.00	0.2288
450.00	0.3417	615.00	0.1765	775.00	0.0741	935.00	1.2716	1190.00	0.1638
455.00	0.3299	620.00	0.1714	780.00	0.0730	940.00	0.6491	1200.00	0.1388
460.00	0.3182								

Table F.19: The spectral reflectivity (R_{Al}) of an Aluminised mirror (Allen, 1976)

λ	R_{Al}	λ	R_{Al}	λ	R_{Al}	λ	R_{Al}	λ	R_{Al}
200.00	0.7200	300.00	0.8200	400.00	0.8500	600.00	0.8900	1000.00	0.9300
220.00	0.7800	320.00	0.8200	450.00	0.8600	650.00	0.8800	2000.00	0.9600
240.00	0.8100	340.00	0.8300	500.00	0.8700	700.00	0.8700	5000.00	0.9700
260.00	0.8200	360.00	0.8300	550.00	0.8800	800.00	0.8500	10000.00	0.9800
280.00	0.8200	380.00	0.8400						

F.3 The EROS B_E,R_E photometric system

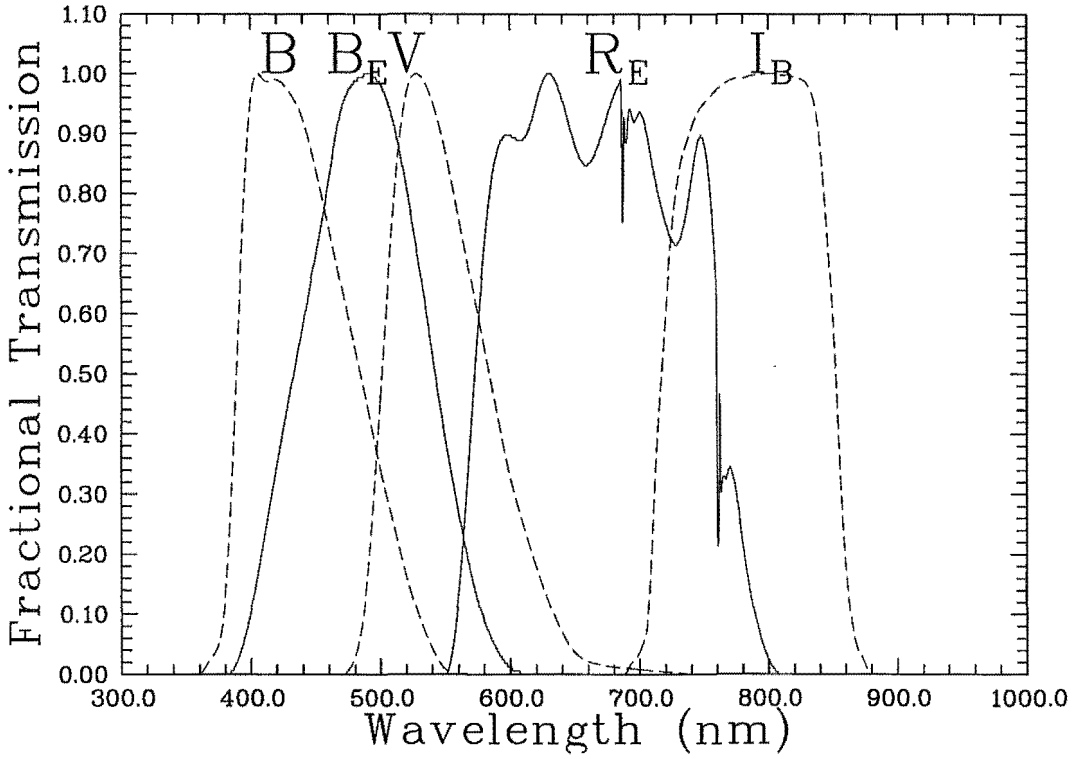

Figure F.1: Normalised response functions of the B_E and R_E EROS photometric system. The ploted response functions include the filter transmission function and the EROS CCD quantum efficiency function (tables F.20 and F.21) and the typical atmosphere transmission function for La Silla (table F.22). Also shown for comparison (dashed lines), are the standard B, V and I normailsed bandpass response functions (tables F.14, F.15 and F.17.)

Table F.20: The transmission function ($T_{B_{\rm E}}$) of the $B_{\rm E}$ filter, as measured from transmission curves provided by the EROS collaboration. These functions include the response function of the EROS CCDs.

λ	$T_{B_{\rm E}}$	λ	$T_{B_{\rm E}}$	λ	$T_{B_{\rm E}}$	λ	$T_{B_{\rm E}}$	λ	$T_{B_{\rm E}}$
380.80	0.0000	461.50	0.2280	482.30	0.2600	541.20	0.1280	620.70	0.0000
420.00	0.1050	466.20	0.2430	501.90	0.2500	581.50	0.0190		

Table F.21: The transmission function ($T_{R_{\rm E}}$) of the $R_{\rm E}$ filter, as measured from transmission curves provided by the EROS collaboration. These functions include the response function of the EROS CCDs.

λ	$T_{R_{\rm E}}$	λ	$T_{R_{\rm E}}$	λ	$T_{R_{\rm E}}$	λ	$T_{R_{\rm E}}$	λ	$T_{R_{\rm E}}$
550.00	0.000	627.70	0.328	672.70	0.297	722.30	0.257	760.40	0.216
583.80	0.270	641.50	0.311	687.70	0.328	732.70	0.270	791.50	0.027
612.70	0.297	657.50	0.277	701.50	0.311	747.70	0.311	830.70	0.000

Table F.22: The transmission function ($T_{\rm LS-Atm}$) of the atmosphere at La Silla (Fluks and Thé, 1992)

λ	$T_{\rm LS-Atm}$	λ	$T_{\rm LS-Atm}$	λ	$T_{\rm LS-Atm}$	λ	$T_{\rm LS-Atm}$	λ	$T_{\rm LS-Atm}$
375.00	0.3849	687.50	0.2100	758.00	0.0390	762.60	0.4888	802.00	0.0361
400.00	0.2900	688.00	0.1065	758.50	0.0426	762.80	0.5288	805.00	0.0494
450.00	0.1805	688.20	0.0653	759.00	0.0521	763.00	0.5149	810.00	0.0799
475.00	0.1537	688.50	0.1187	759.20	0.0832	763.50	0.4969	815.00	0.2083
500.00	0.1389	689.00	0.1436	759.50	0.1723	764.00	0.4408	820.00	0.2614
525.00	0.1275	690.00	0.1434	760.00	0.4454	765.00	0.3840	821.00	0.2746
550.00	0.1217	691.00	0.1161	760.20	0.7774	767.50	0.2952	821.50	0.2765
580.00	0.1128	695.00	0.0993	760.50	0.8762	770.00	0.1585	822.00	0.2744
600.00	0.0940	700.00	0.0657	760.60	0.9334	772.50	0.0892	825.00	0.2073
625.00	0.0762	710.00	0.0593	760.80	0.9100	774.00	0.0552	830.00	0.1096
650.00	0.0614	720.00	0.0737	761.00	0.8390	775.00	0.0386	835.00	0.0608
675.00	0.0502	730.00	0.1146	761.40	0.7633	780.00	0.0325	840.00	0.0357
685.00	0.0549	740.00	0.1126	761.80	0.4677	799.00	0.0298	850.00	0.0212
686.00	0.0772	750.00	0.0528	761.90	0.2344	800.00	0.0310	875.00	0.0170
687.00	0.2651	757.00	0.0356	762.00	0.2273	801.00	0.0333	900.00	0.0127
687.10	0.2626	757.50	0.0372	762.40	0.2561				

Bibliography

Abbe, C. 1867, MNRAS, 27, 262

Al-Naimiy, H. 1978, Ap&SS, 53, 181

Alcock, C., Akerlof, C., Allsman, R., Axelrod, T., Bennet, D., Chan, S., Cook, K., Freeman, K., Griest, K., Marshall, S., Park, H.-S., Perimutter, S., Peterson, B., Pratt, M., Quinn, P., Rodgers, A., Stubbs, C., & Sutherland, W. 1993, Nature, 365, 621, The MACHO Collaboration

Alcock, C., Allsman, R. A., Alves, D. R., Axelrod, T. S., Becker, A., Bennett, D. P., Clayton, G. C., Cook, K. H., Freeman, K. C., Griest, K., Guern, J. A., Kilkenny, D., Lehner, M. J., Marshall, S. L., Minniti, D., Peterson, B. A., Pratt, M. R., Quinn, P. J., Rodgers, A. W., Stubbs, C. W., Sutherland, W., & Welch, D. L. 1996a, APJ, 470, 583

Alcock, C., Allsman, R. A., Axelrod, T. S., Bennett, D. P., Cook, K. H., Freeman, K. C., & Griest, K. 1996b, AJ, 111, 1146

Alcock, C., Allsman, R. A., Axelrod, T. S., Bennett, D. P., Cook, K. H., Freeman, K. C., Griest, K., Marshall, S. L., Peterson, B. A., Pratt, M. R., Quinn, P. J., Reimann, J., Rodgers, A. W., Stubbs, C. W., Sutherland, W., & Welch, D. L. 1995, AJ, 109, 1654

Allen, C. 1976, *Astrophysical Quantites*, Athlone, London, 3rd edition edition

Andersen, J. 1991, A&AR, 3, 91

Andersen, J., Clausen, J., & Nordström, B. 1984, A&A, 134, 147

Ansari, R., Cavalier, F., Moniez, M., Aubourg, E., Bareyre, P., Bréhin, S., Gros, M., Lachièze-Rey, M., Laurent, B., Lesquoy, E., Magneville, C., Milsztajn, A., Moscoso, L., Queinnec, F., Renault, C., Rich, J., Spiro, M., Vigroux, L., Zylberajch, S., Beaulieu, J. P., Ferlet, R., Grison , P., Vidal-Madjar, A., Guibert, J., Moreau, O., Tajahmady, F., Maurice, E., Prévôt, L., & Gry, C. 1996, A&A, 314, 94

Aubourg, E., Bareyre, P., Brehin, S., Gros, M., De Kat, J., Lachieze-Rey, M., Laurent, B., Lesquoy, E., Magneville, C., Milsztajn, A., Moscoso, L., Queinnec, F., Renault, C., Rich, J., Spiro, M., Vigroux, L., Zylberajch, S., Ansari, R., Cavalier, F., Moniez, M., Beaulieu, J. P., Ferlet, R., Grison, P., Vidal-Madjar, A., Guibert, J., Moreau, O., Tajahmady, F., Maurice, E., Prevot, L., & Gry, C. 1995, A&A, 301, 1

Aubourg, E., Bareyre, P., Brehin, S., Gros, M., Lachièze-Rey, M., Laurent, B., Lesquoy, E., Magneville, C., Milsztajn, A., Moscoso, L., Quiennec, F., Rich, J., Spiro, M., Vigroux, L., Zylbrajch, S., Ansari, R., Cavalier, F., Moniez, M., Beaulieu, J.-P., Ferlet, R., Grison, P., Vidal-Madjar, A., Guibert, J., Moreau, O., Tajahmady, F., Maurice, E., Prévot, L., & Gry, C. 1993, Nat, 365, 623

Avni, Y. 1976, APJ, 209, 574

Batten, A. H. 1995, Reports on Progress in Physics, 58, 885

Beaulieu, J. & Sasselov 1997, in press

Beaulieu, J.-P., Grison, P., Tobin, W., Pritchard, J., Ferlet, R., Lepeintre, F., Vidal-Madjar, A., Maurice, E., Prévot, L., Gry, C., Guibert, J., Moreau, O., Tajahmady, F., Aubourg, E., Bareyre, P., Coutures, C., Gros, M., Laurent, B., Lachièze-Rey, M., Lesquoy, E., Magneville, C., Milsztajn, A., Moscoso, L., Quiennec, F., Renault, C., Rich, J., Spiro, M., Vigroux, L., Zylbrajch, S., Ansari, R., Cavalier, F., & Moniez, M. 1995, A&A, 303, 137

Bell, S., Hill, G., Hilditch, R., Clausen, J., & Reynolds, A. 1993, MNRAS, 265, 1047

Bell, S., Hill, G., Hilditch, R., Clausen, J., Reynolds, A., & Giménez, A. 1991, MNRAS, 250, 119

Bessell, M. 1979, PASP, 91, 589

Bessell, M. 1990, PASP, 102, 1181

Bessell, M. 1991, A&A, 242, L17

Bessell, M. 1995, PASP, 107, 672

Bessell, M. & Wickramasinghe, D. 1978, MNRAS, 182, 275

Bohlin, R., Savage, B., & Drake, J. 1978, APJ, 224, 132

Bouchet, P., Lequeux, J., Maurice, E., Prévot, L., & Prévot-Burnichon, M. 1985, A&A, 149, 330

Bradstreet, D. H., Dewarf, L. E., Guinan, E. F., Maloney, F. P., & Maurone, P. A. 1995, BAAS, 187, 4320

Brodie, L. & Forth Inc. 1987, *Starting* FORTH, Prentice-Hall, Inc.

Buonanno, R., Buscema, G., Corsi, C., Ferraro, I., & Iannicola, G. 1983, A&A, 126, 278

Buscombe, W., Gascoigne, S., & de Vaucouleurs, G. 1954, Aust. J. Sci. Suppl. 17(3)

Caldwell, J. A. & Laney, C. D. 1991, in R. Haynes & D. Milne (eds.), *The Magellanic Clouds*, p. 249, Kluwer Academic Publishers

Carbon, D. & Gingerich, O. 1969, in O. Gingerich (ed.), *Theory and Observation of Normal Stellar Atmospheres*, MIT Press

Castelli, F. & Kurucz, R. 1994, A&A, 281, 817

Chambliss, C. 1967a, AJ, 72, 512

Chambliss, C. 1967b, AJ, 72, 518

Charbonnel, C., Meynet, G., Maeder, A., Schaller, G., & Schaerer, D. 1993, A&AS, 101, 415

Claret, A. & Giménez, A. 1990, A&A, 230, 412
Claret, A. & Giménez, A. 1993, A&A, 277, 487
Claret, A., Giménez, A., & Cunha, N. 1995, A&A, 299, 724
Clausen, J. 1996, private communication, Applications : Observing time on the Danish Telescopes at La Scilla : Travel Grants from the Danish ESO-Reseach Fund
Code, A., Davis, J., Bless, R., & Hanbury Brown, R. 1976, AJ, 203, 417
Cook, K. H. 1996, BAAS, 188, 6503
Cousins, A. 1987, SAAO Circulars, (11), 93
Crawford, D. 1975a, AJ, 80, 955
Crawford, D. 1975b, PASP, 87, 481
Crawford, D. 1978, AJ, 83, 48
Crawford, D. 1979, AJ, 84, 1858
Crawford, D. 1993, in D. Kilkenny, E. Lastovica, & J. Menzies (eds.), *Precision Photometry*, p. 18, The South African Astronomical Observatory
Crawford, D. & Barnes, J. 1970, AJ, 75, 978
Crawford, D., Barnes, J., Gibson, J., Golson, J., Perry, C., & Crawford, M. 1972, A&AS, 5, 109
Crotts, A. P. S., Kunkel, W. E., & Heathcote, S. R. 1995, ApJ, 438, 724
Davidge, T. 1987, AJ, 94, 1169
Davidge, T. 1988, AJ, 95, 731
Davidge, T. & Milone, E. 1984, ApJS, 55, 571
De Greve, J. 1993, A&AS, 97, 527
De Greve, J. & de Loore, C. 1992, A&AS, 96, 653
De Greve, J. & Doom, C. 1988, A&AS, 74, 325
de Landtsheer, A. 1983, Ap&SS, 92, 231
de Loore, C. & De Greve, J. 1992, A&AS, 96, 653
de Vaucouleurs, G. 1993, ApJ, 415, 10
Díaz-Cordovés, J., Claret, A., & Giménez, A. 1995, A&AS, 110, 329
Díaz-Cordovés, J. & Giménez, A. 1992, A&A, 259, 227
Doom, C. 1984, A&A, 120, 97
Doom, C. & de Grève, J. 1983, A&A, 120, 97
Duncan, S. 1991, *CCD Photometry of Three Variable Stars in the Small Magellanic Clouds*, Undergraduate Project Report, Physics Department, University of Canterbury, New Zealand
Duncan, S., Tobin, W., Watson, R., & Gilmore, A. 1993, MNRAS, 265, 189
Etzel, P. 1993, in E. Milone (ed.), *Light Curve Modeling of Eclipsing Binary Stars*, p. 113, Springer-Verlag
Fitzpatrick, E. 1986, AJ, 92, 1068
Fluks, M. & Thé, P. 1992, A&A, 255, 477
Gaposchkin, S. 1965, in *The Position of Variable Stars in the Hertzsprung-Russell Diagram*, Kl. Versöffentlichungen der Remeis-Sterwatre, Astronomisches Institut der Universität, Erlangen-Nürnberg, Bd.IV, Nr.40, p. 66, International Astronomical Union, Combined Coloquium of the Commissions 27 and 42
Gaposhkin, S. 1970, *The Large Magellanic Cloud : Its topography of 1830 variable stars*, Research in Space Science SAO Special Report No.310
Gaposhkin, S. 1977, *One Hundred and Eight Eclipsing Variables in the Magellanic Clouds*, Research in Space Science SAO Special Report No. 380
Gardiner, L. T., Sawa, T., & Fujimoto, M. 1994, MNRAS, 266, 567
Garhart, M. 1992, IUE NASA Newsletter, 40, 98
Gilmore, A. & Kilmartin, P. 1994, *Coordinates for MCEBs*, private communication
Gilmore, A. & Kilmartin, P. 1996, *Coordinates for MCEBs*, private communication
Gilmore, A. & Tobin, W. 1989, *Temperature sensitivity of the CE200 electronics unit*, Mt John Photometrics CCD System Use and Performance Note 5, Department of Physics and Astronomy, University of Canterbury, New Zealand
Giménez, A. & Bastero, M. 1995, Ap&SS, 226, 99
Giménez, A., Clausen, J., Guinan, E., Maloney, F., Bradstreet, D., Storm, J., & Tobin, W. 1994, Experimental Astronomy, 5, 181
Giménez, A. & Garcia-Pelayo, J. 1983, Ap&SS, 92, 203
Graham, J. 1972, AJ, 77, 144
Graham, J. 1982, PASP, 94, 244
Graham, J. & Slettlebak, A. 1973, AJ, 78, 295
Greenhill, J., Watson, R., Tobin, W., Pritchard, J., & Clark, M. 1995, MNRAS, 274, L59
Grison, P., Beaulieu, J.-P., Pritchard, J., Tobin, W., Ferlet, R., Vidal-Madjar, A., Guibert, J., Alard, C., Moreau, O., Tajahmady, F., Maurice, E., Prévot, L., Gry, C., Aubourg, E., Bareyre, P., Brehin, S., Gros, M., Lachièze-Rey, M., Laurent, B., Lesquoy, E., Magneville, C., Milsztajn, A., Moscoso, L., Quiennec, F., Rich, J., Spiro, M., Vigroux, L., Zylbrajch, S., Ansari, R., Cavalier, F., & Moniez, M. 1995, A&AS, 109, 447
Guinan, E. 1977, AJ, 82, 51
Guinan, E. 1993, in K. Leung & I.-S. Nha (eds.), *New Frontiers in Binary Star Research*, p. 38, ASP Conference Series

Guinan, E. 1995, *Effective temperature of HV 2241's primary component*, private communication
Guinan, E. 1996, *HST observations of MCEBs*, private communication
Hanuschik, R. W. & Schmidt-Kaler, T. 1991, A&A, 249, 36
Harris, W., Fitzgerald, M., & Reed, B. 1981, PASP, 93, 507
Heber, U., Hunger, K., Jonas, G., & Kudritzki, R. 1984, A&A, 130, 119
Herczeg, T. J. 1982, in Zdeněk Kopal and Jürgen Rahe (ed.), *Binary and Multiple Stars as Tracers of Stellar Evolution*, Vol. 98 of *Recent Developments of Space Science and of General Geophysics and Astrophysics*, p. 145, IAU Coloquium No. 69, D. Riedel Publishing Company, Dordrecht : Holland / Boston : USA / London : England
Hilditch, R. & Bell, S. 1987, MNRAS, 229, 529
Howarth, I. 1983, MNRAS, 203, 301
Iben, Jr, I. 1965, AJ, 141, 993
Imhoff, C. 1996, *Regarding the uncertainty in the* IUE *flux calibration*, private communication
Jacoby, G. (ed.) 1990, *CCDs in Astronomy*, Vol. 8 of *ASP Conference Series*, Astronomical Society of the Pacific
Jensen, K., Clausen, J., & Giménez, A. 1988, A&AS, 74, 331
Johnson, H. 1965, APJ, 141, 923
Johnson, H. & Morgan, W. 1953, APJ, 117, 313
Keep, L.-B. 1995, *Eclipsing Binary Stars in the Large Magellanic Clouds*, Part III Honours Project, University of Canterbury, New Zealand
Keppens, R. 1997, A&A, 318, 275
Kilkenny, D. 1977a, MNRAS, 178, 369
Kilkenny, D. 1977b, MNRAS, 181, 611
Kilkenny, D. & Hill, P. 1975, MNRAS, 173, 625
Kilkenny, D., Hill, P., & Brown, A. 1977, MNRAS, 178, 123
Kilkenny, D. & Laing, J. 1992, MNRAS, 255, 308
Kilkenny, D. & Menzies, J. 1989, South African Astron. Obs. Circ. no. 13, 25
Koorneef, J. 1982, A&A, 107, 247
Kopal, Z. 1959, *Close Bianry Systems*, Vol. Five of *The International Astrophysics Series*, Chapman & Hall Ltd
Kurucz, R. 1979, APJS, 40, 1
Kurucz, R. 1993, in E. Milone (ed.), *Light Curve Modeling of Eclipsing Binary Stars*, p. 93, Springer-Verlag
Landolt, A. 1983, AJ, 88, 439
Landolt, A. 1992, AJ, 104, 340
Lang, K. 1992, *Astrophysical Data; Planets and Stars*, Springer-Verlag
Latham, D., Mazeh, T., Davis, R., Stefanik, R., & Abt, H. 1991, AJ, 101, 625
Leavitt, H. 1912, Harvard Circular, (173)
Lequeux, J. 1997, *Interstellar Extinction in the Magellanic Clouds*, private communication
Leung, K.-C. 1974, AJ, 79, 852
Lubow, S. & Shu, F. 1975, APJ, 198, 383
Lubow, S. & Shu, F. 1976, APJ, 207, L53
Manfroid, J. 1995, A&AS, 113, 587
Manfroid, J. 1996, A&AS, 118, 391
Marsh, S. 1971, *Master's thesis*, Department of Physics, University of Canterbury, Christchurch, New Zealand
McCall, M. L. 1993, APJ, 417, L75
McGee, R. & Milton, J. 1966, Australian J. Phys., Astrophys. Suppl., (2)
McGee, R. & Newton, L. 1982, Proc. Australian Astr. Soc. 4, 308
Mégessier, C. 1995, A&A, 296, 771
Menzies, J., Cousins, A., Banfield, R., & Laing, J. 1989, South African Astron. Obs. Circ. no. 13, 1
Menzies, J., Marang, F., & Westerhuys, J. 1990, South African Astron. Obs. Circ. no. 14, 33
Milone, E. 1993, in K.-C. Leung & I.-S. Nha (eds.), *New Frontiers in Binary Star Research*, Vol. 38 of *ASP Conference Series*, p. 91, Astronomical Society of the Pacific
Milone, E. 1996, *Kurucz Model Atmosphere Subroutine for the WD code*, private communication, Email: from EFM dated 960201
Mochnacki, S. 1971, *Master's thesis*, Department of Physics, University of Canterbury, Christchurch, New Zealand
Mochnacki, S. & Doughty, N. 1972a, MNRAS, 156, 51
Mochnacki, S. & Doughty, N. 1972b, MNRAS, 156, 243
Nichols, J. & Linsky, J. 1996, AJ, 111, 517
Niemela, V. 1986, in C. de Loore, A. Willis, & P. Laskarides (eds.), *Luminous Stars and Associations in Galaxies*, IAU, (IAU Symposium 116) Spectroscopic Binaries in the LMC
Niemela, V. & Bassino, L. 1994, APJ, 437, 332
Ostreicher, M., Gochermann, J., & Schmidt-Kaler, T. 1995, A&AS, 112, 495
Paczynski, B. 1986, APJ, 304, 1
Pagel, B. 1993, in B. Baschek, G. Klare, & J. Lequeux (eds.), *New Aspects of Magellanic Cloud Research*, p. 24, Springer-Verlag
Panagia, N., Gilmozzi, R., Macchetto, F., Adorf, H. M., & Kirshner, R. P. 1991, APJ, 380, L23

Payne-Gaposchkin, C. 1971, *The Variable Stars of the Large Magellanic Cloud*, Smithsonian Contributions to Astrophysics

Payne-Gaposchkin, C. & Gaposchkin, S. 1966, *Variable Stars in the Small Magellanic Cloud*

Pollard, K. 1989a, *Evaluation of the Linearity of the Mt John CCD*, Mt John Photometrics CCD System Use and Performance Note 2, Department of Physics and Astronomy, University of Canterbury, New Zealand

Pollard, K. 1989b, *Evaluation of the Spectral Response for various operating temperatures of the Mt John CCD*, Mt John Photometrics CCD System Use and Performance Note 3, Department of Physics and Astronomy, University of Canterbury, New Zealand

Popper, D. 1984, AJ, 89, 132

Press, W. H., Flannery, B. P., Teukolsky, S. A., & Vetterling, W. T. 1980, *Numerical Recipes: The Art of Scientific Computing*, Cambridge University Press

Prévot, M., Lequeux, J., Maurice, E., Prévot, L., & Rocca-Volmerange, B. 1984, A&A, 132, 389

Pritchard, J. 1993, *McLellan Telescope f/8 Seeing Values in the Green*, Mt John Photometrics CCD System Use and Performance Note 12, Department of Physics and Astronomy, University of Canterbury, New Zealand

Pritchard, J., Tobin, W., & Clark, M. 1994, Experimental Astronomy, 5, 43

Rieutord, M. & Zahn, J.-P. 1997, ApJ, 474, 760

Ritter, H. 1990, A&AS, 85, 1179

Russell, H. 1956, Vistas Astron., 2, 1177

Savage, B., Massa, D., Meade, M., & Wesselius, P. 1985, ApJS, 59, 397

Schaerer, D., Meynet, G., Maeder, A., & Schaller, G. 1993, A&AS, 98, 523

Schaifers, K. & Voight, H. (eds.) 1982a, *Numerical Data and Functional Relationships in Science and Technology*, Vol. 2 of *New Series*, pp 44–90, Landolt-Börnstein, New Series, Volume 2, Astronomy and Astrophysics, extension and Supplement to Volume 1 Subvolume b, Stars and Star Clusters

Schaifers, K. & Voight, H. (eds.) 1982b, *Numerical Data and Functional Relationships in Science and Technology*, Vol. 2 of *New Series*, pp 451–456, Landolt-Börnstein, New Series, Volume 2, Astronomy and Astrophysics, extension and Supplement to Volume 1 Subvolume b, Stars and Star Clusters

Schaller, G., Schaerer, D., Meynet, G., & Maeder, A. 1992, A&AS, 96, 269

Schechter, P., Mateo, M., & Saha, A. 1993, PASP, 105, 342

Schmidt-Kaler 1992, ASP Conferenec Series, 30, 195

Schmidt-Kaler, T. 1993, in B. Baschek, G. Klare, & J. Lequeux (eds.), *New Aspects of Magellanic Cloud Research*, p. 24, Springer-Verlag

Schwering, P. & Israel, F. 1991, A&A, 246, 231

Seaton, M. 1979, MNRAS, 187, 73P

Shapley, H. & Nail, V. 1953, Proc. Nat. Acad. Sci. (39), 1

Sterken, C. & Manfroid, J. 1992, *Astronomical Photometry: A Guide*, Vol. 175 of *The Recent developments of Space Science and of General Geophysics and Astrophysics*, Kluwer Academic Publishers

Stetson, P. 1987, PASP, 99, 191

Stetson, P. 1989, Highlights of Astronomy, 8, 635

Stetson, P. 1992, in D. Worrall, C. Biemesderfer, & J. Barnes (eds.), *Astronomical Data Analysis Software and Systems I*, ASP Conference Series, p. 297, Astronomical Society of the Pacific

Stetson, P. 1994a, in MIDAS *Manual*, Vol. B: Data Reduction, pp 11–1, European Southern Observatory

Stetson, P. 1994b, PASP, 106, 250

Stetson, P., Davis, L., & Crabtree, D. 1989, in G. Jacoby (ed.), *CCDs in Astronomy*, ASP Conference Series, p. 289, Astronomical Society of the Pacific

Straižys 1992, *Multicolor Stellar Photometry*, Vol. 15 of *Pachart Astronomy and Astrophysics Series*, Pachart Publishing House, Tucson, Arizona

Strohmeier, W. 1977, *Variable Stars, Their Discoverers and First Compilers: From 1006 to 1975*, Veröffentlichungen, der Remeis-Sternwarte Bamberg, Astronomisches Institut der Universität, Erlangen-Nürnberg, Band XII, Nr. 129

Sybesma, C. H. B. 1985, A&A, 142, 171

Sybesma, C. H. B. 1986a, A&A, 159, 108

Sybesma, C. H. B. 1986b, A&A, 168, 147

Tassoul, J.-L. & Tassoul, M. 1992, ApJ, 395, 259

Tobin, W. 1989, *Time keeping on the Photometrics CCD System*, Mt John Photometrics CCD System Use and Performance Note 7, Department of Physics and Astronomy, University of Canterbury, New Zealand

Tobin, W. 1991a, Southern Stars, 34 No. 8, 421

Tobin, W. 1991b, Proc. Astron. Soc. Aust. 9, 164

Tobin, W. 1992, *Gain, Noise And Related Characteristics Of The Mt John Photometrics CCD System*, Mt John Photometrics CCD System Use and Performance Note 10, Department of Physics and Astronomy, University of Canterbury, New Zealand

Tobin, W. 1994, Experimental Astronomy, 5, 67

Tobin, W. 1997a, *Foreground reddenings for HV 982, HV 1620 and HV 2241*, private communication

Tobin, W. 1997b, *New ephemerides for HV 982, HV 1620 and HV 2241*, private communication

Tobin, W., Duncan, S., West, S., & Gilmore, A. 1993a, MNRAS, 260, 777

Tobin, W. & Evans, G. (eds.) 1996, *Stars in a Cluster*, Department of Physics & Astronomy, University of Canterbury, Christchurch, New Zealand
Tobin, W., Kershaw, G., Ritchie, R., Ma, L., Graham, G., & Hemmingsen, S. 1993b, in I. Elliot & C. Butler (eds.), *Poster papers on stellar photometry*, p. 153, DIAS, Dublin
Tobin, W., Pritchard, J., Zambri, M., Keep, L.-B., & L.Skuljan 1997, in press
Underhill, A. 1981, AJ, 244, 963
van den Bergh, S. 1992, PASP, 104, 861
Van Hamme, W. 1993, AJ, 106, 2096
Wade, R. & Rucinski, S. 1985, A&AS, 60, 471
Watson, R., West, S., Tobin, W., & Gilmore, A. 1992, MNRAS, 258, 527
West, S. 1991, *Master's thesis*, University of Canterbury, New Zealand
West, S., Tobin, W., & Gilmore, A. 1992, MNRAS, 254, 419
Westerlund, B. 1990, A&AR, 2, 29
Westerlund, B. 1997, *The Magellanic Clouds*, Cambridge University Press, in press
Wetzel, M. 1953, Ann. Harv. Coll. Obs. 109, 58
Wilson, R. 1979, APJ, 234, 1054
Wilson, R. 1983, Ap&SS, 92, 229
Wilson, R. 1990, APJ, 356, 613
Wilson, R. 1992a, in K. Leung (ed.), *New Frontiers in interacting Binary Star Research*, ASP Conference Series, p. 91, Astronomical Society of the Pacific
Wilson, R. 1992b, *Documentation of Eclipsing Binary Computer Model (Revision of 1992:May)*
Wilson, R. 1993a, in K.-C. Leung & I.-S. Nha (eds.), *New Frontiers in Binary Star Research*, Vol. 38 of *ASP Conference Series*, p. 91, Astronomical Society of the Pacific
Wilson, R. 1993b, in E. Milone (ed.), *Light Curve Modeling of Eclipsing Binary Stars*, p. 7, Springer-Verlag
Wilson, R. 1994, PASP, 106, 921
Wilson, R. & Biermann, P. 1976, A&A, 48, 349
Wilson, R. & Devinney, E. 1971, APJ, 166, 605
Wilson, R. & Sofia, S. 1976, APJ, 203, 182